Study of Bent-tail radio galaxies and their corelation with galaxy clusters

Tapan Kumar Sasmal

Relativity and Cosmology Research Center,
Department of Physics, Jadavpur University,
Kolkata 700032, India.

Supervisor
Dr. Soumen Mondal

Thesis submitted for the degree of
Doctor of Philosophy (Science)
of the
Jadavpur University

September, 2022

JADAVPUR UNIVERSITY
KOLKATA-700032, INDIA

CERTIFICATE FROM THE SUPERVISOR

This is to certify that the thesis entitled **"Study of Bent-tail radio galaxies and their corelation with galaxy clusters"** submitted by **Tapan Kumar Sasmal (Index No.: 231/18/Phys/26, Registration No.: SOPHY-1123118)** who got his name registered on **9th October 2018** for the award of Ph.D. (Science) Degree of Jadavpur University, is absolutely based upon his own work under the supervision of **Dr. Soumen Mondal**, Associate Professor, Department of Physics, Jadavpur University and that neither this thesis nor any part of it has been submitted for either any degree/diploma or any other academic award anywhere before.

Soumen Mondal
8/9/2022

Dr. Soumen Mondal
Associate Professor,
Department of Physics,
Jadavpur University,
Kolkata-700032, India

Dr. Soumen Mondal
Associate Professor
Department of Physics
Jadavpur University
Kolkata - 700032

DECLARATION

I do hereby declare that the work embodied in this thesis entitled **"Study of Bent-tail radio galaxies and their corelation with galaxy clusters"** which is being submitted for the degree of Doctor of Philosophy (Science) has been carried out by me in the Relativity and Cosmology Research Centre (RCRC), PG Science Building, Department of Physics, Jadavpur University, Kolkata. Neither the thesis nor any part thereof has been presented anywhere earlier for any degree/diploma or academic award whatsoever.

Date: 08.09.2022
Kolkata, India

Tapan Kumar Sasmal
.....

Tapan Kumar Sasmal
PhD Research Scholar,
Department of Physics,
Jadavpur University,
Index No.: 231/18/Phys/26,
Registration No.: SOPHY1123118

ABSTRACT OF THE THESIS

submitted by
Tapan Kumar Sasmal, Index No.: 231/18/Phys/26
for the Degree of Doctor of Philosophy (Science) in the Department of Physics and
entitled
"Study of Bent-tail radio galaxies and their corelation with galaxy clusters"

September 2022

The Bent-tail (BT) radio galaxy is sub-class of radio galaxies where the primary lobes are being bent in the intercluster weather due to strong interactions between the radio jets and their respective intracluster medium. Based on the bending angle between the two lobes, BT sources are classify in two catagory narrow-angle tail (NAT) and wide-angle tail (WAT). The opening angle between the two lobes for NAT sources is less than 90 degree and for WAT sources it is greater than 90 degree. NAT radio sources are characterized by tails bent in a narrow V-like shape and in the case of WAT radio galaxies are such that the WATs exhibit wide "C-like morphologies.

We systematically search for BT radio galaxies from Very Large Array Faint Images of the Radio Sky at Twenty-Centimeters (VLA FIRST) survey database at 1400 MHz and LOFAR Two-metre Sky Survey First Data Release (LoTSS DR1) at 144 MHz frequency. From FIRST survey, We catalog of 717 new BT sources, among which 287 are NATs and 430 are WATs. Optical counterparts are found for 359 BT sources from FIRST survey. From LoTSS DR1, we found 82 BT sources, among which 10 are NATs and 72 are WATs. The various physical properties and statistical studies like luminosities, spectral index, power etc are also done of these BT sources.

Bent tail (BT) radio sources are radio galaxies which have jets that show a characteristic C, V or L-shape that is believed to be due to ram pressure caused by the motion of the galaxy through the ambient medium. They are generally found in galaxy clusters in the local Universe. They have already been used in observations as tracers of galaxy clusters at redshifts of up to z $\sim$ 1. In this work, we also try to find out the corelation between the BT soureces and the surrounding medium. We found that 50 out of 82 HT sources are associated with known galaxy clusters from LoTSS DR1. We listed the masses of the known cluster and found cluster masses $M \geq 10^{14.5} M_{\odot}$ contains 34% of BT galaxies while cluster masses $M \leq 10^{14.5} M_{\odot}$ contain 80% of BT galaxies for LoTSS sample.

In this thesis, we also repoted ninteen Miscellaneous Radio Sources (MRG), a new morphology of radio sources from FIRST and LoTSS DR1. This type of radio sources differs from other known morphological radio galaxies like FR-I, FR-II double-lobed , Bent-Tail, winged, HYMORS, and DDRG. This peculier type of radio galaxy are first reported in this thesis.

LIST OF PUBLICATIONS

(A) In Peer-Reviewed Journals:

1. **Tapan K. Sasmal**, Soumen Bera, Sabyasachi Pal, and Soumen Mondal, *A New Catalog of HeadTail Radio Galaxies from the VLA FIRST Survey*, 2022, **ApJS**, 259, 31
   DOI: 10.3847/1538-4365/ac4473

2. Soumen Bera, **Tapan K. Sasmal**, Dusmanta Patra, and Soumen Mondal, *"Winged" Radio Sources from LOFAR Two-meter Sky Survey First Data Release (LoTSS DR1)*, 2022, **ApJS**, 260, 7
   DOI: 10.3847/1538-4365/ac5cc4

3. Soumen Bera, Sabyasachi Pal, **Tapan K. Sasmal**, and Soumen Mondal, *FIRST Winged Radio Galaxies with X and Z Symmetry*, 2020, **ApJS**, 251, 9
   DOI: 10.3847/1538-4365/abb367

4. **Tapan K. Sasmal**, Soumen Bera, Soumen Mondal, *Miscellaneous Radio Galaxies from LOFAR survey*, 2021, accepted in **Astronomische Nachrichten**

5. **Tapan K. Sasmal**, Soumen Bera, Soumen Mondal, *A Catalog of Bent-Tail Radio Galaxies from LoTSS DR1 and their Correlation with Associated Clusters*, 2022, **MNRAS**, review report submitted

6. Soumen Bera, **Tapan K. Sasmal**, Soumen Mondal, Dusmanta Patra, *MRG: A FIRST look at the Miscellaneous Radio Galaxies*, 2022, **JAA**, submitted

(B) In Conference Proceedings:

1. **Tapan K. Sasmal**, Soumen Bera, Sabyasachi Pal, and Soumen Mondal, *Discovery of Four Miscellaneous Radio Galaxies From LoTSS DR1*, 2020, **Journal of Physics: Conference Series**, 1579, 012021
   DOI: 10.1088/1742-6596/1579/1/012021

2. Soumen Bera, Sabyasachi Pal, **Tapan K. Sasmal**, Soumen Mondal, and Dusmanta Patra, *MRG: The Miscellaneous Radio Galaxies from the FIRST Survey*, 2020, **Journal of Physics: Conference Series**, 1579, 012023
   DOI: 10.1088/1742-6596/1579/1/012023

ACKNOWLEDGEMENT

To my elder brother, Ratan Sasmal

I would like to thank my family, for forming and affirming me. To my dad 'Mahitosh Sasmal' and to my mother 'Durgarani Sasmal' – without whom it is inconceivable that I would have made it this far, To my family member who perished along the journey, and has made it this far, "You shall be missed. Dada you have gone too soon".

I would like to express my sincere gratitude to my supervisor Dr. Soumen Mondal for the continuous support of my PhD study and research work. His guidance helped me in all the time of research and writing of papers.

I would like to thank Soumen Bera for giving me all-time support and motivation for the research work as well as for personal problems. He always helps me to papers writing, review writing, how to move with new problems .....everything. This journey would not have been possible without his support. Whenever I fell down, he always stand with me and give me a boost. Thanks for helping me all the time.

I will like to thank Dusmanta da for the valuable advice and suggestions that enhanced the quality of my research work. To all the students and post-docs that I have had the pleasure to meet during this journey.

Thanks to Jadavpur University for giving me the opportunity to do research work and providing me with the financial means to complete this work.

Last but not the least, I would like to thank my friends Nilimesh, Kallol, Tridib, Avijit, Naresh da, Chayan, Suman and Sangita di who always support me.

Contents

List of Abbreviations

2MASS	The Two Micron All-Sky Survey
2MASX	The Two Micron All Sky Survey Extended Objects–Final Release
3C	The Third (3rd) Cambridge catalogue of Radio Sources
4C	The Fourth (4th) Cambridge catalogue of Radio Sources
5C	The Fifth (5th) Cambridge catalogue of Radio Sources
6C	The Sixth (6th) Cambridge catalogue of Radio Sources
7C	The Seventh (7th) Cambridge catalogue of Radio Sources
8C	The Eighth (8th) Cambridge catalogue of Radio Sources
9C	The Ninth (9th) Cambridge catalogue of Radio Sources
ABELL	Abell Clusters of Galaxies
AGN	Active Galactic Nucleus
AIPS	The Astronomical Image Processing System
ALMA	Atacama Large Millimeter Array
APMUKS	Automated Plate Measurement United Kingdom Schmidt
ASK	Automatic Spectroscopic K-means-based Classication
ASKAP	The Australian Square Kilometre Array Pathfinder
ASTRON	The Netherlands Institute for Radio Astronomy
ATATS	The Allen Telescope Array Twenty-centimeter Survey
ATHENA	Advanced Telescope for High-ENergy Astrophysics
ATCA	The Australia Telescope Compact Array
AUI	Associated Universities, Inc.
B2	The second (2nd) radio survey catalog of the Bologna 'Northern Cross' telescope
B3	The third (3rd) radio survey catalog of the Bologna 'Northern Cross' telescope
BH	Black Hole
BLR	Broad Line Region
BT	Bent-Tail
BTRS	Bent-Tail Radio Sources
CMB	The Cosmic Microwave Background
Cul	The radio source catalog from all Culgoora Lists
DDRG	Double-Double Radio Galaxy
DSS	The Digital Sky Survey
DSS2	The Digital Sky Survey 2
EE	Eye Estimation
EMU	The Evolutionary Map of the Universe
ERG	Episodic Radio Galaxy
ESA	The European Space Agency

EUVE	The Extreme Ultraviolet Explorer
EVLA	Expanded Very Large Array
FAST	The Five hundred meter Aperture Spherical Telescope
FFT	The Fast Fourier Transform
FIRST	The Faint Images of the Radio Sky at Twenty-Centimeters
FR-I	Fanaroff-Riley Class I
FR-II	Fanaroff-Riley Class II
FR0	Fanaroff-Riley Class 0
FRB	Fast Radio Burst
GALEXASC	Galaxy Evolution Explorer All-sky Catalog
GALEXMSC	Galaxy Evolution Explorer Medium-deep Sky Catalog
GIN	Galaxy Identication Number
GLEAM	Galactic and Extragalactic All-sky MWA
GMBCG	Gaussian Mixture Brightest Cluster Galaxy
GMRT	The Giant Metrewave Radio Telescope
GRG	Giant Radio Galaxy
GWB	Gravitational Wave Background
HALCA	Highly Advanced Laboratory for Communications and Astronomy
HBA	High Band Antenna
HETDEX	Hobby-Eberly Telescope Dark Energy Experiment
HST	The Hubble Space Telescope
HYMORS	HYbrid MOrphology Radio Sources
ICM	Intra-Cluster Medium
IGM	InterGalactic Medium
ILT	International LOFAR Telescope
IPAC	The Infrared Processing and Analysis Center
IR	InfraRed
ISM	InterStellar Medium
IUE	The International Ultraviolet Explorer
JAXA	The Japan Aerospace Exploration Agency
JWST	The James Webb Space Telescope
LBA	Low Band Antenna
LCRS	Las Campanas Redshift Survey
LINER	Low-Ionization Nuclear Emission-line Region
LOFAR	The LOw-Frequency ARray
LoLSS	The LoFAR LBA Sky Survey
LoTSS	The LoFAR Two-metre Sky Survey
LoTSS DR1	The LoFAR Two-meter Sky Survey First Data Release
LoTSS DR2	The LoFAR Two-meter Sky Survey Second Data Release
MaxBCG	Maximum likelihood redshift Brightest Cluster Galaxy

MBH	Massive Black Hole
MGC	Millennium Galaxy Catalogue
MHD	MagnetoHydroDynamic
MRG	Miscellaneous Radio Galaxy
MSSS	The LOFAR Multifrequency Snapshot Sky Survey
MVS	Manual Visual Search
NASA	The National Aeronautics and Space Administration
NASA IRTF	The NASA Infrared Telescope Facility
NAT	Narrow Angle Tail radio source
NCRA	The National Centre for Radio Astrophysics
NED	The NASA/IPAC Extragalactic Database
NGC	New General Catalogue
NLR	Narrow Line Region
NRAO	The National Radio Astronomy Observatory
NVSS	The NRAO VLA Sky Survey
ORC	Odd Radio Circle
OSO	Orbiting Solar Observatory
OVV	Optically Violently Variable
PKS	The Parkes Catalogue of Radio Sources
PMN	Parkes–MIT–NRAO
QSO	Quasi-Stellar Object
RC	Reference Catalogue, a catalog of nearby galaxies
RG	Radio Galaxy
RGZ	Radio Galaxy Zoo
ROSAT	The RÖntgenSATellit
RRAT	Rotating RAdio Transient
RXTE	The Rossi X-ray Timing Explorer
SAGAN	Search and Analysis of Giant radio galaxies with Associated Nuclei
Sco X-1	Scorpius X-1
SDSS	The Sloan Digital Sky Survey
SFR	Star-Forming Region
SKA	The Square Kilometre Array
SMBH	SuperMassive Black Hole
SNR	SuperNova Remnant
SPRINT-A	The Spectroscopic Planet Observatory for Recognition of Interaction of Atmosphere
SSTSL2	Spitzer Space Telescope Source List version 4.2
TGSS	The TIFR GMRT Sky Survey
TGSS ADR	The TIFR GMRT Sky Survey Alternative Data Release
TGSS ADR1	The TIFR GMRT Sky Survey Alternative Data Release 1

TIFR	The Tata Institute of Fundamental Research
TONS08	Texas–Oxford NVSS Structure 08 h region
TONS08w	TONS08 wider survey
TXS	The Texas Survey of Radio Sources
uGMRT	The upgraded Giant Metrewave Radio Telescope
UHF	Ultra-High Frequency
UKIRT	The United Kingdom Infra-Red Telescope
UV	UltraViolet
VHF	Very High Frequency
VISTA	The Visible and Infrared Survey Telescope for Astronomy
VLBI	The Very Long Baseline Interferometry
VLA	The Karl G. Jansky Very Large Array
VLSS	The VLA Low-Frequency Sky Survey
VLSSr	The VLA Low-frequency Sky Survey Redux
VSA	The Very Small Array
WAT	Wide Angle Tail radio source
WB	WISE Blazar-like Radio-loud Sources
WIRO	The Wyoming Infrared Observatory
WISE	The Wide-field Infrared Survey Explorer
WRG	Winged Radio Galaxy
XMM	The X-ray Multi-Mirror Mission
XRG	X-shaped Radio Galaxy
XRISM	The X-Ray Imaging and Spectroscopy Mission
ZRG	Z-shaped Radio Galaxy

List of Figures

List of Tables

Chapter 1

Introduction

The knowledge of the Universe, including how it evolves, how it could have originated, and where we believe it will end, has advanced significantly over time. Natural phenomenon are predicted and explained although there are till gaps in our understanding, the big picture has yet to clear.

In this work, we search Bent-tail (BT) radio sources from different surveys data which are publicly available. We also study the environment of these BT sources. We find out the corelation between thse BT samples and the cluster which are associated with the BT sources. We have used the surveys data from Very Large Aarray (VLA) telescopes Faint Images of the Radio Sky at Twenty-cm (VLA FIRST) and LOw Frequency ARray Two-metre Sky Survey First Data Release (LoTSS DR1). Some basic radio and optical properties of these BT sources are estimated.

BTs are extended radio galaxies whose radio jets show a characteristic 'C'-like shaped morphology which can be as severe as 'V'-like shaped in cases of a high degree of bending. The bending of these types of sources is thought to be a result of the ram pressure exerted on the jets by ambient gas when the relative velocity between the ambient gas and the radio galaxy is large. These are conditions that are predominantly found within galaxy groups and clusters.

BTs first appeared in 1968, when NGC 1265, IC 310, 3C 129 and 3C 465 were observed (Ryle & Windram(1968), MacDonald et al.(1968)). They were classified into two groups, NATs with opening angles less than 90° and WATs, whose opening angles are greater than 90°. These opening angles gave rise to a U-shape for NATs and V-shape for WATs (Rudnick & Owen(1976), Valentijn(1979)). These classes are discussed later in the chapter.

BTs are believed to have a broad range of bending angles, which depend on the ram pressure exerted by the environment and the degree of stiffness of the radio jet. Most of the BTs found in the early days were in rich Abell clusters (Ryle & Windram(1968), MacDonald et al.(1968), Miley et al.(1972)). These Abell clusters

are characterised by high velocity dispersion and high ICM densities compared to the less massive galaxy groups. This was initially a significant contributing factor to the belief that ram pressure exerted on the galaxy due to its motion through the ICM, is the cause of the jet bending.

A similar study have already done using observations with the Very Large Array (VLA) faint images of the radio sky at twenty-centimetre (FIRST) survey (Blanton et al.(2000)). They managed to find galaxy groups and clusters using BT radio sources in their samples.The results of Blanton et al.(2000) and Wing & Blanton(2011) were successfully used to find galaxy clusters up to a redshift of ≈ 1 (Blanton et al.(2003)). These results also showed that BTs are also likely to be found in galaxy groups. This is promising for their use as tracers of galaxy clusters and groups at high redshift. With an improved spatial resolution of $\sim 1''$ and a sensitivity of ~ 10 Jy, radio surveys, such as the SKA-MID, may find ~ 100 000 BTs in the local Universe and at high redshift ($z \geq 8$) (Dehghan et al.(2011). This method will thus yield even better results.

To study BT sources and its environments, an understanding of an active galactic nucleus (AGN), its host galaxy and group/cluster environment are needed. To better understand an AGN one has to understand its nuclear activity, where a supermassive blackhole (SMBH) accretes gas and forms radio jets whose luminosity can be observed at great distances. The bending of these jets is what characterises BTs have. This becomes a study of different aspects of extra-galactic astronomy as well as their evolution and how they come together to form the observed BTs phenomenon.

The new generation of radio telescopes, like the low frequency array (LOFAR), the SKA and its pathfinders Karoo array telescope (MeerKAT) and the Australia square kilometer array pathfinder (ASKAP), have sensitivity and sampling speed that will yield a wealth of new radio sources (Agudo et al.(2015), Prandoni & Seymour(2015)). A large number of the sources in continuum surveys are expected to be extended radio sources, with AGN jets which can be detected up to high redshift (Amarantidis et al.(2019)). The VLA FIRST Survey (Becker et al.(1995)), discussed later in this chapter, has yielded most of the known BTs. These BTs are thought to be a result of the ram pressure exerted on the jets by ambient ICM/IGM gas of high density when the relative velocity between the ambient gas and the radio galaxy is large. These are conditions that are found within galaxy groups and clusters. If BTs are found in clusters, then observing a BT at high redshift would help to locate where clusters can be observed. Optical and Near-infrared (NIR) surveys are not effective at finding the most massive galaxy clusters far beyond $z = 1.2$ (Ascaso et al.(2014)). The advantage of using radio telescopes to locate BTs, hence galaxy clusters, is that the sensitivity of radio telescopes would allow the observation of number of BTs up to redshift $z \geq 2$. Finding BTs

at high redshift would aid in the investigation of the number density of high mass clusters and how they vary with redshift.

1.1 Galaxies

Astronomy has mostly been an observational activity since humans utilised the Sun, Moon, and stars to determine time, the seasons, and the day of the week. In ancient times the naked eye was used and later on Galileos telescope ushered in an era of assisted observations. These observations considerably profited from the study of optics and served as the inspiration, at least in part, for the advancement in physics. As a result, additional stars were discovered and classified in an attempt to understand them.

Up to the invention of photographic plates, which allowed for a more reliable comparison of stellar fluxes, the comparison of stars at this period was purely subjective. The ability to understand more about the basic properties of stars was increased by the discovery of spectroscopy and the more reliable comparison of fluxes. Theoretical developments in physics have enhanced the scientific field of astronomy and raised new issues that need to improve the optical telescopes and technology.

The window of the electromagnetic radiation emitted by celestial bodies rapidly expanded with William Herschel's discovery of infrared light in 1800 and the birth of infrared astronomy bring on after three decades. Only in the beginning of the twentieth century were the first infrared observations made of stars other than the Sun. After the Second World War, the radio observations were started. X-Ray observations were begain from 1962. Unlike of point-like stars, some of the celestial bodies which were fuzzy or "nebulous" were seen using optical telescopes.

In 1924, Edwin Hubble determined the distance to M33 to be 285 kpc using observations of the period-luminosity relation in Cepheids. He discovered a similar outcome for M31, proving that these spiral nebulae were extragalactic (Hubble(1926)). With this, the studies of galaxy started to develop into their own field of astronomical research. A long period of trying to improve the morphological classification of galaxies and assigning certain physical characteristics to the different morphological classes followed as the number of known galaxies in the Universe increased.

One of the primary areas of study in extragalactic astronomy over the last decade or so has been the development of galaxy formation and evolution models. AGN feedback and star formation have occurred in them (Fabian(2012), Combes(2017)). One of the key questions that is still subject to active research is how the galaxies are formed in the early Universe. The two main conflicting

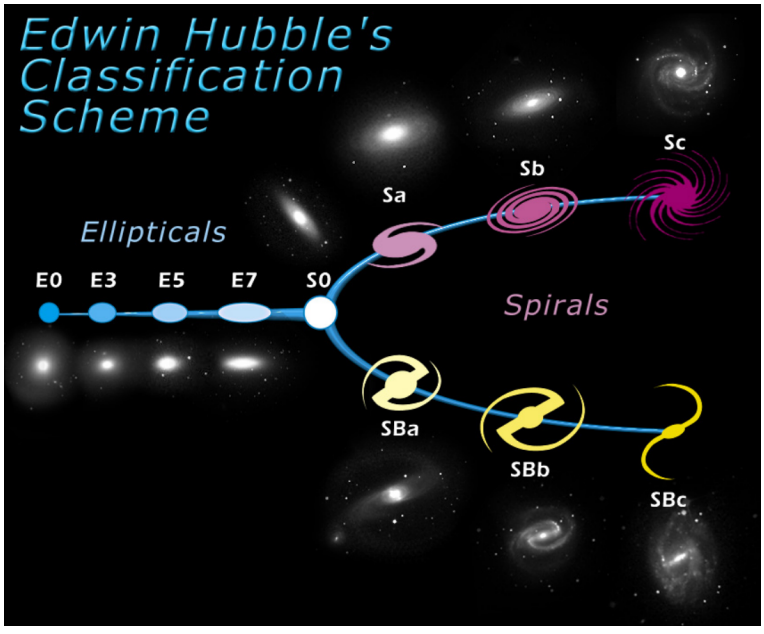

Figure 1.1: The Hubble tuning fork diagram showing the basic classification of galaxies into ellipticals, lenticulars, spirals and barred spirals. Image credit:https://www.spacetelescope.org/images/heic9902o/.

theories are the monolithic formation process, which believes that galaxies develop by the dissipative collapse of proto-galaxies, and the hierarchical structure formation, which argues that the huge galaxies visible today evolved via the merging of smaller structures (Fabian(2012), Kravtsov & Borgani(2012)). The radio emission from AGNs, is confined to galaxies with older spheroidal populations.

1.1.1 Galaxy Classification

A galaxy is made up of stars, stellar remnants, dark matter, gas, and dust that are gravitationally bonded together. This definition has changed throughout time as more information about the Galaxy and other topics has become available. Hubble(1926) was the first to categorise galaxies into three types when they were first spotted with photographic plates: elliptical, spiral, and barred spiral. Further research resulted in the classification of lenticular galaxies (type S0), which stand in between elliptical and spiral galaxies (Hubble et al.(2013)). The sequence of events represented in Figure 1.1 demonstrates the many features of elliptical, lenticular, spiral, and irregular galaxies as well as how they were believed to move from one type to another at the time. The general classes of elliptical, lenticular, spiral and irregular galaxies are discussed below.

Elliptical galaxies

A prolate spheroid shape and a low (less than 1%) cold molecular gas concentration are characteristics of elliptical galaxies (Blanton & Moustakas(2009)). The elliptical galaxies are characterised by old stellar populations and a smooth surface brightness profile. The shape of their isophotes is characterised by the de Vaucouleurs profile (de Vaucouleurs(1948)), which is equivalent to a Sersic index of n=4 (Sersic (1968)). They are known as early-type galaxies (ETGs) when they are combined with lenticulars. This is because they are mentioned first in the Hubble tuning fork diagram. They were once thought to be gas and dust-free. However, with more advanced instruments like the Hubble Space Telescope (HST), it has been discovered that this simplified description is incorrect. Although they may rotate quickly or slowly, all early-type galaxy (ETG) morphologies are supported by random velocity anisotropy. Their surface brightness is dominated by their spheroidal component.

Many of the ellipticals that were previously thought to be free of both dust and gas have been seen to contain both. In ellipticals, faint dust lanes have occasionally been seen that are perpendicular to the galaxy's primary axis. Let's just state that some elliptical galaxies have been incorrectly categorised and that their main difference from S0 galaxies is the absence of the dust lane. The star masses larger than $10^{10} M_{\odot}$, the galaxy luminosity function reveals that elliptical and lenticular galaxies are more common (Blanton & Moustakas(2009)).

The biggest galaxies in the universe are elliptical galaxies, which are situated in the cores of galaxy clusters and groups. Because SMBH mass corresponds with the mass of the spheroidal component of galaxies, such as galaxy bulges, these also contain the most massive SMBHs in the Universe. The other elliptical forms are dwarf ellipticals and dwarf spheroidals, which are significantly less massive.

Lenticular galaxies

These ETGs belong to a different class and are distinguished by the existence of a dust lane that may be completely covered by the spheroidal component. The spheroidal component of lenticulars (S0) shares the same characteristics as ellipticals and bulges of spirals. The spheroidal component of lenticulars (S0) resembles spiral bulges and ellipticals in appearance. They occasionally show the existence of a bar structure, which Hubble thought classified them as a class in between spirals and ellipses (Sparke & Gallagher (2006)). Compared to spiral galaxies, S0 galaxies have less dust than those galaxies (van & Franx (1995)).

The variation of bulge to disc ratios suggests that lenticulars could have funda-

mental differences in how they are formed depending on their environments. More information about lenticulars see Kormendy & Kennicutt(2004) and Kormendy & Ho(2013). The fraction of lenticulars in the local universe is approximately 20% of the total population of galaxies (Wilman & Erwin (2012)).

Spiral galaxies

Spiral galaxies have a more complicated structure than elliptical and lenticular galaxies. The centre of spirals typically has a bulge that is surrounded by a flat revolving disc that extends considerably farther than the bulge component. Both the bulge and the disc are surrounded by a globular cluster-typical spherical halo. The spiral arms are supported by rotation instead of the anisotropy of stellar motions that supports the bulge component and ETGs. At star masses smaller than $10^{10} M_{\odot}$, the galaxy luminosity function reveals that spiral galaxies are more prevalent (Blanton & Moustakas(2009)).

The disc contains stars, gas and dust. The spiral structure is believed to be a result of density waves in the disc or alternatively shock waves which give rise to a new generation of stars. It gives spiral arms with characteristic in blue colour, arising from massive, hot stars. Spirals dominate the local universe where their populations have been estimated to be 67% of galaxies with stellar mass greater than the Milky Way galaxy.

The Hubble classification scheme, as visually presented in Figure 1.1 groups spirals based on the spread of the spiral arms, the separation of the bulge with the arms, the bulge-to-disc ratio and the presence of bars (Sandage et al.(1975)). Regular spirals are designated as (S) and barred spirals along their major axis are (SB). In both designations the scheme defines those with arms very near to a relatively large bulge as a and the designation moves to b and c type spiral galaxies as the bulge becomes smaller whereas the arms are more well defined and stretched outwards (de Vaucouleurs et al.(1991)). The surface brightness of spirals also follows the Sersic profile but with the galaxy concentration index, n, set to 1.

Irregular galaxies

Irregular galaxies have no real symmetry and are neither bulge or disc dominated. They were originally left out of the Hubble classification system and were gradually introduced as the number of galaxies observed increased, culminating in the Hubble-de Vaucouleurs galaxy morphology scheme shown in Figure 1.2. The motion of the stars in irregulars is highly stochastic with no rotational motion (Sparke & Gallagher (2006)). They generally contain the highest amount of gas

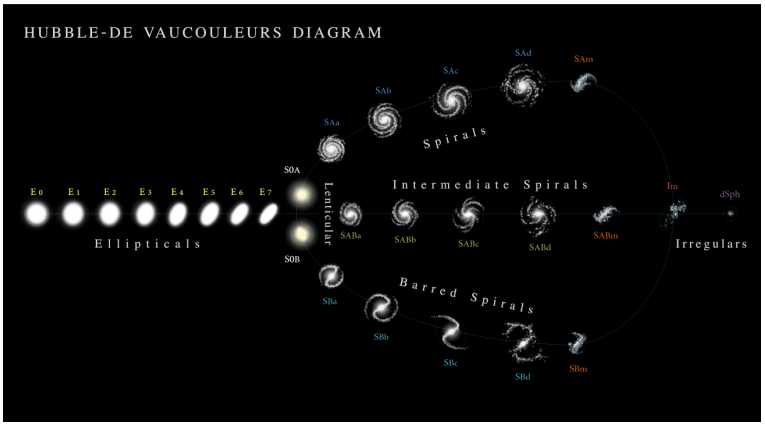

Figure 1.2: The Hubble-de Vaucouleurs galaxy classification diagram including the addition of new classes of barred lenticulars and irregular galaxies to ellipticals, lenticulars, spirals and barred spirals. Image credit:https://en.wikipedia.org/wiki/File:Hubble-Vaucouleurs.png by A. Ciccolella

which drives star formation. As a result, they have a very blue photometric colour due to a very young stellar population. They are one of the primary additions by de Vaucouleurs et al.(1991) to the Hubble-de Vaucouleurs classification scheme.

Peculiar galaxies

Peculiar galaxies are galaxies that have a shape, size, or content that is different from the normal ellipticals, spirals, and irregulars in the Hubble classification system. They often result from galaxy interactions, or sometimes show some other feature such as a jet emerging from the nucleus, low surface brightness or even unusual amounts of dust (Arp & Madore (1987)). They are designated p or pec in addition to their main classification type.

The two main types of peculiar galaxies are interacting galaxies and active galactic nuclei (AGN). The first type of peculiar galaxy are the interacting galaxies, which are those galaxies whose structure has been altered by the gravitational attraction of neighboring galaxies or have undergone galaxy-galaxy collision (Lynds & Toomre (1976), Higdon et al.(2011)). These include the special case of ring galaxies where a small galaxy collides nearly along the rotational axis with a larger spiral galaxy thus temporarily changing the appearance of the spiral galaxy (Lynds & Toomre (1976), Higdon et al.(2010)). As the smaller galaxy passes through the disk of the spiral, its gravitation pulls in stars and interstellar material from the outer disk of the large galaxy and as it departs, this material moves back outward

and triggers major star formation and the appearance of a ring.

The second group of peculiar galaxies are those whose appearances and characteristics have been modified by internal processes, mostly AGN activity (Arp(1966)). Spiral galaxies have interstellar medium (ISM) densities are higher than for elliptical galaxies. When AGN jets go off in the cores of spiral galaxies, as is the case in Seyfert galaxies, the galaxy core increases its luminosity and the ISM gets an energy injection that shocks the gas, heating it to high temperatures and stirring it simultaneously (Paliya et al.(2014)). This is also coupled with a much higher degree of variability in the radiation of the galaxy as the radiation is produced within a relatively small region.

1.2 AGNs

The observed AGN population is divided into different categories for historical reasons depending on the members' observing ability. This creates a situation where classification is more historical than pragmatic. Since the first categorization was based solely on observation, it was unable to distinguish between the underlying physical processes. This is made worse by the fact that each observational wavelength regime has a tendency to name the different types of AGN in accordance with their exact requirements. Members of the same optical AGN class have occasionally ended up with separate X-ray classes and a different set of requirements in the radio domain while belonging to the same optical AGN class. The unified theory of AGNs, which characterised them based on the observer's point of view of the inclination angle to the AGN, was introduced to resolve this.

AGNs are classified based on the presence of at least one of the following observed properties,

- compact nuclear region much brighter than a region of the same size in a normal galaxy

- non-stellar (non-thermal) continuum emission

- strong emission lines

- presence or absence of a jet

- variability in continuum emission and/or in emission lines on relatively short time scales

The AGNs with radio jets are considered as radio-loud when they have a ratio of 5 GHz luminosity to B-band luminosity that is greater than 10. The prevalence of radio-loudness in AGNs is very dependent on the stellar mass of the host. According to Best et al.(2005), the fraction of radio-loud AGNs with 1.4 GHz luminosity greater than 10^{23} WHz^{-1}, the fraction of radio-loud AGNs is nearly zero for host galaxies of stellar mass of $10^{10} M_{\odot}$ and rises to above 30% for host galaxies of mass greater 5 $\times 10^{11} M_{\odot}$.

1.2.1 AGN Jets

In astronomy, jets may be found on three different scales: sub-parsec, parsec, and kiloparsec. The gravitational potential well in solar mass type black hole systems, also known as micro-quasars, is sufficient to produce jets with lengths ranging from astronomical unit (AU) scale to a fraction of a sub-parsec. Parsec scale jets are found in SMBH mass type systems in the cores of AGNs and have lengths that vary from a parsec to a few hundred parsecs. It is observed that they are constrained inside the host galaxies. Although their length scales range from a few kiloparsecs to more than a megaparsec, SMBH mass type systems in the cores of AGNs also contain kiloparsec scale jets.

According to Antonucci(1993), an Astrophysical jet system consists of a black-hole, an accretion disc, a torus (in the case of AGN jets) and a relativistic jet.

1.2.2 Unification Scheme

By applying a few simple assumptions, the difference between type-I and type-II AGNs may be explained by the existence of a dusty torus in the core of the host galaxy of an AGN (Netzer(2015)). This unification scheme is known as the IR-optical-UV-X-ray unification scheme. Type-I AGNs contains a bright, central non-stellar point-source radiation that is visible in a broad wavelength range and broad (10^3 kms^{-1} – $10^{4.3}$ kms^{-1}) permitted and semi-forbidden emission lines and generally do not show narrow emission lines. On the other hand, typer-II AGNs have strong narrow emission lines ($\leq 10^3$ kms^{-1}). They show clear signs of photo-ionization by a non-stellar radiation source.

In addition to the dusty torus, the radio unification concept also invokes a relativistic jet. The 10% of all high-ionization AGNs include this combination. The jet is released near to the SMBH with the symmetry axis of the SMBH and torus system in alignment (Urry et al.(2003), Tadhunter(2008)). Compact and extended radio AGNs have both been predicted using the radio unification scheme.

1.2.3 The bending equation

The degree of the bending of Narrow Angle Tails (NATs) and Wide Angle Tail (WATs) due to ram pressure is governed by the bending equation which depends on the jet velocity, galaxy velocity with respect to the ICM, jet density and the density of the ambient medium.

The bending equation arises from the analytical solution of the conservation of momentum, mass and energy equation of the jet in the ICM

$$\frac{\partial v_{jet}}{\partial t} + (v_{jet}.\nabla)v_{jet} = \frac{1}{\rho_{jet}}\nabla P \tag{1-1}$$

assuming time independence (De Young(1991), Freeland & Wilcots (2011)). It yields

$$\frac{\rho_{jet}v_{jet}^2}{R_{bend}} = \frac{\rho_{ICM}v_{gal}^2}{R_P} \tag{1-2}$$

where ρ_{jet} is the density of the jet, v_{jet} is the velocity of the jet, ρ_{ICM} is the density of the ICM, v_{gal} is the velocity of the galaxy, R_{bend} is the radius of curvature of the deflected jet and R_P is the pressure scale height of the jet material (the radius of the jet is used as the pressure scale height, which is useful when comparing the observability of the jet curvature given the width of the jet)(Burns & Owen(1980), ODea & Owen(1985), Jones & Owen(1979), Begelman et al.(1979)). It is the model that is used to determine where NATs and WATs are likely to be found in the Universe. Details of NAT and WAT are discussed later.

1.3 Bent-Tail Radio Sources (BTRSs)

The radio jets of AGN interact with the intra-cluster medium (ICM) to produce BTRSs. In galaxy clusters, the ICM, a low density, high temperature plasma, serves as a propagation medium for radio jets. Numerous physical factors, beginning with the radio emission produced during jet formation, have an impact on the presence and shape of BTRSs. This process is necessary for gas accretion onto a SMBH, jet collimation, which keeps the radio jet collimated up to distances greater than 100 kpc. The bending is caused by the jet's interaction with the surrounding medium, which depends on the characteristics and motions of the intra-cluster medium in galaxy clusters or the intergalactic medium (IGM) in galaxy groups. The BTRS NGC 1265 and its luminous radio core (shown in red colour) is shown in Figure 1.3. The NGC1265 has a host which is an elliptical galaxy with a stellar component with a mass of $M_* \approx 2.5{\times}10^{11} M_\odot$.

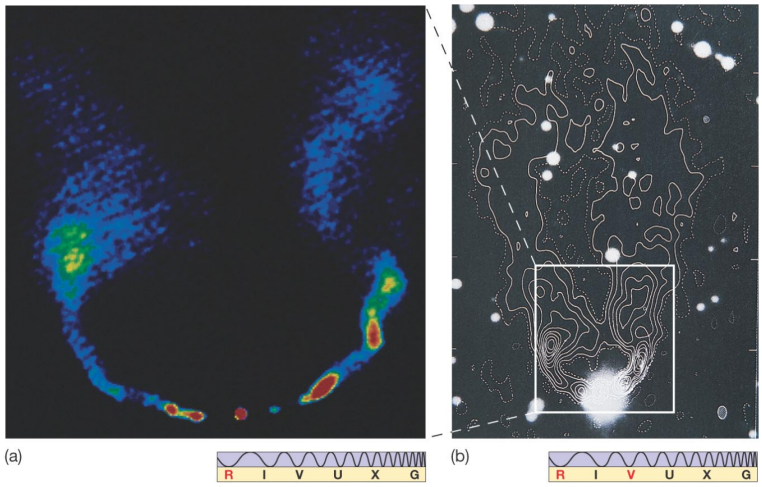

Figure 1.3: The radio image of NGC 1265 showing the basic bent morphology that is typical of BTRSs. On the left the core of the radio image is shown with the highest radio intensity shown in red. On the right the radio contours superimposed on the optical image are shown. It can be seen that, as in many extended radio sources, the radio emission covers a volume many times greater than the extent of the galaxys stellar component. Image credit: Pearson Education, Inc

The study of BTRSs relies on the understanding of the inner cores of galaxies and the role played by SMBHs in jet formation as well as the role played by the ICM and IGM in the bending of galaxy jets. With the correlations between SMBH masses and their host galaxies suggesting a potential co-evolution of galaxies and their SMBHs as well as an effect of AGN feedback in quenching of star formation, to study how the galaxies are evolved over time, environments in which they evolved have to be considered. Studying the galaxies as a function of redshift requires the ability to identify different environments such as galaxy clusters in the distant Universe.

Optical surveys such as the Sloan Digital Sky Survey (SDSS) (York et al.(2000)) have yielded an extensive list of galaxy clusters and groups in the nearby Universe (Koester et al.(2007)). The limitation of optical surveys is that their depth, with current optical telescopes, becomes severely limited beyond the redshift of ~ 0.3. The detection of galaxy clusters via X-Ray emission also suffers from a similar impediment beyond the redshift of ~ 1. Radio surveys can go much further than this with respect to depth (Becker et al.(1995)) and that fact was taken advantage of by attempting to use radio galaxies as tracers of galaxy clusters and groups at high redshift (Blanton et al.(2000), Wing & Blanton(2011)).

BTRSs have been used as possible tracers of galaxy clusters at high redshift

(Blanton et al.(2000), Blanton et al.(2001), Blanton et al.(2003)). This has led to an interest in using them as probes to Intra-group medium (IGM) density in galaxy groups in the nearby Universe as there is currently no method for constraining IGM density analogous to using X-ray luminosity of the ICM to constrain the ICM density (Freeland et al.(2008), Morsony et al.(2013)).

The discussion of the processes involved in the bending of jets is dominated by jet power, length of the jet, particle speeds as well as the magnetic fields in the jets and in the ICM (Kaiser et al.(1997)). These are influenced by SMBH masses and their accretion rates. The length of the jet is influenced by the age of the jet and the mechanisms that are responsible for maintaining their collimation (Antognini et al.(2012)). These are active areas of research and they are still believed to depend on the type of Fanaroff-Riley type radio galaxies (FRGs) being studied. They are also believed to be dependent on the galaxy environment, with clusters and groups producing different fractions of FRGs.

These complications make trying to establish average characteristics of AGN radio jets challenging. This work represents a first step in establishing a method for a statistical study of the interaction of AGN jets and their cluster and group environments. These statistics can be compared to observational results of such all-sky radio surveys as the VLA FIRST survey (Becker et al.(1995)) for validation. Their predictions can be used to constrain the number of BTRSs that will be found by the square kilometre array (SKA).

First Bent-tail sources described by Ryle & Windram(1968). The BT sources also known as Head-Tail (HT) sources. Blanton et al.(2000) reported a total of 384 bent-double radio sources from VLA Faint Images of the Radio Sky at Twenty Centimeters (FIRST) survey data. The optical environments around double-lobed radio sources was studied by Wing & Blanton(2011). Their samples contain 384 visually selected bent samples (from Blanton et al.(2000)), 1546 automatically selected bent samples (from Proctor(2006)), 3232 straight samples (from Proctor(2006)) and 3348 single component samples from the FIRST catalog. They found that 78% of the time the visually selected bent sources were associated with clusters or rich groups. The association rate drops to 59%, 43%, and 29% for auto-bent, straight, and single-component samples, respectively. Dehghan et al.(2014) presented a catalog of 56 BT sources from Australia Telescope Large Area Survey (ATLAS) at 1.4 GHz. Pateno-Mahler et al.(2017) found 190 galaxy-cluster candidates from the study of the surrounding fields of 646 bent, double-lobed radio sources in The Spitzer catalog. Using LoTSS DR1 value-added catalog (Williams et al.(2019)), Mingo et al.(2019) carried out morphological investigation of radio loud AGN. Initially, they selected 5805 extended radio-loud AGN then morphologically classify them into FR-I, FR-II, NAT, WAT and core-D based on machine learning algorithm (PYTHON code) and then visual inspection. By visual inspec-

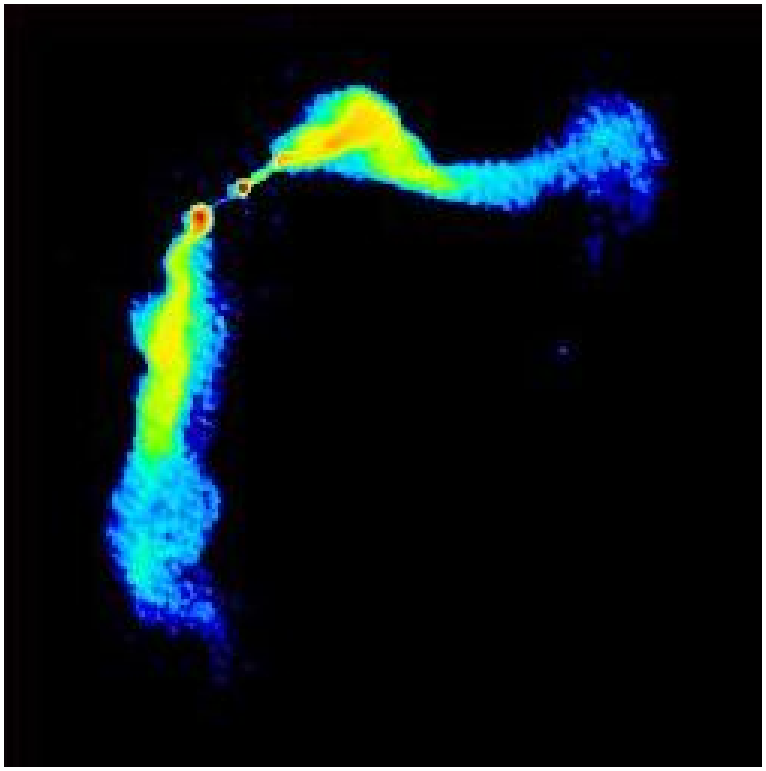

Figure 1.4: Images of the Wide Angle Tail (WAT) galaxy 3C 465. The opening angle between the opposite jets is the reason for which it is termed as Wide. Images are taken from O'Dea & Owen(1986), Owen & Rudnick(1976)

tion, they cataloged 264 NATs, 95% of which have $z \leq 0.8$ and 195 WATs, 1% of which at $z \geq 0.8$.

1.3.1 Wide Angle Tail (WAT)

WATs were first defined as a class by Owen & Rudnick(1976). The study of extragalactic radio jets was still in its early stages at the time. Their study was largely to separate the different opening angles observed in tailed galaxies. Their sample of six WAT galaxies suggested that WATs were found in Abell Clusters of all classes and that they showed a strong tendency to be associated with the BCG (Owen & Rudnick(1976)).

O'Donoghue et al.(1993) further defined the class using a sample of 11 VLA galaxies in 6 cm and 20 cm radio wavelength observation. They also compared the adiabatic and the kinetic flow dynamics that could be responsible for jet bending. O'Donoghue et al.(1993) found WATs to generally share the following observa-

tional characteristics that include the Owen & Rudnick(1976) definition,

- They have a characteristic C-shape morphology that begins at the hotspot.
- They are large structures that extend beyond 50 kpc.
- Preferentially found in galaxy clusters without cooling cores.
- Found close to the core of the cluster where the space velocity of the galaxy is low.
- Show a distinct jet-hotspot transition, where the jet suddenly goes from being narrow and faint to being broader and brighter. That transition is neither found in FR I or FR II radio galaxies.
- They have radio power close to the FR I/FR II break.

O'Donoghue et al.(1993) compared the kinetic and the adiabatic models of jet flows and their abilities to fully explain the dynamics of radio jets. They found that they both did not sufficiently account for jet bending and that at most, each model would only be partially applicable to the jet dynamics. They found that there are other models that might be more suitable to explain the behaviour of AGN jets.

The kinetic model assumes that the radio luminosity is caused by the conversion of some kinetic energy flux of the jet into radiation (Eilek et al.(1984). The kinetic model leads to much higher average jet velocity due to the less dramatic deceleration of the jets at the beginning stages. The slow decay of the velocity field of the jet necessitates an artificial numerical method of ensuring the jet velocity of zero at the end of the jet tail (O'Donoghue et al.(1993)).

The adiabatic model assumes an absence of buoyancy forces and that the radio luminosity of the jet is solely due to the acceleration of relativistic electrons from the central SMBH engine. The magnetic field and the flow thermal energy are assumed to play no part in re-accelerating the electrons in the jet. O'Donoghue et al.(1993) found that the initial velocity of the jet must be close to 0.2 c for feasible radiative efficiency.

In both models the deceleration of the jet is assumed to be caused by the entrainment of the ambient matter by the jet. The adiabatic model was found to result in electron travel times that were about an order of magnitude larger than the travel times calculated from spectral aging. This was a similar result to

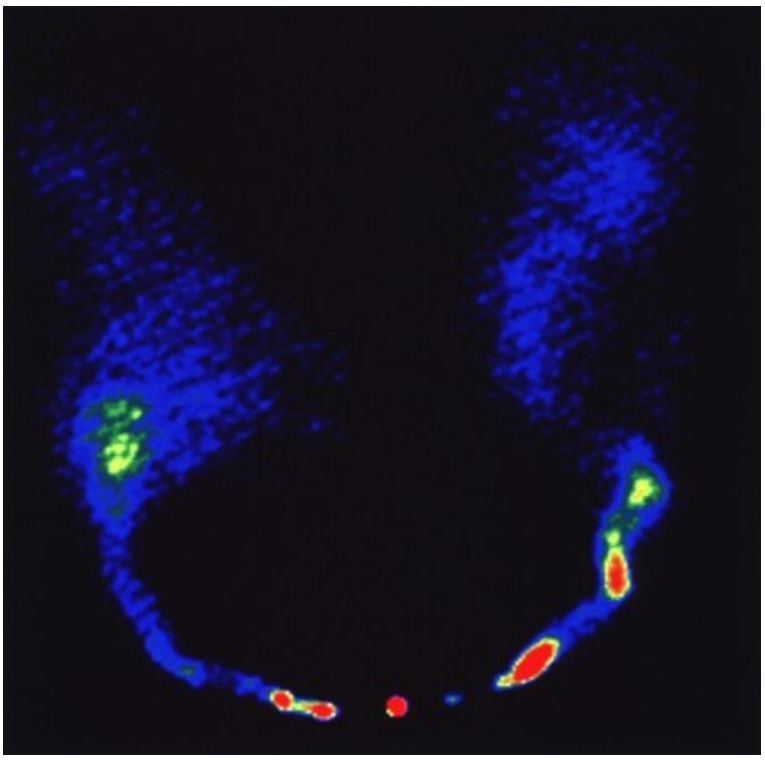

Figure 1.5: Images of the Narrow Angle Tail (NAT) galaxy NGC 1265. The opening angle between the opposite jets is the reason for which it is termed as narrow. Images are taken from O'Dea & Owen(1986), Owen & Rudnick(1976)

3C 75 found by Owen et al.(1985). This could only be mitigated by modelling the presence of strong magnetic fields in the jet cocoons, which implies that the kinetic energy flux is not the only source of radio power in AGN jets (O'Donoghue et al.(1993)).

A total of 47 WAT candidates were cataloged by Missaglia et al.(2019), using a combination of National Radio Astronomy Observatory/Very Large Array Sky Survey (NVSS), FIRST and the Sloan Digital Sky Survey (SDSS) databases. There have also been some individual studies about special types of HT radio galaxies, as found in the literature.

1.3.2 Narrow Angle Tail (NAT)

ODea & Owen(1985) used the very large array (VLA) radio telescope at 1.4 GHz to study NATs to discern global properties that could be used to define the group. They found several correlations that were consistent with the hypothesis that NAT

jets are bent by the interaction of their radio luminous plasma with the ICM (Miley et al.(1972)). ODea & Owen(1985) found a bi-modal distribution of NATs in their sample. The two groups are NATs whose length was 15 kpc $\leq$ length $\leq$ 50 kpc that showed a correlation between the integrated power at 1.4 GHz and the length of the radio jets and a small number (4 NATs) of powerful sources that had a length $\geq$ 100 kpc. There were no intermediate length sources of 50 $\leq$ length $\leq$ 100 kpc that suggested a continuum distribution of jet lengths (ODea & Owen(1985)). The shorter length jets were all found, with the VLA resolution, to be still expanding within the ISM of their respective galaxies.

Venkatesan et al.(1994) found NATs to also reside in poor Abell clusters where the radial velocity of the galaxy is less than 300 km s^{-1} . These results were consistent with ODea & Owen(1985) where the lowest radial velocities of NATs hosts in the poorest Abell clusters were also lower than 300 km s^{-1} . Such low radial velocities would cause jet bending only in extremely dense environments. The poor clusters are also not known to possess high densities. Other possible causes for bending due to ICM motion would be galaxy infall. That would cause a particular galaxy to have a higher relative velocity than the circular velocity the cluster mass can cause (Venkatesan et al.(1994)).

Recently, a multifrequency property of an interacting NAT radio galaxy, J0037+18, was presented by Patra et al.(2019) using the Giant Meterwave Radio Telescope (GMRT) and VLA data.

1.4 BTRS and Galaxy Cluster

As previously mentioned, the galaxy populations are influenced by their environments. The AGN populations in different environments also reflect this dichotomy and most AGN are found in galaxy clusters and groups. Galaxy clusters are the most massive gravitationally bound structures in the Universe. They are the building blocks of the cosmic web and are the link between astrophysics and cosmology. On the low mass end of galaxy clusters are galaxy groups.

These types of objects (BTs) are usually found in the environment of rich clusters of galaxies (Burns(1990)). They are supposed to be moving through the intracluster medium (ICM) with sufficient velocities for the tails to bend by the action of ram pressure (ODea & Owen(1985)). In this way, the primary origin for the bending of the jet is supposed to be the dynamic pressure that pushes back the jets; and the reason for this pressure is the high-velocity motion of the associated galaxy through the surrounding ICM. This ram-pressure model was first mentioned by Begelman et al.(1979). Later this ram-pressure model was well explained by many authors (Baldwin et al.(1985), Vallee(1981)). A buoyancy force was also

invoked to understand the bending of the jets. When the material density of the radio jets is less than the density of the surrounding medium, the buoyancy force comes into action; it pushes the lobes to the regions of the ICM where the density of the jet is equal to that of the surrounding medium and thus bends the jets (Gull & Northover(1973), Sakelliou et al.(1996)). There is an alternative theory wherein the distortion of jets occurs as the result of the high velocity of the ICM due to a merger of clusters (Burns(1990), Roettiger et al.(1996), Blanton et al.(2000), Mao et al.(2009), Dehghan et al.(2014)). These models can be used to probe unknown galaxy clusters with the presence of a BT source.

In every cluster or group, resides a brightest cluster/group galaxy (BCG) which is usually found close to the cluster/group core. It is the most massive member of the agglomeration. Best et al. (2007) found that, in the SDSS clusters and groups, BCGs were more likely to host a radio-loud AGN than field galaxies. The lower stellar mass BCGs ($M_* \leq 10^{11} M_\odot$) are over an order of magnitude more likely to be radio-loud (where the 5 GHz flux is more than 10 times brighter that B-magnitude flux) than other galaxies of the same mass. This ratio falls off slightly to just below a factor of two for high-mass ($M_* \geq 5{\times}10^{11} M_\odot$) BCGs of similar mass.

BT sources are more found in rich environments than other morphology classes and regular FR-IIs are almost zero association. The possible reason for this is the movement of the host galaxy through ICM as a result jets and tails are curves or bends in the opposite direction of movement. Hao et al.(2010) review the population of radio galaxies and radio-loud quasars from a current observational perspective. they show the fraction of radio galaxies at $z \leq 0.4$ associated with SDSS galaxy clusters (M $\geq 10^{14} M_\odot$) are different for different morphology classes (i.e. FR-I, FR-II, NAT and WAT). BT sources are more found in rich environments than other morphology classes and regular FR-IIs are almost zero association.

To investigate whether their BT sample reside in a rich environment, Mingo et al.(2019) cross-matched their 459 BT sample with Croston et al.(2019) catalog. They found that BT candidates are associated with galaxy cluster with cluster matching fraction are 48% and 49% for WAT and NAT sources respectively.

Vos et al.(2021) study the ram pressure interaction between radio galaxies and the intracluster medium. They analyse a sample of 208 highly bends NAT in the cluster. The sample they selected from the morphological catalog of Mingo et al.(2019). They found tails of NATs are distributed anisotropically with a strong tendency to be bent radially away from the cluster within $7R_{500}$ of cluster centre i.e. they are predominantly on radially inbound orbits. Jets of NATs bent towards the cluster core within $0.5R_{500}$ i.e. outbound sources fade away soon after passing pericentre Vos et al.(2021).

1.5 BTRS Samples from Radio Surveys

Many radio surveys of extragalactic sources have been done since the dawn of radio astronomy. Only a few of the recent surveys have significantly increased the size of the sample of known BTRSs. VLA FIRST and LoTSS and their contribution to BTRS statistics are discussed below.

1.5.1 VLA FIRST

In 1943 April the "amateur" radio astronomer Grote Reber began the systematic survey of the radio Universe. Using a backyard telescope with a beamwidth of 16 degree operating at a frequency of 150 MHz, he spent most of the following year mapping the northern sky to a flux density threshold of a few thousand janskys. The results, published in the Astrophysical Journal in the form of strip chart recorded reproductions (Rebber 1944), revealed several areas of enhanced emission lying along the plane of the Milky Way, demonstrated that the emission centroid lay 30 degree from the then-used zero point of Galactic longitute, and provided the first image of the universe outside the traditional window.

Fifty years latter, in 1993 April, Becker et al.(1995) began FIRST survey at radio wavelengths. To produce Faint Images of the Radio Sky at Twenty centimeters taken approximately the same ammount of time as Reber's work, but the finak map have 10^8 more resolution elements and reached a sensitivity $5{\times}10^6$ times higher. Using the NRAO Very Large Array (VLA) in its B configuration, It covered 10,575 deg^2 of the northern galactic cap to a flux density limit of 1.0 mJy with and angular resolution of $5''$. They acquire 3-minute snapshots covering a hexagonal grid using 2×7 3-MHz frequency channels centered at 1365 and 1435 MHz.

This survey includes an area of RA 7.0h to 17.5h and DEC –8.0 deg to +57.6 deg in north galactic cap and RA 20.4h to 4.0h, DEC –11.5 deg to +15.4 deg in the south sky. Roughly 65,000 three-minute snapshot images were obtained over this period. All of the work published to date, including the FIRST catalog, has been based on images constructed by co-adding these snapshots with appropriate weightings (for details, see White et al.(1996)); this process yielded images with a uniform noise level of 0.15 mJy.

The final catalog contains 946,432 sources with a source detection threshold of 1 mJy, yielding a source density of 90 deg^{-2} . The astrometric accuracy of the cataloged sources is better than $1''$. The co-added maps have $1''.8$ pixels and an angular resolution of $5''.4$. The FWHM of VLAs primary beam is $30'$. The catalog also assigns a sidelobe probability to each source. It must be noted that, for this study, we have made use of the 14dec17 version of the catalog available on

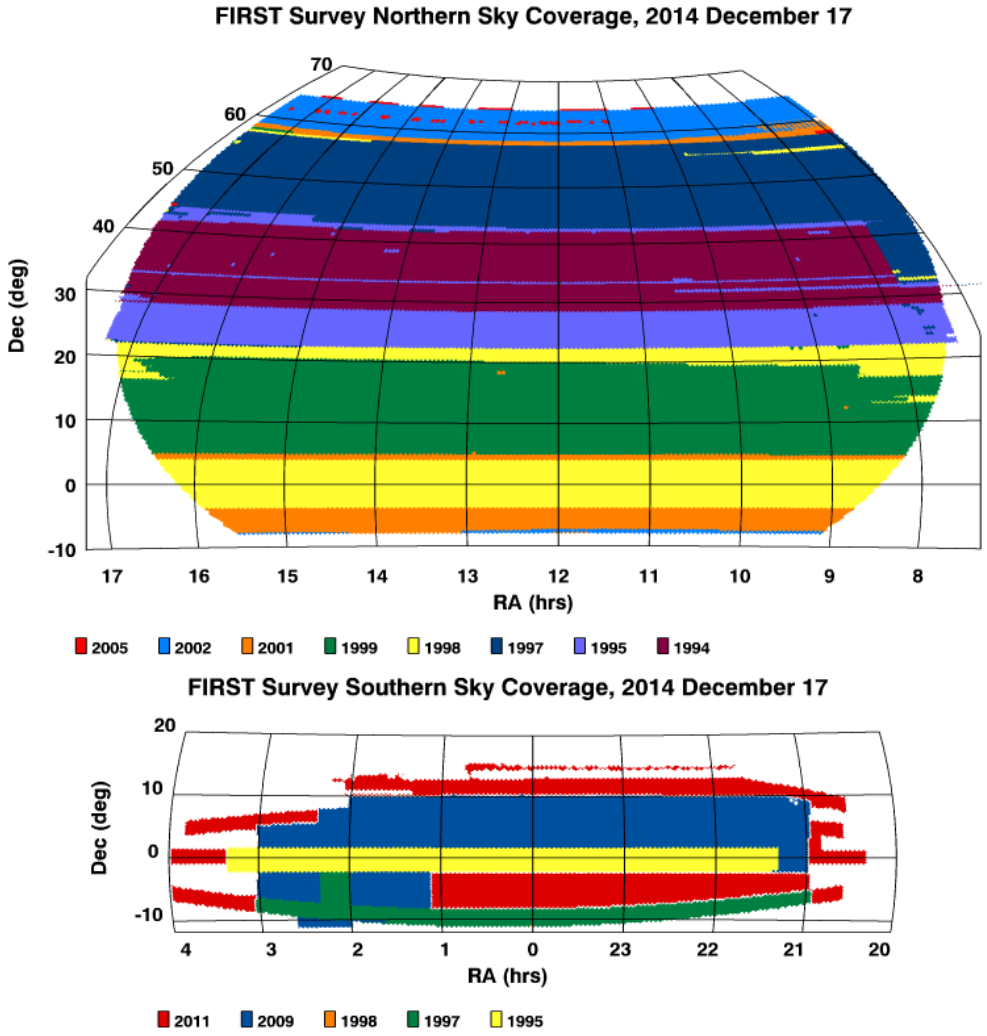

Figure 1.6: This images shows the northern and southern sky coverage of FIRST survey, 2014 december 17. Different colours indicates different years from 1995 to 2014.

Date	Frequencies	Bandpass	Integration
Before 2011	1365, 1435 MHz	2x7 3-MHz channels	180 seconds
2011	1335, 1730 MHz	2x64 2-MHz channels	60 seconds

Figure 1.7: The frequency difference between the new and older FIRST data are shown in this table. The bandpass and integration time are also compared befoe and after 2011.

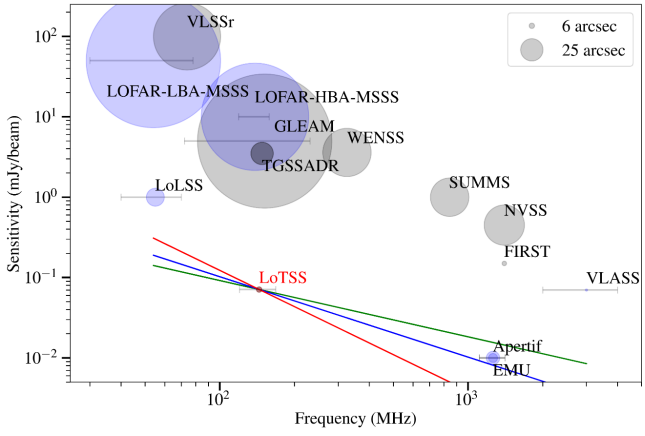

Figure 1.8: Image rms, frequency, and angular resolution (linearly propor- tional to the radius of the markers) of LoTSS-DR1 in comparison to a selection of existing wide-area completed (grey) and upcoming (blue) radio surveys. The horizontal lines show the frequency coverage for surveys with large fractional bandwidths. The green, blue, and red lines show an equivalent sensitivity to LoTSS for compact radio sources with spectral indices of -0.7, -1.0, and -1.5, respectively.

the FIRST surveys Web site http://sundog.stsci.edu/first/catalogs/readme.html. The sky coverage of the FIRST survey in different years are shown in the figure 1.6.

1.5.2 LoTSS DR1

The LOFAR Two-metre Sky Survey (LoTSS; Shimwell et al.(2019)) is one of the surveys that probe deeply into new parameter space have enormous discovery potential. It is an ongoing or recently completed survey that is exploiting the unique capabilities of the LOw Frequency ARray (LOFAR; van et al.(2013)) to produce a sensitive, high-resolution radio survey of the northern sky with a frequency coverage of 120–168 MHz (see figure 1.8). The survey was primarily motivated by the potential of low-frequency observations to facilitate breakthroughs in research areas such as the formation and evolution of massive black holes (e.g. Wilman et al.(2008), Best et al.(2014)) and clusters of galaxies (e.g. Cassano et al.(2010), Brunetti et al.(2014)). However, there are many other important scientific drivers of the survey, and there is active research in areas such as high redshift radio sources, galaxy clusters, active galactic nuclei, star forming galaxies, gravitational lensing, galactic radio emission, cosmological studies, magnetic fields, transients and recombination lines.

The LoTSS survey is very wide-area low-frequency radio surveys that are pro-

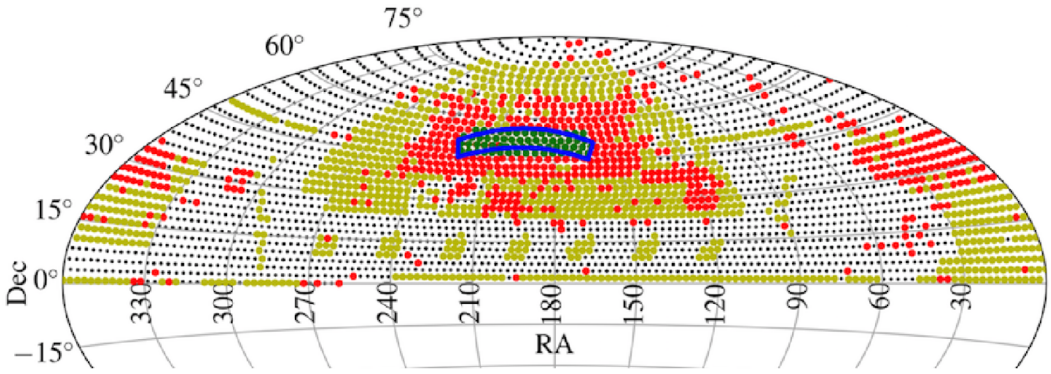

Figure 1.9: Status of the LoTSS observations as of May 2018. The green dots show the images that are presented in LoTSS DR1. The red, yellow, and black dots show the observed pointings (but yet unpublished), pointings presently scheduled for observation between May 2018 and May 2020, and unobserved pointings, respectively. The HETDEX Spring Field region is outlined in blue. The vast majority of the completed coverage (20% of the northern sky) and upcoming observations (an additional 30% of the northern sky) are regions with low Galactic extinction.

viding important scientific and technical insights. Other such surveys include the Multifrequency Snapshot Sky Survey (MSSS; Heald et al.(2015)), TIFR GMRT Sky Survey alternative data release (TGSS-ADR1; Intema et al.(2017)), GaLactic and Extragalactic All-sky MWA (GLEAM; Wayth et al.(2015)), LOFAR Low-band Sky Survey (LoLSS; de Gasperin et al.(2019)), and the Very Large Array Low-frequency Sky Survey Redux (VLSSr; Lane et al.(2014)).

Here, our centre of attention is the first data release of LOFAR (LoTSS DR1), which covers a radio sky of 424 square degrees or eventual coverage of 2% in the region of HETDEX Spring Field (Shimwell et al.(2019), Williams et al.(2019)). Individually this survey includes ranges of right ascension (R.A.) 10h45m00s to 15h30m00s and declination (decl.) 45°00′00″ to 57°00′00″. It is developed by using a fully automated direction-dependent calibration and imaging pipeline. It has median sensitivity of $S_{144MHz} = 71\ \mu Jy$ beams^{-1} and the point-source completeness is 90% at an integrated ux density of 0.45 mJy. The angular resolution of the images is 6″ with the positional accuracy is within 0.2″(Shimwell et al.(2019)). In figure 1.9 shows the sky coverage of full LoTSS survey. The blue region shows the only coverage area of LoTSS DR1 and rest is ongoing, yet to published.

In Figure 1.11, we see a comparison between the LoTSS and other radio surveys, such as NVSS and FIRST, for a GRG. The top image (a) is an optical-radio overlay with a blue colour indicating LoTSS low frequency 6″ resolution map on the optical

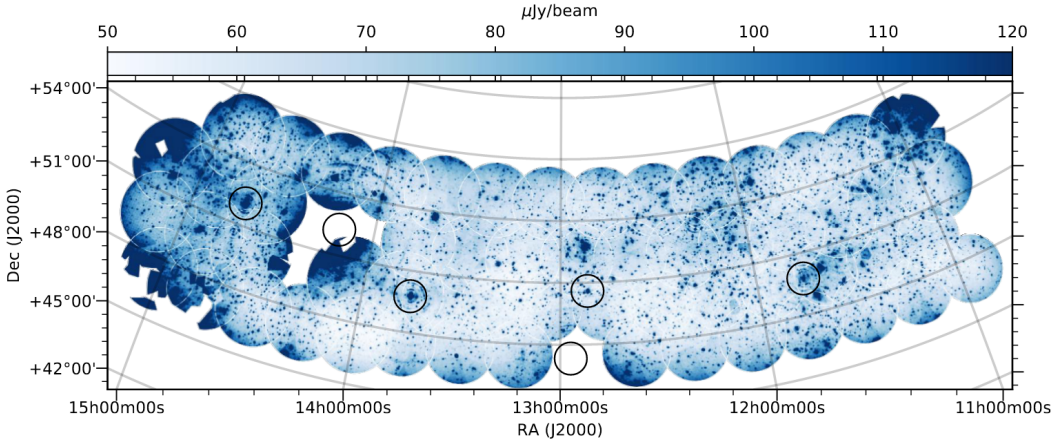

Figure 1.10: Noise image of the LoTSS-DR1 where the median noise level is 71 Jy $beam^{-1}$. Many of the regions with high noise levels are caused by dynamic-range limitations. Sources from the revised 3C catalogue of radio sources (Bennet(1962)) are overplotted as black circles to show the location of potentially problematic object.

SDSS tri-colour image. In the bottom image (b), the same source is shown as it is observed in NVSS and FIRST. NVSS, though highly sensitive to large-scale diffuse emission, fails to reveal the finer details across the source and cannot properly resolve the core due to its coarser resolution of 45″. The FIRST survey on the other hand has high resolution, which manages to resolve the core and hence helps in identifying the host AGN and galaxy but misses out on almost all the diffuse emission of the lobes and hence it alone cannot be used to identify RGs. The LoTSS data provides with both high resolution as well as high sensitivity and does not resolve out structures revealing finer details of the emission of large-scale jets. The image (Figure 1.11) clearly show the radio core and jets feeding the giant radio lobes and the hotspots. This clearly illustrates the excellence of LoTSS and its great potential in unveiling interesting sources.

Following cosmology parameters, we have used in this thesis; $H_0 = 67.4$ km s^{-1} Mpc^{-1}, $\Omega_m = 0.315$ and $\Omega_{vac} = 0.685$ Ag18. The spectral index (α) is defined by $S_\nu \propto \nu^\alpha$ where S_ν is the flux density.

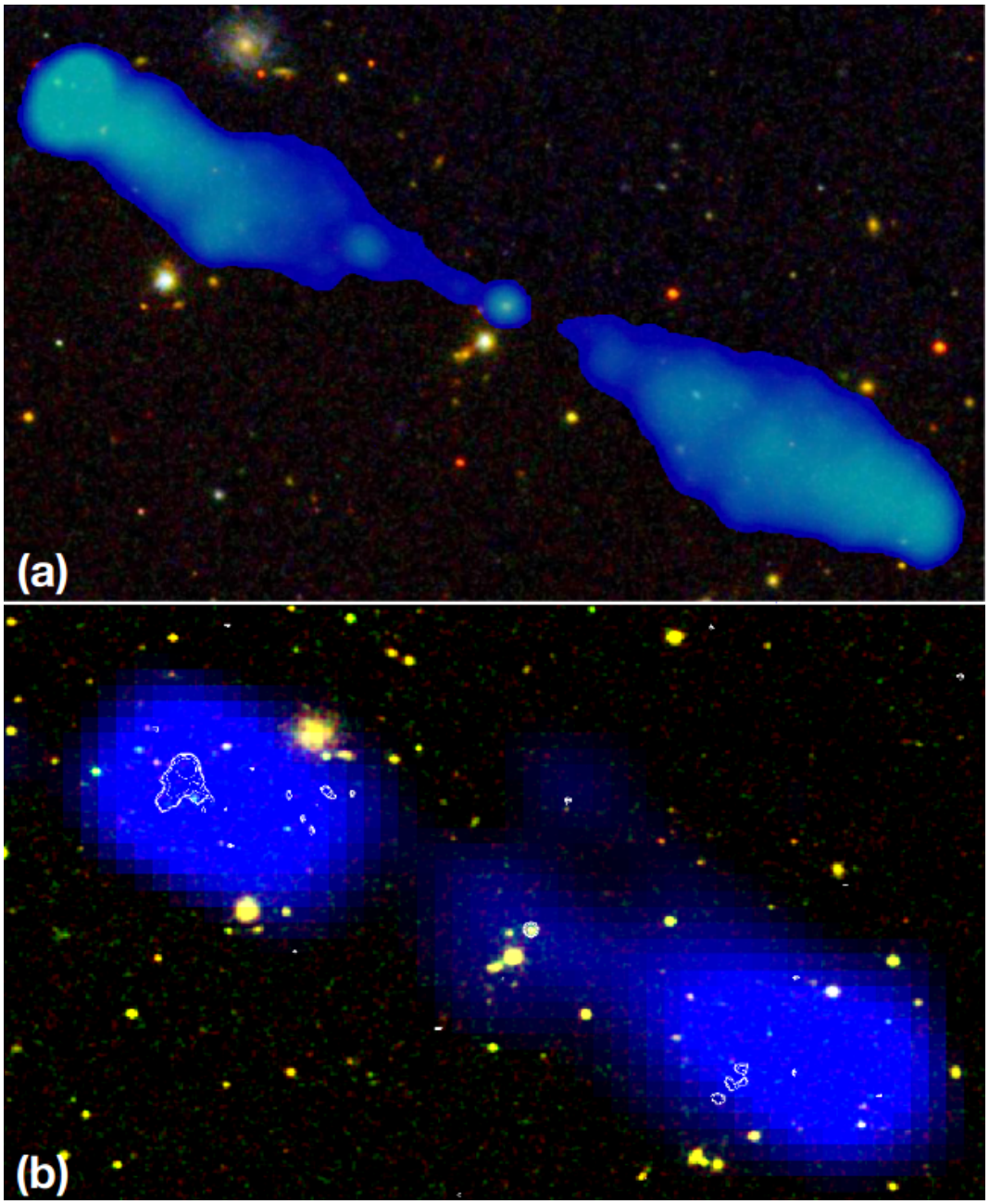

Figure 1.11: Panel a: colour composite image of 1.86 Mpc long GRG J105817.90+514017.70 made using LoTSS-DR1 144 MHz radio and optical SDSS image. Panel b: colour composite image of the same object with optical and radio overlay, where blue represents 1400 MHz NVSS image with 45″ resolution and white contours from the 1400 MHz FIRST survey having 5″ resolution superimposed on optical SDSS image. The LoTSS 144 MHz 6″ resolution image shown in top panel clearly resolves the core and jet and also highlights the diffuse parts of the lobes, which is missed by the FIRST and unresolved in NVSS.

Chapter 2

Radio Telescope and instruments

In this work, we study the bent-tail radio galaxies and their environment using data from two different telescopes, Karl G. Jansky Very Large Array (VLA) and Low Frequency Array (LOFAR). Our investigation is done by visual inspection. The details of these telescopes are described in the following two sections.

2.1 Karl G. Jansky Very Large Array (VLA)

Astronomers at NRAO realised that they required a system of radio dishes to complement the work of our massive, single-dish telescopes as early as the 1960s. An array is a collection of numerous radio antennas that observe together, thus forming a single, enormous telescope. To study and establish optimum communications, correlation, and atmospheric correction methods, NRAO originally constructed the Green Bank Interferometer. This four-element array assisted NRAO in preparing for a Very Large Array of 27 telescopes over the 1960s and the 1970s.

2.1.1 Location

The VLA is located in central New Mexico on the Plains of San Agustin, between the towns of Magdalena and Datil, 50 miles (80 km) west of Socorro. Northwest of Socorro in the state of New Mexico lies a flat desert region known as the Plains of San Agustin. Mountains surround the Plains, acting as a natural rock fortress that blocks off a large amount of radio interference from cities even hundreds of miles away.

Figure 2.1: This is the image of one of 27 antenna of Very Large Array

Figure 2.2: This image shows the 'Y'-shape array of VLA. Each array contains nine telescopes.

2.1.2 Design

The VLA consists of 28 antennas, 27 are operational and one is spare. Each antenna has an 82-foot dish with 8 receivers tucked inside and weighs 209 metric tons. The dish rotates and tilts up and down on an altitude-azimuth mount, which seen on a traditional tripod tilts up and down and spins around. The image of one of the 28 antennas is shown in figure 2.1.

The unique 'Y' shape of the VLA serves a definite purpose. The array gets wider means its eye gets bigger and it can see more details in space. The iconic shape of VLA gives there lovely long arms of nine telescopes each. We also have the freedom to extend our arms to get a closer look when necessary. The 'Y' shape array of VLA is shown in figure 2.2.

The telescopes are mounted on rails. Three times a year, telescopes are picked up and transported down their track one at a time by a specially made rail truck called a transporter. The four most popular designs are A (biggest) through D (tightest), where all of the dishes are placed within 600 metres (2,000 feet) of the central point. The VLA lengthens each of its legs from two-thirds of a mile to 23 miles over the period of 16 months.

2.1.3 Charecteristies

Each of the VLAs 28 25-meter parabolic dish antennas use 10 receivers:

74 MHz	Band 4	8.4 GHz	X Band
327 MHz	P Band	15 GHz	Ku Band
1.4 GHz	L Band	22 GHz	K Band
3 GHz	S Band	33 GHz	Ka Band
5 GHz	C Band	43 GHz	Q Band

The frequency coverage of VLA is 74 MHz to 50 GHz (400 cm to 0.7 cm). The angular resolution can be reached between 0.2 and 0.04 arcseconds. The collecting area of VLA is 13,250 square metre (142,600 sq ft).

The electronics devices in the 1970s-era s were replaced with state-of-the-art equipment. After a ten-year upgrading effort, the VLA's technological capabilities increased by up to 8,000 times in 2011. On March 31, 2012, the VLA was renamed officially the 'Karl G. Jansky Very Large Array'.

The VLA is a multi-purpose telescope made to investigate a wide variety of astronomical objects, such as radio galaxies, quasars, pulsars, supernova remnants, gamma-ray bursts, radio-emitting stars, the sun, planets, astrophysical masers,

black holes, and hydrogen gas, which makes up a significant portion of the Milky Way galaxy as well as other galaxies.

Numerous major surveys of radio sources, such as the NRAO VLA Sky Survey (NVSS), Faint Images of the Radio Sky at Twenty Centimeters (FIRST) and VLA Sky Survey (VLASS), have been conducted using this instruments.

2.2 LOw Frequency ARray (LOFAR)

The LOw-Frequency ARray, or LOFAR, is a modern radio interferometer being built in the northern Netherlands and throughout Europe. The LOFAR spans the mostly untapped low-frequency region from 10-240 MHz and offers a variety of distinctive observation abilities because of its revolutionary phased-array construction. In the low-frequency radio domain, LOFAR provides unmatched sensitivity and angular resolution due to its dense core array and extended interferometric baselines. The International LOFAR Telescope (ILT) foundation jointly manages the LOFAR facilities as an observatory accessible to the astronomy community. The automated processing pipelines used by LOFAR, one of the earliest radio observatories, allow it to provide its user community with properly calibrated research results.

2.2.1 Location

ASTRON, the Institute for Radio Astronomy in the Netherlands, has developed and constructed the LOFAR. The infrastructure that enables top-tier radio astronomical research has been distributed over different research institudes. In 2010, Queen Beatrix of The Netherlands officially inaugurated it and since then, ASTRON has been in charge of running it on behalf of the International LOFAR Telescope (ILT) collaboration. A total of 40 LOFAR stations has been constructed which are spreaded from the core location situated at village of Exloo to the outside of the northeastern Netherlands. In addition, five further stations have been installed in Germany, and one station has been constructed in each France, Sweden, and the United Kingdom.

2.2.2 System overview

ASTRON created the cutting-edge radio telescope LOFAR to enable a wide spectrum of astrophysical research in the lowest frequency radio regime. LOFAR is an interferometric array of dipole antenna stations dispersed across the Netherlands and Europe that can operate in the frequency range of 10-240 MHz (equivalent to

Figure 2.3: An aerial image of the Superterp, the LOFAR core's heart centre, taken in August 2011. The six core stations that make up the Superterp are all contained within the big circular island. In the top right and lower left corners of the picture, three more LOFAR core stations can be seen. These core stations each include two substations with 24 high-band antenna tiles each and a field of 96 low-band antennas. This image is taken from van et al.(2013).

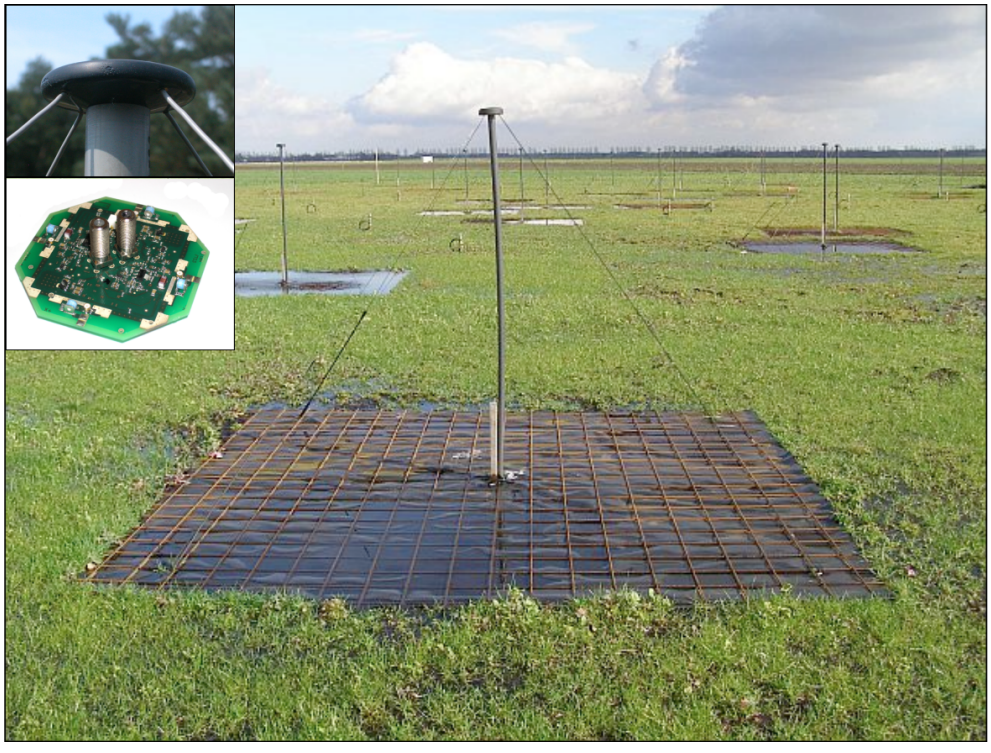

Figure 2.4: A picture of a single LOFAR LBA dipole with the ground plane included. The moulded cap holding the LNA electronics and the wire attachment points are shown in the inset photos. This image is taken from van et al.(2013).

Figure 2.5: A single LOFAR HBA tile in close-up. The real dipole assembly has been partially revealed by removing the protective cover. It is possible to see the circular dipole rotation process. This image is taken from van et al.(2013).

wavelengths of 30-1.2 m). These stations have no moving parts and, due to the effectively all-sky coverage of the component dipoles, give LOFAR a large field-of-view (FoV). The signals from separate dipoles are digitally merged into a phased array at the station level. The equipment is flexible and enables quick repointing of the telescope as well as simultaneous viewing of numerous, independent regions of the sky due to electronic beam-forming techniques. The main projects of LOFAR are the epoch of reionization, deep extragalactic surveys, transient radio phenomena and pulsars, ultra high-energy cosmic rays, cosmic magnetism and solar physics and space weather.

2.2.3 Array configuration

The receiving devises of LOFAR are two types: small and relatively low-cost antennas that together cover the 30240 MHz operating bandpass. 48 different stations comprised of these antennas are located throughout the northern Netherlands, as well as in Germany, France, the UK, and Sweden. In the northeastern Dutch

province of Drenthe, the bulk of these stations 40 in total are dispersed throughout a region measuring about 180 km in diameter and focused close to the town of Exloo. The majority of the array is located in the Netherlands, with a strong central concentration of 24 stations located within a radius of 2 km referred to as the core. Six stations are located on a 320 m-diameter island known as the "Superterp" in the centre of the core. The word "terp" is a local term for an elevated location used for buildings as protection against rising water. In Fig. 2.3, several Superterp stations are displayed.

2.2.4 Stations

Similar fundamental tasks are carried out jointly by both the LOFAR antenna stations and the radio dishes of a traditional interferometric telescopes. These stations offer collecting area, raw sensitivity, pointing, and tracking capabilities, much as conventional radio dishes.

The Low Band Antennas (LBAs), are intended to operate from the ionospheric cutoff of the 'radio window' about 10 MHz up to the beginning of the commercial FM radio band at roughly 90 MHz and are used by LOFAR at the lowest frequencies. This range is operationally constrained to 30-80 MHz by default due to the existence of significant Radio Frequency Interference (RFI) at the lowest frequencies and the vicinity to the FM band at the higher end. Particularly, the LBA antenna's omnidirectional response enables the simultaneous observation of the whole visible sky. On timeframes of seconds, all-sky maps may be produced by simply correlating the LBA dipoles in a certain LOFAR station. This innovative capacity is helpful for a variety of scientific goals, such as investigations of the Milky Way's massive Galactic emission and all-sky radio transient monitoring. In figure 2.4 shows a single LOFAR LBA dipole antenna with the ground plane.

An entirely different mechanical design has been used to cover the upper end of the LOFAR spectral response. The 110250 MHz band has been chosen as the optimal operating range for the LOFAR High Band Antenna (HBA). In reality, the frequency band is only operable between 110 and 240 MHz since the frequency range above that is heavily polluted by Radio frequency Interference (RFI). A single HBA tile is made up of an analogue beam-former made up of delay units and summators, as well as a square, 4x4 element (dual polarised), phased array with built-in amplifiers. The signal received from the MAC system determines the length of the 5 bit time delay, which can range from 0 to 15 ns. Each tile has 16 aluminium antenna components and is 5 metres by 5 metres in size. It is built on an expanded polystyrene framework. The space between tiles is 15 cm due to the 5.15 m between tile centres. A close picture of LOFAR HBA antenna is shown in

figure 2.5.

Two flexible polypropylene foil layers that overlap provides weather protection for the tile's contents. The construction includes a lightweight ground plane made of a 5x5 cm wire mesh. The generated signals are sent to the receiver unit in the electronics cabinet through coaxial wires, similar to the LBAs.

Chapter 3

FIRST Bent-Tail Sources

Bent-tail (BT) radio sources (which include the classes of head-tail galaxies, wide-angle tails and narrow-angle tails) are a class of radio galaxy in which the jets are expelled from the central supermassive black hole have been bent or significantly distorted from their typical linear trajectory. The complex morphologies of BT radio sources can be explained by environmental effects, the most significant of which is the exertion of strong ram pressures on the jets caused by the relative motion of the host galaxy through a dense medium. This motion may be a galaxy moving through a dense medium, or by the medium itself moving across the galaxy. A radio galaxy with a large peculiar velocity moving through the intra-cluster medium (ICM) of its host cluster may produce jet distortions, provided the velocity and density of the ICM are high enough (Miley et al.(1972), Rudnick & Owen(1976), Burns(1990)). These distortions may also be caused by violent movement of the ICM due to the merger history of the cluster (Burns(1990), Roettiger et al.(1996), Burns et al.(1996)). This makes BT radio sources a potentially useful tool for probing galaxy interactions on large scales with several studies showing that they tend to reside in galaxy clusters (Blanton et al.(2000), Mao et al.(2009), Wing & Blanton(2011), Dehghan et al.(2014)).

In this chapter, we discuss the search methodology and results of Bent-tail sources from VLA FIRST survey at 1400 MHz. A few radio and optical properties of BT sample are also discussed here.

3.1 Methedology

3.1.1 Samples Selection

Here, the samples are selected from VLA FIRST survey data which are cataloged NRAO Very Large Array (VLA) in its B-configuration (VLA B) (Becker et al.(1995)). The sky coverage of the FIRST survey is 10,575 square degrees, which

is equivalent to 25% of all the sky area. In north galactic cap, the survey covers an area of RA 7.0h to 17.5h and DEC –8.0 deg to +57.6 deg, a total of 8,444 square degrees and in south sky. Similarly, in the south sky RA changes to 20.4h to 4.0h and DEC –11.5 deg to +15.4 deg, a total of 2,131 square degrees. It has a typical rms 0.15 mJy and an angular resolution of 5″ (Becker et al.(1995)). In the 10,500 square degree region surveyed as of the December 2014 catalog release, FIRST detected approximately 946,432 radio sources. The total FIRST sky is mapped with 3-minute snapshots covering a hexagonal grid using 2×7 3-MHz frequency channels centered at 1365 and 1435 MHz[1]. The cleaning and calibration of the raw data is done using an automated pipeline based largely on routines in the Astronomical Image Processing System (AIPS)[2]. At the same operating frequency (1400 MHz), The FIRST has a nine times better resolution for the NRAO VLA Sky Survey (NVSS). NVSS has angular resolution of 45″ and a rms of $\sim$ 0.45 mJy (Condon et al.(1998)). As a result, FIRST will be the ideal choice for studying the morphologies of a large number of moderately weak radio sources.

3.1.2 Search Strategy

The FIRST's excellent sensitivity and resolution allow us to explore new fainter samples of various types of radio galaxies such as 'wing' radio galaxy (Cheung(2007), Bera et al.(2020)), Bent-Tail radio galaxy (Mingo et al.(2019)) and Giant Radio Galaxy (Dabhade et al.(2020)). In this search, we only looked for radio galaxies with Bent-tail morphology.

We followed the same selection criterion as Cheung(2007), Bera et al.(2020). Cheung(2007) searched for X- shaped radio galaxies from the FIRST survey and he filtered those radio sources whose angular sizes are greater or equals to 15″. Later, Bera et al.(2020) searched for X-shaped, or winged, radio sources from the FIRST survey (2014 data release). They shortlisted the sources with angular sizes greater or equals to 10″. Our searched BT sources may have a single component or multi components (more than one component). For multi components sources, angular size of any components must be greater or equals to 10″.

The FIRST catalog includes a total of 946,432 radio sources. The higher resolution of the FIRST images (5″) provides us with a sufficient number of BT morphology. From the FIRST catalog, we separated the sources that have an angular size greater or equals to 10″ (i.e. atleast twice the convolution beam size). To select the sources, a self made filtering script have been built. Employing it a total of 95,243 sources were filtered. Then, we carefully examined each image

[1]http://sundog.stsci.edu/first/description.html
[2]http://info.cv.nrao.edu/aips/

and identified candidates whose radio jets were twisted into 'C', 'V' or 'L'-like structures.

3.1.3 Finding the Optical Counterparts and Properties

The SDSS (York et al. 2000) is a drift-scan survey of the northern and southern Galactic cap. The SDSS cataloged photometry in five bands (ugriz) for over five million unique sources and spectra of over a million sources as of data release 12 (DR12; Alam et al. 2015). The DR12 includes photometric and spectoscopic redshifts computed using a new hybrid technique that produces substantially more accurate findings than past data releases for every extragalactic object in the SDSS catalog.

The FIRST survey was designed to cover the same sky area as the SDSS. This makes it simple to search the SDSS for optical counterparts for all of the FIRST sources from the samples we have described above. Because of positional accuracy of both SDSS and FIRST is less than one arcsec, we also search for an associated optical source within a very narrow area around each radio source. Because of the enormous number of sources in the SDSS catalog, it's important to identify optical sources that are likely to be situated close to in projection area of the BT radio source. To do so, we used the SDSS to search for all optical sources that were within two arcmin radius of the core of the radio sources. We discovered that a radius of 2 arcmin maximised the chances of identifying a right optical counterpart.

The radio jets are emitted from central core of a galaxy at which an active galactic nucleus (AGN) is located. Generally, an optical galaxy is found in the central region of a radio source and is known as an optical host galaxy. Based on the relative position of radio morphology and optical source, the optical counterparts of our BT sources were selected visually. We overlaid the FIRST image of the source on the respective DSS2 red image in gray scale. In some situations, no optical counterparts can be identified, hence we adopt our best guess "eye-estimated" position as the central spot for those sources. For NATs, optical counterparts were found for 149 sources out of a total of 287 sources. For WATs, optical counterparts were found for 210 sources out of a total of 430 sources.

3.2 Result

Here, we reported a total of 717 new Bent-tail sources from FIRST survey. Based on the bending angle between the two radio jets, BT sources are classified into two subclasses, NAT and WAT. NAT sources are those with a bending angle less than 90 degrees, while WAT sources are those with a bending angle more than or equal

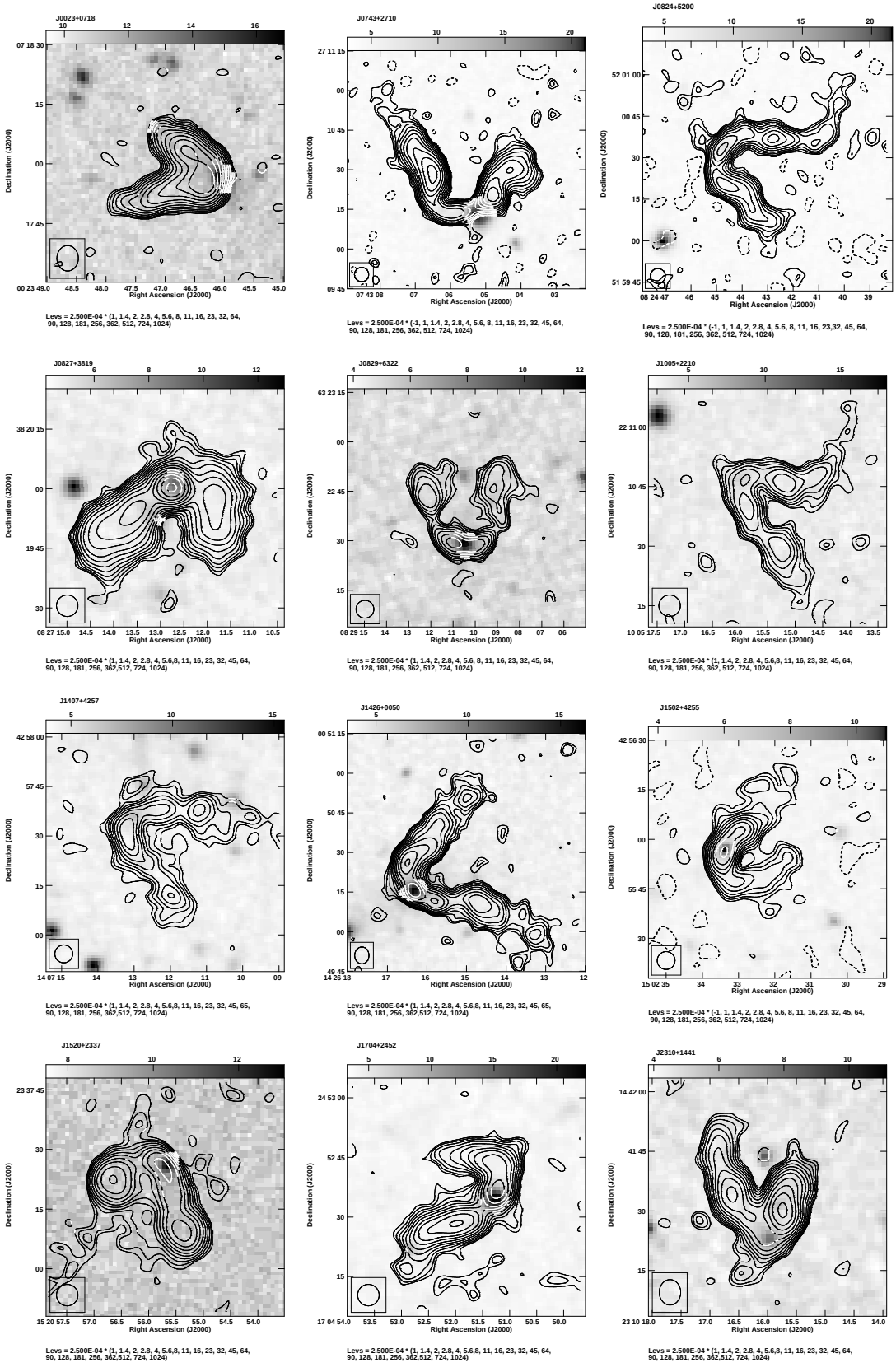

Figure 3.1: FIRST image of a sample of twelve Narrow Angle Tail (NAT) radio sources (contours) overlaid on the DSS2 red image (gray scale).

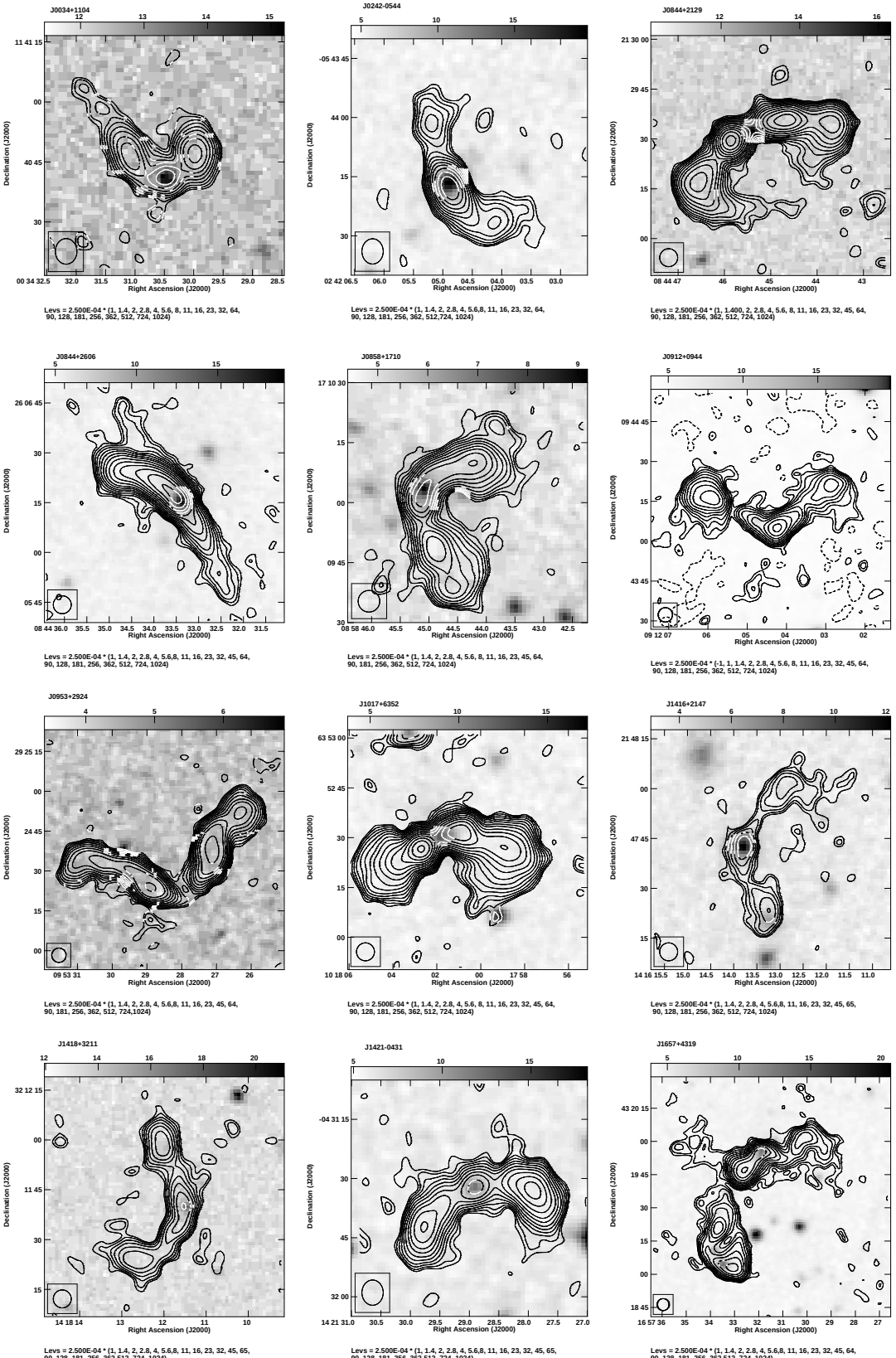

Figure 3.2: FIRST image of a sample of twelve Narrow Angle Tail (WAT) radio sources (contours) overlaid on the DSS2 red image (gray scale).

to 90 degrees. The angle was calculated by measuring the angle formed at the centre (optical counterpart or eye estimated) by the outward vectors (direction) of the two radio jets. Among our BT sample, NAT and WAT sources are 287 and 430, respectively. We determine the spectral indices and radio luminosities of all HT candidates using the available radio and optical data. Some statistical properties of these candidates are also studied in this work.

Table 3.1 and table 3.2 (given at the end of the chapter) contain a list of all WAT and NAT sources, respectively. Sample images of 12 NAT and WAT sources are shown in Figures 1 and 2, respectively. In addition, we show a histogram of the angle distributions of the NAT and WAT sources in Figure 3.3. All sources are listed in their respective table in the ascending order of the R.A. (J2000.0). Column 1 and column 2 represents serial number and source name. Column 3 and column 4 indicates the R.A. and Decl. of the source. One can find the sources by seaching with these coordinates of the sources. Column 5 is the reference column of the optical host galaxy from where the optical counterparts are taken. In column 6, we estimate the redshift of the BT candidates from the SDSS, Two Micron All-Sky Survey eXtended (2MASX), and Two Micron All Sky Survey (2MASS) catalogs. There were redshifts found for 261 of the 717 BT sources, including 153 WATs and 108 NATs. In column 7, we list the integrated flux densities of the BT sources from NVSS data. For flux measurements, we take NVSS flux instead of FIRST though both are observed same frequency (1400 MHz) because, (i) In comparison to the B-configuration FIRST survey (with a resolution of 5 arcsec and astrometrical errors of 0 51 arcsec), NVSS has a low resolution VLA D configuration (with a resolution of 45 arcsec and 17 arcsec astrometric accuracy). As a result, FIRST accurately detects small-scale structures while estimating flux for extended sources. NVSS measures more accurate fluxes for extended sources and can discover low-surface-brightness objects missed by FIRST, but has less accurate positional measurements and cannot distinguish small-scale structures. (ii) The FIRST survey is sensitive to flux-density loss due to its high resolution and lack of antennas with short spacing. In colimn 9, two-point spectral indexes (α_{150}^{1400}) between 150 MHz (TIFR GMRT Sky Survey) and 1400 MHz (NVSS) are computed. We have also calculated the luminosity of the BT sources with known redshifts in column 10. The morphological types (FRs) of NATs and WATs are shown in column 11 using our best eye estimation: "I" represent FR-I type and "II" represents FR-II type.

Of the 717 sources in our sample, 77 are present in the Blanton(2000) sample (marked as 'a'), 42 are in the Wing & Blanton(2011) sample (marked as 'b'), 103(32 WAT and 71 NAT) are in the Proctor(2011) sample (marked as 'c') and 24 are present in the Pateno-Mahler et al.(2017) sample (marked as 'd'), as noted in Table 3.1 and Table 3.2.

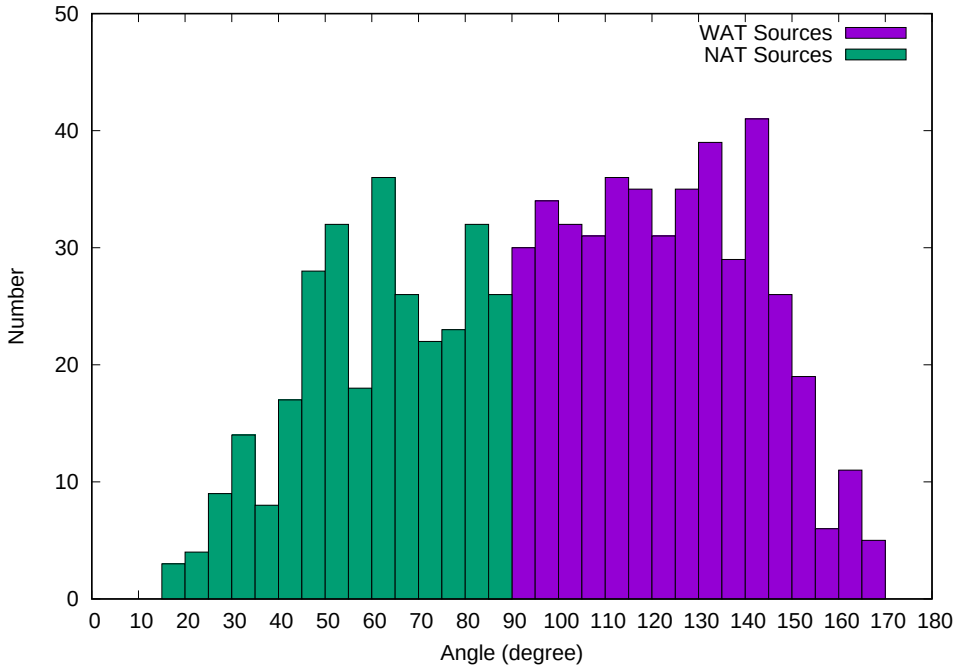

Figure 3.3: Histogram showing the angle distribution of narrow-angle tail (NAT) and wide-angle tail (WAT) sources. Left panel is for NAT sources (green color) and right panel is for WAT sources (violet color).

3.2.1 Bending angle

The angle between two distinct jet axes linking the core was used to measure the bending angle of sources. Depending on the bending angle of these sources, we classified all bent-tail sources in our sample into two groups: 'wide-angle tailed' galaxy and 'narrow-angle tailed' galaxy. The bending angle are measured for all BT sources.

Figure 4.2 shows a histogram illustrating the distribution of bending angles for both NAT and WAT type sources presented in this paper. The majority of NAT sources had an 60 degrees. With a peak between $145 - -150$ degree, WAT sources provided a wide range of angles between the two jets.

3.2.2 Spectral Index (α_{150}^{1400})

The energy distribution of relativistic electrons is represented by the spectral index (α_{150}^{1400}) of a radio source, hence its measurement should ideally cover a wide frequency range. It is generally known that the radio flux density varies with frequency as $S_\nu \propto \nu^\alpha$ for synchrotron radiation, unless it is affected by radiative

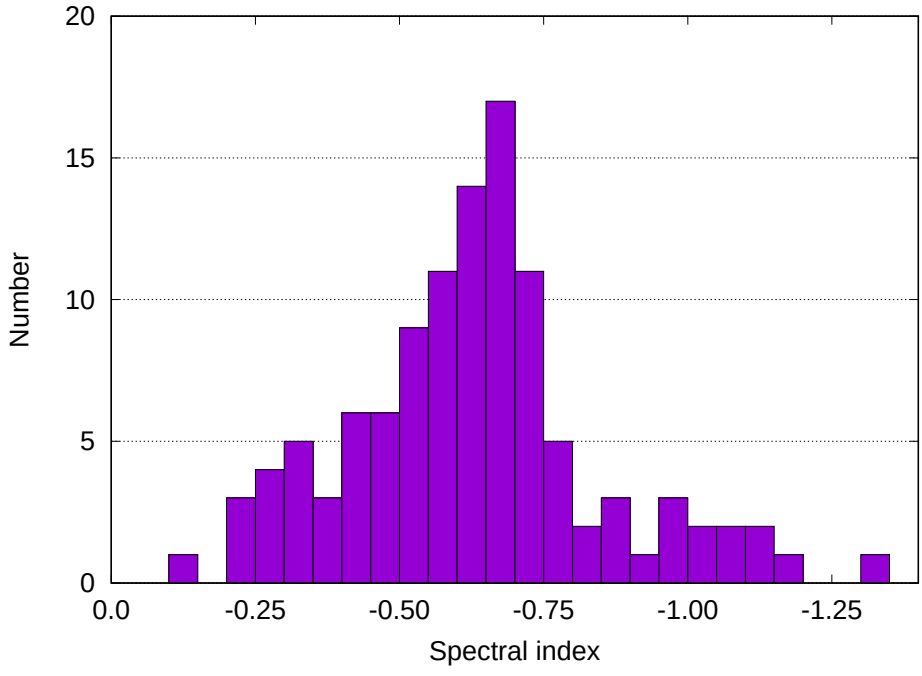

Figure 3.4: The histogram shows spectral index (α_{150}^{1400}) distribution of NAT candidates.

losses and optical depth effects.

Here, we calculate two points spectral index (α_{150}^{1400}) for our newly discovered NAT and WAT sources between two frequencies 150 MHz and 1400 MHz. The equation $S_\nu \propto \nu^\alpha$ is used for the measurements of spectral index where S_ν is the radiative flux density at a given frequency ν and α be the spectral index. The spectral indexes available for WATs and NATs are 195 and 112, respectively, and are reported in Tables 3.2 and Table 3.1. The rest of the sources were not detectable in the TGSS 150 MHz map due to the greater rms in the TGSS images.

The spectral index α_{150}^{1400} distribution of our 112 NAT sources are shown in figure 3.4. The histogram demonstrates that the overall range of α_{150}^{1400} is from –1.33 to –0.11 for NATs candidates. J1235+0741 has the lowest spectral index of NAT sources, with α_{150}^{1400} = –1.33 and J0734+3611 has the highest spctral index with α_{150}^{1400} = –0.11. The histogram shows a peak near α_{150}^{1400} = –0.65.

Figure 3.5 presents the distribution of the spectral index (α_{150}^{1400}) of 195 WAT sources. The histogram shows a overall span of (α_{150}^{1400}) is from –1.27 to –0.15. Among the WAT sources, J1300+2916 has the lowest spectral index with α_{150}^{1400} = –1.27 and J1457+0232 has the highest spectral index with α_{150}^{1400} = –0.15. The histogram shows two peaks near α_{150}^{1400} = –0.60 and –0.75.

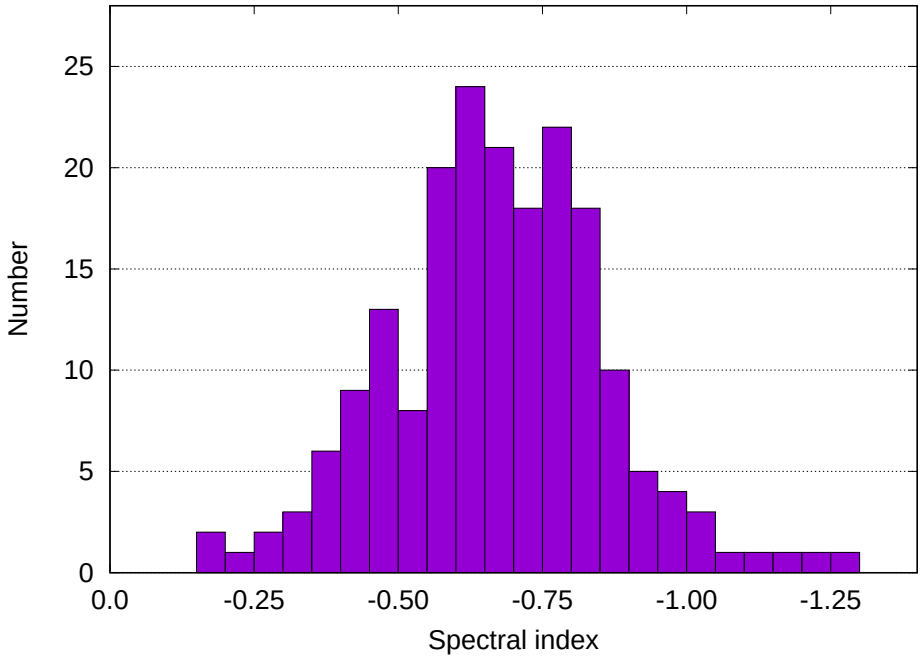

Figure 3.5: The histogram shows spectral index (α_{150}^{1400}) distribution of WAT candidates.

The spectral index (α_{150}^{1400}) of NAT sources has mean and median values of the –0.62. Similarly, the mean and median values for WAT sources are –0.67. That means spectral index values of our newly discovered NAT and WAT sources are similar to normal sized radio galaxies (Oort et al.(1988), Gruppioni et al.(1997), Kapahi et al.(1998), Ishwara-Chandra et al.(2010), Mahony et al.(2016)). In the work of Oort et al.(1988), they surveyed the Lynx field with the Westerbork Synthesis Radio Telescope (WSRT) at 325 MHz and 1400 MHz. Gruppioni et al.(1997) surveyed the Marano field using the Australia Telescope Compact Array (ATCA) at 1.4 GHz and 2.4 GHz. Kapahi et al.(1998) surveyed the Molonglo Radio Catalogue sources with the VLA at L and S bands. In the work of Ishwara-Chandra et al.(2010), they surveyed LBDS-Lynx field by using Giant Metrewave Radio Telescope (GMRT) at 150 MHz and other archival data from GMRT at 325 MHz and 610 MHz frequency along with the data from other surveys like WENSS, NVSS and FIRST. Mahony et al.(2016) surveyed the Lockman Hole field using LOFAR 150 MHz and WSRT 1.4 GHz.

3.2.3 Radio Luminosity (L_{rad})

The characteristic parameter that defines the strength of the radio jets is the radio luminosity (L_{rad}). Using certain empirical relationships, one may easily estimate the surface brightness of an extragalactic radio source from its radio luminosity (Heeschen(1966)). The radio luminosity value is used to determine the FR dichotomy.

The radio luminosity (L_{rad}) is calculated from the equation,

$$L_{rad} = 1.2 \times 10^{27} D_{Mpc}^2 S_0 \nu_0^{-\alpha} (1+z)^{-(1+\alpha)} \times (\nu_u^{(1+\alpha)} - \nu_l^{(1+\alpha)})(1+\alpha)^{-1} ergs^{-1}$$

(3-1)

where D_{Mpc} is luminosity distance to the source (Mpc), S_0 is the flux density (Jy) at a given frequency ν_0 (Hz), z is the redshift of the radio galaxy, α is the spectral index ($S \propto \nu^{\alpha}$) and ν_u (Hz) and ν_l (Hz) are the upeer and lower cut-off frequencies (O'Dea & Owen(1987)). In our calculation, we assume the upper and lower cutoff frequencies as 100 GHz and 10 MHz, respectively.

The radio luminosity distribution of the NATs and WATs in our sample with known redshifts (z) is plotted in Figure Figure 3.6. It's worth noting that the data points in this graph are congested in one place. Malmquist bias is largely responsible for the apparent increase in luminosity with redshift. There are 129 data points plotted here, 42 of which are NATs and 87 of which are WATs. The radio luminosities of the sources at 1400 MHz are in the order of 10^{43} erg s^{-1}, which is comparable to that of a typical radio galaxy.

The most luminous NAT source is J2348+1157 with $L_{rad} = 3.96 \times 10^{44}$ erg s^{-1} and the most luminous WAT source is J1607+4825 with $L_{rad} = 2.20 \times 10^{45}$ erg s^{-1}. Similarly the least luminous NAT source is J1353+3305 with $L_{rad} = 1.13 \times 10^{42}$ erg s^{-1} and the least luminous WAT source is J1253+0604 with $L_{rad} = 1.47 \times 10^{38}$ erg s^{-1}. For WAT sources, the mean $LogL$ (erg s^{-1})and median $LogL$ (erg s^{-1}) values of luminosity are 1.03 and 0.37, respectively. Similarly, for NAT sources, the mean $LogL$ (erg s^{-1})and median $LogL$ (erg s^{-1}) values of luminosity are 0.66 and 0.43, respectively.

3.2.4 Fanaroff-Riley Classes

Visual inspection is used to classify the FR catagories of the sources for our case. We examine the flux-density distribution of each HT radio source individually.

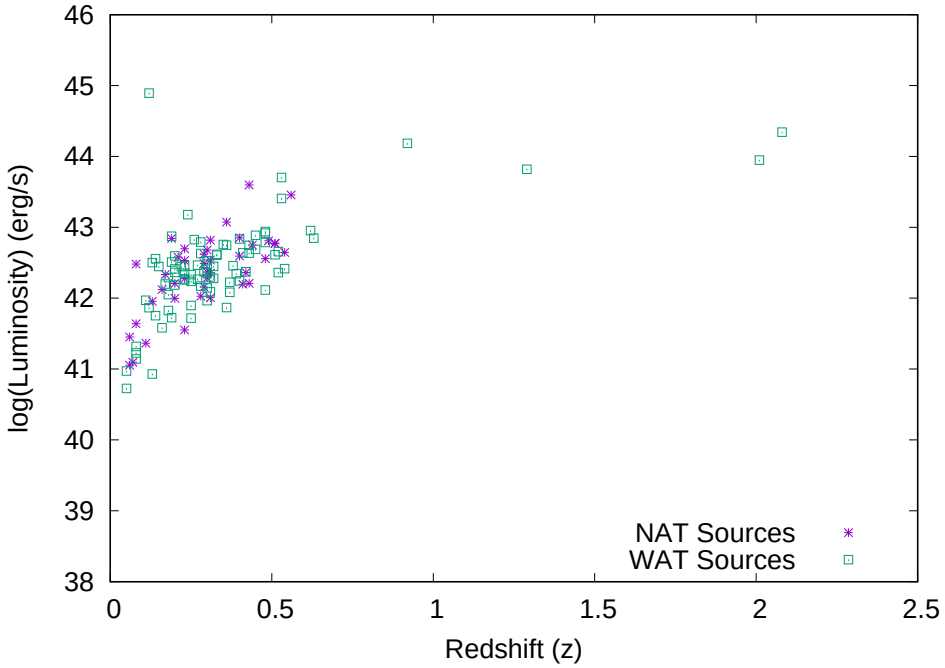

Figure 3.6: The plot shows the distribution of radio luminosity (L_{rad}) of WAT and NAT sources with redshifts (z).

We see if the source flux density is higher in the centre than on the edges, or if the edges are more radio bright than the centre. The edge-brightened cases were assigned to the FR-II type, while the edge-darkened and diffuse cases were assigned to the FR-I type. We did not identify them as FR-I or FR-II type if no conclusion could be reached on the relative flux between the edges and the central core. Note that the luminosity criterion was not used in this categorization. Among all the HTs from our catalog, 266(37%) sources are FR-I types and 317(44%) are FR-II types.

3.3 Discussion

The redshifts are calculated for 108 of the 287 NAT sources (38%). Six sources have redshift values larger than 0.5 among the NAT candidates ($z \geq 0.5$). Among all NATs, J1418+0515 has the highest redshift value of 0.583845 ± 0.000178, while J1334+2537 has the lowest redshift value of 0.04. Redshifts are also recognised for 153 WATs out of 430 (36%). Among all WAT sources, fourteen candidates have redshift values larger than 0.5 ($z \geq 0.5$). The source, J1051+0051 has highest redshift value 2.00660 +/- 0.00500 (Croom et al.(2004)) among all WATs as well

as all BT candidates in our cataloges. J1250+1133 is another high redshift WAT source with redshift $z = 1.28500$ +/- 0.00000 (Richards et al.(2009)). J1253+0604 is the closest WAT source with redshift $z = 0.000255$..

J1143+5201, the brightest BT source, has a flux (F_{1400}) of 2541 mJy. This source is also the most bright of all WATs. J1217+0340 is the brightest NAT source, with a flux (F_{1400}) of 1225 mJy. Higher-resolution observations will improve the dynamical study and other characteristics of such sources.

3.4 Conclusion and Summery

We carefully studied each of the 95,243 individual sources from the VLA FIRST survey at 1400 MHz in the most recent data release (2014 December 17). The sample resulted in a total of 717 BT sources based on visual morphology of the radio sources. A minority are single-component, but the most are multi-component candidates. Based on their bending angles between the two jets, we separated BT samples in two catagories, NAT and WAT. There are 287 NAT sources and 480 WAT sources among all BT sources. For the optical counterpart, we visually cross-matched our BT sample with SDSS data. 359 sources had optical counterparts, including 149 NATs and 210 WATs.

We classified our BT sources into two categories, FR-I and FR-II, based on a visual analysis of the flux distribution over the sources. 266 (37% of all BTs) are of the FR-I type, while 317 (44% of all BTs) are of the FR-II type. Due to their complex flux distributions, we were unable to categorise 134 (19%) sources as either FR-I or FR-II. 95 (75 %) of the BT sources had a sharp spectral index between 150 and 1400 MHz.

BT sources have previously been catalogued by many authors using pattern-recognition technology or visual inspection. The current catalog includes several sources which is not included in earlier catalogs. By using solely visual search, our catalog is the first to contain the largest number of BT sources (717) to date. This collection of BT sources will be useful in a wide range of statistical analyses in the future.

Owen & Rudnick(1976) were the first to discover bent radio sources in the Abell cluster. Following that, we noticed that HT radio sources are located in such cluster contexts in the majority of our identifications. Blanton(2000) cataloged 384 bent-double sources by visually inspecting 3200 multicomponent sources from the FIRST survey's April 1997 data release catalog. The author used BT samples as a galaxy cluster tracer. They discovered 102 clusters in the Abell database across the entire sample area. Bent-double sources were detected in 5% of the clusters in their study. Wing & Blanton(2011) used the SDSS to cross-correlate their radio

samples with their optical surroundings around double-lobed radio sources. They found that visually selected bent radio sources (as contrast to straight or single-component sources) are more frequently linked with galaxy clusters in all samples, with 78 percent of visually selected bent sources identified in cluster environments. Pateno-Mahler et al.(2017) used the Clusters Occupied by Bent Radio AGN survey to look for galaxy clusters in the surrounding fields of 646 bent, double-lobed radio galaxies. They discovered 190 galaxy-cluster candidates (mainly at high redshift) from the surrounding fields of their sample using galaxy overdensity measurements. As a result, bent radio sources are a useful tool for spotting rich galaxy clusters. Our catalogue will be extremely valuable in the search for galactic clusters.

Table 3.1

Table 3.1: **Candidate Wide Angle Tail Radio Sources**

Catalog Number	Name	R.A. (J2000.0)	Decl. (J2000.0)	Ref.	Redshift (z)	F_{1400} (mJy)	F_{150} (mJy)	α_{150}^{1400}	L (erg s^{-1}) ($\times 10^{43}$)	FR Type (I/II)	Other Catalogs
1	J0001–0826	00 01 15.11	–08 26 46.2	SDSS	0.33†	156	—	—	—	—	—
2	J0007+0536	00 07 05.88	+05 36 02.3	EE	—	307	—	—	—	I	8
3[a]	J0017–0149	00 17 32.28	–01 49 23.7	EE	—	91	—	—	—	II	—
4	J0020–0950	00 20 08.01	–09 50 53.3	EE	—	11	—	—	—	I	1
5	J0027+0224	00 27 19.11	+02 24 28.9	2MASX	0.13*	133	—	—	—	—	1, 2
6	J0034+1140	03 34 30.50	+11 40 40.9	SDSS	—	18	—	—	—	—	—
7	J0035–0834	00 35 03.48	–08 34 39.2	2MASS	—	387	—	—	—	II	8
8	J0041–0651	00 41 10.52	–06 51 05.2	EE	—	48	—	—	—	—	1
9[ac]	J0041+0028	00 41 52.16	+00 28 34.9	SDSS	0.15†	94	—	—	—	II	13, 15
10	J0044+1026	00 44 58.90	+10 26 44.2	EE	—	226	—	—	—-	—	—
11	J0045–0701	00 45 47.96	–07 01 40.7	EE	—	123	—	—	—	II	22
12	J0046–0805	00 46 36.48	–08 05 45.6	EE	—	15	—	—	—	II	1
13	J0057–0100	00 57 29.38	–01 00 59.1	EE	—	30	—	—	—	—	—
14	J0057–0336	00 57 33.71	–03 36 09.6	2MASX	0.16†	86	—	—	—	I	1, 2, 16
15[a]	J0103+0041	01 03 29.65	+00 41 01.8	EE	—	155	641	–0.63	—	I	—
16[ad]	J0120+0021	01 20 58.94	+00 21 39.2	EE	—	45	185	–0.63	—	II	—
17	J0158–0215	01 58 30.16	–02 15 30.4	SDSS	0.44†	23	—	—	—	II	—
18[d]	J0159–0119	01 59 55.52	–01 19 59.9	EE	—	23	—	—	—	I	—
19	J0212–0450	02 12 16.55	–04 50 38.8	EE	—	156	—	—	—	II	—
20	J0224+0659	02 24 28.64	+06 59 23.2	EE	—	776	1965	–0.41	—	I	—
21	J0229+0429	02 29 02.09	+04 29 03.3	2MASX	0.19†	34	—	—	—	II	1, 2, 8
22	J0233–0321	02 33 17.70	–03 21 00.6	EE	—	662	—	—	—	II	4
23	J0242–0544	02 42 04.91	–05 44 17.0	2MASX	0.14†	65	—	—	—	I	8, 16
24[c]	J0245–0648	02 45 57.86	–06 48 55.91	EE	—	29	—	—	—	—	14
25[a]	J0248–0113	02 48 08.57	–01 13 44.2	SDSS	0.28†	23	—	—	—-	—	—
26	J0308–0607	03 08 50.29	–06 07 37.2	2MASX	—	88	—	—	—	—	1
27	J0312–0633	03 12 55.23	–06 33 43.1	EE	—	170	—	—	—	II	—
28	J0313–0631	03 13 29.05	–06 31 19.5	EE	—	87	—	—	—	—	1
29	J0318–0810	03 18 00.43	–08 10 20.5	EE	—	24	—	—	—	—	—
30[a]	J0320+0059	03 20 29.23	+00 59 44.9	EE	—	75	392	–0.74	—	I	–
31	J0331–0730	03 31 31.48	–07 30 01.8	EE	—	56	—	—	—	II	1
32	J0332+0024	03 32 36.25	+00 24 57.2	EE	—	15	58	–0.60	—	I	1
33	J0334+0102	03 34 00.64	+01 02 15.9	SDSS	0.38†	6	—	—	—	—	—
34	J0335–0719	03 35 48.23	–07 19 12.5	EE	—	84	—	—	—	II	—
35	J0703+6014	07 03 11.18	+60 14 23.1	2MASX	—	54	155	–0.47	—	I	1
36	J0704+6228	07 04 22.20	+62 28 13.2	EE	—	44	205	–0.69	—	I	1
37	J0715+4829	07 15 19.07	+48 29 32.0	EE	—	39	—	—	—	—	—
38	J0717+4405	07 17 26.66	+44 05 02.3	EE	—	223	770	–0.55	—	—	—
39	J0719+5519	07 19 36.64	+55 19 42.8	EE	—	62	425	–0.86	—	—	1
40	J0723+3323	07 23 59.55	+33 23 20.2	EE	—	151	525	–0.56	—	I	6, 1, 2
41	J0724+3639	07 24 19.13	+36 39 56.7	EE	—	52	168	–0.52	—	I	—
42	J0726+3102	07 26 49.96	+31 02 04.0	2MASX	—	143	887	–0.82	—	I	—
43	J0733+4213	07 33 12.73	+42 13 00.9	EE	—	275	—	—	—	—	—
44[a]	J0734+2933	07 34 06.21	+29 33 16.5	EE	—	106	610	–0.78	—	I	—
45	J0736+1857	07 36 17.12	+18 57 10.2	2MASX	—	139	994	–0.88	—	I	1, 2
46[a]	J0741+2620	07 41 01.20	+26 20 36.6	EE	—	10	64	–0.83	—	—	—
47	J0744+1658	07 44 59.31	+16 58 59.7	EE	—	41	107	–0.43	—	II	1
48	J0744+4353	07 44 42.18	+43 53 07.8	EE	—	17	59	–0.56	—	I	1
49	J0748+2324	07 48 45.09	+23 24 45.7	SDSS	0.19†	515	3238	–0.82	7.48	—	—
50	J0748+4849	07 48 30.52	+48 49 55.1	EE	—	12	—	—	—	—	1

Notes— a, b, c and d are denoted the soucres present in Blanton(2000), Wing & Blanton(2011), Proctor(2011) and Pateno-Mahler et al.(2017), respectively.

† and $*$ are represents spectroscopic and photometric redshifts, respectively.

References– 1: NRAO VLA Sky Survey (NVSS; Condon et al.(1998)); 2:VLA Low-Frequency Sky Survey (VLSS; Cohen et al.(2007)); 3: 3C Be62, Ed59; 4: 4C Pi65, Go67, Ca69; 5: 5C Ke66, Po68, Po69, Wi70, Pe75, Wa77, Sc81, Be82; 6: 6C Ba85, Ha88, Ha90, Ha91, Ha93a, Ha93b; 7: 7C Mc90, Ko94, Wa96, Ve98; 8: Parkes-MIT-NRAO Radio Survey (PMN; Gr94); 9: The Parkes Catalogue of Radio Sources (PKS; Bolton et al.(1964)); 10: Texas Survey of Radio Sources (TXS; Douglas et al.(1996)); 11: Cul Sl95; 12: 87GB Gr91; 13: Automatic Spectroscopic K-means-based classification (ASK; Sánchez et al.(2011)); 14: 2 Micron All Sky Survey Extended objects - Final Release (2MASX; Skrutskie et al.(2006)); 15:GALaxy Evolution eXplorer All-Sky Survey Source Catalog (GALEXASC; Agüeros et al.(2005)); 16: GALaxy Evolution eXplorer Medium Imaging Survey Catalog (GALEXMSC; Agüeros et al.(2005)); 17: Gaussian Mixture Brightest Cluster Galaxy (GMBCG; Ha10); 18: Gaussian Mixture Brightest Cluster Galaxy (MaxBCG; Ko07); 19: New General Catalogue (NGC; Dreyer(1888)); 20: B2 Co70, Co72, Co73, Fa74; 21: B3 Fi85.

Table 3.1: **Candidate Wide Angle Tail Radio Sources**

Catalog Number	Name	R.A. (J2000.0)	Decl. (J2000.0)	Ref.	Redshift (z)	F_{1400} (mJy)	F_{150} (mJy)	α_{150}^{1400}	L (erg s^{-1}) ($\times 10^{43}$)	FR Type (I/II)	Other Catalogs
51	J0750+1741	07 50 49.80	+17 41 41.9	EE	—	79	460	–0.79	—	II	2
52	J0750+5841	07 50 18.30	+58 41 36.3	2MASX	—	46	200	–0.66	—	I	1, 6
53	J0750+5856	07 50 05.16	+58 56 59.4	GALEX	—	92	—	—	—	I	—
54[a]	J0752+3750	07 52 28.25	+37 50 56.7	EE	—	380	2557	–0.85	—	II	4
55	J0755+1909	07 55 11.29	+19 09 36.9	SDSS	0.31†	35	132	–0.59	2.00	I	20
56	J0757+5824	07 57 38.30	+58 24 37.5	2MASX	—	19	—	—-	—	—	1
57[ac]	J0806+2531	08 06 11.29	+25 31 37.8	EE	—	129	—	—	—	—	—
58	J0811+1029	08 11 40.88	+10 29 27.3	2MASX	—	81	469	–0.78	—	—	1
59	J0813+4347	08 13 00.11	+43 47 48.6	2MASX	0.13†	337	—	—	—	—	6, 13
60	J0814+4300	08 14 03.34	+43 00 12.9	EE	—	64	294	–0.68	—	—	—
61	J0815+3840	08 15 12.34	+38 40 45.4	2MASX	0.13†	500	3313	–0.85	3.18	II	13
62[c]	J0816+5716	08 16 59.33	+57 16 28.8	2MASX	0.20†	143	718	–0.72	2.58	II	1, 2, 6
63	J0818+3858	08 18 22.16	+38 58 40.4	EE	—	52	276	–0.74	—	—	—
64[c]	J0818+4956	08 18 00.73	+49 56 11.8	SDSS	0.28†	125	1144	–0.99	4.25	II	1, 20
65	J0819+1849	08 19 01.55	+18 49 18.2	EE	—	59	358	–0.81	—	—	1
66[d]	J0819+3332	08 19 28.70	+33 32 47.4	EE	—	6	40	–0.85	—	—	—
67	J0820+3034	08 20 32.51	+30 34 49.8	EE	—	446	4473	–1.03	—	I	6
68	J0822+1435	08 22 58.44	+14 35 47.5	EE	—	7	—	—	—	—	—
69	J0826+0359	08 26 08.51	+03 59 03.6	SDSS	0.20†	57	—	—	—	II	13, 20
70	J0830+0836	08 30 16.63	+08 36 53.4	EE	—	51	110	–0.34	—	II	1
71	J0831+3914	08 31 08.01	+39 14 28.1	EE	—	73	—	—	—	—	1
72	J0833+1027	08 33 45.45	+10 27 53.1	2MASX	0.29†	42	—	—	—	II	1, 2
73	J0833+4940	08 33 10.17	+49 40 05.3	2MASX	0.05†	43	157	–0.58	0.05	I	1, 13
74	J0834+0019	08 34 09.58	+00 19 48.6	EE	—	28	44	–0.20	—	—	—
75[d]	J0837+6020	08 37 34.89	+60 20 46.6	EE	—	16	—	—	—	II	1
76[b]	J0839+0609	08 39 13.94	+06 09 44.9	SDSS	0.41†	26	60	–0.37	4.35	I	1
77	J0840+3826	08 40 10.61	+38 26 27.5	SDSS	—	120	621	–0.74	—	I	—
78[c]	J0841–0202	08 41 32.00	–02 03 19.7	EE	—	35	—	—	—	II	—
79	J0841+1235	08 41 58.63	+12 35 12.4	SDSS	0.31†	15	—	—	—	I	—
80	J0841+5258	08 41 02.16	+52 58 54.1	SDSS	0.52†	27	115	–0.65	4.52	I	1
81[c]	J0844+2129	08 44 45.33	+21 29 30.7	SDSS	—	120	631	–0.74	—	II	—
82	J0844+2606	08 44 33.40	+26 06 15.1	2MASX	0.11†	100	251	–0.41	0.93	I	2, 10, 13
83[c]	J0846–0131	08 46 55.05	–01 31 42.7	EE	—	28	—	—	—	I	1
84	J0847+3147	08 47 58.72	+31 47 54.3	EE	—	164	—	—	—	II	—
85	J0851+6227	08 51 59.09	+62 27 57.5	SDSS	0.92*	281	1908	–0.86	152.79	I	15
86	J0852+5639	08 52 15.76	+56 39 15.2	SDSS	0.40†	22	127	–0.78	1.75	II	1, 20
87	J0855+3454	08 55 34.71	+34 54 30.9	SDSS	—	66	—	—	—	—	1
88	J0856+2152	08 56 16.87	+21 52 52.8	SDSS	0.38†	40	220	–0.76	2.87	I	1
89	J0856+4951	08 56 18.71	+49 51 06.4	SDSS	0.62†	37	167	–0.67	8.98	I	1
90	J0858+1710	08 58 45.11	+17 10 03.1	2MASX	0.33†	66	—	—	—	II	2, 20
91	J0858+5740	08 58 03.85	+57 40 13.8	SDSS	0.45†	62	253	–0.63	7.70	—	1, 6, 12
92	J0859–0251	08 59 54.39	–02 51 40.0	GALEX	—	404	—	—	—	—	4
93	J0900+1614	09 00 31.97	+16 14 25.6	SDSS	—	48	—	—	—	I	14, 21
94	J0900+5056	09 00 52.57	+50 56 22.6	2MASX	0.20†	224	—	—	—	II	13, 20
95	J0902+1819	09 02 16.30	+18 19 04.3	EE	—	79	434	–0.76	—	I	—
96[a]	J0903+3230	09 03 00.64	+32 30 40.7	EE	—	85	—	—	—	I	—
97	J0904+5834	09 04 57.31	+58 34 49.9	SDSS	0.27†	25	—	—	—	I	1, 20
98	J0907+0234	09 07 04.23	+02 34 38.1	EE	—	40	160	–0.62	—	I	1
99	J0908+3437	09 08 47.17	+34 37 39.8	SDSS	0.36†	16	—	—	—	I	1
100[ac]	J0910+3841	09 10 42.23	+38 41 25.6	SDSS	—	85	377	–0.67	—	I	15, 20
101	J0912+0534	09 12 35.82	+05 33 55.2	EE	—	17	41	–0.39	—	II	—
102[c]	J0912+0944	09 12 04.76	+09 44 07.4	SDSS	0.24†	61	—	—	15.09	—	1
103	J0913+5208	09 13 15.78	+52 08 55.0	2MASX	0.19†	227	1537	–0.86	3.23	I	13
104	J0916+0808	09 16 47.53	+08 08 47.9	SDSS	—	38	98	–0.42	—	I	1, 16
105[d]	J0916+5844	09 16 08.58	+58 44 38.1	SDSS	—	790	4426	–0.77	—	II	1, 2, 6
106	J0917+0350	09 17 23.81	+03 50 04.4	SDSS	—	32	146	–0.68	—	II	1
107	J0917+4322	09 17 12.29	+43 22 48.9	SDSS	—	57	229	–0.62	—	I	—
108	J0923+0759	09 24 01.47	+07 58 51.1	EE	—	51	—	—	—	II	—
109	J0924–0524	09 24 27.17	–05 24 34.5	EE	—	69	—	—	—	—	—
110	J0924+0627	09 24 04.91	+06 27 15.6	SDSS	0.20†	48	123	–0.42	1.53	I	1, 13

Table 3.1: **Candidate Wide Angle Tail Radio Sources**

Catalog Number	Name	R.A. (J2000.0)	Decl. (J2000.0)	Ref.	Redshift (z)	F_{1400} (mJy)	F_{150} (mJy)	α_{150}^{1400}	L (erg s^{-1}) ($\times 10^{43}$)	FR Type (I/II)	Other Catalogs
111	J0924+2326	09 24 20.75	+23 26 33.9	EE	—	32	138	–0.65	—	I	—
112	J0925–0557	09 25 31.68	–05 57 38.5	EE	—	43	—	—	—	II	1
113[c]	J0926+0309	09 26 44.19	+03 09 19.7	SDSS	0.23†	112	—	—	—	I	13
114	J0927+4109	09 27 17.98	+41 09 21.8	EE	—	14	61	–0.66	—	—	—
115	J0928–0507	09 28 51.88	–05 07 17.5	EE	—	139	—	—	—	II	8
116	J0933+0600	09 33 24.84	+06 00 40.1	EE	—	102	472	–0.68	—	II	—
117	J0934+1829	09 34 34.29	+18 29 30.5	2MASX	0.25†	54	180	–0.54	2.15	II	1, 13
118	J0935–0325	09 35 23.36	–03 25 47.0	EE	—	128	—	—	—	—	—
119	J0935+1124	09 35 22.76	+11 24 57.5	EE	—	34	—	—	—	II	—
120	J0936–0627	09 36 02.19	–06 27 59.1	EE	—	106	—	—	—	II	—
121	J0937+0245	09 37 43.70	+02 45 40.2	EE	—	31	—	—	—	—	—
122	J0937+5800	09 37 28.52	+58 00 13.4	EE	—	20	116	–0.79	—	II	1
123	J0940+1510	09 40 13.55	+15 10 53.2	SDSS	0.63†	26	104	–0.62	7.02	I	1
124	J0940+4826	09 40 06.91	+48 26 49.2	SDSS	0.42†	22	89	–0.62	2.35	I	1
125[d]	J0941+0814	09 41 42.11	+08 14 00.5	EE	—	38	150	–0.61	—	I	—
126	J0941+5751	09 41 46.01	+57 51 24.2	EE	—	109	—	—	—	I	—
127	J0943+0611	09 43 09.45	+06 11 31.8	SDSS	—	9	—	—	—	II	—
128	J0944–0234	09 44 33.77	–02 34 16.8	EE	—	45	—	—	—	II	1
129	J0946–0705	09 46 29.26	–07 05 31.3	EE	—	50	—	—	—	—	1
130	J0946+3604	09 46 44.44	+36 04 54.4	EE	—	74	598	–0.93	—	I	6, 13, 14
131[c]	J0947+0044	09 47 07.56	+00 44 16.6	2MASX	0.26†	57	—	—	—	II	1
132[c]	J0947+5251	09 47 15.39	+52 50 57.9	EE	—	52	—	—	—	II	—
133	J0950–0437	09 50 18.42	–04 37 40.6	EE	—	18	—	—	—	I	1
134[ac]	J0953+2924	09 53 27.88	+29 24 19.8	EE	—	159	—	—	—	II	—
135	J0954+4304	09 54 25.87	+43 04 16.1	SDSS	0.48†	57	213	–0.59	8.70	II	—
136	J0954+6241	09 54 55.45	+62 41 30.2	2MASX	0.23†	93	468	–0.72	2.26	I	1, 2, 6, 13
137	J0955–0247	09 55 13.50	–02 47 15.6	SDSS	—	61	—	—	—	II	—
138	J0955+1102	09 55 51.61	+11 02 33.4	SDSS	0.28†	33	127	–0.60	1.48	II	—
139	J0957–0645	09 57 20.04	–06 45 07.9	EE	—	12	—	—	—	—	—
140	J0959–0454	09 59 03.53	–04 54 09.5	EE	—	70	—	—	—	I	1
141	J0959+5641	09 59 56.85	+56 41 14.6	EE	—	21	77	–0.58	—	II	—
142	J0959+5751	09 59 37.65	+57 51 57.2	2MASX	0.08†	51	147	–0.47	0.21	II	1, 7
143	J1001+4902	10 01 53.57	+49 20 33.2	2MASX	—	41	—	—	—	II	1
144	J1002+4756	10 02 44.00	+47 56 20.2	SDSS	—	10	47	–0.69	—	II	1, 15
145	J1003+3730	10 03 46.59	+37 30 56.5	2MASX	—	57	206	–0.57	—	—	1, 6, 12
146	J1005+6022	10 05 01.01	+60 22 03.8	2MASX	0.23†	61	221	–0.58	1.87	I	1, 6, 13
147	J1007+2904	10 07 15.78	+29 40 49.1	EE	—	17	52	–0.50	—	I	—
148	J1008+0142	10 08 44.59	+01 42 11.4	EE	—	178	1040	–0.79	—	II	8
149[c]	J1009+0337	10 09 43.50	+03 37 22.7	2MASX	0.11†	185	—	—	—	II	15
150	J1010–0601	10 10 57.71	–06 01 25.2	EE	—	31	–	—	—	I	—
151	J1018+0348	10 18 52.13	+03 48 56.1	EE	—	13	—	—	—	—	—
152	J1019+0019	10 19 39.05	+00 19 46.1	EE	—	53	—	—	—	II	—
153	J1020+4828	10 20 56.98	+48 28 30.6	EE	—	208	—	—	—	II	2
154	J1021+0024	10 21 41.19	+00 24 47.6	SDSS	—	26	78	–0.49	—	—	1
155	J1026+3259	10 26 22.33	+32 59 11.6	2MASX	0.24†	76	—	—	—	I	13, 20
156	J1031–0640	10 31 30.66	–06 40 28.1	EE	—	30	—	—	—	II	1
157	J1032+0144	10 32 40.96	+01 44 30.3	EE	—	37	161	–0.66	—	—	
158[ab]	J1032+3045	10 32 58.75	+30 45 39.4	SDSS	0.42†	23	109	–0.70	1.67	II	1, 7
159	J1032+5505	10 32 01.09	+55 05 54.4	EE	—	10	48	–0.70	—	I	1
160	J1033+0755	10 33 39.59	+07 55 30.2	EE	—	29	273	–1.00	—	II	—
161	J1033+1923	10 33 08.11	+19 23 55.6	2MASX	0.19†	30	129	–0.65	0.53	II	1, 13
162	J1035+3406	10 35 11.38	+34 06 24.6	SDSS	0.53†	129	461	–0.57	25.53	I	—
163	J1038+4148	10 38 27.38	+41 48 43.5	EE	—	48	111	– 0.37	—	—	—
164[c]	J1039–0645	10 39 47.12	–06 45 24.9	2MASS	—	47	—	—	—	II	—
165[a]	J1039+3338	10 39 16.34	+33 38 29.4	SDSS	0.36†	10	42	–0.64	0.74	—	1, 20
166	J1045+5250	10 45 44.05	+52 50 17.1	2MASX	0.26†	29	—	—	—	—	—
167	J1046+0538	10 46 43.42	+05 38 38.8	SDSS	0.30†	51	253	–0.71	2.26	—	1
168	J1046+5434	10 46 41.67	+54 34 25.2	EE	—	53	—	—	—	—	1
169	J1047–0059	10 47 07.57	–00 59 20.9	EE	—	19	—	—	—	II	—
170[b]	J1050+3040	10 50 10.5	+30 40 00	2MASS	0.25†	58	703	–1.12	1.73	—	17

Table 3.1: **Candidate Wide Angle Tail Radio Sources**

Catalog Number	Name	R.A. (J2000.0)	Decl. (J2000.0)	Ref.	Redshift (z)	F_{1400} (mJy)	F_{150} (mJy)	α_{150}^{1400}	L (erg s^{-1}) ($\times 10^{43}$)	FR Type (I/II)	Other Catalogs
171	J1051+0051	10 51 35.32	+00 51 33.8	SDSS	2.01*	21	213	–1.04	88.65	II	1
172	J1054+5425	10 54 30.26	+54 25 05.8	2MASX	0.18†	92	282	–0.50	1.95	II	1, 7, 10, 13
173	J1103+0356	11 03 32.44	+03 56 23.8	EE	—	101	—	—	—	II	—
174	J1105+5943	11 05 24.26	+59 43 41.9	2MASX	0.36†	89	504	–0.78	5.60	II	1, 2, 6, 7
175[ab]	J1108+2610	11 08 12.46	+26 10 33.8	2MASX	0.17†	122	584	–0.70	1.58	I	1, 2, 7, 10
176	J1112+0346	11 12 44.34	+03 46 32.5	EE	—	15	—	—	—	II	—
177	J1114+3625	11 14 01.78	+34 25 03.2	SDSS	0.57†	82	—	—	—	II	—
178	J1115+0613	11 15 10.07	+06 13 03.9	EE	—	12	74	–0.81	—	II	1
179	J1116–0435	11 16 06.35	–04 35 39.4	EE	—	33	—	—	—	II	1
180	J1116+4516	11 16 54.16	+45 16 17.6	2MASX	—	62	276	–0.67	—	I	—
181	J1118–0556	11 18 00.7	–05 56 25.5	EE	—	63	—	—	—	II	1
182[abc]	J1118+3115	11 18 33.52	+31 15 16.3	EE	—	324	1998	–0.81	—	—	—
183	J1123–0700	11 23 51.34	–07 00 00.3	GALEX	—	28	183	–0.84	—	—	1
184	J1125+0314	11 25 08.80	+03 14 52.2	SDSS	—	12	—	—	—	I	1
185[ab]	J1125+3618	11 25 23.73	+36 18 24.3	2MASX	0.28†	45	—	—	—	—	1
186	J1125+5827	11 25 39.13	+58 27 34.2	2MASX	0.25†	20	172	–0.96	0.52	II	1
187[a]	J1126+2638	11 26 30.83	+26 38 05.5	EE	—	91	330	–0.58	—	II	—
188	J1126+5925	11 26 46.63	+59 25 49.9	EE	—	31	238	–0.91	0.87	I	6
189	J1129+0550	11 29 02.74	+05 50 49.9	SDSS	0.32*	19	43	–0.36	1.90	II	—
190[ab]	J1130+2524	11 30 48.83	+25 24 35.6	2MASX	0.14	96	—	—	—-	II	1, 13
191	J1130+5457	11 30 50.30	+54 57 44.0	EE	—	20	100	–0.72	—	II	1
192	J1131+0435	11 31 40.91	+04 35 20.8	EE	—	36	90	–0.41	0.40	II	—
193	J1131–0600	11 31 56.47	–06 00 12.1	EE	—	88	—	—	—	II	—
194	J1138+2012	11 38 00.00	+20 12 22.6	EE	—	64	248	–0.61	—	I	—
195	J1138+2039	11 38 50.25	+20 39 18.4	SDSS	0.18†	67	267	–0.62	1.12	I	1, 13
196[c]	J1143+0729	11 43 39.85	+07 29 59.6	2MASX	0.10†	70	—	—	—	II	13, 15, 20
197	J1143+1525	11 43 16.54	+15 25 13.2	2MASX	—	15	—	—	—	—	1
198	J1144–0114	11 44 57.93	–01 14 34.4	EE	—	32	—	—	—	I	1
199	J1144+5833	11 44 48.08	+58 33 50.4	SDSS	0.34†	47	—	—	—	II	—
200[c]	J1145–0757	11 45 53.08	–07 57 53.6	EE	—	51	—	—	—	II	1
201	J1146–0504	11 46 21.91	–05 04 48.2	EE	—	109	—	—	—	—	—
202	J1147+5421	11 47 28.97	+54 21 37.3	SDSS	—	70	375	–0.75	—	I	1, 2, 6, 10
203[ab]	J1148+2332	11 48 33.14	+23 32 25.9	2MASX	0.18†	40	160	–0.62	0.67	I	1, 13, 20
204	J1149–0144	11 49 28.17	–01 44 41.6	EE	—	63	—	—	—	II	—
205	J1149+3136	11 49 36.32	+31 36 32.5	EE	—	10	—	—	—	—	1
206	J1150+5728	11 50 56.08	+57 28 06.5	SDSS	0.54*	16	85	–0.75	2.61	I	1, 16
207[ac]	J1152+3405	11 52 43.66	+34 05 33.9	EE	—	35	—	—	—	II	—
208[a]	J1154+3635	11 54 34.82	+36 35 39.9	2MASX	0.11†	42	—	—	—	II	1, 6, 13
209	J1155–0125	11 55 00.48	–01 25 52.0	2MASX	—	112	—	—	—	I	9
210	J1158+0037	11 58 21.34	+00 37 08.1	EE	—	22	—	—	—	II	—
211	J1158+0946	11 58 54.01	+09 46 31.9	EE	—	20	50	–0.41	—	II	1
212	J1159–0127	11 59 40.93	–01 27 15.1	EE	—	92	—	—	—	I	—
213	J1201+3257	12 01 51.87	+32 57 01.3	EE	—	158	—	—	—	II	6
214	J1204+4834	12 04 45.05	+48 34 59.9	EE	—	29	190	–0.84	—	II	—
215[a]	J1205+3204	12 05 14.01	+32 04 41.4	EE	—	185	—	—	—	II	6
216[ab]	J1209+2420	12 09 38.29	+24 20 38.4	EE	—	35	134	–0.60	—	I	—
217[a]	J1209+3708	12 09 24.08	+37 08 49.5	GALEX	—	101	477	–0.70	—	I	6
218	J1210+4812	12 10 28.26	+48 12 57.5	EE	—	38	216	–0.78	—	I	—
219[b]	J1211+0607	12 11 10.99	+06 07 44.2	2MASX	0.14†	36	88	–0.40	0.56	I	13
220	J1213–0327	12 13 45.43	–03 27 09.5	EE	—	26	—	—	—	II	1
221	J1213+5612	12 13 18.95	+56 12 54.1	EE	—	13	—	—	—	I	1
222	J1216+0342	12 16 40.13	+03 42 31.5	2MASX	0.08†	20	—	—	—	I	13
223	J1219+0014	12 19 05.57	+00 14 16.4	SDSS	0.41†	16	—	—	—	I	1
224	J1220+4759	12 20 13.15	+47 59 46.8	2MASX	0.30†	56	—	—	—	I	1
225	J1221–0113	12 21 59.88	–01 13 59.3	SDSS	—	72	—	—	—	II	—
226	J1221–0108	12 21 59.66	–01 08 00.8	SDSS	0.24*	56	—	—	—	II	—
227	J1230+1144	12 30 11.43	+11 44 45.3	EE	—	385	1421	–0.58	—	II	—
228	J1232+3130	12 32 11.44	+31 30 58.1	SDSS	0.35†	80	320	–0.62	5.72	I	1
229	J1233+1928	12 33 16.72	+19 28 50.4	2MASX	0.23†	106	452	–0.65	2.86	II	13
230[a]	J1233+3559	12 33 24.51	+35 59 15.5	EE	—	16	252	–1.23	—	—	1

Table 3.1: **Candidate Wide Angle Tail Radio Sources**

Catalog Number	Name	R.A. (J2000.0)	Decl. (J2000.0)	Ref.	Redshift (z)	F_{1400} (mJy)	F_{150} (mJy)	α_{150}^{1400}	L (erg s^{-1}) ($\times 10^{43}$)	FR Type (I/II)	Other Catalogs
231	J1235+5625	12 35 07.09	+56 25 05.6	SDSS	0.39*	116	631	–0.76	—	I	—
232	J1237+2013	12 37 20.33	+20 13 52.6	EE	—	19	103	–0.76	—	I	1
233[b]	J1241+2734	12 41 08.79	+27 34 47.1	EE	—	177	—	—	—	II	—
234	J1242+4041	12 42 47.76	+40 41 44.3	SDSS	0.45†	43	204	–0.70	4.87	I	—
235	J1246+5453	12 46 47.53	+54 53 15.2	2MASX	0.08†	40	136	–0.55	0.14	I	1, 13
236	J1247+4042	12 47 01.00	+40 42 02.3	SDSS	—	75	304	–0.62	—	I	—
237	J1249+0143	12 49 48.06	+01 43 19.5	EE	—	77	—	—	—	—	—
238[ab]	J1249+3038	12 49 42.23	+30 38 37.9	2MASX	0.19†	86	—	—	—	I	13
239	J1250–0132	12 50 03.80	–01 32 25.0	2MASX	0.08*	384	—	—	—	II	14
240	J1250+0839	12 50 10.59	+08 39 52.7	SDSS	0.35†	13	—	—	—	II	1
241	J1250+1133	12 50 13.31	+11 33 08.0	SDSS	1.29*	53	280	–0.74	65.91	I	16
242	J1251–0123	12 51 18.15	–01 23 12.5	EE	—	26	—	—	—	—	—
243	J1253+0604	12 53 26.70	+06 04 39.7	SDSS	2.55E–4†	46	292	–0.82	1.47E–5	II	1, 2
244	J1254+6134	12 54 31.99	+61 34 5.6	SDSS	—	54	—	—	—	II	1, 15
245	J1255+0152	12 55 17.00	+01 52 59.5	EE	—	8	—	—	—	II	—
246	J1256+0125	12 56 22.78	+01 25 16.0	SDSS	—	164	—	—	—	II	—
247	J1259+4617	12 59 41.85	+46 17 39.9	SDSS	0.42†	13	—	—	—	I	—
248	J1300+2916	13 00 58.31	+29 16 34.2	SDSS	0.52†	10	171	–1.27	2.29	I	1
249	J1301–0649	13 01 35.45	–06 49 58.1	EE	—	110	—	—	—	I	—
250[c]	J1304+1855	13 04 09.29	+18 55 48.7	2MASX	0.20†	52	100	–0.29	2.31	—	1
251	J1306–0539	13 06 30.4	–05 39 26.2	EE	—	22	—	—	—	II	—
252[a]	J1306+3338	13 06 07.11	+33 38 13.5	SDSS	0.30†	22	68	–0.50	1.39	I	1, 5
253[c]	J1307+5651	13 07 43.70	+56 51 03.3	2MASX	0.25†	136	—	—	—	II	13
254	J1308+0829	13 08 36.40	+08 29 00.7	EE	—	13	66	–0.73	—	I	—
255	J1315+0612	13 15 17.25	+06 12 57.3	SDSS	0.26*	45	123	–0.45	1.80	II	14
256	J1319+5443	13 19 52.38	+54 43 08.6	SDSS	0.37†	16	71	–0.67	1.21	I	—
257	J1320–0341	13 20 31.33	–03 41 05.6	EE	—	55	—	—	—	II	—
258	J1321–0637	13 21 40.56	–06 37 11.5	EE	—	16	—	—	—	—	1
259[ab]	J1325+3419	13 25 23.51	+34 19 24.5	EE	—	23	—	—	—	I	1
260	J1327+0007	13 27 57.47	+00 07 47.4	EE	—	56	—	—	—	II	—
261	J1329–0511	13 29 23.93	–05 11 15.2	EE	—	13	—	—	—	I	1
262[c]	J1333–0657	13 33 38.09	–06 57 56.4	EE	—	32	—	—	—	II	—
263	J1333+0944	13 33 25.85	+09 44 31.9	SDSS	0.32†	24	—	—	—	I	1
264[c]	J1333+5427	13 33 35.23	+54 27 43.5	2MASX	0.11†	183	—	—	—	II	2, 6, 13
265	J1336+0047	13 36 05.49	+00 47 26.6	2MASX	0.27†	59	185	–0.51	2.91	I	—
266	J1337–0803	13 37 32.72	–08 03 36.8	EE	—	48	—	—	—	—	1
267	J1339–0726	13 39 02.73	–07 26 43.4	EE	—	63	—	—	—	—	1
268	J1340+5439	13 40 48.19	+54 39 49.4	EE	—	80	243	–0.50	—	II	1
269	J1341–0116	13 41 21.03	–01 16 14.3	EE	—	25	—	—	—	II	—
270	J1345–0451	13 45 22.29	–04 51 49.8	EE	—	61	—	—	—	II	—
271	J1345+0855	13 45 04.67	+08 55 07.2	EE	—	14	—	—	—	II	1
272	J1345+3655	13 45 54.08	+36 55 03.1	EE	—	213	1383	–0.84	—	—	—
273	J1345+5332	13 45 46.01	+53 32 48.9	EE	—	434	—	—	—	II	—
274	J1345+6110	13 45 03.06	+61 10 31.6	SDSS	0.51†	19	55	–0.47	4.10	I	—
275[c]	J1351–0548	13 51 20.54	–05 48 50.4	EE	—	349	—	—	—	—	—
276	J1351+0712	13 51 44.72	+07 12 17.0	SDSS	—	126	1938	–1.19	—	I	—
277	J1353–0732	13 53 30.31	-07 32 16.7	2MASX	—	26	—	—	—	II	1
278	J1354+0528	13 54 42.27	+05 28 56.1	2MASX	0.08†	40	112	–0.46	0.16	I	1, 13, 15
279	J1355+1758	13 55 47.13	+17 58 45.0	SDSS	0.33†	29	52	–0.26	4.05	I	—
280	J1359+2808	13 59 05.03	+28 08 09.9	EE	—	75	383	–0.73	—	I	—
281	J1401+0740	14 01 23.41	+07 40 40.1	SDSS	0.27†	16	43	–0.44	0.78	—	1
282[c]	J1401+2833	14 01 48.60	+28 33 17.9	EE	—	105	157	–0.18	—	II	—
283	J1401+3256	14 01 08.86	+32 56 00.5	EE	—	16	115	–0.88	—	I	—
284	J1401+5654	14 01 09.98	+56 54 20.6	SDSS	—	43	—	—	—	I	—
285	J1406+0211	14 06 05.67	+02 11 53.9	EE	—	15	45	–0.49	—	I	1
286	J1408+0511	14 08 53.71	+05 11 24.6	EE	—	8	—	—	—	II	1
287	J1408+4540	14 08 06.63	+45 40 54.6	EE	—	10	—	—	—	I	—
288	J1410–0636	14 10 55.79	–06 36 39.5	EE	—	114	—	—	—	I	—
289	J1410+5846	14 10 54.06	+58 46 55.4	SDSS	0.48†	45	201	–0.67	6.09	I	15
290	J1411–0731	14 11 38.33	–07 31 43.6	EE	—	51	—	—	—	II	—

Table 3.1: **Candidate Wide Angle Tail Radio Sources**

Catalog Number	Name	R.A. (J2000.0)	Decl. (J2000.0)	Ref.	Redshift (z)	F_{1400} (mJy)	F_{150} (mJy)	α_{150}^{1400}	L (erg s^{-1}) ($\times 10^{43}$)	FR Type (I/II)	Other Catalogs
291	J1411+1048	14 11 29.33	+10 48 59.1	2MASX	0.16†	28	106	–0.59	0.38	II	1, 13
292	J1411+4535	14 11 10.93	+45 35 18.1	EE	—	37	86	–0.37	—	—	1
293	J1412+0043	14 12 20.57	+00 43 14.9	EE	—	9	—	—	—	—	—
294	J1412+0153	14 12 51.75	+01 53 51.4	EE	—	18	131	–0.89	—	I	1
295	J1412+0257	14 12 09.48	+02 57 51.8	SDSS	—	23	—	—	—	II	15
296	J1412+2157	14 12 53.65	+21 57 43.9	EE	—	38	140	–0.58	—	I	1
297	J1415+2326	14 15 38.85	+23 26 50.7	EE	—	22	175	–0.93	—	I	—
298	J1416+2147	14 16 13.79	+21 47 42.8	2MASX	0.19†	11	—	—	—	I	—
299	J1417+0114	14 17 52.89	+01 14 42.7	SDSS	0.38†	13	—	—	—	I	—
300	J1419+4657	14 19 40.16	+46 57 29.9	SDSS	0.48†	67	362	–0.75	8.27	I	—
301^{c}	J1420–0622	14 20 31.37	–06 22 43.4	EE	—	26	—	—	—		
302	J1422+0825	14 22 58.90	+08 25 18.8	EE	—	16	—	—	—	I	—
303	J1424+0025	14 24 20.20	+00 25 34.0	EE	—	158	714	–0.67	—	I	8
304^{b}	J1424+0403	14 24 46.46	+04 03 45.6	SDSS	0.36†	20	—	—	—	II	—
305	J1425+5545	14 25 47.10	+55 45 26.1	EE	—	47	280	–0.80	—	—	1
306	J1426+4102	14 26 39.46	+41 02 48.9	SDSS	0.36†	41	—	—	—	I	—
307^{a}	J1429+2336	14 29 19.16	+23 36 16.7	SDSS	—	83	—	—	—	II	—
308^{b}	J1433+1913	14 33 20.47	+19 13 29.0	2MASX	0.21†	23	—	—	—	II	1, 13
309	J1435+5507	14 35 28.46	+55 07 52.1	2MASX	0.14†	480	3017	–0.82	3.59	II	2, 6, 13, 16
310	J1437+1950	14 37 37.96	+19 50 11.9	EE	—	70	274	–0.61	—	II	—
311	J1438+0926	14 38 07.58	+09 26 11.7	SDSS	0.33†	60	213	–0.57	4.16	II	—
312	J1438+4753	14 38 40.48	+47 53 56.8	SDSS	—	47	—	—	—	II	—
313	J1440+1342	14 40 02.86	+13 42 17.9	SDSS	—	11	—	—	—	II	—
314	J1443–0111	14 43 47.49	–01 11 36.9	EE	—	8	—	—	—	I	—
315	J1443+5201	14 43 02.78	+52 01 37.3	EE	0.14†	2541	—	—	—	I	1, 2, 10, 14
316	J1444–0311	14 44 57.45	–03 11 51.3	EE	—	370	—	—	—	II	—
317	J1444–0542	14 44 29.96	–05 42 48.8	EE	—	70	—	—	—	I	—
318^{a}	J1445+2951	14 45 12.73	+29 51 36.9	EE	—	30	141	–0.69	—	I	1
319	J1445+6357	14 45 38.45	+63 57 33.8	SDSS	0.30†	22	123	–0.77	0.92	II	—
320	J1446+1402	14 46 33.83	+14 02 11.9	2MASX	0.12†	22	—	—	78.17	I	1, 13
321	J1446+4319	14 46 00.93	+43 19 12.8	SDSS	—	8	51	0.83	—	—	—
322	J1448+5944	14 48 38.85	+59 44 52.0	2MASX	0.28†	130	465	–0.57	6.20	II	—
323^{c}	J1450+1447	14 50 01.50	+14 47 47.7	2MASX	0.30†	90	—	—	—	II	1
324^{c}	J1450+2728	14 50 22.52	+27 28 20.5	2MASX	0.12†	86	280	–0.53	0.73	II	7, 13, 15
325	J1452+0636	14 52 30.11	+06 36 45.0	EE	—	20	—	—	—	II	—
326	J1452+1707	14 52 22.84	+17 07 17.9	SDSS	0.04†	174	—	—	—	II	13
327^{b}	J1457+0232	14 57 22.66	+02 32 56.4	2MASX	0.15†	78	110	–0.15	2.79	II	1, 13, 16
328	J1457+3140	14 57 55.85	+31 40 57.1	EE	—	73	—	—	—	II	—
329^{ab}	J1459+2754	14 59 00.23	+27 54 00.8	2MASX	0.23†	16	—	—	—	I	1, 13
330	J1501+2134	15 01 28.25	+21 34 23.8	EE	0.26†	228	1378	–0.80	6.70	II	1, 2, 9
331	J1504+1409	15 04 43.54	+14 09 25.8	EE	—	6	—	—	—	—	—
332	J1505+0253	15 05 50.75	+02 53 04.6	2MASX	0.05†	42	89	–0.34	0.09	I	1, 15
333^{c}	J1510+0544	15 10 56.07	+05 44 41.7	EE	—	552	7719	–1.18	—	I	20
334	J1511+3633	15 11 25.92	+36 33 36.0	2MASX	0.16*	144	—	—	—	I	13, 16, 20
335	J1512+0612	15 12 54.82	+06 12 11.7	2MASX	0.17†	28	—	—	—	II	1, 13, 20
336	J1512+1513	15 12 20.61	+15 13 51.3	EE	—	66	266	–0.62	—	—	1
337	J1512+3654	15 12 18.26	+36 54 18.8	2MASX	0.29†	52	220	–0.64	2.36	II	1, 16, 20
338^{a}	J1520+2329	15 20 01.08	+23 29 05.2	SDSS	0.48†	10	48	–0.70	1.30	II	1, 20
339^{ac}	J1521+3157	15 21 26.98	+31 57 33.3	2MASX	0.31†	82	—	—	—	II	20
340	J1521+5104	15 21 25.02	+51 04 03.1	EE	—	273	2201	–0.93	—	I	1
341	J1524+1321	15 24 43.44	+13 21 21.3	EE	—	6	—	—	—	I	—
342	J1528+0714	15 28 18.54	+07 14 09.3	SDSS	0.39†	24	—	—	—	I	1, 20
343	J1529–0431	15 29 18.88	–04 31 38.3	EE	—	33	—	—	—	II	—
344	J1532+0028	15 32 52.09	+00 28 09.4	SDSS	—	29	—	—	—	I	—
345	J1532+4658	15 32 01.76	+46 58 52.8	SDSS	0.32†	25	51	–0.32	2.80	II	1
346	J1533+5700	15 33 46.37	+57 00 11.9	2MASX	0.22†	110	449	–0.63	2.79	I	1, 2, 6, 20
347	J1534+0556	15 34 39.48	+05 56 17.5	SDSS	—	43	125	–0.48	—	I	14, 20
348	J1536–0201	15 36 44.82	–02 01 36.8	EE	—	241	—	—	—	—	1
349	J1537+4051	15 37 52.75	+40 51 30.6	EE	—	15	84	–0.77	—	—	—
350	J1538+3557	15 38 56.78	+35 57 09.6	SDSS	—	168	—	—	—	I	20

Table 3.1: **Candidate Wide Angle Tail Radio Sources**

Catalog Number	Name	R.A. (J2000.0)	Decl. (J2000.0)	Ref.	Redshift (z)	F_{1400} (mJy)	F_{150} (mJy)	α_{150}^{1400}	L (erg s^{-1}) ($\times 10^{43}$)	FR Type (I/II)	Other Catalogs
351	J1539–0215	15 39 59.25	–02 15 10.2	SDSS	—	34	—	—	—	I	—
352	J1539–0544	15 39 23.41	–05 44 42.9	EE	—	20	—	—	—	I	1
353	J1539+0450	15 39 04.01	+04 50 56.9	SDSS	0.17†	8	—	—	—	II	1, 13
354^{c}	J1545–0249	15 45 48.80	–02 49 38.6	EE	—	51	—	—	—	II	—
355	J1548+5813	15 48 26.29	+58 13 14.0	SDSS	—	455	2630	–0.78	—	—	1, 2, 6, 16
356	J1550+1200	15 50 34.84	+12 00 40.8	2MASX	0.30†	57	190	–0.54	3.37	I	1
357	J1551+0609	15 51 40.33	+06 09 16.7	2MASX	0.31†	21	77	–0.58	1.23	I	1, 17, 20
358	J1554+5819	15 54 51.41	+58 19 09.5	EE	—	10	—	—	—	I	1
359	J1559–0143	15 59 20.03	–01 43 33.39	EE	—	52	—	—	—	I	—
360	J1601+3155	16 0130.74	+31 55 32.4	SDSS	—	19	113	–0.80	—	I	—
361	J1606+5610	16 06 04.55	+56 10 44.7	EE	—	17	103	–0.81	—	—	—
362	J1607+4825	16 07 28.21	+48 25 35.2	SDSS	0.97†	59	378	–0.83	220.26	I	1, 15
363	J1608+0141	16 08 03.55	+01 41 54.34	EE	—	516	3282	–0.83	—	I	—
364	J1609+5844	16 09 29.98	+58 44 08.0	SDSS	0.39†	21	70	–0.54	2.23	I	1
365	J1616+0926	16 16 53.17	+09 26 35.7	SDSS	0.20†	225	1197	–0.75	3.94	II	13, 20
366	J1620+4740	16 20 06.81	+47 40 45.7	SDSS	—	132	—	—	—	II	—
367	J1621+1140	16 21 23.34	+11 40 12.5	EE	—	18	124	–0.86	—	I	1
368^{a}	J1625+3026	16 25 31.80	+30 26 39.4	EE	—	207	1103	–0.75	—	II	—
369	J1625+4456	16 25 23.87	+44 56 23.4	SDSS	0.40†	66	240	–0.58	6.85	II	20
370	J1625+4813	16 25 12.80	+48 13 03.4	EE	—	43	166	–0.60	—	II	—
371	J1631+0531	16 31 10.28	+05 31 50.3	2MASX	0.15†	44	—	—	—	II	1, 2, 21
372	J1631+0535	16 31 42.43	+05 35 23.1	EE	—	12	—	—	—	II	—
373	J1633+1710	16 33 51.11	+17 10 54.5	SDSS	0.35†	33	—	—	—	II	1
374^{b}	J1635+2020	16 35 17.08	+20 20 48.5	2MASX	0.15†	80	—	—	—	I	1
375	J1635+4309	16 35 16.22	+43 09 55.9	EE	—	26	—	—	—	I	—
376	J1641+1004	16 41 08.91	+10 04 42.3	EE	—	211	1230	–0.79	—	I	—
377	J1645+1046	16 45 00.34	+10 46 40.1	SDSS	—	23	—	—	—	II	—
378	J1645+5842	16 45 22.51	+58 42 55.8	EE	—	62	556	–0.98	—	—	1
379^{ab}	J1650+3202	16 50 07.71	+32 02 09.0	SDSS	0.30†	43	119	–0.45	30.3	II	1
380	J1651+3500	16 51 25.35	+35 00 36.2	EE	—	157	473	–0.49	—	I	—
381	J1655+5217	16 55 18.47	+52 17 23.8	EE	—	63	470	–0.90	—	II	1
382^{a}	J1657+2746	16 57 47.88	+27 46 09.5	2MASX	—	18	66	–0.58	—	I	1
383	J1659+2955	16 59 36.94	+29 55 17.2	SDSS	—	77	846	–1.07	—	II	15
384	J1701+4959	17 01 37.10	+49 59 14.6	EE	—	12	—	—	—	I	—
385	J1705+5109	17 05 26.41	+51 09 35.4	EE	0.53*	342	2570	–0.90	50.27	—	1, 2, 10
386	J1708+4723	17 08 51.55	+47 23 35.5	EE	—	5	—	—	—	I	1
387	J1718+4202	17 18 02.23	+42 02 11.5	SDSS	0.41†	17	—	—	—	II	—
388^{a}	J1719+3547	17 19 36.39	+35 47 06.98	SDSS	0.26*	33	91	–0.45	1.85	I	—
389	J1723+4757	17 23 51.91	+47 57 32.7	EE	—	14	—	—	—	—	1
390	J1727+4030	17 27 55.04	+40 30 23.5	EE	—	12	67	–0.77	—	—	—
391	J1743+6342	17 43 41.98	+63 42 37.3	EE	—	13	—	—	—	—	—
392	J2020+0026	20 20 53.29	+00 26 26.1	EE	—	17	—	—	—	II	1
393	J2031+0107	20 31 24.60	+01 07 14.8	EE	—	26	131	–0.72	—	—	—
394	J2056+0205	20 56 37.87	+02 05 45.8	EE	—	47	—	—	—	I	—
395^{a}	J2127–0127	21 27 10.80	–01 27 21.2	2MASX	0.18†	75	—	—	—	II	—
396	J2127+0042	21 27 22.52	+00 42 57.7	2MASX	0.13†	11	49	–0.67	0.08	I	1, 13
397	J2131–0555	21 31 53.07	–05 55 55.0	2MASX	—	39	—	—	—	II	—
398	J2138–0545	21 38 19.97	–05 45 44.2	EE	—	87	—	—	—	I	—
399	J2139+1008	21 39 46.25	+10 08 28.0	2MASX	0.22†	87	—	—	—	—	1
400	J2142–0549	21 42 36.85	–05 49 43.3	EE	—	50	—	—	—	—	1
401	J2142+1017	21 42 03.49	+10 17 21.8	2MASX	0.07†	98	—	—	—	II	2, 10
402	J2145–0659	21 45 03.51	–06 59 24.7	EE	—	26	—	—	—	II	—
403	J2147+1215	21 47 11.37	+12 15 15.8	SDSS	—	20	—	—	—	II	1
404	J2148–0825	21 48 01.28	–08 25 27.5	2MASX	0.13†	92	—	—	—	II	13
405	J2150–0744	21 50 10.33	–07 44 17.8	EE	—	22	—	—	—	II	1
406	J2158–0507	21 58 52.69	–05 07 35.8	EE	—	37	—	—	—	II	—
407	J2201–0451	22 01 39.25	–04 51 36.9	EE	—	23	—	—	—	I	1
408	J2202–0101	22 02 04.86	–01 01 01.4	2MASX	0.18†	72	—	—	—	I	13
409^{a}	J2207–0102	22 07 30.82	–01 02 46.1	EE	—	13	—	—	—	I	—
410	J2210–0152	22 10 04.77	–01 52 33.9	GALEX	—	39	—	—	—	I	—

Table 3.1: **Candidate Wide Angle Tail Radio Sources**

Catalog Number	Name	R.A. (J2000.0)	Decl. (J2000.0)	Ref.	Redshift (z)	F_{1400} (mJy)	F_{150} (mJy)	α_{150}^{1400}	L (erg s^{-1}) ($\times 10^{43}$)	FR Type (I/II)	Other Catalogs
411	J2213–0854	22 13 12.43	–08 54 37.1	EE	—	632	—	—	—	I	—
412	J2214–0447	22 14 44.07	–04 47 33.6	EE	—	24	—	—	—	I	1
413	J2215–0757	22 15 49.46	–07 57 39.9	2MASX	0.21†	24	—	—	—	I	1, 13
414	J2218+0230	22 18 07.20	+02 30 33.2	EE	—	36	256	–0.88	—	II	1
415	J2221–0747	22 21 16.81	–07 47 42.6	SDSS	—	85	—	—	—	II	8
416^{a}	J2248+0052	22 48 12.59	+00 52 52.8	SDSS	0.41†	16	—	—	—	II	—
417	J2250–0141	22 50 47.02	–01 41 17.2	2MASX	0.11†	127	—	—	—	II	1, 16
418^{a}	J2301+0037	23 01 35.06	+00 37 13.1	SDSS	0.43†	47	177	–0.59	5.58	I	20
419	J2306–0357	23 06 31.11	–03 57 45.2	EE	—	103	—	—	—	—	—
420	J2312–0919	23 12 12.16	–09 19 28.6	SDSS	0.83†	180	—	—	—	II	1, 2, 8, 10
421	J2315–0300	23 15 27.84	–03 00 05.1	EE	—	73	—	—	—	II	—
422	J2319–0737	23 19 19.27	–07 37 34.5	EE	—	70	—	—	—	II	—
423	J2320–0433	23 20 49.50	–04 33 58.5	EE	—	101	—	—	—	I	1
424	J2328+0038	23 28 54.12	+00 38 48.8	SDSS	0.43	24	57	–0.39	4.32	I	—
425	J2334–0759	23 34 55.59	–07 59 14.4	EE	—	15	—	—	—	II	—
426	J2337–0900	23 37 34.47	–09 00 15.4	SDSS	—	96	—	—	—	—	—
427	J2344–0658	23 44 42.31	–06 58 09.8	EE	—	82	—	—	—	I	1
428	J2349–0812	23 49 44.66	–08 12 08.6	EE	—	13	—	—	—	II	1
429^{a}	J2350–0117	23 50 28.43	–01 17 02.0	2MASX	0.19†	50	—	—	—	I	1, 16
430	J2356+0119	23 56 36.26	+01 19 29.1	EE	—	23	—	—	—	II	—

Table 3.2

Table 3.2: **Candidate Narrow Angle Tail Radio Sources**

Catalog Number	Name	R.A. (J2000.0)	Decl. (J2000.0)	Ref.	Redshift (z)	F_{1400} (mJy)	F_{150} (mJy)	α_{150}^{1400}	L (erg s^{-1}) ($\times 10^{43}$)	FR Type (I/II)	Other Catalogs
1	J0012–0607	00 12 48.62	–06 07 03.1	2MASX	0.20†	66	—	—	—	II	15
2	J0017+0827	00 17 37.70	+08 27 52.9	EE	—	55	—	—	—	I	—
3	J0020+0004	00 20 14.18	+00 04 48.0	EE	—	170	457	–0.44	—	I	16
4	J0023+0717	00 23 46.06	+07 17 55.5	2MASX	0.25†	74	—	—	—	I	1, 2, 10
5^{c}	J0041–0925	00 41 49.95	–09 25 48.6	GALEX	—	35	—	—	—	II	—
6	J0047+1034	00 47 11.24	+10 34 58.2	2MASS	—	24	—	—	—	—	—
7	J0054+0302	00 54 43.83	+03 02 10.5	SDSS	0.41†	18	192	–1.06	1.58	—	1
8	J0056–0119	00 56 30.55	–01 19 19.9	EE	—	162	—	—	—	—	—
9^{ac}	J0056–0120	00 56 02.70	–01 20 03.5	CGCG	0.04†	370	—	—	—	II	8, 11, 14, 16
10	J0111+1141	01 11 40.13	+11 41 34.1	EE	—	13	—	—	—	II	—
11	J0140+0223	01 40 23.32	+02 23 56.7	EE	—	33	294	–0.98	—	II	—
12	J0148+0000	01 48 07.84	+00 00 52.2	EE	—	33	120	–0.58	—	II	—
13	J0148+0142	01 48 17.75	+01 42 54.3	EE	—	15	31	–0.32	—	I	—
14	J0150–0818	01 50 43.47	–08 18 36.7	SDSS	—	55	—	—	—	II	1
15	J0212–0155	02 12 42.34	–01 55 47.7	EE	—	43	—	—	—	I	—
16^{c}	J0216–0245	02 16 19.98	–02 45 26.7	EE	—	122	—	—	—	I	1
17	J0223+0640	02 23 27.58	+06 40 39.1	GALEX	—	81	—	—	—	II	4
18	J0231+0531	02 31 17.02	+05 31 09.7	2MASX	—	31	262	–0.95	—	I	1, 12
19	J0256–0542	02 56 20.02	–05 42 49.5	GALEX	—	38	—	—	—	II	1
20	J0317–0816	03 17 41.97	–08 16 39.8	EE	—	73	—	—	—	—	—
21	J0323–0814	03 23 04.96	–08 14 16.6	EE	—	16	—	—	—	—	—
22	J0334–0109	03 34 34.09	–01 09 52.3	2MASX	0.14†	87	—	—	—	II	13, 16
23	J0335+0420	03 35 05.72	+04 20 17.1	EE	—	33	128	–0.61	—	II	—
24	J0337+0421	03 37 50.21	+04 21 04.2	SDSS	0.51*	30	115	–0.60	—	I	1
25	J0340–0111	03 40 31.47	–01 11 40.6	EE	—	6	—	—	—	—	1
26	J0349–0648	03 49 28.97	–06 48 00.1	EE	—	37	—	—	—	I	13
27	J0356+0013	03 56 50.87	+00 13 23.2	EE	—	254	—	—	—	II	—
28	J0703+5147	07 03 36.36	+51 47 17.1	EE	—	64	296	–0.68	—	I	1
29	J0709+4331	07 09 06.53	+43 31 35.4	EE	—	14	66	–0.69	—	II	1
30	J0714+3634	07 14 49.33	+36 34 49.8	EE	—	144	608	–0.64	—	II	—
31	J0718+4820	07 18 25.52	+48 20 20.6	EE	—	95	—	—	—	II	—
32	J0720+3617	07 20 11.94	+36 17 49.6	SDSS	—	21	—	—	—	I	—
33^{c}	J0729+5949	07 29 30.39	+59 49 52.0	2MASS	—	54	—		—	—	—
34	J0731+3251	07 31 13.85	+32 51 15.1	EE	—	42	—	—	—	I	1
35	J0732+4208	07 32 01.32	+42 08 29.9	SDSS	0.29†	16	33	–0.32	1.43	I	—
36	J0732+6150	07 32 19.53	+61 50 03.9	2MASX	—	102	324	–0.52	—	II	—
37^{c}	J0734+3611	07 34 41.42	+36 11 37.2	SDSS	—	62	80	–0.11	—	II	—
38	J0738+3846	07 38 54.99	+38 46 23.4	EE	—	145	—	—	—	II	17
39^{c}	J0738+4159	07 38 49.51	+41 59 07.5	2MASX	0.18†	104	—	—	—	II	13, 20
40^{c}	J0743+2710	07 43 06.29	+27 10 14.2	SDSS	—	111	—	—	—	II	—
41	J0754+3951	07 54 42.69	+39 51 39.1	2MASX	0.29†	37	63	–0.24	4.16	II	1
42^{c}	J0756+6030	07 56 42.43	+60 30 40.2	EE	—	13	75	–0.78	—	—	6
43	J0802+3904	08 02 22.95	+39 04 21.3	EE	—	30	—	—	—	II	—
44	J0803+3951	08 03 44.68	+39 51 00.0	EE	—	20	104	–0.74	—	I	1
45	J0809+0934	08 09 26.10	+09 34 03.8	2MASX	0.23†	16	99	–0.82	0.35	I	1, 13, 20
46	J0811+3810	08 11 18.94	+38 10 08.7	EE	—	90	327	–0.58	—	—	—
47^{a}	J0819+2522	08 19 38.66	+25 22 22.8	EE	—	53	286	–0.75	—	I	—
48^{c}	J0819+5746	08 19 39.25	+57 46 06.6	EE	—	32	—	—	—	II	—
49	J0819+5804	08 19 11.01	+58 04 20.9	EE	—	23	—	—	—	—	—
50	J0820+1642	08 20 41.53	+16 42 30.2	EE	—	23	56	–0.40	—	—	—

Notes— a, b, c and d are denoted the soucres present in Blanton(2000), Wing & Blanton(2011), Proctor(2011) and Pateno-Mahler et al.(2017), respectively.
† and $*$ are represents spectroscopic and photometric redshifts, respectively.

References– 1: NRAO VLA Sky Survey (NVSS; Condon et al.(1998)); 2:VLA Low-Frequency Sky Survey (VLSS; Cohen et al.(2007)); 3: 3C Be62, Ed59; 4: 4C Pi65, Go67, Ca69; 5: 5C Ke66, Po68, Po69, Wi70, Pe75, Wa77, Sc81, Be82; 6: 6C Ba85, Ha88, Ha90, Ha91, Ha93a, Ha93b; 7: 7C Mc90, Ko94, Wa96, Ve98; 8: Parkes-MIT-NRAO Radio Survey (PMN; Gr94); 9: The Parkes Catalogue of Radio Sources (PKS; Bolton et al.(1964)); 10: Texas Survey of Radio Sources (TXS; Douglas et al.(1996)); 11: Cul Sl95; 12: 87GB Gr91; 13: Automatic Spectroscopic K-means-based classification (ASK; Sánchez et al.(2011)); 14: 2 Micron All Sky Survey Extended objects - Final Release (2MASX; Skrutskie et al.(2006)); 15:GALaxy Evolution eXplorer All-Sky Survey Source Catalog (GALEXASC; Agüeros et al.(2005)); 16: GALaxy Evolution eXplorer Medium Imaging Survey Catalog (GALEXMSC; Agüeros et al.(2005)); 17: Gaussian Mixture Brightest Cluster Galaxy (GMBCG; Ha10); 18: Gaussian Mixture Brightest Cluster Galaxy (MaxBCG; Ko07); 19: New General Catalogue (NGC; Dreyer(1888)); 20: B2 Co70, Co72, Co73, Fa74; 21: B3 Fi85.

Table 3.2: **Candidate Narrow Angle Tail Radio Sources**

Catalog Number	Name	R.A. (J2000.0)	Decl. (J2000.0)	Ref.	Redshift (z)	F_{1400} (mJy)	F_{150} (mJy)	α_{150}^{1400}	L (erg s^{-1}) ($\times 10^{43}$)	FR Type (I/II)	Other Catalogs
51[c]	J0824+5200	08 24 44.68	+52 00 33.8	SDSS	0.30†	54	—	—	—	I	20
52	J0826+1531	08 26 23.62	+15 31 26.6	EE	—	49	83	–0.24	—	—	—
53	J0827+0816	08 27 30.03	+08 16 26.1	EE	—	21	—	—	—	I	—
54[b]	J0827+3820	08 27 12.91	+38 20 02.3	GALEX	—	152	—	—	—	II	—
55[ac]	J0828+2436	08 28 39.63	+24 36 55.8	EE	—	122	—	—	—	II	—
56[c]	J0829+6322	08 29 10.55	+63 22 28.5	2MASX	—	36	—	—	—	I	1, 15
57	J0830+2155	08 30 50.27	+21 55 57.8	EE	—	17	—	—	—	I	—
58	J0834+3945	08 34 30.09	+39 45 09.5	EE	—	102	513	–0.72	—	I	2
59	J0844+2538	08 44 47.54	+25 38 23.7	EE	—	11	54	–0.71	—	—	—
60	J0846+2024	08 46 47.94	+20 24 48.9	EE	—	48	—	—	—	—	—
61[c]	J0850+1349	08 50 53.72	+13 49 00.3	EE	—	137	—	—	—	II	—
62	J0851+1615	08 51 10.34	+16 15 30.6	SDSS	0.66†	27	—	—	—	I	—
63[c]	J0857+1704	08 57 57.06	+17 04 47.3	2MASX	0.33†	63	—	—	—	—	2, 20
64	J0858+1620	08 58 39.90	+16 20 08.8	EE	—	30	64	–0.34	—	II	1, 20
65[c]	J0901+0259	09 01 25.81	+02 59 28.8	2MASS	0.19†	281	—	—	—	II	13
66[ab]	J0902+3505	09 02 30.30	+35 05 11.0	SDSS	—	15	—	—	—	—	1
67[c]	J0903+4509	09 03 05.38	+45 09 59.7	SDSS	0.21†	130	403	–0.51	3.79	—	20
68	J0914+0824	09 14 50.71	+08 24 42.7	EE	—	77	378	–0.71	—	I	1
69	J0916+1729	09 16 42.69	+17 29 20.4	EE	—	56	219	–0.61	—	II	—
70	J0916+3818	09 16 48.04	+38 18 06.2	EE	—	336	1457	–0.66	—	I	6
71	J0919–0129	09 19 40.43	–01 29 50.3	EE	—	25	—	—	—	I	—
72	J0921+0723	09 21 04.79	+07 23 38.3	SDSS	0.30†	41	72	–0.25	4.79	I	—
73	J0922–0724	09 22 39.18	–07 24 27.5	EE	—	101	—	—	—	I	1
74[c]	J0927+5423	09 27 04.27	+54 23 46.6	2MASX	0.12†	199	—	—	—	—	13, 16
75	J0933+1341	09 33 28.30	+13 41 37.5	EE	—	35	147	–0.64	—	I	1
76	J0936+0340	09 36 43.62	+03 40 44.1	SDSS	—	14	—	—	—	II	1
77[a]	J0940+2530	09 40 56.39	+25 30 59.5	EE	—	19	241	–1.14	—	I	—
78	J0942+1523	09 42 14.45	+15 22 56.3	EE	—	94	1255	–1.16	—	I	1
79[c]	J0944–0616	09 44 54.86	–06 16 07.9	2MASX	—	87	—	—	—	II	1
80[c]	J0951+1802	09 51 13.21	+18 02 08.8	EE	—	168	—	—	—	II	—
81[ac]	J0953+2924	09 53 27.88	+29 24 19.8	EE	—	162	—	—	—	II	—
82[c]	J1005+2210	10 05 15.91	+22 10 47.5	EE	—	23	—	—	—	I	—
83	J1005+3000	10 05 00.53	+30 00 04.4	EE	—	24	—	—	—	II	—
84	J1006+0850	10 06 28.48	+08 50 12.3	EE	—	34	122	–0.57	—	I	—
85	J1010+2145	10 10 42.61	+21 45 57.3	EE	—	20	94	–0.69	—	II	1
86	J1011–0607	10 11 34.79	–06 07 51.5	EE	—	23	—	—	—	II	1
87	J1013+5532	10 13 07.16	+55 32 01.6	EE	—	27	120	–0.67	—	II	—
88[c]	J1014+0038	10 14 41.93	+00 38 01.5	EE	—	59	—	—	—	II	—
89[c]	J1014+4945	10 14 36.20	+49 45 32.6	2MASX	0.21†	412	—	—	—	I	6, 13
90[a]	J1015+2627	10 15 18.55	+26 27 54.9	EE	—	78	161	–0.32	—	II	—
91	J1016+0930	10 16 05.97	+09 30 12.3	SDSS	0.20†	85	391	–0.68	1.62	II	13
92	J1016+4708	10 16 06.64	+47 08 06.6	EE	—	56	222	–0.62	—	II	—
93	J1017+6352	10 18 01.89	+63 52 30.1	2MASX	0.23†	222	1349	–0.81	4.96	II	1, 2, 6, 16
94[a]	J1022+3758	10 22 54.28	+37 58 16.6	2MASX	0.23†	40	94	–0.38	1.88	—	13
95	J1023+0851	10 23 22.59	+08 51 26.9	EE	—	47	—	—	—	II	1
96	J1032+0514	10 32 21.43	+05 14 21.8	SDSS	—	19	48	–0.42	—	I	14
97[a]	J1032+3152	10 32 15.87	+31 52 35.7	SDSS	0.33†	56	—	—	—	I	1
98[a]	J1032+3502	10 32 01.62	+35 02 52.9	2MASX	0.12†	30	—	—	—	—	7, 13
99	J1035+5907	10 35 41.52	+59 07 07.7	SDSS	0.47†	9	—	—	—	II	20
100	J1040+1548	10 40 20.07	+15 48 33.4	EE	—	18	39	–0.35	—	II	1
101[ac]	J1042+2907	10 42 54.72	+29 07 17.5	EE	—	64	—	—	—	I	—
102	J1043–0553	10 43 18.94	–05 53 52.5	2MASS	—	352	—	—	—	—	—
103	J1043+0847	10 43 44.72	+08 47 49.8	SDSS	—	51	224	–0.66	—	—	—
104	J1043+0947	10 43 26.16	+09 47 11.8	SDSS	0.43†	18	130	–0.88	1.62	II	1, 20
105[c]	J1045+1258	10 45 01.48	+12 58 02.8	SDSS	0.30†	56	318	–0.78	2.33	II	20
106	J1046+0902	10 46 47.92	+09 02 56.6	SDSS	—	16	110	–0.86	—	II	1
107	J1046+1631	10 46 56.15	+16 31 25.9	SDSS	0.30†	33	112	–0.56	1.92	I	1
108	J1048+1857	10 48 45.26	+18 57 57.8	2MASX	0.13†	88	282	–0.52	0.90	II	13
109[c]	J1051+0503	10 51 29.91	+05 03 24.2	2MASX	0.22	89	—	—	—	II	13, 16
110	J1055+1432	10 55 40.80	+14 32 20.2	EE	—	58	—	—	—	—	—

Table 3.2: **Candidate Narrow Angle Tail Radio Sources**

Catalog Number	Name	R.A. (J2000.0)	Decl. (J2000.0)	Ref.	Redshift (z)	F_{1400} (mJy)	F_{150} (mJy)	α_{150}^{1400}	L (erg s^{-1}) ($\times 10^{43}$)	FR Type (I/II)	Other Catalogs
111	J1056+1128	10 56 14.77	+11 28 42.7	SDSS	0.42†	22	92	–0.64	2.30	II	—
112^{c}	J1104+4726	11 04 44.46	+47 26 56.8	EE	—	67	—	—	—	II	1, 6
113	J1105+1235	11 05 28.85	+12 35 14.6	EE	—	66	—	—	—	II	—
114^{ab}	J1109+3252	11 09 56.70	+32 52 05.9	EE	—	22	—	—	—	II	—
115	J1110+1159	11 10 06.16	+11 59 43.2	2MASX	0.13†	122	—	—	—	II	15, 13
116^{c}	J1131+2125	11 31 22.88	+21 25 56.5	EE	—	193	—	—	—	II	—
117^{c}	J1131+0128	11 31 31.07	+01 28 27.8	2MASX	0.24†	55	—	—	—	II	—
118^{b}	J1131+3908	11 31 57.05	+39 08 00.1	SDSS	0.23†	30	—	—	—	II	1, 13
119	J1132+1344	11 32 40.23	+13 44 26.2	EE	—	11	—	—	—	II	1
120^{c}	J1133+4903	11 33 59.34	+49 03 45.5	EE	—	427	—	—	—	II	6
121^{a}	J1137+3000	11 37 33.28	+30 00 06.6	EE	—	8	45	–0.77	—	—	1
122	J1143+1641	11 43 12.27	+16 41 39.3	SDSS	—	11	49	–0.67	—	I	—
123	J1144+3710	11 44 33.74	+37 10 06.5	EE	—	1070	—	—	—	II	4, 6
124	J1145+1529	11 45 22.20	+15 29 43	EE	—	34	—	—	—	II	—
125^{c}	J1152+4229	11 52 37.64	+42 29 04.7	EE	—	38	—	—	—	II	6
126	J1154+1009	11 54 16.57	+10 09 40.4	EE	—	46	188	–0.63	—	II	1
127^{b}	J1156+2048	11 56 38.83	+20 48 47.5	2MASX	0.15†	19	—	—	—	I	1, 13
128^{c}	J1201–0703	12 01 25.73	–07 03 10.9	2MASX	—	207	—	—	—	II	8
129^{c}	J1202+5801	12 02 02.76	+58 01 48.1	EE	—	855	—	—	—	I	4
130^{c}	J1204+2013	12 04 01.70	+20 13 55.7	EE	—	76	—	—	—	I	—
131	J1208+3425	12 08 28.56	+34 25 09.4	EE	—	80	605	–0.91	—	II	6
132^{c}	J1209+5715	12 09 00.38	+57 15 30.5	EE	—	30	—	—	—	—	17
133	J1211+0707	12 11 56.28	+07 07 29.2	2MASX	0.14†	164	—	—	—	II	2, 13, 16
134	J1215+3243	12 15 50.25	+32 43 13.0	EE	—	60	208	–0.56	—	I	—
135	J1217+0336	12 17 31.4	+03 36 57.0	SDSS	0.08†	22	—	—	—	—	4
136^{c}	J1217+0340	12 17 40.19	+03 40 02.1	EE	—	1125	—	—	—	II	—
137	J1220+0203	12 20 13.94	+02 03 52.2	EE	—	711	—	—	—	II	—
138^{c}	J1222–0449	12 22 23.69	–04 49 35.4	EE	—	169	—	—	—	II	—
139^{c}	J1225+3737	12 25 25.15	+37 37 28.7	EE	—	252	—	—	—	II	—
140	J1227+4928	12 27 32.29	+49 28 44.0	2MASX	0.12†	124	—	—	—	—	20, 21
141^{c}	J1229+1140	12 29 51.29	+11 40 40.4	SDSS	0.08†	781	—	—	—	II	—
142^{a}	J1231+3850	12 31 45.98	+38 50 30.9	2MASX	—	67	—	—	—	II	16
143^{a}	J1234+4012	12 34 56.52	+40 12 54.4	SDSS	0.49†	46	212	–0.68	6.43	I	1
144	J1235+0741	12 35 37.39	+07 41 10.5	EE	—	8	157	–1.33	—	I	—
145	J1235+5314	12 35 28.51	+53 14 57.7	EE	—	26	293	–1.08	—	I	—
146	J1239+1423	12 39 16.13	+14 23 09.7	SDSS	0.37†	8	—	—	—	I	1
147	J1241+6056	12 41 48.03	+60 56 39.4	2MASX	0.23†	16	—	—	—	—	1, 13
148	J1242+5022	12 42 08.74	+50 22 12.8	EE	—	57	—	—	—	I	—
149	J1243–0726	12 43 10.27	–07 26 09.2	EE	—	59	—	—	—	I	—
150^{ab}	J1246+3005	12 46 51.53	+30 05 31.1	EE	—	127	519	–0.63	—	I	1
151	J1247–0249	12 47 51.48	–02 49 51.6	EE	—	159	—	—	—	II	1
152	J1247+0119	12 47 54.54	+01 19 56.5	EE	—	29	—	—	—	—	—
153^{c}	J1247+0931	12 47 24.16	+09 31 08.9	2MASX	0.19†	117	—	—	—	II	13
154^{b}	J1249+0713	12 49 50.79	+07 13 13.5	EE	—	33	123	–0.59	—	II	1
155^{c}	J1249+5004	12 49 18.69	+50 04 49.5	2MASX	0.25†	220	—	—	—	II	13
156	J1256+0126	12 56 28.28	+01 26 04.7	EE	—	13	67	–0.73	—	I	—
157^{b}	J1259+4906	12 59 30.22	+49 06 00.6	EE	—	15	46	–0.50	—	I	—
158	J1301+2818	13 01 10.80	+28 18 29.8	EE	—	10	—	—	—	I	5, 21
159^{c}	J1308+5311	13 08 33.03	+53 11 19.4	SDSS	0.32†	21	—	—	—	I	—
160	J1311+1922	13 11 17.46	+19 22 46.3	2MASX	0.19†	36	—	—	—	I	13, 21
161	J1313+0220	13 13 41.05	+02 20 36.7	EE	—	7	—	—	—	—	—
162^{c}	J1313+1745	13 13 36.78	+17 45 28.6	2MASX	0.23†	92	273	–0.49	3.39	II	1, 13
163^{c}	J1317+1910	13 17 39.52	+19 10 20.8	SDSS	0.27†	160	—	—	—	II	—
164^{ab}	J1317+3144	13 17 56.76	+31 44 47.0	2MASX	0.21†	30	—	—	—	I	—
165	J1319+5807	13 19 26.90	+58 07 25.3	SDSS	0.31†	31	—	—	—	II	—
166	J1322+1132	13 22 46.31	+11 32 15.9	SDSS	0.21†	57	—	—	—	II	13
167	J1327–0440	13 27 05.57	–04 40 47.2	EE	—	39	—	—	—	I	—
168^{c}	J1330+0649	13 30 31.07	+06 49 33.8	SDSS	0.28†	152	—	—	—	I	18
169	J1330+1904	13 30 46.50	+19 04 44.5	EE	—	67	—	—	—	II	—
170	J1334+1728	13 34 48.60	+17 28 12.3	EE	—	40	—	—	—	II	—

Table 3.2: **Candidate Narrow Angle Tail Radio Sources**

Catalog Number	Name	R.A. (J2000.0)	Decl. (J2000.0)	Ref.	Redshift (z)	F_{1400} (mJy)	F_{150} (mJy)	α_{150}^{1400}	L (erg s^{-1}) ($\times 10^{43}$)	FR Type (I/II)	Other Catalogs
171	J1334+2537	13 34 37.09	+25 37 20.1	2MASX	0.30	28	—	—	—	II	—
172[c]	J1342+1226	13 42 44.59	+12 26 55.6	2MASX	0.22†	30	—	—	—	I	13
173	J1348+3726	13 48 47.55	+37 26 34.2	2MASS	0.21*	71	—	—	—	—	20
174	J1349+4207	13 49 48.35	+42 07 03.7	SDSS	0.23†	39	—	—	—	II	13
175	J1349+4828	13 49 36.07	+48 28 44.0	SDSS	0.50†	29	90	–0.51	5.88	I	—
176	J1351+0023	13 51 33.47	+00 23 27.6	EE	—	49	—	—	—	II	—
177[c]	J1353+0942	13 53 39.85	+09 42 13.5	2MASX	0.13†	59	—	—	—	II	—
178	J1353+3305	13 53 02.05	+33 05 28.5	2MASX	0.06†	48	136	–0.47	0.11	I	13, 15
179	J1357+0732	13 57 45.57	+07 32 23.7	SDSS	0.11†	49	277	–0.77	0.23	—	13
180	J1358+0352	13 58 57.2	+03 52 26.8	EE	—	64	276	–0.65	—	II	—
181	J1359–0102	13 59 50.7	–01 02 38.9	SDSS	0.35†	30	—	—	—	—	—
182	J1359+4443	13 59 59.4	+44 43 57.5	EE	—	22	—	—	—	II	—
183	J1403+0610	14 03 13.29	+06 10 08.3	2MASX	0.08†	355	555	–0.20	3.03	I	8, 10, 13, 15
184[bc]	J1406+4041	14 06 03.79	+40 41 47.8	SDSS	—	220	1098	–0.31	—	II	14
185	J1407+4257	14 07 13.04	+42 57 35.7	SDSS	—	32	—	—	—	I	—
186[c]	J1413+4844	14 13 30.45	+48 44 26.9	EE	—	72	218	–0.50	—	II	—
187[c]	J1414+1746	14 14 55.75	+17 46 07.9	SDSS	—	78	349	–0.67	—	I	—
188	J1418+0515	14 18 09.17	+05 15 15.5	SDSS	0.58†	31	—	—	—	II	—
189[ab]	J1418+3211	14 18 11.51	+32 11 39.3	SDSS	0.36†	30	—	—	—	I	—
190	J1419+2008	14 19 20.69	+20 08 41.3	EE	—	22	—	—	—	II	—
191[ab]	J1420+2500	14 20 41.85	+25 00 35.0	SDSS	0.36†	139	483	–0.56	11.85	II	—
192	J1421–0431	14 21 28.90	–04 31 31.9	EE	—	61	—	—	—	II	—
193[b]	J1421+6100	14 21 36.93	+61 00 24.6	2MASX	0.31†	21	101	–0.70	1.01	II	1
194[c]	J1426+0050	14 26 16.34	+00 50 15.4	2MASX	0.12†	60	—	—	—	I	13, 16
195[a]	J1428+3953	14 28 07.32	+39 53 17.2	SDSS	0.51†	36	145	–0.62	5.97	II	—
196	J1432+1247	14 32 25.38	+12 47 24.6	SDSS	0.56†	72	139	–0.29	28.65	II	—
197	J1435+4758	14 35 54.89	+47 58 19.2	2MASX	0.25†	6	—	—	—	II	1
198	J1439+4931	14 39 09.78	+49 31 37.6	EE	—	93	230	–0.40	—	—	—
199	J1442+2945	14 42 28.67	+29 45 56.4	EE	—	110	—	—	—	I	—
200	J1444+5406	14 44 53.30	+54 06 17.2	SDSS	—	71	—	—	—	II	—
201	J1451+1622	14 51 44.40	+16 22 46.9	EE	—	16	—	—	—	I	—
202	J1452+0733	14 52 38.29	+07 33 31.6	SDSS	0.40†	33	58	–0.25	7.10	I	—
203	J1452+5022	14 52 15.40	+50 22 25.0	SDSS	0.09†	150	—	—	—	II	—
204	J1458+1006	14 58 42.16	+10 06 24.2	EE	—	58	—	—	—	II	1
205	J1500+1241	15 00 50.73	+12 41 47.7	EE	—	82	—	—	—	I	—
206[b]	J1502+4255	15 02 33.40	+42 55 56.5	SDSS	0.29†	42	104	–0.41	3.08	II	—
207	J1505+1546	15 05 47.86	+15 46 50.8	SDSS	—	22	—	—	—	—	—
208[abc]	J1509+3327	15 09 57.37	+33 27 15.0	2MASX	0.12†	59	—	—	—	II	13
209[c]	J1514+1017	15 14 49.36	+10 17 03.2	2MASX	0.06†	192	921	–0.70	0.28	II	1, 2, 10, 13
210[ab]	J1520+2337	15 20 55.66	+23 37 25.2	SDSS	0.31†	44	191	–0.66	2.26	II	—
211	J1524+0957	15 24 41.55	+09 57 36.8	EE	—	83	285	–0.55	—	I	—
212	J1526+0438	15 26 14.82	+04 38 30.2	SDSS	—	20	59	–0.48	—	II	—
213	J1530–0703	15 30 58.15	–07 03 29.9	EE	—	150	—	—	—	II	—
214[ab]	J1530+3210	15 30 30.66	+32 10 56.6	SDSS	—	30	82	–0.45	—	II	—
215	J1530+4525	15 30 08.02	+45 25 52.8	EE	—	55	—	—	—	II	—
216[c]	J1536–0205	15 36 31.19	–02 05 06.3	2MASX	0.16*	95	—	—	—	II	13, 21
217	J1539+1805	15 39 28.61	+18 05 59.2	SDSS	0.31*	117	451	–0.60	6.57	II	—
218	J1541+0301	15 41 41.70	+03 01 03.0	SDSS	0.06†	19	—	—	—	II	14
219[c]	J1544+1755	15 44 09.94	+17 55 04.8	2MASX	0.21†	166	—	—	—	I	13, 20
220	J1544+6042	15 44 46.24	+60 42 19.9	EE	—	16	—	—	—	I	—
221	J1545–0237	15 45 47.40	–02 37 59.6	EE	—	12	—	—	—	I	1
222[c]	J1545+0309	15 45 53.98	+03 09 12.3	2MASX	0.21†	24	—	—	—	II	1, 13, 20
223[a]	J1546+2620	15 46 30.86	+26 20 31.3	EE	—	12	—	—	—	I	—
224[a]	J1548+3610	15 48 49.35	+36 10 35.4	SDSS	0.23†	120	—	—	—	II	13
225[c]	J1550+1516	15 50 20.46	+15 16 14.1	SDSS	0.14†	80	—	—	—	I	13
226	J1551+4025	15 51 54.65	+40 25 18.9	EE	—	21	91	–0.66	—	—	—
227[c]	J1553+1530	15 53 45.53	+15 30 13.6	2MASX	0.13†	141	—	—	—	II	1, 13, 20
228	J1555+0326	15 55 32.43	+03 26 57.9	2MASX	0.20†	46	178	–0.61	0.99	II	1, 13
229	J1555+0446	15 55 18.73	+04 46 26.9	SDSS	0.54†	21	73	–0.56	4.41	II	—
230	J1555+4531	15 55 22.00	+45 31 00.8	2MASX	0.07†	44	140	–0.52	0.12	I	1, 13

Table 3.2: **Candidate Narrow Angle Tail Radio Sources**

Catalog Number	Name	R.A. (J2000.0)	Decl. (J2000.0)	Ref.	Redshift (z)	F_{1400} (mJy)	F_{150} (mJy)	α_{150}^{1400}	L (erg s^{-1}) ($\times 10^{43}$)	FR Type (I/II)	Other Catalogs
231	J1558+5857	15 58 30.11	+58 57 59.1	EE	—	18	219	–1.12	—	I	—
232	J1600+2300	16 00 09.68	+23 00 56.2	SDSS	0.43†	17	—	—	—	—	20
233^{ac}	J1603+2857	16 03 38.33	+28 57 48.6	SDSS	0.28†	21	70	–0.54	1.06	II	20
234	J1603+3133	16 03 40.50	+31 33 00.7	SDSS	0.40†	37	131	–0.57	3.93	II	1, 20
235^{ab}	J1607+3442	16 07 23.84	+34 42 10.9	2MASX	0.29†	60	—	—	—	—	1, 20
236	J1609+6144	16 09 30.66	+61 44 19.5	EE	—	32	150	–0.69	—	I	1
237	J1610+1203	16 10 39.03	+12 03 18.8	SDSS	—	54	511	–1.01	—	I	1, 2, 16
238	J1611+0415	16 11 02.89	+04 15 03.1	SDSS	0.31†	40	97	–0.40	3.45	II	—
239	J1613+1921	16 13 35.02	+19 21 05.8	SDSS	—	199	803	–0.62	—	II	—
240^{b}	J1616+0906	16 16 10.48	+09 06 55.3	2MASX	0.17†	172	871	–0.73	2.15	II	1, 2, 13, 16, 20
241^{ac}	J1616+4226	16 16 37.83	+42 26 55.7	SDSS	—	171	—	—	—	II	20
242	J1623+1110	16 23 46.00	+11 10 47.4	EE	—	18	52	–0.48	—	I	—
243	J1623+4618	16 23 43.99	+46 18 02.6	EE	—	25	84	–0.54	—	I	—
244^{c}	J1625+0932	16 25 23.45	+09 32 29.2	SDSS	—	37	—	—	—	I	14
245^{c}	J1634+0626	16 34 02.06	+06 26 39.3	2MASX	—	101	—	—	—	I	—
246^{c}	J1639+5346	16 39 30.32	+53 46 54.9	EE	—	638	—	—	—	I	—
247^{bc}	J1640+3247	16 40 53.90	+32 47 28.4	SDSS	0.14†	62	—	—	—	I	13
248	J1640+4634	16 40 44.33	+46 34 06.5	SDSS	—	16	—	—	—	II	21
249	J1643+1406	16 43 30.08	+14 06 14.2	2MASX	0.18†	56	—	—	—	—	—
250	J1650+3303	16 50 36.46	+33 03 00.1	2MASX	0.16†	48	93	–0.30	1.32	II	1, 13
251^{ac}	J1652+3055	16 52 05.38	+30 55 17.0	EE	—	92	—	—	—	I	1
252^{c}	J1657+4319	16 57 32.98	+43 19 42.1	EE	—	104	—	—	—	I	1
253	J1700+4442	17 00 47.39	+44 42 42.0	SDSS	0.48†	27	124	–0.68	3.60	II	20
254^{c}	J1703+4139	17 03 32.97	+41 39 57.6	EE	—	56	—	—	—	II	1
255^{ac}	J1704+2452	17 04 51.26	+24 52 33.6	SDSS	—	41	202	–0.71	—	I	1
256^{a}	J1710+4022	17 10 13.72	+40 22 03.4	SDSS	0.44†	32	82	–0.42	5.61	I	—
257	J1713+6347	17 13 16.01	+63 47 37.5	2MASX	0.08†	21	78	–0.59	0.43	—	13, 21
258^{c}	J1721+4726	17 21 52.24	+47 26 36.8	EE	—	49	—	—	—	II	—
259	J1725+4949	17 25 52.31	+49 49 11.7	EE	—	30	133	–0.67	—	—	—
260	J1726+4530	17 26 13.09	+45 30 28.8	EE	—	16	84	–0.74	—	I	—
261	J1728+4045	17 28 02.55	+40 45 47.1	2MASX	—	48	164	–0.55	—	I	1
262^{c}	J1729+5415	17 29 21.19	+54 15 26.1	2MASX	0.08†	64	—	—	—	II	7, 13, 15
263	J1730+5923	17 30 43.60	+59 23 26.5	EE	—	12	—	—	—	—	—
264	J1733+4229	17 33 43.25	+42 29 12.1	EE	—	22	—	—	—	II	—
265	J2058+0930	20 58 45.62	+09 30 09.9	2MASX	—	167	428	–0.42	—	—	1, 2, 8, 10
266	J2102–0145	21 02 14.61	–01 45 09.5	EE	—	30	—	—	—	II	—
267	J2126–0710	21 26 16.07	–07 10 46.4	2MASX	0.11*	134	—	—	—	I	1
268	J2137–0134	21 37 26.40	–01 34 14.7	EE	—	13	53	–0.63	—	I	—
269	J2139–0742	21 39 26.27	–07 42 23.4	EE	—	29	—	—	—	I	—
270	J2152+0907	21 52 50.62	+09 07 59.7	2MASX	0.11†	54	—	—	—	I	—
271^{ab}	J2154+0037	21 54 22.62	+00 37 10.8	EE	—	32	235	–0.89	—	—	21
272	J2155+0846	21 55 26.18	+08 46 48.5	2MASX	0.15†	122	—	—	—	II	8
273	J2155+1231	21 55 41.97	+12 31 28.6	SDSS	0.19†	488	4589	–1.00	6.97	I	13, 20
274	J2159–0542	21 59 34.35	–05 42 54.3	EE	—	18	—	—	—	I	1
275	J2222+1435	22 22 35.28	+14 35 35.4	EE	—	24	—	—	—	I	—
276	J2224+0126	22 24 21.97	+01 26 31.3	EE	—	40	366	–0.99	—	I	1
277	J2234+0552	22 34 24.76	+05 52 42.5	2MASX	0.17†	75	—	—	—	II	8, 10
278	J2239–0322	22 39 36.63	–03 22 38.1	EE	—	16	—	—	—	II	—
279^{c}	J2239–0932	22 39 02.43	–09 32 35.6	EE	—	180	—	—	—	II	2
280	J2300+1426	23 00 46.83	+14 26 02.8	2MASX	0.15†	137	—	—	—	II	1, 13
281	J2304–0952	23 04 29.26	–09 52 04.8	SDSS	—	77	—	—	—	II	20
282	J2310–0326	23 10 22.50	–03 26 58.8	EE	—	24	—	—	—	II	—
283	J2310+1441	23 10 15.98	+14 41 22.3	SDSS	—	43	—	—	—	I	20
284	J2332–0744	23 32 06.89	–07 44 44.9	EE	—	20	—	—	—	—	—
285	J2332+1016	23 32 36.03	+10 16 27.8	2MASX	0.25†	106	—	—	—	I	—
286^{a}	J2346–0154	23 46 54.00	–01 54 09.4	EE	—	83	—	—	—	II	—
287	J2348+1157	23 48 02.21	+11 57 22.9	SDSS	0.43†	385	1800	–0.70	39.65	I	1, 2, 10

Chapter 4

Bent-tail Sources from LoTSS DR1

The radio jets are a characteristic of the energy that is being ejected from centrally active galactic nuclei (AGN). The structure and alignment of the radio jets define the morphology of a radio galaxy. A double-lobed radio galaxy has a very straightforward and symmetric structure with two radio jets pointing in opposing directions from a common centre, When the two radio jets happen to be bent in the same direction, a deformed structure may occasionally be observed. This group of radio sources is frequently referred to as Bent-tail (BT) radio sources, Head-tail (HT) radio sources, or 'C-shaped radio sources (Ryle & Windram(1968), Rudnick & Owen(1976), Blanton et al.(2000), Proctor(2011), Dehghan et al.(2014), Sasmal et al.(2022)). Their jets are twisted into 'V', 'C', or 'L'-like shapes, which is the main orientation of these kinds of radio galaxies. When two jets are bent in the same direction in an extremely dense cluster medium, bent-tail radio sources are created. The dynamic pressure that pushes the jets back is what causes them to bend. The jets are bent in the same direction by the action of ram pressure when these sources move through the Intra-cluster medium (ICM) at adequate velocities (ODea & Owen(1985)).

In this chapter, using the high-resolution LOFAR Two-Meter Sky Survey First Data Release (LoTSS DR1), we aim to produce a catalog of BT radio sources. Consequently, we discussed the morphological details, characteristics and some statistical properties of BT radio galaxies.

4.1 METHODOLOGY

4.1.1 The LOFAR Survey Data: LoTSS DR1

The survey data should be used to have a higher resolution when working with diffuse emission sources. LOFAR Two-Meter Sky Servey (LoTSS) with frequency coverage of 120-168 MHz and is performed using the high-band antennas (HBA)

of LOFAR is used in this scenario Shimwell et al.(2019). The first data release of LOFAR (LoTSS DR1), which eventually covered 2% of the radio sky in the vicinity of HETDEX Spring Field, is the focus of our attention (Shimwell et al.(2019), Williams et al.(2019)). It is built by using a completely automated direction-dependent calibration and imaging pipeline. The angular resolution is $6''$, while their positional accuracy is $0.2''$. Its point-source completeness is 90% at an integrated flux density of 0.45 mJy, and its median sensitivity is $S_{144MHz} = 71\ \mu Jy$ beams^{-1} (Shimwell et al.(2019)). This survey contains individual right ascension (R.A.) ranges of 10h45m00s to 15h30m00s and declination (decl.) $45°00'00''$ to $57°00'00''$(Shimwell et al.(2019)). High resolution and high sensitive LoTSS data provides more details about core information and large scale diffuse emission. The detail of LoTSS survey is also discussed in the introduction section. The LoTSS DR1 could be used to search for a variety of radio sources due to its 501000 times better sensitivity and 530 times higher resolution compared to other low-frequency wide-area surveys (like GLEAM; Wayth et al.(2015), TGSS; Intema et al.(2017), MESS; Heald et al.(2015), and VLSSr; Lane et al.(2014)).

4.1.2 Search Metheod

The source density in LoTSS is a factor of 10 times larger than that in the most sensitive existing extremely wide-area radio-continuum surveys. LoTSS DR1 has catalog a total of 325,694 sources that are recorded with a signal at least five times the noise level (Shimwell et al.(2019)). Here, we're looking for bent-tail candidates with moderate luminosity and size. The sources in the catalog that have an angular size greater than or equal to $12''$ (i.e. at least twice the convolution beam size) are initially identified. To short out the sources ($> 12''$), a custom filtering script has been developed. The script was shorlisted with 18,500 sources. The fields of each image were then visually examined to identify possible BT radio galaxies. From the LoTSS DR1 survey, which is reported in this study, we can confidently identify a significant number of bent sources. Of the LoTSS sources, 73% have optical identifications (Williams et al.(2019)) and 51% have either spectroscopic or photometric redshifts (Duncan et al.(2019)). In the Williams et al.(2019) value added catalog, various optical properties of the host galaxies were discussed. We adopted the redshift and flux values from the value added catalog.

4.1.3 Identifying and Defining the NAT and WAT Sources

By manual-visual inspection, we detected radio galaxies with bent tails whose jets diverge from a conventional linear trajectory. We carefully inspect each source to look for potential bent-tail sources with jets bent 'V', 'C', or 'L'-like structures.

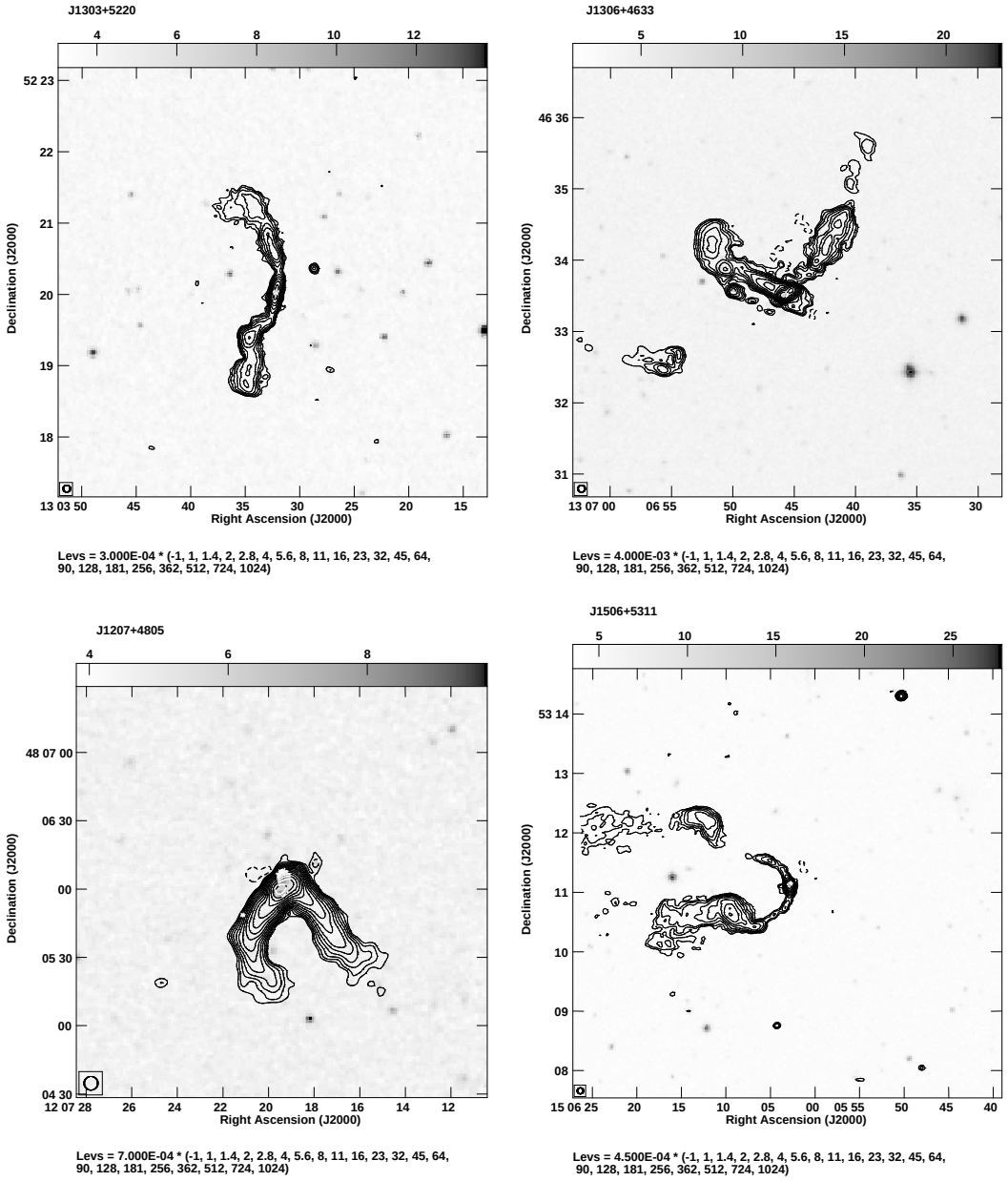

Figure 4.1: This is a sample contour images of bent-tail sources from LoTSS. The above two images are example of two wide angle tail sources. The lower panel shows the example of two narrow angle tail sources. This image is drawn by overlaid radio image (contour) on the DSS2 red image (gray scale). The lower level of contours are drawn from minimum 5 times of the local rms noise. We chose minimum contour level in such a way to get reliable radio structure of the sources.

Depending on the angle of bending between the two radio jets, the BT sources are divided into two subclasses: wide-angle tail (WAT) and narrow-angle tail (NAT). We classify sources as WAT if the bending angle is higher than or equal to 90 degrees. NAT sources are sources with an angle less than 90 degrees. We calculate the angle formed at the centre (optical counterpart) by the two radio jet outward-vectors. It should be mentioned that depending on the projection effect or the source's direction to the sky's plane, a specific WAT source may appear as a NAT source on our radio map.

4.2 RESULT

We were able to create a catalog of 82 bent-tail radio sources, including 72 WAT candidates and 10 NAT candidates from first data release of LoTSS. Among our 82 BT sources, 32 BT sources (27 WATs and 5 NATs) were reported by Mingo et al.(2019) which are marked as 'a' in Table 4.1. Using existing radio and optical data, we estimated spectral indices and radio luminosities for our BT source. We analyzed a number of statistical properties of these identified NAT and WAT candidates.

Figure 4.1 is the sample images of four bent-tail radio sources.

In Table 4.1, we present a list of all WAT and NAT sources from LoTSS DR1. Columns (3) and (4) are Right Ascension (J2000.0) and Declination (J2000.0) of the sources. Column (5) indicates the references of the optical host galaxies. The redshifts of the host galaxies are mentioned in column (6), when available. In column (7) and column (8) are the fluxes of the BT sources at 144 MHz and 1400 MHz frequencies, respectively. The spectral indices between two frequencies of 144 MHz and 1400 MHz are mentioned in column (9). We also calculated the luminosities of the BT sources, which are mensioned in column (10). Column (11) is other catalog column where the sources already known in other literature.

4.2.1 Angle Between Two Jets of BT Galaxies

For each bent-tail candidate, we carefully measured the angle between two jets. The angle of the source is defined as the angle formed by the two lobe's axes at the centre of the radio source. We discovered 72 WAT and 10 NAT sources, whose bending angles are larger or less than 90 degree, respectively. J1506+5311 has the largest bending angle in terms of NAT candidates (40 degree), while J1523+5255 has the lowest bending angle in terms of WAT candidates (160 degree).

In Figure 4.2, we present a histogram of the angle distribution of the WAT and NAT sources. The histogram displays its peak with 16 (19.5%) BT sources at an

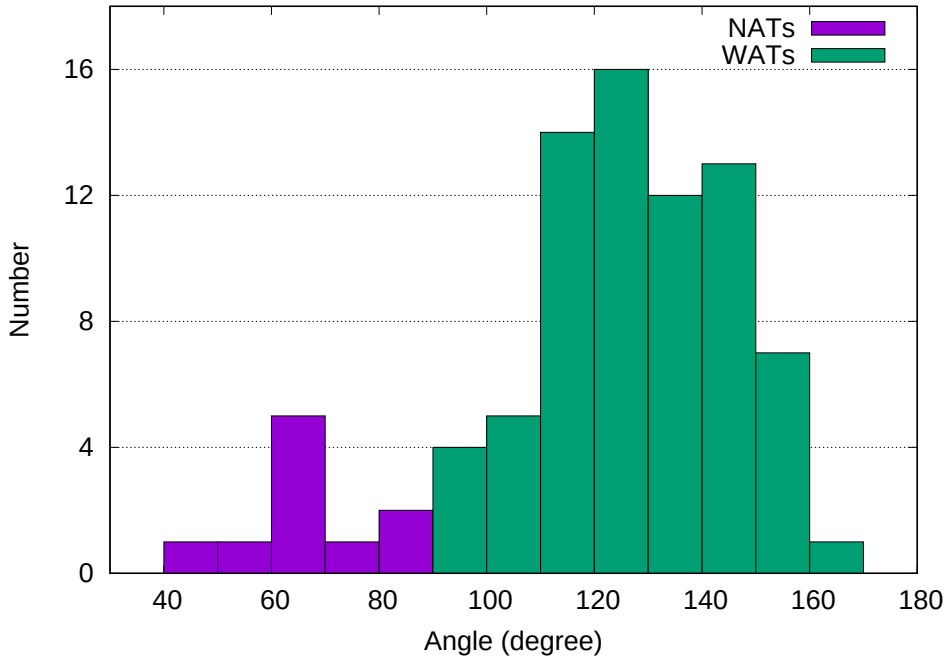

Figure 4.2: Histogram showing the angle distribution of narrow-angle tail (NAT) and wide-angle tail (WAT) sources. Left panel is for NAT sources (green color) and right panel is for WAT sources (violet color).

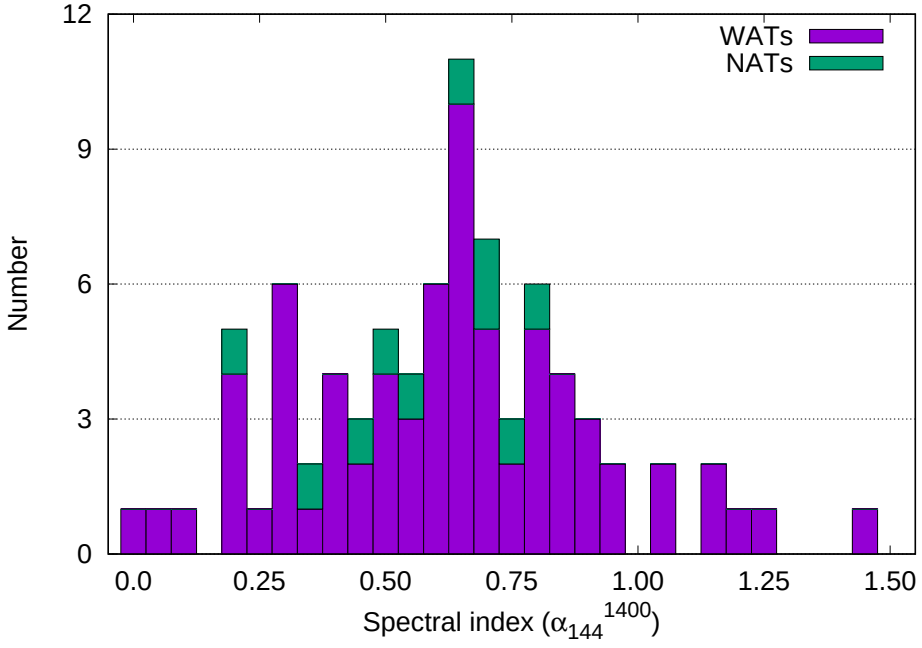

Figure 4.3: The above histogram shows spectral index (α_{144}^{1400}) variation with number of our discovered NATs (green colour) and WATs (violet colour) radio galaxies using NVSS and LoTSS fluxes. Here, we taken absolute value of spectral index.

angle between 120 and 130 degree.

4.2.2 Spectral Index (α_{144}^{1400})

We calculated the two-point spectral index (α_{144}^{1400}) for bent-tail sources by combining the high frequency (1400 MHz) NVSS and low frequency (144 MHz) LoTSS. Equation $S_\nu \propto \nu^\alpha$ is used to calculate the spectral index, where S_ν is the radiative flux density at a particular frequency ν and α be the spectral index. For each NAT and WAT source listed in column (9) of Table 4.1, the spectral index is calculated. To calculate spectral index, LoTSS flux values are directly taken from the value-added catalog while NVSS flux values are calculated using NVSS cutout images. We calculated the integrated flux value of each NVSS cutout image by Astronomical Image Processing System (AIPS)[1] software.

Figure 4.3 shows the spectral index (α_{144}^{1400}) distribution 72 WATs and 10 NATs with violet and green colour, respectively. The histogram shows its peak near $\alpha_{144}^{1400} = -0.65$. The histogram displays that the whole range of α_{144}^{1400} for NAT

[1]http://info.cv.nrao.edu/aips/

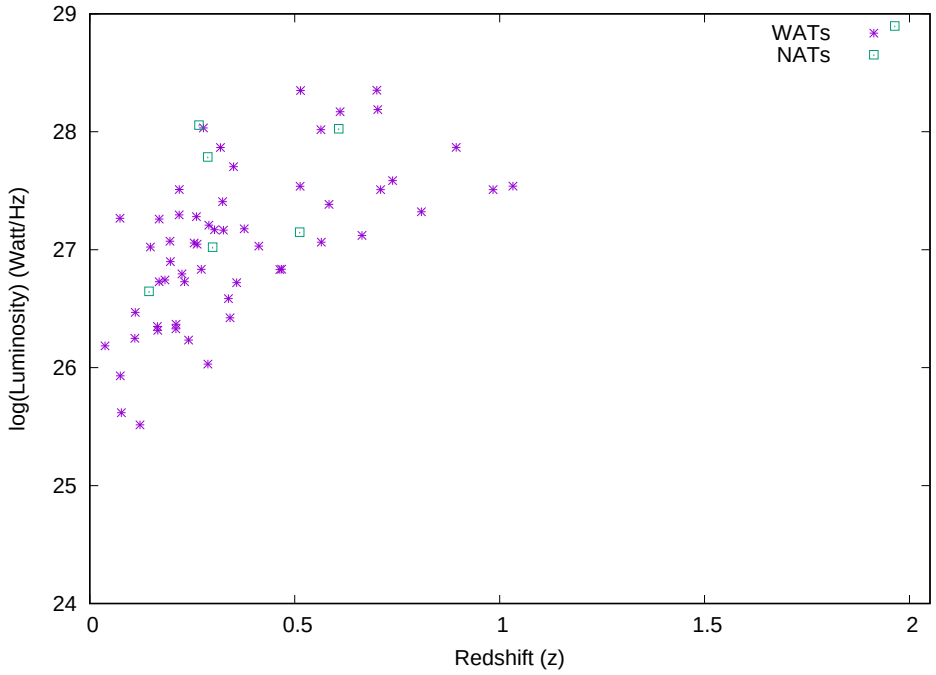

Figure 4.4: The above figure shows distribution of radio luminosity (L_{144MHz}) of our WAT (blue colour) and NAT (green colour) samples with redshifts (z). Here, we use $LogL_{144MHz}$ values in the unit of W Hz^{-1}.

sources is between – 0.21 and – 0.78. Among the NAT sources, J1325+5544 has the lowest spectral index (α_{144}^{1400} = – 0.78) and J1505+4706 has the highest spectral index (α_{144}^{1400} = – 0.21). Similarly, the total range of spectral index (α_{144}^{1400}) for WAT candidates is – 1.45 to – 0.02. J1142+4718 has the highest spectral index with α_{144}^{1400} = – 0.02 and J1459+5333 has the lowest spectral index with α_{144}^{1400} =– 1.45.

4.2.3 Radio Luminosity (L_{rad})

We have calculated the radio luminosity (L_{144}) of all BT candidates in LoTSS (when the value of z is available) using the standard formula (Heeschen(1966)):

$$L_{rad} = 1.2 \times 10^{27} D_{Mpc}^2 S_0 \nu_0^{-\alpha} (1+z)^{-(1+\alpha)} \times (\nu_u^{(1+\alpha)} - \nu_l^{(1+\alpha)})(1+\alpha)^{-1} ergs^{-1} \quad (4\text{-}1)$$

Where D_{Mpc} is the luminosity distance to the source (Mpc), S_0 is the flux density (Jy) at a specific frequency ν_0 (Hz), z is the radio galaxy's redshift, α is its spectral index ($S \propto \nu^{\alpha}$) and ν_u (Hz) and ν_l (Hz) are the upper and lower cut-off frequencies (O'Dea & Owen(1987)). We used 100 GHz and 10 MHz as the upper and lower cutoff frequencies in our calculation.

We ploted the distribution of radio luminosities of our NAT and WAT candidates with known redshift (z) as shown in figure 4.4. Here we ploted a total of 65 data points, out of which 58 WATs and 7 NATs from our table. The WAT candidate J1142+4718 has highest value of luminosity with L_{rad} = 2.25×10^{28} W Hz^{-1} and the NAT candidate J1325+5544 has highest value of luminosity with L_{rad} = 7.88×10^{28} W Hz^{-1}. The lowest value of luminosities of NAT (J1506+5311) and WAT (J1224+4906) are 4.43×10^{26} W Hz^{-1} and 3.27×10^{25} W Hz^{-1}, respectively.

Here, we plot a total of 65 data points, out of which 58 WATs and 7 NATs from our table where redshift are available. For NAT sources, the mean $LogL$ (W Hz^{-1})and median $LogL$ (W Hz^{-1}) values of luminosity are 27.65 and 27.78, respectively. Similarly, for WAT sources, the mean $LogL$ (W Hz^{-1})and median $LogL$ (W Hz^{-1}) values of luminosity are 27.05 and 27.06 respectively.

4.3 DISCUSSION

Among our 82 bent-tail candidates, the WAT source J1306+4633 has highest flux value F_{144MHz}= 2757.8 mJy. J1051+5523 (WAT) and J1245+4859 (NAT) are the other two sources with flux values larger than 1000 mJy at 144 MHz, with flux values 1097.6 mJy and 1000.8 mJy, respectively. So, most of our BT candidates are brighest compare to other radio sources.

Redshifts of the radio sources are beautifully eatimate by Duncan et al.(2019). We adopted redshift values directly from value added catalog (Williams et al.(2019)). Redshift was found for a total of 65 sources out of 82 (79%) sources. In this case, spectroscopic redshift is preferred over photometric redshift. In 17 sources (14 WAT and 3 NAT) no spectroscopic redshift could be determined, hence we used photometric redshifts instead. Redshift values for 45 sources (60%) are less than 0.5. With a redshift value of 1.9641, the NAT source J1325+5544 is the farthest away, and from the WAT, J1344+5553 is the one that is nearest with a redshift value of 0.03734.

All the previous studies (Oort et al.(1988), Gruppioni et al.(1997), Kapahi et al.(1998), Ishwara-Chandra et al.(2010), Mahony et al.(2016)) found a mean spectral index of radio galaxies in the range –0.7 to –0.8, with –0.75 usually considered to be the typical spectral index for radio galaxies (RGs). Oort et al.(1988) surveyed the Lynx field with the Westerbork Synthesis Radio Telescope (WSRT) at 325 MHz and 1400 MHz. Mahony et al.(2016) found radio galaxies with spectral indices in the range –0.5 to –1.5 with median = –0.78 and Ishwara-Chandra et al.(2010) found radio galaxies with spectral indices in the range –0.5 to –2.5 with median = –0.78. The mean and median of the spectral indices of bent-tail galaxies presented in the current chapter are close to the spectral index of a typical radio galaxy, which implies that RGs and bent-tail radio galaxies are similar in terms of the properties of their spectral index. The mean and median values of the spectral index of WATs are – 0.63 and – 0.64 respectively. Similarly for NAT sources mean and median values are – 0.56 and – 0.60 respectively. Missaglia et al.(2019) cataloged a list of 47 WAT sources using VLA FIRST and NVSS data. In their paper Missaglia et al.(2019), they mention the general value for the spectral index of –0.7, typical of lobes and plumes of radio galaxies. The GMRT spectral observation (in 240 and 610 MHz) of seven HT galaxies is presented by Sebastian et al.(2017), where we can see the two points spectral index value lie in the range – 0.20 to – 2.31. In Sasmal et al.(2022) catalog, the mean spectral index value for BT sample is –0.65. The mean and median values of the spectral index of NAT sources is –0.62. Similarly, for WAT sources the mean and median values is –0.67. These show that the mean and median bent-tail sources in our sample are nearly the same as those of other bent-tail sources found from the other radio surveys.

We estimate L_{144} for 58 WATs and 7 NATs from our database based on the availability of redshift value. The mean and median values demonstrate that WATs and NATs have the same radio luminosity distribution, indicating that they have jet kinetic powers of a similar order. As a result, the radio luminosity of WATs and NATs is of the same order, suggesting that the regulating conditions in the core engines of WATs and NATs may be the same. The mean $LogL$ (erg/sec)and median $LogL$ (erg/sec) values of luminosity for WAT candidates in Sasmal et al.(2022) are 1.03 and 0.37, respectively. Similarly, for NAT sources, the mean $LogL$ (erg/sec)and median $LogL$ (erg/sec) values of luminosity are 0.66 and 0.43, respectively. For easy comparison, all the luminosities from different surveys are converted to that at 144 MHz using the LoTSS survey.

For the confirmation of these sources, high-resolution observations are required. The number of NATs and WATs in a new catalog has significantly increased. With high-resolution observations, we will find more of these sources in the future.

4.4 CONCLUSION

We look for Bent-tail radio galaxies from LoTSS DR1 at 144 MHz. Our main findings in this work are as follows.

(i) A total of 82 candidate bent-tail radio sources are discovered, of which 72 are WATs and 10 are NATs. This discovery helps us to increase the number of known WATs and NATs significantly and opens up the possibility of followup observations of these sources with high-resolution deep radio observations and observations in other wavelengths.

(ii) Optical counterparts are identified for 58 out of 72 WATs (80 percent) and 7 out of 10 ZRGs (70 percent).

(iii) Most of the bent-tail sources show a steep spectral index between 144 and 1400 MHz and only few percent of the sources show a flat spectrum. The mean and median values of spectral index are lies in the range of normal radio galaxies.

(iv) The WATs and NATs identified in the present study are slightly more luminous compared with those detected from the FIRST survey at 1400 MHz. The average value of luminosities of WATs and NATs are close to the FR-I and FR-II division as found previously.

(v) The present sample does not give any conclusive evidence about the origin bent-tail morphologies, though some of the models seem to work well for a group of sources. In Section 4.1.3 , we discussed different models for different subclasses of bent-tail radio sources.

This type of source is common, as evidenced by the discovery of numerous

NATs and WATs, and we expect discovering more such objects with upcoming deeper and higher-resolution surveys. For a deeper understanding of the nature of these sources, high-resolution multifrequency observations are encouraged.

Table 4.1: Here, we list all the 72 WATs and 10 NATs from LoTSS DR 1. The columns (3) and (4) are Right Ascension (J2000.0) and Declination (J2000.0), which indicate the probable center of the host galaxies which are taken from value added catalog. Column (5) is the reference of the optical identification. In redshift (z) column (column 6) '*' represents photometric redshift where spectoscopic redshift is not found. In column (7) is the flux value at 144 MHz in mJy (F_{144}). In column (8), we measure the flux value at 1400 MHz frequency (F_{1400}) from NVSS. Column (9) represent two point spectral index (α_{144}^{1400}) between 1400 MHz (NVSS) flux and 144 MHz (LoTSS) flux. In column (10) we have also calculated luminosity (L) of the sources with known redshift in W Hz^{-1}. Column (11) is the other catalog column where the sources already known in other literature. 'a' represent sources in Mingo et al.(2019) catalog.

Table 4.1: **Bent-tail Radio Sources from LoTSS DR1**

Cat. Num.	Name	R.A. (J2000.0)	Decl. (J2000.0)	Optical ID Reference	Redshift (z)	F_{144} (mJy)	F_{1400} (mJy)	α_{144}^{1400}	L (W Hz^{-1}) ($\times 10^{26}$)	Others Catalog
(1)	(2)	(3)	(4)	(5)	(6)	(7)	(8)	(9)	(10)	(11)
W1	J1049+4619	10 49 55.05	+46 19 23.0	PanSTARRs	0.350794	497.1	109	–0.67	50.63	1, 4, 7, 9, 15
W2	J1051+5041	10 51 58.34	+50 41 48.8	AllWISE	—	65.2	19	–0.54	—	1, 5
W3	J1051+5523	10 51 55.09	+55 23 29.0	PanSTARRs	0.073927	1097.6	524	–0.32	18.49	1, 5, 6
W4	J1057+4749	10 57 28.34	+47 49 24.0	PanSTARRs	0.183403	63.5	27	–0.38	5.53	1, 10
W5	J1101+5603	11 01 08.94	+56 03 21.9	AllWISE	—	108.9	17	–0.82	—	—
W6	J1105+4800	11 05 04.75	+48 00 33.4	PanSTARRs	0.894000*	40.7	14	–0.47	73.67	1
W7[a]	J1107+4801	11 07 22.78	+48 01 02.1	PanSTARRs	0.664100*	73.9	7	–1.04	13.23	—
W8	J1112+5151	11 12 20.73	+51 51 24.0	AllWISE	—	32.4	8	–0.61	—	1
W9	J1113+4952	11 13 17.04	+49 52 16.0	PanSTARRs	0.610775	142.6	57	–0.40	147.89	1
W10	J1114+4610	11 14 17.63	+46 10 58.9	—	—	203.5	26	–0.90	—	1, 4
W11[a]	J1115+4729	11 15 28.30	+47 29 11.1	—	—	19.3	15	–0.11	—	1
W12	J1115+4835	11 15 42.08	+48 35 00.2	PanSTARRs	0.074324	440.1	64	–0.85	0.85	1, 10
W13[a]	J1117+5051	11 17 56.28	+50 51 04.7	PanSTARRs	0.318815	52.1	46	–0.05	73.44	1
W14[a]	J1117+5636	11 17 25.92	+56 36 48.6	PanSTARRs	0.342334	44.3	7	–0.81	2.64	1
W15[a]	J1120+4714	11 20 05.48	+47 14 00.8	PanSTARRs	0.109900*	210.6	47	–0.66	1.77	1
W16[a]	J1120+4745	11 20 51.78	+47 45 15.2	PanSTARRs	—	583.4	89	–0.83	—	1, 2, 4
W17	J1120+5308	11 20 39.98	+53 08 10.8	PanSTARRs	1.032300*	15.4	5	–0.49	34.56	1
W18[a]	J1120+5516	11 20 16.83	+55 16 27.1	PanSTARRs	0.513096	82.4	25	–0.52	34.52	1
W19	J1121+4822	11 21 56.49	+48 22 02.7	—	—	48.0	23	–0.32	—	—
W20	J1121+5421	11 21 13.61	+54 21 36.4	PanSTARRs	0.210208	74.1	15	–0.70	2.13	1, 10
W21	J1124+5546	11 24 25.85	+55 46 07.6	PanSTARRs	0.809018	35.0	7	–0.71	20.97	1
W22[a]	J1127+5031	11 27 36.74	+50 31 40.7	PanSTARRs	0.338420	41.2	9	–0.67	3.84	1
W23	J1127+5533	11 27 18.35	+55 33 29.0	PanSTARRs	0.984100*	5.0	3	–0.22	32.30	1
W24	J1132+5056	11 32 50.67	+50 56 59.0	PanSTARRs	0.358569	67.7	12	–0.76	5.25	1
W25[a]	J1142+4718	11 42 27.66	+47 18 30.3	PanSTARRs	0.700500*	26.1	25	–0.02	224.97	1
W26	J1147+4805	11 47 47.75	+48 05 58.0	PanSTARRs	0.702800	65.8	34	–0.29	154.26	1
W27	J1147+4917	11 47 51.79	+49 17 18.3	PanSTARRs	0.241000*	45.1	9	–0.71	1.71	1
W28[a]	J1147+5548	11 47 16.12	+55 48 10.2	AllWISE	—	29.2	6	–0.70	—	—
W29	J1154+4948	11 54 13.41	+49 48 46.07	PanSTARRs	0.288353	45.3	4	–1.07	1.07	1
W30	J1208+5457	12 08 05.83	+54 57 54.5	PanSTARRs	0.463974	80.9	9	–0.96	6.79	1
W31[a]	J1217+5334	12 17 37.52	+53 34 41.4	PanSTARRs	0.195732	786.2	112	–0.86	11.80	1, 2, 4, 9
W32[a]	J1220+4603	12 20 17.03	+46 03 47.0	PanSTARRs	0.110975	124.3	47	–0.43	2.94	1
W33	J1220+5334	12 20 49.17	+53 34 44.8	—	—	154.2	47	–0.52	—	—
W34	J1224+4906	12 24 12.79	+49 06 00.7	PanSTARRs	0.122400*	107.8	6	–1.27	0.33	1
W35	J1224+5419	12 24 49.37	+54 19 32.1	PanSTARRs	0.467984	73.1	9	–0.92	6.83	1
W36[a]	J1225+4904	12 25 41.00	+49 04 27.8	PanSTARRs	0.261906	188.5	44	–0.64	11.13	—
W37	J1236+5525	12 36 48.05	+55 25 08.8	PanSTARRs	0.324225	249.5	61	–0.62	25.57	1, 4
W38	J1238+4838	12 38 57.80	+48 38 23.5	—	—	113.7	25	–0.66	—	1
W39	J1242+5021	12 42 08.44	+50 21 42.3	PanSTARRs	0.147895	321.1	106	–0.49	10.53	1, 4
W40	J1247+4852	12 47 42.03	+48 52 16.1	PanSTARRs	0.210588	224.6	15	–1.19	2.33	3, 17
W41	J1249+4953	12 49 40.21	+49 53 51.0	—	—	144.4	26	–0.75	—	1
W42[a]	J1257+4854	12 57 46.81	+48 54 51.9	PanSTARRs	0.260368	576.6	93	–0.80	19.09	—
W43	J1303+4744	13 03 47.72	+47 44 00.8	PanSTARRs	0.217920	66.6	42	–0.20	19.72	1, 11
W44	J1303+4935	13 03 28.05	+49 35 56.6	PanSTARRs	0.254710	239.3	51	–0.68	11.41	1
W45	J1303+5219	13 03 33.75	+52 19 56.4	PanSTARRs	0.272003	98.2	24	–0.62	6.82	11, 12

References– 1:NVSS Condon et al.(1998); 2:VLA Low-Frequency Sky Survey (VLSS; Cohen et al.(2007));3:5C Ke66, Po68, Po69, Wi70, Pe75, Wa77, Pe78, Sc81, Be82, Be88; 4:6C Baldwin et al.(1985), Ha88, Ha90, Ha91, Ha93a, Ha93b; 5:7C Mc90, Ko94, Wa96, Ve98; 6:The Parkes Catalog of Radio Sources (PKS; Bolton et al.(1964)); 7:Texas Survey of Radio Sources (TXS; Douglas et al.(1996)); 8:Cul Slee(1995); 9:87GB Gr91; 10:Automatic Spectroscopic K-means-based classification (ASK; Sánchez et al.(2011)); 11:2 Micron All Sky Survey Extended objects - Final Release (2MASX; Skrutskie et al.(2006)); 12:GALaxy Evolution eXplorer All-Sky Survey Source Catalog (GALEXASC; Agüeros et al.(2005)); 13:GALaxy Evolution eXplorer Medium Imaging Survey Catalog (GALEXMSC; Agüeros et al.(2005));14:New General Catalog (NGC; Dreyer(1888));15:B3 Ficarra et al.(1985);16:Wide-field Infrared Survey Explorer (WISE; Chung et al.(2011), Rebull et al.(2011));17:2 Micron All Sky Survey Point Source Catalog - Final Release (2MASS; Skrutskie et al.(2006))

Table 4.1: **Bent-tail Radio Sources from LoTSS**

Cat. Num.	Name	R.A. (J2000.0)	Decl. (J2000.0)	Optical ID Reference	Redshift (z)	F_{144} (mJy)	F_{1400} (mJy)	α_{1400}^{144}	L (W Hz^{-1}) ($\times 10^{26}$)	Others Catalog
(1)	(2)	(3)	(4)	(5)	(6)	(7)	(8)	(9)	(10)	(11)
W46	J1306+4634	13 06 45.32	+46 34 02.7	PanSTARRs	0.218359	2757.8	211	–1.13	32.36	1, 15
W47	J1306+5144	13 06 12.02	+51 44 06.5	PanSTARRs	0.277312	356.7	180	–0.30	107.84	1, 2, 9
W48[a]	J1312+4714	13 12 45.61	+47 14 53.9	PanSTARRs	0.225151	261.7	42	–0.80	6.23	—
W49	J1315+4840	13 15 29.23	+48 40 55.5	PanSTARRs	0.514087	115.9	75	–0.19	223.34	1, 4
W50	J1325+5617	13 25 04.38	+56 17 42.3	—	—	107	43	–0.40	—	1
W51[a]	J1329+5246	13 29 11.10	+52 46 04.5	PanSTARRs	0.412396	155.8	19	–0.92	10.73	1
W52	J1330+4730	13 30 32.27	+47 30 54.2	PanSTARRs	0.326122	118.7	32	–0.58	14.64	13
W53[a]	J1344+5553	13 44 42.65	+55 53 03.8	PanSTARRs	0.037340	333.6	166	–0.31	1.53	—
W54[a]	J1346+5250	13 46 08.90	+52 50 05.3	—	—	98.1	63	–0.19	—	1, 17
W55[a]	J1347+5021	13 47 01.85	+50 22 10.1	PanSTARRs	0.709600*	52.1	13	–0.61	32.34	1, 17
W56	J1351+5216	13 51 52.95	+52 16 18.8	PanSTARRs	0.165942	36.5	14	–0.42	2.07	1
W57[a]	J1351+5439	13 51 37.33	+54 39 46.4	PanSTARRs	0.563901	92.1	42	–0.34	104.21	—
W58	J1359+4905	13 59 44.71	+49 05 52.6	PanSTARRs	0.165200*	92.7	23	–0.61	2.23	1
W59	J1426+5547	14 26 06.07	+55 47 15.5	PanSTARRs	0.738800*	66.5	15	–0.65	38.58	1
W60	J1428+5520	14 28 43.48	+55 20 58.7	PanSTARRs	0.290652	220.1	51	–0.64	16.15	13
W61[a]	J1431+4744	14 31 50.54	+47 43 55.2	—	—	112.8	64	–0.25	—	1
W62[a]	J1431+5518	14 31 16.92	+55 18 57.9	PanSTARRs	0.565100*	33.3	8	–0.63	11.57	1
W63	J1434+4951	14 34 43.55	+49 51 38.8	PanSTARRs	0.196541	168.5	49	–0.54	7.92	—
W64	J1439+5631	14 39 19.12	+56 31 39.8	—	—	22.7	11	–0.32	—	13, 16, 17
W65	J1446+4841	14 46 07.05	+48 41 49.9	PanSTARRs	0.376757	365.0	27	–1.14	15.05	1
W66[a]	J1451+4841	14 51 47.28	+48 41 23.5	PanSTARRs	0.231262	211.7	34	–0.80	5.35	1
W67	J1459+4947	14 59 43.01	+49 47 18.9	PanSTARRs	0.169449	781.5	184	–0.64	18.16	1, 2
W68	J1459+5333	14 59 35.07	+53 33 50.1	PanSTARRs	0.076957	352.0	13	–1.45	0.41	1
W69[a]	J1506+5354	15 06 27.68	+53 54 45.6	PanSTARRs	0.304365	126.7	36	–0.55	14.77	1
W70[a]	J1510+5146	15 10 00.15	+51 46 07.7	PanSTARRs	0.169300*	259.0	57	–0.66	5.35	1, 14
W71[a]	J1512+5147	15 12 16.35	+51 47 31.8	PanSTARRs	0.583700*	143.7	19	–0.89	24.24	1
W72[a]	J1523+5255	15 23 28.43	+52 55 02.6	—	—	345.2	50	–0.85	—	1, 17
N1	J1132+5459	11 32 01.17	+54 59 06.3	PanSTARRs	0.512300*	25.6	9	–0.46	14.07	1
N2	J1142+4622	11 42 51.44	+46 22 52.4	—	—	379	172	–0.35	—	—
N3[a]	J1203+5100	12 03 39.98	+51 01 01.2	PanSTARRs	0.299619	89.3	26	–0.54	10.52	1
N4	J1207+4805	12 07 19.27	+48 05 53.6	—	—	418.5	84	–0.71	—	1, 2
N5[a]	J1219+5055	12 19 06.86	+50 55 19.8	PanSTARRs	0.607600*	148	49	–0.49	106.09	—
N6[a]	J1245+4859	12 45 43.52	+48 59 26.4	PanSTARRs	0.287956	1000.8	210	–0.69	61.10	3
N7[a]	J1325+5544	13 25 51.86	+55 44 03.3	PanSTARRs	1.964100*	206.5	35	–0.78	788.26	1, 17
N8[a]	J1428+4839	14 28 59.97	+48 39 07.6	PanSTARRs	—	393	72	–0.75	—	1, 4
N9	J1505+4706	15 05 38.47	+47 06 22.4	PanSTARRs	0.26656	264	163	–0.21	114.01	1, 17
N10	J1506+5311	15 06 03.10	+53 11 09.3	PanSTARRs	0.14469	299	66	–0.66	4.43	1

Chapter 5

BT Sources and their host environments

The biggest gravitationally bound structures in the Universe are galaxy clusters. In order to track the large-scale structure of the Universe, they are created near dark matter concentrations where sheets and filaments of the cosmic web interact. If we are to understand the evolution of the Universe on large scales, the observational evidences for the formation of galaxy clusters are required however such events are critical to observe.

Traditionally, optical searches for galaxy overdensities are used to find galaxy clusters, followed by photometric or spectroscopic measurements. A different method is to search for the diffuse ICM's X-ray thermal emission. Both of these methods are restricted to finding clusters in the nearby universe (z=0.2), as cosmological dimming effects make it challenging to observe clusters at a greater distance.

Since even modestly sensitive radio observations may detect radio galaxies up to high redshifts, the use of BT radio sources as galaxy cluster indicators shares this capacity to discover more distant clusters. Blanton et al.(2003) found galaxy cluster in the local Universe (up to z=1) by using BT radio sources. Growing evidence from researchers (such as Dehghan et al.(2014)) suggests that BT radio candidates may be utilised to identify galaxy clusters during their formative phases and that they are successful at detecting more distant clusters up to z=2.

This chapter aims to determine the efficacy of detecting distant clusters by correlating BT radio sources identified in the high-resolution LoTSS DR1 radio catalog with known galaxy clusters from the literature.

5.1 Sample selection and sample properties

Our sample of bent-tail radio sources is taken from first data release of LOFAR Two-metre Sky Servey (LoTSS DR1). The sky coverage of LoTSS DR1 is 424

square degrees or eventual coverage of 2% in the region of HETDEX Spring Field (Shimwell et al.(2019), Williams et al.(2019)). The angular resolution of the images is 6″ with the positional accuracy is within 0.2″ and the frequency coverage is 120-168 MHz that is being conducted with the high-band antennas (HBA) of LOFAR (Shimwell et al.(2019)). To study the environment of bent-tail sources, we selected 82 BT sample from LoTSS first data release. The selection process of BT sample are described in chapter 4. The radio and optical properties also explain in the chapter.

5.2 Matching Bent-tail Candidates with known Clusters

For each BT candidate, we conducted a search of neighbouring clusters. We used a search radius of 1 Mpc at each source's redshift to cross-match each BT sample with the cluster catalog. Using this search technique, we identify 43 known clusters, showed in Table 5.1, that are correlated to 65 BT sources whose redshifts are known. For our BT sample, the overall cross-matching fraction is 68%. For example, the cluster match percentages for the WAT and NAT samples are 68 percent (38 out of 56) and 71 percent (5 out of 7) respectively.

The cluster catalogs feature many observational techniques using frequencies as optical and X-ray. We listed a total of 143 clusters from various cluster catalogs in Table 5.1. Among them 19 clusters are obtained from the Gaussian Mixture Brightest Cluster Galaxy (CMBCG) (Hao et al.(2010)) cluster catalog (optical), CMBCG include 55,880 clusters in the main cluster catalog. 68 out of 143 clusters are derived from the Wen+Han+Liu (WHL) cluster catalog (Wen & Han(2015), WHL contain 158,103 clusters (X-ray frequency), 20 clusters are taken from Northern Sky optical Cluster (NSC; Smith et al.(2012)) cluster catalogs (optical), 8 clusters obtain from Abell Clusters of Galaxies (ABELL; Lopes et al.(2004)) cluster catalogs (optical), 5 clusters taken from Northern Sky optical Cluster Survey (NSCS; Von et al.(2007)) cluster catalogs (optical), 5 clusters taken from Multi-Scale Probability Mapping (MSPM; Smith et al.(2012)) cluster catalogs (optical), 3 clusters are taken from Sloan Digital Sky Survey C4 Cluster Catalog (based on Data Release 3) (SDSS–C4–DR3; Von et al.(2007)) cluster catalogs (optical), 1 cluster is taken from RedMapper Cluster (RM; Rozo et al.(2015)) cluster catalogs (optical) and 1 cluster is taken from the maximum likelihood redshift Brightest Cluster Galaxy (MaxBCG; Koester et al.(2007)) cluster catalogs (optical), 1 cluster is taken from Super-CLuster (SCL; Einasto et al.(2011)) catalog (optical and x-ray), 1 cluster is taken from Estrada+Annis+Diehl ([EAD2007] Estrada et al.(2007) (optical) cluster catalog, 1 cluster is taken from Swift X-ray Telescope Cluster Survey (SWXCS; Liu et al.(2015) catalog (x-ray) and 1 cluster is taken from 400 Square Degree ROSAT PSPC Galaxy Cluster Survey (400d; Vikhlinin

et al.(1998)) cluster catalog.

We determine the linear separations between BT radio sources and link them to known clusters that are located within 1 Mpc of the search radius. For WAT and NAT, we find the smallest physical distances are 7.59 Kpc and 6.94 Kpc, respectively. The cluster radius from optical luminosity (r_{500}) and newly defined cluster richness $R_{L*_{500}}$ of 53 WHL clusters (15 WHL clusters are not in the Wen & Han(2015)) are listed in Table 5.1 (taken from Wen & Han(2015)). The cluster masses M_{500} are also calculated where available.

Most of the clusters has comparatively low masses. The highest massive cluster we find with mass M_{500}=10.64×$10^{14}M_{\odot}$. Almost all (52 out of 53) BT candidates are associated with known clusters or groups in relatively low mass clusters (of the order of $10^{14}M_{\odot}$). Only one BT candidate is associated with known high-mass clusters (greater than $10^{15}M_{\odot}$).

In our catalog, the massive clusters associated with the WAT (J1306+4634) and NAT (J1219+5055) sources are WHL J130650.0+463333 and WHL J121912.2+505135 with masses (M_{500}) 10.64×$10^{14}M_{\odot}$ and 8.66×$10^{14}M_{\odot}$ respectively. Similarly, low mass clusters associated with the WAT (J1242+5021) and NAT (J1203+5101) sources are WHL J124207.4+502147 and WHL J120339.9+510022 with masses (M_{500}) 0.53×$10^{14}M_{\odot}$ and 1.70×$10^{14}M_{\odot}$, respectively. Figure 5.1 shows the histogram of fraction i.e. number of clusters to the total number of clusters with known mass with $\log[M_{host}/M_{\odot}]$. This plot shows the peak between 14 to 14.5 i.e. most of our BT sources has masses between $10^{14}M_{\odot}$ to $10^{14.5}M_{\odot}$.

Among all BT sources, WAT source J1344+5553 contain highest number (thirteen) of surrounding galaxy clusters WHL J134450.3+554741, WHL J134455.9+554537, 400d J1343+5546, WHL J134448.8+560531, WHL J134316.3+560006, WHL J134314.7 +560001, ABELL 1783, WHL J134527.2+553724, SDSS-C4-DR3 3007, SWXCS J134340+5537.4, WHL J134642.9+560040, WHL J134316.1+553656 and MSPM 01743 with the distances from the host galaxy 253.07 kpc, 354.29 kpc, 546.75 kpc, 576.47 kpc, 645.62 kpc, 652.82 kpc, 774.48 kpc, 788.42 kpc, 830.24 kpc, 860.65 kpc, 932.84 kpc and 945.62 kpc, respectively.

5.3 Discussion

Mguda et al.(2015) demonstrate through simulations that BT galaxies are associated with massive clusters and estimate that BT may be found up to 400 kpc from the centre of the cluster with 13.5≤ $\log M_{\odot}$ ≤14.0 and clusters mass over $10^{15}M_{\odot}$ should include about 7 BT galaxies. According to Mguda et al.(2015), 40% of BT galaxies are found in clusters with masses of $M \geq 10^{14.5}M_{\odot}$. Out of 65 galaxies with known redshifts in our sample, we detected clusters for 43 BT sources. For

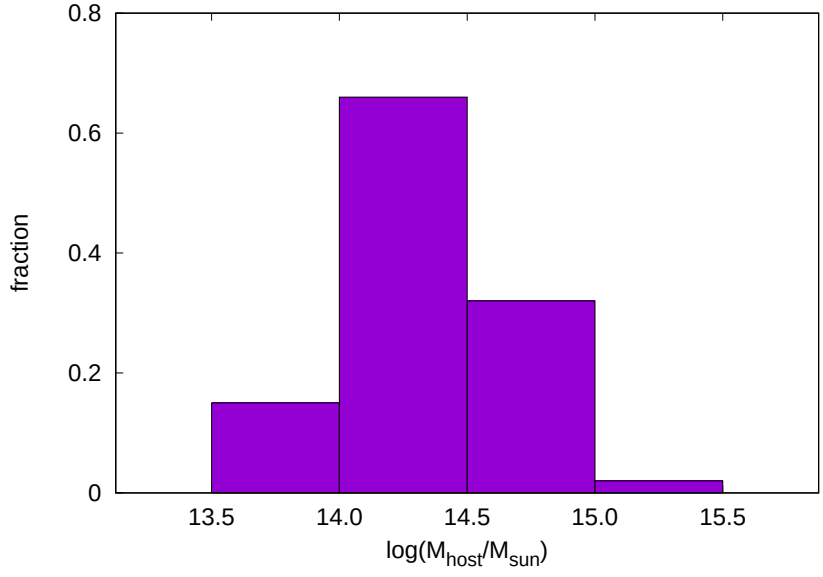

Figure 5.1: The histogram is a plot of fraction (number of cluster to total number of clusters with known mass) with $\log[M_{host}/M_{\odot}]$.

a total of 53 clusters, cluster mass has been measured. We identified 12 clusters with mass $M \geq 10^{14.5} M_{\odot}$ and 41 clusters with mass $M \leq 10^{14.5} M_{\odot}$ out of a total of 53 clusters. A high mass cluster's share of BT sources is 43:12, whereas a low mass cluster's ratio is 43:41. Therefore, it is evident that 3.42 represents the low mass to high mass cluster ratio for our BT sources.

Mingo et al.(2019) cross-matched 459 BT sample from LoTSS DR1 with Croston et al.(2019) cluster catalog to explore at the environment of the BT sample. For WAT and NAT sources, they discovered that the cluster matching percentage is 48% and 49%, respectively. The matching fractions for WAT and NAT candidates in our sample grow to 68% and 71%, respectively. We draw the conclusion that our sample is more closely related with galaxy clusters based on this comparison.

The simulation results by Mguda et al.(2015) are not entirely supported by our data. Additionally, our result has boosted the cluster matching percentages from Mingo et al.(2019) sample. The histogram plot of number of cluster to total number of clusters with known mass of our BT samples with $\log[M_{host}/M_{\odot}]$ is shown in figure 5.1. This plot shows its peak between 14 to 14.5 of $\log[M_{host}/M_{\odot}]$.

Our sample size of 65 BT galaxies with known redshifts and the sky coverage of LoTSS DR1 (424 square degrees) may have an influence on our findings. Below is a discussion of several potential causes for these.

Galaxy clusters can be identified using bent-tail sources as a tracer. Our find-

ings supported the hypothesis. While classifying, our BT sources' projection effects can be affected. A bent source may look straight when reprojected because symmetrical sources stay symmetrical throughout reprojection. We list them as BT candidates based on any radio source's jets bending. Due to projection effects, BT sources with significant jets (up to a few degrees) of the line-of-sight would seem straight and would be removed from our sample. So, based on our best estimation, only a very small percentage of our BT jets appear straight in the sky.

The number of BT sources that may be detected at any one moment largely depends on the AGN's duty cycle for producing bent jets. According to Mguda et al.(2015), cluster masses $M \geq 10^{14.5} M_{\odot}$ will contain at least one BT source at some point in their lifetimes.The search radius is an additional factor. In comparison to Vos et al.(2021), our search radius of 1 Mpc at the redshift of each source is unsatisfactory. Due to the short sample size and restricted search area of our sample, we unable to draw any conclusions on the orientation of the tails for the BT sources as Vos et al.(2021).

Our BT sources are chosen entirely by visual inspection. Several candidates exhibit BT asymmetries or slight jet bending. Perhaps some of our samples were incorrectly categorised. High-resolution observation is thus required for the validation in order to reduce the error.

5.4 Conclusion

We create a catalog of known cluster corelated to bent-tail radio sources. The 82 bent-tail sample are selected from LoTSS DR1 which is described in details at chapter 4. The galaxy clusters can be identified by using bent-tail radio galaxies. Out of the 65 BTs, we find that 43 are associated with known galaxy clusters. All of these known cluster's masses fall between $0.53 \times 10^{14} M_{\odot} \leq M \leq 10.64 \times 10^{14} M_{\odot}$ with known redshift of 65 BT galaxies. We find that whereas cluster masses $M \geq 10^{14.5} M_{\odot}$ only include 28% of BT galaxies, cluster masses $M \leq 10^{14.5} M_{\odot}$ contain 95% of BT galaxies. Therefore, we draw a conclusion that the probability of finding BT galaxies in low mass galaxy clusters is ~ 3.5 times to high mass galaxy clusters. Our results suggest that BT galaxies may be found in low mass clusters (in the order of $\times 10^{14} M_{\odot}$) region or lower density environments.

Table 5.1 LoTSS BTs in galaxy clusters: Cloumns (1) and (2) are source name and source redshift. Colum (3) is associated clusters name crossponding to the source. Columns (4) and (5) are R.A. and Dec. of the cluster. Column (6) is redshift of the crossponding clusters. '*' represent photometric redshifts and rest are spectoscopic. Column (7) is the angular separation in arcmin of source and cluster. Column (8) is the linear distance between host BT and associate clusters (D_{cl}) in Kpc. Column (9) and column (10) are represents (r_{500}) and (R_{L*}) which are taken from WHL galaxy cluster catalog Wen & Han(2015). (r_{500}) is the radius within which the mean density of a cluster is 500 times of the critical density of the universe and (R_{L*}) is newly define cluster richness parameter. In column (11), we computed cluster mass (M_{500}) (the mass of the cluster within (r_{500})) from Equation 2 of Wen & Han(2015).

Table 5.1: **LoTSS bent-tail galaxy clusters**

Source Name	Source Redshift (z)	Cluster Name	RA_{cl} (deg)	Dec_{cl} (deg)	Cluster Redshift (z)	Angular Sep. (arcmin)	D_{cl} (Kpc)	r_{500} (Mpc)	R_{L*}	M_{500} ($\times 10^{14} M_{\odot}$)
(1)	(2)	(3)	(4)	(5)	(6)	(7)	(8)	(9)	(10)	(11)
J1049+4619	0.350794	WHL J104955.4+461912	162.48073	46.31987	0.3508	0.200	61.41	0.73	30.58	1.71
		GMBCG J162.45523+46.37205	162.45523	46.37205	0.3530*	3.105	953.34	—	—	—
J1051+5523	0.073927	WHL J105147.4+552309	162.94750	55.38570	0.0738	1.1440	100.08	0.87	34.53	1.95
		WHL J105231.4+552319	163.13083	55.38861	0.3630*	5.1590	451.32	—	—	—
		WHL J105236.7+552407	163.15296	55.40193	0.3235	5.9430	519.91	0.85	36.99	2.10
		WHL J105116.2+552913	162.81749	55.48690	0.7010	7.9540	695.84	0.64	31.64	1.78
		ABELL 1112	163.08683	55.55093		10.244	896.17	—	—	—
		GMBCG J163.12160+55.23930	163.12160	55.23930	0.3850*	10.334	904.04	—	—	—
		NSC J105206+551310	163.02780	55.21959	0.0609*	10.439	913.23	—	—	—
J1057+4749	0.183403	MSPM 05580	164.42320	47.83900	0.0873	2.411	461.88	—	—	—
J1105+4800	0.894000*	—	—	—	—	—	—	—	—	—
J1107+4801[a]	0.664100*	—	—	—	—	—	—	—	—	—
J1113+4952	0.610775	—	—	—	—	—	—	—	—	—
J1115+4835	0.074324	MSPM 02053	168.92680	48.59270	0.07443	0.562	49.39	—	—	—
		SDSS-C4-DR3 3408	168.92094	48.57265	0.07400	0.668	58.71	—	—	—
		NSCS J111554+483541	168.97500	48.59472	0.0739S	2.085	183.25	—	—	—
		SCL 260	168.70450	48.52740	—	9.391	825.37	—	—	—
J1117+5051[a]	0.318815	GMBCG J169.48266+50.84749	169.48266	50.84749	0.3180*	0.240	69.19	—	—	—
		WHL J111745.3+505013	169.43875	50.83694	0.3870*	1.936	558.15	—	—	—
		WHL J111744.2+504943	169.43420	50.82850	0.3207	2.346	676.36	1.00	69.40	4.16
J1117+5636[a]	0.342334	—	—	—	—	—	—	—	—	—
J1120+4714[a]	0.109900*	GMBCG J170.02097+47.23593	170.02092	47.23593	0.1350	0.162	20.20	—	—	—
		WHL J112012.6+471132	170.05250	47.19222	0.1117*	2.759	344.07	1.07	63.38	3.77
		NSC J112020+471017	170.10154	47.17422	0.0710*	4.792	597.61	—	—	—
		ABELL 1222	170.11917	47.15942	0.1126	5.934	740.25	—	—	—
		GMBCG J170.15363+47.15517	170.15363	47.15517	0.1850*	7.110	886.68	—	—	—
J1120+5308	1.032300	—	—	—	—	—	—	—	—	—
J1120+5516[a]	0.513096	—	—	—	—	—	—	—	—	—
J1121+5421	0.210208	WHL J112113.6+542133	170.30658	54.35928	0.2122	0.050	10.66	0.68	20.68	1.12
J1124+5546	0.809018	—	—	—	—	—	—	—	—	—
J1127+5031[a]	0.338420	WHL J112737.5+503200	171.90640	50.53344	0.3384	0.352	105.58	0.65	22.65	1.24
J1127+5533	0.984100*	—	—	—	—	—	—	—	—	—
J1132+5056	0.358569	WHL J113250.7+505705	173.21115	50.95139	0.3586	0.100	31.14	0.63	18.73	1.01
J1142+4718[a]	0.700500*	—	—	—	—	—	—	—	—	—
J1147+4805	0.702800	—	—	—	—	—	—	—	—	—
J1147+4917	0.241000*	—	—	—	—	—	—	—	—	—
J1154+4948	0.288353	WHL J115412.9+494858	178.55375	49.81583	0.2873	0.190	51.13	0.67	21.80	1.19
J1208+5457	0.463974	—	—	—	—	—	—	—	—	—
J1217+5334[a]	0.195732	WHL J121737.8+533428	184.40743	53.57452	0.1953	0.222	44.77	0.80	28.97	1.62
		NSCS J121735+533415	184.39583	53.57083	0.3400	0.578	116.57	—	—	—
		NSCS J121755+533254	184.47917	53.54833	0.3400+	3.153	635.94	—	—	—
		WHL J121802.7+533345	184.51144	53.56248	0.4313	3.861	778.74	0.54	12.67	0.66
J1220+4603[a]	0.110975	NSC J122011+460658	185.04610	46.11634	0.1719*	3.360	422.54	—	—	—
		NSC J122006+460710	185.02658	46.11933	0.1976*	3.849	484.04	—	—	—
		WHL J122036.6+460146	185.15266	46.02942	0.6715*	3.956	497.49	0.63	27.49	1.53
		WHL J121954.1+460225	184.97533	46.04017	0.3176	4.212	529.68	0.55	10.63	0.55
		GMBCG J185.01899+46.13467	185.01899	46.13467	0.265*	4.810	604.88	—	—	—
		MaxBCG J185.01069+45.97200	185.01069	45.97201	0.25655*	6.013	756.12	—	—	—

Table 5.1

Table 5.1: **LoTSS bent-tail galaxy clusters**

Source Name	Source Redshift (z)	Cluster Name	RA_{cl} (deg)	Dec_{cl} (deg)	Cluster Redshift (z)	Angular Sep. (arcmin)	D_{cl} (Kpc)	r_{500} (Mpc)	R_{L*}	M_{500} ($\times 10^{14} M_{\odot}$)
(1)	(2)	(3)	(4)	(5)	(6)	(7)	(8)	(9)	(10)	(11)
J1224+4906	0.122400*	WHL J122418.6+490550	186.07743	49.09719	0.1012	0.965	132.13	0.64	46.49	0.88
		NSC J122403+490530	186.01447	49.09193	0.1528*	1.604	219.63	—	—	—
		NSC J122358+490418	185.99463	49.07161	0.1847*	2.873	393.38	—	—	—
		GMBCG J185.96312+49.12210	185.96312	49.12210	0.3700*	3.778	517.30	—	—	—
		WHL J122348.9+490214	185.95361	49.03724	0.2218	5.443	745.28	0.79	28.21	1.57
		GMBCG J185.90979+49.05996	185.90979	49.05996	0.2110*	6.135	840.03	—	—	—
J1224+5419	0.467984	WHL J122450.7+541929	186.20708	54.32778	0.4672	0.140	51.11	0.98	71.72	4.31
		WHL J122446.9+541709	186.19524	54.28596	0.3318	2.405	877.95	0.67	15.17	0.80
J1225+4904[a]	0.261906	GMBCG J186.41756+49.07704	186.41755	49.07704	0.2740*	0.205	82.03	—	—	—
J1236+5525	0.324225	WHL J123647.3+552511	189.19708	55.41944	0.3231	0.108	31.49	0.80	32.86	1.85
		NSCS J123644+552626	189.18333	55.44056	0.2100+	1.409	410.80	—	—	—
		NSC J123630+552310	189.12700	55.38611	0.1714*	3.184	928.33	—	—	—
		GMBCG J189.29170+55.39860	189.29170	55.39860	0.2660*	3.351	977.01	—	—	—
J1242+5021	0.147895	WHL J124207.4+502147	190.53078	50.36295	0.1489	0.183	29.41	0.52	10.28	0.53
		NSC J124203+502529	190.51535	50.42495	0.2061*	3.867	621.48	—	—	—
		NSC J124139+502431	190.41279	50.40847	0.1944*	5.457	877.02	—	—	—
J1247+4852	0.210588	WHL J124743.2+485156	191.93001	48.86562	0.2095	0.383	29.70	0.94	55.86	3.29
		RM J124743.2+485156.2	191.93000	48.86562	0.2205*	0.383	29.70	—	—	—
		ABELL 1615	191.90792	48.86833	0.2133*	0.700	54.29	—	—	—
		GMBCG J191.96209+48.85500	191.96209	48.85500	0.1910*	1.751	135.80	—	—	—
		WHL J124644.5+485254	191.68530	48.88173	0.3279	9.485	735.62	0.62	14.27	0.75
		WHL J124638.8+485332	191.66158	48.89229	0.3367*	10.476	812.47	—	—	—
		WHL J124636.1+485036	191.65042	48.84333	0.3481*	10.972	850.94	—	—	—
J1257+4854[a]	0.260368	WHL J125746.3+485447	194.44272	48.91298	0.2636	0.126	31.53	0.92	48.16	2.80
		NSC J125741+485449	194.42134	48.91376	0.2366*	0.935	233.97	—	—	—
		GMBCG J194.47003+48.86499	194.47003	48.86499	0.3090*	3.125	781.97	—	—	—
		WHL J125807.4+485610	194.53070	48.93608	0.5011	3.618	905.34	0.66	22.51	1.23
J1303+4744	0.217920	GMBCG J195.99926+47.72834	195.99926	47.72834	0.3770*	2.059	451.27	—	—	—
J1303+4935	0.254710	WHL J130327.7+493558	195.86541	49.59943	0.2547	0.061	15.02	0.66	17.22	0.92
		NSC J130314+493837	195.80927	49.64363	0.1325*	3.488	859.01	—	—	—
J1303+5219	0.272003	WHL J130300.9+521054	195.75356	52.18170	0.4858	10.345	970.41	0.61	10.87	0.56
J1306+4634	0.218359	WHL J130650.0+463333	196.70832	46.55927	0.2291*	0.941	206.57	1.41	165.77	10.64
		ABELL 1682	196.72792	46.55611	0.2259	1.749	383.97	—	—	—
		GMBCG J196.70330+46.60084	196.70330	46.60084	0.4150*	2.092	459.23	—	—	—
		NSC J130639+463208	196.66350	46.53558	0.2508*	2.177	477.89	—	—	—
		GMBCG J196.75262+46.56389	196.75262	46.56389	0.3370*	2.640	579.53	—	—	—
		WHL J130657.3+463206	196.73875	46.53500	0.2081*	2.833	621.90	—	—	—
		[EAD2007] 037	196.76500	46.56330	0.2466*	3.152	691.93	—	—	—
J1306+5144	0.277312	WHL J130612.2+514407	196.55083	51.73528	0.2850*	0.029	7.59	0.98	53.93	3.16
J1312+4714[a]	0.225151	WHL J131245.4+471440	198.18920	47.24446	0.2237	0.233	52.35	0.77	26.97	1.50
J1315+4840	0.514087	WHL J131527.6+484025	198.86500	48.67361	0.5072*	0.575	220.72	1.03	81.90	4.97
		WHL J131519.9+484146	198.83304	48.69611	0.5897	1.751	672.15	0.82	61.23	3.63
J1329+5246[a]	0.412396	—	—	—	—	—	—	—	—	—
J13303+4730	0.326122	WHL J133032.6+473053	202.63583	47.51472	0.3261	0.059	17.27	0.72	22.42	1.23
		WHL J133037.2+473001	202.65497	47.50015	0.4939	1.221	357.41	0.52	14.80	0.78
J1344+5553[a]	0.037340	WHL J134450.3+554741	206.20964	55.79478	0.1544	5.483	253.07	0.59	12.26	0.64
		WHL J134455.9+554537	206.23292	55.76028	0.1630*	7.676	354.29	—	—	—
		400d J1343+5546	205.87083	55.78806	0.0690	11.846	546.75	—	—	—
		WHL J134448.8+560531	206.20346	56.09205	0.6166	12.490	576.47	0.63	24.73	1.36
		WHL J134316.3+560006	205.81792	56.00167	0.4866*	13.988	645.62	—	—	—
		WHL J134314.7+560001	205.81111	56.00024	0.4830	14.144	652.82	0.79	39.67	2.27
		ABELL 1783	205.93875	55.63917	0.0690	16.780	774.48	—	—	—
		WHL J134527.2+553724	206.36324	55.62345	0.6216	16.863	778.31	0.57	13.37	0.70
		SDSS-C4-DR3 3007	205.93759	55.63379	0.0682	17.082	788.42	—	—	—
		SWXCS J134340+5537.4	205.91581	55.62332	0.0680*	17.988	830.24	—	—	—
		WHL J134642.9+560040	206.67860	56.01115	0.6154	18.467	860.65	0.58	24.96	1.38
		WHL J134316.1+553656	205.81708	55.61556	0.0678	20.211	932.84	—	—	—
		MSPM 01743	205.88420	55.58710	0.0682	20.408	945.62	—	—	—

Table 5.1

Table 5.1: **LoTSS bent-tail galaxy clusters**

Source Name	Source Redshift (z)	Cluster Name	RA_{cl} (deg)	Dec_{cl} (deg)	Cluster Redshift (z)	Angular Sep. (arcmin)	D_{cl} (Kpc)	r_{500} (Mpc)	R_{L*}	M_{500} ($\times 10^{14} M_{\odot}$)
(1)	(2)	(3)	(4)	(5)	(6)	(7)	(8)	(9)	(10)	(11)
J1347+5022[a]	0.709600*	WHL J134708.2+502222	206.78415	50.37281	0.5746	1.032	458.76	0.70	33.36	1.88
J1351+5216	0.165942	WHL J135156.1+521542	207.98360	52.26159	0.1653	0.780	137.83	0.66	20.34	1.10
J1351+5439[a]	0.563901	WHL J135133.2+543943	207.88820	54.66191	0.5641	0.605	243.15	—	—	—
J1359+4905	0.165200*	WHL J135949.8+490516	209.95741	49.08800	0.1260*	1.022	179.94	—	—	—
		NSC J135946+490706	209.94202	49.11845	0.1088*	1.251	220.26	—	—	—
		MSPM 10188	209.89450	49.11760	0.1548	2.021	355.84	—	—	—
		WHL J135946.1+490350	209.94208	49.06361	0.3690	2.073	364.99	1.02	70.33	4.22
		WHL J135936.7+490919	209.90278	49.15537	0.1077	3.688	649.34	0.61	15.83	0.83
J1426+5547	0.738800*	—	—	—	—	—	—	—	—	—
J1428+5520	0.290652	WHL J142843.4+552045	217.18083	55.34556	0.2893	0.245	66.30	0.66	19.76	1.07
J1431+5518[a]	0.565100*	—	—	—	—	—	—	—	—	—
J1434+4951	0.196541	GMBCG J218.67368+49.85134	218.67368	49.85134	0.2040*	0.641	129.69	—	—	—
		WHL J143433.3+495500	218.63875	49.91667	0.2349*	3.738	756.31	—	—	—
		NSC J143457+495528	218.73849	49.92461	0.1996*	4.419	894.10	—	—	—
		GMBCG J218.78324+49.90218	218.78324	49.90218	0.1860*	4.654	941.65	—	—	—
J1446+4841	0.376757	—	—	—	—	—	—	—	—	—
J1451+4841	0.231262	—	—	—	—	—	—	—	—	—
J1459+4947	0.169449	WHL J145943.2+494716	224.93017	49.78770	0.1705	0.065	11.68	1.12	83.76	5.09
		ABELL 2011	224.95838	49.75236	0.1800*	2.450	440.35	—	—	—
J1459+5333	0.076957	NSC J145935+533319	224.89918	53.55542	0.0699*	0.521	47.27	—	—	—
		SDSS-C4-DR3 3613	224.90166	53.57254	0.0750	0.554	50.27	—	—	—
		MSPM 05374	224.92240	53.53220	0.07501	2.121	192.45	—	—	—
		WHL J145907.3+533427	224.78040	53.57408	0.2656	4.168	378.20	0.69	20.51	1.11
J1506+5354[a]	0.304365	WHL J150624.1+535503	226.60042	53.91745	0.3044	0.600	167.62	0.62	16.04	0.54
J1510+5146[a]	0.169300*	WHL J151003.4+514612	227.51418	51.76987	0.2073	0.507	91.06	0.84	30.94	1.74
		WHL J150934.8+514635	227.39499	51.77639	0.5778	3.948	709.13	—	—	—
J1512+5147[a]	0.583700*	—	—	—	—	—	—	—	—	—
J1132+5459	0.512300*	—	—	—	—	—	—	—	—	—
J1203+5101[a]	0.299619	WHL J120340.7+510047	180.91958	51.01306	0.3030*	0.262	72.41	—	—	—
		WHL J120339.9+510022	180.91646	51.00602	0.2965	0.659	182.13	0.81	30.27	1.70
		ABELL 1454	180.96174	51.02169	0.3400*	1.728	477.58	—	—	—
		GMBCG J180.98159+51.05794	180.98159	51.05794	0.3310*	3.471	959.31	—	—	—
J1219+5055[a]	0.607600*	WHL J184.801+50.9098	184.77720	50.91310	0.5271*	0.547	227.76	—	—	—
		WHL J121912.2+505435	184.80086	50.90981	0.5523	1.122	467.18	1.15	137.00	8.66
		GMBCG J184.80005+50.93515	184.80005	50.93515	0.4710*	1.125	510.07	—	—	—
		WHL J121917.6+505432	184.82333	50.90889	0.5347*	1.871	779.05	—	—	—
J1245+4859[a]	0.287956	WHL J124543.7+485902	191.43216	48.98396	0.2864	0.404	108.61	0.95	48.19	2.80
J1325+5544[a]	1.964100*	—	—	—	—	—	—	—	—	—
J1505+4706	0.26656	WHL J150538.1+470617	226.40856	47.10485	0.2648	0.108	27.49	1.0	74.29	4.47
		ABELL 2024	226.37374	47.12389	0.2203	1.831	466.05	—	—	—
J1506+5311	0.14469	WHL J150602.9+531108	226.51206	53.18540	0.1414	0.044	6.94	0.81	32.89	1.85
		WHL J150611.6+531101	226.54823	53.18365	0.2983	1.277	201.51	0.70	26.55	1.74

Chapter 6

MRG: A FIRST look at the Miscellaneous Radio Galaxies

A rare example of an unusual and uncommon source with peculiar radio morphology is a miscellaneous radio galaxy. These sources have unusual and distinctive jet alignment and direction. The source morphology is unusual from other known radio sources due to the unique irregular jet propagation. In this chapter we report fifteen miscellaneous sources from a symmetric search of the VLA Faint Images of the Radio Sky at Twenty-Centimeters (VLA FIRST) survey at 1.4 GHz. We describe these radio galaxy's morphological structure, nature, visualisation features, and distinctions from other classes of radio galaxy. We also compare their radio morphology in other radio surveys e.g. at 325 MHz in Westerbork Northern Sky Survey (WENSS) and at 150 MHz in TIFR GMRT Sky Survey (TGSS).

6.1 Identifying the MRGs

From the FIRST survey, we shortlisted the sources whose angular sizes are greater than or equal to 10 arcsec. The details of the FIRST survey are discussed in the introduction section (Becker et al.(1995)). This is the only selection criterion we

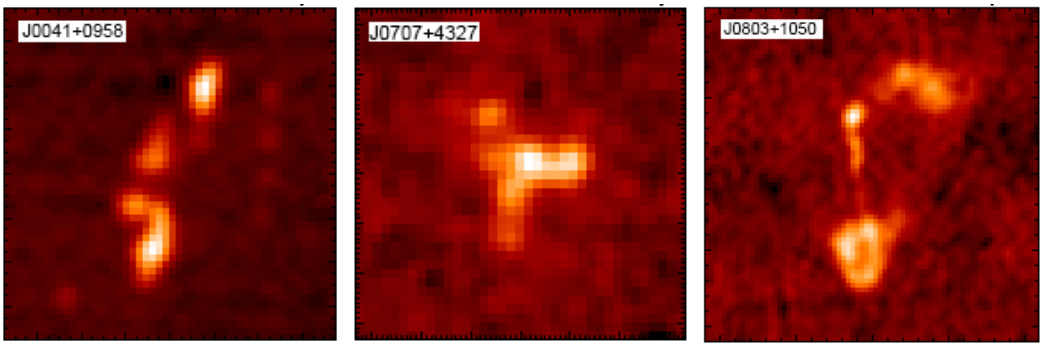

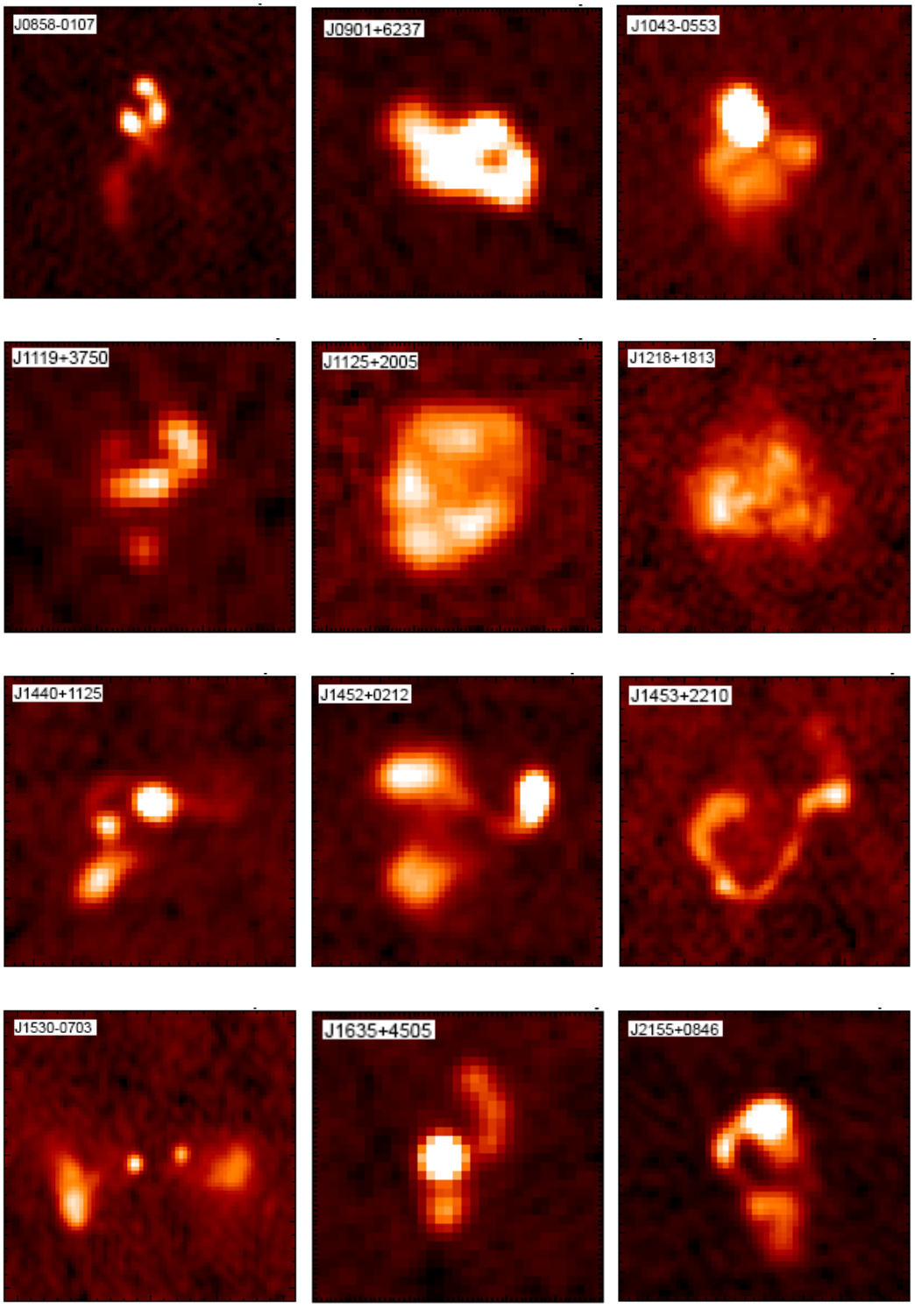

Figure 6.1: Color stamp images of the fifteen FIRST MRG candidates.

have used to find reliable and moderate radio sources. We get 95,243 radio sources from the FIRST dataset by implying this selection cut. Then we visually examined each of the sources to find out miscellaneous morphology. We also compared the morphology of these miscellaneous candidates in TGSS and WENSS surveys. The details of the identification of the MRGs is same as bent-tail radio sources from FIRST survey and discussed in chapter 3.

6.2 Result

A total of fifteen sources that appears to be MRG candidates in the FIRST database is reported. We have studied the morphology of each source from the FIRST image. We also have collected the respective redshift of the sources from their corresponding optical counterparts, if available. The flux density of each source are measured from the TGSS at 150 MHz, 1400 MHz fulx from NVSS and the respective spectral index between 1400 MHz and 150 MHz (α_{150}^{1400}) are calculated.

We have estimated the radio luminosity of each source. To calculate the radio luminosity (L_{rad}) we use the following relation adopted from O'Dea & Owen(1987).

$$L_{rad} = 1.2 \times 10^{27} D_{Mpc}^2 S_0 \nu_0^{-\alpha} (1+z)^{-(1+\alpha)} \times (\nu_u^{(1+\alpha)} - \nu_l^{(1+\alpha)})(1+\alpha)^{-1} ergs^{-1} \quad (6\text{-}1)$$

where D_{Mpc} is luminosity distance to the source (Mpc), S_0 is the flux density (Jy) at a given frequency ν_0 (Hz), z is the red-shift of the radio galaxy, α is the spectral index and ν_u (Hz), and ν_l (Hz) are the upper and lower cutoff frequencies. In our calculation, we assume the upper and lower cutoff frequencies as 15 GHz and 100 MHz, respectively.

The basic parameters of the MRG are mentioned in Table 6.1, and the color images extracted from the FIRST catalog are shown in Figure 6.1. The MRGs are cataloged in Table 6.1 in the ascending order of Right Ascension (RA). Table 1 contains the following columns; column 1: Catalog Number, column 2: Name, column 3: RA (J2000.0), column 4: Declination (J2000.0), column 5: Position Reference, column 6: Red-shift (z), column 7: Angular size (θ) in arc-second (Major Axis), column 8: Linear Size (l) in Mpc, column 9: flux density at 1400 MHz in mJy (F_{1400}), column 10: flux density in TGSS at 150 MHz in mJy (F_{150}) , column 11: spectral index (α_{150}^{1400}), column 12: Luminosity in erg/s (L), column 13: Other Catalog.

Table 6.1: **Candidates of FIRST Miscellaneous Radio Source**

Sl. No.	Name	R.A. (J2000.0)	Decl. (J2000.0)	Ref.	z	θ (arcsec)	l (Mpc)	F_{1400} (mJy)	F_{150} (mJy)	α_{150}^{1400}	L (erg/s) ($\times 10^{41}$)	Oth Cat
1	J0041+0958	00 41 31.26	+09 58 33.8	EE	—	68	—	56.6	—	—	—	1
2	J0707+4327	07 07 11.67	+43 27 09.6	EE	—	35	—	22.5	85.5	−0.60	—	1
3	J0803+1050	08 03 37.68	+10 50 42.4	SDSS	0.142	112	0.379	85.2	663.1	−0.92	3.44	1
4	J0858–0107	08 58 28.92	−01 07 17.3	2MASX	—	75	—	101.9	448.0	−0.66	—	1, 2
5	J0901+6237	09 01 12.56	+62 37 18.5	SDSS	—	42	—	184.6	771.8	−0.64	—	1
6	J1043–0553	10 43 18.94	−05 53 52.5	WISE	0.549	52	0.826	334.4	1427.1	−0.65	280.82	1, 2 3, 4
7	J1119+3750	11 19 46.88	+37 50 51.3	EE	0.485	31	0.425	27.1	182.4	−0.85	17.27	1
8	J1125+2005	11 25 54.82	+20 05 03.4	EE	—	50	—	111.0	856.8	−0.91	—	1
9	J1218+1813	12 18 04.89	+18 13 53.6	SDSS	0.140	83	0.276	126.8	1056.2	−0.95	4.97	1, 2 5
10	J1440+1125	14 40 20.78	+11 25 07.1	SDSS	0.311	68	0.553	119.9	578.7	−0.70	27.57	1
11	J1452+0212	14 52 24.11	+02 12 01.2	EE	—	63	—	201.8	970.9	−0.70	—	1, 2 4, 5
12	J1453+2210	14 53 17.40	+22 10 55.8	SDSS	—	85	—	96.2	495.1	−0.73	—	1
13	J1530–0703	15 30 58.88	−07 03 32.4	2MASS	—	102	—	110.3	598.8	−0.76	—	1
14	J1636+4505	16 36 40.99	+45 05 51.3	EE	—	38	—	75.0	561.4	−0.90	—	1, 2 3, 6 7
15	J2155+0846	21 55 26.16	+08 46 48.4	SDSS	0.150	58	0.208	125.5	776.7	−0.82	5.72	1

References: (1) NVSS: Condon et al.(1998); (2) VLSS: Cohen et al.(2007), Helmboldt et al.(2008); (3) TXS: Douglas et al.(1996); (4) PMN: Griffith et al.(1994); (5) 87GB: Gregory & Condon(1991); (6) B3: Ficarra et al.(1985); (7) 6C: Baldwin et al.(1985), Hales et al.(1988), Hales et al.(1990), Hales et al.(1991), Hales et al.(1993a), Hales et al.(1993b); PKS: Bolton et al.(1964); SDSS: Fan et al.(1999), Tumlinson et al.(2013); 2MASS: Skrutskie et al.(2006); 2MASX: Skrutskie et al.(2006); WISE: Chung et al.(2011), Rebull et al.(2011)

6.2.1 Notes on individual sources

1. **J0041+0958**

The source seems to be a DDRG. In the general morphology of a DDRG, there are two pairs of lobes with a common center in a straight line Schoenmakers et al.(2000). The radio source, J0041+0958, also has four clear lobes, but the inner and outer sets of lobes are not in a straight line. The outer south lobe is straight in line with the inner pairs, while the outer north lobe deviates from the straight line towards the west direction. This deviation of the north side outer lobe indicates that this source is different from a DDRG. Such morphology may be due to massive objects like galaxy clusters or massive black holes in the east direction, as the north side of the outer lobe bents towards the west direction. There is no optical counterpart found for this source and no data found in TGSS at 150 MHz and WENSS at 325 MHz for J0041+0958.

2. **J0707+4327:**

The radio source contains three arms that are symmetrically oriented in three directions, giving the source a 'spinner' like shape. The radio lobes are elongated towards the west, north, and south-east (SE) direction. The measured angles between the lobes of west and north, north and SE, SE and west are 110, 125 and 125 degrees, respectively. We notice that at 1.4 GHz, the SE and north lobes have

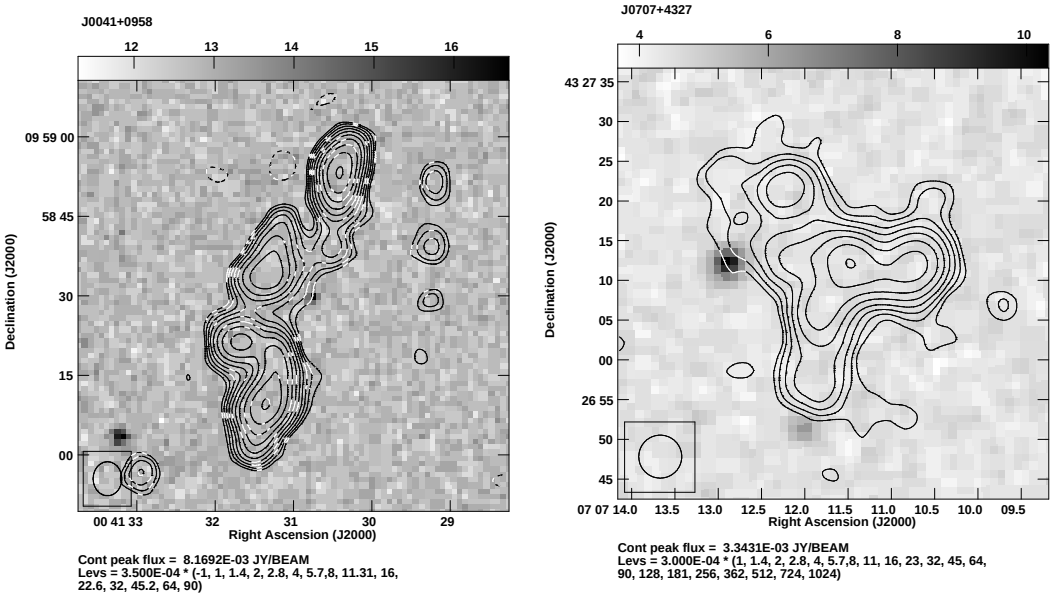

Figure 6.2: FIRST image of the candidate miscellaneous radio sources (contours) J0041+0958 and J0707+4327, overlaid on the DSS2 red image (grayscale). The contours are drawn from $\sim 3\sigma$ ($\geq 3.0 \times 10^{-4}$ Jy) to ensure a reliable structure. The contours are increased by factors of $\sqrt{2}$.

nearly equal flux with the values 5.7 mJy and 5.8 mJy, respectively, while the west lobe has a comparatively higher flux density with a value of 6.9 mJy. We measure the flux density of the central core of a value of 4.0 mJy at 1.4 GHz. We have cross-checked this source at other frequencies for such a 'spinner' like structure, and it looks like a point source both in TGSS and WENSS due to poor resolution. Re-orientation of any of the jets or restarting jet activity in a different direction may be the reason behind such peculiar morphology.

3. **J0803+1050:**

On the two sides of the central region, the jets of this radio source have two different forms of bent structure. The top jet of the source is exactly like 'S', while the shape of the lower half is like a sharp 'U'. A small 'wing' towards the east direction from the lower 'U'-shaped portion is also seen. SDSS J080337.68+105042.4 is the optical counterpart of the radio source Fan et al.(1999), with a red-shift value of 0.142356 Sánchez et al.(2011). The source has an angular size of $\sim 112''$ which corresponds to a linear size of 0.38 Mpc. We found that the galaxy cluster WHL J080337.7+105042 (Wen et al.(2010)) is very near with an angular separation of $\sim 0.1''$ to the source and probably associated with the source. The radio luminosity of the object has a moderate value of 3.44 $\times 10^{41}$ erg/s. We have not found any counterpart in WENSS at 325 MHz. The TGSS survey at 150 MHz has not enough resolution to observe such morphology as seen in FIRST.

4. **J0858–0107:**

On the two sides of the central region, the jets of this radio source have two different forms of bent structure. The morphology of this radio source looks quite fascinating. The upper section of the jet has a 'C'-shaped structure, though the tail towards the north is further extended. The top lobe is significantly brighter than the lower. WHL J085829.2–010704, a galaxy cluster Wen et al.(2010) is present on the upper lobe. This object is mentioned as NVSS J085829-010720 in NVSS catalog (Condon et al.(1998)), though the lack of resolution of NVSS could not resolve out such miscellaneous morphology. The structure of this source looks to be a point-like source in both NVSS and TGSS survey, while no counterpart found in WENSS.

5. **J0901+6237:**

The main jets are oriented from NW to SE when the wings are in SW to NE direction. As shown in the color image, the NW main jet bends southward and

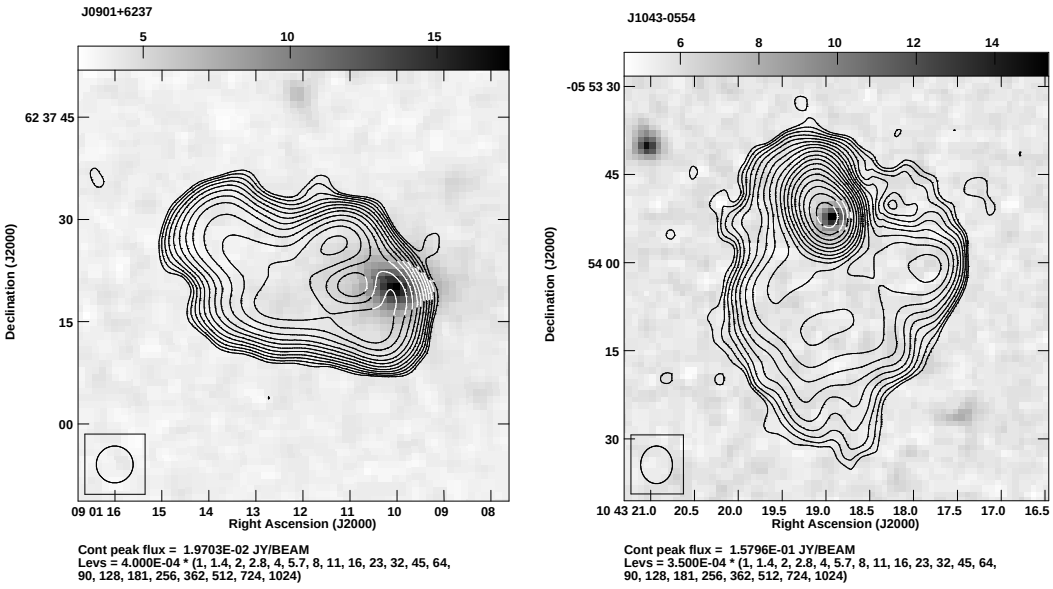

Figure 6.3: FIRST image of the candidate miscellaneous radio sources (contours) of J0901+6237 and J1043-0553, overlaid on the DSS2 red image (grayscale). The contours are drawn from $\sim 3\sigma$ ($\geq 3.0 \times 10^{-4}$ Jy) to ensure a reliable structure. The contours are increased by factors of $\sqrt{2}$.

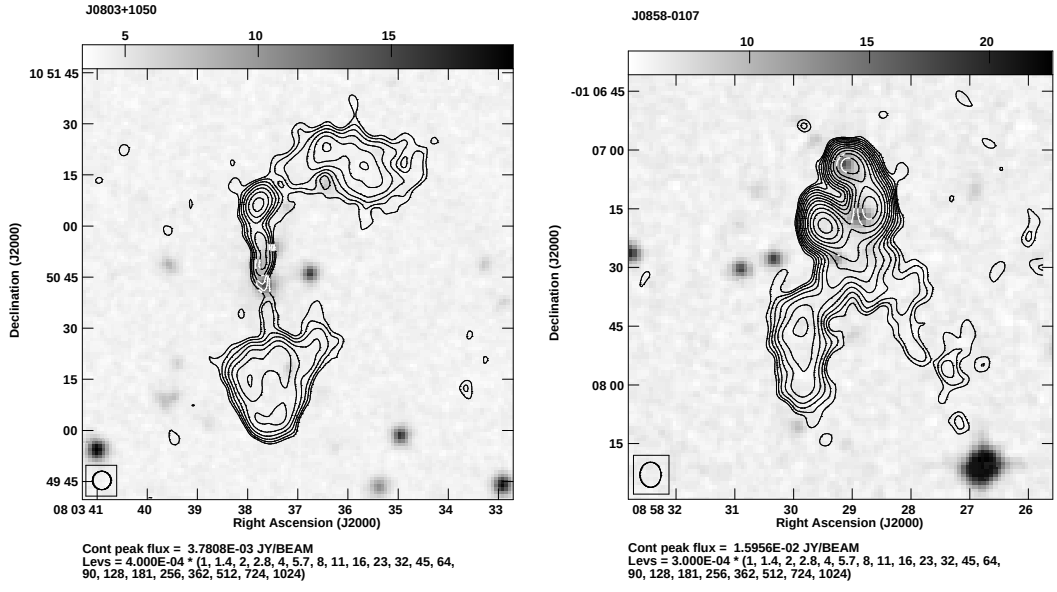

Figure 6.4: FIRST image of the candidate miscellaneous radio sources (contours) J0803+1050 and J0858-0107, overlaid on the DSS2 red image (grayscale). The contours are drawn from $\sim 3\sigma$ ($\geq 3.0 \times 10^{-4}$ Jy) to ensure a reliable structure. The contours are increased by factors of $\sqrt{2}$.

collides with the SW wing. In WENSS and TGSS, the source is found to be a point-like source.

6. **J1043–0553:**

The object J1043–0554 is a quasar LQAC 160-005 001 Souchay et al.(2012). It may be a head-tail source with a 'U'-shaped extension along NE direction. At the SE edge of the source, a radio-loud region is spotted. The radio flux density of this radio hot-spot is found to be 243.9 mJy at 1.4 GHz, while the total radio flux is 334.4 mJy. It is also cataloged as UVQS J104318.95-055352.5 (Monroe et al.(2016)) and as TXS 1040–056 with flux value of 658.0 mJy at 365 MHz (Douglas et al.(1996)). No data is found in WENSS, while the source detected as a point-like source in TGSS.

7. **J1119+3750:**

The radio source J1119+3750 appears to be like the English alphabet 't'. Inside the radio source, three optical galaxies are found. The optical galaxy SDSS

J111946.94+3
75038.6 (Fan et al.(1999)) with red-shift 0.486700 (Blanton et al.(2000)) lies in the north secondary lobe, while SDSS J111947.
40+375058.9 (Fan et al.(1999)) with a red-shift value of 0.486218 ± 0.000261 [1] is noticed inside the south secondary lobe. The primary jet forming the tail 't' contains the optical galaxy SDSS J111946.26+375055 (Fan et al.(1999)). We use the EE location as a position coordinate of the source because the above three optical galaxies have not coincided with the center. The north and south secondary lobes have flux values of 2.7 mJy and 1.7 mJy at 1.4 GHz. We noticed a point-like morphology of this radio source in the TGSS and WENSS survey rather than such miscellaneous structure.

8. **J1125+2005:**

The source J1125+2005 looks like to be a radio cloud. So it is probably an H I region. The morphology of this radio source matches with crab nebula Velusamy & Roshi(1991) [2]. In the color image, four distinct radio hot spots are noticed. A multi-wavelength deep-field study is needed to understand the nature of this source. We have not found any optical counterpart for this exciting source. It has an angular size of $\sim 50''$. Previously the source is catalog as NVSS J112554+200505 in NVSS catalog Condon et al.(1998).

9. **J1218+1813:**

The radio emission from this source appears to be like a cloud. SDSS J121804.89+ 181353.6 is the optical counterpart of this object (Fan et al.(1999)). Both 2MASS J12180539+
1813466 (Skrutskie et al.(2006)) and 2MASS J12180420+1813455 (Skrutskie et al.(2006)) are inside the radio-emitting region and maybe also consider as the optical counterparts. Like the previous one, J1125+2005, it may also be an H I region source. The TGSS image for this source also shows a similar radio cloud-like structure, but no counterpart is found in WENSS.

10. **J1440+1125:**

The orientation of the outward jets of the source is along the north-east and west direction. The north-east jet looks compact, while the west jet has a diffused structure. In the central part, a bent structure like 'C' is seen. The edges are

[1] http://www.sdss.org/dr5/products/catalogs/index.html
[2] http://images.nrao.edu/393

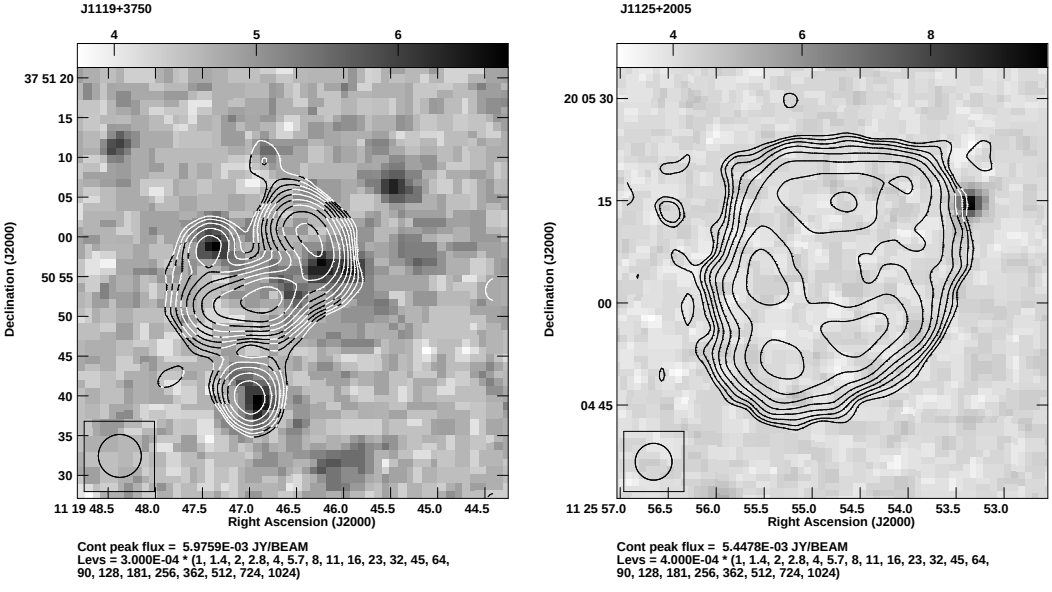

Figure 6.5: FIRST image of the candidate miscellaneous radio sources (contours) J1119+3750 and J1125+2005, overlaid on the DSS2 red image (grayscale). The contours are drawn from $\sim 3\sigma$ ($\geq 3.0 \times 10^{-4}$ Jy) to ensure a reliable structure. The contours are increased by factors of $\sqrt{2}$.

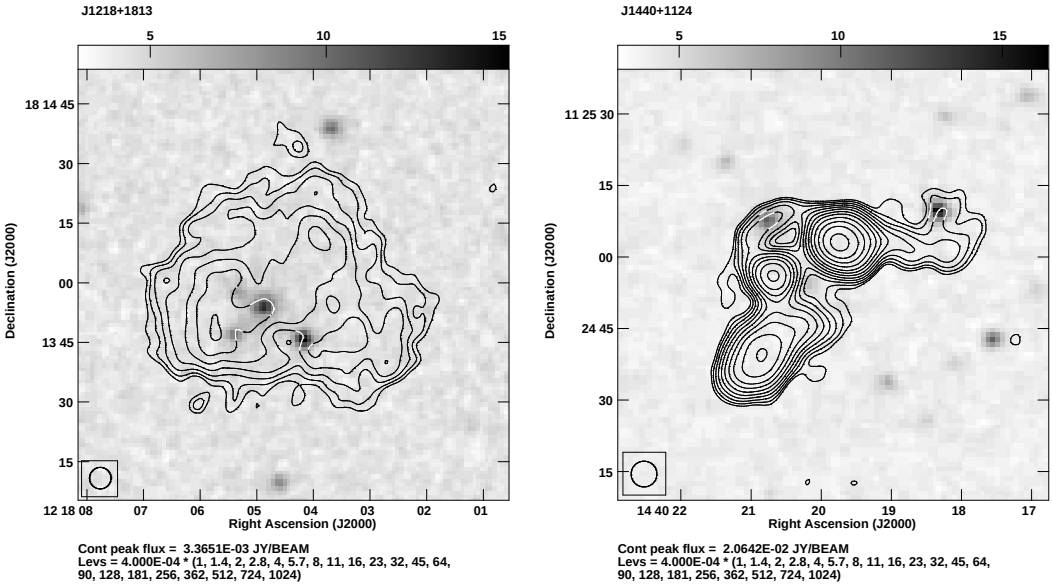

Figure 6.6: FIRST image of the candidate miscellaneous radio sources (contours) J1218+1813 and J1440+1125, overlaid on the DSS2 red image (grayscale). The contours are drawn from $\sim 3\sigma$ ($\geq 3.0 \times 10^{-4}$ Jy) to ensure a reliable structure. The contours are increased by factors of $\sqrt{2}$.

brighter compared to the arched region of the central 'C' shaped region. WHL J144020.8+112507 Wen et al.(2010), the galaxy cluster is located at an angular distance 0.04 arcmin from the optical counterpart, SDSS J144020.78+112507.1 (Fan et al.(1999)). The galaxy cluster is probably associated with this exciting radio source. TGSS data is available, and the source is not resolved, while no counterpart is found in WENSS at 325 MHz.

11. **J1452+0212:**

This fascinating radio object consists of three clear radio lobes, and the three lobes are nearly equispaced in our projected plane. Starting from an anti-clockwise direction, the angle between the west, south and north lobes are 110, 105 and 145 degrees, respectively. At 1.4 GHz, the radio source has a total radio flux of 201.8 mJy. The flux densities for the south, north and west lobes are 76.3 mJy, 61.6 mJy and 64.1 mJy. SDSS J145222.58+021203.4 (Fan et al.(1999)) may be the optical counterpart for this radio source. This miscellaneous three-lobe morphology is not seen in any other survey.

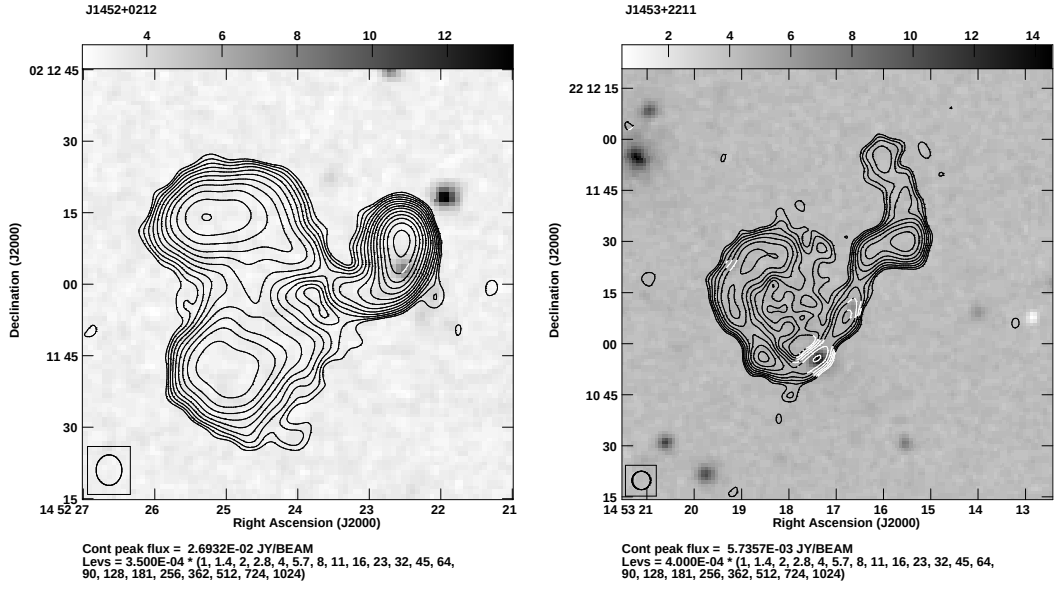

Figure 6.7: FIRST image of the candidate miscellaneous radio sources (contours) J1452+0212 and J1453+2210, overlaid on the DSS2 red image (grayscale). The contours are drawn from $\sim 3\sigma$ ($\geq 3.0 \times 10^{-4}$ Jy) to ensure a reliable structure. The contours are increased by factors of $\sqrt{2}$.

12. **J1453+2210:**

The bending of the jet of J1453+2210 is very special. Looking at the morphology of the jets from the center, the jets initially are steep and directed towards the south direction, and after that, both the jets go flat towards the west. The western half of the jet extends once again to the south, making it somewhat unique to the entire jet structure. In the TGSS survey, an extended structure is found, but the lack of resolution fails to give a detailed structure, but no counterpart is found in WENSS.

13. **J1530–0703:**

The primary alignment of the radio jets is directed towards the east to west direction. Both of the radio jets have a compact core towards a common center and diffuse edges in the opposite direction. Interestingly the east lobe is further extended towards north to south and makes the overall morphology of the radio source a special one. In the NVSS catalog, the two lobes are cataloged as two different sources, the east one is known as NVSS J153100–070343 (Condon

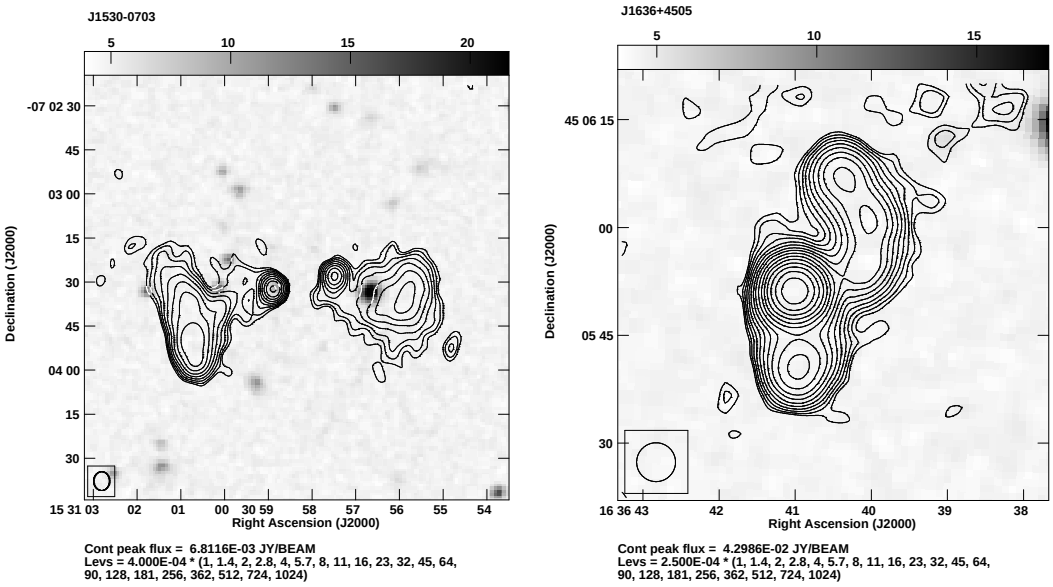

Figure 6.8: FIRST image of the candidate miscellaneous radio sources (contours) J1530-0703 and J1636+4505, overlaid on the DSS2 red image (grayscale). The contours are drawn from $\sim 3\sigma$ ($\geq 3.0 \times 10^{-4}$ Jy) to ensure a reliable structure. The contours are increased by factors of $\sqrt{2}$.

et al.(1998)) when the west one is named as NVSS J153056-070333 (Condon et al.(1998)). Two distinguishable lobes are seen in TGSS but the resolved structure is not found. There is no database found in WENSS.

14. **J1636+4505:**

The radio jet has a distinct hotspot in the middle, with two jets pointing north and south. The radio jet in the south bent like a 'C' form, whereas the north jet is a typical straight jet. The source is unique due to this jet formation. The flux density of the south and north jet has a value of 16.0 mJy and 11.3 mJy, respectively. The central region is relatively radio-loud and has flux 47.5 mJy at 1.4 GHz. We have not found any optical counterpart for this exotic radio source. The source looks like a point source from the other survey, like WENSS at 325 MHz and TGSS at 150 MHz.

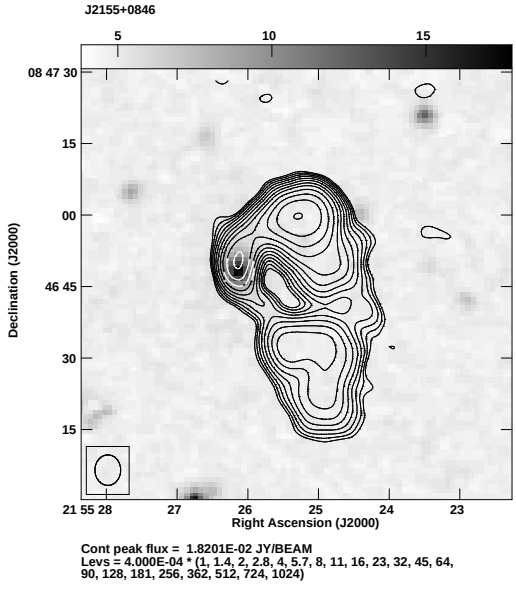

Figure 6.9: FIRST image of the candidate J2155+0846 miscellaneous radio source (contours) overlaid on the DSS2 red image (grayscale). The contours are drawn from $\sim 3\sigma$ ($\geq 3.0 \times 10^{-4}$ Jy) to ensure a reliable structure. The contours are increased by factors of $\sqrt{2}$.

15. **J2155+0846:**

The bent upper jet of the object J2155+0846, with a straight lower jet, yields the whole source a mirror image of question mark ('?') like shape. The upper bent jet is brighter than the lower straight one. RM J215526.2+08464
8.4 (Rykoff et al.(2014)), a galaxy cluster, is associated with the source. In the TGSS survey, a point-like structure is detected, while there is no data found in WENSS.

6.3 Discussion and Conclusion

The main objective of this study is to find radio sources that are unique in morphology. Morphology of these sources is somehow different from the known class and subclass of radio sources like FR-I, FR-II double-lobed radio source, head-tail radio source, winged radio source, HYMORS and DDRG. A symmetric search of 95,243 sources from the FIRST catalog, a sample of fifteen sources is selected as the MRG candidates. We have enlisted the corresponding optical counterpart from SDSS and also check the morphology of the selected fifteen candidates with TGSS

and WISE. As the resolution of the two surveys mentioned above is poorer than FIRST, the MRGs are unresolved and look like point source for most cases.

The spectral index (α) is a measure of the radiative flux density (S) on frequency (ν). Observationally, it is noted that radio sources follow a gaussian distribution (dispersion ± 0.11) with the mean spectral index have values in between – 0.63 to – 0.89 (Williams & Bridle(1967)). Later, the spectral index range for extended radio source is redefined as $-1.8 < \alpha < -0.6$ (McGee & Newton(1972), McGee et al.(1976), Ennis et al.(1982), Milne et al.(1980)). A relative deep study shows $-1.3 < \alpha < -0.5$ with concentraion at the value $- - 0.8$[3]. The α_{150}^{1400} for the MRGs are estimated in Table 6.1 and found that it varies between – 0.60 and – 0.95. This range implies that α of our MRG candidates falls nicely in the defined range of typical radio galaxies. We also estimated the radio luminosity $\sim (10^{41} - 10^{43})$ erg/s and this is also typical for a radio source.

The mechanism behind such unique structures of the radio sources should be different and not clear to us. We can conclude the following points as the probable reasons behind such miscellaneous morphology:

— For a radio source, its morphology depends on the orientation and structure of the jet. The jets ejected from the central core (AGN) need not be symmetric. There may be differences in shape, size, luminosity and sometimes in the composition also.

— The environment on both sides of the central core (AGN) within which the jets propagate may be different. The discrepancy on the two side affects the propagation of the jets in two different ways.

— Through the process of propagation, the jets encounter several interactions with the Inter Galactic Medium (IGM) and (/or) Inter Cluster Medium (ICM). The interacting ICM or IGM are not identical, so the interactions for each jet are different, causing different morphology.

— Along with these, we may also include the black flow of plasma, the reorientation of jets, the spin-flip, the merging of two binary sources, the presence of massive cluster – as the probable reasons. Any of these above-listed reasons or any combination of the reasons may cause such unusual miscellaneous radio morphology. Further multi-frequency observations are needed to explain these morphologies.

The search of these miscellaneous sources may lead to new insights into radio galaxy evolution and interactions with cluster environments. In this regard, we have also search a similar kind of search for such sources from LOFAR Two Metre Sky Survey first data release (LoTSS DR1), presented in the next chapter.

[3]https://ned.ipac.caltech.edu/level5/Sept04/Kellermann2/Kellermann1_3.html

Chapter 7

Miscellaneous Radio Galaxies from LOFAR survey

The miscellaneous radio galaxies (MRGs) are the another new type of radio galaxies which are different from known types of radio galaxies . MRGs are very unique due to their peculiar morphological radio structure. The details of the MRGs are discussed in introductin section. Using the LOFAR Two Metre Sky Survey (LoTSS DR1) data, we report four new MRGs through a visual identification process. Here, we go through their morphological structure, visual variations, and characteristics that set them apart from other subclasses of radio galaxy. We compare their morphological structure to that of other widely used sky surveys, including the Westerbork Northern Sky Survey (WENSS) at 325 MHz (Becker et al.(1995)), the TIFR GMRT Sky Survey alternative data release 1 (TGSS ADR 1) at 150 MHz (Intema et al.(2017)), the NRAO Very Large Array (VLA) Sky Survey (NVSS) at 1.4 GHz (Condon et al.(1998)), and the VLA Faint Images of the Radio Sky at Twenty-Centimeters (VLA FIRST) Survey at 1.4 GHz (Becker et al.(1995)). We also study the presence and association known clusters which are located within 1 Mpc radius of the core of MRG.

7.1 METHODOLOGY

A total of 325,694 radio galaxies are cataloged in preliminary data release of LOFAR Two-metre Sky Survey (LoTSS DR1). The sky coverage of LoTSS is 424 square degree and the operating frequency is 144 MHz (Shimwell et al.(2019)). The angular resolution of the images is $6''$ and the positional accuracy is within $0.2''$ (Shimwell et al.(2019)). LOFAR has a median sensitivity of $S_{144MHz} = 71\ \mu Jy$ beam^{-1} and the point-source completeness is 90% at an integrated flux density of 0.45 mJy (Shimwell et al.(2019)). More details about LoTSS DR1 are mension in chapter 1.

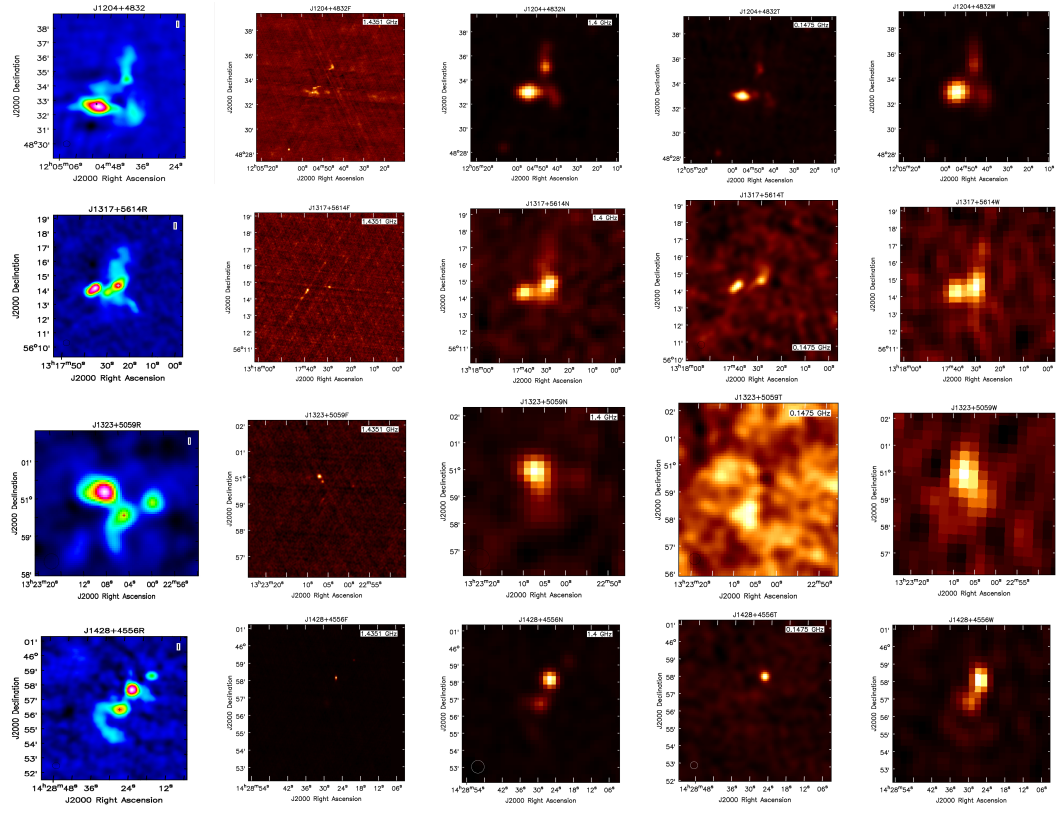

Figure 7.1: A comparison between LoTSS DR1, FIRST, NVSS, TGSS and WENSS images of four miscellaneous radio galaxies. The upper panel is the radio cutout images of MRG J1204+4832. From left to right, the radio images are from LoTSS DR1, FIRST, NVSS, TGSS and WENSS surveys, respectively for each panel. The second upper panel is the radio images of J1317+5614 in different surveys. In the third panel, radio iamges of J1323+5059 are shown. In the lower panel, the radio images of J1428+4556 are shown. From these figures, It is seen that the morphology of the MRG sources are prominent in LOFAR cutout due to its high resolution.

The selection criterion of MRGs are same as bent-tail from LoTSS. the details of selection criterion is discussed in chapter 4. First, we separate those source whose angular size greater or equal to 12″. Then visually inspect each shortlisted sources. We consider those candidate as miscellaneous whose morphological structure is different from known radio morphology like BT, XRG, ZRG, DDRG and HYMORS in LoTSS frequency.

Here, only the LoTSS DR1 data are used to determine the MRGs. It is essential to review the relevant source images in various surveys in order to study source morphology at different frequencies. Regardless of the source's morphology in the FIRST, NVSS, TGSS, or WENSS data, no sources are excluded.

7.1.1 Identification of optical counterpart

A common location for an optical galaxy, sometimes referred to as the optical host galaxy, is near the centre of a radio source. The specific optical host galaxy that corresponds to the radio source is the optical counterpart. The optical galaxy is selected as the optical counterpart by our eye inspection based on the relative position in the radio map at the core region. The optical counterparts are identified from the Sloan Digital Sky Survey (SDSS) data catalog,(Gunn et al.(2006)). We make use of SDSS data from (Alam et al.(2015)) of data release 12 (DR12). By looking through the optical galaxy close to the central core, the optical counterpart is found. Images captured by the SDSS-i band are utilised to identify optical counterparts. For infrared counterpart, Wide-field Infrared Survey Explorer All-Sky (WISEA) and Two Micron All Sky Survey (2MASS) infrared surveys are used.

7.1.2 Crosscheck with other radio surveys

We also study these MRG sources in the FIRST, NVSS, TGSS, and WENSS surveys in order to analyse and compare the morphologies for our MRG candidates. The coverage area of the FIRST survey is 10,575 square degrees in the north and south Galactic caps near 1.4 GHz (White et al.(1996)). The typical rms and angular resolution of FIRST survey are 0.15 mJy and 5″, respectively (Becker et al.(1995).) The NRAO Very Large Array (VLA) Sky Survey (NVSS) has an rms of ∼0.45 mJy and an angular resolution of 45″ (Condon et al.(1998)). At VLA-D configuration, the NVSS survey has the largest angular scale of 970 arcsec. The sky coverage of TGSS ADR1 is 36,900 square degree and a frequency 147.5 MHz. This survey has a typical rms and angular resolution of 3.5 mJy and 25″, respectively (Intema et al.(2017)). The TGSS ADR1 has sky coverage of 36,900 square degree and a frequency 147.5 MHz. This survey has a typical rms and angular resolution of 3.5 mJy and 25″ respectively Intema et al.(2017). While at

Table 7.1: Candidates of Miscellaneous Radio Galaxies from LoTSS.
Here, we list our four identified MRGs from LoTSS DR 1. The columns (3) and (4) are Right Ascension (J2000.0) and Declination (J2000.0), which indicate the probable centre of the host galaxies. Column (5) is position Reference, we have mentioned the catalog name from where the optical counterpart was found. The redshift (z) is presented in column 6. In colums (7) and (8), we list the measured flux densities at 144 MHz (LoTSS) and 1400 MHz (NVSS) in mJy, respectively. Column (9) represent two-point spectral index (α_{144}^{1400}) between 144 MHz and 1400 MHz. In columns (10) and (11) we have calculated radio luminosity (L) and power (P) of the sources with known redshift in erg/sec and W/Hz respectively. Column (12) is the other catalog column, where the source is already known in other literature.

Sl. No.	Name	R.A. (J2000.0)	Decl. (J2000.0)	Ref.	z	F_{144} (mJy)	F_{1400} (mJy)	α_{144}^{1400}	L (erg/s) ($\times 10^{41}$)	P (W/Hz) ($\times 10^{25}$)	Oth Cat
1	J1204+4832	12 04 55.02	+48 32 56.9	SDSS	0.0656	2956.3	118.1	–1.42	3.57	3.45	NVSS
2	J1317+5614	13 17 29.13	+56 14 43.1	SDSS	0.1076	368.8	12.7	–1.47	1.33	1.25	NVSS
3	J1323+5059	13 23 05.08	+50 59 11.5	SDSS	0.3395	131.2	13.4	–1.02	6.94	5.41	—
4	J1428+4556	14 28 28.98	+45 56 44.1	SDSS	0.4162	312.6	28.4	–1.06	25.39	21.17	NVSS, B3

References: (I) NRAO VLA Sky Survey (NVSS): Condon et al.(1998); (II) Sloan Digital Sky Survey (SDSS): Fan et al.(1999), Tumlinson et al.(2013); (III) Third Bologna Catalog of radio sources (B3): Ficarra et al.(1985);

625 MHz the Westerbork Northern Sky Survey (WENSS) has the resolution and rms value as 54″ and ∼18 mJy (5 σ_{rms}) respectively (Rengelink et al.(1997)). While the resolution and rms value of the Westerbork Northern Sky Survey (WENSS) at 625 MHz are 54 arcsec and 18 mJy (5 σ_{rms}), respectively (Rengelink et al.(1997)).

7.2 RESULT

From a visual examination of the LoTSS DR1 database, we present here four miscellaneous radio galaxies. These sources differ in their morphology from well-known features like "Winged" radio galaxies, Bent-tail (BT) radio galaxies, Hybride Morphology (HYMORS) and Double-Double radio galaxies (DDRGs). They are classified as miscellaneous since none of the known sub-classes match the orientations of their jets. In this study, we describe these new MRGs' different properties, including their morphological structure, external appearance, and general nature.

The high frequency (1400 MHz) NVSS and low frequency (144 MHz) LoTSS flux densities are used to compute the two-point spectral indices (α_{1400}^{144}) for MRGs. The task "tvstat" in the Astronomical Image Processing System (AIPS)[1] is used to calculate the intregated flux density values of MRGs (Greisen(1998)). We calculate the spectral index (α_{1400}^{144}) by using the equation $S_\nu \propto \nu^\alpha$ where S_ν is the radiative flux density at a given frequency ν. We calculate the spectral index (α_{1400}^{144}) for all MRGs, which are mentioned in column 9 of Table 7.1

We calculate the radio luminosity (L_{rad}) of each MRGs using the following equation O'Dea & Owen(1987).

[1]http://www.aips.nrao.edu/index.shtml

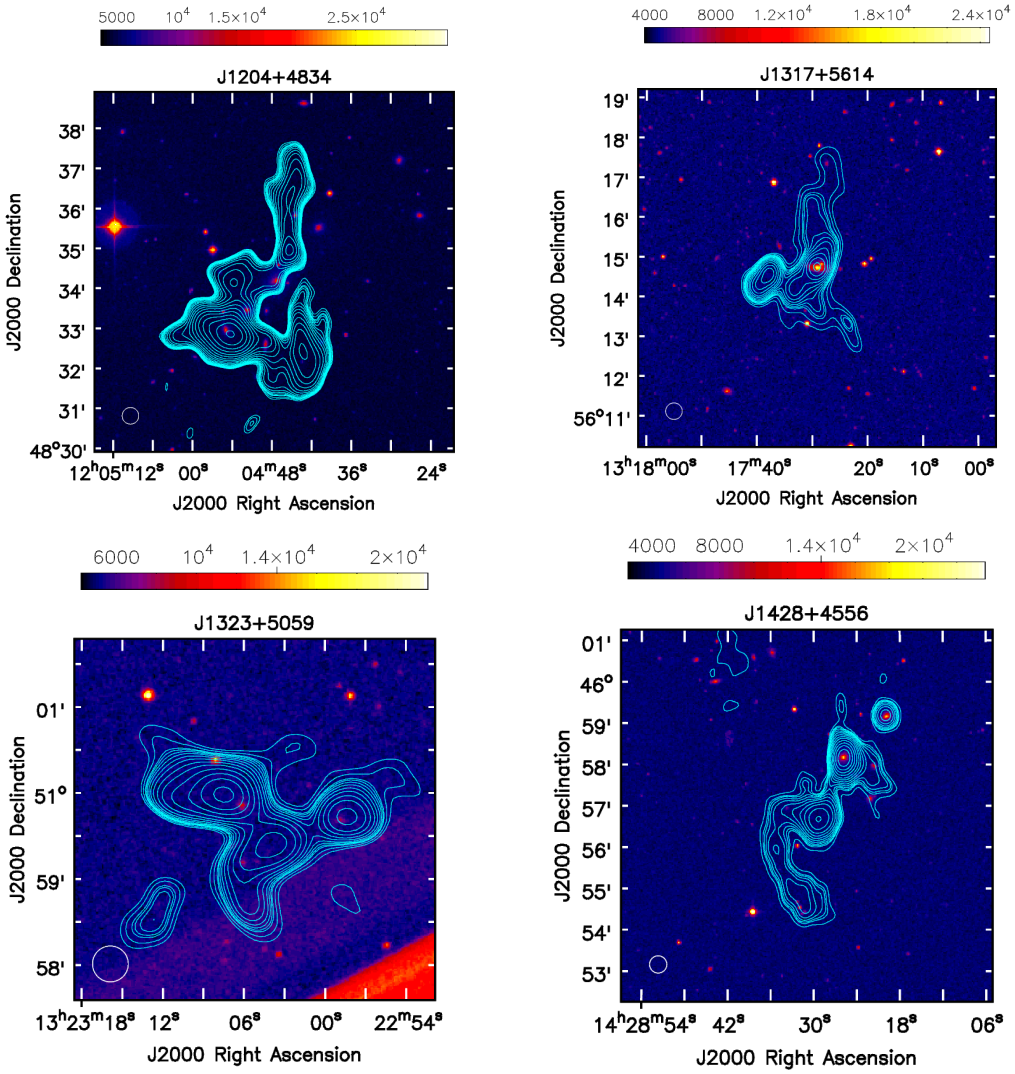

Figure 7.2: LoTSS radio images with resolution 6″ of miscellaneous radio galaxies (white contours) overlaid on the optical SDSS i-band images. The level of contours are $3 \times \sigma$, where σ denotes local RMS noise. The contour levels are increased by factors of $\sqrt{2}$.

$$L_{rad} = 1.2 \times 10^{27} D^2_{Mpc} S_0 \nu_0^{-\alpha} (1+z)^{-(1+\alpha)} \times (\nu_u^{(1+\alpha)} - \nu_l^{(1+\alpha)})(1+\alpha)^{-1} erg/s \quad (7\text{-}1)$$

where D_{Mpc} is luminosity distance to the source (Mpc), S_0 is the flux density (Jy) at a given frequency ν_0 (Hz), z is the red-shift of the radio galaxy, α is the spectral index and ν_u (Hz) and ν_l (Hz) are the upper and lower cut-off frequencies. In our calculation, we assume the upper and lower cutoff frequencies as 100 GHz and 10 MHz respectively. We calculate the radio luminosity (L_{rad}) for all MRGs which are mentioned in column 10 of Table 7.1. The radio power is calculated using the following formula, given by Donoso et al.(2009)

$$P_\nu = 4\pi D_L^2 S_\nu (1+z)^{(\alpha-1)} \quad (7\text{-}2)$$

where D_L is the luminosity distance, S_ν is the radio flux density at a frequency ν, $(1+z)^{(\alpha-1)}$ is the standard k-correction used in radio astronomy. The estimated power is presented in column (11) of Table 7.1.

7.2.1 Notes on individual sources

1. **J1204+4832:** A "triangular" shape is observed on the source's overall contour radio map. The radio lobes are individually extended in three directions: south, north-west (NW), and east. The LOFAR image shows that the source's centre has a radio null zone since there is no radio emission from the central region. The radio source's optical counterpart is found to be the optical galaxy SDSS J122055.01+483256.8 (Fan et al.(1999)). The relative infrared (IR) counterparts are WISEA J120455.03+483257.3 (Chung et al.(2011))and 2MASS J12045500+4832568 (Skrutskie et al.(2006)). The spectroscopic redshift of radio source is 0.06565 ± 0.00019 with a magnitude (g filter) value 16.5 (Alam et al.(2015)). The galaxy cluster WHL J120447.4+483412, which is located at 1.772 arcmin from the source's centre, may be associated to the radio source (Wen et al.(2010)). 7 arcmin is the angular size of the MRG. Note that the task 'tvdist' in AIPS is used to measure the angular size. AIPS task "tvdist" calculates the angular distance between two sky locations. To complete the task, one must select two points from which angular distance can be calculated. Here, we select those two locations along with the reliable radio emission's greatest angular extent. The MRG's predicted linear size is 628 kpc. In the imaging field of the FIRST survey at 1.4 GHz, we detected no valid radio emission. The radio image of WENSS at 325 MHz has a triangular form that is fairly similar to the LoTSS image. The core region is not as visible in the corresponding WENSS radio image as it is observed in the LoTSS data. The triangle shape with a rather bright lobe facing east is visible in the radio

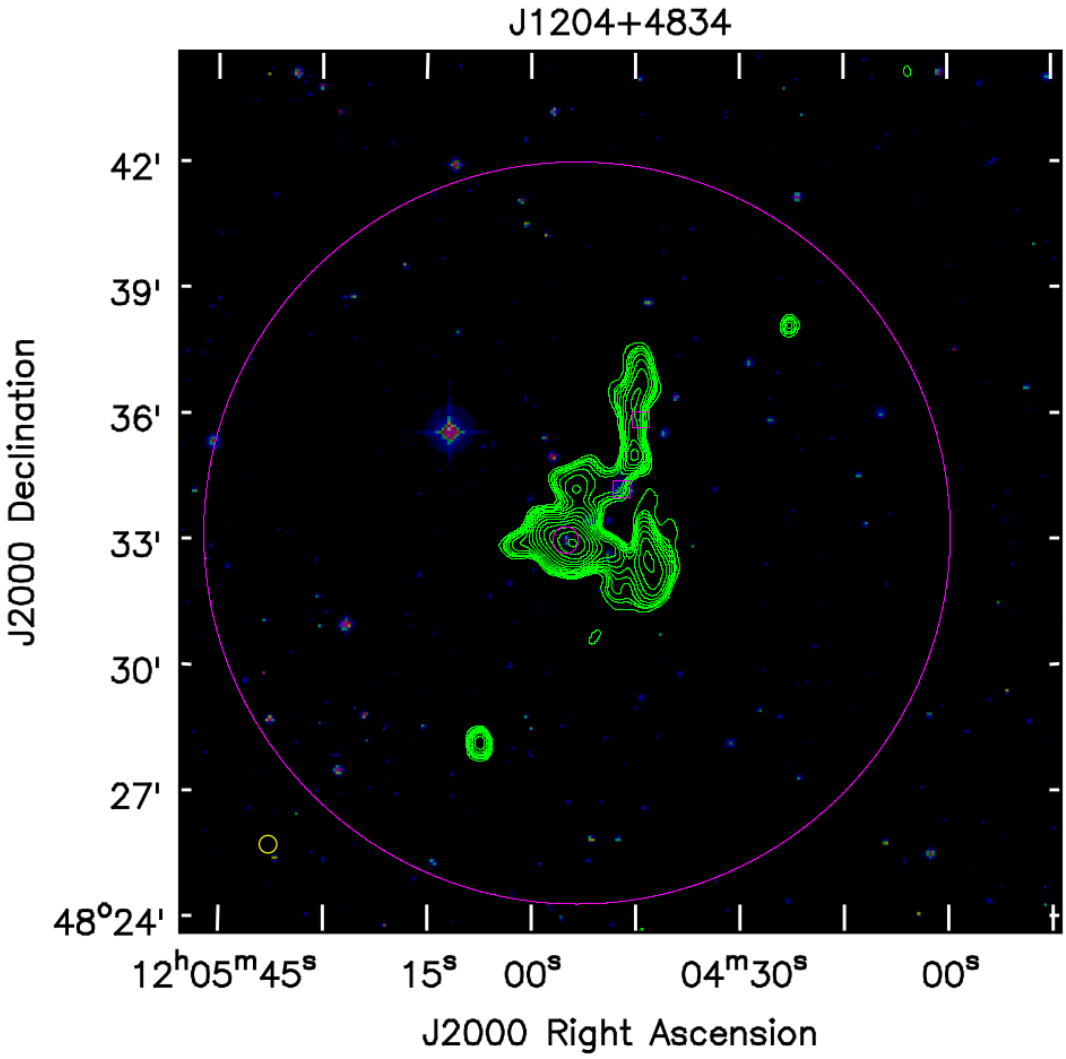

Figure 7.3: The above figure show the presence of nearby known galaxy clusters for the identified miscellaneous radio sources J1204+4832. LoTSS radio image of miscellaneous radio galaxies overlaid on the optical SDSS i-band images. The circles denote optical counterparts of the sources and the boxes indicate associated clusters of the sources with in 1 Mpc.

contour image. In comparison to the WENSS data, the radio image is extremely noticeable in the NVSS data at 1.4 GHz. Although the centre loop-like structure is not apparent, the NVSS picture reveals three lobes pointing south, northwest, and east. The NVSS image's NW edge is observed to be twisted at the edge towards the direction of the north. The 150 MHz TGSS radio map displays a picture that is quite similar to the NVSS image.

2. **J1317+5614:**

The source has an asymmetric lobe, a pair of primary lobes, and two pairs of secondary lobes. The radio source's secondary lobes are pointed in the north-south direction, while the primary lobes are oriented in east-west. The southwest (SW) direction is where the attractive asymmetric lobe is situated. All of the lobes are ejected from the centre, according to the LoTSS radio map. Although the source first seems to be a radio source with "wings," the presence of the asymmetric lobe gives the source an unique form and makes it a possibility for miscellaneous radio sources. The source's optical counterpart is the optical galaxy SDSS J131729.13+561443.1 (Fan et al.(1999)). The equivalent IR counterparts of the sources are 2MASS J13172914+5614434 (Skrutskie et al.(2006)) and WISEA J131729.09+561443.3 (Chung et al.(2011)). The source has a spectroscopic redshift of 0.107570 ± 0.000151 with a magnitude of 16.2 in the g filter (Alam et al.(2015)). The source has angular size of 6 arcmin which crossponds to linear size 908 kpc. The MRG is a Giant Radio Galaxy (GRG) candidate since it has a linear length larger than 700 kpc (Willis et al.(1974), Dabhade et al.(2020)). An extended (from north to south) emission is discovered in WENSS, when a little spot of the radio emission is observed in the FIRST picture. Although the lobes are not as symmetrical as in the LoTSS data, the radio picture from WENSS also shows a lobe extension towards the east. However, according to the NVSS data, the source is an extended "C"-type source with lobe expansion to the south and east (Sasmal et al.(2022)). But, the TGSS map did not contain any such extended emission. The TGSS picture displays two neighbouring radio emission areas, the east of which is linear and the west of which has a minute curved structure pointing towards north.

3. **J1323+5059:**

An overall "triangular" form is seen in the radio picture. In the projected plane, the three lobes are rather equally pointed in three different directions: west, north-east (NE), and south-east (SE). The SE lobe's edge is twisted in a southerly direction. Additionally, a little lobe extension in the east that connects to the SE lobe is seen. SDSS J132306.24+505950.8 is the source's optical counterpart (Fan et al.(1999)). The IR counterparts of the source are identified to be 2MASS J13230505+5059117 (Skrutskie et al.(2006)) and WISEA J132305.10+505911.6

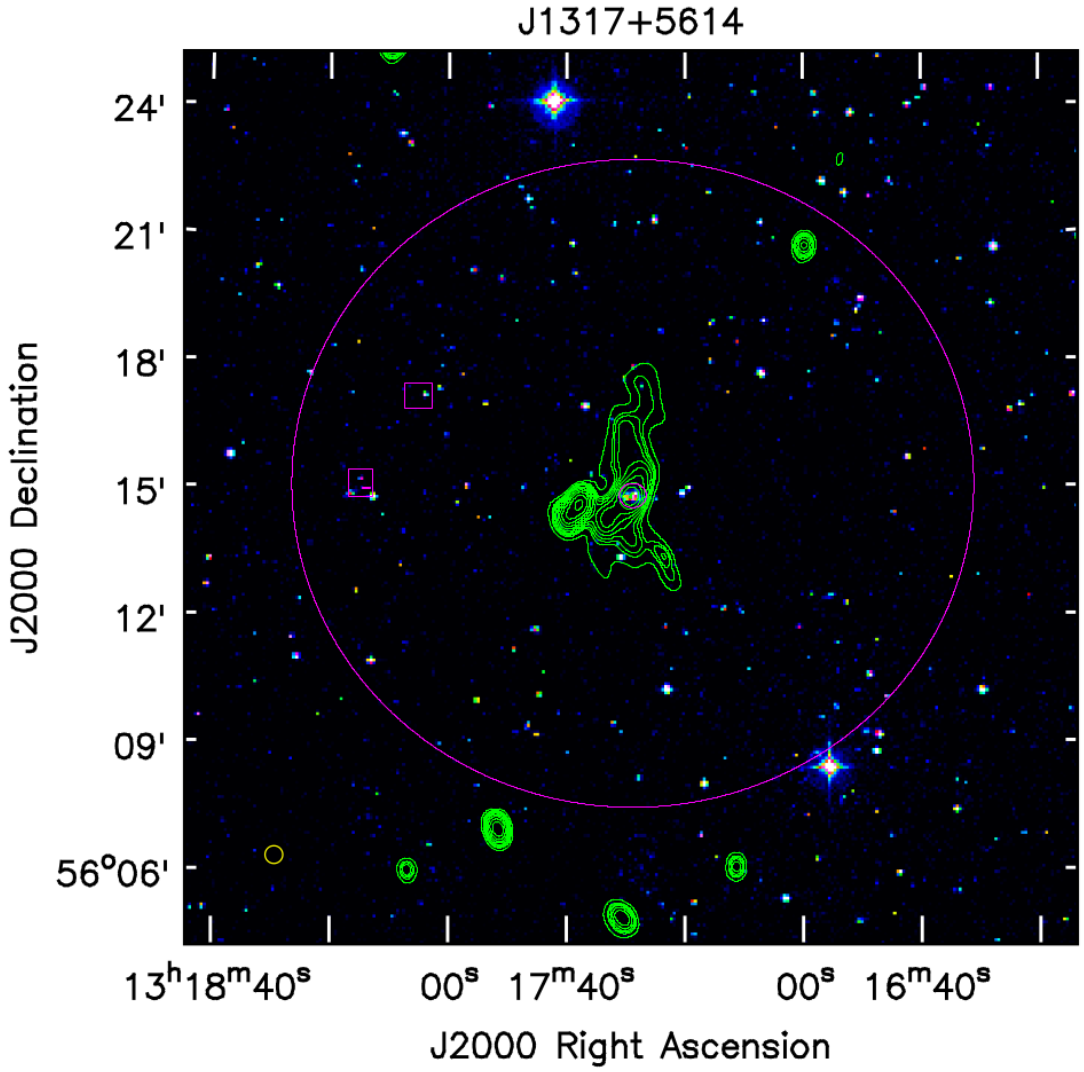

Figure 7.4: The above figures show the presence of nearby known galaxy clusters for the identified miscellaneous radio sources J1317+5614. LoTSS radio image of miscellaneous radio galaxies overlaid on the optical SDSS i-band images. The circles denote optical counterparts of the sources and the boxes indicate associated clusters of the sources with in 1 Mpc.

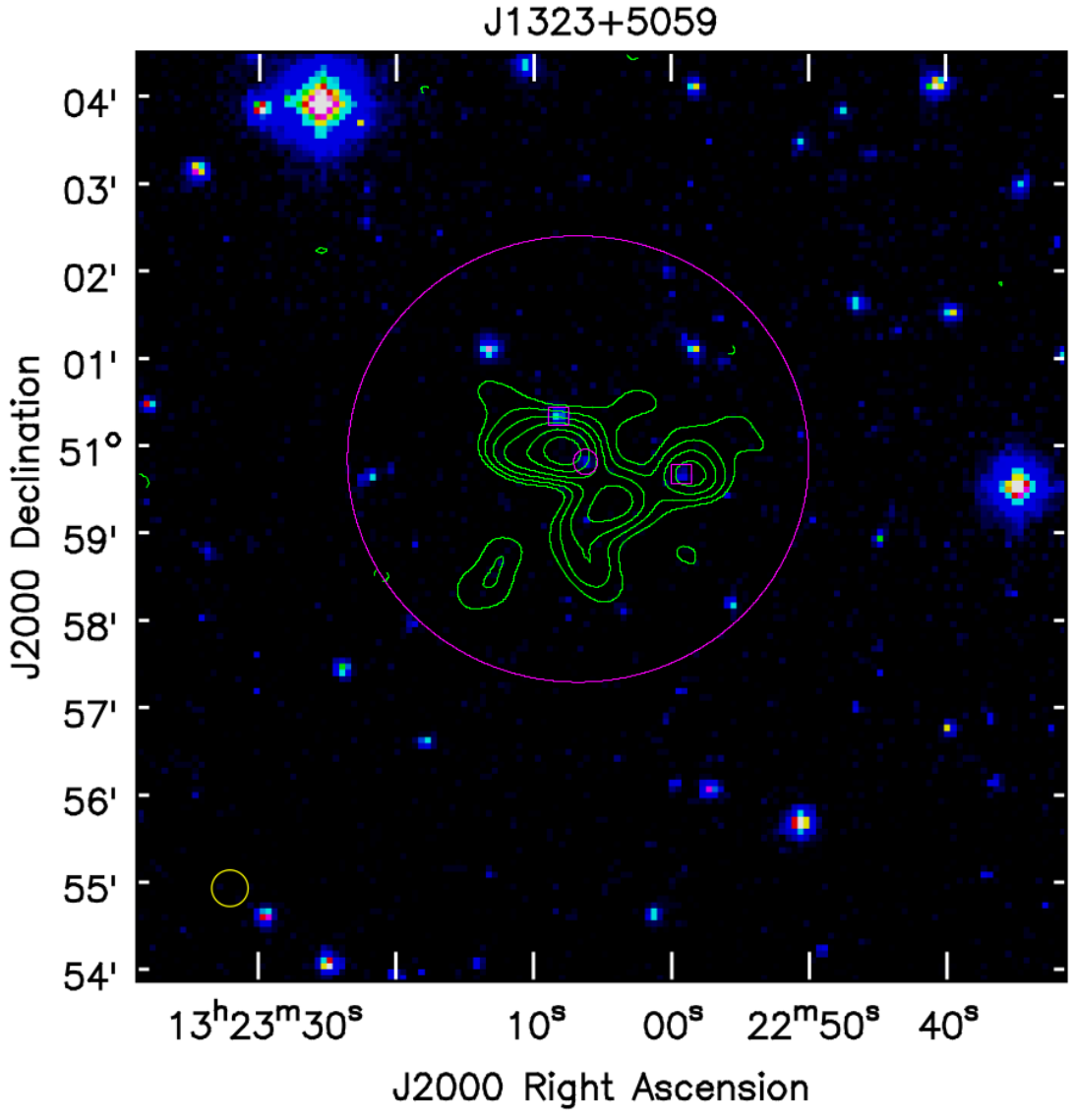

Figure 7.5: The above figures show the presence of nearby known galaxy clusters for the identified miscellaneous radio sources J1323+5059. LoTSS radio image of miscellaneous radio galaxies overlaid on the optical SDSS i-band images. The circles denote optical counterparts of the sources and the boxes indicate associated clusters of the sources with in 1 Mpc.

(Chung et al.(2011)). It is found that the source has a redshift with the value 0.33955 ± 0.00008 Al15. The galaxy cluster WHL J132306.3+505951, which is situated 0.686 arcmin away from its optical counterpart, may be associated with the radio source (Wen et al.(2010)). The source is approximately 5 arcmin in angular dimension. When compared to the WENSS, which exhibits an expanded radio emission, the FIRST image exhibits no radio emission at 1.4 GHz. No miscellaneous nature is seen in WENSS at 325 MHz. A diffused radio emission from north to south with a bit towards the west is only found in WENSS image. A point-like object with a little lobe stretched westward may be seen in the NVSS picture of this radio source. A diffuse radio emission area is visible in the source direction on the TGSS picture at 150 MHz. No appropriate morphology is seen in TGSS.

4. **J1428+4556:**

The radio source's principal alignment runs from northwest to southeast. According to the radio picture, the source has three lobes pointing in the principal direction. The centre lobe, which holds the optical counterpart, is attached to a round, point-like component of the lobe that faces northwest. There is an extension of the core region's lobe to the west. The bottom lobe, which faces southeast, is the one that is the longest. The lobe arced and looked a radio source in the shape of a "C" (Sasmal et al.(2022)). The source is consider as the miscellaneous radio source due to the direction and extent of these three lobes. The optical equivalent of the radio source is discovered to be SDSS J142826.95+455641.4 (Fan et al.(1999)). The corresponding IR counterpart for this radio source is WISEA J142826.94+455641.3 (Chung et al.(2011)). The source has a spectroscopic redshift of 0.416175 ± 0.000101 with a magnitude value 21.4 (g filter) (Alam et al.(2015)). The angular size of of the source is 5.7 arcmin, which corresponds to a projected linear size of 3.972 Mpc. The linear size indicates the candidature of the sources are a giant radio galaxy (GRG). The FIRST data shows a point like emission at 1.4 GHz frequency. The source has an extended emission similar to the LOFAR image in WENSS at 325 MHz. The 'C'-shape at the lower part of the radio image also found in WENSS. Through WENSS, the source is not resolved enough like LoTSS DR1. The bottom arched area is not visible in the NVSS data. The unique morphology is also missed due to the lack of resolution. The source looks like a double-double radio source (Schoenmakers et al.(2000)). In the TGSS map at 150 MHz, the source seems to be a point source.

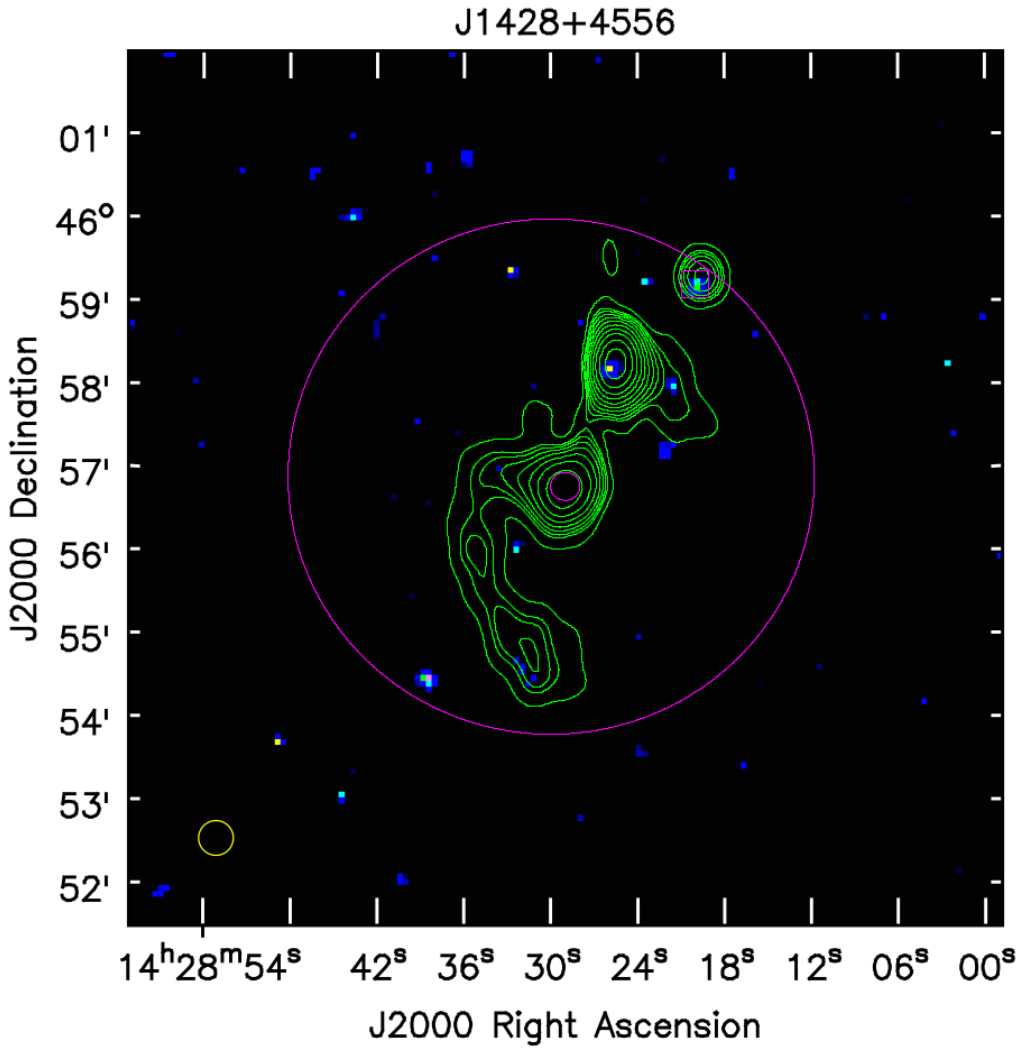

Figure 7.6: The above figures show the presence of nearby known galaxy clusters for the identified miscellaneous radio sources J1428+4556. LoTSS radio image of miscellaneous radio galaxies overlaid on the optical SDSS i-band images. The circles denote optical counterparts of the sources and the boxes indicate associated clusters of the sources with in 1 Mpc.

Table 7.2: List of associated galaxy clusters of the Miscellaneous Radio Sources.

MRG Candidate	Nearby Galaxy Cluster	s_θ (arcmin)	s_l (kpc)	z	z_{flag}	z_{ref}	Cross-identification
J1204+4832	WHL J120447.4+483412	1.772	148.01	0.0655	PHOT	Yoon et al.(2008)	[YSS2008] 166
	MSPM 01799	3.365	281.07	0.065	—	Smith et al.(2012)	—
J1317+5614	GMBCG J199.54965+56.27219	6.156	753.56	0.452	PHOT	Hao et al.(2010)	—
	WHL J131818.0+561527	6.827	836.92	0.4526	PHOT	Wen et al.(2010)	—
J1323+5059	WHL J132306.3+505951	0.006	1.80	0.3629	PHOT	Wen & Han(2015)	—
	GMBCG J200.74564+50.99458	0.398	119.63	0.360	PHOT	Hao et al.(2010)	—
J1428+4556	SDSS-C4-DR3 3131	2.893	256.40	0.075	—	Von et al.(2007)	[YSS2008] 194

References: (I) WHL (Wen+Han+Liu) (Wen et al.(2010)), (II) [YSS2008] (Yoon+Schawinski+Sheen) (Yoon et al.(2008)), (III) MSPM (MultiScale Probability Mapping) (Smith et al.(2012)), (IV) NSC (Northern Sky optical Cluster) (Gal et al.(2003)), (V) GMBCG (Gaussian Mixture Brightest Cluster Galaxy) (Hao et al.(2010)), (VI) SDSS-C4-DR3 (Sloan Digital Sky Survey C4 Cluster Catalog (based on Data Release 3)) Von et al.(2007), (VII) NSCS (Northern Sky optical Cluster Survey) (Gal et al.(2003)).

7.2.2 The presence of Nearby galaxy clusters

Table 7.2 lists and describes the galaxy clusters that are closest to the MRG sources. Here, we define a source's nearby region as a hypothetical spherical zone with a radius of 1 Mpc that surrounds the relevant source. At each source's redshift, we employed a search radius of 1 Mpc. For each of the MRGs, we place an optical host galaxy in the centre of a circle with a radius of 1 Mpc in Figures 7.3,7.4,7.5,7.6. In Figures 7.3,7.4,7.5,7.6 the locations of the discovered neighbouring galaxy clusters are shown and denoted by square boxes. The position of the optical source is shown by the circles in mensioned figures. The diameter is chosen based on the actual size of the sources (we maintain the diameter greater than the source size). The names of the galaxy clusters are listed in column (2) of Table 7.2. The results of our calculations for the angular and linear separations between the MRG centre and cluster are shown in columns (3) and (4), respectively. The galaxy cluster's redshift is mentioned in column (5) along with the redshift flag (z_{flag}) and a redshift reference in columns (6) and (7). z_{flag} in this context refers to the redshifts' quality, i.e., whether they are photometric (PHOT), spectroscopic (SPEC), or estimated. For the galaxy cluster shown in column (2), we give additional cross-identifications from the literature in column (8).

Except for the source J1317+5614, we identify at least one galaxy cluster for each MRG that is inside the source's physical limits. When the source has an angular size of 6 arcmin, the closest galaxy cluster, GMBCG J199.54965+56.27219 (Hao et al.(2010)), is situated at a distance of 6.156 arcmin. The galaxy cluster WHL J120447.4+483412 (Wen & Han(2015)) is situated at a distance of 1.772 arcmins from the optical centre of the MRG for the source J1204+4832. Calculations reveal a linear separation of 148.01 kpc. The closest galaxy cluster, WHL J132306.3+505951 (Wen & Han(2015)) is likewise situated within one arcmin (0.686) of the source,s (J1323+5059) optical centre. SDSS-C4-DR3 3131 (Von et al.(2007)), which is situated at an angular distance of 2.893 arcmin, is the nearest galaxy cluster to the MRG J1428+4556.Galaxy clusters are seen for the

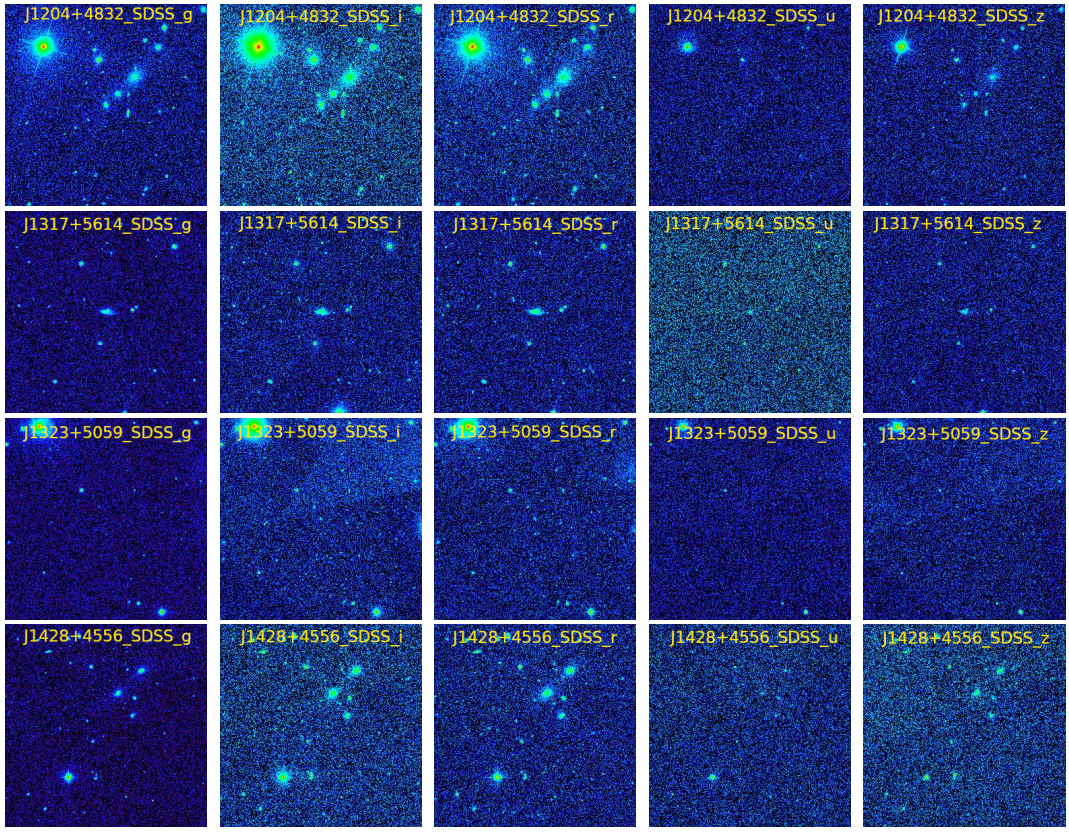

Figure 7.7: The images show the SDSS optical counterparts of our four MRGs in different bands. Here, we show five optical band images i.e. g, i, r, u, and z for each source. The optical pictures in the various bands did not reveal any irregularities. They are similar to the optical counterparts of conventional radio galaxies.

four MRGs in the designated neighbouring locations, suggesting that they may be related to the MRGs.

Where applicable, we additionally make note of a few fundamental cluster parameters. We show four parameters from the cluster catalog provided by Wen & Han(2015), such as: r_{500}, R_{L*500}, M_{500} and N_{500}. r_{500} is the cluster radius from optical luminosity, R_{L*500} is the cluster richness, M_{500} is the cluster mass within r_{500} and N_{500} is the number of all member galaxies within r_{500}. These values are available for the three clusters WHL J120447.4+483412, J120503.3+482142, J132306.3+505951. The values of r_{500}, R_{L*500}, M_{500} and N_{500} fo the cluster WHL J120447.4+483412 are 0.70, 15.53, 0.82 and 9 respectively, when M_{500} is presented in the unit of $\times 10^{14} M_{\odot}$. For J120503.3+482142, the corresponding values are 0.64, 15.65, 0.83, and 8. The corresponding parameter values for the cluster WHL J132236.6+505611 are 0.61, 18.67, 1.01, and 7, whereas for WHL J132211.8+505430 they are 0.57, 7.41, 0.37, and 5. The three clusters WHL J131818.0+561527, WHL J131722.2+560448, and WHL J132224.6+505656 have respective cluster richness factors of 7.12, 8.89, and 9.96 based on Wen & Han(2015).

Finding the connection between MRGs and their associated galaxy clusters is motivated by a variety of factors: (i) determining the specific AGN feedback modes, (ii) triggering of AGN activity, (iii) determining the physical condition of the radio jet, (iv) by employing these sources to follow the galaxy cluster at a high redshift, (v) evaluating model of source dynamics and environmental effects. We are looking for any association between MRGs and associated clusters because MRGs are a novel class of radio sources. For each MRG, we have discovered that at least one cluster is related to a radius of 1 Mpc. Since our sample size is too little to draw any conclusions from the aforementioned activities.We must examine a large number of MRG samples in order to draw any conclusions.

7.3 DISCUSSION AND CONCLUSION

Here, we list the radio sources which has a particular radio morphology using LoTSS DR1 at 144 MHz. Each source has a distinct morphology that differs from other known typical radio galaxies with structures like FR-I, FR-II double-lobed radio galaxies, Head-Tail radio galaxies, winged radio sources, HYMORS, and DDRG. We choose four radio sources as possible miscellaneous radio source after manually and visually searching among 18,500 sources from the LoTSS DR1. We also compared the morphology of MRGs with FIRST, NVSS, TGSS and WENSS as well as their correlative visual counterpart from SDSS.

The spectral index (α) is a measure of the radiative flux density (S) at a

frequency (ν). Observationally, it is noted that radio sources follow a gaussian distribution (dispersion ± 0.11) with the mean spectral index have the values in between – 0.63 to – 0.89 Williams & Bridle(1967). Later, the spectral index range for extended radio source is redefined as $-1.8 < \alpha < -0.6$ McGee & Newton(1972), McGee et al.(1976), Ennis et al.(1982), Milne et al.(1980). A relative deep study shows $-1.3 < \alpha < -0.5$ with concentration at the value – 0.8[2]. The spectral index (α_{144}^{1400}) for the MRGs are estimated in Table 7.1 and found that it varies between – 1.02 and – 1.47. This range implies that α of our MRG candidates fall well in the defined range of typical radio galaxies. The MRG, J1317+5614 has the lowest spectral index (α_{144}^{1400}) value –1.47 and J1323+5059 has the highest spectral index (α_{144}^{1400}) value –1.02.

We estimate the radio luminosity (L_{rad}) of MGRs as mentioned above. J1428+4556 is the most luminous MRG with luminosity $L_{rad} = 2.54 \times 10^{42}$ erg/s and J1317+5614 is the less luminous MRG with luminosity $L_{rad} = 1.33 \times 10^{41}$ erg/s. The luminosity of J1204+4832 is calculated as 3.57×10^{41} erg/s. The mean value of logL for radio sources are calculated by Nilsson et al.(1993) as 41.72 erg/s. For our MRG candidates, four available logL values are 41.55 (J1204+4832), 41.12 (J1317+5614) 41.84 (J1323+5059) and 42.40 (J1428+4556). These logL values reffer that our MRG sources have luminosity values little less than the average luminosities as given by Nilsson et al.(1993). We also calculate the radio power (P) of the MRGs at 144 MHz and found that J1428+4556 has the highest power 2.12×10^{26} W/Hz. The power of J1204+4832, J1317+5614 and J1323+5059 are found as 3.45×10^{25} W/Hz, 1.25×10^{25} W/Hz and 5.41×10^{25} W/Hz respectively. Dabhade et al.(2020) evaluated the average radio power (logP value) for the LOFAR sources as 25.95 log(W/Hz). In our case the logP values are 25.54 (J1204+4832), 25.10 (J1317+5614) and 26.32 (J1428+4556). These values are quite relatable to the value found by Dabhade et al.(2020).

The linear dimensions for the three available sources, J1204+4832, J1317+5614, J1323+5059 and J1428+4556, are 628 kpc, 908 kpc, 2.69 Mpc and 3.97 Mpc, respectively. There is a real possibility of any misidentification because the sources are sufficiently large. It's possible that the sources we took into account are the result of several radio sources. The sources are positioned in the sky in such a way that the radio map of those two or more radio sources seems to be a single source in the projected plane. The several MRG candidates may represent the lobes of various radio emitters, however they were only seen as one source.

The following is a potential explanation for the unusual morphology of radio sources.

[2]https://ned.ipac.caltech.edu/level5/Sept04/Kellermann2/Kellermann1_3.html

(i) The jet structure and alignment affect a source's radio morphology. There is interaction between the jets to the intracluster medium (ICM) or intergalactic medium (IGM), and the jets released from the central core are not always equal. Since the ICM or IGM may differ, the interaction on the opposing jets is not expected to be the same. An asymmetric radio jet structure might result from this. An unusual morphology might result from the asymmetric structure.

(ii) A galaxy passes through a definite number of phases starting from birth as it evolves. The galaxy's structure and morphology change with time in each phase. Since MRGs differ from existing structures, this would suggest that they are in a unique stage or passing through a unique phase of evolution.

(iii) These irregular structure of MRGs may have more than one explanation. The effects of bouncing, plasma backflow, and ram pressure caused by the relatively high-speed motion, together with phenomena such as galaxy merger, shift in spin axis, may combine to produce such unique shape.

The literature lacks more comprehensive information on the MRG sources. As shown in Fig. 7.1, we compare the radio structures for each MRG at FIRST, NVSS, TGSS, and WENSS. Despite the fact that data at those many frequencies is often accessible, the resolution is insufficient to determine the fine miscellaneous structure as shown in LOFAR. The optical host galaxies of these MRGs are shown in Figure 7.3 in a variety of bands, including g, r, I u, and z from SDSS. There are no anomalies in the optical morphology. For each MRG, the optical host galaxies seem normal. We want to perform further observations at various radio wavelengths. Depending on the characteristics of the spectral indices and the break frequency, this will assist in estimating the spectral indices, which provides some significant information about the ages of the sources. We may create a spectral index map based on the source's location. We can also figure out the radiative age of the sources and the magnetic field inside the lobes (Patra et al.(2019)). The sources' deeper morphology will become more apparent with higher resolution observation. This will assist in better understanding of the sources' overall morphology. Along with these a multiwavelength study (optical, infrared, X-ray) for these sources may give more information and the nature of the associated optical and infrared counterpart of the MRGs.Therefore, further multi-frequency observations with better resolution are needed to explain these morphologies of MRGs.

Chapter 8

Summery and Future Prospective

The radio morphology of the sources may become distorted possible due to the relative motion between the host galaxy and the surrounding intracluster medium (ICM) or via interaction with a neighboring galaxy. Common distortions in FR I sources include wide-angle tail (WAT) and narrow- angle tail (NAT) morphologies, which have large and small opening angles, respectively. The classical explanation for the bending of the lobes is the ram pressure exerted by the ICM as a galaxy with a signicant peculiar velocity moves through a cluster (Owen & Rudnick(1976)). In an alternate explanation the ICM is in motion rather than the galaxy, since WATs are often associated with cD galaxies that have small peculiar velocities relative to the immediately surrounding cluster (Burns et al.(1996), Roettiger et al.(1996), Burns et al,(1993)). In this scenario, the ICM is set in motion by the merging of clusters or smaller subclumps ; evidence for this view is found in the alignment of X-ray emission contours with the bending of the lobes (Gomez et al,(1997)). FR II sources may also become distorted; sometimes the distortions appear symmetric and may result from ICM interaction, whereas at other times the sources have an asymmetric appearance most likely caused by interaction with a neighboring galaxy (Rector et al.(1995)).

Galaxy clusters are at the junction between astrophysics and cosmology in that they form the building blocks of cosmological large scale structure and are also the environments where the most massive galaxies form. Their abundance, internal structure and distribution in the Universe carry an imprint of the initial linear density perturbations and the cosmic expansion history. These linear perturbations of the density field are assumed to be Gaussian in nature. This astounding regularity is borne out in the tight scaling relations between cluster properties and cluster mass and the universality of the cluster mass function as well as its bias when expressed as a function of the peak height (v) of the initial Gaussian perturbations of the collapsing objects of any given mass (Kravtsov & Borgani(2012)).

With increasing redshift, optical and X-ray survey techniques for finding galaxy

clusters lose their effectiveness, and a targeted approach is warranted. In particular, radio galaxies can be used as cluster signposts. Deltorn et al,(1997) has identifed clusters around powerful 3C sources at redshifts greater than 1.2, and Deltorn et al,(1997) discovered a cluster of galaxies around 3 CR 184 at z $\sim$ 0.996. Clusters of varying richness have also been seen around the radio galaxies studied by Hill & Lilly(1991) and by Zirbel(1997), among other. However, some kinds of radio galaxies are more often associated with clusters than others and are therefore more efficient tracers of these high-density environments.

8.1 Summary

In this work, it has been shown the searched method of Bent-tail and Miscellaneous radio galaxies from FIRST and FOFAR (LoTSS DR1) surveys and discuss the results. We also study the environment of BT and MRG sample from LoTSS DR1. We reported 799 BT sources and 19 MRG sources from these two surveys. This is the largest sample of BT sources till date. MRGs are first identified by our group and reported in the literature. Some of the radio and optical properties of these sources are discussed here.

First, we presente the visually selected sample of 717 bent-tail sources from the latest data release (2014 December 17) of FIRST survey at 1400 MHz. Our classification revealed that 287 are NATs and 480 are WATs. For NAT and WAT sources the opening angle between the jets are less and greater than 90 degree respectively. Among the BT sources, $\sim$ 37% are FR-I and $\sim$ 44% are FR-II; where FR refers to Fanaroff & Riley(1974) classification scheme: FR-I sources usually have bright radio cores and lobes that fade at the edges, FR-II sources have dim or absent cores, and are brightest at the edges of their lobes. The highest redshift value of WAT as well as BT sample (J1051+0051) is 2.00660 $\pm$ 0.00500 (Croom et al.(2004)). Another high-redshift WAT source is J1250+1133 with redshift z = 1.28500 $\pm$ 0.00000 (Richards et al.(2009)). The spectral index between 150 MHz and 1400 MHz are calculated for these BT sample and found that $\sim$ 75% have steep spectrum.

Second, we presente another sample of 82 BT sources from LoTSS DR1 data set. Among them 10 are NATs and 72 are WAT candidates. Optical counterparts are found for 65 BT sources. Redshift is found for total of 79% of BT sources. Total 60% sources have redshift value of less than 0.5. The highest redshift value of NAT source J1325+5544 is 1.9641, while the WAT source J1344+5553 is the closest one with a redshift value 0.03734. The optical counterparts and redshifts of the radio sources in LoTSS DR1 catalog are estimated by Duncan et al.(2019). Most of the sources shows a steep spectral index between the frequencies of 144

MHz and 1400 MHz.

Third, we study the environment of the LoTSS BT sample. we develop a catalog of known galaxy clusters that are associated with BT sources. We cross matched our BT sample with known cluster catalog of Gaussian Mixture Brightest Cluster Galaxy (CMBCG;Hao et al.(2010)), Wen+Han+Liu (WHL;Wen & Han(2015)), Northern Sky optical Cluster (NSC; Smith et al.(2012)), Abell Clusters of Galaxies (ABELL; Lopes et al.(2004)), Northern Sky optical Cluster Survey (NSCS; Von et al.(2007)), MultiScale Probability Mapping (MSPM; Smith et al.(2012)), Sloan Digital Sky Survey C4 Cluster Catalog (based on Data Release 3) (SDSS–C4–DR3; Von et al.(2007)), RedMapper Cluster (RM; Rozo et al.(2015)), maximum likelihood redshift Brightest Cluster Galaxy (MaxBCG; Koester et al.(2007)), Super-CLuster (SCL; Einasto et al.(2011)), Estrada+Annis+Diehl ([EAD2007] Estrada et al.(2007), Swift X-ray Telescope Cluster Survey (SWXCS; Liu et al.(2015), 400 Square Degree ROSAT PSPC Galaxy Cluster Survey (400d; Vikhlinin et al.(1998)). We found that 43 out of 65 BT sources are associated with known galaxy clusters. We found that 28% of BT sources are associated with galaxy clusters with masses $M \geq 10^{14.5} M_{\odot}$ and 95% of BT sources are associated with galaxy clusters with masses $M \leq 10^{14.5} M_{\odot}$. From this result we conclude that the probability of finding BT galaxies in low mass galaxy clusters is ~ 3.5 times to high mass galaxy clusters.

Forth, we reporte new type of radio sources, Miscellaneous Radio Sources (MRG) from FIRST and LoTSS DR1 respectively. The morphology of this type of sources differs from other known typical radio galaxies with structures like double-lobed radio galaxies, Head-Tail radio galaxies and winged radio sources. By visual inspection, we reported fiften MRG from FIRST survey and four MRG from LoTSS DR1. Some radio and optical properties of these MRG are also discuss here.

8.2 Future Prospective

Future work will be based on expanding the scope of this work. The potential of the sample of radio sources presented here has not been realized. There are several new directions that can be taken with the data, and we outiles the possibilities below.

The LOFAR telescope observes the low frequency emission from the Universe up to $z \sim 2$ and the Jansky Very Large Array (JVLA) will serve a similar purpose at the gigahertz regime. The SKA pathfinders, MeerKAT and ASKAP, when fully operational, will extend these radio studies through better survey speed and sensitivity. The low frequency studies will reveal old electron populations in the cores of galaxy clusters at $z \approx 2$ and in AGN jets, whereas gigahertz frequencies will map

the interactions of jets with ICM plasma and use detailed Faraday rotation observations to reveal the magnetic field structure of the plasma. The low frequency luminosity has been found to correlate with SMBH mass and it has been found that a bigger sample of SMBH mass measurements of low radio frequency galaxies is needed to constrain the correlation. Studying relativistic jets in AGNs is one of the key science goals of the SKA. This field is still subject to active research and has many open questions with respect to the detailed physics of AGN jets. The resolution and sensitivity of the SKA will facilitate the study of AGN jets in great detail up to the epoch or re-ionisation. Agudo et al. (2015) lists some of the outstanding research questions as

• The particle composition of the ejecta plasma at different scales and its evolution along the jet.

• The influence of magnetic fields on jet formation, collimation and how it is maintained over a distance of hundreds of kpc.

• The influence of the jet-IGM feedback on group/cluster evolution.

• The 3-dimensional distribution of jet flow parameters like velocity, magnetic structure and emissivity.

• Why are jets produced efficiently in some cases and not others, and how does blackhole mass and accretion mode relate to jet power?

Understanding the physical nature of these jets will allow the use of BTRSs not only as tracers of clusters and groups at high z but as probes of the ICM density and magnetic structure in the host clusters. The optical and NIR methods of SMBH mass measurement methods at high redshift are essential to probing the last point. The multiwavelength approach is the only viable one for these fundamental jet physics studies.

The increased sensitivity and angular resolution of sub-millimeter ALMA telescope has already extended the distance to galaxies for which the blackhole mass can be measured via molecular gas dynamics in the cores of ETGs. This will increase the statistical sample size of measured blackhole masses and potentially allow for more SMBH masses measured via two or more methods. The next generation of optical and NIR telescopes like the TMT, OWL and E-ELT will achieve the same objective in the optical and NIR regimes. The ability to cross-reference SMBH masses obtained via different methods will improve the modeling and con-

strain uncertainties in the assumptions used in the models.

The ansatz that BTRSs are caused by ram pressure experienced by AGN jets against the IGM will be better constrained when tested against observations of the next generation radio telescopes, particularly the SKA. Detailed observations of the jet plasma as well as the IGM itself will be able to measure the particle content, flow velocity, jet age and magnetic field structure and strength with enough resolution and for a big enough sample of AGN jets to allow better modelling of the plasma physics of jets and likely be able to pinpoint where and why jets bend. The study pursued in this work will then have to be able to allow for more accurate physics in the future as well as the separation between different types of radio galaxies. The old population of particles in radio lobes of AGN jets will help in the study of the impact of the radio jets on the environment. This includes the degree to which the jets enrich the IGM with metals, the role of the jets in the cooling flows of clusters/groups and the role of the shocks, generated by the jets, in the heating of the IGM.

The use of BTs as tracers of galaxy clusters at high redshift has been tested for $z \geq 1$. It has worked reasonably well for galaxies in $z \leq 1$ clusters but it has yet to be proven in deep (z up to ≥ 2) large scale radio surveys . Only 50% of galaxies in the low redshift Universe are in clusters, with the rest being in the field and in groups. This work is a first step in bringing together the numerical studies of bent jets with the observational success of this method at $z \leq 1$.

The highest redshift quasars that are found in the SDSS survey is $z \geq 6$. The search for galaxy clusters is not supposed to extend much beyond $z = 2$. According to the hierarchical structure formation paradigm, the earliest they could have formed is $z \approx 2$. Before then, they had not virialised and are proto-clusters. Mguda et al (2021) shown that SMBH masses can be measured up to $z \approx 3$ using the virial mass estimator method which has a scatter of 0.5 dex. Blackhole mass and accretion rate are the primary driving forces in the study of AGN jet formation. The ability to measure SMBH masses at high z allows the comparison of jet formation at high z with jet formation in the local Universe. This is important when testing the ansatz that jet formation does not change with redshift.

Determining the particle content of the jet ejecta, allows for its use in probing the density of the ICM. At high z, this would be an excellent method to determine cluster density. Modeling interactions between radio jets and the environments requires a constraint on the particle content of the jets or the gas density of the environment. It may be possible, with the next generation of telescopes, to constrain gas density which would allow the use of BTs to measure the particle content of jet ejecta.

Bibliography

Agüeros, M. A., Ivezić, Ž., Covey, K. R., et al. 2005, The Astronomical Journal, 130, 1022

Agudo I., Boettcher M., Falcke H. D. E., Georganopoulos M., Ghisellini G., Giovannini G., Giroletti M., Gurvits L., Gmez J. L., Laing R., Lister D., Stawarz L., Vlahakis N., Wardle J., 2015, Advancing Astrophysics with the Square Kilometre Array (AASKA14), p. 93

Aghanim, N., Akrami, Y., Ashdown, M., et al. 2018, astro-ph: 1807.06209

Alam S. et al., 2015, , 219, 12A

Albareti Franco D., Allende Prieto Carlos, Almeida Andres, et al., 2017, , 233, 25

Amarantidis S., Afonso J., Messias H., Henriques B., Griffin A., Lacey C., Lagos C. d. P., Gonzalez-Perez V., Dubois Y., Volonteri M., Matute I., Pappalardo C., Qin Y., Chary R.-R., Norris R. P., 2019, , 485, 2694

Antonucci R., 1993, Annual Review of Astronomy and Astrophysics, 31, 473

Antognini J., Bird J., Martini P., 2012, , 756, 116

Arp H., 1966, , 14, 1

Arp, H., 1967, AJ, 148, 321

Arp H. C., Madore B., 1987, A catalogue of southern peculiar galaxies and associations

Ascaso B., Wittman D., Dawson W., 2014, , 439, 1980

Baan, W. A., & McKee, M. R., A&A, 143, 136

Baldwin, J. E., Boysen, R. C., Hales, S. E. G., et. al 1985, , 217, 717

Baldwin J. E., Boysen R. C., Hales S. E. G., Jennings J. E., Waggett P. C., Warner P. J., Wilson D. M. A., 1985, , 217, 717

Banfield J. K. et al., 2015, ,453, 2326

Bassi T. et al, 2018, MNRAS, 481, 5236

Bennett, A. S. 1962, , 68, 163

Begelman M. C., Rees M. J., Blandford R. D., 1979, Nature, 279, 770

Benn, C. R., Gruff, G., Vigotti, M., & Wall, J. V. 1982, , 200, 747

Benn, C. R., Grueff, G., Vigotti, M., & Wall, J. V. 1988, , 230, 1

Becker, R. H., White, R. L., & Helfand, D. J. 1995, , 450, 559

Begelman M. C., Rees M. J., Blandford R. D., 1979, , 279, 770

Bennett, A. S. 1962, , 68, 163

Begelman M. C., Rees M. J., Blandford R. D., 1979, , 279, 770

Bera, S., Pal, S., Sasmal, T., K. & Mondal, S., , 251, 9

Bera S., Sasmal T. K., Patra D. & Mondal S., 2022, ApJS, 260, 7

Best P. N., Kauffmann G., Heckman T. M., Brinchmann J., Charlot S., Ivezi ., White S. D. M., 2005, , 362, 25

Best, P. N., Ker, L. M., Simpson, C., Rigby, E. E., & Sabater, J. 2014, , 445, 955

Blanton E. L., Gregg M. D., Helfand D. J., Becker R. H., White R. L., 2000, , 531, 118

Blanton, E. L. 2000, PhD thesis, Columbia Univ.

Blanton E. L., Gregg M. D., Helfand D. J., Becker R. H., Leighly K. M., 2001, , 121, 2915

Blanton E. L., Gregg M. D., Helfand D. J., Becker R. H., White R. L., 2003, , 125, 1635

Blanton M. R., Moustakas J., 2009, Annual Review of Astronomy and Astrophysics, 47, 159

Bolton, J., Gardner, F., & Mackey, M. 1964, Australian J. Phys., 17, 340

van Breugel W. & Fomalont E. B., 1984, ApJ, 282, 55

van Breugel, W., Balick, B., Heckman, T., Miley, G., & Helfand, D.,1983, AJ, 88, 40

Brunetti, G., & Jones, T. W. 2014, , 23, 1430007

Burns J. O., Owen F. N., 1980, , 85, 204

Burns, J. O. 1990, , 99, 14

Burns, J. O., Rhee, G., Roettiger, K., & Owen, F. 1993, in ASP Conf. Ser. 51, Observational Cosmology, ed. G. Chincarini, A. Iovino, T. Maccacaro, & D. Maccagni (San Francisco : ASP), 407

Burns J. O., Ledlow M. J., Loken C., Klypin A., Voges W., Bryan G. L., Norman M. L., White R. A., 1996, , 467, L49

Cassano, R., Brunetti, G., Rttgering, H. J. A., & Brggen, M. 2010, A&A, 509, A68

Caswell, J. L., & Crowther, J. H. 1969, , 145, 181

Cheung, C. C., 2007, ApJ, 133, 2097

Chung, S. M., Eisenhardt, P. R., Gonzalez, A. H., et al. 2011, , 743, 10

Cohen, A. S., Lane, W. M., Cotton, W. D., et al. 2007, , 134, 1245

Colla, G., Fanti, C., Ficarra, A., et al. 1970, A&AS, 1, 281

Colla, G., Fanti, C., Fanti, R., et al. 1972, A&AS, 7, 1

Colla, G., Fanti, C., Fanti, R., et al. 1973, A&AS, 11, 291

Combes F., 2017, Frontiers in Astronomy and Space Sciences, 4, 10

Condon, J. J., Cotton, W. D., Greisen, E. W., et al. 1998, , 115, 1693

Croom, S. M., Smith, R., J., et al. 2004, , 349, 1397-1418

Croston J. H. et al., 2019, A&A, 622, A10

Dabhade, P., R ottgering, H. J. A., Bagchi, J., et al. 2020, A&A, 635, A5

de Vaucouleurs G., 1948, Annales dAstrophysique, 11, 247

de Vaucouleurs G., de Vaucouleurs A., Corwin Jr. H. G., Buta R. J., Paturel G., Fouqu P., 1991, Third Reference Catalogue of Bright Galaxies. Volume I: Explanations and references. Volume II: Data for galaxies between 0 h and 12 h . Volume III: Data for galaxies between 12 h and 24 h .

De Young D. S., 1991, , 371, 69

Dehghan S., Johnston-Hollitt M., Mao M., Norris R. P., Miller N. A., Huynh M., 2011, Journal of Astrophysics and Astronomy, 32, 491

Dehghan et al., 2014, , 148, 75

de Gasperin, F., Dijkema, T. J., Drabent, A., et al. 2019, A&A, 622, A5 (LOFAR SI)

Deltorn, J.-M., Le Fvre, O., Crampton, D., & Dickinson, M. 1997, , 483, L21

Douglas, J. N., Bash, F. N., Bozyan, F. A., Torrence G. W., & Wolfe, C. 1996, , 111, 1945

Donoso E., Best P. N., Kauffmann G., 2009, MNRAS, 392, 617

Dreyer, J. L. E. 1888, MmRAS, 49, 1

Duncan K. J. et al., 2019, A&A, 622, A3

Edge, D. O., Shakeshaft, J. R., McAdam, W. B., Baldwin, J. E., & Archer, S. 1959, , 68, 37

Eilek J. A., Burns J. O., ODea C. P., Owen F. N., 1984, , 278, 37

Eilek J. A. & Owen F. N., 2002, , 567, 202

Einasto, M., Einasto, J., Tago, E., Muller, V., & Andernach, H., 2011, , 122, 2222

Ennis D. J., Neugebauer G. & Werner M., 1982, Astrophys. J. 262, 460

Estrada et al., 2007, , 660, 1176

Fanaroff, B. L. & Riley, J. M., 1974, , 167, 31

Fan X. et al., 1999, AJ 118, 1

Fabian A., 2012, Annual Review of Astronomy and Astrophysics, 50, 455

Ficarra A., Grueff G., Tomassetti G., 1985, A&A, 59, 255

Freeland E., Cardoso R. F., Wilcots E., 2008, , 685, 858

Freeland E., Wilcots E., 2011, , 738, 145

Ficarra, A., Grueff, G., & Tomassetti, G. 1985, A&A, 59, 255

Gal R. R., de Carvalho R. R., Lopes P. A. A., Djorgovski S. G., Brunner R. J., Mahabal A., Odewahn S. C., 2003, AJ, 125, 2064

Gal R. R., Lopes P. A. A., de Carvalho R. R., Kohl-Moreira J. L., Capelato H. V., Djorgovski S. G., 2009, AJ, 137, 2981

Gawroński M. P., Marecki A., Kunert-Bajraszewska M., Kus A. J., 2006, A&A, 447, 63

Garon, Avery F.; Rudnick, Lawrence; Wong, O. Ivy et al, 2018, , 157, 126

de Gasperin F., 2017, MNRAS, 467, 2234

Gawroński M. P., Marecki A., Kunert-Bajraszewska M., Kus A. J., 2006, A&A, 447, 63

Ghisellini G., Celotti A., Tavecchio F., Haardt F., Sbarrato T., 2014, , 438, 2694

Gizani N. A. B., Leahy J. P., 1999, NewAR, 99, 639

Gizani N. A. B., Garrett M. A., Leahy J. P., 2002, J. Astrophys. Astr., 23,89

Gomez, P. L., Pinkney, J., Burns, J. O., Wang, Q., Owen, F. N., & Voges, W. 1997, , 474, 580

Gopal-Krishna & Wiita P.J., 2000, A&A, 363, 507

Gower, J. F. R., Scott, P. F., & Wills, D. 1967, MmRAS, 71, 49

Gregory, P. C., & Condon, J. J. 1991, , 75, 1011

Griffith, M. R., Wright, A. E., Burke, B. F., & Ekers, R. D. 1994, , 90, 179

Gruppioni et al. 1997,, 286, 470

Greisen, E. W. 1998, in Astronomical Data Analysis Software and Systems VII, eds. R. Albrecht, R. N. Hook, & H. A. Bushouse, ASP Conf. Ser., 145, 204

Gull, S. F. & Northover, K. J. E., 1973, , 244, 80

Gunn, J, E., Walter, A. S., Edward, J. M., et al. 2006, , 131, 2332

Hardcastle, M. J., Sakelliou I. & Worrall D. M., 2005, , 359, 1007

Hardcastle, M. J. & Croston, J. H. 2020, New AR, 88, 101539

Hales, S. E. G., Baldwin, J. E., & Warner, P. J. 1988, , 234, 919

Hales, S. E. G., Masson, C. R., Warner, P. J., & Baldwin, J. E. 1990, , 246, 256

Hales, S. E. G., Mayer, C. J., Warner, P. J., & Baldwin, J. E. 1991, , 251, 46

Hales, S. E. G., Baldwin, J. E., & Warner, P. J. 1993a, , 263, 25

Hales, S. E. G., Masson, C. R., Warner, P. J., Baldwin, J. E., & Green, D. A. 1993b, , 262, 1057

Hao Jiangang, McKay Timothy A., Koester Benjamin P. et al., 2010, , 191, 254

Hewett, Paul C. & Wild, Vivienne., , 2010, 405, 2302

Heeschen, D. S. 1966, , 146, 517H

Helmboldt J. F., Kassim N. E., Cohen A. S., Lane W. M., Lazio T. J., 2008, ApJS, 174, 313

Heald, G. H., Pizzo, R. F., Orr, E., et al. 2015, A&A, 582, A123

Hill, G. J., & Lilly, S. J. 1991, , 367, 1 (HL91)

Higdon J. L., Higdon S. J. U., 2010, in Smith B., Higdon J., Higdon S., Bastian N., eds, Galaxy Wars: Stellar Populations and Star Formation in Interacting Galaxies Vol. 423 of Astronomical Society of the Pacific Conference Series, Why Are Ring Galaxies Interesting?. p. 12

Higdon J. L., Higdon S. J. U., Rand R. J., 2011, , 739, 97

Hubble E. P., 1926, , 64

Hubble E., Kirshner R., Carroll S., 2013, The Realm of the Nebulae. Mrs. Hepsa Ely Silliman memorial lectures, Yale University Press

Intema, H. T., Jagannathan, P., Mooley, K. P., & Frail, D. A. 2017, A&A, 598, A78

Ishwara-Chandra C. H., Sirothia S. K., Wadadekar Y., et al. 2010, , 405, 436

Jones T. W., Owen F. N., 1979, , 234, 818

Joshi S. A., Nandi S., Saikia D. J., Ishwara-Chandra C. H., Konar C., 2011, 414, 1397

Kaiser C. R., Alexander P., 1997, , 286, 215

Kaiser C. R., Dennett-Thorpe J., Alexander P., 1997, , 292, 723

Kapahi V. K., Athreya R. M., van Breugel W., et al. 1998, 118, 275

Kapińska A. D. et al., 2017, AJ, 154, 16

Kenderdine, S., Ryle, M. S., & Pooley, G. G., 1966, , 134, 189

Kollgaard, R. I., Brinkmann, W., Chester, M. M., et al. 1994, , 93, 145

Koester B. P., McKay T. A. Annis J., Wechsler R. H et al., 2007, , 660, 239

Kormendy J., Kennicutt Jr. R. C., 2004, ARA&A, 42, 603

Koester B. P., McKay T. A., Annis J. e. a., 2007, , 660, 239

Kormendy J., Ho L. C., 2013, &A, 51, 511

Kravtsov A. V., Borgani S., 2012, &A, 50, 353

Lane, W. M., Cotton, W. D., van Velzen, S., et al. 2014, , 440, 327

Leahy J. P. & Parma P., 1992, in Extragalactic Radio Sources: From Beams toJets, ed. J. Roland, H. Sol, & G. Pelletier (Cambridge: Cambridge Univ.Press), 307

Leahy, J. P. & Williams, A. G., 1984, MNRAS, 210, 929

Ledlow M.J., Owen F.N., 1996, AJ 112, 9

Liu et al., 2015, , 216, 15

Lopes P. A. A., de Carvalho R. R., Gal R. R. et al., 2004, , 128, 1017

Lopes P. A. A., de Carvalho R. R., Kohl-Moreira J. L., Jones C., 2009, , 392, 135

Lynds R., Toomre A., 1976, , 209, 382

MacDonald G. H., Kenderdine S., Neville A. C., 1968, , 138, 259

Mao et al, 2009, , 392, 1070

Mao M. Y., Johnston-Hollitt M., Stevens J. B., & Wotherspoon S. J., 2009, , 392, 1070

Mahony E. K., Morganti R., Prandoni I., et al. 2016, , 463, 2997

McGee R. X. & Newton L. M., 1972, Aust. J. Phys. 25, 619

McGee R. X., Newton L. M. & Butler P. W., 1976, Aust. J. Phys., 29, 329

Merritt D., Ekers R. D., 2002, Science, 297, 1310

McGilchrist, M. M., Baldwin, J. E., Riley, J. M., et al. 1990, , 246, 110

Mguda et al., 2015, , 446, 3310

Miley G. K., Perola G. C., van der Kruit P. C., van der Laan H., 1972, , 237, 269

Milne, D. K. Caswell J. L. & Haynes R. F., 1980, MNRAS, 191, 469

Mingo B. et al., 2019, , 488, 2701

Missaglia, V., et al. 2019, A&A, 626, A8

Morsony B. J., Miller J. J., Heinz S., Freeland E., Wilcots E., Brggen M., Ruszkowski M., 2013, , 431, 781

Monroe T. R., Prochaska J. X., Tejos N., Worseck G., Hennawi J. F., Schmidt T., Tumlinson J., Shen Y., 2016, AJ, 152, 11

Nagai H., Suzuki K., Asada K. et al., PASJ, 2010, 62, L11

Nilsson K., Valtonen M. J., Kotilainen J., Jaakkola T., 1993, ApJ, 413, 453

Netzer H., 2015, Annual Review of Astronomy and Astrophysics, 53, 365

Norris R. P., Intema H. T., Kapińska A. D. et al, 2021, PASA, 38, 3N

Norris, R. P., Collier, J. D., Crocker, R., M., et al, 2022, MNRAS, 513, 1, 1300

O'Brien, Andrew N., Norris, Ray P., Tothill, Nick F. H. & Filipovi, Miroslav D., 2018 , 481, 5247

ODea C. P. & Owen F. N., 1985, , 90, 954

ODea C. P., 1985, , 295, 80

ODea C. P., Owen F. N., 1986, , 301, 841

O'Dea, C. P., & Owen, F. N. 1987, , 316, 95

ODonoghue A. A., Eilek J. A., Owen F. N., 1993, , 408, 428

O'Donoghue, A. A., Owen, F. N. & Eilek, J. A. 1990, , 72, 75

O'Donoghue, A. A., Eilek, J. A. & Owen, F. N. 1993, , 408, 428

Oort M. J. A., Steemers W. J. G., & Windhorst R. A., 1988, A&AS, 73, 103

Owen, F. N. & Rudnick, L., 1976, , 205, L1

Owen F. N., ODea C. P., Inoue M., Eilek J. A., 1985, , 294, L85

Paliya V. S., Sahayanathan S., Parker M. L., Fabian A. C., Stalin C. S., Anjum A., Pand ey S. B., 2014, , 789, 143

Prandoni I., Seymour N., 2015, in Advancing Astrophysics with the Square Kilometre Array (AASKA14) Revealing the Physics and Evolution of Galaxies and Galaxy Clusters with SKA Continuum Surveys. p. 67

Paterno-Mahler, R., Blanton, E. L., Brodwin, M., et al. 2017, , 844, 11

Patra, D., Pal, S., Konar, C., et al. 2019, , 364, 72

Paterno-Mahler, R., Blanton, E. L., Brodwin, M., et al. 2017, , 844, 11

Pearson, T. 1975, , 171, 475

Pearson, T., & Kus, A. J. 1978, , 182, 273

Pilkington, J. D. H., & Scott, J. F. 1965, MmRAS, 69, 183

Pooley, G. G., & Kenderdine, S. 1968, , 139, 529

Pooley, G. G. 1969, , 144, 101

Proctor, D. D. 2006, , 165, 95

Prandoni I., Seymour N., 2015, in Advancing Astrophysics with the Square Kilometre Array (AASKA14) Revealing the Physics and Evolution of Galaxies and Galaxy Clusters with SKA Continuum Surveys. p. 67

Rengelink R. B., Tang Y., de Bruyn A. G., Miley G. K., Bremer M. N., Roettgering H. J. A., Bremer M. A. R., 1997, A&A Supplement series, 124, 259

Rodŕiguez L. F., Carrasco-Gonźalez C., Montes G., Tapia M., 2014, AJ, 148, 5

Proctor, D. D. 2011, , 194, 2

Rector, T. A., Stocke, J. T., & Ellingson, E. 1995, , 110, 1492

Rebull, L. M., Koenig, X. P., Padgett, D. L. et al. 2011, , 196, 19

Richards, G. T., Myers, A., D., Gray, A., G., et al. 2009, , 180, 68-83

Roettiger, K., Burns, J. O. & Loken, C. 1996, , 473, 651

Rozo E., Rykoff E. S., Becker M., Reddick R. M., Wechsler R. H., 2015, , 453, 38

Rudnick L. & Owen F. N., 1976, , 203, 107

Ryle M., & Windram M. D., 1968, , 138, 1

Rykoff E. S. et al., 2014, ApJ, 785, 33

Sandage A., Sandage M., Kristian J., 1975, Galaxies and the Universe

Sakelliou I., Merrifield M. R., & McHardy, I. M. 1996, , 283, 673

Saikia D. J., Konar C. & Kulkarni V. K., 2006, MNRAS, 366,1391

Sasmal T. K., Pal S., Bera S., & Mondal S., , sumbitted

Sasmal T. K., Bera S., Pal S., & Mondal S., , sumbitted

Sasmal T. K., Bera S., et al., 2022, , 259, 31

Sánchez, A. J., Aguerri, J. A. L., Muñoz − $Tuñón, C., \& Huertas - Company, M.$2011, , 735, 15

Schuch, N. 1981, , 196, 695

Schoenmakers A. P., de Bruyn A. G., Röttgering H. J. A., van der Laan H. & Kaiser C. R., 2000, MNRAS, 315, 371

Schlafly, E. F.& Finkbeiner, D. P., 2011, ApJ, 737, 13

Sersic J. L., 1968, Atlas de galaxias australes

Sebastian, B., Lal, D. V., & Rao, A., P., 2017, , 154, 169

Shimwell T. W., Rttgering H. J. A., Best P. N., et al. 2017, A&A, 598, A104

Shulevski, A., Morganti, R., Barthe, P. D., et al. 2015, A&A, 579, A27

Shimwell, T. W., Tasse, C., Hardcastle, M. J., et al. 2019, A&A, 622, A1

Skrutskie M. F. et al., 2006, AJ, 131, 1163

Skrutskie, M. F., Cutri, R. M., Stiening, R, et al. 2006, , 131, 1163

Slee, O. 1995, Australian J. Phys., 48, 143

Smith Anthony G., Hopkins Andrew M., Hunstead Richard W., Pimbblet Kevin A., 2012a, , 422, 25

Souchay J.,Andrei A. H.,Barache C., Bouquillon S.,Suchet D., Taris F. and Peralta R., 2012, A&A, 537, A99

Sparke L. S., Gallagher III J. S., 2006, Galaxies in the Universe - 2nd Edition

Srivastava, S., & Singal, A. K. 2020, , 493, 3811

Tadhunter C., 2008, New Astronomy Reviews (), 52, 227

Tumlinson J. et al., 2013, ApJ, 777, 33

Urry C. M., 2003, in American Astronomical Society Meeting Abstracts 202 Vol. 202 of American Astronomical Society Meeting Abstracts, Grand Unification of Active Galaxies. p. 22.01

Valentijn E. A., 1979, A&A, 78, 367

Vallee, J. P., 1981, 22, 193

van Dokkum P. G., Franx M., 1995, , 110, 2027

van Haarlem, M. P., Wise, M. W., Gunst, A. W., et al. 2013, A&A, 556, A2

Velusamy T., Roshi A., 1991, Current Science, 60, 120

Venkatesan T. C. A., Batuski D. J., Hanisch R. J., Burns J. O., 1994, , 436, 67

Vessey, S. J., & Green, D. A. 1998, , 294, 607

Vikhlinin et al., 1998, , 502, 558

Von Der Linden Anja, Best Philip N., Kauffmann Guinevere, White Simon D. M. , 2007, , 379, 867

Vos, K. de., Hatch, N. A., Merrifield, M. R., & Mingo, B., 2021, MNRAS Letter, 506, L55

Waggett, P., 1977, , 181, 547

Waldram, E. M., Yates, J. A., Riley, J. M., & Warner, P. J. 1996, , 282, 779

Wayth, R. B., Lenc, E., Bell, M. E., et al. 2015, , 32, e025

Wen Z. L., Han J. L., Liu F. S., ApJs, 2009, 187, 272

Wen Z. L., Han J. L., Liu F. S., 2010, ApJS, 187, 272

Wen, Z. L. & Han, J., L., 2015, , 807, 178

Williams P. J. S., & Bridle A. H., 1967, The Observatory, 87, 280

Willis A. G., Strom R. G., Wilson A. S., 1974, Nature, 250, 625

Willson, M. 1970, , 151, 1

Wilman, R. J., Miller, L., Jarvis, M. J., et al. 2008, , 388, 1335

Wing, Joshua D. & Blanton, Elizabeth L. 2001, , 141, 24

Wing, Joshua D. & Blanton, Elizabeth L. 2011, , 141, 24

Willson, M. 1970, , 151, 1

Wilman D. J., Erwin P., 2012, , 746, 160

Williams W. L. et al., 2019, A&A, 622, A2

White, R. L., Becker, R. H., Helfand, D. J., & Gregg, M. D. 1996, , 475, 479

Williams P. J. S., & Bridle A. H., 1967, The Observatory, 87, 280

Yang, X., Joshi, R., Gopal-Krishna, et al. 2019, ApJS, 245, 17

Yoon J. H., Schawinski K., Sheen Y., Ree C. H., Yi S. K., 2008, ApJS, 176, 414

York D. G., Adelman J., Anderson Jr. J. E., Anderson S. F., Annis J., Bahcall N. A., SDSS Collaboration 2000, , 120, 1579

Zirbel, E. L. 1997, , 476, 489 (Z97)

Zier C., 2005, MNRAS, 364, 583

Appendix A

All contour images of FIRST WAT sources

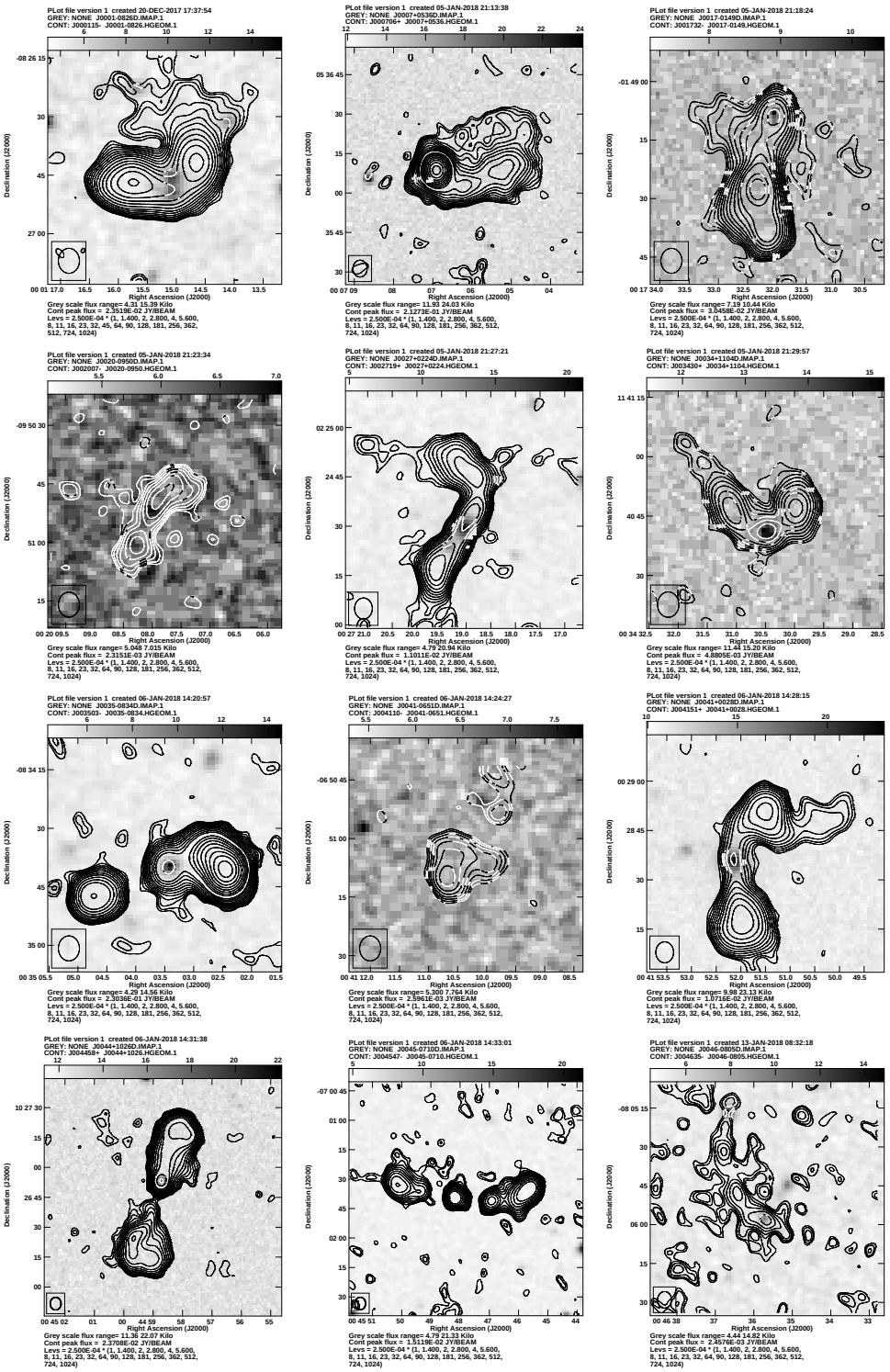
PLot file version 1 created 20-DEC-2017 17:37:54
GREY: NONE J0001-0826D.IMAP.1
CONT: J000115- J0001-0826.HGEOM.1
Declination (J2000)
Right Ascension (J2000)
Grey scale flux range= 4.31 15.39 Kilo
Cont peak flux = 2.3519E-02 JY/BEAM
Levs = 2.500E-04 * (1, 1.400, 2, 2.800, 4, 5.600, 8, 11, 16, 23, 32, 45, 64, 90, 128, 181, 256, 362, 512, 724, 1024)
PLot file version 1 created 05-JAN-2018 21:13:38
GREY: NONE J0007+0536D.IMAP.1
CONT: J000706+ J0007+0536.HGEOM.1
Declination (J2000)
Right Ascension (J2000)
Grey scale flux range= 11.93 24.03 Kilo
Cont peak flux = 2.1273E-01 JY/BEAM
Levs = 2.500E-04 * (1, 1.400, 2, 2.800, 4, 5.600, 8, 11, 16, 23, 32, 64, 90, 128, 181, 256, 362, 512, 724, 1024)
PLot file version 1 created 05-JAN-2018 21:18:24
GREY: NONE J0017-0149D.IMAP.1
CONT: J001732- J0017-0149.HGEOM.1
Declination (J2000)
Right Ascension (J2000)
Grey scale flux range= 7.19 10.44 Kilo
Cont peak flux = 3.0458E-02 JY/BEAM
Levs = 2.500E-04 * (1, 1.400, 2, 2.800, 4, 5.600, 8, 11, 16, 23, 32, 64, 90, 128, 181, 256, 362, 512, 724, 1024)
PLot file version 1 created 05-JAN-2018 21:23:34
GREY: NONE J0020-0950D.IMAP.1
CONT: J002007- J0020-0950.HGEOM.1
Declination (J2000)
Right Ascension (J2000)
Grey scale flux range= 5.048 7.015 Kilo
Cont peak flux = 2.3151E-03 JY/BEAM
Levs = 2.500E-04 * (1, 1.400, 2, 2.800, 4, 5.600, 8, 11, 16, 23, 32, 64, 90, 128, 181, 256, 362, 512, 724, 1024)
PLot file version 1 created 05-JAN-2018 21:27:21
GREY: NONE J0027+0224D.IMAP.1
CONT: J002719+ J0027+0224.HGEOM.1
Declination (J2000)
Right Ascension (J2000)
Grey scale flux range= 4.79 20.94 Kilo
Cont peak flux = 1.1011E-02 JY/BEAM
Levs = 2.500E-04 * (1, 1.400, 2, 2.800, 4, 5.600, 8, 11, 16, 23, 32, 64, 90, 128, 181, 256, 362, 512, 724, 1024)
PLot file version 1 created 05-JAN-2018 21:29:57
GREY: NONE J0034+1104D.IMAP.1
CONT: J003430+ J0034+1104.HGEOM.1
Declination (J2000)
Right Ascension (J2000)
Grey scale flux range= 11.44 15.20 Kilo
Cont peak flux = 4.8805E-03 JY/BEAM
Levs = 2.500E-04 * (1, 1.400, 2, 2.800, 4, 5.600, 8, 11, 16, 23, 32, 64, 90, 128, 181, 256, 362, 512, 724, 1024)
PLot file version 1 created 06-JAN-2018 14:20:57
GREY: NONE J0035-0834D.IMAP.1
CONT: J003503- J0035-0834.HGEOM.1
Declination (J2000)
Right Ascension (J2000)
Grey scale flux range= 4.29 14.56 Kilo
Cont peak flux = 2.3038E-01 JY/BEAM
Levs = 2.500E-04 * (1, 1.400, 2, 2.800, 4, 5.600, 8, 11, 16, 23, 32, 64, 90, 128, 181, 256, 362, 512, 724, 1024)
PLot file version 1 created 06-JAN-2018 14:24:27
GREY: NONE J0041-0651D.IMAP.1
CONT: J004110- J0041-0651.HGEOM.1
Declination (J2000)
Right Ascension (J2000)
Grey scale flux range= 5.300 7.764 Kilo
Cont peak flux = 2.5961E-03 JY/BEAM
Levs = 2.500E-04 * (1, 1.400, 2, 2.800, 4, 5.600, 8, 11, 16, 23, 32, 64, 90, 128, 181, 256, 362, 512, 724, 1024)
PLot file version 1 created 06-JAN-2018 14:28:15
GREY: NONE J0041+0028D.IMAP.1
CONT: J004151+ J0041+0028.HGEOM.1
Declination (J2000)
Right Ascension (J2000)
Grey scale flux range= 9.98 23.13 Kilo
Cont peak flux = 1.0716E-02 JY/BEAM
Levs = 2.500E-04 * (1, 1.400, 2, 2.800, 4, 5.600, 8, 11, 16, 23, 32, 64, 90, 128, 181, 256, 362, 512, 724, 1024)
PLot file version 1 created 06-JAN-2018 14:31:38
GREY: NONE J0044+1026D.IMAP.1
CONT: J004458+ J0044+1026.HGEOM.1
Declination (J2000)
Right Ascension (J2000)
Grey scale flux range= 11.36 22.07 Kilo
Cont peak flux = 2.3708E-02 JY/BEAM
Levs = 2.500E-04 * (1, 1.400, 2, 2.800, 4, 5.600, 8, 11, 16, 23, 32, 64, 90, 128, 181, 256, 362, 512, 724, 1024)
PLot file version 1 created 06-JAN-2018 14:33:01
GREY: NONE J0045-0710D.IMAP.1
CONT: J004547- J0045-0710.HGEOM.1
Declination (J2000)
Right Ascension (J2000)
Grey scale flux range= 4.79 21.33 Kilo
Cont peak flux = 1.5119E-02 JY/BEAM
Levs = 2.500E-04 * (1, 1.400, 2, 2.800, 4, 5.600, 8, 11, 16, 23, 32, 64, 90, 128, 181, 256, 362, 512, 724, 1024)
PLot file version 1 created 13-JAN-2018 08:32:18
GREY: NONE J0046-0805D.IMAP.1
CONT: J004635- J0046-0805D.HGEOM.1
Declination (J2000)
Right Ascension (J2000)
Grey scale flux range= 4.44 14.82 Kilo
Cont peak flux = 2.4576E-03 JY/BEAM
Levs = 2.500E-04 * (1, 1.400, 2, 2.800, 4, 5.600, 8, 11, 16, 23, 32, 64, 90, 128, 181, 256, 362, 512, 724, 1024)

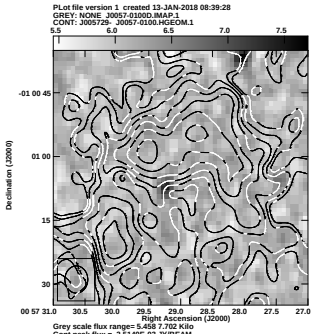
PLot file version 1 created 13-JAN-2018 08:39:28
GREY: NONE J0057-0100D.IMAP.1
CONT: J005729- J0057-0100.HGEOM.1
Declination (J2000)
Right Ascension (J2000)
Grey scale flux range= 5.458 7.702 Kilo
Cont peak flux = 2.514OE-03 JY/BEAM
Levs = 2.500E-04 * (1, 1.400, 2, 2.800, 4, 5.600, 8, 11, 16, 23, 32, 64, 90, 128, 181, 256, 362, 512, 724, 1024)

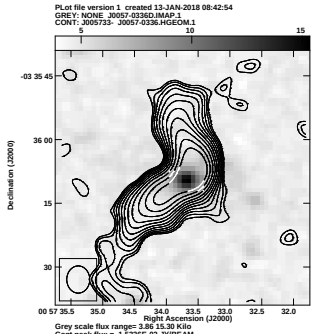
PLot file version 1 created 13-JAN-2018 08:42:54
GREY: NONE J0057-0336D.IMAP.1
CONT: J005733- J0057-0336.HGEOM.1
Declination (J2000)
Right Ascension (J2000)
Grey scale flux range= 3.86 15.30 Kilo
Cont peak flux = 1.5326E-02 JY/BEAM
Levs = 2.500E-04 * (1, 1.400, 2, 2.800, 4, 5.600, 8, 11, 16, 23, 32, 64, 90, 128, 181, 256, 362, 512, 724, 1024)

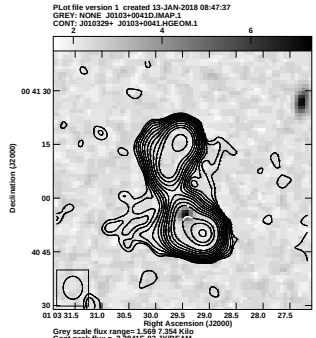
PLot file version 1 created 13-JAN-2018 08:47:37
GREY: NONE J0103+0041D.IMAP.1
CONT: J010329+ J0103+0041.HGEOM.1
Declination (J2000)
Right Ascension (J2000)
Grey scale flux range= 1.569 7.354 Kilo
Cont peak flux = 3.3841E-02 JY/BEAM
Levs = 2.500E-04 * (1, 1.400, 2, 2.800, 4, 5.600, 8, 11, 16, 23, 32, 64, 90, 128, 181, 256, 362, 512, 724, 1024)

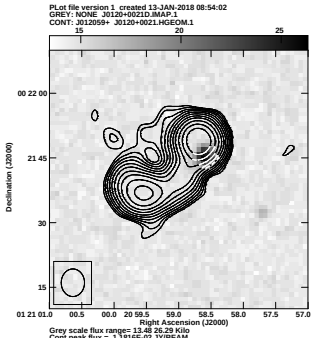
PLot file version 1 created 13-JAN-2018 08:54:02
GREY: NONE J0120+0021D.IMAP.1
CONT: J012059+ J0120+0021.HGEOM.1
Declination (J2000)
Right Ascension (J2000)
Grey scale flux range= 13.48 26.29 Kilo
Cont peak flux = 1.3816E-02 JY/BEAM
Levs = 2.500E-04 * (1, 1.400, 2, 2.800, 4, 5.600, 8, 11, 16, 23, 32, 64, 90, 128, 181, 256, 362, 512, 724, 1024)

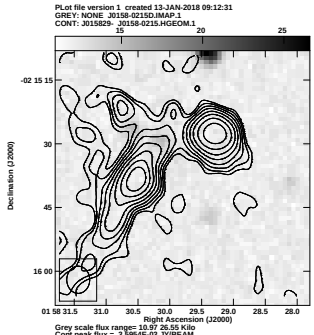
PLot file version 1 created 13-JAN-2018 09:12:31
GREY: NONE J0158-0215D.IMAP.1
CONT: J015829- J0158-0215.HGEOM.1
Declination (J2000)
Right Ascension (J2000)
Grey scale flux range= 10.97 26.55 Kilo
Cont peak flux = 3.5954E-03 JY/BEAM
Levs = 2.500E-04 * (1, 1.400, 2, 2.800, 4, 5.600, 8, 11, 16, 23, 32, 64, 90, 128, 181, 256, 362, 512, 724, 1024)

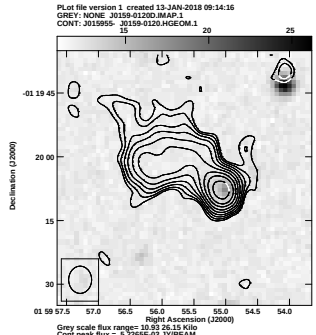
PLot file version 1 created 13-JAN-2018 09:14:16
GREY: NONE J0159-0120D.IMAP.1
CONT: J015955- J0159-0120.HGEOM.1
Declination (J2000)
Right Ascension (J2000)
Grey scale flux range= 10.93 26.15 Kilo
Cont peak flux = 5.2265E-03 JY/BEAM
Levs = 2.500E-04 * (1, 1.400, 2, 2.800, 4, 5.600, 8, 11, 16, 23, 32, 64, 90, 128, 181, 256, 362, 512, 724, 1024)

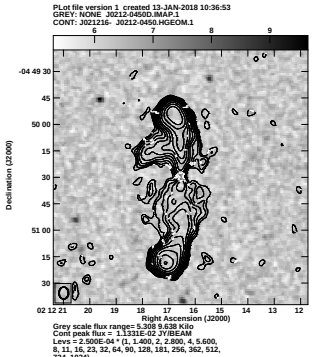
PLot file version 1 created 13-JAN-2018 10:36:53
GREY: NONE J0212-0450D.IMAP.1
CONT: J021216- J0212-0450.HGEOM.1
Declination (J2000)
Right Ascension (J2000)
Grey scale flux range= 5.309 9.638 Kilo
Cont peak flux = 1.1331E-02 JY/BEAM
Levs = 2.500E-04 * (1, 1.400, 2, 2.800, 4, 5.600, 8, 11, 16, 23, 32, 64, 90, 128, 181, 256, 362, 512, 724, 1024)

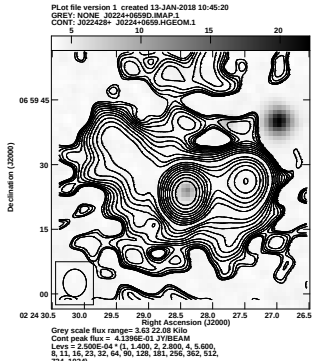
PLot file version 1 created 13-JAN-2018 10:45:20
GREY: NONE J0224+0659D.IMAP.1
CONT: J022429+ J0224+0659.HGEOM.1
Declination (J2000)
Right Ascension (J2000)
Grey scale flux range= 3.63 22.08 Kilo
Cont peak flux = 4.1396E-01 JY/BEAM
Levs = 2.500E-04 * (1, 1.400, 2, 2.800, 4, 5.600, 8, 11, 16, 23, 32, 64, 90, 128, 181, 256, 362, 512, 724, 1024)

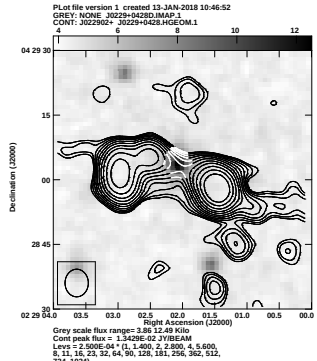
PLot file version 1 created 13-JAN-2018 10:46:52
GREY: NONE J0229+0428D.IMAP.1
CONT: J022902+ J0229+0428.HGEOM.1
Declination (J2000)
Right Ascension (J2000)
Grey scale flux range= 3.86 12.49 Kilo
Cont peak flux = 1.3429E-02 JY/BEAM
Levs = 2.500E-04 * (1, 1.400, 2, 2.800, 4, 5.600, 8, 11, 16, 23, 32, 64, 90, 128, 181, 256, 362, 512, 724, 1024)

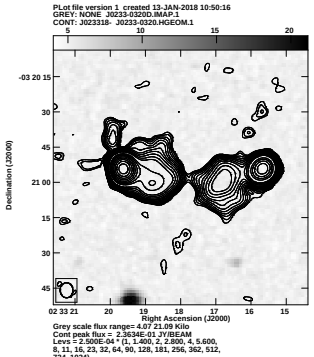
PLot file version 1 created 13-JAN-2018 10:50:16
GREY: NONE J0233-0320D.IMAP.1
CONT: J023318- J0233-0320.HGEOM.1
Declination (J2000)
Right Ascension (J2000)
Grey scale flux range= 4.07 21.09 Kilo
Cont peak flux = 2.3634E-01 JY/BEAM
Levs = 2.500E-04 * (1, 1.400, 2, 2.800, 4, 5.600, 8, 11, 16, 23, 32, 64, 90, 128, 181, 256, 362, 512, 724, 1024)

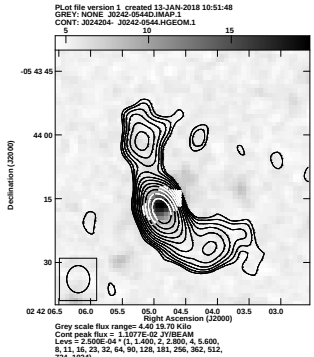
PLot file version 1 created 13-JAN-2018 10:51:48
GREY: NONE J0242-0544D.IMAP.1
CONT: J024204- J0242-0544.HGEOM.1
Declination (J2000)
Right Ascension (J2000)
Grey scale flux range= 4.40 19.70 Kilo
Cont peak flux = 1.1077E-02 JY/BEAM
Levs = 2.500E-04 * (1, 1.400, 2, 2.800, 4, 5.600, 8, 11, 16, 23, 32, 64, 90, 128, 181, 256, 362, 512, 724, 1024)

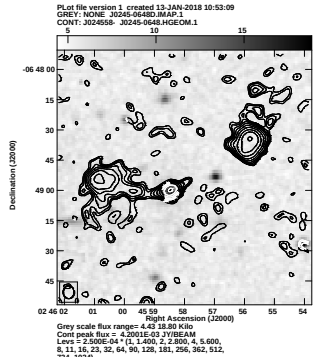
PLot file version 1 created 13-JAN-2018 10:53:09
GREY: NONE J0245-0648D.IMAP.1
CONT: J024558- J0245-0648.HGEOM.1
Declination (J2000)
Right Ascension (J2000)
Grey scale flux range= 4.43 18.80 Kilo
Cont peak flux = 4.2001E-03 JY/BEAM
Levs = 2.500E-04 * (1, 1.400, 2, 2.800, 4, 5.600, 8, 11, 16, 23, 32, 64, 90, 128, 181, 256, 362, 512, 724, 1024)

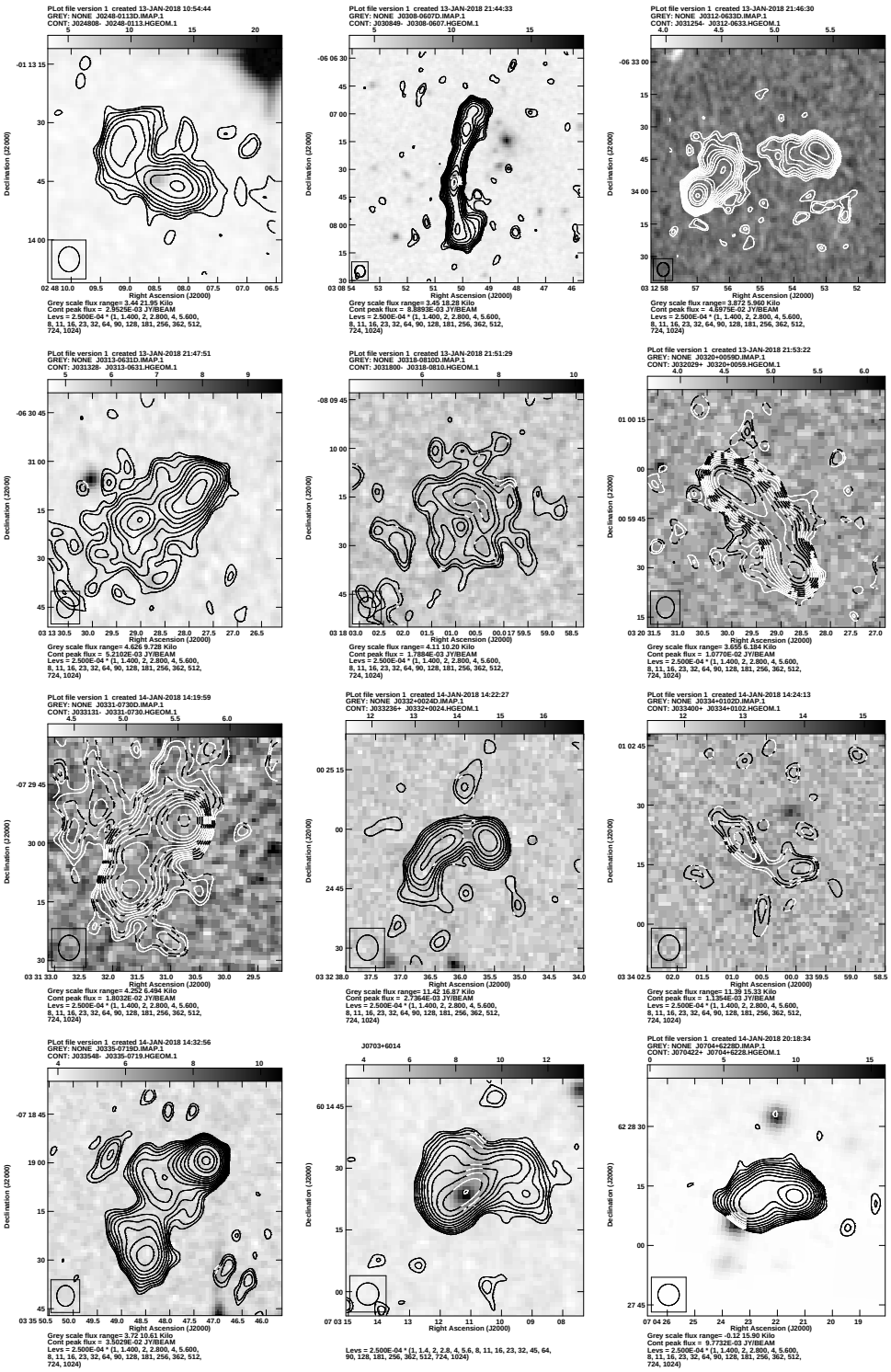
PLot file version 1 created 13-JAN-2018 10:54:44
GREY: NONE J0248-0113D.IMAP.1
CONT: J024808- J0248-0113.HGEOM.1
Declination (J2000)
Right Ascension (J2000)
Grey scale flux range= 3.44 21.95 Kilo
Cont peak flux = 2.9526E-03 JY/BEAM
Levs = 2.500E-04 * (1, 1.400, 2, 2.800, 4, 5.600, 8, 11, 16, 23, 32, 64, 90, 128, 181, 256, 362, 512, 724, 1024)
PLot file version 1 created 13-JAN-2018 21:44:33
GREY: NONE J0308-0607D.IMAP.1
CONT: J030848- J0308-0607.HGEOM.1
Declination (J2000)
Right Ascension (J2000)
Grey scale flux range= 3.45 18.28 Kilo
Cont peak flux = 8.8893E-03 JY/BEAM
Levs = 2.500E-04 * (1, 1.400, 2, 2.800, 4, 5.600, 8, 11, 16, 23, 32, 64, 90, 128, 181, 256, 362, 512, 724, 1024)
PLot file version 1 created 13-JAN-2018 21:46:30
GREY: NONE J0312-0633D.IMAP.1
CONT: J031254- J0312-0633.HGEOM.1
Declination (J2000)
Right Ascension (J2000)
Grey scale flux range= 3.872 5.960 Kilo
Cont peak flux = 4.6975E-02 JY/BEAM
Levs = 2.500E-04 * (1, 1.400, 2, 2.800, 4, 5.600, 8, 11, 16, 23, 32, 64, 90, 128, 181, 256, 362, 512, 724, 1024)
PLot file version 1 created 13-JAN-2018 21:47:51
GREY: NONE J0313-0631D.IMAP.1
CONT: J031328- J0313-0631.HGEOM.1
Declination (J2000)
Right Ascension (J2000)
Grey scale flux range= 4.626 9.728 Kilo
Cont peak flux = 5.2102E-03 JY/BEAM
Levs = 2.500E-04 * (1, 1.400, 2, 2.800, 4, 5.600, 8, 11, 16, 23, 32, 64, 90, 128, 181, 256, 362, 512, 724, 1024)
PLot file version 1 created 13-JAN-2018 21:51:29
GREY: NONE J0318-0810D.IMAP.1
CONT: J031800- J0318-0810.HGEOM.1
Declination (J2000)
Right Ascension (J2000)
Grey scale flux range= 4.11 10.20 Kilo
Cont peak flux = 1.7884E-03 JY/BEAM
Levs = 2.500E-04 * (1, 1.400, 2, 2.800, 4, 5.600, 8, 11, 16, 23, 32, 64, 90, 128, 181, 256, 362, 512, 724, 1024)
PLot file version 1 created 13-JAN-2018 21:53:22
GREY: NONE J0320+0059D.IMAP.1
CONT: J032029+ J0320+0059.HGEOM.1
Declination (J2000)
Right Ascension (J2000)
Grey scale flux range= 3.655 6.184 Kilo
Cont peak flux = 1.0770E-02 JY/BEAM
Levs = 2.500E-04 * (1, 1.400, 2, 2.800, 4, 5.600, 8, 11, 16, 23, 32, 64, 90, 128, 181, 256, 362, 512, 724, 1024)
PLot file version 1 created 14-JAN-2018 14:19:59
GREY: NONE J0331-0730D.IMAP.1
CONT: J033131- J0331-0730.HGEOM.1
Declination (J2000)
Right Ascension (J2000)
Grey scale flux range= 4.252 6.494 Kilo
Cont peak flux = 1.8032E-02 JY/BEAM
Levs = 2.500E-04 * (1, 1.400, 2, 2.800, 4, 5.600, 8, 11, 16, 23, 32, 64, 90, 128, 181, 256, 362, 512, 724, 1024)
PLot file version 1 created 14-JAN-2018 14:22:27
GREY: NONE J0332+0024D.IMAP.1
CONT: J033236+ J0332+0024.HGEOM.1
Declination (J2000)
Right Ascension (J2000)
Grey scale flux range= 11.42 16.87 Kilo
Cont peak flux = 2.7364E-03 JY/BEAM
Levs = 2.500E-04 * (1, 1.400, 2, 2.800, 4, 5.600, 8, 11, 16, 23, 32, 64, 90, 128, 181, 256, 362, 512, 724, 1024)
PLot file version 1 created 14-JAN-2018 14:24:13
GREY: NONE J0334+0102D.IMAP.1
CONT: J033400+ J0334+0102.HGEOM.1
Declination (J2000)
Right Ascension (J2000)
Grey scale flux range= 11.39 15.33 Kilo
Cont peak flux = 1.1354E-03 JY/BEAM
Levs = 2.500E-04 * (1, 1.400, 2, 2.800, 4, 5.600, 8, 11, 16, 23, 32, 64, 90, 128, 181, 256, 362, 512, 724, 1024)
PLot file version 1 created 14-JAN-2018 14:32:56
GREY: NONE J0335-0719D.IMAP.1
CONT: J033548- J0335-0719.HGEOM.1
Declination (J2000)
Right Ascension (J2000)
Grey scale flux range= 3.72 10.61 Kilo
Cont peak flux = 3.5029E-02 JY/BEAM
Levs = 2.500E-04 * (1, 1.400, 2, 2.800, 4, 5.600, 8, 11, 16, 23, 32, 64, 90, 128, 181, 256, 362, 512, 724, 1024)
J0703+6014
Declination (J2000)
Right Ascension (J2000)
Levs = 2.500E-04 * (1, 1.4, 2, 2.8, 4, 5.6, 8, 11, 16, 23, 32, 45, 64, 90, 128, 181, 256, 362, 512, 724, 1024)
PLot file version 1 created 14-JAN-2018 20:18:34
GREY: NONE J0704+6228D.IMAP.1
CONT: J0704Z2+ J0704+6228.HGEOM.1
Declination (J2000)
Right Ascension (J2000)
Grey scale flux range= -0.12 15.90 Kilo
Cont peak flux = 9.7732E-03 JY/BEAM
Levs = 2.500E-04 * (1, 1.400, 2, 2.800, 4, 5.600, 8, 11, 16, 23, 32, 64, 90, 128, 181, 256, 362, 512, 724, 1024)

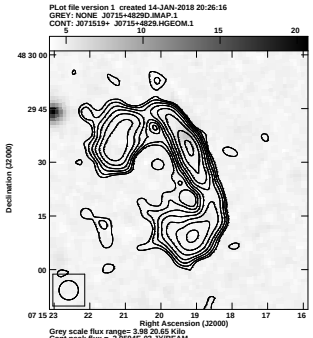
PLot file version 1 created 14-JAN-2018 20:26:16
GREY: NONE J0715+4829D.IMAP.1
CONT: J0715I9+ J0715+4829.HGEOM.1
Declination (J2000)
Right Ascension (J2000)
Grey scale flux range= 3.98 20.65 Kilo
Cont peak flux = 2.5504E-03 JY/BEAM
Levs = 2.500E-04 * (1, 1.400, 2, 2.800, 4, 5.600, 8, 11, 16, 23, 32, 64, 90, 128, 181, 256, 362, 512, 724, 1024)

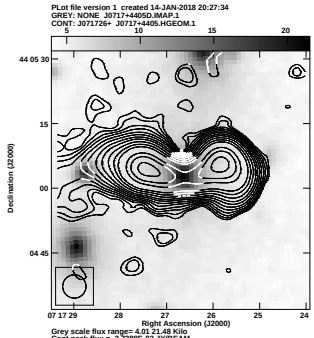
PLot file version 1 created 14-JAN-2018 20:27:34
GREY: NONE J0717+4405D.IMAP.1
CONT: J0717I26+ J0717+4405.HGEOM.1
Declination (J2000)
Right Ascension (J2000)
Grey scale flux range= 4.01 21.48 Kilo
Cont peak flux = 3.7389E-02 JY/BEAM
Levs = 2.500E-04 * (1, 1.400, 2, 2.800, 4, 5.600, 8, 11, 16, 23, 32, 64, 90, 128, 181, 256, 362, 512, 724, 1024)

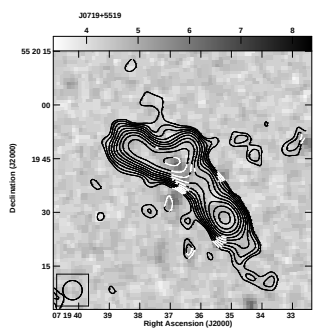
J0719+5519
Declination (J2000)
Right Ascension (J2000)
Levs = 2.500E-04 * (1, 1.4, 2, 2.8, 4, 5.6, 8, 11, 16, 23, 32, 45, 64, 90, 128, 181, 256, 362, 512, 724, 1024)

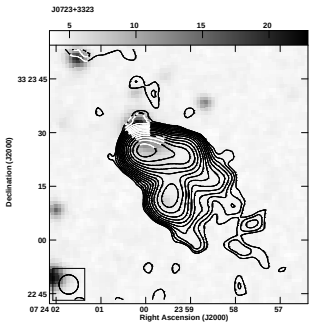
J0723+3323
Declination (J2000)
Right Ascension (J2000)
Levs = 2.500E-04 * (1, 1.4, 2, 2.8, 4, 5.7, 8, 11, 16, 23, 32, 45, 64, 90, 128, 181, 256, 362, 512, 724, 1024)

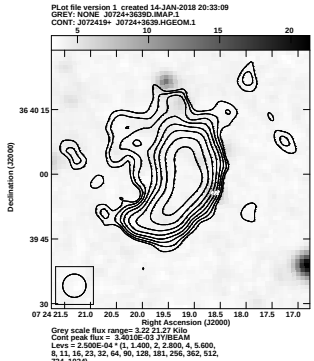
PLot file version 1 created 14-JAN-2018 20:33:09
GREY: NONE J0724+3639D.IMAP.1
CONT: J0724I9+ J0724+3639.HGEOM.1
Declination (J2000)
Right Ascension (J2000)
Grey scale flux range= 3.22 21.27 Kilo
Cont peak flux = 3.4010E-03 JY/BEAM
Levs = 2.500E-04 * (1, 1.400, 2, 2.800, 4, 5.600, 8, 11, 16, 23, 32, 64, 90, 128, 181, 256, 362, 512, 724, 1024)

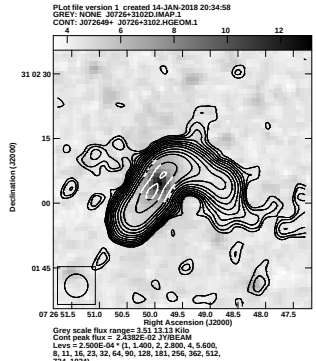
PLot file version 1 created 14-JAN-2018 20:34:58
GREY: NONE J0726+3102D.IMAP.1
CONT: J0726I8+ J0726+3102.HGEOM.1
Declination (J2000)
Right Ascension (J2000)
Grey scale flux range= 3.51 13.13 Kilo
Cont peak flux = 2.4382E-02 JY/BEAM
Levs = 2.500E-04 * (1, 1.400, 2, 2.800, 4, 5.600, 8, 11, 16, 23, 32, 64, 90, 128, 181, 256, 362, 512, 724, 1024)

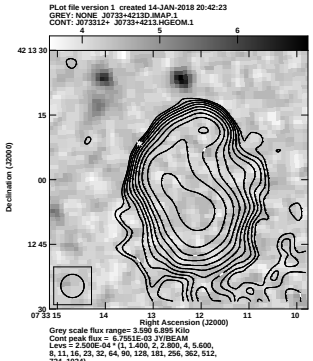
PLot file version 1 created 14-JAN-2018 20:42:23
GREY: NONE J0733+4213D.IMAP.1
CONT: J0733I2+ J0733+4213.HGEOM.1
Declination (J2000)
Right Ascension (J2000)
Grey scale flux range= 3.590 6.895 Kilo
Cont peak flux = 6.7851E-03 JY/BEAM
Levs = 2.500E-04 * (1, 1.400, 2, 2.800, 4, 5.600, 8, 11, 16, 23, 32, 64, 90, 128, 181, 256, 362, 512, 724, 1024)

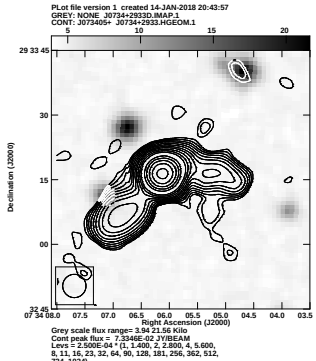
PLot file version 1 created 14-JAN-2018 20:43:57
GREY: NONE J0734+2933D.IMAP.1
CONT: J0734O5+ J0734+2933.HGEOM.1
Declination (J2000)
Right Ascension (J2000)
Grey scale flux range= 3.94 21.56 Kilo
Cont peak flux = 7.3346E-02 JY/BEAM
Levs = 2.500E-04 * (1, 1.400, 2, 2.800, 4, 5.600, 8, 11, 16, 23, 32, 64, 90, 128, 181, 256, 362, 512, 724, 1024)

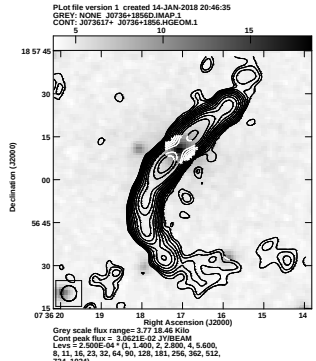
PLot file version 1 created 14-JAN-2018 20:46:35
GREY: NONE J0736+1856D.IMAP.1
CONT: J0736I7+ J0736+1856.HGEOM.1
Declination (J2000)
Right Ascension (J2000)
Grey scale flux range= 3.77 18.46 Kilo
Cont peak flux = 3.0621E-02 JY/BEAM
Levs = 2.500E-04 * (1, 1.400, 2, 2.800, 4, 5.600, 8, 11, 16, 23, 32, 64, 90, 128, 181, 256, 362, 512, 724, 1024)

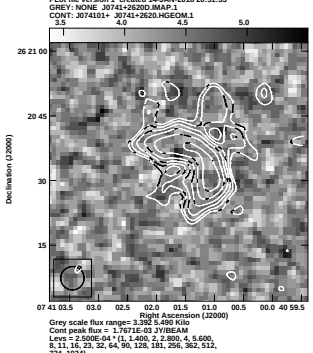
PLot file version 1 created 14-JAN-2018 20:51:33
GREY: NONE J0741+2620D.IMAP.1
CONT: J0741O1+ J0741+2620.HGEOM.1
Declination (J2000)
Right Ascension (J2000)
Grey scale flux range= 3.392 5.490 Kilo
Cont peak flux = 1.7671E-03 JY/BEAM
Levs = 2.500E-04 * (1, 1.400, 2, 2.800, 4, 5.600, 8, 11, 16, 23, 32, 64, 90, 128, 181, 256, 362, 512, 724, 1024)

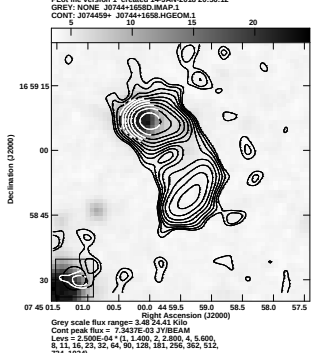
PLot file version 1 created 14-JAN-2018 20:56:12
GREY: NONE J0744+1658D.IMAP.1
CONT: J0744I59+ J0744+1658.HGEOM.1
Declination (J2000)
Right Ascension (J2000)
Grey scale flux range= 3.48 24.41 Kilo
Cont peak flux = 7.3437E-03 JY/BEAM
Levs = 2.500E-04 * (1, 1.400, 2, 2.800, 4, 5.600, 8, 11, 16, 23, 32, 64, 90, 128, 181, 256, 362, 512, 724, 1024)

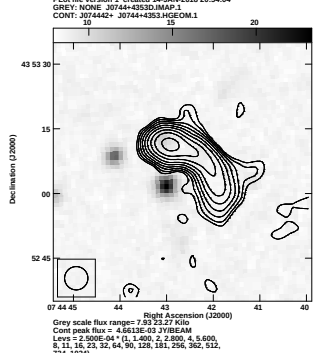
PLot file version 1 created 14-JAN-2018 20:54:04
GREY: NONE J0744+4353D.IMAP.1
CONT: J0744I2+ J0744+4353.HGEOM.1
Declination (J2000)
Right Ascension (J2000)
Grey scale flux range= 7.93 22.27 Kilo
Cont peak flux = 4.6613E-03 JY/BEAM
Levs = 2.500E-04 * (1, 1.400, 2, 2.800, 4, 5.600, 8, 11, 16, 23, 32, 64, 90, 128, 181, 256, 362, 512, 724, 1024)

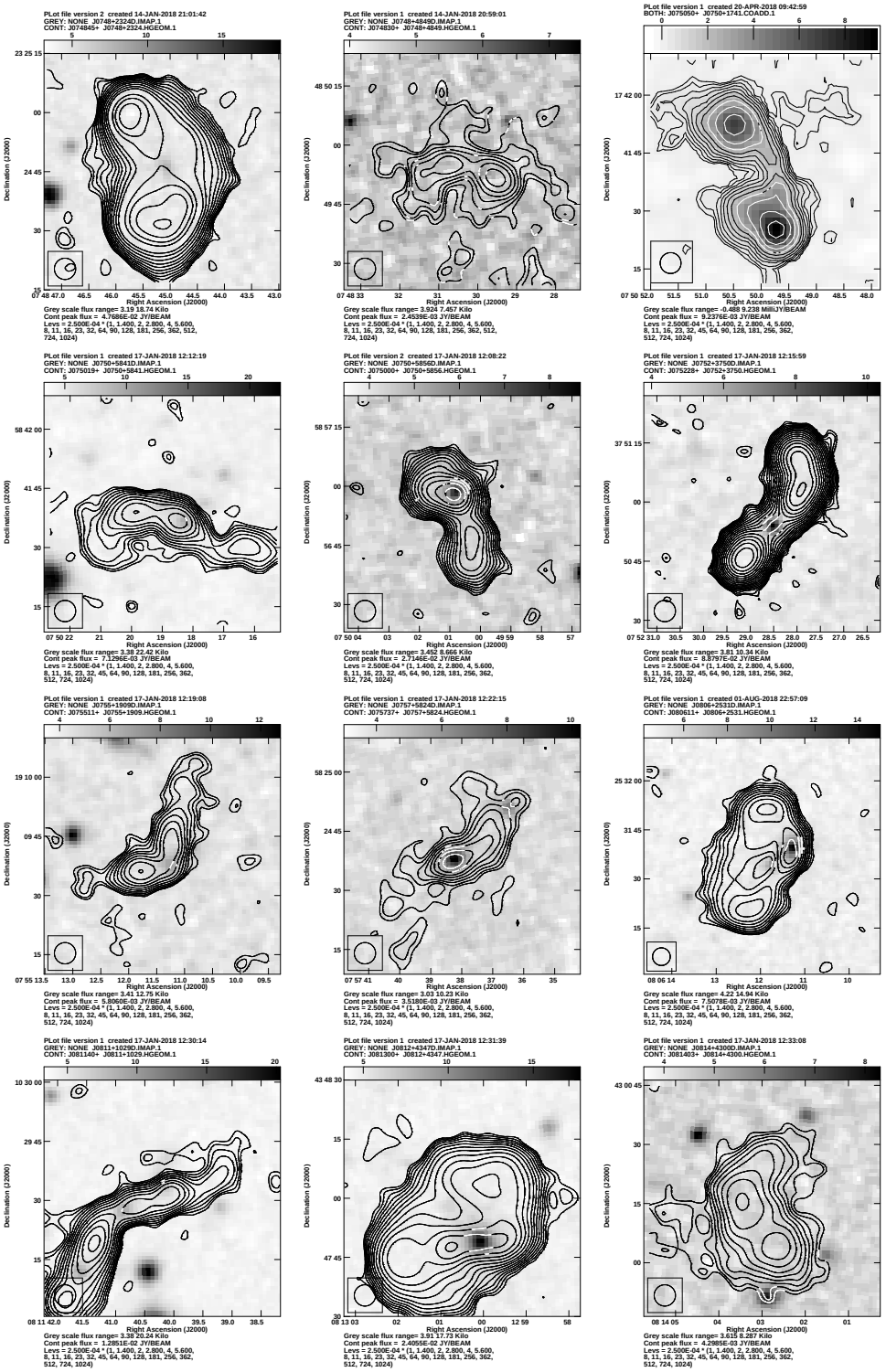
PLot file version 2 created 14-JAN-2018 21:01:42
GREY: NONE J0748+2324D.IMAP.1
CONT: J0748+ J0748+2324.HGEOM.1
Grey scale flux range= 3.19 18.74 Kilo
Cont peak flux = 4.7886E-02 JY/BEAM
Levs = 2.500E-04 * (1, 1.400, 2, 2.800, 4, 5.600, 8, 11, 16, 23, 32, 64, 90, 128, 181, 256, 362, 512, 724, 1024)
PLot file version 1 created 14-JAN-2018 20:59:01
GREY: NONE J0748+4849D.IMAP.1
CONT: J0748+ J0748+4849.HGEOM.1
Grey scale flux range= 3.924 7.457 Kilo
Cont peak flux = 2.4539E-03 JY/BEAM
Levs = 2.500E-04 * (1, 1.400, 2, 2.800, 4, 5.600, 8, 11, 16, 23, 32, 64, 90, 128, 181, 256, 362, 512, 724, 1024)
PLot file version 1 created 20-APR-2018 09:42:59
BOTH: J0750+ J0750+1741.COADD.1
Grey scale flux range= -0.488 9.238 MilliJY/BEAM
Cont peak flux = 9.2376E-03 JY/BEAM
Levs = 2.500E-04 * (1, 1.400, 2, 2.800, 4, 5.600, 8, 11, 16, 23, 32, 45, 64, 90, 128, 181, 256, 362, 512, 724, 1024)
PLot file version 1 created 17-JAN-2018 12:12:19
GREY: NONE J0750+5841D.IMAP.1
CONT: J0750+ J0750+5841.HGEOM.1
Grey scale flux range= 3.38 22.42 Kilo
Cont peak flux = 7.1296E-03 JY/BEAM
Levs = 2.500E-04 * (1, 1.400, 2, 2.800, 4, 5.600, 8, 11, 16, 23, 32, 45, 64, 90, 128, 181, 256, 362, 512, 724, 1024)
PLot file version 2 created 17-JAN-2018 12:08:22
GREY: NONE J0750+5856D.IMAP.1
CONT: J0750+ J0750+5856.HGEOM.1
Grey scale flux range= 3.452 8.666 Kilo
Cont peak flux = 2.7146E-02 JY/BEAM
Levs = 2.500E-04 * (1, 1.400, 2, 2.800, 4, 5.600, 8, 11, 16, 23, 32, 45, 64, 90, 128, 181, 256, 362, 512, 724, 1024)
PLot file version 1 created 17-JAN-2018 12:15:59
GREY: NONE J0752+3750D.IMAP.1
CONT: J0752+ J0752+3750.HGEOM.1
Grey scale flux range= 3.81 10.34 Kilo
Cont peak flux = 8.8797E-02 JY/BEAM
Levs = 2.500E-04 * (1, 1.400, 2, 2.800, 4, 5.600, 8, 11, 16, 23, 32, 45, 64, 90, 128, 181, 256, 362, 512, 724, 1024)
PLot file version 1 created 17-JAN-2018 12:19:08
GREY: NONE J0755+1909D.IMAP.1
CONT: J0755+ J0755+1909.HGEOM.1
Grey scale flux range= 3.41 12.75 Kilo
Cont peak flux = 5.8060E-03 JY/BEAM
Levs = 2.500E-04 * (1, 1.400, 2, 2.800, 4, 5.600, 8, 11, 16, 23, 32, 45, 64, 90, 128, 181, 256, 362, 512, 724, 1024)
PLot file version 1 created 17-JAN-2018 12:22:15
GREY: NONE J0757+5824D.IMAP.1
CONT: J0757+ J0757+5824.HGEOM.1
Grey scale flux range= 3.03 10.23 Kilo
Cont peak flux = 3.5180E-03 JY/BEAM
Levs = 2.500E-04 * (1, 1.400, 2, 2.800, 4, 5.600, 8, 11, 16, 23, 32, 45, 64, 90, 128, 181, 256, 362, 512, 724, 1024)
PLot file version 1 created 01-AUG-2018 22:57:09
GREY: NONE J0806+2531D.IMAP.1
CONT: J0806+ J0806+2531.HGEOM.1
Grey scale flux range= 4.22 14.94 Kilo
Cont peak flux = 7.5078E-03 JY/BEAM
Levs = 2.500E-04 * (1, 1.400, 2, 2.800, 4, 5.600, 8, 11, 16, 23, 32, 45, 64, 90, 128, 181, 256, 362, 512, 724, 1024)
PLot file version 1 created 17-JAN-2018 12:30:14
GREY: NONE J0811+1029D.IMAP.1
CONT: J0811+ J0811+1029.HGEOM.1
Grey scale flux range= 3.38 20.24 Kilo
Cont peak flux = 1.2851E-02 JY/BEAM
Levs = 2.500E-04 * (1, 1.400, 2, 2.800, 4, 5.600, 8, 11, 16, 23, 32, 45, 64, 90, 128, 181, 256, 362, 512, 724, 1024)
PLot file version 1 created 17-JAN-2018 12:31:39
GREY: NONE J0812+4347D.IMAP.1
CONT: J0813+ J0812+4347.HGEOM.1
Grey scale flux range= 3.91 17.73 Kilo
Cont peak flux = 2.4056E-02 JY/BEAM
Levs = 2.500E-04 * (1, 1.400, 2, 2.800, 4, 5.600, 8, 11, 16, 23, 32, 45, 64, 90, 128, 181, 256, 362, 512, 724, 1024)
PLot file version 1 created 17-JAN-2018 12:33:08
GREY: NONE J0814+4300D.IMAP.1
CONT: J0814+ J0814+4300.HGEOM.1
Grey scale flux range= 3.615 8.287 Kilo
Cont peak flux = 4.2985E-03 JY/BEAM
Levs = 2.500E-04 * (1, 1.400, 2, 2.800, 4, 5.600, 8, 11, 16, 23, 32, 45, 64, 90, 128, 181, 256, 362, 512, 724, 1024)
Declination (J2000)
Right Ascension (J2000)

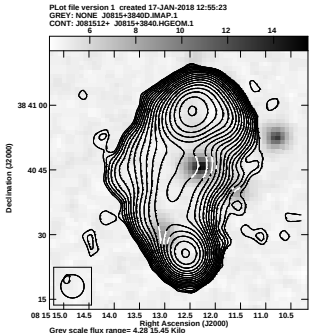
PLot file version 1 created 17-JAN-2018 12:55:23
GREY: NONE J0815+3840D.IMAP.1
CONT: J0815I2+ J0815+3840.HGEOM.1
Declination (J2000)
Right Ascension (J2000)
Grey scale flux range= 4.28 15.45 Kilo
Cont peak flux = 9.4226E-02 JY/BEAM
Levs = 2.500E-04 * (1, 1.400, 2, 2.800, 4, 5.600, 8, 11, 16, 23, 32, 45, 64, 90, 128, 181, 256, 362, 512, 724, 1024)

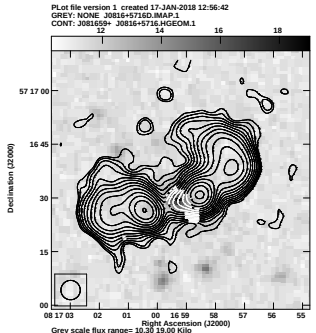
PLot file version 1 created 17-JAN-2018 12:56:42
GREY: NONE J0816+5716D.IMAP.1
CONT: J0816I9+ J0816+5716.HGEOM.1
Declination (J2000)
Right Ascension (J2000)
Grey scale flux range= 10.30 19.00 Kilo
Cont peak flux = 2.4761E-02 JY/BEAM
Levs = 2.500E-04 * (1, 1.400, 2, 2.800, 4, 5.600, 8, 11, 16, 23, 32, 45, 64, 90, 128, 181, 256, 362, 512, 724, 1024)

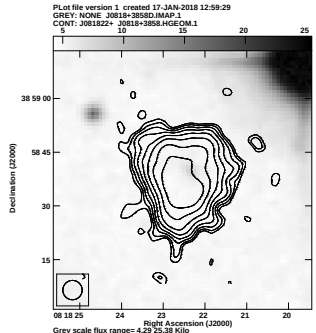
PLot file version 1 created 17-JAN-2018 12:59:29
GREY: NONE J0818+3858D.IMAP.1
CONT: J0818I2+ J0818+3858.HGEOM.1
Declination (J2000)
Right Ascension (J2000)
Grey scale flux range= 4.29 25.38 Kilo
Cont peak flux = 3.7772E-03 JY/BEAM
Levs = 2.500E-04 * (1, 1.400, 2, 2.800, 4, 5.600, 8, 11, 16, 23, 32, 45, 64, 90, 128, 181, 256, 362, 512, 724, 1024)

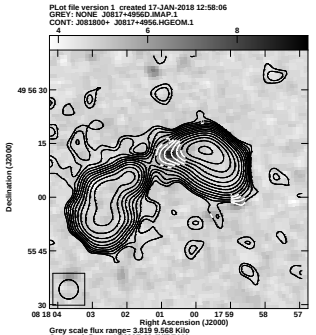
PLot file version 1 created 17-JAN-2018 12:58:06
GREY: NONE J0817+4956D.IMAP.1
CONT: J0818I0+ J0817+4956.HGEOM.1
Declination (J2000)
Right Ascension (J2000)
Grey scale flux range= 3.819 9.568 Kilo
Cont peak flux = 1.7020E-02 JY/BEAM
Levs = 2.500E-04 * (1, 1.400, 2, 2.800, 4, 5.600, 8, 11, 16, 23, 32, 45, 64, 90, 128, 181, 256, 362, 512, 724, 1024)

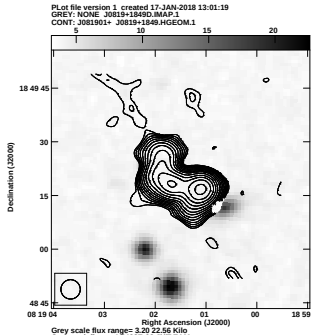
PLot file version 1 created 17-JAN-2018 13:01:19
GREY: NONE J0819+1849D.IMAP.1
CONT: J0819I1+ J0819+1849.HGEOM.1
Declination (J2000)
Right Ascension (J2000)
Grey scale flux range= 3.20 22.56 Kilo
Cont peak flux = 1.9438E-02 JY/BEAM
Levs = 2.500E-04 * (1, 1.400, 2, 2.800, 4, 5.600, 8, 11, 16, 23, 32, 45, 64, 90, 128, 181, 256, 362, 512, 724, 1024)

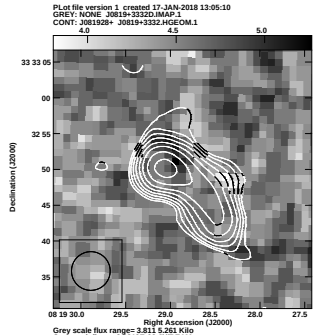
PLot file version 1 created 17-JAN-2018 13:05:10
GREY: NONE J0819+3332D.IMAP.1
CONT: J0819I2+ J0819+3332.HGEOM.1
Declination (J2000)
Right Ascension (J2000)
Grey scale flux range= 3.811 5.261 Kilo
Cont peak flux = 3.2318E-03 JY/BEAM
Levs = 2.500E-04 * (1, 1.400, 2, 2.800, 4, 5.600, 8, 11, 16, 23, 32, 45, 64, 90, 128, 181, 256, 362, 512, 724, 1024)

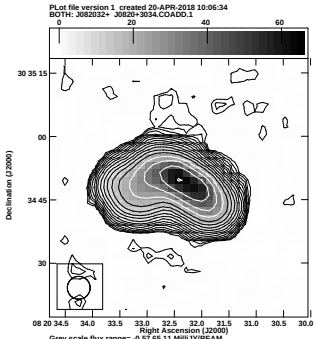
PLot file version 1 created 20-APR-2018 10:06:34
BOTH: J0820I2+ J0820+3034.COADD.1
Declination (J2000)
Right Ascension (J2000)
Grey scale flux range= -0.57 65.11 MILLI/BEAM
Cont peak flux = 6.5110E-02 JY/BEAM
Levs = 2.500E-04 * (1, 1.400, 2, 2.800, 4, 5.600, 8, 11, 16, 23, 32, 45, 64, 90, 128, 181, 256, 362, 512, 724, 1024)

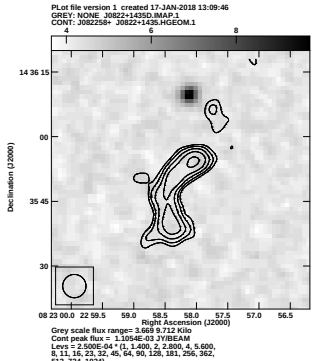
PLot file version 1 created 17-JAN-2018 13:09:46
GREY: NONE J0822+1435D.IMAP.1
CONT: J0822I5+ J0822+1435.HGEOM.1
Declination (J2000)
Right Ascension (J2000)
Grey scale flux range= 3.669 9.712 Kilo
Cont peak flux = 1.1054E-03 JY/BEAM
Levs = 2.500E-04 * (1, 1.400, 2, 2.800, 4, 5.600, 8, 11, 16, 23, 32, 45, 64, 90, 128, 181, 256, 362, 512, 724, 1024)

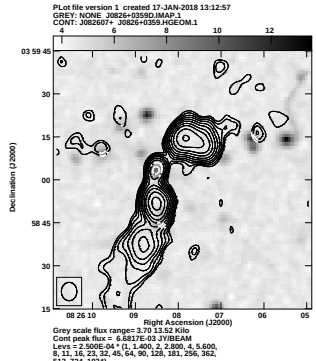
PLot file version 1 created 17-JAN-2018 13:12:57
GREY: NONE J0826+0359D.IMAP.1
CONT: J0826I7+ J0826+0359.HGEOM.1
Declination (J2000)
Right Ascension (J2000)
Grey scale flux range= 3.70 13.52 Kilo
Cont peak flux = 6.6817E-03 JY/BEAM
Levs = 2.500E-04 * (1, 1.400, 2, 2.800, 4, 5.600, 8, 11, 16, 23, 32, 45, 64, 90, 128, 181, 256, 362, 512, 724, 1024)

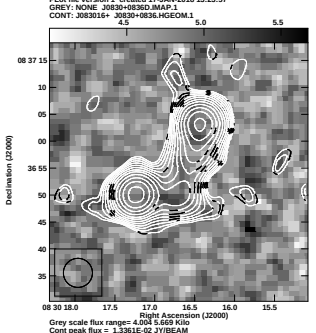
PLot file version 1 created 17-JAN-2018 13:23:57
GREY: NONE J0830+0836D.IMAP.1
CONT: J0830I6+ J0830+0836.HGEOM.1
Declination (J2000)
Right Ascension (J2000)
Grey scale flux range= 4.004 5.669 Kilo
Cont peak flux = 1.3361E-02 JY/BEAM
Levs = 2.500E-04 * (1, 1.400, 2, 2.800, 4, 5.600, 8, 11, 16, 23, 32, 45, 64, 90, 128, 181, 256, 362, 512, 724, 1024)

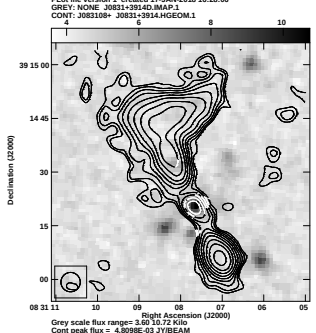
PLot file version 1 created 17-JAN-2018 16:28:06
GREY: NONE J0831+3914D.IMAP.1
CONT: J0831I8+ J0831+3914.HGEOM.1
Declination (J2000)
Right Ascension (J2000)
Grey scale flux range= 3.60 10.72 Kilo
Cont peak flux = 4.8098E-03 JY/BEAM
Levs = 2.500E-04 * (1, 1.400, 2, 2.800, 4, 5.600, 8, 11, 16, 23, 32, 45, 64, 90, 128, 181, 256, 362, 512, 724, 1024)

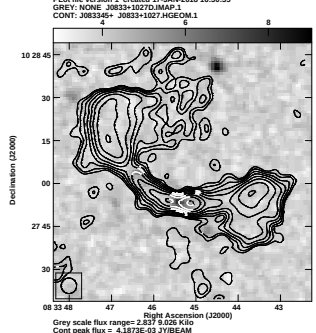
PLot file version 1 created 17-JAN-2018 16:30:35
GREY: NONE J0833+1027D.IMAP.1
CONT: J0833I4+ J0833+1027.HGEOM.1
Declination (J2000)
Right Ascension (J2000)
Grey scale flux range= 2.837 9.026 Kilo
Cont peak flux = 4.1873E-03 JY/BEAM
Levs = 2.500E-04 * (1, 1.400, 2, 2.800, 4, 5.600, 8, 11, 16, 23, 32, 45, 64, 90, 128, 181, 256, 362, 512, 724, 1024)

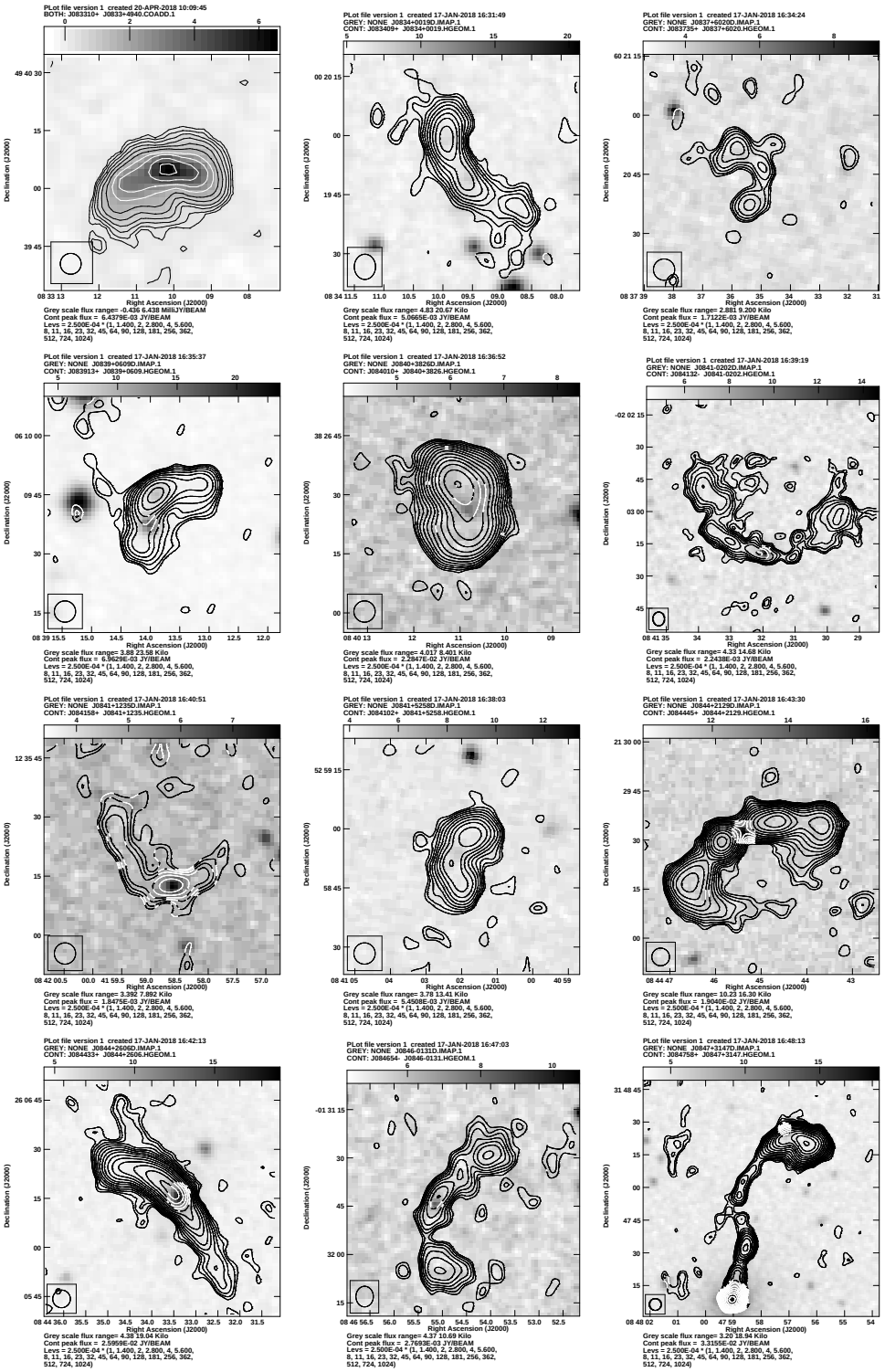
PLot file version 1 created 20-APR-2018 10:09:45
BOTH: J083310+ J0833+4940.COADD.1
Declination (J2000)
Right Ascension (J2000)
Grey scale flux range= -6.439 6.438 MilliJY/BEAM
Cont peak flux = 6.4379E-03 JY/BEAM
Levs = 2.500E-04 * (1, 1.400, 2, 2.800, 4, 5.600, 8, 11, 16, 23, 32, 45, 64, 90, 128, 181, 256, 362, 512, 724, 1024)
PLot file version 1 created 17-JAN-2018 16:31:49
GREY: NONE J0834+0019D.IMAP.1
CONT: J083409+ J0834+0019.HGEOM.1
Declination (J2000)
Right Ascension (J2000)
Grey scale flux range= -4.83 20.67 Kilo
Cont peak flux = 5.0665E-03 JY/BEAM
Levs = 2.500E-04 * (1, 1.400, 2, 2.800, 4, 5.600, 8, 11, 16, 23, 32, 45, 64, 90, 128, 181, 256, 362, 512, 724, 1024)
PLot file version 1 created 17-JAN-2018 16:34:24
GREY: NONE J0837+6020D.IMAP.1
CONT: J083735+ J0837+6020.HGEOM.1
Declination (J2000)
Right Ascension (J2000)
Grey scale flux range= 2.881 9.200 Kilo
Cont peak flux = 1.7122E-03 JY/BEAM
Levs = 2.500E-04 * (1, 1.400, 2, 2.800, 4, 5.600, 8, 11, 16, 23, 32, 45, 64, 90, 128, 181, 256, 362, 512, 724, 1024)
PLot file version 1 created 17-JAN-2018 16:35:37
GREY: NONE J0839+0609D.IMAP.1
CONT: J083913+ J0839+0609.HGEOM.1
Declination (J2000)
Right Ascension (J2000)
Grey scale flux range= 3.88 23.58 Kilo
Cont peak flux = 6.9629E-03 JY/BEAM
Levs = 2.500E-04 * (1, 1.400, 2, 2.800, 4, 5.600, 8, 11, 16, 23, 32, 45, 64, 90, 128, 181, 256, 362, 512, 724, 1024)
PLot file version 1 created 17-JAN-2018 16:36:52
GREY: NONE J0840+3826D.IMAP.1
CONT: J084010+ J0840+3826.HGEOM.1
Declination (J2000)
Right Ascension (J2000)
Grey scale flux range= 4.017 8.401 Kilo
Cont peak flux = 2.2847E-02 JY/BEAM
Levs = 2.500E-04 * (1, 1.400, 2, 2.800, 4, 5.600, 8, 11, 16, 23, 32, 45, 64, 90, 128, 181, 256, 362, 512, 724, 1024)
PLot file version 1 created 17-JAN-2018 16:39:19
GREY: NONE J0841-0202D.IMAP.1
CONT: J084132- J0841-0202.HGEOM.1
Declination (J2000)
Right Ascension (J2000)
Grey scale flux range= 4.33 14.68 Kilo
Cont peak flux = 2.2438E-03 JY/BEAM
Levs = 2.500E-04 * (1, 1.400, 2, 2.800, 4, 5.600, 8, 11, 16, 23, 32, 45, 64, 90, 128, 181, 256, 362, 512, 724, 1024)
PLot file version 1 created 17-JAN-2018 16:40:51
GREY: NONE J0841+1235D.IMAP.1
CONT: J084158+ J0841+1235.HGEOM.1
Declination (J2000)
Right Ascension (J2000)
Grey scale flux range= 3.392 7.892 Kilo
Cont peak flux = 1.8475E-03 JY/BEAM
Levs = 2.500E-04 * (1, 1.400, 2, 2.800, 4, 5.600, 8, 11, 16, 23, 32, 45, 64, 90, 128, 181, 256, 362, 512, 724, 1024)
PLot file version 1 created 17-JAN-2018 16:38:03
GREY: NONE J0841+5258D.IMAP.1
CONT: J084102+ J0841+5258.HGEOM.1
Declination (J2000)
Right Ascension (J2000)
Grey scale flux range= 3.78 13.41 Kilo
Cont peak flux = 5.4508E-03 JY/BEAM
Levs = 2.500E-04 * (1, 1.400, 2, 2.800, 4, 5.600, 8, 11, 16, 23, 32, 45, 64, 90, 128, 181, 256, 362, 512, 724, 1024)
PLot file version 1 created 17-JAN-2018 16:43:30
GREY: NONE J0844+2129D.IMAP.1
CONT: J084445+ J0844+2129.HGEOM.1
Declination (J2000)
Right Ascension (J2000)
Grey scale flux range= 10.23 16.30 Kilo
Cont peak flux = 1.9040E-02 JY/BEAM
Levs = 2.500E-04 * (1, 1.400, 2, 2.800, 4, 5.600, 8, 11, 16, 23, 32, 45, 64, 90, 128, 181, 256, 362, 512, 724, 1024)
PLot file version 1 created 17-JAN-2018 16:42:13
GREY: NONE J0844+2606D.IMAP.1
CONT: J084433+ J0844+2606.HGEOM.1
Declination (J2000)
Right Ascension (J2000)
Grey scale flux range= 4.38 19.04 Kilo
Cont peak flux = 2.5959E-02 JY/BEAM
Levs = 2.500E-04 * (1, 1.400, 2, 2.800, 4, 5.600, 8, 11, 16, 23, 32, 45, 64, 90, 128, 181, 256, 362, 512, 724, 1024)
PLot file version 1 created 17-JAN-2018 16:47:03
GREY: NONE J0846-0131D.IMAP.1
CONT: J084654- J0846-0131.HGEOM.1
Declination (J2000)
Right Ascension (J2000)
Grey scale flux range= 4.37 10.69 Kilo
Cont peak flux = 2.7693E-03 JY/BEAM
Levs = 2.500E-04 * (1, 1.400, 2, 2.800, 4, 5.600, 8, 11, 16, 23, 32, 45, 64, 90, 128, 181, 256, 362, 512, 724, 1024)
PLot file version 1 created 17-JAN-2018 16:48:13
GREY: NONE J0847+3147D.IMAP.1
CONT: J084758+ J0847+3147.HGEOM.1
Declination (J2000)
Right Ascension (J2000)
Grey scale flux range= 3.20 18.94 Kilo
Cont peak flux = 3.3155E-02 JY/BEAM
Levs = 2.500E-04 * (1, 1.400, 2, 2.800, 4, 5.600, 8, 11, 16, 23, 32, 45, 64, 90, 128, 181, 256, 362, 512, 724, 1024)

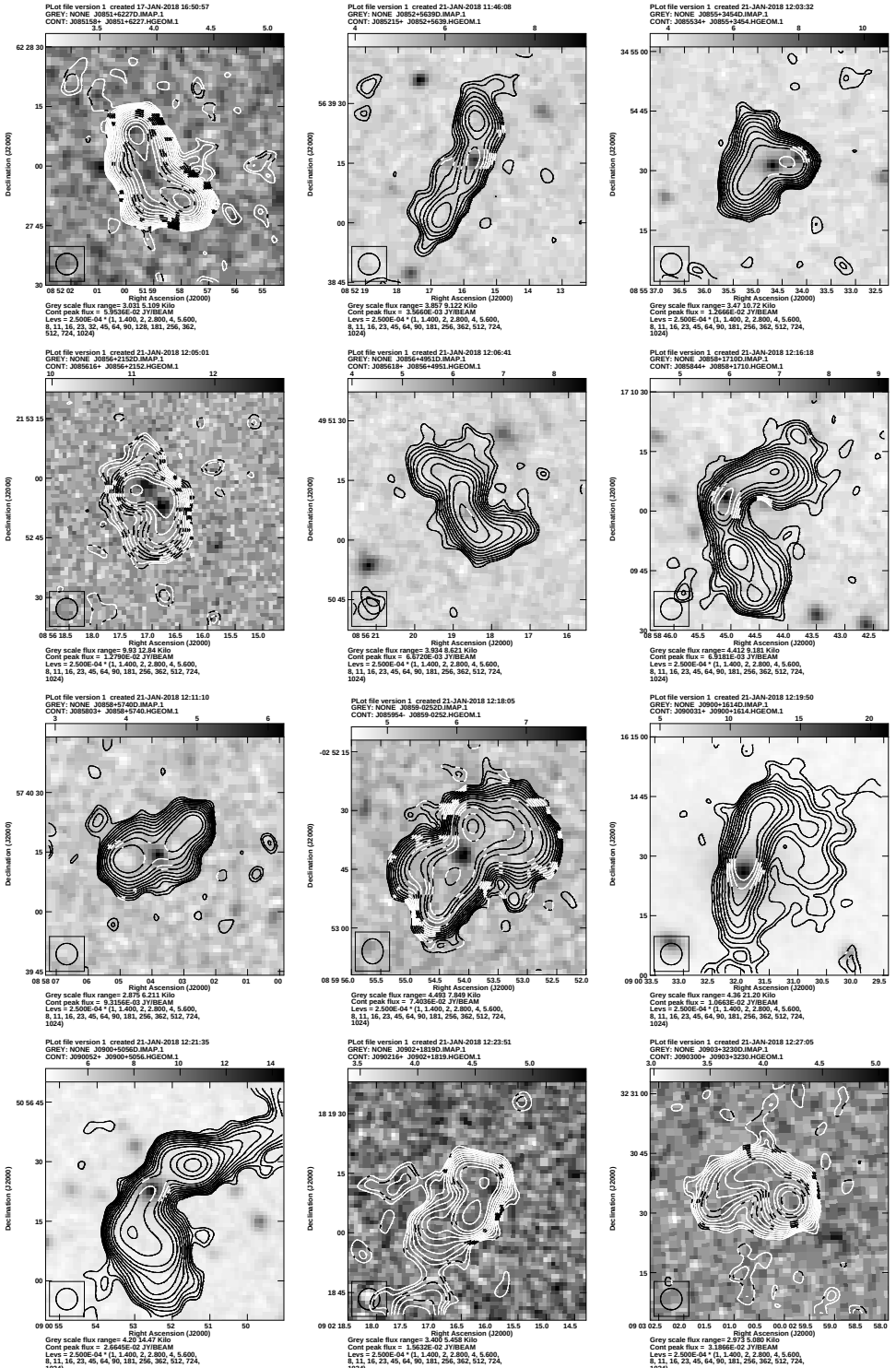
PLot file version 1 created 17-JAN-2018 16:50:57
GREY: NONE J0851+6227D.IMAP.1
CONT: J0851S8+ J0851+6227.HGEOM.1
Grey scale flux range= 3.031 5.109 Kilo
Cont peak flux = 5.9536E-02 JY/BEAM
Levs = 2.500E-04 * (1, 1.400, 2, 2.800, 4, 5.600, 8, 11, 16, 23, 32, 45, 64, 90, 128, 181, 256, 362, 512, 724, 1024)
PLot file version 1 created 21-JAN-2018 11:46:08
GREY: NONE J0852+5639D.IMAP.1
CONT: J0852I5+ J0852+5639.HGEOM.1
Grey scale flux range= 3.857 9.122 Kilo
Cont peak flux = 3.9660E-03 JY/BEAM
Levs = 2.500E-04 * (1, 1.400, 2, 2.800, 4, 5.600, 8, 11, 16, 23, 45, 64, 90, 181, 256, 362, 512, 724, 1024)
PLot file version 1 created 21-JAN-2018 12:03:32
GREY: NONE J0855+3454D.IMAP.1
CONT: J0855S3+ J0855+3454.HGEOM.1
Grey scale flux range= 3.47 10.72 Kilo
Cont peak flux = 1.2666E-02 JY/BEAM
Levs = 2.500E-04 * (1, 1.400, 2, 2.800, 4, 5.600, 8, 11, 16, 23, 45, 64, 90, 181, 256, 362, 512, 724, 1024)
PLot file version 1 created 21-JAN-2018 12:05:01
GREY: NONE J0856+2152D.IMAP.1
CONT: J0856I6+ J0856+2152.HGEOM.1
Grey scale flux range= 9.93 12.84 Kilo
Cont peak flux = 1.2790E-02 JY/BEAM
Levs = 2.500E-04 * (1, 1.400, 2, 2.800, 4, 5.600, 8, 11, 16, 23, 45, 64, 90, 181, 256, 362, 512, 724, 1024)
PLot file version 1 created 21-JAN-2018 12:06:41
GREY: NONE J0856+4951D.IMAP.1
CONT: J0856I8+ J0856+4951.HGEOM.1
Grey scale flux range= 3.934 8.621 Kilo
Cont peak flux = 6.6720E-03 JY/BEAM
Levs = 2.500E-04 * (1, 1.400, 2, 2.800, 4, 5.600, 8, 11, 16, 23, 45, 64, 90, 181, 256, 362, 512, 724, 1024)
PLot file version 1 created 21-JAN-2018 12:16:18
GREY: NONE J0858+1710D.IMAP.1
CONT: J0858I4+ J0858+1710.HGEOM.1
Grey scale flux range= 4.412 9.181 Kilo
Cont peak flux = 6.9181E-03 JY/BEAM
Levs = 2.500E-04 * (1, 1.400, 2, 2.800, 4, 5.600, 8, 11, 16, 23, 45, 64, 90, 181, 256, 362, 512, 724, 1024)
PLot file version 1 created 21-JAN-2018 12:11:10
GREY: NONE J0858+5740D.IMAP.1
CONT: J0858I3+ J0858+5740.HGEOM.1
Grey scale flux range= 2.875 6.211 Kilo
Cont peak flux = 9.3156E-03 JY/BEAM
Levs = 2.500E-04 * (1, 1.400, 2, 2.800, 4, 5.600, 8, 11, 16, 23, 45, 64, 90, 181, 256, 362, 512, 724, 1024)
PLot file version 1 created 21-JAN-2018 12:18:05
GREY: NONE J0859-0252D.IMAP.1
CONT: J0859S4- J0859-0252.HGEOM.1
Grey scale flux range= 4.493 7.849 Kilo
Cont peak flux = 7.4036E-02 JY/BEAM
Levs = 2.500E-04 * (1, 1.400, 2, 2.800, 4, 5.600, 8, 11, 16, 23, 45, 64, 90, 181, 256, 362, 512, 724, 1024)
PLot file version 1 created 21-JAN-2018 12:19:50
GREY: NONE J0900+1614D.IMAP.1
CONT: J0900I1+ J0900+1614.HGEOM.1
Grey scale flux range= 4.36 21.20 Kilo
Cont peak flux = 1.0663E-02 JY/BEAM
Levs = 2.500E-04 * (1, 1.400, 2, 2.800, 4, 5.600, 8, 11, 16, 23, 45, 64, 90, 181, 256, 362, 512, 724, 1024)
PLot file version 1 created 21-JAN-2018 12:21:35
GREY: NONE J0900+5056D.IMAP.1
CONT: J0900I2+ J0900+5056.HGEOM.1
Grey scale flux range= 4.20 14.47 Kilo
Cont peak flux = 2.6645E-02 JY/BEAM
Levs = 2.500E-04 * (1, 1.400, 2, 2.800, 4, 5.600, 8, 11, 16, 23, 45, 64, 90, 181, 256, 362, 512, 724, 1024)
PLot file version 1 created 21-JAN-2018 12:23:51
GREY: NONE J0902+1819D.IMAP.1
CONT: J0902I6+ J0902+1819.HGEOM.1
Grey scale flux range= 3.400 5.458 Kilo
Cont peak flux = 1.5632E-02 JY/BEAM
Levs = 2.500E-04 * (1, 1.400, 2, 2.800, 4, 5.600, 8, 11, 16, 23, 45, 64, 90, 181, 256, 362, 512, 724, 1024)
PLot file version 1 created 21-JAN-2018 12:27:05
GREY: NONE J0903+3230D.IMAP.1
CONT: J0903I0+ J0903+3230.HGEOM.1
Grey scale flux range= 2.973 5.080 Kilo
Cont peak flux = 3.1866E-02 JY/BEAM
Levs = 2.500E-04 * (1, 1.400, 2, 2.800, 4, 5.600, 8, 11, 16, 23, 45, 64, 90, 181, 256, 362, 512, 724, 1024)
Declination (J2000)
Right Ascension (J2000)

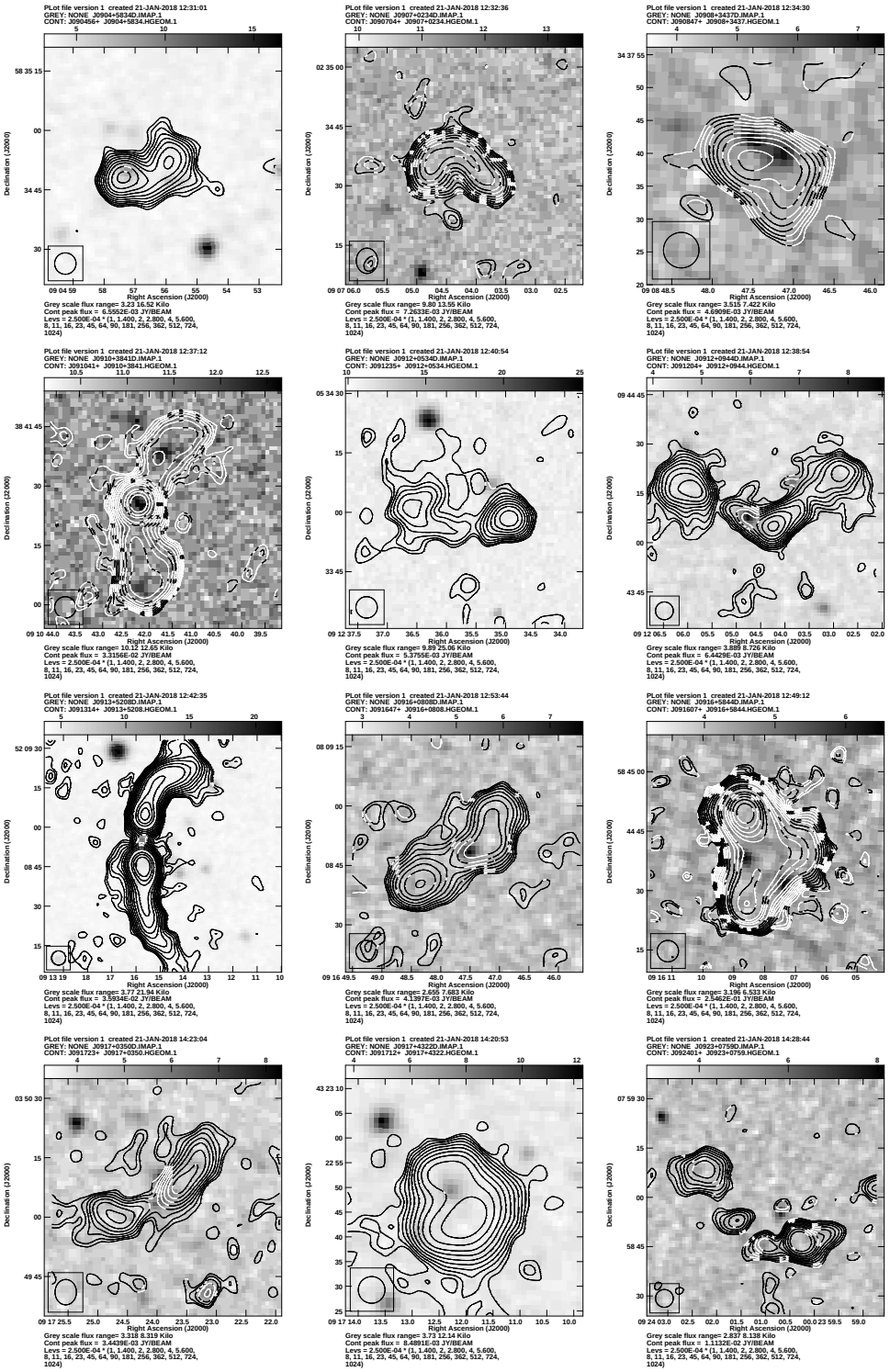
PLot file version 1 created 21-JAN-2018 12:31:01
GREY: NONE J0904+5834D.IMAP.1
CONT: J0904S6+ J0904+5834.HGEOM.1
Declination (J2000)
Right Ascension (J2000)
Grey scale flux range= 3.23 16.52 Kilo
Cont peak flux = 6.5552E-03 JY/BEAM
Levs = 2.500E-04 * (1, 1.400, 2, 2.800, 4, 5.600, 8, 11, 16, 23, 45, 64, 90, 181, 256, 362, 512, 724, 1024)
PLot file version 1 created 21-JAN-2018 12:32:36
GREY: NONE J0907+0234D.IMAP.1
CONT: J0907O4+ J0907+0234.HGEOM.1
Declination (J2000)
Right Ascension (J2000)
Grey scale flux range= 9.80 13.55 Kilo
Cont peak flux = 7.2633E-03 JY/BEAM
Levs = 2.500E-04 * (1, 1.400, 2, 2.800, 4, 5.600, 8, 11, 16, 23, 45, 64, 90, 181, 256, 362, 512, 724, 1024)
PLot file version 1 created 21-JAN-2018 12:34:30
GREY: NONE J0908+3437D.IMAP.1
CONT: J0908A7+ J0908+3437.HGEOM.1
Declination (J2000)
Right Ascension (J2000)
Grey scale flux range= 3.515 7.422 Kilo
Cont peak flux = 4.6909E-03 JY/BEAM
Levs = 2.500E-04 * (1, 1.400, 2, 2.800, 4, 5.600, 8, 11, 16, 23, 45, 64, 90, 181, 256, 362, 512, 724, 1024)
PLot file version 1 created 21-JAN-2018 12:37:12
GREY: NONE J0910+3841D.IMAP.1
CONT: J091041+ J0910+3841.HGEOM.1
Declination (J2000)
Right Ascension (J2000)
Grey scale flux range= 10.12 12.65 Kilo
Cont peak flux = 3.3156E-02 JY/BEAM
Levs = 2.500E-04 * (1, 1.400, 2, 2.800, 4, 5.600, 8, 11, 16, 23, 45, 64, 90, 181, 256, 362, 512, 724, 1024)
PLot file version 1 created 21-JAN-2018 12:40:54
GREY: NONE J0912+0534D.IMAP.1
CONT: J091235+ J0912+0534.HGEOM.1
Declination (J2000)
Right Ascension (J2000)
Grey scale flux range= 9.89 25.06 Kilo
Cont peak flux = 5.3755E-03 JY/BEAM
Levs = 2.500E-04 * (1, 1.400, 2, 2.800, 4, 5.600, 8, 11, 16, 23, 45, 64, 90, 181, 256, 362, 512, 724, 1024)
PLot file version 1 created 21-JAN-2018 12:38:54
GREY: NONE J0912+0944D.IMAP.1
CONT: J0912O4+ J0912+0944.HGEOM.1
Declination (J2000)
Right Ascension (J2000)
Grey scale flux range= 3.888 8.726 Kilo
Cont peak flux = 6.4429E-03 JY/BEAM
Levs = 2.500E-04 * (1, 1.400, 2, 2.800, 4, 5.600, 8, 11, 16, 23, 45, 64, 90, 181, 256, 362, 512, 724, 1024)
PLot file version 1 created 21-JAN-2018 12:42:35
GREY: NONE J0913+5208D.IMAP.1
CONT: J091314+ J0913+5208.HGEOM.1
Declination (J2000)
Right Ascension (J2000)
Grey scale flux range= 3.77 21.94 Kilo
Cont peak flux = 3.5934E-02 JY/BEAM
Levs = 2.500E-04 * (1, 1.400, 2, 2.800, 4, 5.600, 8, 11, 16, 23, 45, 64, 90, 181, 256, 362, 512, 724, 1024)
PLot file version 1 created 21-JAN-2018 12:53:44
GREY: NONE J0916+0808D.IMAP.1
CONT: J091647+ J0916+0808.HGEOM.1
Declination (J2000)
Right Ascension (J2000)
Grey scale flux range= 2.655 7.683 Kilo
Cont peak flux = 4.1397E-03 JY/BEAM
Levs = 2.500E-04 * (1, 1.400, 2, 2.800, 4, 5.600, 8, 11, 16, 23, 45, 64, 90, 181, 256, 362, 512, 724, 1024)
PLot file version 1 created 21-JAN-2018 12:49:12
GREY: NONE J0916+5844D.IMAP.1
CONT: J0916O7+ J0916+5844.HGEOM.1
Declination (J2000)
Right Ascension (J2000)
Grey scale flux range= 3.196 6.533 Kilo
Cont peak flux = 2.5462E-01 JY/BEAM
Levs = 2.500E-04 * (1, 1.400, 2, 2.800, 4, 5.600, 8, 11, 16, 23, 45, 64, 90, 181, 256, 362, 512, 724, 1024)
PLot file version 1 created 21-JAN-2018 14:23:04
GREY: NONE J0917+0350D.IMAP.1
CONT: J091723+ J0917+0350.HGEOM.1
Declination (J2000)
Right Ascension (J2000)
Grey scale flux range= 3.318 8.319 Kilo
Cont peak flux = 3.4439E-03 JY/BEAM
Levs = 2.500E-04 * (1, 1.400, 2, 2.800, 4, 5.600, 8, 11, 16, 23, 45, 64, 90, 181, 256, 362, 512, 724, 1024)
PLot file version 1 created 21-JAN-2018 14:20:53
GREY: NONE J0917+4322D.IMAP.1
CONT: J091712+ J0917+4322.HGEOM.1
Declination (J2000)
Right Ascension (J2000)
Grey scale flux range= 3.73 12.14 Kilo
Cont peak flux = 8.4891E-03 JY/BEAM
Levs = 2.500E-04 * (1, 1.400, 2, 2.800, 4, 5.600, 8, 11, 16, 23, 45, 64, 90, 181, 256, 362, 512, 724, 1024)
PLot file version 1 created 21-JAN-2018 14:28:44
GREY: NONE J0923+0759D.IMAP.1
CONT: J092401+ J0923+0759.HGEOM.1
Declination (J2000)
Right Ascension (J2000)
Grey scale flux range= 2.837 8.138 Kilo
Cont peak flux = 1.1132E-02 JY/BEAM
Levs = 2.500E-04 * (1, 1.400, 2, 2.800, 4, 5.600, 8, 11, 16, 23, 45, 64, 90, 181, 256, 362, 512, 724, 1024)

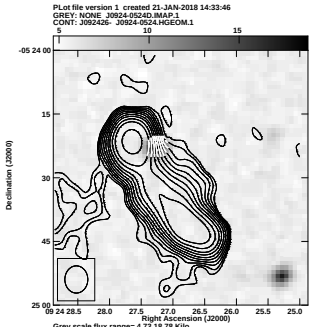
PLot file version 1 created 21-JAN-2018 14:33:46
GREY: NONE J0924-0524D.IMAP.1
CONT: J092426- J0924-0524.HGEOM.1
Declination (J2000)
Right Ascension (J2000)
Grey scale flux range= 4.73 18.78 Kilo
Cont peak flux = 1.5901E-02 JY/BEAM
Levs = 2.500E-04 * (1, 1.400, 2, 2.800, 4, 5.600, 8, 11, 16, 23, 45, 64, 90, 181, 256, 362, 512, 724, 1024)

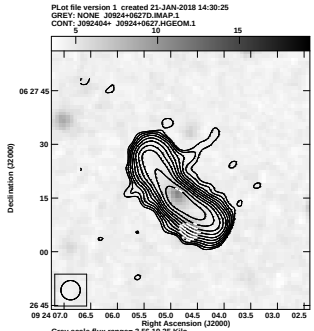
PLot file version 1 created 21-JAN-2018 14:30:25
GREY: NONE J0924+0627D.IMAP.1
CONT: J092404+ J0924+0627.HGEOM.1
Declination (J2000)
Right Ascension (J2000)
Grey scale flux range= 3.56 19.25 Kilo
Cont peak flux = 8.9454E-03 JY/BEAM
Levs = 2.500E-04 * (1, 1.400, 2, 2.800, 4, 5.600, 8, 11, 16, 23, 45, 64, 90, 181, 256, 362, 512, 724, 1024)

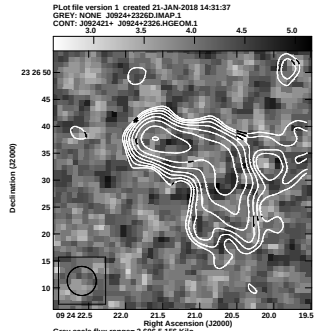
PLot file version 1 created 21-JAN-2018 14:31:37
GREY: NONE J0924+2326D.IMAP.1
CONT: J092421+ J0924+2326.HGEOM.1
Declination (J2000)
Right Ascension (J2000)
Grey scale flux range= 2.606 8.156 Kilo
Cont peak flux = 2.7777E-03 JY/BEAM
Levs = 2.500E-04 * (1, 1.400, 2, 2.800, 4, 5.600, 8, 11, 16, 23, 45, 64, 90, 181, 256, 362, 512, 724, 1024)

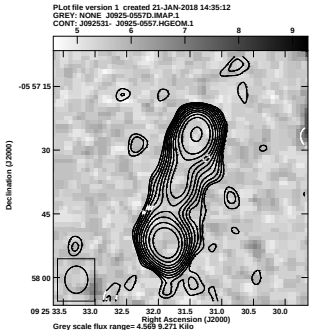
PLot file version 1 created 21-JAN-2018 14:35:12
GREY: NONE J0925-0557D.IMAP.1
CONT: J092531- J0925-0557.HGEOM.1
Declination (J2000)
Right Ascension (J2000)
Grey scale flux range= 4.569 9.271 Kilo
Cont peak flux = 1.2856E-02 JY/BEAM
Levs = 2.500E-04 * (1, 1.400, 2, 2.800, 4, 5.600, 8, 11, 16, 23, 45, 64, 90, 181, 256, 362, 512, 724, 1024)

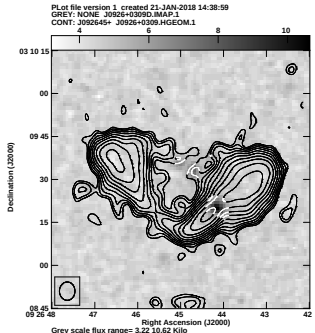
PLot file version 1 created 21-JAN-2018 14:38:59
GREY: NONE J0926+0309D.IMAP.1
CONT: J092645+ J0926+0309.HGEOM.1
Declination (J2000)
Right Ascension (J2000)
Grey scale flux range= 3.22 10.62 Kilo
Cont peak flux = 7.4251E-03 JY/BEAM
Levs = 2.500E-04 * (1, 1.400, 2, 2.800, 4, 5.600, 8, 11, 16, 23, 45, 64, 90, 181, 256, 362, 512, 724, 1024)

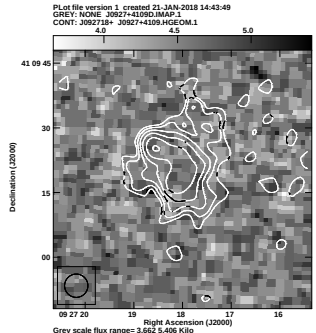
PLot file version 1 created 21-JAN-2018 14:43:49
GREY: NONE J0927+4109D.IMAP.1
CONT: J092718+ J0927+4109.HGEOM.1
Declination (J2000)
Right Ascension (J2000)
Grey scale flux range= 3.662 5.406 Kilo
Cont peak flux = 1.4355E-03 JY/BEAM
Levs = 2.500E-04 * (1, 1.400, 2, 2.800, 4, 5.600, 8, 11, 16, 23, 45, 64, 90, 181, 256, 362, 512, 724, 1024)

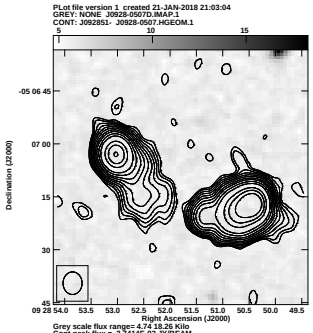
PLot file version 1 created 21-JAN-2018 21:03:04
GREY: NONE J0928-0507D.IMAP.1
CONT: J092851- J0928-0507.HGEOM.1
Declination (J2000)
Right Ascension (J2000)
Grey scale flux range= 4.74 18.26 Kilo
Cont peak flux = 3.7414E-02 JY/BEAM
Levs = 2.500E-04 * (1, 1.400, 2, 2.800, 4, 5.600, 8, 11, 16, 23, 45, 64, 90, 181, 256, 362, 512, 724, 1024)

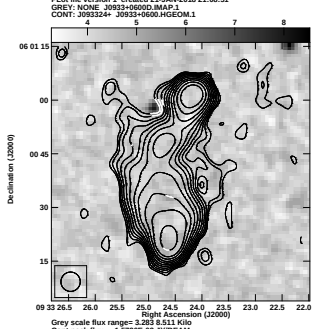
PLot file version 1 created 21-JAN-2018 21:08:51
GREY: NONE J0933+0600D.IMAP.1
CONT: J093324+ J0933+0600.HGEOM.1
Declination (J2000)
Right Ascension (J2000)
Grey scale flux range= 3.283 8.511 Kilo
Cont peak flux = 1.5736E-02 JY/BEAM
Levs = 2.500E-04 * (1, 1.400, 2, 2.800, 4, 5.600, 8, 11, 16, 23, 45, 64, 90, 181, 256, 362, 512, 724, 1024)

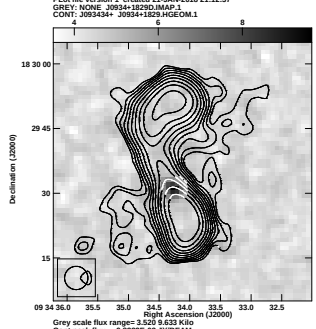
PLot file version 1 created 21-JAN-2018 21:12:37
GREY: NONE J0934+1829D.IMAP.1
CONT: J093434+ J0934+1829.HGEOM.1
Declination (J2000)
Right Ascension (J2000)
Grey scale flux range= 3.520 9.633 Kilo
Cont peak flux = 9.8323E-03 JY/BEAM
Levs = 2.500E-04 * (1, 1.400, 2, 2.800, 4, 5.600, 8, 11, 16, 23, 45, 64, 90, 181, 256, 362, 512, 724, 1024)

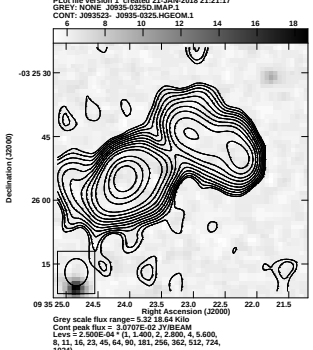
PLot file version 1 created 21-JAN-2018 21:21:17
GREY: NONE J0935-0325D.IMAP.1
CONT: J093523- J0935-0325.HGEOM.1
Declination (J2000)
Right Ascension (J2000)
Grey scale flux range= 5.32 18.64 Kilo
Cont peak flux = 3.0707E-02 JY/BEAM
Levs = 2.500E-04 * (1, 1.400, 2, 2.800, 4, 5.600, 8, 11, 16, 23, 45, 64, 90, 181, 256, 362, 512, 724, 1024)

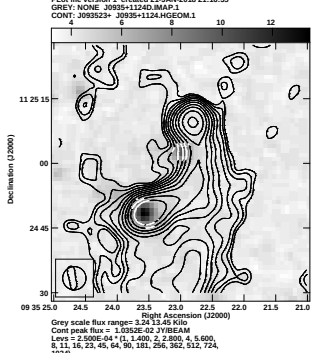
PLot file version 1 created 21-JAN-2018 21:16:35
GREY: NONE J0935+1124D.IMAP.1
CONT: J093523+ J0935+1124.HGEOM.1
Declination (J2000)
Right Ascension (J2000)
Grey scale flux range= 3.24 13.45 Kilo
Cont peak flux = 1.0352E-02 JY/BEAM
Levs = 2.500E-04 * (1, 1.400, 2, 2.800, 4, 5.600, 8, 11, 16, 23, 45, 64, 90, 181, 256, 362, 512, 724, 1024)

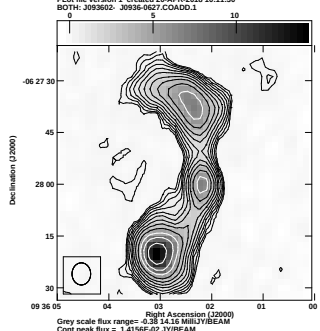
PLot file version 1 created 20-APR-2018 10:11:30
BOTH: J093602- J0936-0627.COADD.1
Declination (J2000)
Right Ascension (J2000)
Grey scale flux range= -0.38 14.16 MilliJY/BEAM
Cont peak flux = 1.4156E-02 JY/BEAM
Levs = 2.500E-04 * (1, 1.400, 2, 2.800, 4, 5.600, 8, 11, 16, 23, 32, 45, 64, 90, 128, 181, 256, 362, 512, 724, 1024)

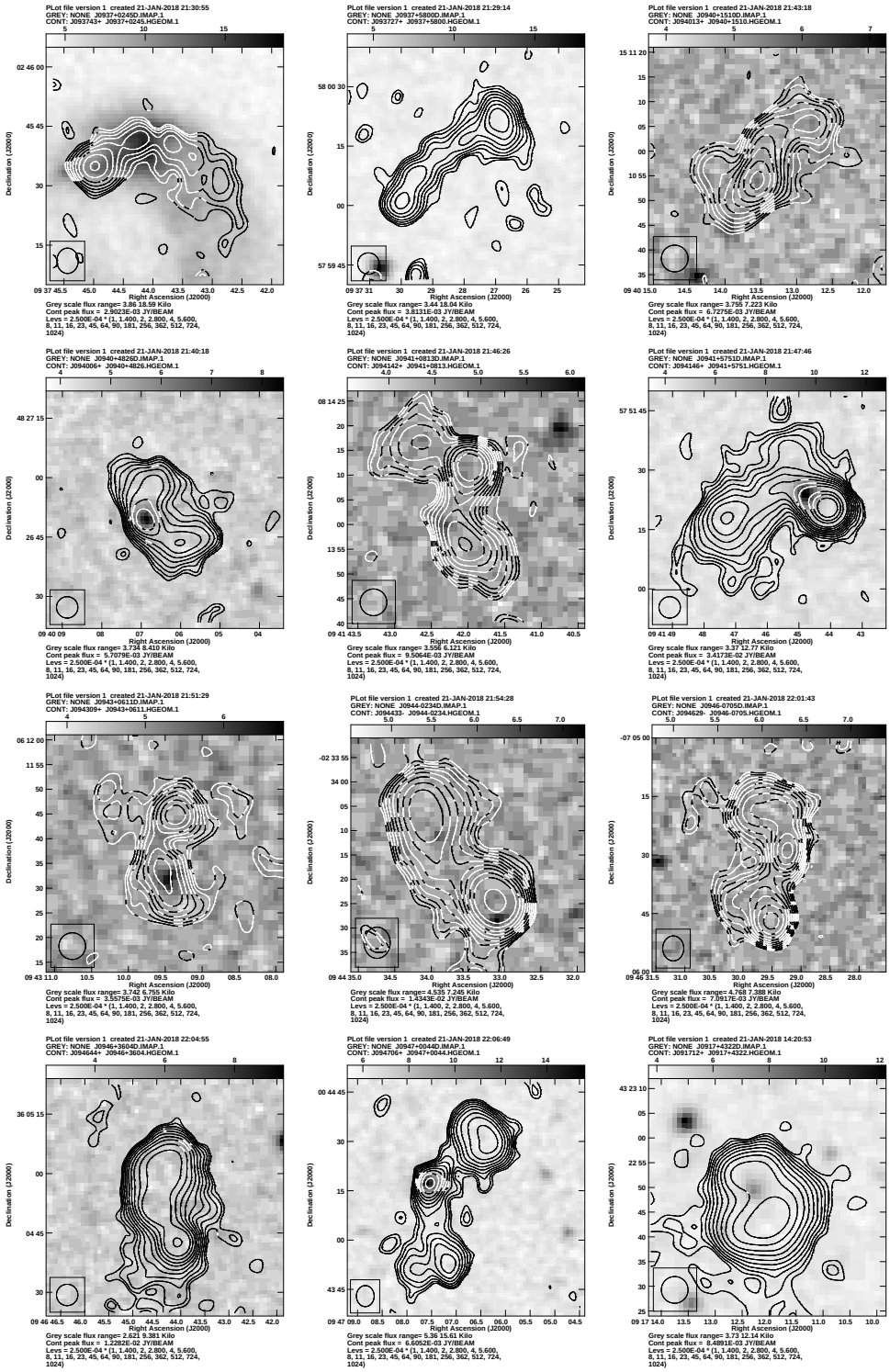
PLot file version 1 created 21-JAN-2018 21:30:55
GREY: NONE J0937+0245D.IMAP.1
CONT: J0937+43+ J0937+0245.HGEOM.1
Declination (J2000)
Right Ascension (J2000)
Grey scale flux range= 3.86 18.59 Kilo
Cont peak flux = 2.9023E-03 JY/BEAM
Levs = 2.500E-04 * (1, 1.400, 2, 2.800, 4, 5.600, 8, 11, 16, 23, 45, 64, 90, 181, 256, 362, 512, 724, 1024)
PLot file version 1 created 21-JAN-2018 21:29:14
GREY: NONE J0937+5800D.IMAP.1
CONT: J0937+27+ J0937+5800.HGEOM.1
Declination (J2000)
Right Ascension (J2000)
Grey scale flux range= 3.44 18.04 Kilo
Cont peak flux = 3.8131E-03 JY/BEAM
Levs = 2.500E-04 * (1, 1.400, 2, 2.800, 4, 5.600, 8, 11, 16, 23, 45, 64, 90, 181, 256, 362, 512, 724, 1024)
PLot file version 1 created 21-JAN-2018 21:43:18
GREY: NONE J0940+1510D.IMAP.1
CONT: J0940+13+ J0940+1510.HGEOM.1
Declination (J2000)
Right Ascension (J2000)
Grey scale flux range= 3.755 7.223 Kilo
Cont peak flux = 6.7275E-03 JY/BEAM
Levs = 2.500E-04 * (1, 1.400, 2, 2.800, 4, 5.600, 8, 11, 16, 23, 45, 64, 90, 181, 256, 362, 512, 724, 1024)
PLot file version 1 created 21-JAN-2018 21:40:18
GREY: NONE J0940+4826D.IMAP.1
CONT: J0940+06+ J0940+4826.HGEOM.1
Declination (J2000)
Right Ascension (J2000)
Grey scale flux range= 3.734 8.410 Kilo
Cont peak flux = 5.7079E-03 JY/BEAM
Levs = 2.500E-04 * (1, 1.400, 2, 2.800, 4, 5.600, 8, 11, 16, 23, 45, 64, 90, 181, 256, 362, 512, 724, 1024)
PLot file version 1 created 21-JAN-2018 21:46:26
GREY: NONE J0941+0813D.IMAP.1
CONT: J0941+42+ J0941+0813.HGEOM.1
Declination (J2000)
Right Ascension (J2000)
Grey scale flux range= 3.556 6.121 Kilo
Cont peak flux = 9.5064E-03 JY/BEAM
Levs = 2.500E-04 * (1, 1.400, 2, 2.800, 4, 5.600, 8, 11, 16, 23, 45, 64, 90, 181, 256, 362, 512, 724, 1024)
PLot file version 1 created 21-JAN-2018 21:47:46
GREY: NONE J0941+5751D.IMAP.1
CONT: J0941+46+ J0941+5751.HGEOM.1
Declination (J2000)
Right Ascension (J2000)
Grey scale flux range= 3.37 12.77 Kilo
Cont peak flux = 3.4173E-02 JY/BEAM
Levs = 2.500E-04 * (1, 1.400, 2, 2.800, 4, 5.600, 8, 11, 16, 23, 45, 64, 90, 181, 256, 362, 512, 724, 1024)
PLot file version 1 created 21-JAN-2018 21:51:29
GREY: NONE J0943+0611D.IMAP.1
CONT: J0943+09+ J0943+0611.HGEOM.1
Declination (J2000)
Right Ascension (J2000)
Grey scale flux range= 3.742 6.755 Kilo
Cont peak flux = 3.5575E-03 JY/BEAM
Levs = 2.500E-04 * (1, 1.400, 2, 2.800, 4, 5.600, 8, 11, 16, 23, 45, 64, 90, 181, 256, 362, 512, 724, 1024)
PLot file version 1 created 21-JAN-2018 21:54:28
GREY: NONE J0944-0234D.IMAP.1
CONT: J0944-33- J0944-0234.HGEOM.1
Declination (J2000)
Right Ascension (J2000)
Grey scale flux range= 4.535 7.245 Kilo
Cont peak flux = 1.4343E-02 JY/BEAM
Levs = 2.500E-04 * (1, 1.400, 2, 2.800, 4, 5.600, 8, 11, 16, 23, 45, 64, 90, 181, 256, 362, 512, 724, 1024)
PLot file version 1 created 21-JAN-2018 22:01:43
GREY: NONE J0946-0705D.IMAP.1
CONT: J0946+29- J0946-0705.HGEOM.1
Declination (J2000)
Right Ascension (J2000)
Grey scale flux range= 4.768 7.388 Kilo
Cont peak flux = 7.9917E-03 JY/BEAM
Levs = 2.500E-04 * (1, 1.400, 2, 2.800, 4, 5.600, 8, 11, 16, 23, 45, 64, 90, 181, 256, 362, 512, 724, 1024)
PLot file version 1 created 21-JAN-2018 22:04:55
GREY: NONE J0946+3604D.IMAP.1
CONT: J0946+4+ J0946+3604.HGEOM.1
Declination (J2000)
Right Ascension (J2000)
Grey scale flux range= 2.621 9.381 Kilo
Cont peak flux = 1.2282E-02 JY/BEAM
Levs = 2.500E-04 * (1, 1.400, 2, 2.800, 4, 5.600, 8, 11, 16, 23, 45, 64, 90, 181, 256, 362, 512, 724, 1024)
PLot file version 1 created 21-JAN-2018 22:06:49
GREY: NONE J0947+0044D.IMAP.1
CONT: J0947+06+ J0947+0044.HGEOM.1
Declination (J2000)
Right Ascension (J2000)
Grey scale flux range= 5.36 15.61 Kilo
Cont peak flux = 6.6052E-03 JY/BEAM
Levs = 2.500E-04 * (1, 1.400, 2, 2.800, 4, 5.600, 8, 11, 16, 23, 45, 64, 90, 181, 256, 362, 512, 724, 1024)
PLot file version 1 created 21-JAN-2018 14:20:53
GREY: NONE J0917+4322D.IMAP.1
CONT: J0917+12+ J0917+4322.HGEOM.1
Declination (J2000)
Right Ascension (J2000)
Grey scale flux range= 3.73 12.14 Kilo
Cont peak flux = 8.4891E-03 JY/BEAM
Levs = 2.500E-04 * (1, 1.400, 2, 2.800, 4, 5.600, 8, 11, 16, 23, 45, 64, 90, 181, 256, 362, 512, 724, 1024)

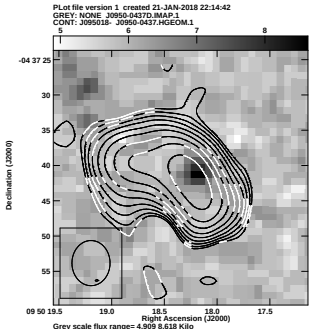
PLot file version 1 created 21-JAN-2018 22:14:42
GREY: NONE J0950-0437D.IMAP.1
CONT: J0950I8- J0950-0437.HGEOM.1
Declination (J2000)
Right Ascension (J2000)
Grey scale flux range= 4.909 8.618 Kilo
Cont peak flux = 5.3238E-03 JY/BEAM
Levs = 2.500E-04 * (1, 1.400, 2, 2.800, 4, 5.600, 8, 11, 16, 23, 45, 64, 90, 181, 256, 362, 512, 724, 1024)

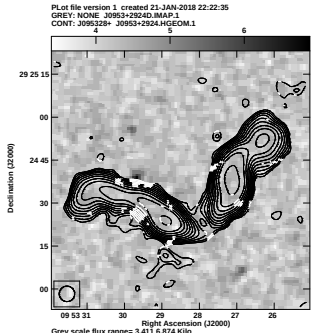
PLot file version 1 created 21-JAN-2018 22:22:35
GREY: NONE J0953+2924D.IMAP.1
CONT: J0953I8+ J0953+2924.HGEOM.1
Declination (J2000)
Right Ascension (J2000)
Grey scale flux range= 3.411 6.674 Kilo
Cont peak flux = 1.5647E-02 JY/BEAM
Levs = 2.500E-04 * (1, 1.400, 2, 2.800, 4, 5.600, 8, 11, 16, 23, 45, 64, 90, 181, 256, 362, 512, 724, 1024)

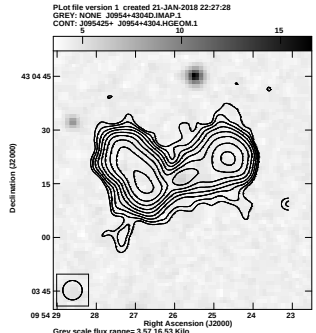
PLot file version 1 created 21-JAN-2018 22:27:28
GREY: NONE J0954+4304D.IMAP.1
CONT: J0954I5+ J0954+4304.HGEOM.1
Declination (J2000)
Right Ascension (J2000)
Grey scale flux range= 3.57 16.53 Kilo
Cont peak flux = 4.5225E-03 JY/BEAM
Levs = 2.500E-04 * (1, 1.400, 2, 2.800, 4, 5.600, 8, 11, 16, 23, 45, 64, 90, 181, 256, 362, 512, 724, 1024)

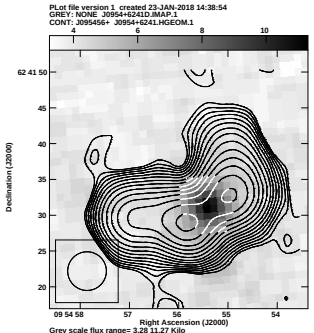
PLot file version 1 created 23-JAN-2018 14:38:54
GREY: NONE J0954+6241D.IMAP.1
CONT: J0954I6+ J0954+6241.HGEOM.1
Declination (J2000)
Right Ascension (J2000)
Grey scale flux range= 3.28 11.27 Kilo
Cont peak flux = 2.5132E-02 JY/BEAM
Levs = 2.500E-04 * (1, 1.400, 2, 2.800, 4, 5.600, 8, 11, 16, 23, 32, 45, 64, 90, 128, 181, 256, 362, 512, 724, 1024)

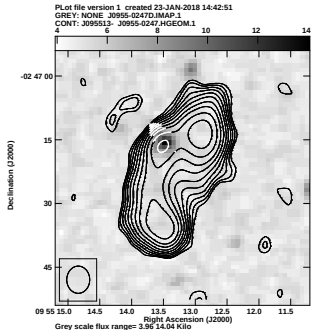
PLot file version 1 created 23-JAN-2018 14:42:51
GREY: NONE J0955-0247D.IMAP.1
CONT: J0955I3- J0955-0247.HGEOM.1
Declination (J2000)
Right Ascension (J2000)
Grey scale flux range= 3.96 14.04 Kilo
Cont peak flux = 7.5957E-03 JY/BEAM
Levs = 2.500E-04 * (1, 1.400, 2, 2.800, 4, 5.600, 8, 11, 16, 23, 32, 45, 64, 90, 128, 181, 256, 362, 512, 724, 1024)

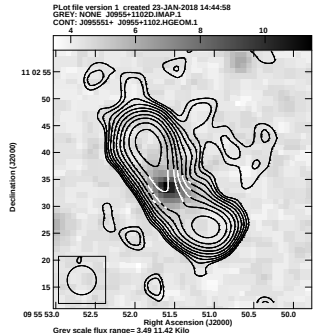
PLot file version 1 created 23-JAN-2018 14:44:58
GREY: NONE J0955+1102D.IMAP.1
CONT: J0955I1+ J0955+1102.HGEOM.1
Declination (J2000)
Right Ascension (J2000)
Grey scale flux range= 3.49 11.42 Kilo
Cont peak flux = 7.7819E-03 JY/BEAM
Levs = 2.500E-04 * (1, 1.400, 2, 2.800, 4, 5.600, 8, 11, 16, 23, 32, 45, 64, 90, 128, 181, 256, 362, 512, 724, 1024)

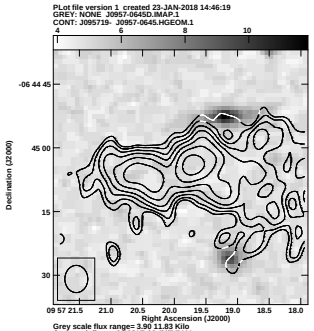
PLot file version 1 created 23-JAN-2018 14:46:19
GREY: NONE J0957-0645D.IMAP.1
CONT: J0957I9- J0957-0645.HGEOM.1
Declination (J2000)
Right Ascension (J2000)
Grey scale flux range= 3.90 11.83 Kilo
Cont peak flux = 2.3681E-03 JY/BEAM
Levs = 2.500E-04 * (1, 1.400, 2, 2.800, 4, 5.600, 8, 11, 16, 23, 32, 45, 64, 90, 128, 181, 256, 362, 512, 724, 1024)

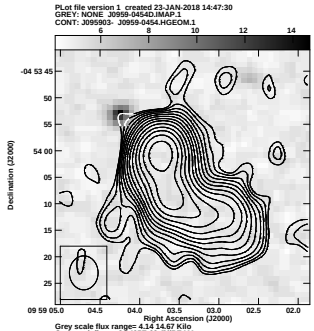
PLot file version 1 created 23-JAN-2018 14:47:30
GREY: NONE J0959-0454D.IMAP.1
CONT: J0959I3- J0959-0454.HGEOM.1
Declination (J2000)
Right Ascension (J2000)
Grey scale flux range= 4.14 14.67 Kilo
Cont peak flux = 2.1465E-02 JY/BEAM
Levs = 2.500E-04 * (1, 1.400, 2, 2.800, 4, 5.600, 8, 11, 16, 23, 32, 45, 64, 90, 128, 181, 256, 362, 512, 724, 1024)

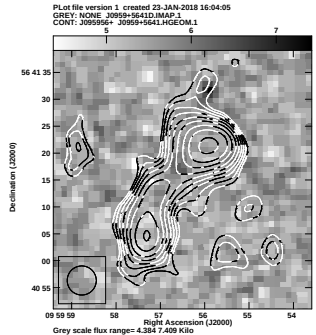
PLot file version 1 created 23-JAN-2018 16:04:05
GREY: NONE J0959+5641D.IMAP.1
CONT: J0959I6+ J0959+5641.HGEOM.1
Declination (J2000)
Right Ascension (J2000)
Grey scale flux range= 4.384 7.409 Kilo
Cont peak flux = 4.5088E-03 JY/BEAM
Levs = 2.500E-04 * (1, 1.400, 2, 2.800, 4, 5.600, 8, 11, 16, 23, 32, 45, 64, 90, 128, 181, 256, 362, 512, 724, 1024)

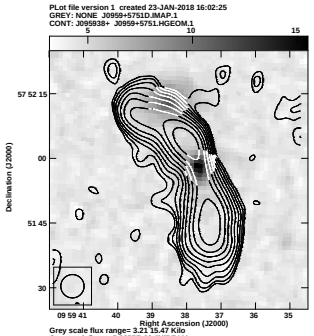
PLot file version 1 created 23-JAN-2018 16:02:25
GREY: NONE J0959+5751D.IMAP.1
CONT: J0959I8+ J0959+5751.HGEOM.1
Declination (J2000)
Right Ascension (J2000)
Grey scale flux range= 3.21 15.47 Kilo
Cont peak flux = 5.6255E-03 JY/BEAM
Levs = 2.500E-04 * (1, 1.400, 2, 2.800, 4, 5.600, 8, 11, 16, 23, 32, 45, 64, 90, 128, 181, 256, 362, 512, 724, 1024)

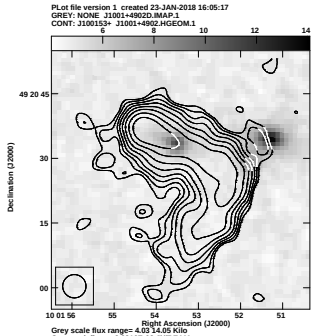
PLot file version 1 created 23-JAN-2018 16:05:17
GREY: NONE J1001+4902D.IMAP.1
CONT: J1001I3+ J1001+4902.HGEOM.1
Declination (J2000)
Right Ascension (J2000)
Grey scale flux range= 4.03 14.05 Kilo
Cont peak flux = 3.9816E-03 JY/BEAM
Levs = 2.500E-04 * (1, 1.400, 2, 2.800, 4, 5.600, 8, 11, 16, 23, 32, 45, 64, 90, 128, 181, 256, 362, 512, 724, 1024)

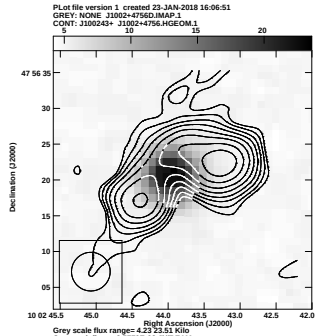
PLot file version 1 created 23-JAN-2018 16:06:51
GREY: NONE J1002+4756D.IMAP.1
CONT: J1002I3+ J1002+4756.HGEOM.1
Declination (J2000)
Right Ascension (J2000)
Grey scale flux range= 4.23 23.51 Kilo
Cont peak flux = 3.5770E-03 JY/BEAM
Levs = 2.500E-04 * (1, 1.400, 2, 2.800, 4, 5.600, 8, 11, 16, 23, 32, 45, 64, 90, 128, 181, 256, 362, 512, 724, 1024)

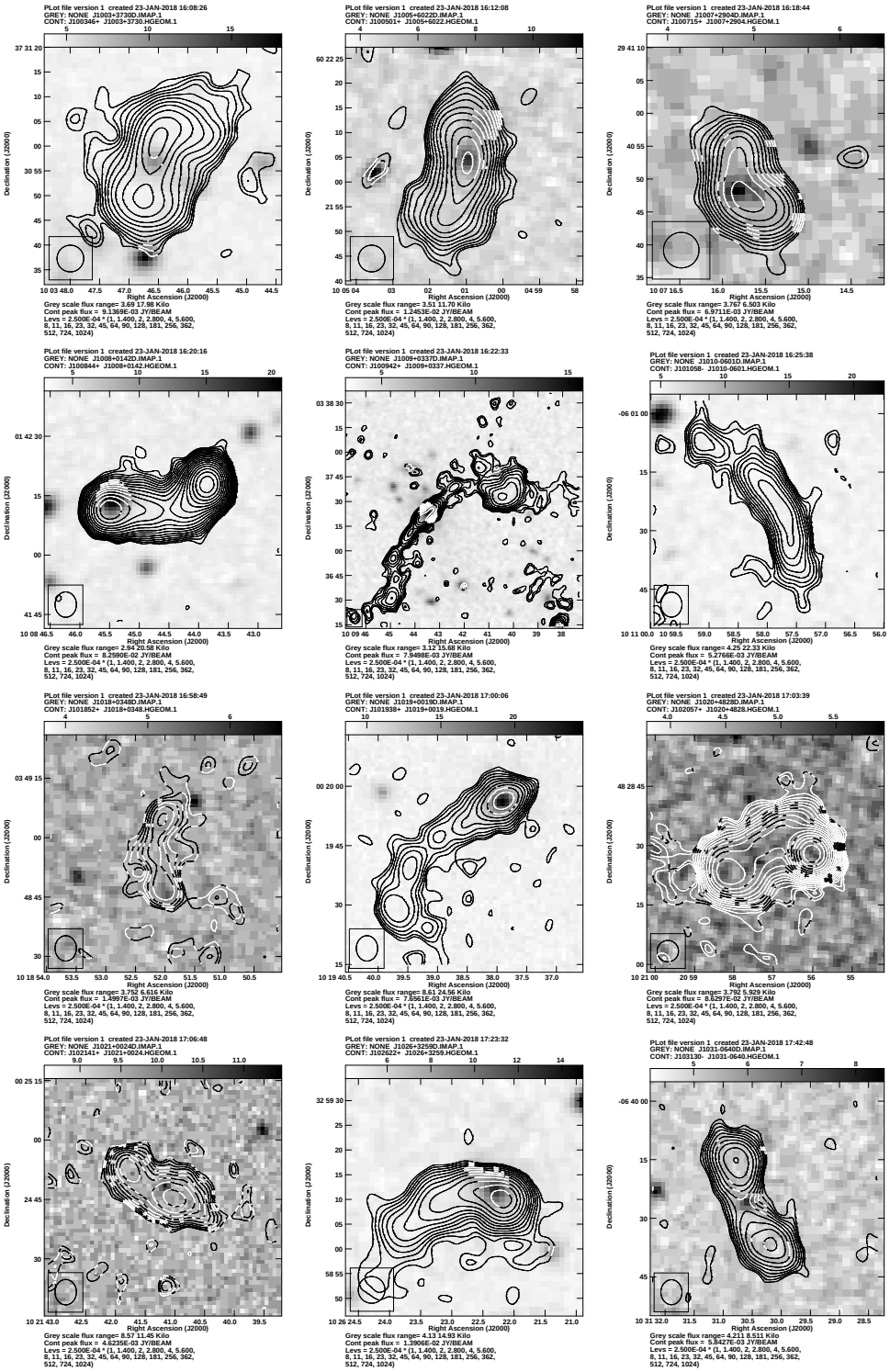
PLot file version 1 created 23-JAN-2018 16:08:26
GREY: NONE J1003+3730D.IMAP.1
CONT: J100346+ J1003+3730.HGEOM.1
Declination (J2000)
Right Ascension (J2000)
Grey scale flux range= 3.69 17.98 Kilo
Cont peak flux = 9.1369E-03 JY/BEAM
Levs = 2.500E-04 * (1, 1.400, 2, 2.800, 4, 5.600, 8, 11, 16, 23, 32, 45, 64, 90, 128, 181, 256, 362, 512, 724, 1024)
PLot file version 1 created 23-JAN-2018 16:12:08
GREY: NONE J1005+6022D.IMAP.1
CONT: J100501+ J1005+6022.HGEOM.1
Declination (J2000)
Right Ascension (J2000)
Grey scale flux range= 3.51 11.70 Kilo
Cont peak flux = 1.2453E-02 JY/BEAM
Levs = 2.500E-04 * (1, 1.400, 2, 2.800, 4, 5.600, 8, 11, 16, 23, 32, 45, 64, 90, 128, 181, 256, 362, 512, 724, 1024)
PLot file version 1 created 23-JAN-2018 16:18:44
GREY: NONE J1007+2904D.IMAP.1
CONT: J100715+ J1007+2904.HGEOM.1
Declination (J2000)
Right Ascension (J2000)
Grey scale flux range= 3.767 6.503 Kilo
Cont peak flux = 6.9711E-03 JY/BEAM
Levs = 2.500E-04 * (1, 1.400, 2, 2.800, 4, 5.600, 8, 11, 16, 23, 32, 45, 64, 90, 128, 181, 256, 362, 512, 724, 1024)
PLot file version 1 created 23-JAN-2018 16:20:16
GREY: NONE J1008+0142D.IMAP.1
CONT: J100844+ J1008+0142.HGEOM.1
Declination (J2000)
Right Ascension (J2000)
Grey scale flux range= 2.94 20.58 Kilo
Cont peak flux = 8.2590E-02 JY/BEAM
Levs = 2.500E-04 * (1, 1.400, 2, 2.800, 4, 5.600, 8, 11, 16, 23, 32, 45, 64, 90, 128, 181, 256, 362, 512, 724, 1024)
PLot file version 1 created 23-JAN-2018 16:22:33
GREY: NONE J1009+0337D.IMAP.1
CONT: J100942+ J1009+0337.HGEOM.1
Declination (J2000)
Right Ascension (J2000)
Grey scale flux range= 3.12 15.68 Kilo
Cont peak flux = 7.9488E-03 JY/BEAM
Levs = 2.500E-04 * (1, 1.400, 2, 2.800, 4, 5.600, 8, 11, 16, 23, 32, 45, 64, 90, 128, 181, 256, 362, 512, 724, 1024)
PLot file version 1 created 23-JAN-2018 16:25:38
GREY: NONE J1010-0601D.IMAP.1
CONT: J101058- J1010-0601.HGEOM.1
Declination (J2000)
Right Ascension (J2000)
Grey scale flux range= 4.25 22.33 Kilo
Cont peak flux = 5.2766E-03 JY/BEAM
Levs = 2.500E-04 * (1, 1.400, 2, 2.800, 4, 5.600, 8, 11, 16, 23, 32, 45, 64, 90, 128, 181, 256, 362, 512, 724, 1024)
PLot file version 1 created 23-JAN-2018 16:58:49
GREY: NONE J1018+0348D.IMAP.1
CONT: J101852+ J1018+0348.HGEOM.1
Declination (J2000)
Right Ascension (J2000)
Grey scale flux range= 3.752 6.616 Kilo
Cont peak flux = 1.4997E-03 JY/BEAM
Levs = 2.500E-04 * (1, 1.400, 2, 2.800, 4, 5.600, 8, 11, 16, 23, 32, 45, 64, 90, 128, 181, 256, 362, 512, 724, 1024)
PLot file version 1 created 23-JAN-2018 17:00:06
GREY: NONE J1019+0019D.IMAP.1
CONT: J101938+ J1019+0019.HGEOM.1
Declination (J2000)
Right Ascension (J2000)
Grey scale flux range= 8.61 24.56 Kilo
Cont peak flux = 7.5561E-03 JY/BEAM
Levs = 2.500E-04 * (1, 1.400, 2, 2.800, 4, 5.600, 8, 11, 16, 23, 32, 45, 64, 90, 128, 181, 256, 362, 512, 724, 1024)
PLot file version 1 created 23-JAN-2018 17:03:39
GREY: NONE J1020+4828D.IMAP.1
CONT: J102057+ J1020+4828.HGEOM.1
Declination (J2000)
Right Ascension (J2000)
Grey scale flux range= 3.792 5.929 Kilo
Cont peak flux = 8.8297E-02 JY/BEAM
Levs = 2.500E-04 * (1, 1.400, 2, 2.800, 4, 5.600, 8, 11, 16, 23, 32, 45, 64, 90, 128, 181, 256, 362, 512, 724, 1024)
PLot file version 1 created 23-JAN-2018 17:06:48
GREY: NONE J1021+0024D.IMAP.1
CONT: J102141+ J1021+0024.HGEOM.1
Declination (J2000)
Right Ascension (J2000)
Grey scale flux range= 8.57 11.45 Kilo
Cont peak flux = 4.6235E-03 JY/BEAM
Levs = 2.500E-04 * (1, 1.400, 2, 2.800, 4, 5.600, 8, 11, 16, 23, 32, 45, 64, 90, 128, 181, 256, 362, 512, 724, 1024)
PLot file version 1 created 23-JAN-2018 17:23:32
GREY: NONE J1026+3259D.IMAP.1
CONT: J102622+ J1026+3259.HGEOM.1
Declination (J2000)
Right Ascension (J2000)
Grey scale flux range= 4.13 14.80 Kilo
Cont peak flux = 1.3906E-02 JY/BEAM
Levs = 2.500E-04 * (1, 1.400, 2, 2.800, 4, 5.600, 8, 11, 16, 23, 32, 45, 64, 90, 128, 181, 256, 362, 512, 724, 1024)
PLot file version 1 created 23-JAN-2018 17:42:48
GREY: NONE J1031-0640D.IMAP.1
CONT: J103130- J1031-0640.HGEOM.1
Declination (J2000)
Right Ascension (J2000)
Grey scale flux range= 4.211 8.511 Kilo
Cont peak flux = 5.8427E-03 JY/BEAM
Levs = 2.500E-04 * (1, 1.400, 2, 2.800, 4, 5.600, 8, 11, 16, 23, 32, 45, 64, 90, 128, 181, 256, 362, 512, 724, 1024)

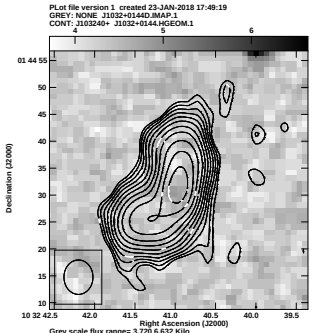
PLot file version 1 created 23-JAN-2018 17:49:19
GREY: NONE J1032+0144D.IMAP.1
CONT: J1032+0144.HGEOM.1
Declination (J2000)
Right Ascension (J2000)
Grey scale flux range= 3.720 6.632 Kilo
Cont peak flux = 1.0166E-02 JY/BEAM
Levs = 2.500E-04 * (1, 1.400, 2, 2.800, 4, 5.600, 8, 11, 16, 23, 32, 45, 64, 90, 128, 181, 256, 362, 512, 724, 1024)

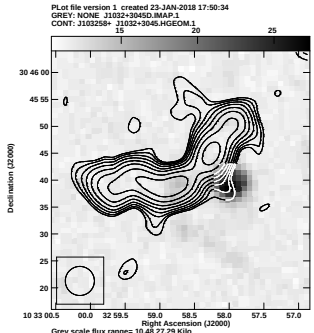
PLot file version 1 created 23-JAN-2018 17:50:34
GREY: NONE J1032+3045D.IMAP.1
CONT: J1032+3045.HGEOM.1
Declination (J2000)
Right Ascension (J2000)
Grey scale flux range= 10.48 27.29 Kilo
Cont peak flux = 3.5272E-03 JY/BEAM
Levs = 2.500E-04 * (1, 1.400, 2, 2.800, 4, 5.600, 8, 11, 16, 23, 32, 45, 64, 90, 128, 181, 256, 362, 512, 724, 1024)

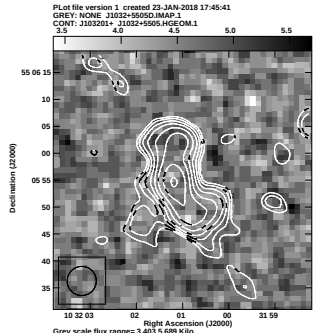
PLot file version 1 created 23-JAN-2018 17:45:41
GREY: NONE J1032+5505D.IMAP.1
CONT: J1032+5505.HGEOM.1
Declination (J2000)
Right Ascension (J2000)
Grey scale flux range= 3.403 5.689 Kilo
Cont peak flux = 2.8542E-03 JY/BEAM
Levs = 2.500E-04 * (1, 1.400, 2, 2.800, 4, 5.600, 8, 11, 16, 23, 32, 45, 64, 90, 128, 181, 256, 362, 512, 724, 1024)

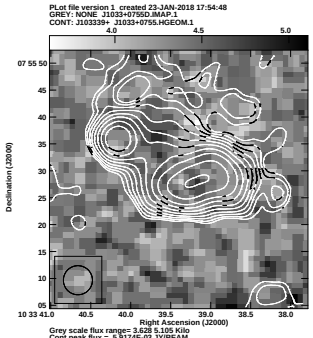
PLot file version 1 created 23-JAN-2018 17:54:48
GREY: NONE J1033+0755D.IMAP.1
CONT: J1033+0755.HGEOM.1
Declination (J2000)
Right Ascension (J2000)
Grey scale flux range= 3.628 5.105 Kilo
Cont peak flux = 5.9174E-03 JY/BEAM
Levs = 2.500E-04 * (1, 1.400, 2, 2.800, 4, 5.600, 8, 11, 16, 23, 32, 45, 64, 90, 128, 181, 256, 362, 512, 724, 1024)

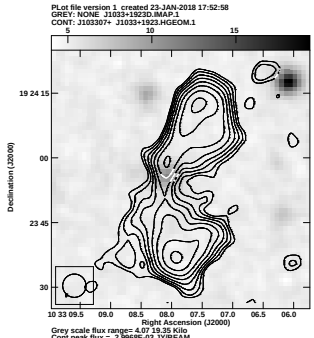
PLot file version 1 created 23-JAN-2018 17:52:58
GREY: NONE J1033+1923D.IMAP.1
CONT: J1033307+ J1033+1923.HGEOM.1
Declination (J2000)
Right Ascension (J2000)
Grey scale flux range= 4.07 19.35 Kilo
Cont peak flux = 2.9968E-03 JY/BEAM
Levs = 2.500E-04 * (1, 1.400, 2, 2.800, 4, 5.600, 8, 11, 16, 23, 32, 45, 64, 90, 128, 181, 256, 362, 512, 724, 1024)

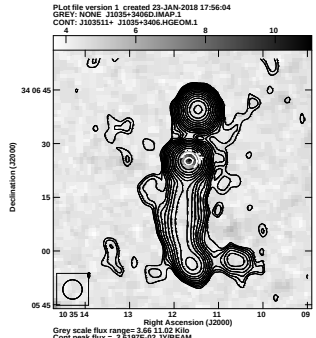
PLot file version 1 created 23-JAN-2018 17:56:04
GREY: NONE J1035+3406D.IMAP.1
CONT: J1035511+ J1035+3406.HGEOM.1
Declination (J2000)
Right Ascension (J2000)
Grey scale flux range= 3.66 11.02 Kilo
Cont peak flux = 3.6197E-02 JY/BEAM
Levs = 2.500E-04 * (1, 1.400, 2, 2.800, 4, 5.600, 8, 11, 16, 23, 32, 45, 64, 90, 128, 181, 256, 362, 512, 724, 1024)

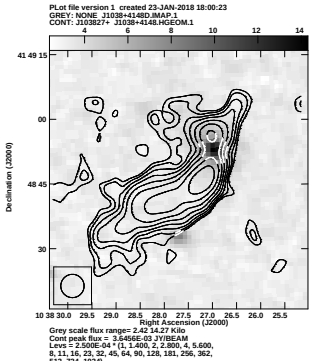
PLot file version 1 created 23-JAN-2018 18:00:23
GREY: NONE J1038+4148D.IMAP.1
CONT: J1038271+ J1038+4148.HGEOM.1
Declination (J2000)
Right Ascension (J2000)
Grey scale flux range= 2.42 14.27 Kilo
Cont peak flux = 3.6366E-03 JY/BEAM
Levs = 2.500E-04 * (1, 1.400, 2, 2.800, 4, 5.600, 8, 11, 16, 23, 32, 45, 64, 90, 128, 181, 256, 362, 512, 724, 1024)

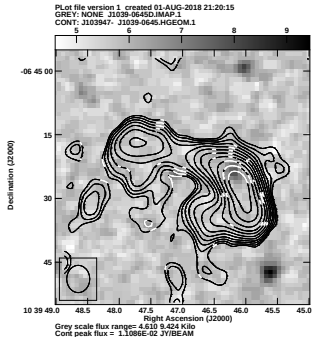
PLot file version 1 created 01-AUG-2018 21:20:15
GREY: NONE J1039-0645D.IMAP.1
CONT: J103947- J1039-0645.HGEOM.1
Declination (J2000)
Right Ascension (J2000)
Grey scale flux range= 4.610 9.424 Kilo
Cont peak flux = 1.1086E-02 JY/BEAM
Levs = 2.500E-04 * (1, 1.400, 2, 2.800, 4, 5.600, 8, 11, 16, 23, 32, 45, 64, 90, 128, 181, 256, 362, 512, 724, 1024)

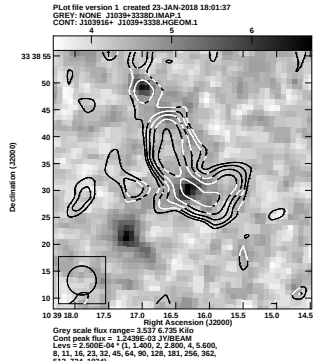
PLot file version 1 created 23-JAN-2018 18:01:37
GREY: NONE J1039+3338D.IMAP.1
CONT: J103916+ J1039+3338.HGEOM.1
Declination (J2000)
Right Ascension (J2000)
Grey scale flux range= 3.537 6.735 Kilo
Cont peak flux = 1.2439E-03 JY/BEAM
Levs = 2.500E-04 * (1, 1.400, 2, 2.800, 4, 5.600, 8, 11, 16, 23, 32, 45, 64, 90, 128, 181, 256, 362, 512, 724, 1024)

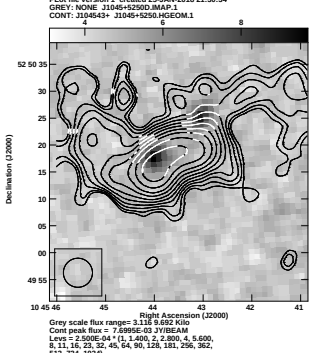
PLot file version 1 created 25-JAN-2018 21:30:34
GREY: NONE J1045+5250D.IMAP.1
CONT: J1045431+ J1045+5250.HGEOM.1
Declination (J2000)
Right Ascension (J2000)
Grey scale flux range= 3.116 9.692 Kilo
Cont peak flux = 7.5995E-03 JY/BEAM
Levs = 2.500E-04 * (1, 1.400, 2, 2.800, 4, 5.600, 8, 11, 16, 23, 32, 45, 64, 90, 128, 181, 256, 362, 512, 724, 1024)

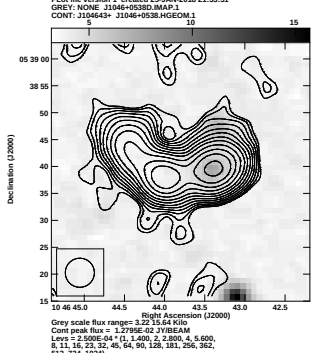
PLot file version 1 created 25-JAN-2018 21:33:31
GREY: NONE J1046+0538D.IMAP.1
CONT: J1046431+ J1046+0538.HGEOM.1
Declination (J2000)
Right Ascension (J2000)
Grey scale flux range= 3.22 15.64 Kilo
Cont peak flux = 1.2795E-02 JY/BEAM
Levs = 2.500E-04 * (1, 1.400, 2, 2.800, 4, 5.600, 8, 11, 16, 23, 32, 45, 64, 90, 128, 181, 256, 362, 512, 724, 1024)

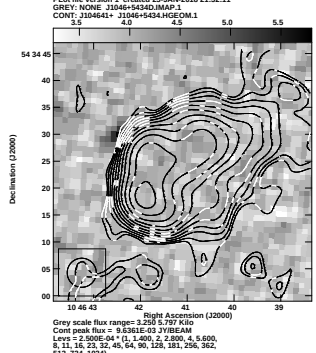
PLot file version 1 created 25-JAN-2018 21:32:11
GREY: NONE J1046+5434D.IMAP.1
CONT: J1046411+ J1046+5434.HGEOM.1
Declination (J2000)
Right Ascension (J2000)
Grey scale flux range= 3.250 5.797 Kilo
Cont peak flux = 9.6361E-03 JY/BEAM
Levs = 2.500E-04 * (1, 1.400, 2, 2.800, 4, 5.600, 8, 11, 16, 23, 32, 45, 64, 90, 128, 181, 256, 362, 512, 724, 1024)

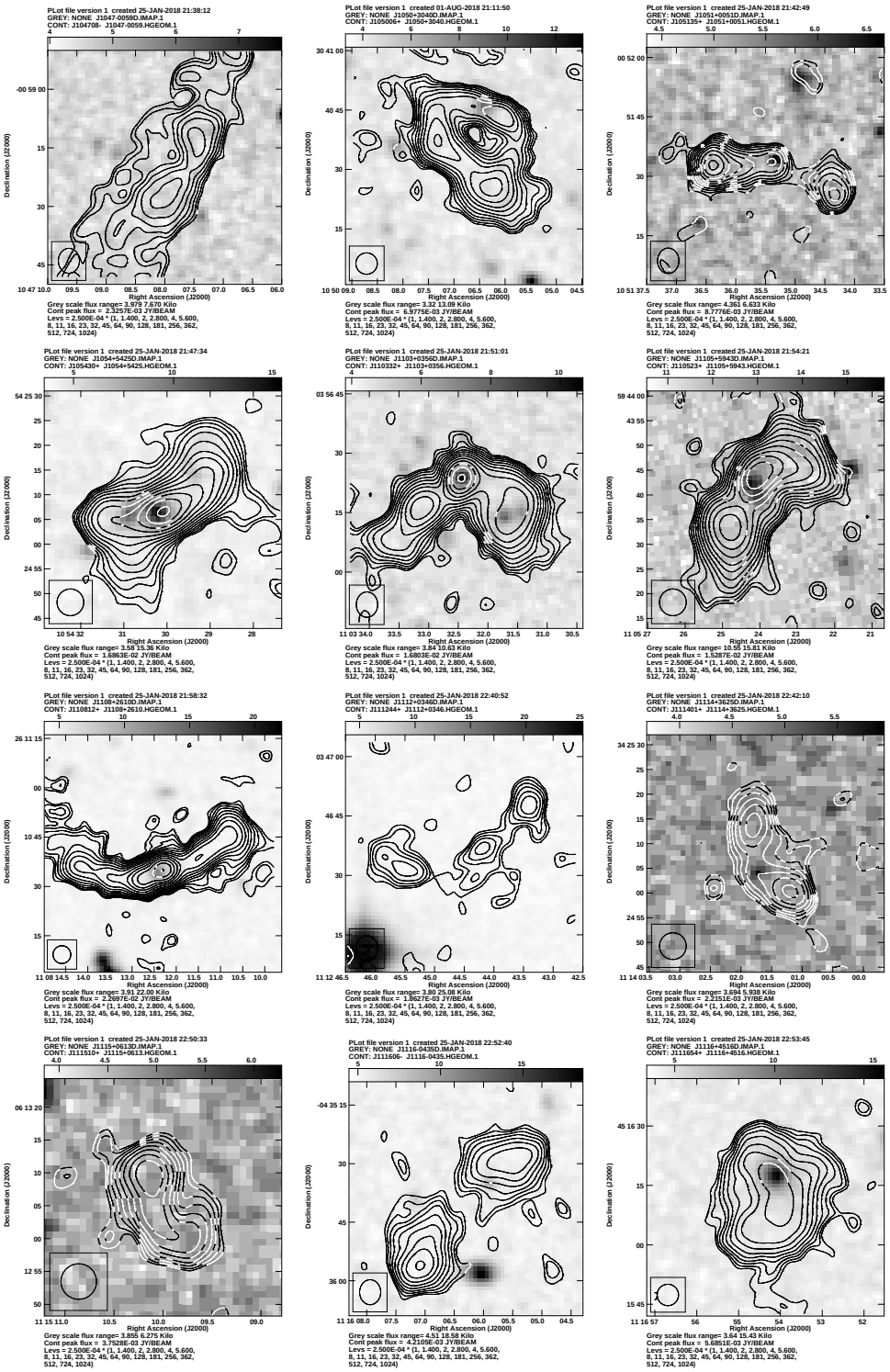
PLot file version 1 created 25-JAN-2018 21:38:12
GREY: NONE J1047-0059D.IMAP.1
CONT: J104708- J1047-0059.HGEOM.1
Grey scale flux range= 3.979 7.670 Kilo
Cont peak flux = 2.3257E-03 JY/BEAM
Levs = 2.500E-04 * (1, 1.400, 2, 2.800, 4, 5.600, 8, 11, 16, 23, 32, 45, 64, 90, 128, 181, 256, 362, 512, 724, 1024)
PLot file version 1 created 01-AUG-2018 21:11:50
GREY: NONE J1050+3040D.IMAP.1
CONT: J105006+ J1050+3040.HGEOM.1
Grey scale flux range= 3.32 13.09 Kilo
Cont peak flux = 6.9775E-03 JY/BEAM
Levs = 2.500E-04 * (1, 1.400, 2, 2.800, 4, 5.600, 8, 11, 16, 23, 32, 45, 64, 90, 128, 181, 256, 362, 512, 724, 1024)
PLot file version 1 created 25-JAN-2018 21:42:49
GREY: NONE J1051+0051D.IMAP.1
CONT: J105135+ J1051+0051.HGEOM.1
Grey scale flux range= 4.361 6.633 Kilo
Cont peak flux = 8.7776E-03 JY/BEAM
Levs = 2.500E-04 * (1, 1.400, 2, 2.800, 4, 5.600, 8, 11, 16, 23, 32, 45, 64, 90, 128, 181, 256, 362, 512, 724, 1024)
PLot file version 1 created 25-JAN-2018 21:47:34
GREY: NONE J1054+5425D.IMAP.1
CONT: J105430+ J1054+5425.HGEOM.1
Grey scale flux range= 3.58 15.36 Kilo
Cont peak flux = 1.6863E-02 JY/BEAM
Levs = 2.500E-04 * (1, 1.400, 2, 2.800, 4, 5.600, 8, 11, 16, 23, 32, 45, 64, 90, 128, 181, 256, 362, 512, 724, 1024)
PLot file version 1 created 25-JAN-2018 21:51:01
GREY: NONE J1103+0356D.IMAP.1
CONT: J110332+ J1103+0356.HGEOM.1
Grey scale flux range= 3.84 10.63 Kilo
Cont peak flux = 1.6803E-02 JY/BEAM
Levs = 2.500E-04 * (1, 1.400, 2, 2.800, 4, 5.600, 8, 11, 16, 23, 32, 45, 64, 90, 128, 181, 256, 362, 512, 724, 1024)
PLot file version 1 created 25-JAN-2018 21:54:21
GREY: NONE J1105+5943D.IMAP.1
CONT: J110523+ J1105+5943.HGEOM.1
Grey scale flux range= 10.55 15.81 Kilo
Cont peak flux = 1.5287E-02 JY/BEAM
Levs = 2.500E-04 * (1, 1.400, 2, 2.800, 4, 5.600, 8, 11, 16, 23, 32, 45, 64, 90, 128, 181, 256, 362, 512, 724, 1024)
PLot file version 1 created 25-JAN-2018 21:58:32
GREY: NONE J1108+2610D.IMAP.1
CONT: J110812+ J1108+2610.HGEOM.1
Grey scale flux range= 3.91 22.00 Kilo
Cont peak flux = 2.2697E-02 JY/BEAM
Levs = 2.500E-04 * (1, 1.400, 2, 2.800, 4, 5.600, 8, 11, 16, 23, 32, 45, 64, 90, 128, 181, 256, 362, 512, 724, 1024)
PLot file version 1 created 25-JAN-2018 22:40:52
GREY: NONE J1112+0346D.IMAP.1
CONT: J111244+ J1112+0346.HGEOM.1
Grey scale flux range= 3.80 25.08 Kilo
Cont peak flux = 1.8627E-03 JY/BEAM
Levs = 2.500E-04 * (1, 1.400, 2, 2.800, 4, 5.600, 8, 11, 16, 23, 32, 45, 64, 90, 128, 181, 256, 362, 512, 724, 1024)
PLot file version 1 created 25-JAN-2018 22:42:10
GREY: NONE J1114+3625D.IMAP.1
CONT: J111401+ J1114+3625.HGEOM.1
Grey scale flux range= 3.694 5.938 Kilo
Cont peak flux = 2.2151E-03 JY/BEAM
Levs = 2.500E-04 * (1, 1.400, 2, 2.800, 4, 5.600, 8, 11, 16, 23, 32, 45, 64, 90, 128, 181, 256, 362, 512, 724, 1024)
PLot file version 1 created 25-JAN-2018 22:50:33
GREY: NONE J1115+0613D.IMAP.1
CONT: J111510+ J1115+0613.HGEOM.1
Grey scale flux range= 3.855 6.275 Kilo
Cont peak flux = 3.7528E-03 JY/BEAM
Levs = 2.500E-04 * (1, 1.400, 2, 2.800, 4, 5.600, 8, 11, 16, 23, 32, 45, 64, 90, 128, 181, 256, 362, 512, 724, 1024)
PLot file version 1 created 25-JAN-2018 22:52:40
GREY: NONE J1116-0435D.IMAP.1
CONT: J111606- J1116-0435.HGEOM.1
Grey scale flux range= 4.51 18.58 Kilo
Cont peak flux = 4.2109E-03 JY/BEAM
Levs = 2.500E-04 * (1, 1.400, 2, 2.800, 4, 5.600, 8, 11, 16, 23, 32, 45, 64, 90, 128, 181, 256, 362, 512, 724, 1024)
PLot file version 1 created 25-JAN-2018 22:53:45
GREY: NONE J1116+4516D.IMAP.1
CONT: J111654+ J1116+4516.HGEOM.1
Grey scale flux range= 3.64 15.43 Kilo
Cont peak flux = 5.6851E-03 JY/BEAM
Levs = 2.500E-04 * (1, 1.400, 2, 2.800, 4, 5.600, 8, 11, 16, 23, 32, 45, 64, 90, 128, 181, 256, 362, 512, 724, 1024)
Declination (J2000)
Right Ascension (J2000)

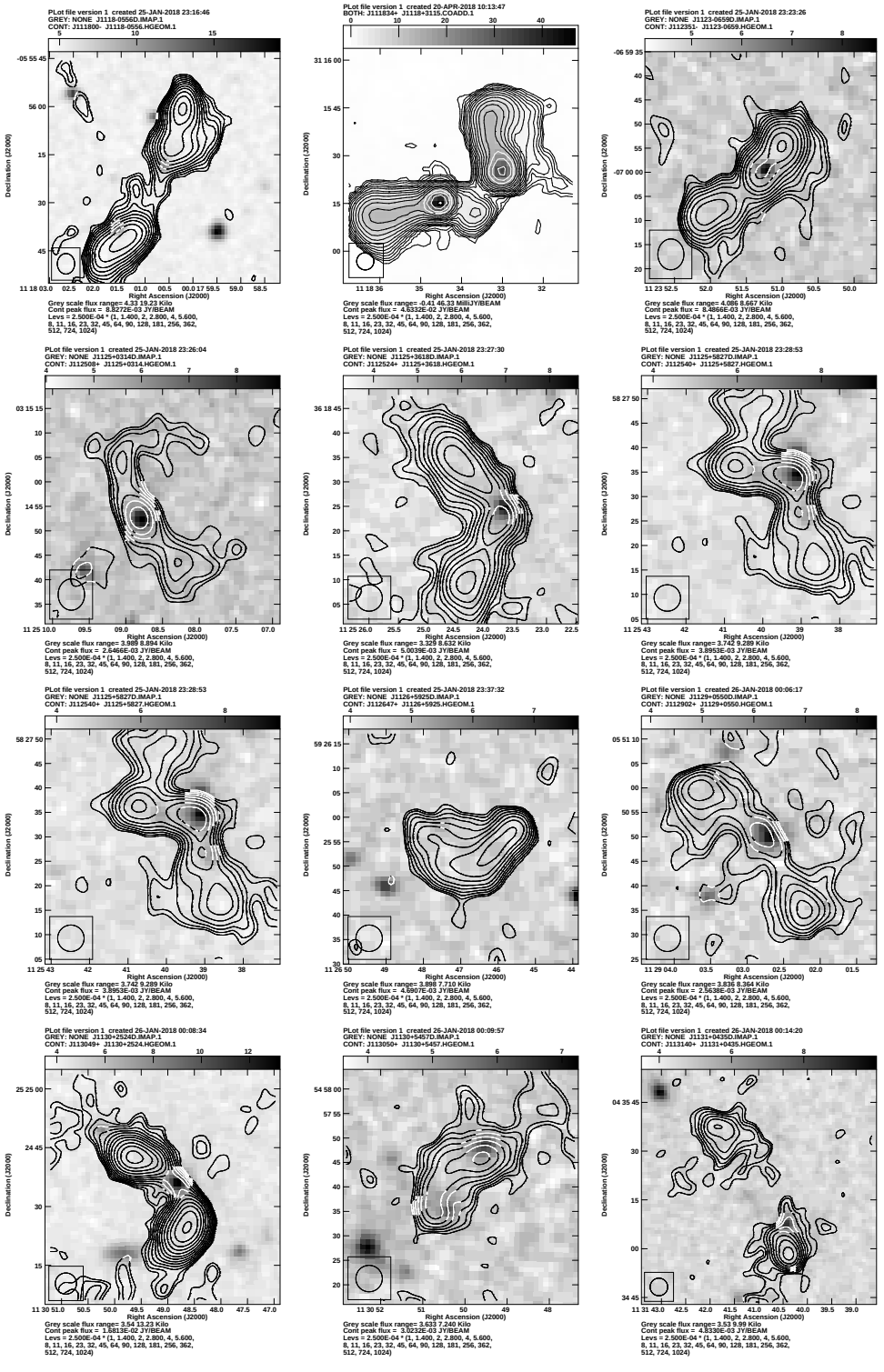
PLot file version 1 created 25-JAN-2018 23:16:46
GREY: NONE J1118-0556D.IMAP.1
CONT: J111800- J1118-0556.HGEOM.1
Declination (J2000)
Right Ascension (J2000)
Grey scale flux range= 4.33 19.23 Kilo
Cont peak flux = 8.8272E-03 JY/BEAM
Levs = 2.500E-04 * (1, 1.400, 2, 2.800, 4, 5.600, 8, 11, 16, 23, 32, 45, 64, 90, 128, 181, 256, 362, 512, 724, 1024)
PLot file version 1 created 20-APR-2018 10:13:47
BOTH: J111834+ J1118+3115.COADD.1
Declination (J2000)
Right Ascension (J2000)
Grey scale flux range= -0.41 46.33 MilliJY/BEAM
Cont peak flux = 4.5332E-02 JY/BEAM
Levs = 2.500E-04 * (1, 1.400, 2, 2.800, 4, 5.600, 8, 11, 16, 23, 32, 45, 64, 90, 128, 181, 256, 362, 512, 724, 1024)
PLot file version 1 created 25-JAN-2018 23:23:26
GREY: NONE J1123-0659D.IMAP.1
CONT: J112351- J1123-0659.HGEOM.1
Declination (J2000)
Right Ascension (J2000)
Grey scale flux range= 4.086 8.667 Kilo
Cont peak flux = 8.4866E-03 JY/BEAM
Levs = 2.500E-04 * (1, 1.400, 2, 2.800, 4, 5.600, 8, 11, 16, 23, 32, 45, 64, 90, 128, 181, 256, 362, 512, 724, 1024)
PLot file version 1 created 25-JAN-2018 23:26:04
GREY: NONE J1125+0314D.IMAP.1
CONT: J112508+ J1125+0314.HGEOM.1
Declination (J2000)
Right Ascension (J2000)
Grey scale flux range= 3.988 8.894 Kilo
Cont peak flux = 2.6466E-03 JY/BEAM
Levs = 2.500E-04 * (1, 1.400, 2, 2.800, 4, 5.600, 8, 11, 16, 23, 32, 45, 64, 90, 128, 181, 256, 362, 512, 724, 1024)
PLot file version 1 created 25-JAN-2018 23:27:30
GREY: NONE J1125+3618D.IMAP.1
CONT: J112524+ J1125+3618.HGEOM.1
Declination (J2000)
Right Ascension (J2000)
Grey scale flux range= 3.328 8.632 Kilo
Cont peak flux = 5.0039E-03 JY/BEAM
Levs = 2.500E-04 * (1, 1.400, 2, 2.800, 4, 5.600, 8, 11, 16, 23, 32, 45, 64, 90, 128, 181, 256, 362, 512, 724, 1024)
PLot file version 1 created 25-JAN-2018 23:28:53
GREY: NONE J1125+5827D.IMAP.1
CONT: J112540+ J1125+5827.HGEOM.1
Declination (J2000)
Right Ascension (J2000)
Grey scale flux range= 3.742 9.289 Kilo
Cont peak flux = 3.8953E-03 JY/BEAM
Levs = 2.500E-04 * (1, 1.400, 2, 2.800, 4, 5.600, 8, 11, 16, 23, 32, 45, 64, 90, 128, 181, 256, 362, 512, 724, 1024)
PLot file version 1 created 25-JAN-2018 23:28:53
GREY: NONE J1125+5827D.IMAP.1
CONT: J112540+ J1125+5827.HGEOM.1
Declination (J2000)
Right Ascension (J2000)
Grey scale flux range= 3.742 9.289 Kilo
Cont peak flux = 3.8953E-03 JY/BEAM
Levs = 2.500E-04 * (1, 1.400, 2, 2.800, 4, 5.600, 8, 11, 16, 23, 32, 45, 64, 90, 128, 181, 256, 362, 512, 724, 1024)
PLot file version 1 created 25-JAN-2018 23:37:32
GREY: NONE J1126+5925D.IMAP.1
CONT: J112647+ J1126+5925.HGEOM.1
Declination (J2000)
Right Ascension (J2000)
Grey scale flux range= 3.898 7.710 Kilo
Cont peak flux = 4.6907E-03 JY/BEAM
Levs = 2.500E-04 * (1, 1.400, 2, 2.800, 4, 5.600, 8, 11, 16, 23, 32, 45, 64, 90, 128, 181, 256, 362, 512, 724, 1024)
PLot file version 1 created 26-JAN-2018 00:06:17
GREY: NONE J1129+0550D.IMAP.1
CONT: J112902+ J1129+0550.HGEOM.1
Declination (J2000)
Right Ascension (J2000)
Grey scale flux range= 3.836 8.364 Kilo
Cont peak flux = 2.5638E-03 JY/BEAM
Levs = 2.500E-04 * (1, 1.400, 2, 2.800, 4, 5.600, 8, 11, 16, 23, 32, 45, 64, 90, 128, 181, 256, 362, 512, 724, 1024)
PLot file version 1 created 26-JAN-2018 00:08:34
GREY: NONE J1130+2524D.IMAP.1
CONT: J113049+ J1130+2524.HGEOM.1
Declination (J2000)
Right Ascension (J2000)
Grey scale flux range= 3.54 13.23 Kilo
Cont peak flux = 1.8813E-02 JY/BEAM
Levs = 2.500E-04 * (1, 1.400, 2, 2.800, 4, 5.600, 8, 11, 16, 23, 32, 45, 64, 90, 128, 181, 256, 362, 512, 724, 1024)
PLot file version 1 created 26-JAN-2018 00:09:57
GREY: NONE J1130+5457D.IMAP.1
CONT: J113050+ J1130+5457.HGEOM.1
Declination (J2000)
Right Ascension (J2000)
Grey scale flux range= 3.633 7.240 Kilo
Cont peak flux = 3.0232E-03 JY/BEAM
Levs = 2.500E-04 * (1, 1.400, 2, 2.800, 4, 5.600, 8, 11, 16, 23, 32, 45, 64, 90, 128, 181, 256, 362, 512, 724, 1024)
PLot file version 1 created 26-JAN-2018 00:14:20
GREY: NONE J1131+0435D.IMAP.1
CONT: J113140+ J1131+0435.HGEOM.1
Declination (J2000)
Right Ascension (J2000)
Grey scale flux range= 3.53 9.99 Kilo
Cont peak flux = 4.8330E-03 JY/BEAM
Levs = 2.500E-04 * (1, 1.400, 2, 2.800, 4, 5.600, 8, 11, 16, 23, 32, 45, 64, 90, 128, 181, 256, 362, 512, 724, 1024)

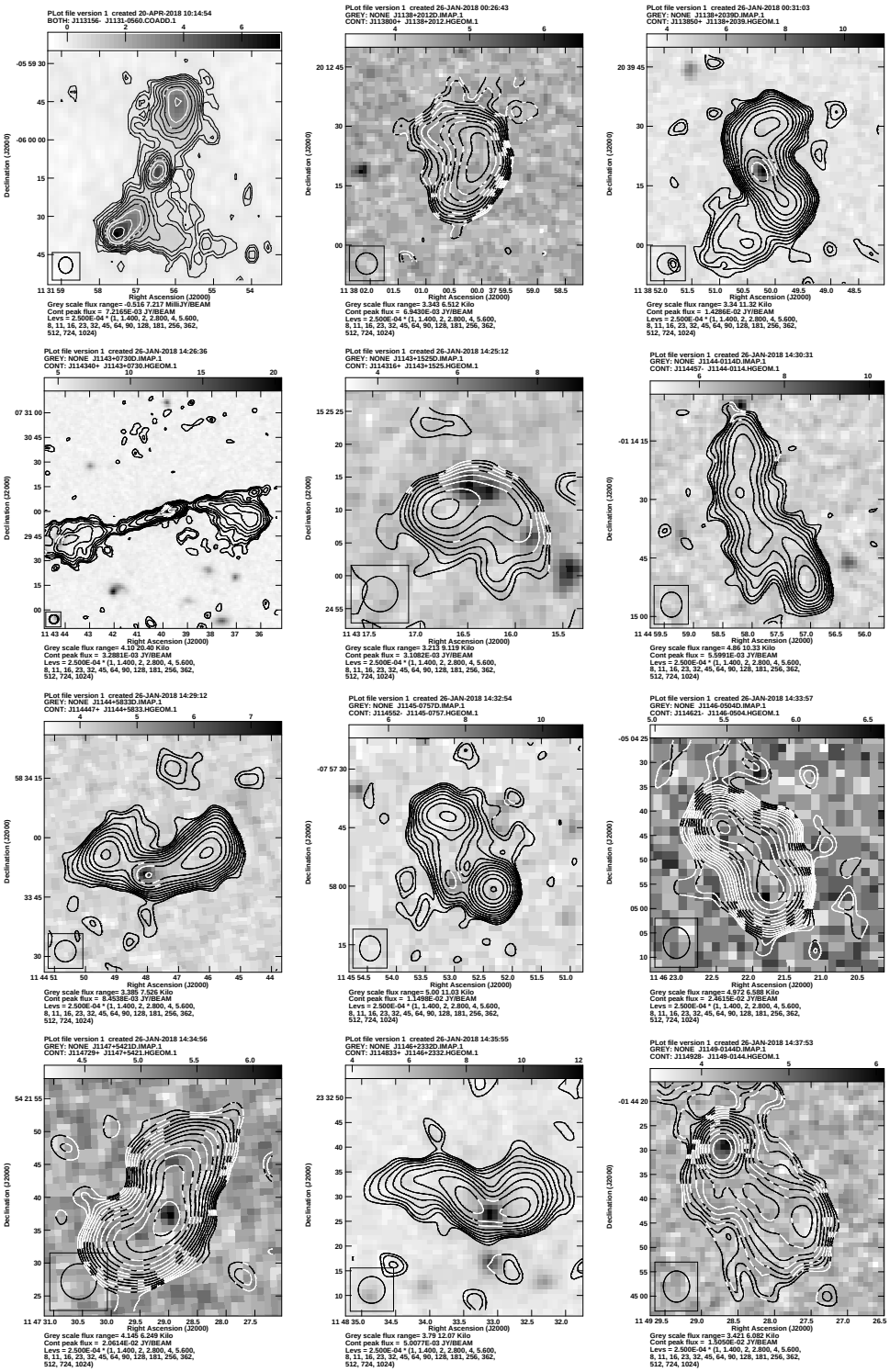
PLot file version 1 created 20-APR-2018 10:14:54
BOTH: J113156- J1131-0560.COADD.1
Declination (J2000)
Right Ascension (J2000)
Grey scale flux range= -0.516 7.217 MILLIY/BEAM
Cont peak flux = 7.2165E-03 JY/BEAM
Levs = 2.500E-04 * (1, 1.400, 2, 2.800, 4, 5.600, 8, 11, 16, 23, 32, 45, 64, 90, 128, 181, 256, 362, 512, 724, 1024)
PLot file version 1 created 26-JAN-2018 00:26:43
GREY: NONE J113B+2012D.IMAP.1
CONT: J113B0+ J113B+2012.HGEOM.1
Declination (J2000)
Right Ascension (J2000)
Grey scale flux range= 3.343 6.512 Kilo
Cont peak flux = 6.9430E-03 JY/BEAM
Levs = 2.500E-04 * (1, 1.400, 2, 2.800, 4, 5.600, 8, 11, 16, 23, 32, 45, 64, 90, 128, 181, 256, 362, 512, 724, 1024)
PLot file version 1 created 26-JAN-2018 00:31:03
GREY: NONE J113B+2039D.IMAP.1
CONT: J113B0+ J113B+2039.HGEOM.1
Declination (J2000)
Right Ascension (J2000)
Grey scale flux range= 3.34 11.32 Kilo
Cont peak flux = 1.4286E-02 JY/BEAM
Levs = 2.500E-04 * (1, 1.400, 2, 2.800, 4, 5.600, 8, 11, 16, 23, 32, 45, 64, 90, 128, 181, 256, 362, 512, 724, 1024)
PLot file version 1 created 26-JAN-2018 14:26:36
GREY: NONE J1143+0730D.IMAP.1
CONT: J114340+ J1143+0730.HGEOM.1
Declination (J2000)
Right Ascension (J2000)
Grey scale flux range= 4.10 20.40 Kilo
Cont peak flux = 3.2881E-03 JY/BEAM
Levs = 2.500E-04 * (1, 1.400, 2, 2.800, 4, 5.600, 8, 11, 16, 23, 32, 45, 64, 90, 128, 181, 256, 362, 512, 724, 1024)
PLot file version 1 created 26-JAN-2018 14:25:12
GREY: NONE J1143+1525D.IMAP.1
CONT: J114316+ J1143+1525.HGEOM.1
Declination (J2000)
Right Ascension (J2000)
Grey scale flux range= 3.213 9.119 Kilo
Cont peak flux = 3.1082E-03 JY/BEAM
Levs = 2.500E-04 * (1, 1.400, 2, 2.800, 4, 5.600, 8, 11, 16, 23, 32, 45, 64, 90, 128, 181, 256, 362, 512, 724, 1024)
PLot file version 1 created 26-JAN-2018 14:30:31
GREY: NONE J1144-0114D.IMAP.1
CONT: J114457- J1144-0114.HGEOM.1
Declination (J2000)
Right Ascension (J2000)
Grey scale flux range= 4.86 10.33 Kilo
Cont peak flux = 5.3991E-03 JY/BEAM
Levs = 2.500E-04 * (1, 1.400, 2, 2.800, 4, 5.600, 8, 11, 16, 23, 32, 45, 64, 90, 128, 181, 256, 362, 512, 724, 1024)
PLot file version 1 created 26-JAN-2018 14:29:12
GREY: NONE J1144+5833D.IMAP.1
CONT: J114447+ J1144+5833.HGEOM.1
Declination (J2000)
Right Ascension (J2000)
Grey scale flux range= 3.385 7.526 Kilo
Cont peak flux = 8.4538E-03 JY/BEAM
Levs = 2.500E-04 * (1, 1.400, 2, 2.800, 4, 5.600, 8, 11, 16, 23, 32, 45, 64, 90, 128, 181, 256, 362, 512, 724, 1024)
PLot file version 1 created 26-JAN-2018 14:32:54
GREY: NONE J1145-0757D.IMAP.1
CONT: J114552- J1145-0757.HGEOM.1
Declination (J2000)
Right Ascension (J2000)
Grey scale flux range= 5.00 11.03 Kilo
Cont peak flux = 1.1488E-02 JY/BEAM
Levs = 2.500E-04 * (1, 1.400, 2, 2.800, 4, 5.600, 8, 11, 16, 23, 32, 45, 64, 90, 128, 181, 256, 362, 512, 724, 1024)
PLot file version 1 created 26-JAN-2018 14:33:57
GREY: NONE J1146-0504D.IMAP.1
CONT: J114621- J1146-0504.HGEOM.1
Declination (J2000)
Right Ascension (J2000)
Grey scale flux range= 4.972 6.588 Kilo
Cont peak flux = 2.4615E-02 JY/BEAM
Levs = 2.500E-04 * (1, 1.400, 2, 2.800, 4, 5.600, 8, 11, 16, 23, 32, 45, 64, 90, 128, 181, 256, 362, 512, 724, 1024)
PLot file version 1 created 26-JAN-2018 14:34:56
GREY: NONE J1147+5421D.IMAP.1
CONT: J114729+ J1147+5421.HGEOM.1
Declination (J2000)
Right Ascension (J2000)
Grey scale flux range= 4.145 6.249 Kilo
Cont peak flux = 2.0614E-02 JY/BEAM
Levs = 2.500E-04 * (1, 1.400, 2, 2.800, 4, 5.600, 8, 11, 16, 23, 32, 45, 64, 90, 128, 181, 256, 362, 512, 724, 1024)
PLot file version 1 created 26-JAN-2018 14:35:55
GREY: NONE J1146+2332D.IMAP.1
CONT: J114833+ J1146+2332.HGEOM.1
Declination (J2000)
Right Ascension (J2000)
Grey scale flux range= 3.79 12.07 Kilo
Cont peak flux = 5.0077E-03 JY/BEAM
Levs = 2.500E-04 * (1, 1.400, 2, 2.800, 4, 5.600, 8, 11, 16, 23, 32, 45, 64, 90, 128, 181, 256, 362, 512, 724, 1024)
PLot file version 1 created 26-JAN-2018 14:37:53
GREY: NONE J1149-0144D.IMAP.1
CONT: J114928- J1149-0144.HGEOM.1
Declination (J2000)
Right Ascension (J2000)
Grey scale flux range= 3.421 6.082 Kilo
Cont peak flux = 1.5050E-02 JY/BEAM
Levs = 2.500E-04 * (1, 1.400, 2, 2.800, 4, 5.600, 8, 11, 16, 23, 32, 45, 64, 90, 128, 181, 256, 362, 512, 724, 1024)

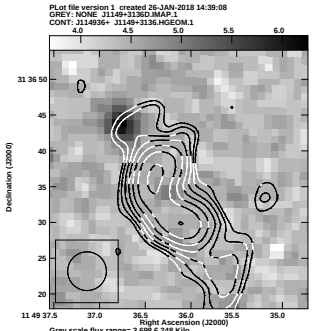
PLot file version 1 created 26-JAN-2018 14:39:08
GREY: NONE J1149+3136D.IMAP.1
CONT: J114936+ J1149+3136.HGEOM.1
Declination (J2000)
Right Ascension (J2000)
Grey scale flux range= 3.698 6.248 Kilo
Cont peak flux = 2.1930E-03 JY/BEAM
Levs = 2.500E-04 * (1, 1.400, 2, 2.800, 4, 5.600, 8, 11, 16, 23, 32, 45, 64, 90, 128, 181, 256, 362, 512, 724, 1024)

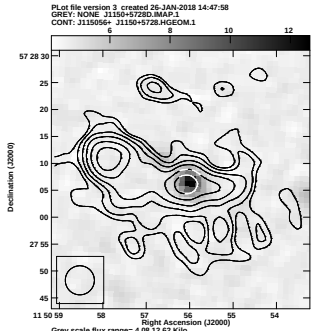
PLot file version 3 created 26-JAN-2018 14:47:58
GREY: NONE J1150+5728D.IMAP.1
CONT: J1150056+ J1150+5728.HGEOM.1
Declination (J2000)
Right Ascension (J2000)
Grey scale flux range= 4.08 12.62 Kilo
Cont peak flux = 1.7781E-03 JY/BEAM
Levs = 2.500E-04 * (1, 1.400, 2, 2.800, 4, 5.600, 8, 11, 16, 23, 32, 45, 64, 90, 128, 181, 256, 362, 512, 724, 1024)

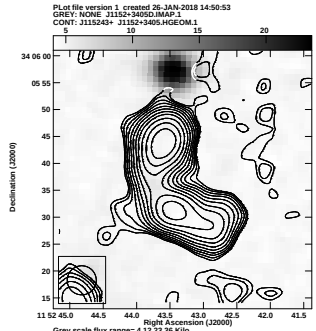
PLot file version 1 created 26-JAN-2018 14:50:53
GREY: NONE J1152+3405D.IMAP.1
CONT: J115243+ J1152+3405.HGEOM.1
Declination (J2000)
Right Ascension (J2000)
Grey scale flux range= 4.12 23.36 Kilo
Cont peak flux = 1.0827E-02 JY/BEAM
Levs = 2.500E-04 * (1, 1.400, 2, 2.800, 4, 5.600, 8, 11, 16, 23, 32, 45, 64, 90, 128, 181, 256, 362, 512, 724, 1024)

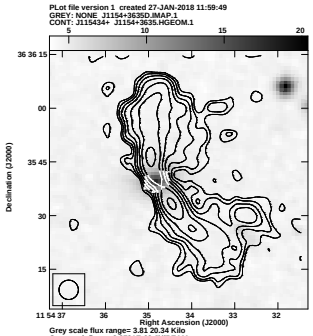
PLot file version 1 created 27-JAN-2018 11:59:49
GREY: NONE J1154+3635D.IMAP.1
CONT: J115434+ J1154+3635.HGEOM.1
Declination (J2000)
Right Ascension (J2000)
Grey scale flux range= 3.81 20.34 Kilo
Cont peak flux = 2.2731E-03 JY/BEAM
Levs = 2.500E-04 * (1, 1.400, 2, 2.800, 4, 5.600, 8, 11, 16, 23, 32, 45, 64, 90, 128, 181, 256, 362, 512, 724, 1024)

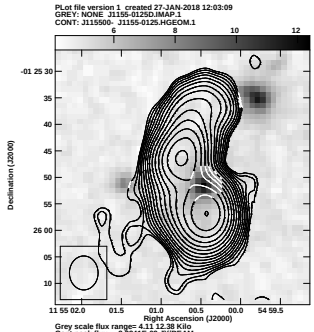
PLot file version 1 created 27-JAN-2018 12:03:09
GREY: NONE J1155-0125D.IMAP.1
CONT: J115500- J1155-0125.HGEOM.1
Declination (J2000)
Right Ascension (J2000)
Grey scale flux range= 4.11 12.38 Kilo
Cont peak flux = 3.2241E-02 JY/BEAM
Levs = 2.500E-04 * (1, 1.400, 2, 2.800, 4, 5.600, 8, 11, 16, 23, 32, 45, 64, 90, 128, 181, 256, 362, 512, 724, 1024)

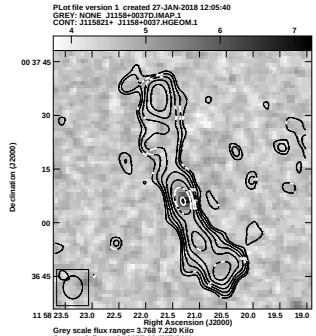
PLot file version 1 created 27-JAN-2018 12:05:40
GREY: NONE J1158+0037D.IMAP.1
CONT: J115821+ J1158+0037.HGEOM.1
Declination (J2000)
Right Ascension (J2000)
Grey scale flux range= 3.768 7.220 Kilo
Cont peak flux = 2.1007E-03 JY/BEAM
Levs = 2.500E-04 * (1, 1.400, 2, 2.800, 4, 5.600, 8, 11, 16, 23, 32, 45, 64, 90, 128, 181, 256, 362, 512, 724, 1024)

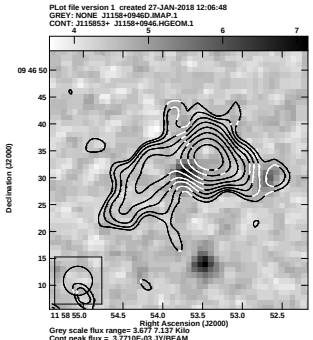
PLot file version 1 created 27-JAN-2018 12:06:48
GREY: NONE J1158+0946D.IMAP.1
CONT: J115853+ J1158+0946.HGEOM.1
Declination (J2000)
Right Ascension (J2000)
Grey scale flux range= 3.677 7.137 Kilo
Cont peak flux = 3.7710E-03 JY/BEAM
Levs = 2.500E-04 * (1, 1.400, 2, 2.800, 4, 5.600, 8, 11, 16, 23, 32, 45, 64, 90, 128, 181, 256, 362, 512, 724, 1024)

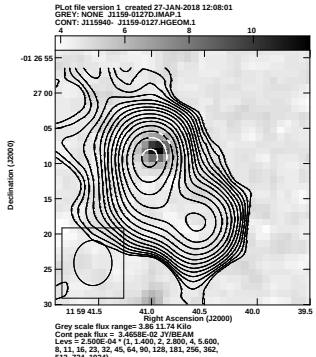
PLot file version 1 created 27-JAN-2018 12:08:01
GREY: NONE J1159-0127D.IMAP.1
CONT: J115940- J1159-0127.HGEOM.1
Declination (J2000)
Right Ascension (J2000)
Grey scale flux range= 3.86 11.74 Kilo
Cont peak flux = 3.4698E-02 JY/BEAM
Levs = 2.500E-04 * (1, 1.400, 2, 2.800, 4, 5.600, 8, 11, 16, 23, 32, 45, 64, 90, 128, 181, 256, 362, 512, 724, 1024)

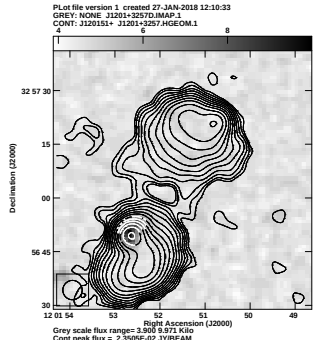
PLot file version 1 created 27-JAN-2018 12:10:33
GREY: NONE J1201+3257D.IMAP.1
CONT: J120151+ J1201+3257.HGEOM.1
Declination (J2000)
Right Ascension (J2000)
Grey scale flux range= 3.900 9.971 Kilo
Cont peak flux = 2.3505E-02 JY/BEAM
Levs = 2.500E-04 * (1, 1.400, 2, 2.800, 4, 5.600, 8, 11, 16, 23, 32, 45, 64, 90, 128, 181, 256, 362, 512, 724, 1024)

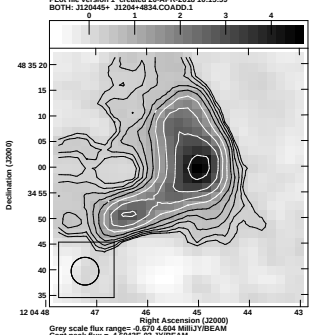
PLot file version 1 created 20-APR-2018 10:15:59
BOTH: J120445+ J1204+4834.COADD.1
Declination (J2000)
Right Ascension (J2000)
Grey scale flux range= -0.670 4.604 MilliJY/BEAM
Cont peak flux = 4.8043E-03 JY/BEAM
Levs = 2.500E-04 * (1, 1.400, 2, 2.800, 4, 5.600, 8, 11, 16, 23, 32, 45, 64, 90, 128, 181, 256, 362, 512, 724, 1024)

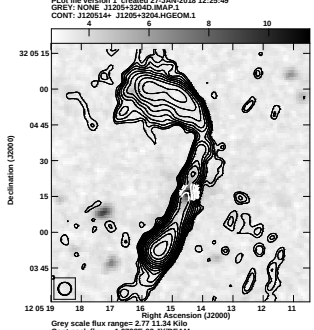
PLot file version 1 created 27-JAN-2018 12:25:49
GREY: NONE J1205+3204D.IMAP.1
CONT: J120514+ J1205+3204.HGEOM.1
Declination (J2000)
Right Ascension (J2000)
Grey scale flux range= 2.77 11.34 Kilo
Cont peak flux = 1.9798E-02 JY/BEAM
Levs = 2.500E-04 * (1, 1.400, 2, 2.800, 4, 5.600, 8, 11, 16, 23, 32, 45, 64, 90, 128, 181, 256, 362, 512, 724, 1024)

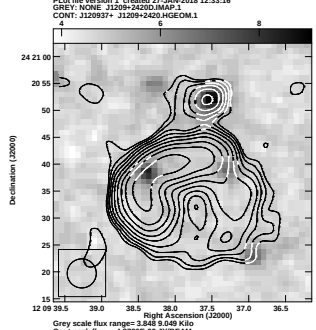
PLot file version 1 created 27-JAN-2018 12:33:16
GREY: NONE J1209+2420D.IMAP.1
CONT: J120937+ J1209+2420.HGEOM.1
Declination (J2000)
Right Ascension (J2000)
Grey scale flux range= 3.848 9.049 Kilo
Cont peak flux = 4.8796E-03 JY/BEAM
Levs = 2.500E-04 * (1, 1.400, 2, 2.800, 4, 5.600, 8, 11, 16, 23, 32, 45, 64, 90, 128, 181, 256, 362, 512, 724, 1024)

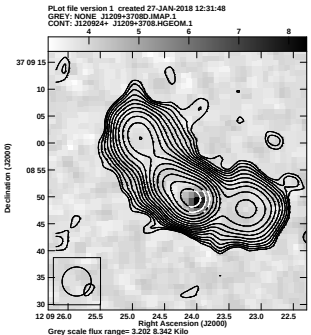

Grey scale flux range= 3.202 8.342 Kilo
Cont peak flux = 4.0465E-02 JY/BEAM
Levs = 2.500E-04 * (1, 1.400, 2, 2.800, 4, 5.600, 8, 11, 16, 23, 32, 45, 64, 90, 128, 181, 256, 362, 512, 724, 1024)

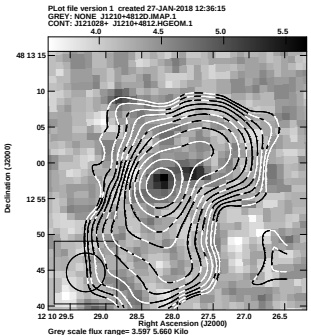

Grey scale flux range= 3.597 5.660 Kilo
Cont peak flux = 1.0713E-02 JY/BEAM
Levs = 2.500E-04 * (1, 1.400, 2, 2.800, 4, 5.600, 8, 11, 16, 23, 32, 45, 64, 90, 128, 181, 256, 362, 512, 724, 1024)

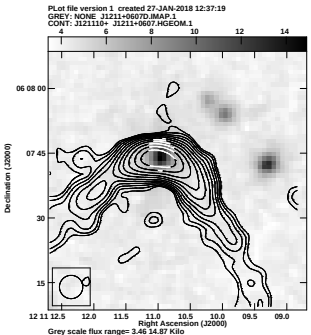

Grey scale flux range= 3.46 14.87 Kilo
Cont peak flux = 1.0893E-02 JY/BEAM
Levs = 2.500E-04 * (1, 1.400, 2, 2.800, 4, 5.600, 8, 11, 16, 23, 32, 45, 64, 90, 128, 181, 256, 362, 512, 724, 1024)

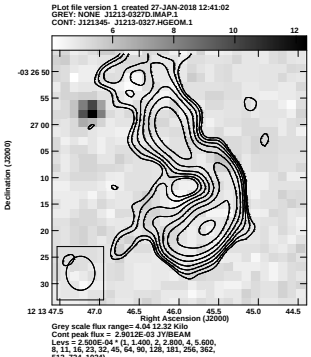

Grey scale flux range= 4.04 12.32 Kilo
Cont peak flux = 2.9012E-03 JY/BEAM
Levs = 2.500E-04 * (1, 1.400, 2, 2.800, 4, 5.600, 8, 11, 16, 23, 32, 45, 64, 90, 128, 181, 256, 362, 512, 724, 1024)

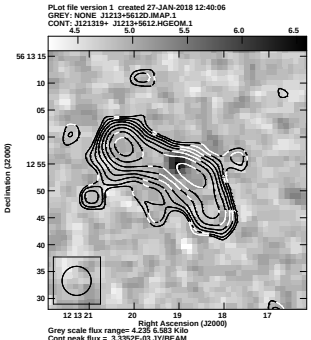

Grey scale flux range= 4.235 6.583 Kilo
Cont peak flux = 3.3352E-03 JY/BEAM
Levs = 2.500E-04 * (1, 1.400, 2, 2.800, 4, 5.600, 8, 11, 16, 23, 32, 45, 64, 90, 128, 181, 256, 362, 512, 724, 1024)

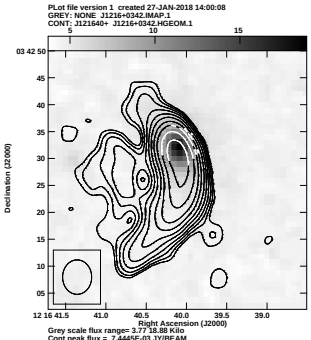

Grey scale flux range= 3.77 18.88 Kilo
Cont peak flux = 7.4445E-03 JY/BEAM
Levs = 2.500E-04 * (1, 1.400, 2, 2.800, 4, 5.600, 8, 11, 16, 23, 32, 45, 64, 90, 128, 181, 256, 362, 512, 724, 1024)

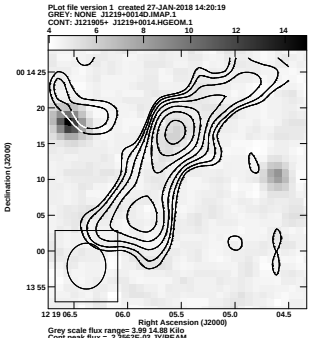

Grey scale flux range= 3.99 14.88 Kilo
Cont peak flux = 2.3562E-03 JY/BEAM
Levs = 2.500E-04 * (1, 1.400, 2, 2.800, 4, 5.600, 8, 11, 16, 23, 32, 45, 64, 90, 128, 181, 256, 362, 512, 724, 1024)

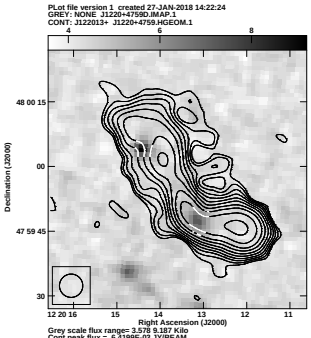

Grey scale flux range= 3.578 9.187 Kilo
Cont peak flux = 6.4198E-03 JY/BEAM
Levs = 2.500E-04 * (1, 1.400, 2, 2.800, 4, 5.600, 8, 11, 16, 23, 32, 45, 64, 90, 128, 181, 256, 362, 512, 724, 1024)

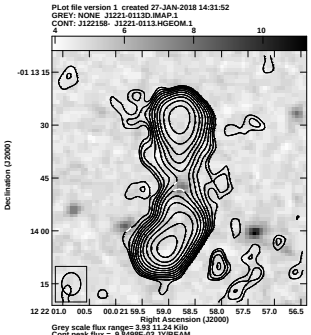

Grey scale flux range= 3.93 11.24 Kilo
Cont peak flux = 9.8498E-03 JY/BEAM
Levs = 2.500E-04 * (1, 1.400, 2, 2.800, 4, 5.600, 8, 11, 16, 23, 32, 45, 64, 90, 128, 181, 256, 362, 512, 724, 1024)

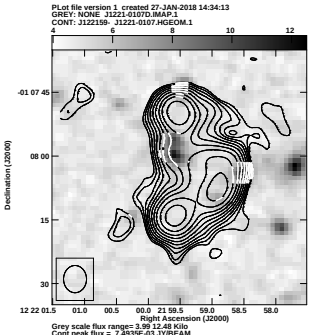

Grey scale flux range= 3.99 12.48 Kilo
Cont peak flux = 7.4935E-03 JY/BEAM
Levs = 2.500E-04 * (1, 1.400, 2, 2.800, 4, 5.600, 8, 11, 16, 23, 32, 45, 64, 90, 128, 181, 256, 362, 512, 724, 1024)

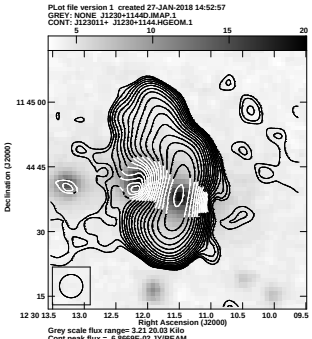

Grey scale flux range= 3.21 20.00 Kilo
Cont peak flux = 6.8669E-02 JY/BEAM
Levs = 2.500E-04 * (1, 1.400, 2, 2.800, 4, 5.600, 8, 11, 16, 23, 32, 45, 64, 90, 128, 181, 256, 362, 512, 724, 1024)

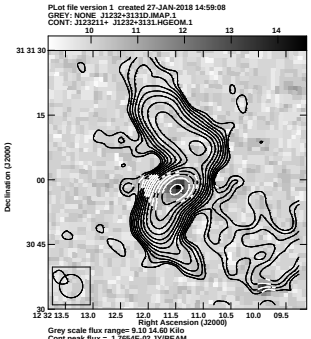

Grey scale flux range= 9.10 14.60 Kilo
Cont peak flux = 1.7654E-02 JY/BEAM
Levs = 2.500E-04 * (1, 1.400, 2, 2.800, 4, 5.600, 8, 11, 16, 23, 32, 45, 64, 90, 128, 181, 256, 362, 512, 724, 1024)

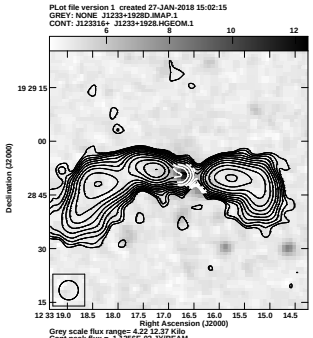
PLot file version 1 created 27-JAN-2018 15:02:15
GREY: NONE J1233+1928D.IMAP.1
CONT: J123316+ J1233+1928.HGEOM.1
Declination (J2000)
Right Ascension (J2000)
Grey scale flux range= 4.22 12.37 Kilo
Cont peak flux = 1.1256E-02 JY/BEAM
Levs = 2.500E-04 * (1, 1.400, 2, 2.800, 4, 5.600, 8, 11, 16, 23, 32, 45, 64, 90, 128, 181, 256, 362, 512, 724, 1024)

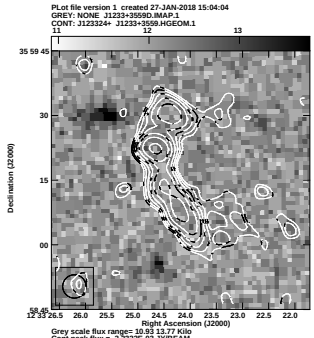
PLot file version 1 created 27-JAN-2018 15:04:04
GREY: NONE J1233+3559D.IMAP.1
CONT: J123324+ J1233+3559.HGEOM.1
Declination (J2000)
Right Ascension (J2000)
Grey scale flux range= 10.93 13.77 Kilo
Cont peak flux = 2.2322E-03 JY/BEAM
Levs = 2.500E-04 * (1, 1.400, 2, 2.800, 4, 5.600, 8, 11, 16, 23, 32, 45, 64, 90, 128, 181, 256, 362, 512, 724, 1024)

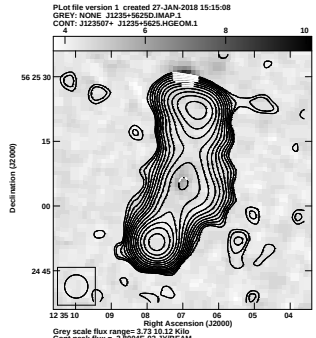
PLot file version 1 created 27-JAN-2018 15:15:08
GREY: NONE J1235+5625D.IMAP.1
CONT: J123507+ J1235+5625.HGEOM.1
Declination (J2000)
Right Ascension (J2000)
Grey scale flux range= 2.73 10.12 Kilo
Cont peak flux = 2.8004E-02 JY/BEAM
Levs = 2.500E-04 * (1, 1.400, 2, 2.800, 4, 5.600, 8, 11, 16, 23, 32, 45, 64, 90, 128, 181, 256, 362, 512, 724, 1024)

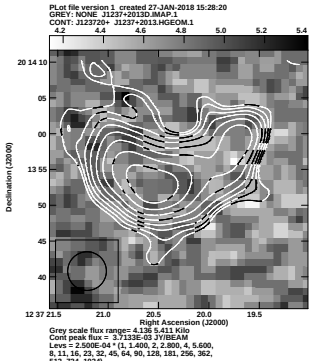
PLot file version 1 created 27-JAN-2018 15:28:20
GREY: NONE J1237+2013D.IMAP.1
CONT: J123720+ J1237+2013.HGEOM.1
Declination (J2000)
Right Ascension (J2000)
Grey scale flux range= 4.136 5.411 Kilo
Cont peak flux = 3.7133E-03 JY/BEAM
Levs = 2.500E-04 * (1, 1.400, 2, 2.800, 4, 5.600, 8, 11, 16, 23, 32, 45, 64, 90, 128, 181, 256, 362, 512, 724, 1024)

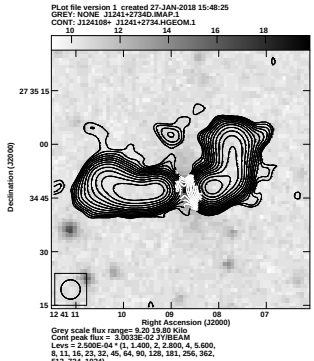
PLot file version 1 created 27-JAN-2018 15:48:25
GREY: NONE J1241+2734D.IMAP.1
CONT: J124108+ J1241+2734.HGEOM.1
Declination (J2000)
Right Ascension (J2000)
Grey scale flux range= 9.20 19.80 Kilo
Cont peak flux = 3.0033E-02 JY/BEAM
Levs = 2.500E-04 * (1, 1.400, 2, 2.800, 4, 5.600, 8, 11, 16, 23, 32, 45, 64, 90, 128, 181, 256, 362, 512, 724, 1024)

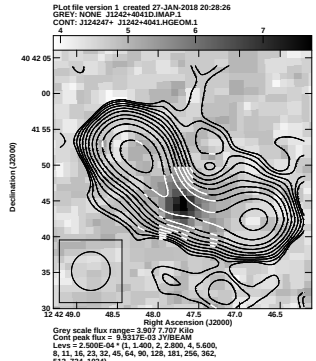
PLot file version 1 created 27-JAN-2018 20:28:26
GREY: NONE J1242+4041D.IMAP.1
CONT: J124247+ J1242+4041.HGEOM.1
Declination (J2000)
Right Ascension (J2000)
Grey scale flux range= 3.907 7.707 Kilo
Cont peak flux = 9.9317E-03 JY/BEAM
Levs = 2.500E-04 * (1, 1.400, 2, 2.800, 4, 5.600, 8, 11, 16, 23, 32, 45, 64, 90, 128, 181, 256, 362, 512, 724, 1024)

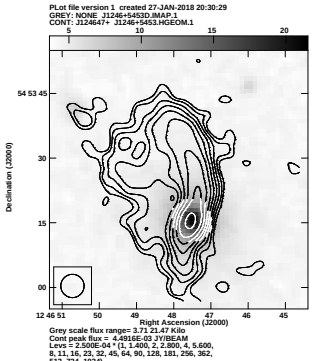
PLot file version 1 created 27-JAN-2018 20:30:29
GREY: NONE J1246+5453D.IMAP.1
CONT: J124647+ J1246+5453.HGEOM.1
Declination (J2000)
Right Ascension (J2000)
Grey scale flux range= 3.71 21.47 Kilo
Cont peak flux = 4.4916E-03 JY/BEAM
Levs = 2.500E-04 * (1, 1.400, 2, 2.800, 4, 5.600, 8, 11, 16, 23, 32, 45, 64, 90, 128, 181, 256, 362, 512, 724, 1024)

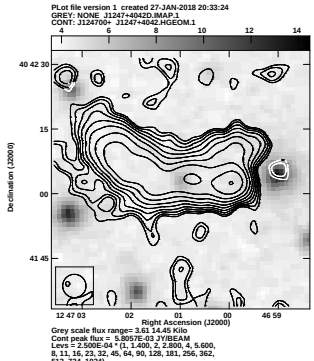
PLot file version 1 created 27-JAN-2018 20:33:24
GREY: NONE J1247+4042D.IMAP.1
CONT: J124700+ J1247+4042.HGEOM.1
Declination (J2000)
Right Ascension (J2000)
Grey scale flux range= 3.61 14.45 Kilo
Cont peak flux = 5.8057E-03 JY/BEAM
Levs = 2.500E-04 * (1, 1.400, 2, 2.800, 4, 5.600, 8, 11, 16, 23, 32, 45, 64, 90, 128, 181, 256, 362, 512, 724, 1024)

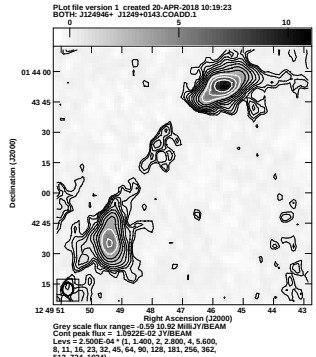
PLot file version 1 created 20-APR-2018 10:19:23
BOTH: J124946+ J1249+0143.COADD.1
Declination (J2000)
Right Ascension (J2000)
Grey scale flux range= -0.59 10.92 MilliJY/BEAM
Cont peak flux = 1.0922E-02 JY/BEAM
Levs = 2.500E-04 * (1, 1.400, 2, 2.800, 4, 5.600, 8, 11, 16, 23, 32, 45, 64, 90, 128, 181, 256, 362, 512, 724, 1024)

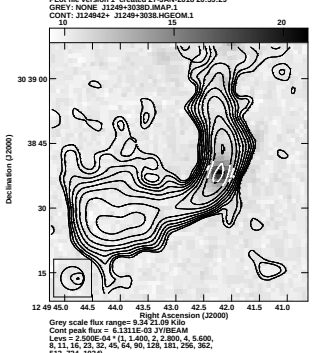
PLot file version 1 created 27-JAN-2018 20:39:29
GREY: NONE J1249+3038D.IMAP.1
CONT: J124942+ J1249+3038.HGEOM.1
Declination (J2000)
Right Ascension (J2000)
Grey scale flux range= 9.34 21.09 Kilo
Cont peak flux = 6.1311E-03 JY/BEAM
Levs = 2.500E-04 * (1, 1.400, 2, 2.800, 4, 5.600, 8, 11, 16, 23, 32, 45, 64, 90, 128, 181, 256, 362, 512, 724, 1024)

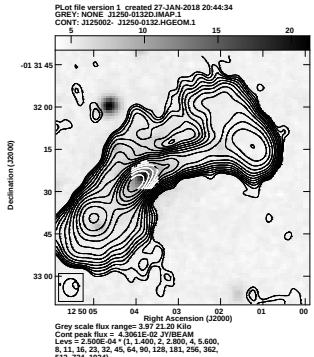
PLot file version 1 created 27-JAN-2018 20:44:34
GREY: NONE J1250-0132D.IMAP.1
CONT: J125002- J1250-0132.HGEOM.1
Declination (J2000)
Right Ascension (J2000)
Grey scale flux range= 3.97 21.20 Kilo
Cont peak flux = 4.3961E-02 JY/BEAM
Levs = 2.500E-04 * (1, 1.400, 2, 2.800, 4, 5.600, 8, 11, 16, 23, 32, 45, 64, 90, 128, 181, 256, 362, 512, 724, 1024)

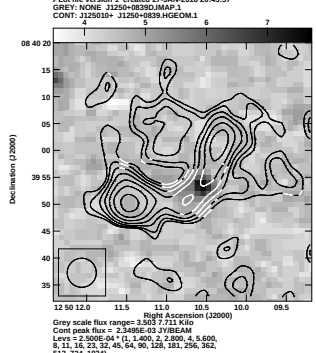
PLot file version 1 created 27-JAN-2018 20:45:57
GREY: NONE J1250+0839D.IMAP.1
CONT: J125010+ J1250+0839.HGEOM.1
Declination (J2000)
Right Ascension (J2000)
Grey scale flux range= 3.503 7.711 Kilo
Cont peak flux = 2.3495E-03 JY/BEAM
Levs = 2.500E-04 * (1, 1.400, 2, 2.800, 4, 5.600, 8, 11, 16, 23, 32, 45, 64, 90, 128, 181, 256, 362, 512, 724, 1024)

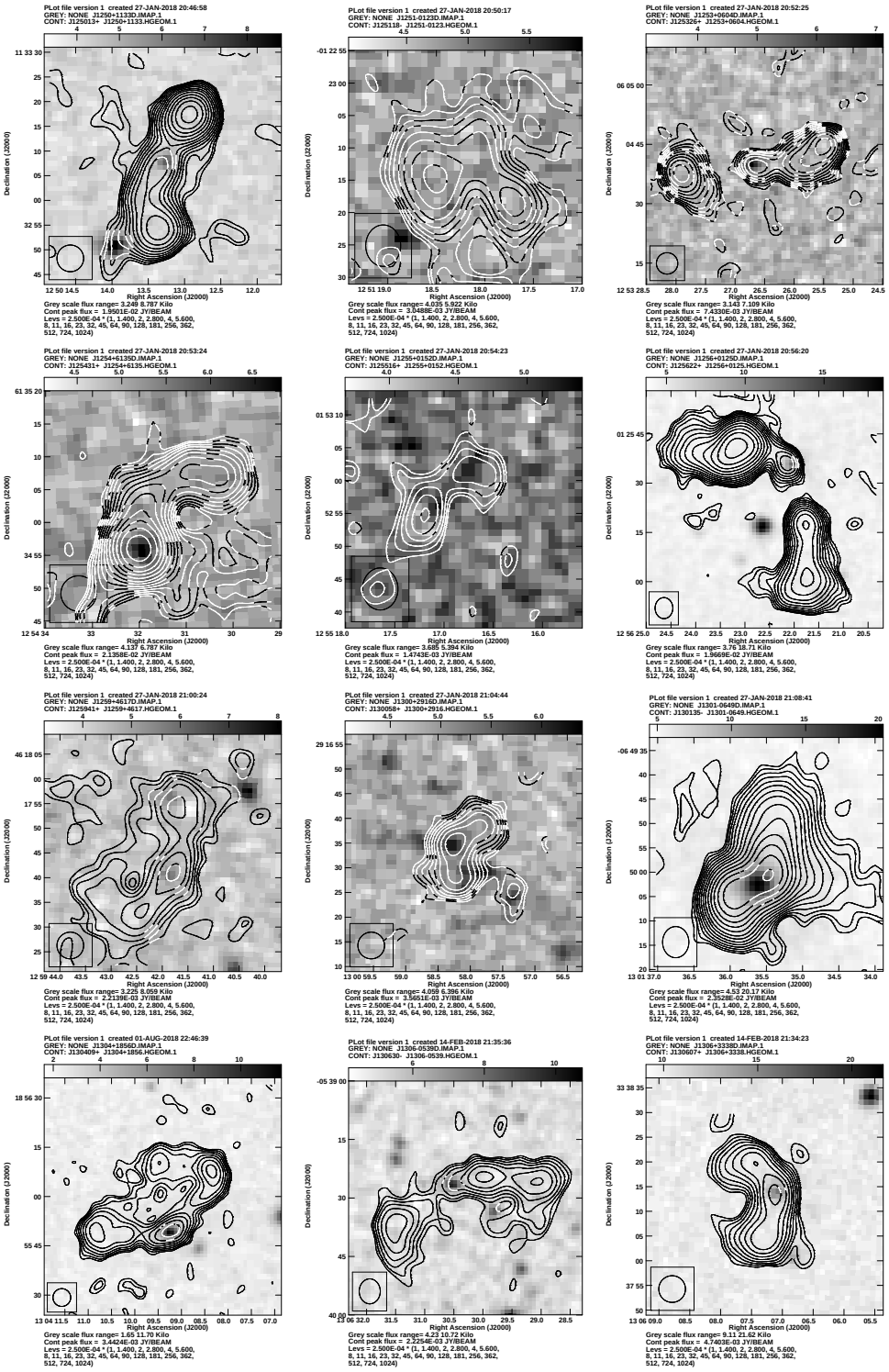
PLot file version 1 created 27-JAN-2018 20:46:58
GREY: NONE J1250+1133D.IMAP.1
CONT: J1250131+ J1250+1133.HGEOM.1
Declination (J2000)
Right Ascension (J2000)
Grey scale flux range= 3.248 8.787 Kilo
Cont peak flux = 1.9501E-02 JY/BEAM
Levs = 2.500E-04 * (1, 1.400, 2, 2.800, 4, 5.600, 8, 11, 16, 23, 32, 45, 64, 90, 128, 181, 256, 362, 512, 724, 1024)
PLot file version 1 created 27-JAN-2018 20:50:17
GREY: NONE J1251-0123D.IMAP.1
CONT: J125118- J1251-0123.HGEOM.1
Declination (J2000)
Right Ascension (J2000)
Grey scale flux range= 4.035 5.922 Kilo
Cont peak flux = 3.0488E-03 JY/BEAM
Levs = 2.500E-04 * (1, 1.400, 2, 2.800, 4, 5.600, 8, 11, 16, 23, 32, 45, 64, 90, 128, 181, 256, 362, 512, 724, 1024)
PLot file version 1 created 27-JAN-2018 20:52:25
GREY: NONE J1252+0604D.IMAP.1
CONT: J125326+ J1253+0604.HGEOM.1
Declination (J2000)
Right Ascension (J2000)
Grey scale flux range= 3.143 7.109 Kilo
Cont peak flux = 7.4330E-03 JY/BEAM
Levs = 2.500E-04 * (1, 1.400, 2, 2.800, 4, 5.600, 8, 11, 16, 23, 32, 45, 64, 90, 128, 181, 256, 362, 512, 724, 1024)
PLot file version 1 created 27-JAN-2018 20:53:24
GREY: NONE J1254+6135D.IMAP.1
CONT: J125431+ J1254+6135.HGEOM.1
Declination (J2000)
Right Ascension (J2000)
Grey scale flux range= 4.137 6.787 Kilo
Cont peak flux = 2.1358E-02 JY/BEAM
Levs = 2.500E-04 * (1, 1.400, 2, 2.800, 4, 5.600, 8, 11, 16, 23, 32, 45, 64, 90, 128, 181, 256, 362, 512, 724, 1024)
PLot file version 1 created 27-JAN-2018 20:54:23
GREY: NONE J1255+0152D.IMAP.1
CONT: J125516+ J1255+0152.HGEOM.1
Declination (J2000)
Right Ascension (J2000)
Grey scale flux range= 3.685 5.394 Kilo
Cont peak flux = 1.4743E-03 JY/BEAM
Levs = 2.500E-04 * (1, 1.400, 2, 2.800, 4, 5.600, 8, 11, 16, 23, 32, 45, 64, 90, 128, 181, 256, 362, 512, 724, 1024)
PLot file version 1 created 27-JAN-2018 20:56:20
GREY: NONE J1256+0125D.IMAP.1
CONT: J125622+ J1256+0125.HGEOM.1
Declination (J2000)
Right Ascension (J2000)
Grey scale flux range= 3.76 18.71 Kilo
Cont peak flux = 1.9669E-02 JY/BEAM
Levs = 2.500E-04 * (1, 1.400, 2, 2.800, 4, 5.600, 8, 11, 16, 23, 32, 45, 64, 90, 128, 181, 256, 362, 512, 724, 1024)
PLot file version 1 created 27-JAN-2018 21:00:24
GREY: NONE J1259+4617D.IMAP.1
CONT: J125941+ J1259+4617.HGEOM.1
Declination (J2000)
Right Ascension (J2000)
Grey scale flux range= 3.225 8.059 Kilo
Cont peak flux = 2.2139E-03 JY/BEAM
Levs = 2.500E-04 * (1, 1.400, 2, 2.800, 4, 5.600, 8, 11, 16, 23, 32, 45, 64, 90, 128, 181, 256, 362, 512, 724, 1024)
PLot file version 1 created 27-JAN-2018 21:04:44
GREY: NONE J1300+2916D.IMAP.1
CONT: J130058+ J1300+2916.HGEOM.1
Declination (J2000)
Right Ascension (J2000)
Grey scale flux range= 4.059 6.396 Kilo
Cont peak flux = 3.5651E-03 JY/BEAM
Levs = 2.500E-04 * (1, 1.400, 2, 2.800, 4, 5.600, 8, 11, 16, 23, 32, 45, 64, 90, 128, 181, 256, 362, 512, 724, 1024)
PLot file version 1 created 27-JAN-2018 21:08:41
GREY: NONE J1301-0649D.IMAP.1
CONT: J130135- J1301-0649.HGEOM.1
Declination (J2000)
Right Ascension (J2000)
Grey scale flux range= 4.53 20.17 Kilo
Cont peak flux = 2.3528E-02 JY/BEAM
Levs = 2.500E-04 * (1, 1.400, 2, 2.800, 4, 5.600, 8, 11, 16, 23, 32, 45, 64, 90, 128, 181, 256, 362, 512, 724, 1024)
PLot file version 1 created 01-AUG-2018 22:46:39
GREY: NONE J1304+1856D.IMAP.1
CONT: J130409+ J1304+1856.HGEOM.1
Declination (J2000)
Right Ascension (J2000)
Grey scale flux range= 1.85 11.70 Kilo
Cont peak flux = 3.4424E-03 JY/BEAM
Levs = 2.500E-04 * (1, 1.400, 2, 2.800, 4, 5.600, 8, 11, 16, 23, 32, 45, 64, 90, 128, 181, 256, 362, 512, 724, 1024)
PLot file version 1 created 14-FEB-2018 21:35:36
GREY: NONE J1306-0539D.IMAP.1
CONT: J130630- J1306-0539.HGEOM.1
Declination (J2000)
Right Ascension (J2000)
Grey scale flux range= 4.23 10.72 Kilo
Cont peak flux = 2.2254E-03 JY/BEAM
Levs = 2.500E-04 * (1, 1.400, 2, 2.800, 4, 5.600, 8, 11, 16, 23, 32, 45, 64, 90, 128, 181, 256, 362, 512, 724, 1024)
PLot file version 1 created 14-FEB-2018 21:34:23
GREY: NONE J1306+3338D.IMAP.1
CONT: J130607+ J1306+3338.HGEOM.1
Declination (J2000)
Right Ascension (J2000)
Grey scale flux range= 9.11 21.62 Kilo
Cont peak flux = 4.7403E-03 JY/BEAM
Levs = 2.500E-04 * (1, 1.400, 2, 2.800, 4, 5.600, 8, 11, 16, 23, 32, 45, 64, 90, 128, 181, 256, 362, 512, 724, 1024)

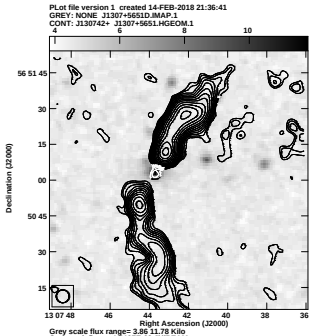
PLot file version 1 created 14-FEB-2018 21:36:41
GREY: NONE J1307+5651D.IMAP.1
CONT: J1307+42+ J1307+5651.HGEOM.1
Declination (J2000)
Right Ascension (J2000)
Grey scale flux range= 3.86 11.78 Kilo
Cont peak flux = 1.8107E-02 JY/BEAM
Levs = 2.500E-04 * (1, 1.400, 2, 2.800, 4, 5.600, 8, 11, 16, 23, 32, 45, 64, 90, 128, 181, 256, 362, 512, 724, 1024)

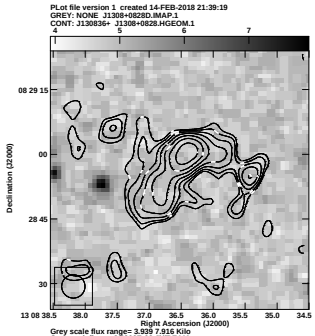
PLot file version 1 created 14-FEB-2018 21:39:19
GREY: NONE J1308+0828D.IMAP.1
CONT: J130836+ J1308+0828.HGEOM.1
Declination (J2000)
Right Ascension (J2000)
Grey scale flux range= 3.939 7.916 Kilo
Cont peak flux = 2.8260E-03 JY/BEAM
Levs = 2.500E-04 * (1, 1.400, 2, 2.800, 4, 5.600, 8, 11, 16, 23, 32, 45, 64, 90, 128, 181, 256, 362, 512, 724, 1024)

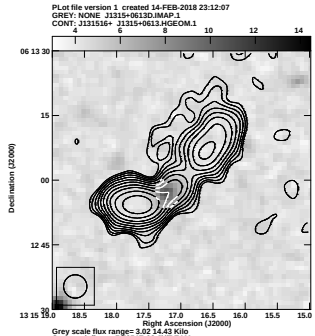
PLot file version 1 created 14-FEB-2018 23:12:07
GREY: NONE J1315+0613D.IMAP.1
CONT: J131516+ J1315+0613.HGEOM.1
Declination (J2000)
Right Ascension (J2000)
Grey scale flux range= 3.92 14.43 Kilo
Cont peak flux = 7.7654E-03 JY/BEAM
Levs = 2.500E-04 * (1, 1.400, 2, 2.800, 4, 5.600, 8, 11, 16, 23, 32, 45, 64, 90, 128, 181, 256, 362, 512, 724, 1024)

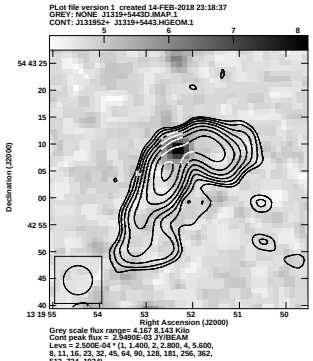
PLot file version 1 created 14-FEB-2018 23:18:37
GREY: NONE J1319+5443D.IMAP.1
CONT: J131952+ J1319+5443.HGEOM.1
Declination (J2000)
Right Ascension (J2000)
Grey scale flux range= 4.167 8.143 Kilo
Cont peak flux = 2.9490E-03 JY/BEAM
Levs = 2.500E-04 * (1, 1.400, 2, 2.800, 4, 5.600, 8, 11, 16, 23, 32, 45, 64, 90, 128, 181, 256, 362, 512, 724, 1024)

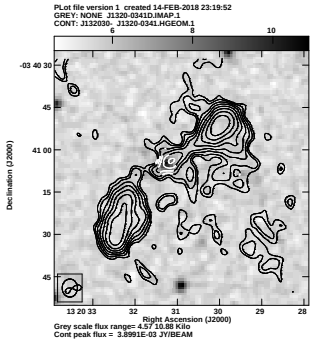
PLot file version 1 created 14-FEB-2018 23:19:52
GREY: NONE J1320-0341D.IMAP.1
CONT: J132030- J1320-0341.HGEOM.1
Declination (J2000)
Right Ascension (J2000)
Grey scale flux range= 4.57 10.88 Kilo
Cont peak flux = 3.8991E-03 JY/BEAM
Levs = 2.500E-04 * (1, 1.400, 2, 2.800, 4, 5.600, 8, 11, 16, 23, 32, 45, 64, 90, 128, 181, 256, 362, 512, 724, 1024)

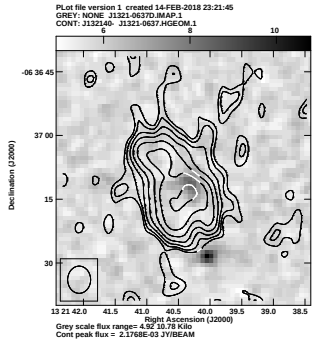
PLot file version 1 created 14-FEB-2018 23:21:45
GREY: NONE J1321-0637D.IMAP.1
CONT: J132140- J1321-0637.HGEOM.1
Declination (J2000)
Right Ascension (J2000)
Grey scale flux range= 4.82 10.78 Kilo
Cont peak flux = 2.1768E-03 JY/BEAM
Levs = 2.500E-04 * (1, 1.400, 2, 2.800, 4, 5.600, 8, 11, 16, 23, 32, 45, 64, 90, 128, 181, 256, 362, 512, 724, 1024)

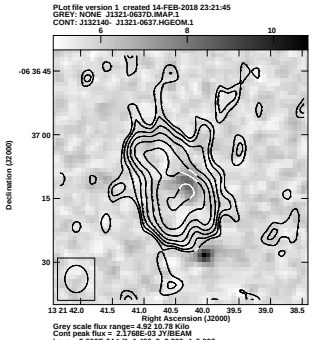
PLot file version 1 created 14-FEB-2018 23:21:45
GREY: NONE J1321-0637D.IMAP.1
CONT: J132140- J1321-0637.HGEOM.1
Declination (J2000)
Right Ascension (J2000)
Grey scale flux range= 4.92 10.78 Kilo
Cont peak flux = 2.1768E-03 JY/BEAM
Levs = 2.500E-04 * (1, 1.400, 2, 2.800, 4, 5.600, 8, 11, 16, 23, 32, 45, 64, 90, 128, 181, 256, 362, 512, 724, 1024)

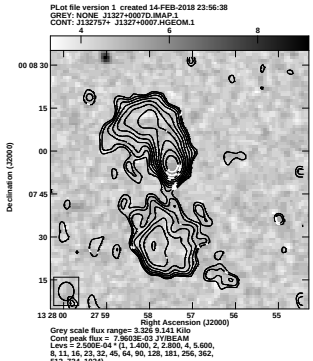
PLot file version 1 created 14-FEB-2018 23:56:38
GREY: NONE J1327+0007D.IMAP.1
CONT: J132757+ J1327+0007.HGEOM.1
Declination (J2000)
Right Ascension (J2000)
Grey scale flux range= 3.326 9.141 Kilo
Cont peak flux = 7.8603E-03 JY/BEAM
Levs = 2.500E-04 * (1, 1.400, 2, 2.800, 4, 5.600, 8, 11, 16, 23, 32, 45, 64, 90, 128, 181, 256, 362, 512, 724, 1024)

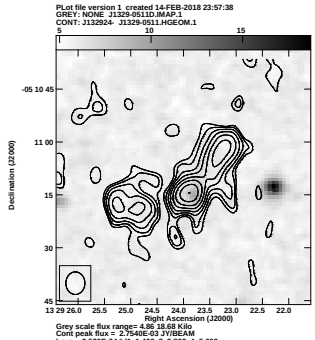
PLot file version 1 created 14-FEB-2018 23:57:38
GREY: NONE J1329-0511D.IMAP.1
CONT: J132924- J1329-0511.HGEOM.1
Declination (J2000)
Right Ascension (J2000)
Grey scale flux range= 4.86 18.68 Kilo
Cont peak flux = 2.7540E-03 JY/BEAM
Levs = 2.500E-04 * (1, 1.400, 2, 2.800, 4, 5.600, 8, 11, 16, 23, 32, 45, 64, 90, 128, 181, 256, 362, 512, 724, 1024)

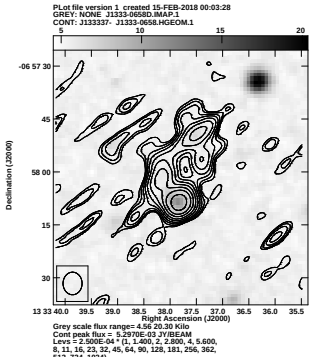
PLot file version 1 created 15-FEB-2018 00:03:28
GREY: NONE J1333-0658D.IMAP.1
CONT: J133337- J1333-0658.HGEOM.1
Declination (J2000)
Right Ascension (J2000)
Grey scale flux range= 4.56 20.30 Kilo
Cont peak flux = 5.2970E-03 JY/BEAM
Levs = 2.500E-04 * (1, 1.400, 2, 2.800, 4, 5.600, 8, 11, 16, 23, 32, 45, 64, 90, 128, 181, 256, 362, 512, 724, 1024)

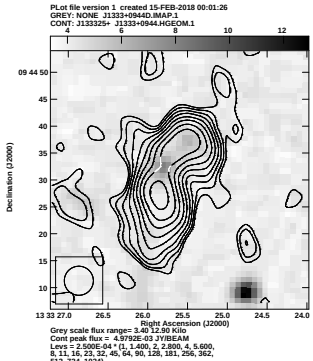
PLot file version 1 created 15-FEB-2018 00:01:26
GREY: NONE J1333+0944D.IMAP.1
CONT: J133325+ J1333+0944.HGEOM.1
Declination (J2000)
Right Ascension (J2000)
Grey scale flux range= 3.40 12.90 Kilo
Cont peak flux = 4.9792E-03 JY/BEAM
Levs = 2.500E-04 * (1, 1.400, 2, 2.800, 4, 5.600, 8, 11, 16, 23, 32, 45, 64, 90, 128, 181, 256, 362, 512, 724, 1024)

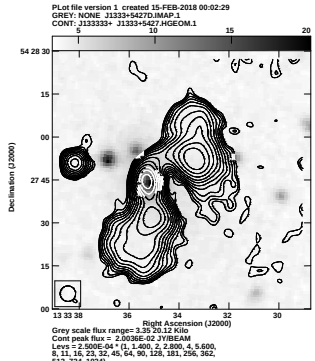
PLot file version 1 created 15-FEB-2018 00:02:29
GREY: NONE J1333+5427D.IMAP.1
CONT: J133333+ J1333+5427.HGEOM.1
Declination (J2000)
Right Ascension (J2000)
Grey scale flux range= 3.35 20.12 Kilo
Cont peak flux = 2.0036E-02 JY/BEAM
Levs = 2.500E-04 * (1, 1.400, 2, 2.800, 4, 5.600, 8, 11, 16, 23, 32, 45, 64, 90, 128, 181, 256, 362, 512, 724, 1024)

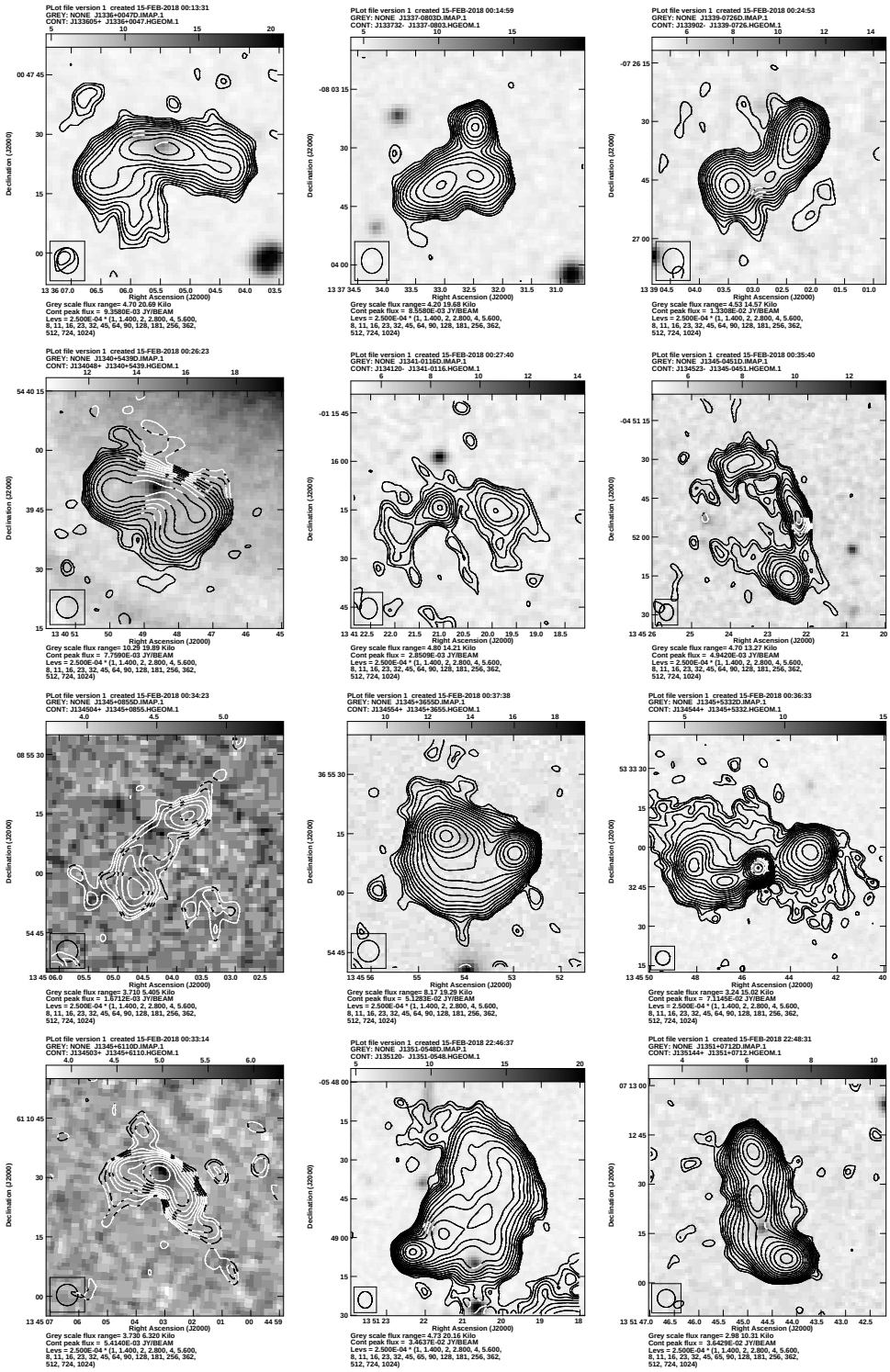
PLot file version 1 created 15-FEB-2018 00:13:31
GREY: NONE J1336+0047D.IMAP.1
CONT: J133605+ J1336+0047.HGEOM.1
Grey scale flux range= 4.70 20.69 Kilo
Cont peak flux = 9.3580E-03 JY/BEAM
Levs = 2.500E-04 * (1, 1.400, 2, 2.800, 4, 5.600, 8, 11, 16, 23, 32, 45, 64, 90, 128, 181, 256, 362, 512, 724, 1024)
PLot file version 1 created 15-FEB-2018 00:14:59
GREY: NONE J1337-0803D.IMAP.1
CONT: J133732- J1337-0803.HGEOM.1
Grey scale flux range= 4.20 19.68 Kilo
Cont peak flux = 8.5580E-03 JY/BEAM
Levs = 2.500E-04 * (1, 1.400, 2, 2.800, 4, 5.600, 8, 11, 16, 23, 32, 45, 64, 90, 128, 181, 256, 362, 512, 724, 1024)
PLot file version 1 created 15-FEB-2018 00:24:53
GREY: NONE J1339-0726D.IMAP.1
CONT: J133902- J1339-0726.HGEOM.1
Grey scale flux range= 4.53 14.57 Kilo
Cont peak flux = 1.3308E-02 JY/BEAM
Levs = 2.500E-04 * (1, 1.400, 2, 2.800, 4, 5.600, 8, 11, 16, 23, 32, 45, 64, 90, 128, 181, 256, 362, 512, 724, 1024)
PLot file version 1 created 15-FEB-2018 00:26:23
GREY: NONE J1340+5439D.IMAP.1
CONT: J134048+ J1340+5439.HGEOM.1
Grey scale flux range= 10.28 19.89 Kilo
Cont peak flux = 7.7590E-03 JY/BEAM
Levs = 2.500E-04 * (1, 1.400, 2, 2.800, 4, 5.600, 8, 11, 16, 23, 32, 45, 64, 90, 128, 181, 256, 362, 512, 724, 1024)
PLot file version 1 created 15-FEB-2018 00:27:40
GREY: NONE J1341-0116D.IMAP.1
CONT: J134120- J1341-0116.HGEOM.1
Grey scale flux range= 4.80 14.21 Kilo
Cont peak flux = 2.8509E-03 JY/BEAM
Levs = 2.500E-04 * (1, 1.400, 2, 2.800, 4, 5.600, 8, 11, 16, 23, 32, 45, 64, 90, 128, 181, 256, 362, 512, 724, 1024)
PLot file version 1 created 15-FEB-2018 00:35:40
GREY: NONE J1345-0451D.IMAP.1
CONT: J134523- J1345-0451.HGEOM.1
Grey scale flux range= 4.70 13.27 Kilo
Cont peak flux = 4.8420E-03 JY/BEAM
Levs = 2.500E-04 * (1, 1.400, 2, 2.800, 4, 5.600, 8, 11, 16, 23, 32, 45, 64, 90, 128, 181, 256, 362, 512, 724, 1024)
PLot file version 1 created 15-FEB-2018 00:34:23
GREY: NONE J1345+0855D.IMAP.1
CONT: J134504+ J1345+0855.HGEOM.1
Grey scale flux range= 3.710 5.405 Kilo
Cont peak flux = 1.8712E-03 JY/BEAM
Levs = 2.500E-04 * (1, 1.400, 2, 2.800, 4, 5.600, 8, 11, 16, 23, 32, 45, 64, 90, 128, 181, 256, 362, 512, 724, 1024)
PLot file version 1 created 15-FEB-2018 00:37:38
GREY: NONE J1345+3655D.IMAP.1
CONT: J134554+ J1345+3655.HGEOM.1
Grey scale flux range= 8.17 19.29 Kilo
Cont peak flux = 5.1283E-02 JY/BEAM
Levs = 2.500E-04 * (1, 1.400, 2, 2.800, 4, 5.600, 8, 11, 16, 23, 32, 45, 64, 90, 128, 181, 256, 362, 512, 724, 1024)
PLot file version 1 created 15-FEB-2018 00:36:33
GREY: NONE J1345+5332D.IMAP.1
CONT: J134544+ J1345+5332.HGEOM.1
Grey scale flux range= 3.24 15.02 Kilo
Cont peak flux = 7.1145E-02 JY/BEAM
Levs = 2.500E-04 * (1, 1.400, 2, 2.800, 4, 5.600, 8, 11, 16, 23, 32, 45, 64, 90, 128, 181, 256, 362, 512, 724, 1024)
PLot file version 1 created 15-FEB-2018 00:33:14
GREY: NONE J1345+6110D.IMAP.1
CONT: J134503+ J1345+6110.HGEOM.1
Grey scale flux range= 3.730 6.320 Kilo
Cont peak flux = 5.4140E-03 JY/BEAM
Levs = 2.500E-04 * (1, 1.400, 2, 2.800, 4, 5.600, 8, 11, 16, 23, 32, 45, 64, 90, 128, 181, 256, 362, 512, 724, 1024)
PLot file version 1 created 15-FEB-2018 22:46:37
GREY: NONE J1351-0548D.IMAP.1
CONT: J135120- J1351-0548.HGEOM.1
Grey scale flux range= 4.73 20.16 Kilo
Cont peak flux = 3.4637E-02 JY/BEAM
Levs = 2.500E-04 * (1, 1.400, 2, 2.800, 4, 5.600, 8, 11, 16, 23, 32, 45, 65, 90, 128, 181, 256, 362, 512, 724, 1024)
PLot file version 1 created 15-FEB-2018 22:48:31
GREY: NONE J1351+0712D.IMAP.1
CONT: J135144+ J1351+0712.HGEOM.1
Grey scale flux range= 2.98 10.31 Kilo
Cont peak flux = 3.6429E-02 JY/BEAM
Levs = 2.500E-04 * (1, 1.400, 2, 2.800, 4, 5.600, 8, 11, 16, 23, 32, 45, 65, 90, 128, 181, 256, 362, 512, 724, 1024)
Declination (J2000)
Right Ascension (J2000)

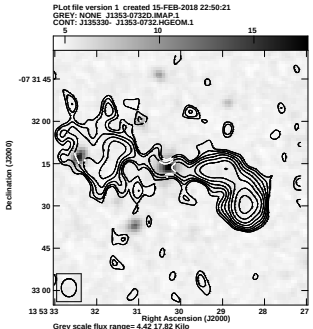
PLot file version 1 created 15-FEB-2018 22:50:21
GREY: NONE J1353-0732D.IMAP.1
CONT: J135330- J1353-0732.HGEOM.1
Declination (J2000)
Right Ascension (J2000)
Grey scale flux range= 4.42 17.82 Kilo
Cont peak flux = 3.2974E-03 JY/BEAM
Levs = 2.500E-04 * (1, 1.400, 2, 2.800, 4, 5.600, 8, 11, 16, 23, 32, 45, 65, 90, 128, 181, 256, 362, 512, 724, 1024)

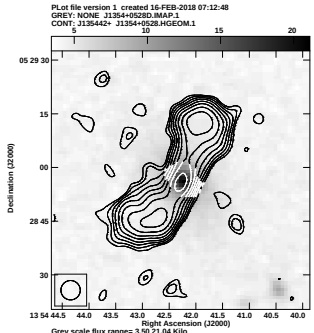
PLot file version 1 created 16-FEB-2018 07:12:48
GREY: NONE J1354+0528D.IMAP.1
CONT: J135442+ J1354+0528.HGEOM.1
Declination (J2000)
Right Ascension (J2000)
Grey scale flux range= 3.50 21.04 Kilo
Cont peak flux = 3.5927E-03 JY/BEAM
Levs = 2.500E-04 * (1, 1.400, 2, 2.800, 4, 5.600, 8, 11, 16, 23, 32, 45, 65, 90, 128, 181, 256, 362, 512, 724, 1024)

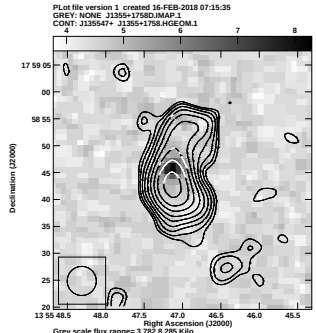
PLot file version 1 created 16-FEB-2018 07:15:35
GREY: NONE J1355+1758D.IMAP.1
CONT: J135547+ J1355+1758.HGEOM.1
Declination (J2000)
Right Ascension (J2000)
Grey scale flux range= 3.782 8.285 Kilo
Cont peak flux = 4.8700E-03 JY/BEAM
Levs = 2.500E-04 * (1, 1.400, 2, 2.800, 4, 5.600, 8, 11, 16, 23, 32, 45, 65, 90, 128, 181, 256, 362, 512, 724, 1024)

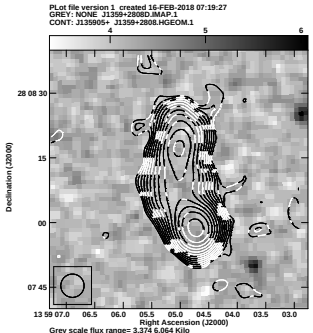
PLot file version 1 created 16-FEB-2018 07:19:27
GREY: NONE J1359+2808D.IMAP.1
CONT: J135905+ J1359+2808.HGEOM.1
Declination (J2000)
Right Ascension (J2000)
Grey scale flux range= 3.374 6.064 Kilo
Cont peak flux = 1.9551E-02 JY/BEAM
Levs = 2.500E-04 * (1, 1.400, 2, 2.800, 4, 5.600, 8, 11, 16, 23, 32, 45, 65, 90, 128, 181, 256, 362, 512, 724, 1024)

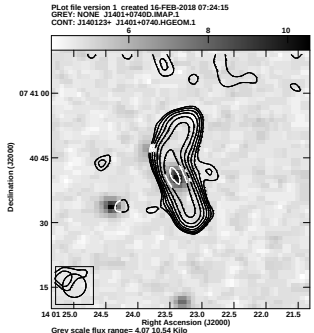
PLot file version 1 created 16-FEB-2018 07:24:15
GREY: NONE J1401+0740D.IMAP.1
CONT: J140123+ J1401+0740.HGEOM.1
Declination (J2000)
Right Ascension (J2000)
Grey scale flux range= 4.07 10.54 Kilo
Cont peak flux = 2.9080E-03 JY/BEAM
Levs = 2.500E-04 * (1, 1.400, 2, 2.800, 4, 5.600, 8, 11, 16, 23, 32, 45, 65, 90, 128, 181, 256, 362, 512, 724, 1024)

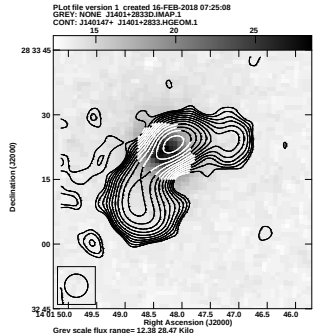
PLot file version 1 created 16-FEB-2018 07:25:08
GREY: NONE J1401+2833D.IMAP.1
CONT: J140147+ J1401+2833.HGEOM.1
Declination (J2000)
Right Ascension (J2000)
Grey scale flux range= 12.38 28.47 Kilo
Cont peak flux = 1.3894E-02 JY/BEAM
Levs = 2.500E-04 * (1, 1.400, 2, 2.800, 4, 5.600, 8, 11, 16, 23, 32, 45, 65, 90, 128, 181, 256, 362, 512, 724, 1024)

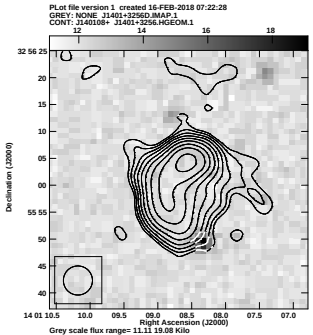
PLot file version 1 created 16-FEB-2018 07:22:28
GREY: NONE J1401+3256D.IMAP.1
CONT: J140108+ J1401+3256.HGEOM.1
Declination (J2000)
Right Ascension (J2000)
Grey scale flux range= 11.11 19.08 Kilo
Cont peak flux = 4.6770E-03 JY/BEAM
Levs = 2.500E-04 * (1, 1.400, 2, 2.800, 4, 5.600, 8, 11, 16, 23, 32, 45, 65, 90, 128, 181, 256, 362, 512, 724, 1024)

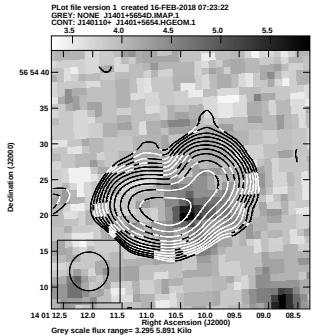
PLot file version 1 created 16-FEB-2018 07:23:22
GREY: NONE J1401+5654D.IMAP.1
CONT: J140110+ J1401+5654.HGEOM.1
Declination (J2000)
Right Ascension (J2000)
Grey scale flux range= 3.295 5.891 Kilo
Cont peak flux = 1.0409E-02 JY/BEAM
Levs = 2.500E-04 * (1, 1.400, 2, 2.800, 4, 5.600, 8, 11, 16, 23, 32, 45, 65, 90, 128, 181, 256, 362, 512, 724, 1024)

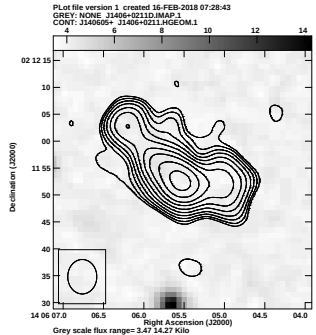
PLot file version 1 created 16-FEB-2018 07:28:43
GREY: NONE J1406+0211D.IMAP.1
CONT: J140605+ J1406+0211.HGEOM.1
Declination (J2000)
Right Ascension (J2000)
Grey scale flux range= 3.47 14.27 Kilo
Cont peak flux = 6.8582E-03 JY/BEAM
Levs = 2.500E-04 * (1, 1.400, 2, 2.800, 4, 5.600, 8, 11, 16, 23, 32, 45, 65, 90, 128, 181, 256, 362, 512, 724, 1024)

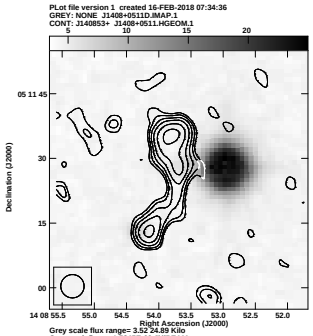
PLot file version 1 created 16-FEB-2018 07:34:36
GREY: NONE J1408+0511D.IMAP.1
CONT: J140853+ J1408+0511.HGEOM.1
Declination (J2000)
Right Ascension (J2000)
Grey scale flux range= 3.52 24.89 Kilo
Cont peak flux = 1.5845E-03 JY/BEAM
Levs = 2.500E-04 * (1, 1.400, 2, 2.800, 4, 5.600, 8, 11, 16, 23, 32, 45, 65, 90, 128, 181, 256, 362, 512, 724, 1024)

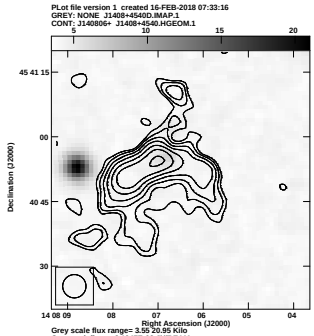
PLot file version 1 created 16-FEB-2018 07:33:16
GREY: NONE J1408+4540D.IMAP.1
CONT: J140806+ J1408+4540.HGEOM.1
Declination (J2000)
Right Ascension (J2000)
Grey scale flux range= 3.95 20.95 Kilo
Cont peak flux = 2.1947E-03 JY/BEAM
Levs = 2.500E-04 * (1, 1.400, 2, 2.800, 4, 5.600, 8, 11, 16, 23, 32, 45, 65, 90, 128, 181, 256, 362, 512, 724, 1024)

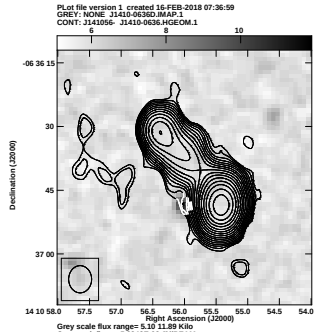
PLot file version 1 created 16-FEB-2018 07:36:59
GREY: NONE J1410-0636D.IMAP.1
CONT: J141056- J1410-0636.HGEOM.1
Declination (J2000)
Right Ascension (J2000)
Grey scale flux range= 5.10 11.89 Kilo
Cont peak flux = 5.9243E-02 JY/BEAM
Levs = 2.500E-04 * (1, 1.400, 2, 2.800, 4, 5.600, 8, 11, 16, 23, 32, 45, 65, 90, 128, 181, 256, 362, 512, 724, 1024)

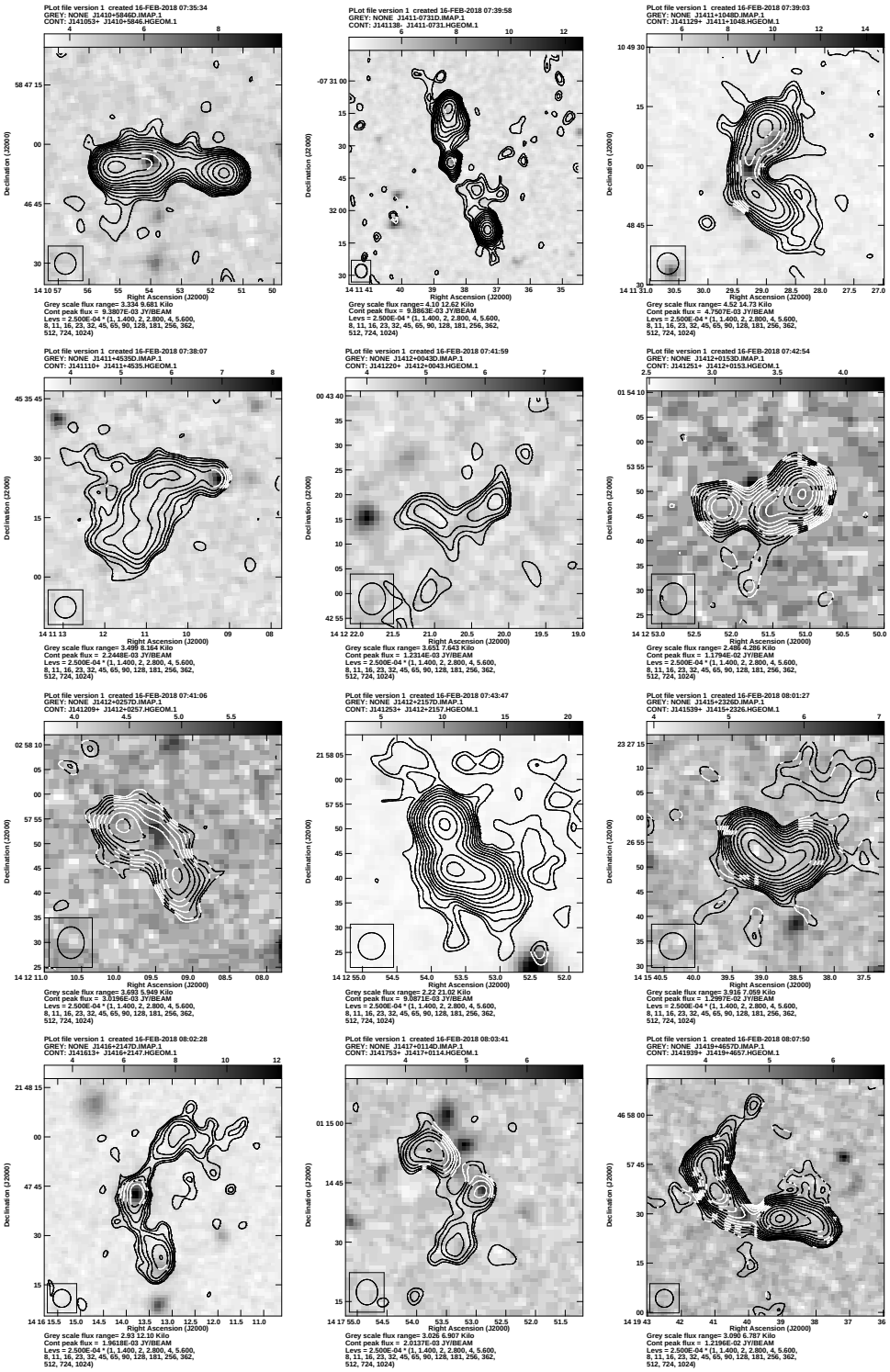
PLot file version 1 created 16-FEB-2018 07:35:34
GREY: NONE J1410+5846D.IMAP.1
CONT: J141053+ J1410+5846.HGEOM.1
Declination (J2000)
Right Ascension (J2000)
Grey scale flux range= 3.334 9.681 Kilo
Cont peak flux = 9.3807E-03 JY/BEAM
Levs = 2.500E-04 * (1, 1.400, 2, 2.800, 4, 5.600, 8, 11, 16, 23, 32, 45, 65, 90, 128, 181, 256, 362, 512, 724, 1024)
PLot file version 1 created 16-FEB-2018 07:39:58
GREY: NONE J1411-0731D.IMAP.1
CONT: J141138- J1411-0731.HGEOM.1
Declination (J2000)
Right Ascension (J2000)
Grey scale flux range= 4.10 12.62 Kilo
Cont peak flux = 9.8863E-03 JY/BEAM
Levs = 2.500E-04 * (1, 1.400, 2, 2.800, 4, 5.600, 8, 11, 16, 23, 32, 45, 65, 90, 128, 181, 256, 362, 512, 724, 1024)
PLot file version 1 created 16-FEB-2018 07:39:03
GREY: NONE J1411+1048D.IMAP.1
CONT: J141129+ J1411+1048.HGEOM.1
Declination (J2000)
Right Ascension (J2000)
Grey scale flux range= 4.52 14.73 Kilo
Cont peak flux = 4.7507E-03 JY/BEAM
Levs = 2.500E-04 * (1, 1.400, 2, 2.800, 4, 5.600, 8, 11, 16, 23, 32, 45, 65, 90, 128, 181, 256, 362, 512, 724, 1024)
PLot file version 1 created 16-FEB-2018 07:38:07
GREY: NONE J1411+4535D.IMAP.1
CONT: J141110+ J1411+4535.HGEOM.1
Declination (J2000)
Right Ascension (J2000)
Grey scale flux range= 3.499 8.164 Kilo
Cont peak flux = 2.2448E-03 JY/BEAM
Levs = 2.500E-04 * (1, 1.400, 2, 2.800, 4, 5.600, 8, 11, 16, 23, 32, 45, 65, 90, 128, 181, 256, 362, 512, 724, 1024)
PLot file version 1 created 16-FEB-2018 07:41:59
GREY: NONE J1412+0043D.IMAP.1
CONT: J141220+ J1412+0043.HGEOM.1
Declination (J2000)
Right Ascension (J2000)
Grey scale flux range= 3.651 7.643 Kilo
Cont peak flux = 1.2314E-03 JY/BEAM
Levs = 2.500E-04 * (1, 1.400, 2, 2.800, 4, 5.600, 8, 11, 16, 23, 32, 45, 65, 90, 128, 181, 256, 362, 512, 724, 1024)
PLot file version 1 created 16-FEB-2018 07:42:54
GREY: NONE J1412+0153D.IMAP.1
CONT: J141251+ J1412+0153.HGEOM.1
Declination (J2000)
Right Ascension (J2000)
Grey scale flux range= 2.486 4.286 Kilo
Cont peak flux = 1.1794E-02 JY/BEAM
Levs = 2.500E-04 * (1, 1.400, 2, 2.800, 4, 5.600, 8, 11, 16, 23, 32, 45, 65, 90, 128, 181, 256, 362, 512, 724, 1024)
PLot file version 1 created 16-FEB-2018 07:41:06
GREY: NONE J1412+0257D.IMAP.1
CONT: J141209+ J1412+0257.HGEOM.1
Declination (J2000)
Right Ascension (J2000)
Grey scale flux range= 3.693 5.949 Kilo
Cont peak flux = 3.0196E-03 JY/BEAM
Levs = 2.500E-04 * (1, 1.400, 2, 2.800, 4, 5.600, 8, 11, 16, 23, 32, 45, 65, 90, 128, 181, 256, 362, 512, 724, 1024)
PLot file version 1 created 16-FEB-2018 07:43:47
GREY: NONE J1412+2157D.IMAP.1
CONT: J141253+ J1412+2157.HGEOM.1
Declination (J2000)
Right Ascension (J2000)
Grey scale flux range= 2.22 21.02 Kilo
Cont peak flux = 9.0871E-03 JY/BEAM
Levs = 2.500E-04 * (1, 1.400, 2, 2.800, 4, 5.600, 8, 11, 16, 23, 32, 45, 65, 90, 128, 181, 256, 362, 512, 724, 1024)
PLot file version 1 created 16-FEB-2018 08:01:27
GREY: NONE J1415+2326D.IMAP.1
CONT: J141539+ J1415+2326.HGEOM.1
Declination (J2000)
Right Ascension (J2000)
Grey scale flux range= 3.916 7.059 Kilo
Cont peak flux = 1.2397E-02 JY/BEAM
Levs = 2.500E-04 * (1, 1.400, 2, 2.800, 4, 5.600, 8, 11, 16, 23, 32, 45, 65, 90, 128, 181, 256, 362, 512, 724, 1024)
PLot file version 1 created 16-FEB-2018 08:02:28
GREY: NONE J1416+2147D.IMAP.1
CONT: J141613+ J1416+2147.HGEOM.1
Declination (J2000)
Right Ascension (J2000)
Grey scale flux range= 2.93 12.10 Kilo
Cont peak flux = 1.9618E-03 JY/BEAM
Levs = 2.500E-04 * (1, 1.400, 2, 2.800, 4, 5.600, 8, 11, 16, 23, 32, 45, 65, 90, 128, 181, 256, 362, 512, 724, 1024)
PLot file version 1 created 16-FEB-2018 08:03:41
GREY: NONE J1417+0114D.IMAP.1
CONT: J141753+ J1417+0114.HGEOM.1
Declination (J2000)
Right Ascension (J2000)
Grey scale flux range= 3.026 6.907 Kilo
Cont peak flux = 2.0137E-03 JY/BEAM
Levs = 2.500E-04 * (1, 1.400, 2, 2.800, 4, 5.600, 8, 11, 16, 23, 32, 45, 65, 90, 128, 181, 256, 362, 512, 724, 1024)
PLot file version 1 created 16-FEB-2018 08:07:50
GREY: NONE J1419+4657D.IMAP.1
CONT: J141939+ J1419+4657.HGEOM.1
Declination (J2000)
Right Ascension (J2000)
Grey scale flux range= 3.090 6.787 Kilo
Cont peak flux = 1.2196E-02 JY/BEAM
Levs = 2.500E-04 * (1, 1.400, 2, 2.800, 4, 5.600, 8, 11, 16, 23, 32, 45, 65, 90, 128, 181, 256, 362, 512, 724, 1024)

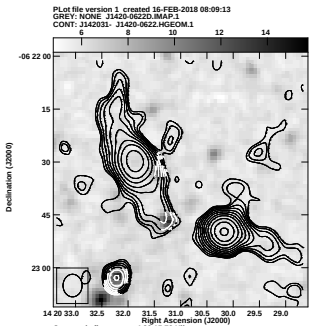
PLot file version 1 created 16-FEB-2018 08:09:13
GREY: NONE J1420-0622D.IMAP.1
CONT: J142031- J1420-0622.HGEOM.1
Declination (J2000)
Right Ascension (J2000)
Grey scale flux range= 4.82 15.72 Kilo
Cont peak flux = 8.5338E-03 JY/BEAM
Levs = 2.500E-04 * (1, 1.400, 2, 2.800, 4, 5.600, 8, 11, 16, 23, 32, 45, 65, 90, 128, 181, 256, 362, 512, 724, 1024)

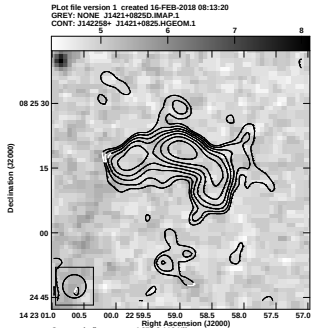
PLot file version 1 created 16-FEB-2018 08:13:20
GREY: NONE J1421+0825D.IMAP.1
CONT: J14259+ J1421+0825.HGEOM.1
Declination (J2000)
Right Ascension (J2000)
Grey scale flux range= 4.27 8.113 Kilo
Cont peak flux = 2.7246E-03 JY/BEAM
Levs = 2.500E-04 * (1, 1.400, 2, 2.800, 4, 5.600, 8, 11, 16, 23, 32, 45, 65, 90, 128, 181, 256, 362, 512, 724, 1024)

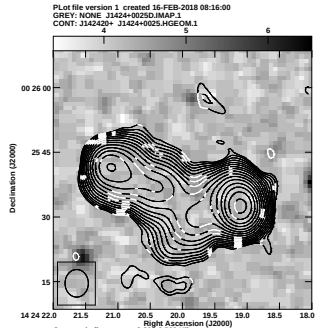
PLot file version 1 created 16-FEB-2018 08:16:00
GREY: NONE J1424+0025D.IMAP.1
CONT: J1424209+ J1424+0025.HGEOM.1
Declination (J2000)
Right Ascension (J2000)
Grey scale flux range= 3.392 6.523 Kilo
Cont peak flux = 5.1294E-02 JY/BEAM
Levs = 2.500E-04 * (1, 1.400, 2, 2.800, 4, 5.600, 8, 11, 16, 23, 32, 45, 65, 90, 128, 181, 256, 362, 512, 724, 1024)

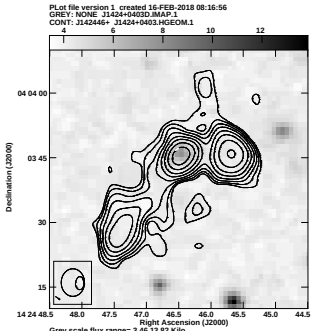
PLot file version 1 created 16-FEB-2018 08:16:56
GREY: NONE J1424+0403D.IMAP.1
CONT: J142446+ J1424+0403.HGEOM.1
Declination (J2000)
Right Ascension (J2000)
Grey scale flux range= 3.46 13.82 Kilo
Cont peak flux = 3.5801E-03 JY/BEAM
Levs = 2.500E-04 * (1, 1.400, 2, 2.800, 4, 5.600, 8, 11, 16, 23, 32, 45, 65, 90, 128, 181, 256, 362, 512, 724, 1024)

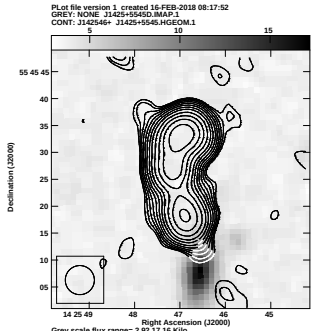
PLot file version 1 created 16-FEB-2018 08:17:52
GREY: NONE J1425+5545D.IMAP.1
CONT: J142546+ J1425+5545.HGEOM.1
Declination (J2000)
Right Ascension (J2000)
Grey scale flux range= 2.92 17.16 Kilo
Cont peak flux = 1.5176E-02 JY/BEAM
Levs = 2.500E-04 * (1, 1.400, 2, 2.800, 4, 5.600, 8, 11, 16, 23, 32, 45, 65, 90, 128, 181, 256, 362, 512, 724, 1024)

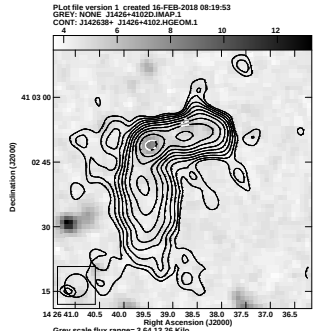
PLot file version 1 created 16-FEB-2018 08:19:53
GREY: NONE J1426+4102D.IMAP.1
CONT: J142638+ J1426+4102.HGEOM.1
Declination (J2000)
Right Ascension (J2000)
Grey scale flux range= 3.64 13.26 Kilo
Cont peak flux = 5.3028E-02 JY/BEAM
Levs = 2.500E-04 * (1, 1.400, 2, 2.800, 4, 5.600, 8, 11, 16, 23, 32, 45, 65, 90, 128, 181, 256, 362, 512, 724, 1024)

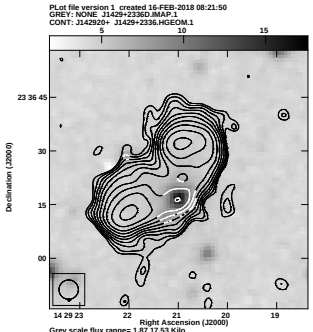
PLot file version 1 created 16-FEB-2018 08:21:50
GREY: NONE J1429+2336D.IMAP.1
CONT: J142920+ J1429+2336.HGEOM.1
Declination (J2000)
Right Ascension (J2000)
Grey scale flux range= 1.87 17.53 Kilo
Cont peak flux = 6.3622E-03 JY/BEAM
Levs = 2.500E-04 * (1, 1.400, 2, 2.800, 4, 5.600, 8, 11, 16, 23, 32, 45, 65, 90, 128, 181, 256, 362, 512, 724, 1024)

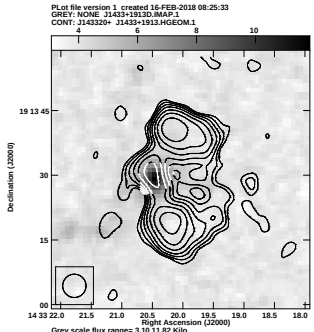
PLot file version 1 created 16-FEB-2018 08:25:33
GREY: NONE J1433+1913D.IMAP.1
CONT: J143320+ J1433+1913.HGEOM.1
Declination (J2000)
Right Ascension (J2000)
Grey scale flux range= 3.10 11.82 Kilo
Cont peak flux = 2.7449E-03 JY/BEAM
Levs = 2.500E-04 * (1, 1.400, 2, 2.800, 4, 5.600, 8, 11, 16, 23, 32, 45, 65, 90, 128, 181, 256, 362, 512, 724, 1024)

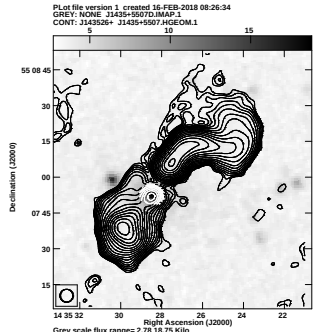
PLot file version 1 created 16-FEB-2018 08:26:34
GREY: NONE J1435+5507D.IMAP.1
CONT: J143526+ J1435+5507.HGEOM.1
Declination (J2000)
Right Ascension (J2000)
Grey scale flux range= 2.78 18.75 Kilo
Cont peak flux = 5.8440E-02 JY/BEAM
Levs = 2.500E-04 * (1, 1.400, 2, 2.800, 4, 5.600, 8, 11, 16, 23, 32, 45, 65, 90, 128, 181, 256, 362, 512, 724, 1024)

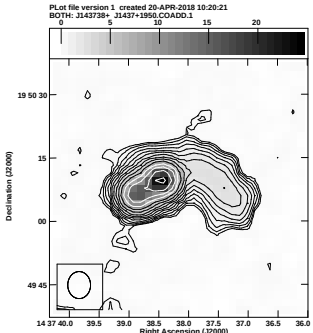
PLot file version 1 created 20-APR-2018 10:20:21
BOTH: J143738+ J1437+1950.COADD.1
Declination (J2000)
Right Ascension (J2000)
Grey scale flux range= -0.41 24.32 MilliJY/BEAM
Cont peak flux = 2.4321E-02 JY/BEAM
Levs = 2.500E-04 * (1, 1.400, 2, 2.800, 4, 5.600, 8, 11, 16, 23, 32, 45, 64, 90, 128, 181, 256, 362, 512, 724, 1024)

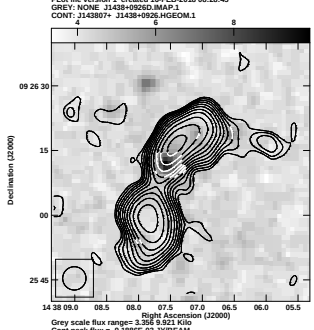
PLot file version 1 created 16-FEB-2018 08:28:45
GREY: NONE J1438+0926D.IMAP.1
CONT: J143807+ J1438+0926.HGEOM.1
Declination (J2000)
Right Ascension (J2000)
Grey scale flux range= 3.356 9.921 Kilo
Cont peak flux = 9.1886E-03 JY/BEAM
Levs = 2.500E-04 * (1, 1.400, 2, 2.800, 4, 5.600, 8, 11, 16, 23, 32, 45, 65, 90, 128, 181, 256, 362, 512, 724, 1024)

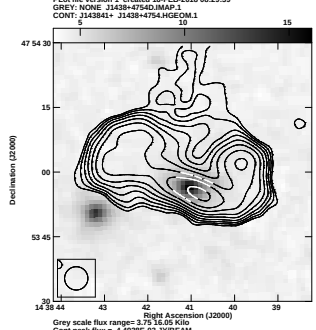
PLot file version 1 created 16-FEB-2018 08:29:39
GREY: NONE J1438+4754D.IMAP.1
CONT: J143841+ J1438+4754.HGEOM.1
Declination (J2000)
Right Ascension (J2000)
Grey scale flux range= 3.75 16.05 Kilo
Cont peak flux = 4.4838E-03 JY/BEAM
Levs = 2.500E-04 * (1, 1.400, 2, 2.800, 4, 5.600, 8, 11, 16, 23, 32, 45, 65, 90, 128, 181, 256, 362, 512, 724, 1024)

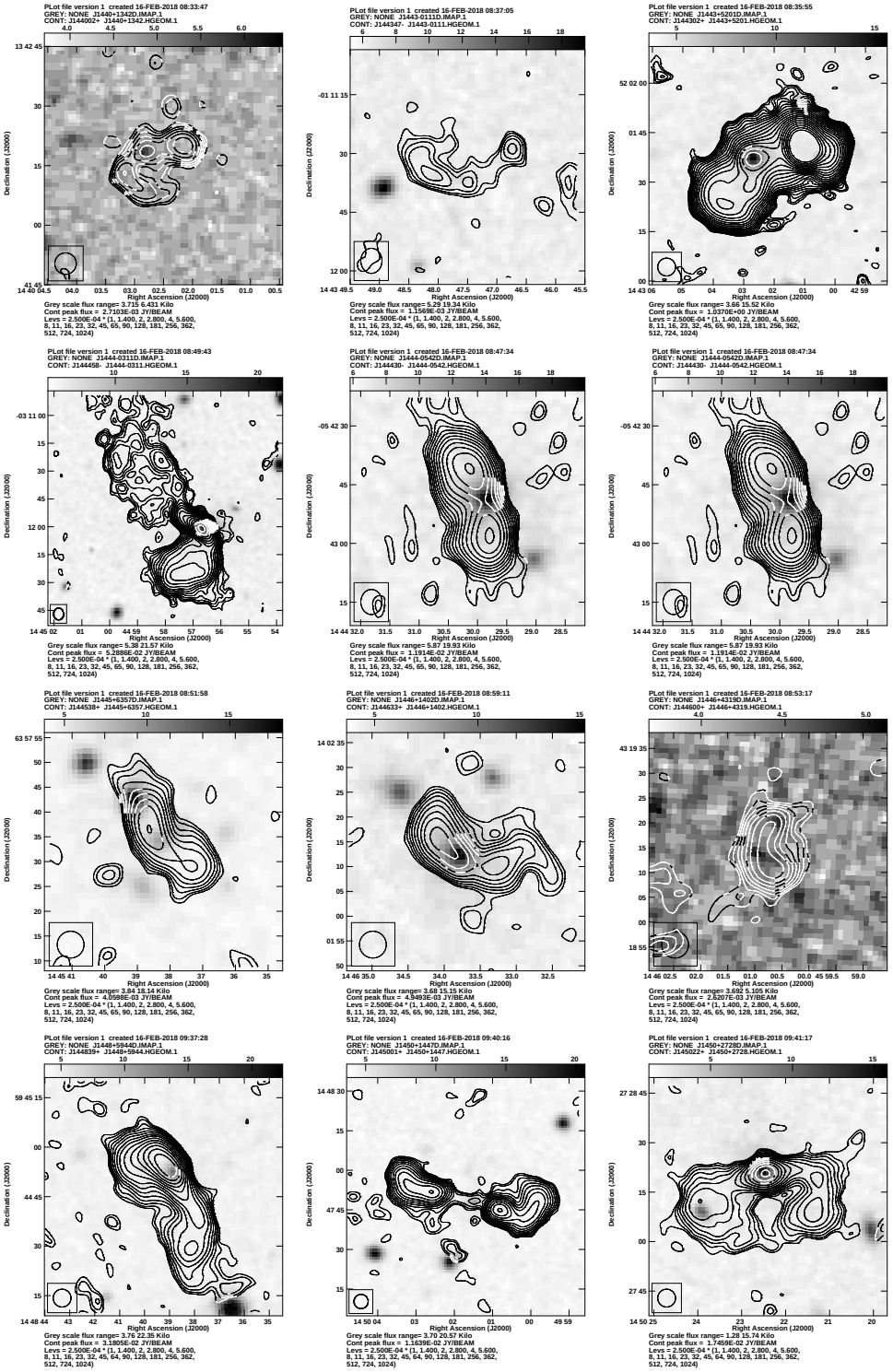
PLot file version 1 created 16-FEB-2018 08:33:47
GREY: NONE J1440+1342D.IMAP.1
CONT: J144002+ J1440+1342.HGEOM.1
Declination (J2000)
Right Ascension (J2000)
Grey scale flux range= 3.715 6.431 Kilo
Cont peak flux = 2.7103E-03 JY/BEAM
Levs = 2.500E-04 * (1, 1.400, 2, 2.800, 4, 5.600, 8, 11, 16, 23, 32, 45, 65, 90, 128, 181, 256, 362, 512, 724, 1024)
PLot file version 1 created 16-FEB-2018 08:37:05
GREY: NONE J1443-0111D.IMAP.1
CONT: J144347- J1443-0111.HGEOM.1
Declination (J2000)
Right Ascension (J2000)
Grey scale flux range= 5.29 19.34 Kilo
Cont peak flux = 1.1569E-03 JY/BEAM
Levs = 2.500E-04 * (1, 1.400, 2, 2.800, 4, 5.600, 8, 11, 16, 23, 32, 45, 65, 90, 128, 181, 256, 362, 512, 724, 1024)
PLot file version 1 created 16-FEB-2018 08:35:55
GREY: NONE J1443+5201D.IMAP.1
CONT: J144302+ J1443+5201.HGEOM.1
Declination (J2000)
Right Ascension (J2000)
Grey scale flux range= 3.66 15.52 Kilo
Cont peak flux = 1.0370E+00 JY/BEAM
Levs = 2.500E-04 * (1, 1.400, 2, 2.800, 4, 5.600, 8, 11, 16, 23, 32, 45, 65, 90, 128, 181, 256, 362, 512, 724, 1024)
PLot file version 1 created 16-FEB-2018 08:49:43
GREY: NONE J1444-0311D.IMAP.1
CONT: J144458- J1444-0311.HGEOM.1
Declination (J2000)
Right Ascension (J2000)
Grey scale flux range= 5.38 21.57 Kilo
Cont peak flux = 5.2898E-02 JY/BEAM
Levs = 2.500E-04 * (1, 1.400, 2, 2.800, 4, 5.600, 8, 11, 16, 23, 32, 45, 65, 90, 128, 181, 256, 362, 512, 724, 1024)
PLot file version 1 created 16-FEB-2018 08:47:34
GREY: NONE J1444-0542D.IMAP.1
CONT: J144430- J1444-0542.HGEOM.1
Declination (J2000)
Right Ascension (J2000)
Grey scale flux range= 5.87 19.93 Kilo
Cont peak flux = 1.1914E-02 JY/BEAM
Levs = 2.500E-04 * (1, 1.400, 2, 2.800, 4, 5.600, 8, 11, 16, 23, 32, 45, 65, 90, 128, 181, 256, 362, 512, 724, 1024)
PLot file version 1 created 16-FEB-2018 08:47:34
GREY: NONE J1444-0542D.IMAP.1
CONT: J144430- J1444-0542.HGEOM.1
Declination (J2000)
Right Ascension (J2000)
Grey scale flux range= 5.87 19.93 Kilo
Cont peak flux = 1.1914E-02 JY/BEAM
Levs = 2.500E-04 * (1, 1.400, 2, 2.800, 4, 5.600, 8, 11, 16, 23, 32, 45, 65, 90, 128, 181, 256, 362, 512, 724, 1024)
PLot file version 1 created 16-FEB-2018 08:51:58
GREY: NONE J1445+6357D.IMAP.1
CONT: J144538+ J1445+6357.HGEOM.1
Declination (J2000)
Right Ascension (J2000)
Grey scale flux range= 3.84 18.14 Kilo
Cont peak flux = 4.0598E-03 JY/BEAM
Levs = 2.500E-04 * (1, 1.400, 2, 2.800, 4, 5.600, 8, 11, 16, 23, 32, 45, 65, 90, 128, 181, 256, 362, 512, 724, 1024)
PLot file version 1 created 16-FEB-2018 08:59:11
GREY: NONE J1446+1402D.IMAP.1
CONT: J144633+ J1446+1402.HGEOM.1
Declination (J2000)
Right Ascension (J2000)
Grey scale flux range= 3.68 15.15 Kilo
Cont peak flux = 4.9483E-03 JY/BEAM
Levs = 2.500E-04 * (1, 1.400, 2, 2.800, 4, 5.600, 8, 11, 16, 23, 32, 45, 65, 90, 128, 181, 256, 362, 512, 724, 1024)
PLot file version 1 created 16-FEB-2018 08:53:17
GREY: NONE J1446+4319D.IMAP.1
CONT: J144600+ J1446+4319.HGEOM.1
Declination (J2000)
Right Ascension (J2000)
Grey scale flux range= 3.692 5.105 Kilo
Cont peak flux = 2.6207E-03 JY/BEAM
Levs = 2.500E-04 * (1, 1.400, 2, 2.800, 4, 5.600, 8, 11, 16, 23, 32, 45, 65, 90, 128, 181, 256, 362, 512, 724, 1024)
PLot file version 1 created 16-FEB-2018 09:37:28
GREY: NONE J1448+5944D.IMAP.1
CONT: J144839+ J1448+5944.HGEOM.1
Declination (J2000)
Right Ascension (J2000)
Grey scale flux range= 3.76 22.35 Kilo
Cont peak flux = 3.1805E-02 JY/BEAM
Levs = 2.500E-04 * (1, 1.400, 2, 2.800, 4, 5.600, 8, 11, 16, 23, 32, 45, 64, 90, 128, 181, 256, 362, 512, 724, 1024)
PLot file version 1 created 16-FEB-2018 09:40:16
GREY: NONE J1450+1447D.IMAP.1
CONT: J145001+ J1450+1447.HGEOM.1
Declination (J2000)
Right Ascension (J2000)
Grey scale flux range= 3.70 20.57 Kilo
Cont peak flux = 1.1639E-02 JY/BEAM
Levs = 2.500E-04 * (1, 1.400, 2, 2.800, 4, 5.600, 8, 11, 16, 23, 32, 45, 64, 90, 128, 181, 256, 362, 512, 724, 1024)
PLot file version 1 created 16-FEB-2018 09:41:17
GREY: NONE J1450+2728D.IMAP.1
CONT: J145022+ J1450+2728.HGEOM.1
Declination (J2000)
Right Ascension (J2000)
Grey scale flux range= 1.28 15.74 Kilo
Cont peak flux = 1.7459E-02 JY/BEAM
Levs = 2.500E-04 * (1, 1.400, 2, 2.800, 4, 5.600, 8, 11, 16, 23, 32, 45, 64, 90, 128, 181, 256, 362, 512, 724, 1024)

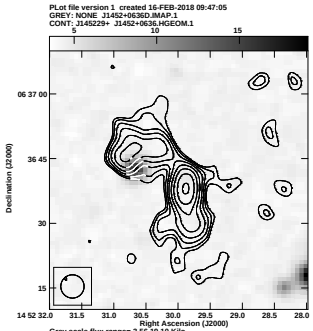
PLot file version 1 created 16-FEB-2018 09:47:05
GREY: NONE J1452+0636D.IMAP.1
CONT: J145229+ J1452+0636.HGEOM.1
Declination (J2000)
Right Ascension (J2000)
Grey scale flux range= 3.56 19.10 Kilo
Cont peak flux = 2.8637E-03 JY/BEAM
Levs = 2.500E-04 * (1, 1.400, 2, 2.800, 4, 5.600, 8, 11, 16, 23, 32, 45, 64, 90, 128, 181, 256, 362, 512, 724, 1024)

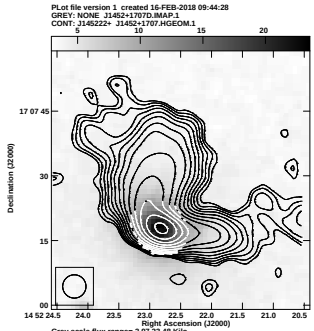
PLot file version 1 created 16-FEB-2018 09:44:28
GREY: NONE J1452+1707D.IMAP.1
CONT: J145222+ J1452+1707.HGEOM.1
Declination (J2000)
Right Ascension (J2000)
Grey scale flux range= 2.97 23.48 Kilo
Cont peak flux = 1.7495E-02 JY/BEAM
Levs = 2.500E-04 * (1, 1.400, 2, 2.800, 4, 5.600, 8, 11, 16, 23, 32, 45, 64, 90, 128, 181, 256, 362, 512, 724, 1024)

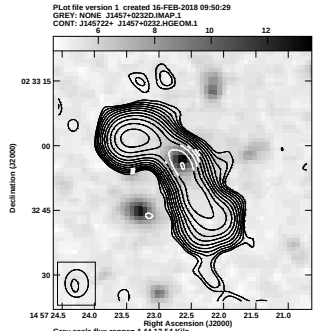
PLot file version 1 created 16-FEB-2018 09:50:29
GREY: NONE J1457+0232D.IMAP.1
CONT: J145722+ J1457+0232.HGEOM.1
Declination (J2000)
Right Ascension (J2000)
Grey scale flux range= 4.44 13.54 Kilo
Cont peak flux = 9.8648E-03 JY/BEAM
Levs = 2.500E-04 * (1, 1.400, 2, 2.800, 4, 5.600, 8, 11, 16, 23, 32, 45, 64, 90, 128, 181, 256, 362, 512, 724, 1024)

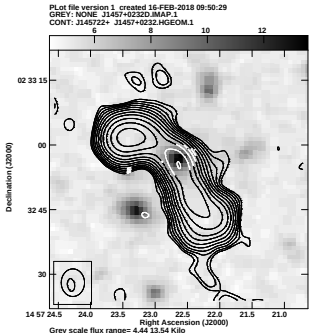
PLot file version 1 created 16-FEB-2018 09:50:29
GREY: NONE J1457+0232D.IMAP.1
CONT: J145722+ J1457+0232.HGEOM.1
Declination (J2000)
Right Ascension (J2000)
Grey scale flux range= 4.44 13.54 Kilo
Cont peak flux = 9.8648E-03 JY/BEAM
Levs = 2.500E-04 * (1, 1.400, 2, 2.800, 4, 5.600, 8, 11, 16, 23, 32, 45, 64, 90, 128, 181, 256, 362, 512, 724, 1024)

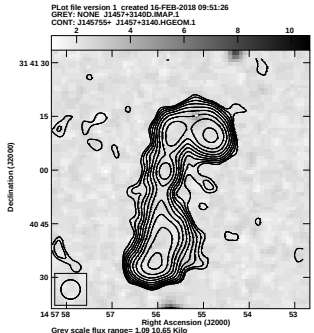
PLot file version 1 created 16-FEB-2018 09:51:26
GREY: NONE J1457+3140D.IMAP.1
CONT: J145755+ J1457+3140.HGEOM.1
Declination (J2000)
Right Ascension (J2000)
Grey scale flux range= 1.09 10.65 Kilo
Cont peak flux = 6.6517E-03 JY/BEAM
Levs = 2.500E-04 * (1, 1.400, 2, 2.800, 4, 5.600, 8, 11, 16, 23, 32, 45, 64, 90, 128, 181, 256, 362, 512, 724, 1024)

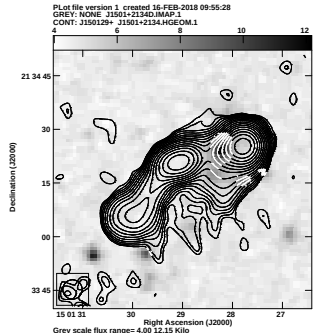
PLot file version 1 created 16-FEB-2018 09:55:28
GREY: NONE J1501+2134D.IMAP.1
CONT: J150129+ J1501+2134.HGEOM.1
Declination (J2000)
Right Ascension (J2000)
Grey scale flux range= 4.00 12.15 Kilo
Cont peak flux = 6.0307E-02 JY/BEAM
Levs = 2.500E-04 * (1, 1.400, 2, 2.800, 4, 5.600, 8, 11, 16, 23, 32, 45, 64, 90, 128, 181, 256, 362, 512, 724, 1024)

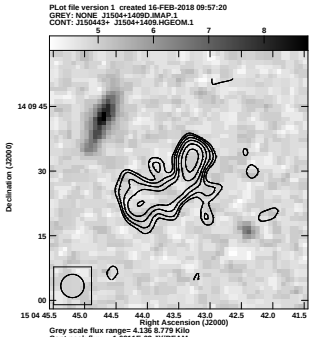
PLot file version 1 created 16-FEB-2018 09:57:20
GREY: NONE J1504+1409D.IMAP.1
CONT: J150443+ J1504+1409.HGEOM.1
Declination (J2000)
Right Ascension (J2000)
Grey scale flux range= 4.136 8.779 Kilo
Cont peak flux = 1.6911E-03 JY/BEAM
Levs = 2.500E-04 * (1, 1.400, 2, 2.800, 4, 5.600, 8, 11, 16, 23, 32, 45, 64, 90, 128, 181, 256, 362, 512, 724, 1024)

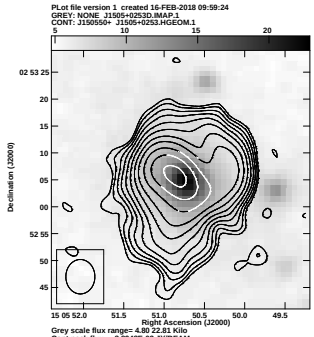
PLot file version 1 created 16-FEB-2018 09:59:24
GREY: NONE J1505+0253D.IMAP.1
CONT: J150550+ J1505+0253.HGEOM.1
Declination (J2000)
Right Ascension (J2000)
Grey scale flux range= 4.80 22.81 Kilo
Cont peak flux = 8.8948E-03 JY/BEAM
Levs = 2.500E-04 * (1, 1.400, 2, 2.800, 4, 5.600, 8, 11, 16, 23, 32, 45, 64, 90, 128, 181, 256, 362, 512, 724, 1024)

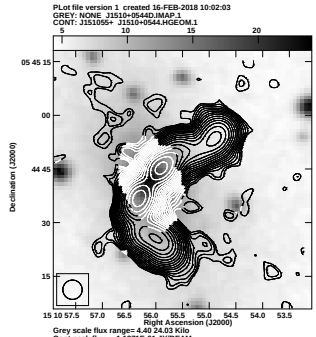
PLot file version 1 created 16-FEB-2018 10:02:03
GREY: NONE J1510+0544D.IMAP.1
CONT: J151055+ J1510+0544.HGEOM.1
Declination (J2000)
Right Ascension (J2000)
Grey scale flux range= 4.40 24.03 Kilo
Cont peak flux = 1.1371E-01 JY/BEAM
Levs = 2.500E-04 * (1, 1.400, 2, 2.800, 4, 5.600, 8, 11, 16, 23, 32, 45, 64, 90, 128, 181, 256, 362, 512, 724, 1024)

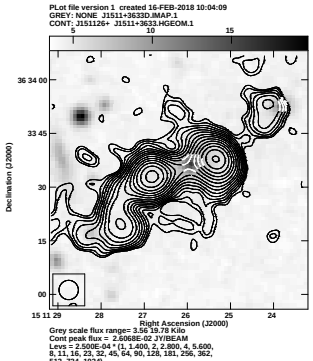
PLot file version 1 created 16-FEB-2018 10:04:09
GREY: NONE J1511+3633D.IMAP.1
CONT: J151126+ J1511+3633.HGEOM.1
Declination (J2000)
Right Ascension (J2000)
Grey scale flux range= 3.56 19.78 Kilo
Cont peak flux = 2.6068E-02 JY/BEAM
Levs = 2.500E-04 * (1, 1.400, 2, 2.800, 4, 5.600, 8, 11, 16, 23, 32, 45, 64, 90, 128, 181, 256, 362, 512, 724, 1024)

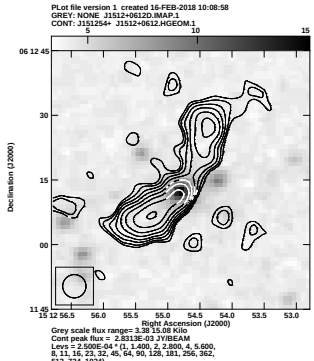
PLot file version 1 created 16-FEB-2018 10:08:58
GREY: NONE J1512+0612D.IMAP.1
CONT: J151254+ J1512+0612.HGEOM.1
Declination (J2000)
Right Ascension (J2000)
Grey scale flux range= 3.38 15.08 Kilo
Cont peak flux = 2.8313E-03 JY/BEAM
Levs = 2.500E-04 * (1, 1.400, 2, 2.800, 4, 5.600, 8, 11, 16, 23, 32, 45, 64, 90, 128, 181, 256, 362, 512, 724, 1024)

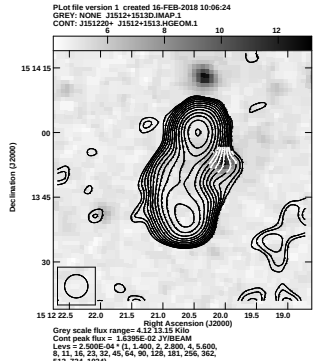
PLot file version 1 created 16-FEB-2018 10:06:24
GREY: NONE J1512+1513D.IMAP.1
CONT: J151220+ J1512+1513.HGEOM.1
Declination (J2000)
Right Ascension (J2000)
Grey scale flux range= 4.12 13.15 Kilo
Cont peak flux = 1.6395E-02 JY/BEAM
Levs = 2.500E-04 * (1, 1.400, 2, 2.800, 4, 5.600, 8, 11, 16, 23, 32, 45, 64, 90, 128, 181, 256, 362, 512, 724, 1024)

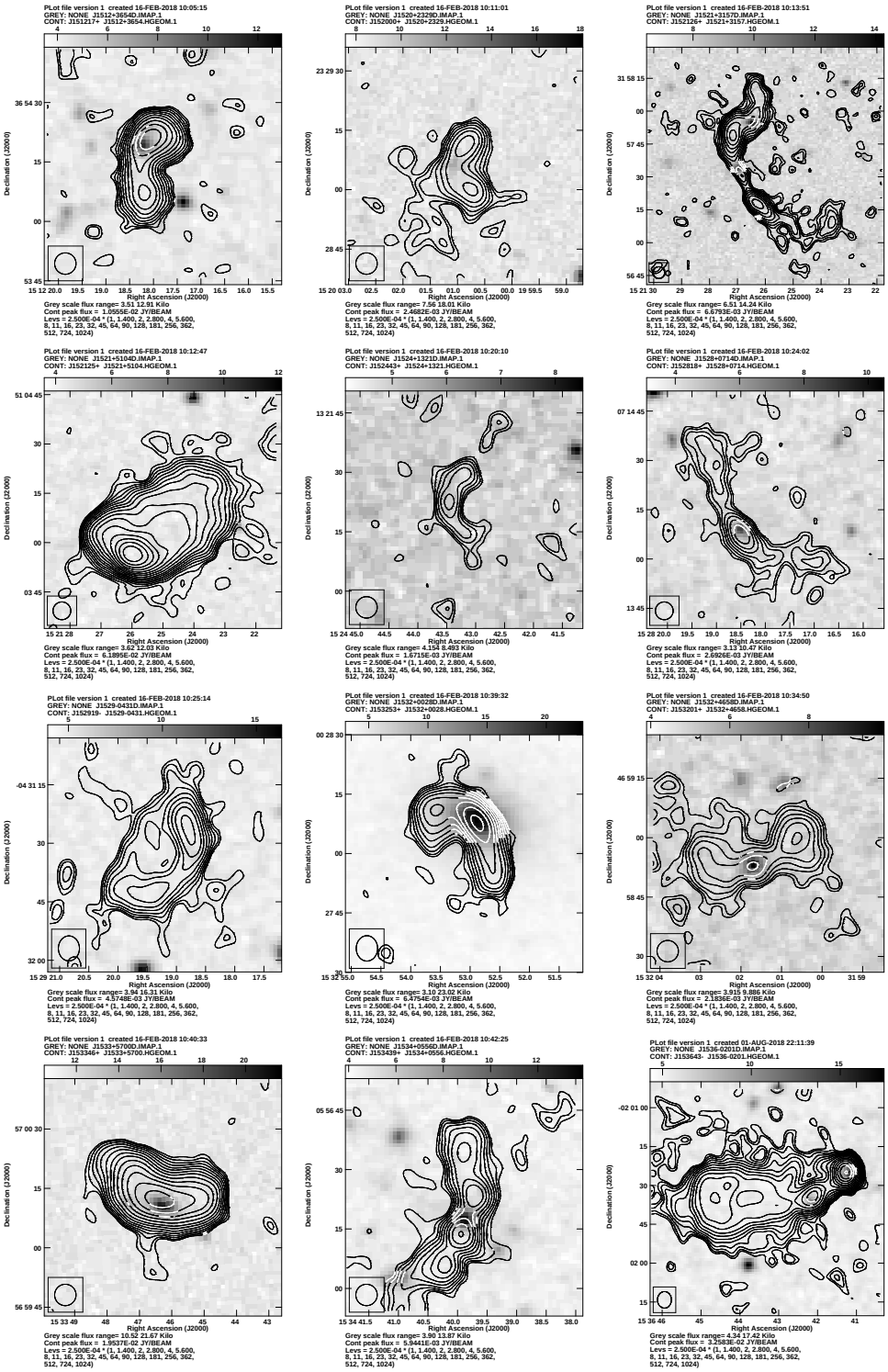
PLot file version 1 created 16-FEB-2018 10:05:15
GREY: NONE J1512+3654D.IMAP.1
CONT: J151217+ J1512+3654.HGEOM.1
Declination (J2000)
Right Ascension (J2000)
Grey scale flux range= 3.51 12.91 Kilo
Cont peak flux = 1.0555E-02 JY/BEAM
Levs = 2.500E-04 * (1, 1.400, 2, 2.800, 4, 5.600, 8, 11, 16, 23, 32, 45, 64, 90, 128, 181, 256, 362, 512, 724, 1024)
PLot file version 1 created 16-FEB-2018 10:11:01
GREY: NONE J1520+2329D.IMAP.1
CONT: J152000+ J1520+2329.HGEOM.1
Declination (J2000)
Right Ascension (J2000)
Grey scale flux range= 7.56 18.01 Kilo
Cont peak flux = 2.4682E-03 JY/BEAM
Levs = 2.500E-04 * (1, 1.400, 2, 2.800, 4, 5.600, 8, 11, 16, 23, 32, 45, 64, 90, 128, 181, 256, 362, 512, 724, 1024)
PLot file version 1 created 16-FEB-2018 10:13:51
GREY: NONE J1521+3157D.IMAP.1
CONT: J152126+ J1521+3157.HGEOM.1
Declination (J2000)
Right Ascension (J2000)
Grey scale flux range= 6.51 14.24 Kilo
Cont peak flux = 6.6793E-03 JY/BEAM
Levs = 2.500E-04 * (1, 1.400, 2, 2.800, 4, 5.600, 8, 11, 16, 23, 32, 45, 64, 90, 128, 181, 256, 362, 512, 724, 1024)
PLot file version 1 created 16-FEB-2018 10:12:47
GREY: NONE J1521+5104D.IMAP.1
CONT: J152125+ J1521+5104.HGEOM.1
Declination (J2000)
Right Ascension (J2000)
Grey scale flux range= 3.62 12.03 Kilo
Cont peak flux = 6.1895E-02 JY/BEAM
Levs = 2.500E-04 * (1, 1.400, 2, 2.800, 4, 5.600, 8, 11, 16, 23, 32, 45, 64, 90, 128, 181, 256, 362, 512, 724, 1024)
PLot file version 1 created 16-FEB-2018 10:20:10
GREY: NONE J1524+1321D.IMAP.1
CONT: J152443+ J1524+1321.HGEOM.1
Declination (J2000)
Right Ascension (J2000)
Grey scale flux range= 4.154 8.493 Kilo
Cont peak flux = 1.6713E-03 JY/BEAM
Levs = 2.500E-04 * (1, 1.400, 2, 2.800, 4, 5.600, 8, 11, 16, 23, 32, 45, 64, 90, 128, 181, 256, 362, 512, 724, 1024)
PLot file version 1 created 16-FEB-2018 10:24:02
GREY: NONE J1528+0714D.IMAP.1
CONT: J152818+ J1528+0714.HGEOM.1
Declination (J2000)
Right Ascension (J2000)
Grey scale flux range= 3.13 10.47 Kilo
Cont peak flux = 2.6926E-03 JY/BEAM
Levs = 2.500E-04 * (1, 1.400, 2, 2.800, 4, 5.600, 8, 11, 16, 23, 32, 45, 64, 90, 128, 181, 256, 362, 512, 724, 1024)
PLot file version 1 created 16-FEB-2018 10:25:14
GREY: NONE J1529-0431D.IMAP.1
CONT: J152919- J1529-0431.HGEOM.1
Declination (J2000)
Right Ascension (J2000)
Grey scale flux range= 3.94 16.31 Kilo
Cont peak flux = 4.5748E-03 JY/BEAM
Levs = 2.500E-04 * (1, 1.400, 2, 2.800, 4, 5.600, 8, 11, 16, 23, 32, 45, 64, 90, 128, 181, 256, 362, 512, 724, 1024)
PLot file version 1 created 16-FEB-2018 10:39:32
GREY: NONE J1532+0028D.IMAP.1
CONT: J153253+ J1532+0028.HGEOM.1
Declination (J2000)
Right Ascension (J2000)
Grey scale flux range= 3.10 23.02 Kilo
Cont peak flux = 6.4754E-03 JY/BEAM
Levs = 2.500E-04 * (1, 1.400, 2, 2.800, 4, 5.600, 8, 11, 16, 23, 32, 45, 64, 90, 128, 181, 256, 362, 512, 724, 1024)
PLot file version 1 created 16-FEB-2018 10:34:50
GREY: NONE J1532+4658D.IMAP.1
CONT: J153201+ J1532+4658.HGEOM.1
Declination (J2000)
Right Ascension (J2000)
Grey scale flux range= 3.915 9.886 Kilo
Cont peak flux = 2.1836E-03 JY/BEAM
Levs = 2.500E-04 * (1, 1.400, 2, 2.800, 4, 5.600, 8, 11, 16, 23, 32, 45, 64, 90, 128, 181, 256, 362, 512, 724, 1024)
PLot file version 1 created 16-FEB-2018 10:40:33
GREY: NONE J1533+5700D.IMAP.1
CONT: J153346+ J1533+5700.HGEOM.1
Declination (J2000)
Right Ascension (J2000)
Grey scale flux range= 10.52 21.67 Kilo
Cont peak flux = 1.9537E-02 JY/BEAM
Levs = 2.500E-04 * (1, 1.400, 2, 2.800, 4, 5.600, 8, 11, 16, 23, 32, 45, 64, 90, 128, 181, 256, 362, 512, 724, 1024)
PLot file version 1 created 16-FEB-2018 10:42:25
GREY: NONE J1534+0556D.IMAP.1
CONT: J153439+ J1534+0556.HGEOM.1
Declination (J2000)
Right Ascension (J2000)
Grey scale flux range= 3.90 13.87 Kilo
Cont peak flux = 5.9441E-03 JY/BEAM
Levs = 2.500E-04 * (1, 1.400, 2, 2.800, 4, 5.600, 8, 11, 16, 23, 32, 45, 64, 90, 128, 181, 256, 362, 512, 724, 1024)
PLot file version 1 created 01-AUG-2018 22:11:39
GREY: NONE J1536-0201D.IMAP.1
CONT: J153643- J1536-0201.HGEOM.1
Declination (J2000)
Right Ascension (J2000)
Grey scale flux range= 4.34 17.42 Kilo
Cont peak flux = 3.2583E-02 JY/BEAM
Levs = 2.500E-04 * (1, 1.400, 2, 2.800, 4, 5.600, 8, 11, 16, 23, 32, 45, 64, 90, 128, 181, 256, 362, 512, 724, 1024)

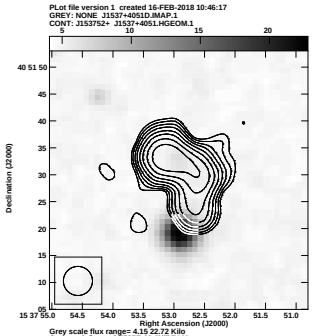
PLot file version 1 created 16-FEB-2018 10:46:17
GREY: NONE J1537+4051D.IMAP.1
CONT: J153752+ J1537+4051.HGEOM.1
Declination (J2000)
Right Ascension (J2000)
Grey scale flux range= 4.15 22.72 Kilo
Cont peak flux = 3.7727E-03 JY/BEAM
Levs = 2.500E-04 * (1, 1.400, 2, 2.800, 4, 5.600, 8, 11, 16, 23, 32, 45, 64, 90, 128, 181, 256, 362, 512, 724, 1024)

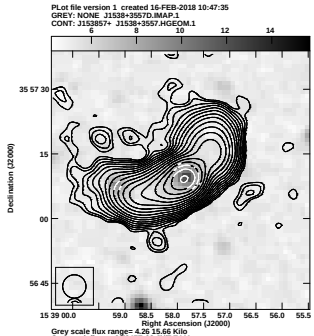
PLot file version 1 created 16-FEB-2018 10:47:35
GREY: NONE J1538+3557D.IMAP.1
CONT: J153857+ J1538+3557.HGEOM.1
Declination (J2000)
Right Ascension (J2000)
Grey scale flux range= 4.26 15.66 Kilo
Cont peak flux = 6.7647E-02 JY/BEAM
Levs = 2.500E-04 * (1, 1.400, 2, 2.800, 4, 5.600, 8, 11, 16, 23, 32, 45, 64, 90, 128, 181, 256, 362, 512, 724, 1024)

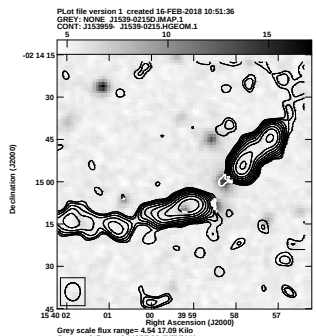
PLot file version 1 created 16-FEB-2018 10:51:36
GREY: NONE J1539-0215D.IMAP.1
CONT: J153959- J1539-0215.HGEOM.1
Declination (J2000)
Right Ascension (J2000)
Grey scale flux range= 4.54 17.09 Kilo
Cont peak flux = 6.1485E-03 JY/BEAM
Levs = 2.500E-04 * (1, 1.400, 2, 2.800, 4, 5.600, 8, 11, 16, 23, 32, 45, 64, 90, 128, 181, 256, 362, 512, 724, 1024)

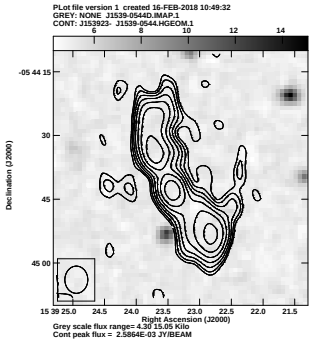
PLot file version 1 created 16-FEB-2018 10:49:32
GREY: NONE J1539-0544D.IMAP.1
CONT: J153923- J1539-0544.HGEOM.1
Declination (J2000)
Right Ascension (J2000)
Grey scale flux range= 4.30 15.05 Kilo
Cont peak flux = 2.5864E-03 JY/BEAM
Levs = 2.500E-04 * (1, 1.400, 2, 2.800, 4, 5.600, 8, 11, 16, 23, 32, 45, 64, 90, 128, 181, 256, 362, 512, 724, 1024)

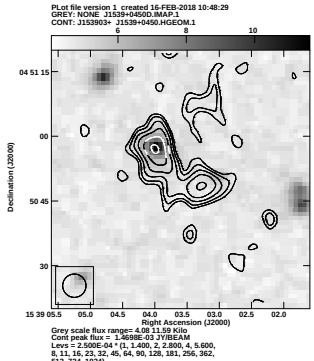
PLot file version 1 created 16-FEB-2018 10:48:29
GREY: NONE J1539+0450D.IMAP.1
CONT: J153903+ J1539+0450.HGEOM.1
Declination (J2000)
Right Ascension (J2000)
Grey scale flux range= 4.08 11.59 Kilo
Cont peak flux = 1.4698E-03 JY/BEAM
Levs = 2.500E-04 * (1, 1.400, 2, 2.800, 4, 5.600, 8, 11, 16, 23, 32, 45, 64, 90, 128, 181, 256, 362, 512, 724, 1024)

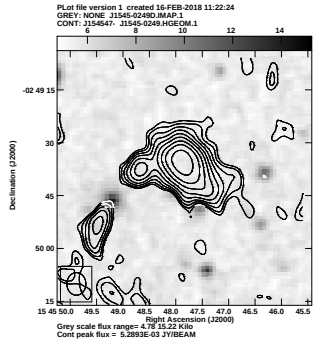
PLot file version 1 created 16-FEB-2018 11:22:24
GREY: NONE J1545-0249D.IMAP.1
CONT: J154547- J1545-0249.HGEOM.1
Declination (J2000)
Right Ascension (J2000)
Grey scale flux range= 4.78 15.22 Kilo
Cont peak flux = 5.2893E-03 JY/BEAM
Levs = 2.500E-04 * (1, 1.400, 2, 2.800, 4, 5.600, 8, 11, 16, 23, 32, 45, 64, 90, 128, 181, 256, 362, 512, 724, 1024)

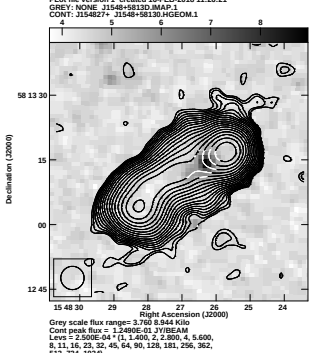
PLot file version 1 created 16-FEB-2018 11:26:21
GREY: NONE J1548+5813D.IMAP.1
CONT: J154827+ J1548+5813.HGEOM.1
Declination (J2000)
Right Ascension (J2000)
Grey scale flux range= 3.760 8.944 Kilo
Cont peak flux = 1.2490E-01 JY/BEAM
Levs = 2.500E-04 * (1, 1.400, 2, 2.800, 4, 5.600, 8, 11, 16, 23, 32, 45, 64, 90, 128, 181, 256, 362, 512, 724, 1024)

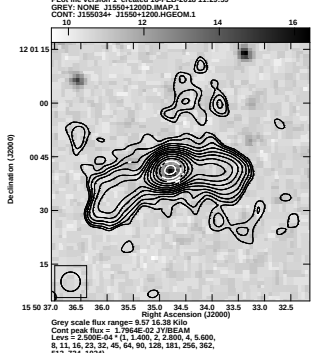
PLot file version 1 created 16-FEB-2018 11:29:59
GREY: NONE J1550+1200D.IMAP.1
CONT: J155034+ J1550+1200.HGEOM.1
Declination (J2000)
Right Ascension (J2000)
Grey scale flux range= 9.57 16.38 Kilo
Cont peak flux = 1.7954E-02 JY/BEAM
Levs = 2.500E-04 * (1, 1.400, 2, 2.800, 4, 5.600, 8, 11, 16, 23, 32, 45, 64, 90, 128, 181, 256, 362, 512, 724, 1024)

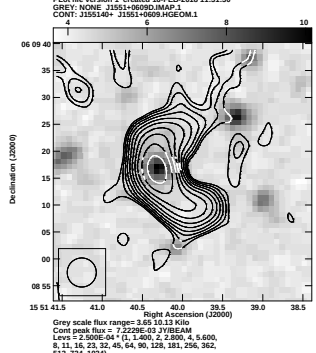
PLot file version 1 created 16-FEB-2018 11:31:30
GREY: NONE J1551+0609D.IMAP.1
CONT: J155140+ J1551+0609.HGEOM.1
Declination (J2000)
Right Ascension (J2000)
Grey scale flux range= 3.65 10.13 Kilo
Cont peak flux = 7.2229E-03 JY/BEAM
Levs = 2.500E-04 * (1, 1.400, 2, 2.800, 4, 5.600, 8, 11, 16, 23, 32, 45, 64, 90, 128, 181, 256, 362, 512, 724, 1024)

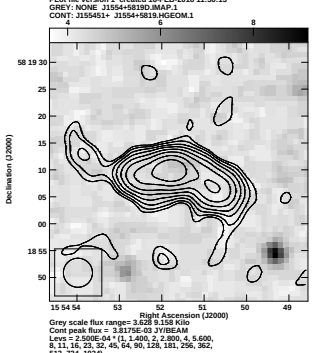
PLot file version 1 created 16-FEB-2018 11:36:13
GREY: NONE J1554+5819D.IMAP.1
CONT: J155451+ J1554+5819.HGEOM.1
Declination (J2000)
Right Ascension (J2000)
Grey scale flux range= 3.628 9.158 Kilo
Cont peak flux = 3.8175E-03 JY/BEAM
Levs = 2.500E-04 * (1, 1.400, 2, 2.800, 4, 5.600, 8, 11, 16, 23, 32, 45, 64, 90, 128, 181, 256, 362, 512, 724, 1024)

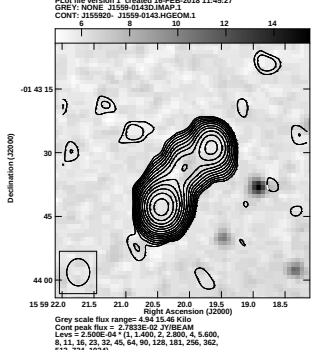
PLot file version 1 created 16-FEB-2018 11:45:27
GREY: NONE J1559-0143D.IMAP.1
CONT: J155920- J1559-0143.HGEOM.1
Declination (J2000)
Right Ascension (J2000)
Grey scale flux range= 4.94 15.46 Kilo
Cont peak flux = 2.7833E-02 JY/BEAM
Levs = 2.500E-04 * (1, 1.400, 2, 2.800, 4, 5.600, 8, 11, 16, 23, 32, 45, 64, 90, 128, 181, 256, 362, 512, 724, 1024)

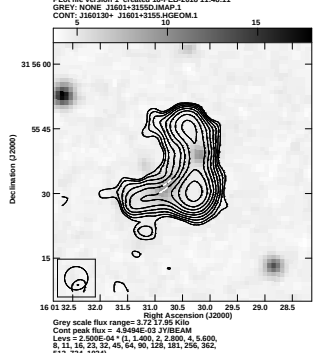
PLot file version 1 created 16-FEB-2018 11:48:11
GREY: NONE J1601+3155D.IMAP.1
CONT: J160130+ J1601+3155.HGEOM.1
Declination (J2000)
Right Ascension (J2000)
Grey scale flux range= 3.72 17.95 Kilo
Cont peak flux = 4.9494E-03 JY/BEAM
Levs = 2.500E-04 * (1, 1.400, 2, 2.800, 4, 5.600, 8, 11, 16, 23, 32, 45, 64, 90, 128, 181, 256, 362, 512, 724, 1024)

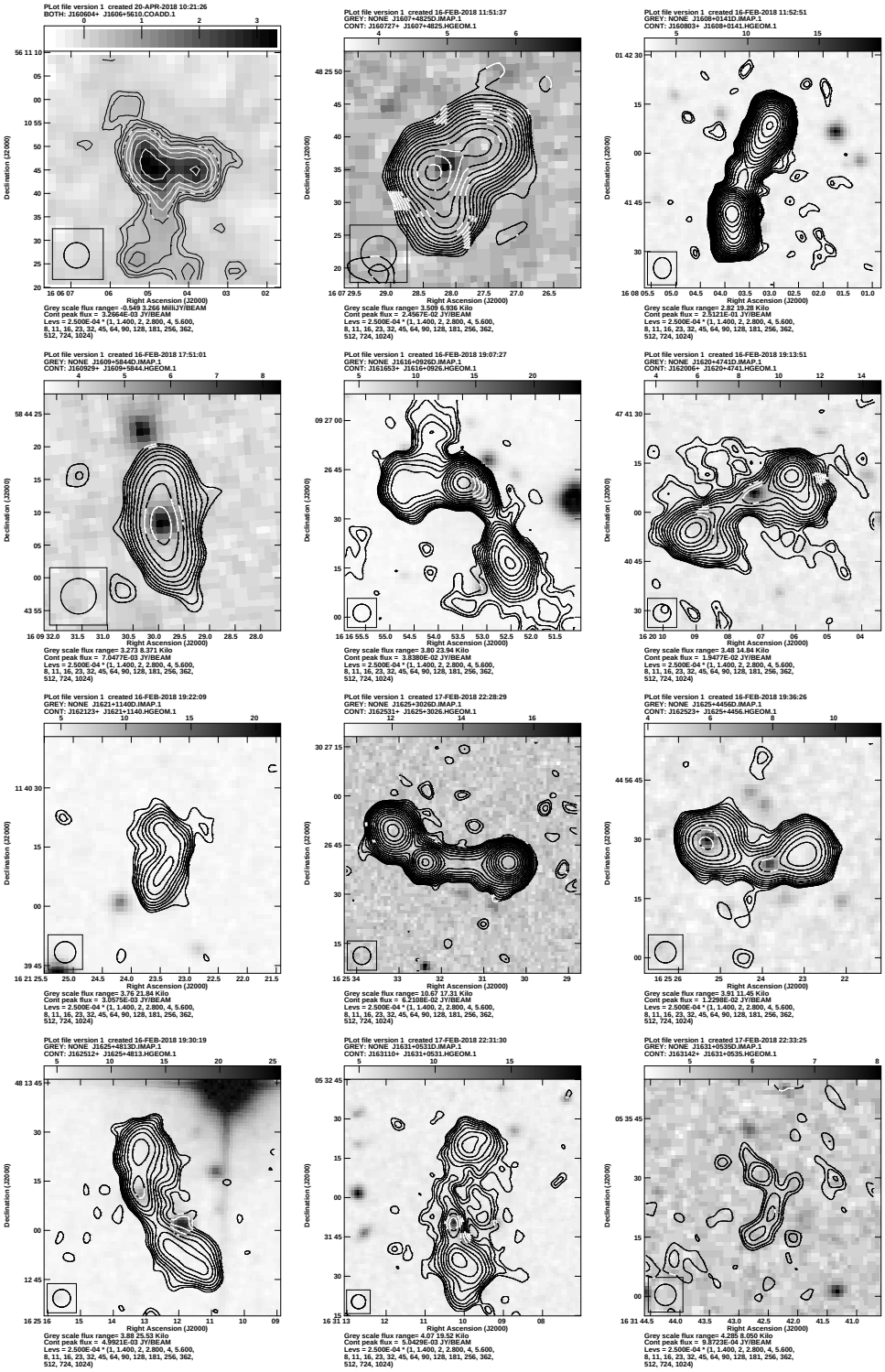
PLot file version 1 created 20-APR-2018 10:21:26
BOTH: J1606O4+ J1606+5610.COADD.1
Declination (J2000)
Right Ascension (J2000)
Grey scale flux range= -0.549 3.266 MilliJY/BEAM
Cont peak flux = 3.2664E-03 JY/BEAM
Levs = 2.500E-04 * (1, 1.400, 2, 2.800, 4, 5.600, 8, 11, 16, 23, 32, 45, 64, 90, 128, 181, 256, 362, 512, 724, 1024)
PLot file version 1 created 16-FEB-2018 11:51:37
GREY: NONE J1607+4825D.IMAP.1
CONT: J160727+ J1607+4825.HGEOM.1
Declination (J2000)
Right Ascension (J2000)
Grey scale flux range= 3.509 6.936 Kilo
Cont peak flux = 2.4567E-02 JY/BEAM
Levs = 2.500E-04 * (1, 1.400, 2, 2.800, 4, 5.600, 8, 11, 16, 23, 32, 45, 64, 90, 128, 181, 256, 362, 512, 724, 1024)
PLot file version 1 created 16-FEB-2018 11:52:51
GREY: NONE J1608+0141D.IMAP.1
CONT: J160803+ J1608+0141.HGEOM.1
Declination (J2000)
Right Ascension (J2000)
Grey scale flux range= 2.82 19.28 Kilo
Cont peak flux = 2.5121E-01 JY/BEAM
Levs = 2.500E-04 * (1, 1.400, 2, 2.800, 4, 5.600, 8, 11, 16, 23, 32, 45, 64, 90, 128, 181, 256, 362, 512, 724, 1024)
PLot file version 1 created 16-FEB-2018 17:51:01
GREY: NONE J1609+5844D.IMAP.1
CONT: J160929+ J1609+5844.HGEOM.1
Declination (J2000)
Right Ascension (J2000)
Grey scale flux range= 3.273 8.371 Kilo
Cont peak flux = 7.0477E-03 JY/BEAM
Levs = 2.500E-04 * (1, 1.400, 2, 2.800, 4, 5.600, 8, 11, 16, 23, 32, 45, 64, 90, 128, 181, 256, 362, 512, 724, 1024)
PLot file version 1 created 16-FEB-2018 19:07:27
GREY: NONE J1616+0926D.IMAP.1
CONT: J161653+ J1616+0926.HGEOM.1
Declination (J2000)
Right Ascension (J2000)
Grey scale flux range= 3.80 23.94 Kilo
Cont peak flux = 3.8380E-02 JY/BEAM
Levs = 2.500E-04 * (1, 1.400, 2, 2.800, 4, 5.600, 8, 11, 16, 23, 32, 45, 64, 90, 128, 181, 256, 362, 512, 724, 1024)
PLot file version 1 created 16-FEB-2018 19:13:51
GREY: NONE J1620+4741D.IMAP.1
CONT: J162006+ J1620+4741.HGEOM.1
Declination (J2000)
Right Ascension (J2000)
Grey scale flux range= 3.48 14.84 Kilo
Cont peak flux = 1.9477E-02 JY/BEAM
Levs = 2.500E-04 * (1, 1.400, 2, 2.800, 4, 5.600, 8, 11, 16, 23, 32, 45, 64, 90, 128, 181, 256, 362, 512, 724, 1024)
PLot file version 1 created 16-FEB-2018 19:22:09
GREY: NONE J1621+1140D.IMAP.1
CONT: J162123+ J1621+1140.HGEOM.1
Declination (J2000)
Right Ascension (J2000)
Grey scale flux range= 3.76 21.84 Kilo
Cont peak flux = 3.0575E-03 JY/BEAM
Levs = 2.500E-04 * (1, 1.400, 2, 2.800, 4, 5.600, 8, 11, 16, 23, 32, 45, 64, 90, 128, 181, 256, 362, 512, 724, 1024)
PLot file version 1 created 17-FEB-2018 22:28:29
GREY: NONE J1625+3026D.IMAP.1
CONT: J162531+ J1625+3026.HGEOM.1
Declination (J2000)
Right Ascension (J2000)
Grey scale flux range= 10.67 17.31 Kilo
Cont peak flux = 6.2108E-02 JY/BEAM
Levs = 2.500E-04 * (1, 1.400, 2, 2.800, 4, 5.600, 8, 11, 16, 23, 32, 45, 64, 90, 128, 181, 256, 362, 512, 724, 1024)
PLot file version 1 created 16-FEB-2018 19:36:26
GREY: NONE J1625+4456D.IMAP.1
CONT: J162523+ J1625+4456.HGEOM.1
Declination (J2000)
Right Ascension (J2000)
Grey scale flux range= 3.91 11.45 Kilo
Cont peak flux = 1.2286E-02 JY/BEAM
Levs = 2.500E-04 * (1, 1.400, 2, 2.800, 4, 5.600, 8, 11, 16, 23, 32, 45, 64, 90, 128, 181, 256, 362, 512, 724, 1024)
PLot file version 1 created 16-FEB-2018 19:30:19
GREY: NONE J1625+4813D.IMAP.1
CONT: J162512+ J1625+4813.HGEOM.1
Declination (J2000)
Right Ascension (J2000)
Grey scale flux range= 3.88 25.53 Kilo
Cont peak flux = 4.9921E-03 JY/BEAM
Levs = 2.500E-04 * (1, 1.400, 2, 2.800, 4, 5.600, 8, 11, 16, 23, 32, 45, 64, 90, 128, 181, 256, 362, 512, 724, 1024)
PLot file version 1 created 17-FEB-2018 22:31:30
GREY: NONE J1631+0531D.IMAP.1
CONT: J163110+ J1631+0531.HGEOM.1
Declination (J2000)
Right Ascension (J2000)
Grey scale flux range= 4.07 19.52 Kilo
Cont peak flux = 5.0429E-03 JY/BEAM
Levs = 2.500E-04 * (1, 1.400, 2, 2.800, 4, 5.600, 8, 11, 16, 23, 32, 45, 64, 90, 128, 181, 256, 362, 512, 724, 1024)
PLot file version 1 created 17-FEB-2018 22:33:25
GREY: NONE J1631+0535D.IMAP.1
CONT: J163142+ J1631+0535.HGEOM.1
Declination (J2000)
Right Ascension (J2000)
Grey scale flux range= 4.285 8.050 Kilo
Cont peak flux = 9.8723E-04 JY/BEAM
Levs = 2.500E-04 * (1, 1.400, 2, 2.800, 4, 5.600, 8, 11, 16, 23, 32, 45, 64, 90, 128, 181, 256, 362, 512, 724, 1024)

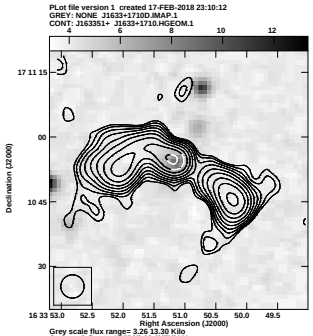
PLot file version 1 created 17-FEB-2018 23:10:12
GREY: NONE J1633+1710D.IMAP.1
CONT: J163351+ J1633+1710.HGEOM.1
Declination (J2000)
Right Ascension (J2000)
Grey scale flux range= 3.26 13.30 Kilo
Cont peak flux = 4.3586E-03 JY/BEAM
Levs = 2.500E-04 * (1, 1.400, 2, 2.800, 4, 5.600, 8, 11, 16, 23, 32, 45, 64, 90, 128, 181, 256, 362, 512, 724, 1024)

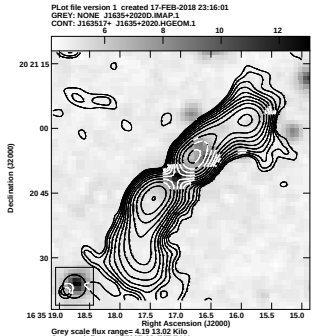
PLot file version 1 created 17-FEB-2018 23:16:01
GREY: NONE J1635+2020D.IMAP.1
CONT: J1635175+ J1635+2020.HGEOM.1
Declination (J2000)
Right Ascension (J2000)
Grey scale flux range= 4.19 13.02 Kilo
Cont peak flux = 1.2590E-02 JY/BEAM
Levs = 2.500E-04 * (1, 1.400, 2, 2.800, 4, 5.600, 8, 11, 16, 23, 32, 45, 64, 90, 128, 181, 256, 362, 512, 724, 1024)

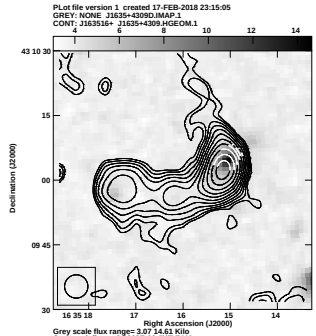
PLot file version 1 created 17-FEB-2018 23:15:05
GREY: NONE J1635+4309D.IMAP.1
CONT: J1635162+ J1635+4309.HGEOM.1
Declination (J2000)
Right Ascension (J2000)
Grey scale flux range= 3.07 14.61 Kilo
Cont peak flux = 9.8963E-03 JY/BEAM
Levs = 2.500E-04 * (1, 1.400, 2, 2.800, 4, 5.600, 8, 11, 16, 23, 32, 45, 64, 90, 128, 181, 256, 362, 512, 724, 1024)

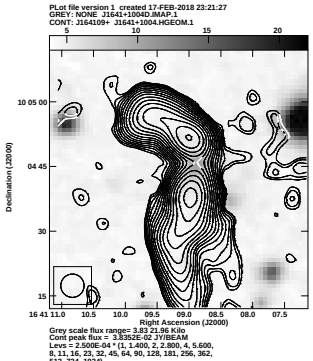
PLot file version 1 created 17-FEB-2018 23:21:27
GREY: NONE J1641+1004D.IMAP.1
CONT: J164109+ J1641+1004.HGEOM.1
Declination (J2000)
Right Ascension (J2000)
Grey scale flux range= 3.83 21.96 Kilo
Cont peak flux = 3.8352E-02 JY/BEAM
Levs = 2.500E-04 * (1, 1.400, 2, 2.800, 4, 5.600, 8, 11, 16, 23, 32, 45, 64, 90, 128, 181, 256, 362, 512, 724, 1024)

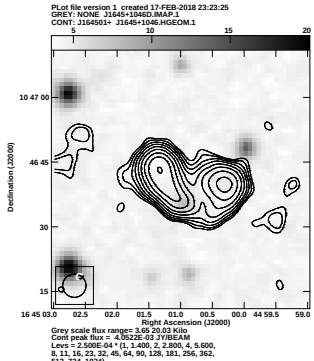
PLot file version 1 created 17-FEB-2018 23:23:25
GREY: NONE J1645+1046D.IMAP.1
CONT: J164501+ J1645+1046.HGEOM.1
Declination (J2000)
Right Ascension (J2000)
Grey scale flux range= 3.65 20.03 Kilo
Cont peak flux = 4.0522E-03 JY/BEAM
Levs = 2.500E-04 * (1, 1.400, 2, 2.800, 4, 5.600, 8, 11, 16, 23, 32, 45, 64, 90, 128, 181, 256, 362, 512, 724, 1024)

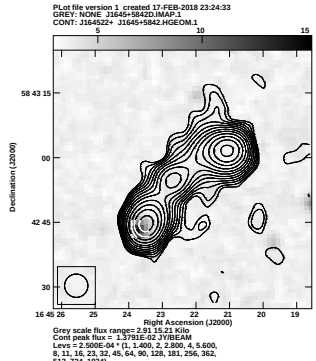
PLot file version 1 created 17-FEB-2018 23:24:33
GREY: NONE J1645+5842D.IMAP.1
CONT: J164522+ J1645+5842.HGEOM.1
Declination (J2000)
Right Ascension (J2000)
Grey scale flux range= 2.91 15.21 Kilo
Cont peak flux = 1.3791E-02 JY/BEAM
Levs = 2.500E-04 * (1, 1.400, 2, 2.800, 4, 5.600, 8, 11, 16, 23, 32, 45, 64, 90, 128, 181, 256, 362, 512, 724, 1024)

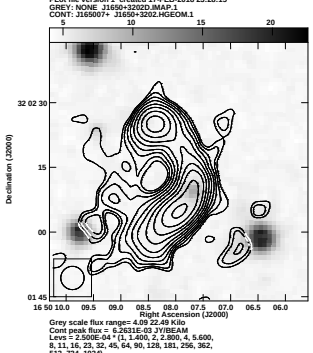
PLot file version 1 created 17-FEB-2018 23:28:15
GREY: NONE J1650+3202D.IMAP.1
CONT: J165007+ J1650+3202.HGEOM.1
Declination (J2000)
Right Ascension (J2000)
Grey scale flux range= 4.09 22.49 Kilo
Cont peak flux = 6.2631E-03 JY/BEAM
Levs = 2.500E-04 * (1, 1.400, 2, 2.800, 4, 5.600, 8, 11, 16, 23, 32, 45, 64, 90, 128, 181, 256, 362, 512, 724, 1024)

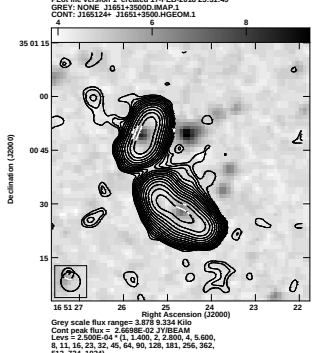
PLot file version 1 created 17-FEB-2018 23:31:49
GREY: NONE J1651+3500D.IMAP.1
CONT: J165124+ J1651+3500.HGEOM.1
Declination (J2000)
Right Ascension (J2000)
Grey scale flux range= 3.878 9.334 Kilo
Cont peak flux = 2.8698E-02 JY/BEAM
Levs = 2.500E-04 * (1, 1.400, 2, 2.800, 4, 5.600, 8, 11, 16, 23, 32, 45, 64, 90, 128, 181, 256, 362, 512, 724, 1024)

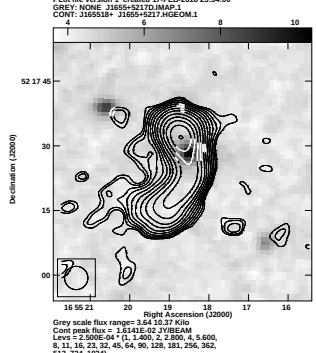
PLot file version 1 created 17-FEB-2018 23:34:00
GREY: NONE J1655+5217D.IMAP.1
CONT: J165518+ J1655+5217.HGEOM.1
Declination (J2000)
Right Ascension (J2000)
Grey scale flux range= 3.64 10.37 Kilo
Cont peak flux = 1.6141E-02 JY/BEAM
Levs = 2.500E-04 * (1, 1.400, 2, 2.800, 4, 5.600, 8, 11, 16, 23, 32, 45, 64, 90, 128, 181, 256, 362, 512, 724, 1024)

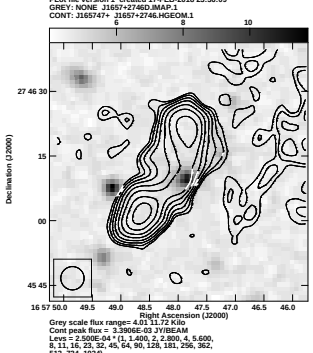
PLot file version 1 created 17-FEB-2018 23:36:09
GREY: NONE J1657+2746D.IMAP.1
CONT: J165747+ J1657+2746.HGEOM.1
Declination (J2000)
Right Ascension (J2000)
Grey scale flux range= 4.01 11.72 Kilo
Cont peak flux = 3.3906E-03 JY/BEAM
Levs = 2.500E-04 * (1, 1.400, 2, 2.800, 4, 5.600, 8, 11, 16, 23, 32, 45, 64, 90, 128, 181, 256, 362, 512, 724, 1024)

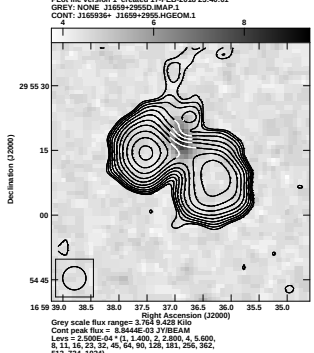
PLot file version 1 created 17-FEB-2018 23:40:01
GREY: NONE J1659+2955D.IMAP.1
CONT: J165936+ J1659+2955.HGEOM.1
Declination (J2000)
Right Ascension (J2000)
Grey scale flux range= 3.764 9.428 Kilo
Cont peak flux = 8.9444E-03 JY/BEAM
Levs = 2.500E-04 * (1, 1.400, 2, 2.800, 4, 5.600, 8, 11, 16, 23, 32, 45, 64, 90, 128, 181, 256, 362, 512, 724, 1024)

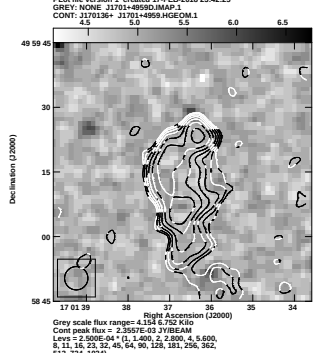
PLot file version 1 created 17-FEB-2018 23:42:25
GREY: NONE J1701+4959D.IMAP.1
CONT: J170136+ J1701+4959.HGEOM.1
Declination (J2000)
Right Ascension (J2000)
Grey scale flux range= 4.154 6.752 Kilo
Cont peak flux = 2.3957E-03 JY/BEAM
Levs = 2.500E-04 * (1, 1.400, 2, 2.800, 4, 5.600, 8, 11, 16, 23, 32, 45, 64, 90, 128, 181, 256, 362, 512, 724, 1024)

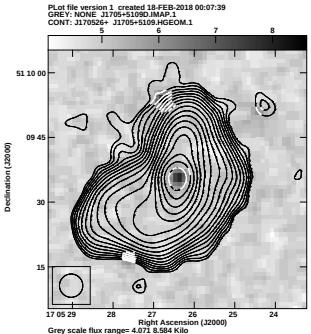
PLot file version 1 created 18-FEB-2018 00:07:39
GREY: NONE J170+5108D.IMAP.1
CONT: J170526+ J1705+5109.HGEOM.1
Declination (J2000)
Right Ascension (J2000)
Grey scale flux range= 4.071 8.584 Kilo
Cont peak flux = 8.7256E-02 JY/BEAM
Levs = 2.500E-04 * (1, 1.400, 2, 2.800, 4, 5.600,
8, 11, 16, 23, 32, 45, 64, 90, 128, 181, 256, 362,
512, 724, 1024)

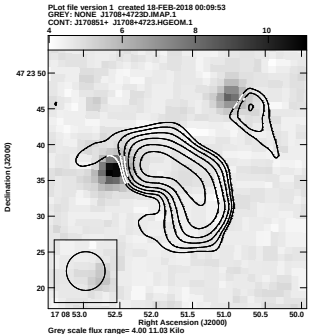
PLot file version 1 created 18-FEB-2018 00:09:53
GREY: NONE J170+4723D.IMAP.1
CONT: J170851+ J1708+4723.HGEOM.1
Declination (J2000)
Right Ascension (J2000)
Grey scale flux range= 4.00 11.03 Kilo
Cont peak flux = 1.3179E-03 JY/BEAM
Levs = 2.500E-04 * (1, 1.400, 2, 2.800, 4, 5.600,
8, 11, 16, 23, 32, 45, 64, 90, 128, 181, 256, 362,
512, 724, 1024)

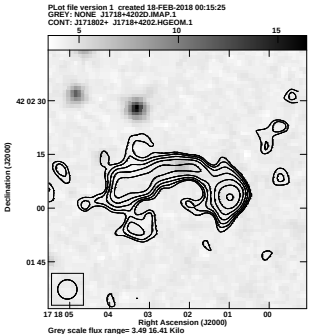
PLot file version 1 created 18-FEB-2018 00:15:25
GREY: NONE J171+4202D.IMAP.1
CONT: J171802+ J1718+4202.HGEOM.1
Declination (J2000)
Right Ascension (J2000)
Grey scale flux range= 3.49 16.41 Kilo
Cont peak flux = 2.0622E-03 JY/BEAM
Levs = 2.500E-04 * (1, 1.400, 2, 2.800, 4, 5.600,
8, 11, 16, 23, 32, 45, 64, 90, 128, 181, 256, 362,
512, 724, 1024)

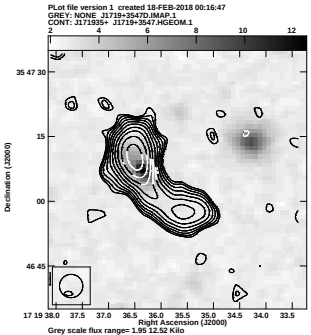
PLot file version 1 created 18-FEB-2018 00:16:47
GREY: NONE J1719+3547D.IMAP.1
CONT: J171935+ J1719+3547.HGEOM.1
Declination (J2000)
Right Ascension (J2000)
Grey scale flux range= 1.95 12.52 Kilo
Cont peak flux = 7.0682E-03 JY/BEAM
Levs = 2.500E-04 * (1, 1.400, 2, 2.800, 4, 5.600,
8, 11, 16, 23, 32, 45, 64, 90, 128, 181, 256, 362,
512, 724, 1024)

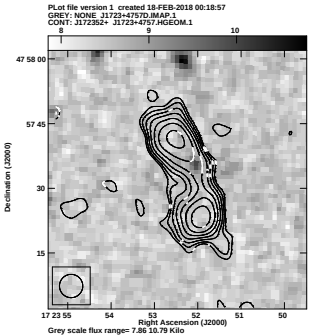
PLot file version 1 created 18-FEB-2018 00:18:57
GREY: NONE J1723+4757D.IMAP.1
CONT: J172352+ J1723+4757.HGEOM.1
Declination (J2000)
Right Ascension (J2000)
Grey scale flux range= 7.86 16.79 Kilo
Cont peak flux = 2.5898E-03 JY/BEAM
Levs = 2.500E-04 * (1, 1.400, 2, 2.800, 4, 5.600,
8, 11, 16, 23, 32, 45, 64, 90, 128, 181, 256, 362,
512, 724, 1024)

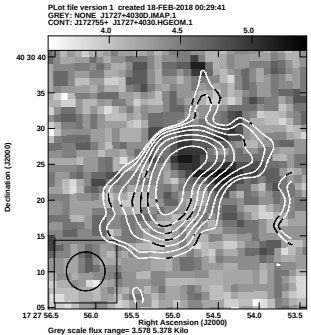
PLot file version 1 created 18-FEB-2018 00:29:41
GREY: NONE J1727+4030D.IMAP.1
CONT: J172755+ J1727+4030.HGEOM.1
Declination (J2000)
Right Ascension (J2000)
Grey scale flux range= 3.578 5.378 Kilo
Cont peak flux = 2.6965E-03 JY/BEAM
Levs = 2.500E-04 * (1, 1.400, 2, 2.800, 4, 5.600,
8, 11, 16, 23, 32, 45, 64, 90, 128, 181, 256, 362,
512, 724, 1024)

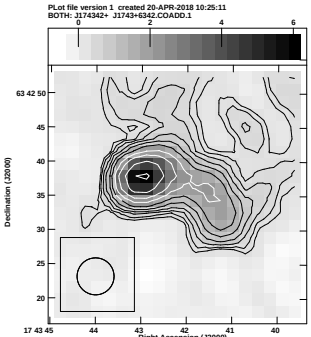
PLot file version 1 created 20-APR-2018 10:25:11
BOTH: J174342+ J1743+6342.COADD.1
Declination (J2000)
Right Ascension (J2000)
Grey scale flux range= -0.500 6.031 MilliJY/BEAM
Cont peak flux = 6.0312E-03 JY/BEAM
Levs = 2.500E-04 * (1, 1.400, 2, 2.800, 4, 5.600,
8, 11, 16, 23, 32, 45, 64, 90, 128, 181, 256, 362,
512, 724, 1024)

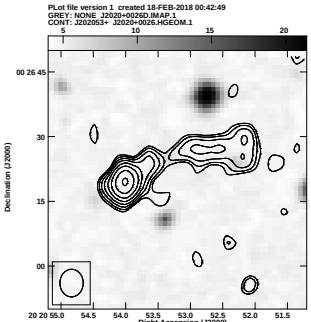
PLot file version 1 created 18-FEB-2018 00:42:49
GREY: NONE J202D+0026D.IMAP.1
CONT: J202053+ J202D+0026.HGEOM.1
Declination (J2000)
Right Ascension (J2000)
Grey scale flux range= 4.05 21.36 Kilo
Cont peak flux = 2.8633E-03 JY/BEAM
Levs = 2.500E-04 * (1, 1.400, 2, 2.800, 4, 5.600,
8, 11, 16, 23, 32, 45, 64, 90, 128, 181, 256, 362,
512, 724, 1024)

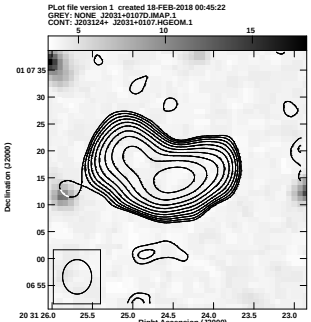
PLot file version 1 created 18-FEB-2018 00:45:22
GREY: NONE J2031+0107D.IMAP.1
CONT: J203124+ J2031+0107.HGEOM.1
Declination (J2000)
Right Ascension (J2000)
Grey scale flux range= 3.30 18.08 Kilo
Cont peak flux = 7.4643E-03 JY/BEAM
Levs = 2.500E-04 * (1, 1.400, 2, 2.800, 4, 5.600,
8, 11, 16, 23, 32, 45, 64, 90, 128, 181, 256, 362,
512, 724, 1024)

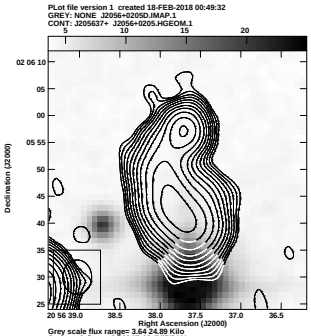
PLot file version 1 created 18-FEB-2018 00:49:32
GREY: NONE J205E+0205D.IMAP.1
CONT: J205637+ J205E+0205.HGEOM.1
Declination (J2000)
Right Ascension (J2000)
Grey scale flux range= 3.64 24.89 Kilo
Cont peak flux = 9.8094E-03 JY/BEAM
Levs = 2.500E-04 * (1, 1.400, 2, 2.800, 4, 5.600,
8, 11, 16, 23, 32, 45, 64, 90, 128, 181, 256, 362,
512, 724, 1024)

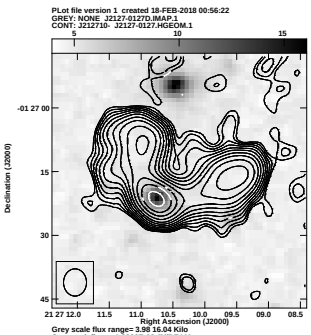
PLot file version 1 created 18-FEB-2018 00:56:22
GREY: NONE J2127-0127D.IMAP.1
CONT: J212710- J2127-0127.HGEOM.1
Declination (J2000)
Right Ascension (J2000)
Grey scale flux range= 3.98 16.04 Kilo
Cont peak flux = 1.2920E-02 JY/BEAM
Levs = 2.500E-04 * (1, 1.400, 2, 2.800, 4, 5.600,
8, 11, 16, 23, 32, 45, 64, 90, 128, 181, 256, 362,
512, 724, 1024)

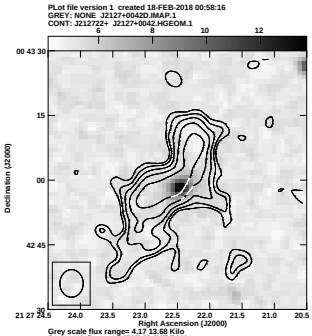
PLot file version 1 created 18-FEB-2018 00:58:16
GREY: NONE J2127+0042D.IMAP.1
CONT: J212722+ J2127+0042.HGEOM.1
Declination (J2000)
Right Ascension (J2000)
Grey scale flux range= 4.17 13.68 Kilo
Cont peak flux = 1.3452E-03 JY/BEAM
Levs = 2.500E-04 * (1, 1.400, 2, 2.800, 4, 5.600,
8, 11, 16, 23, 32, 45, 64, 90, 128, 181, 256, 362,
512, 724, 1024)

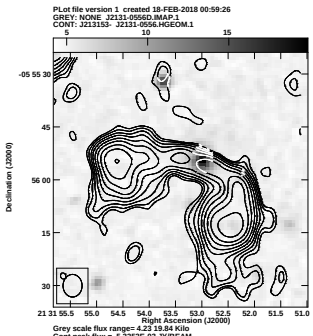
PLot file version 1 created 18-FEB-2018 00:59:26
GREY: NONE J2131-0556D.IMAP.1
CONT: J213153- J2131-0556.HGEOM.1
Declination (J2000)
Right Ascension (J2000)
Grey scale flux range= 4.23 19.84 Kilo
Cont peak flux = 5.3252E-03 JY/BEAM
Levs = 2.500E-04 * (1, 1.400, 2, 2.800, 4, 5.600, 8, 11, 16, 23, 32, 45, 64, 90, 128, 181, 256, 362, 512, 724, 1024)

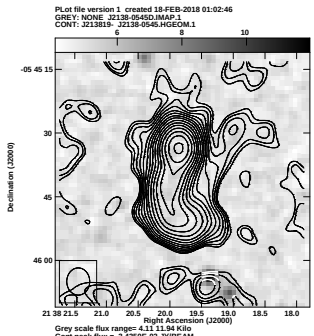
PLot file version 1 created 18-FEB-2018 01:02:46
GREY: NONE J2138-0545D.IMAP.1
CONT: J213819- J2138-0545.HGEOM.1
Declination (J2000)
Right Ascension (J2000)
Grey scale flux range= 4.11 11.94 Kilo
Cont peak flux = 3.4380E-02 JY/BEAM
Levs = 2.500E-04 * (1, 1.400, 2, 2.800, 4, 5.600, 8, 11, 16, 23, 32, 45, 64, 90, 128, 181, 256, 362, 512, 724, 1024)

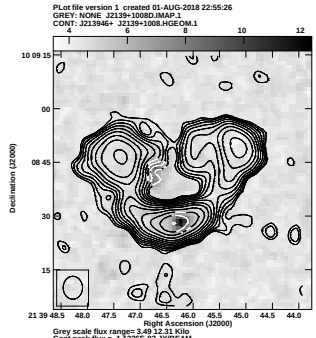
PLot file version 1 created 01-AUG-2018 22:55:26
GREY: NONE J2139+1008D.IMAP.1
CONT: J213946+ J2139+1008.HGEOM.1
Declination (J2000)
Right Ascension (J2000)
Grey scale flux range= 3.49 12.31 Kilo
Cont peak flux = 1.1320E-02 JY/BEAM
Levs = 2.500E-04 * (1, 1.400, 2, 2.800, 4, 5.600, 8, 11, 16, 23, 32, 45, 64, 90, 128, 181, 256, 362, 512, 724, 1024)

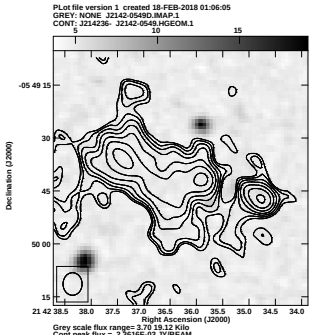
PLot file version 1 created 18-FEB-2018 01:06:05
GREY: NONE J2142-0549D.IMAP.1
CONT: J214236- J2142-0549.HGEOM.1
Declination (J2000)
Right Ascension (J2000)
Grey scale flux range= 3.70 19.12 Kilo
Cont peak flux = 2.3616E-03 JY/BEAM
Levs = 2.500E-04 * (1, 1.400, 2, 2.800, 4, 5.600, 8, 11, 16, 23, 32, 45, 64, 90, 128, 181, 256, 362, 512, 724, 1024)

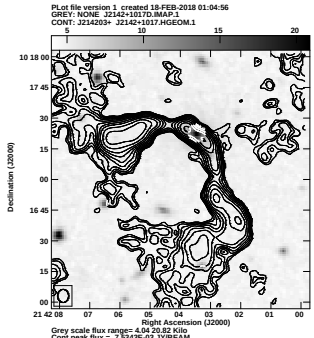
PLot file version 1 created 18-FEB-2018 01:04:56
GREY: NONE J2142+1017D.IMAP.1
CONT: J214203+ J2142+1017.HGEOM.1
Declination (J2000)
Right Ascension (J2000)
Grey scale flux range= 4.04 20.82 Kilo
Cont peak flux = 7.5343E-03 JY/BEAM
Levs = 2.500E-04 * (1, 1.400, 2, 2.800, 4, 5.600, 8, 11, 16, 23, 32, 45, 64, 90, 128, 181, 256, 362, 512, 724, 1024)

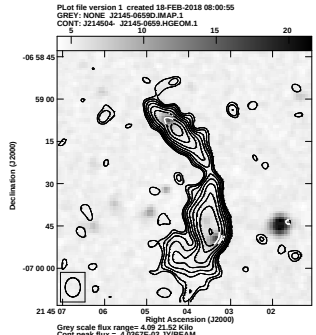
PLot file version 1 created 18-FEB-2018 08:00:55
GREY: NONE J2145-0659D.IMAP.1
CONT: J214504- J2145-0659.HGEOM.1
Declination (J2000)
Right Ascension (J2000)
Grey scale flux range= 4.09 21.52 Kilo
Cont peak flux = 4.0367E-03 JY/BEAM
Levs = 2.500E-04 * (1, 1.400, 2, 2.800, 4, 5.600, 8, 11, 16, 23, 32, 45, 64, 90, 128, 181, 256, 362, 512, 724, 1024)

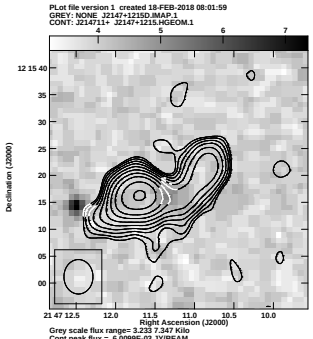
PLot file version 1 created 18-FEB-2018 08:01:59
GREY: NONE J2147+1215D.IMAP.1
CONT: J214711+ J2147+1215.HGEOM.1
Declination (J2000)
Right Ascension (J2000)
Grey scale flux range= 3.233 7.347 Kilo
Cont peak flux = 6.0099E-03 JY/BEAM
Levs = 2.500E-04 * (1, 1.400, 2, 2.800, 4, 5.600, 8, 11, 16, 23, 32, 45, 64, 90, 128, 181, 256, 362, 512, 724, 1024)

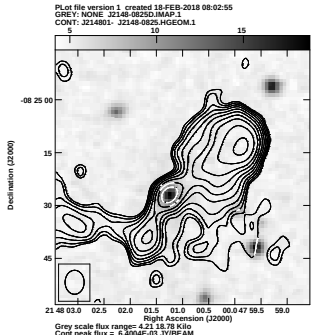
PLot file version 1 created 18-FEB-2018 08:02:55
GREY: NONE J2148-0825D.IMAP.1
CONT: J214801- J2148-0825.HGEOM.1
Declination (J2000)
Right Ascension (J2000)
Grey scale flux range= 4.21 18.78 Kilo
Cont peak flux = 6.4004E-03 JY/BEAM
Levs = 2.500E-04 * (1, 1.400, 2, 2.800, 4, 5.600, 8, 11, 16, 23, 32, 45, 64, 90, 128, 181, 256, 362, 512, 724, 1024)

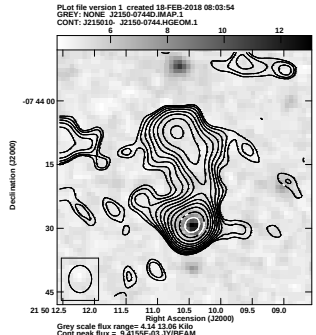
PLot file version 1 created 18-FEB-2018 08:03:54
GREY: NONE J2150-0744D.IMAP.1
CONT: J215010- J2150-0744.HGEOM.1
Declination (J2000)
Right Ascension (J2000)
Grey scale flux range= 4.14 13.06 Kilo
Cont peak flux = 9.4155E-03 JY/BEAM
Levs = 2.500E-04 * (1, 1.400, 2, 2.800, 4, 5.600, 8, 11, 16, 23, 32, 45, 64, 90, 128, 181, 256, 362, 512, 724, 1024)

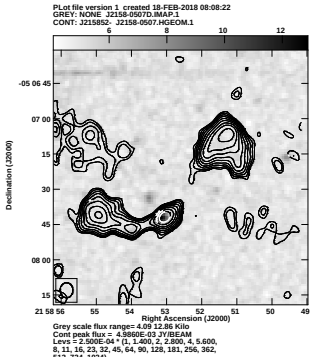
PLot file version 1 created 18-FEB-2018 08:08:22
GREY: NONE J2158-0507D.IMAP.1
CONT: J215852- J2158-0507.HGEOM.1
Declination (J2000)
Right Ascension (J2000)
Grey scale flux range= 4.09 12.86 Kilo
Cont peak flux = 4.9860E-03 JY/BEAM
Levs = 2.500E-04 * (1, 1.400, 2, 2.800, 4, 5.600, 8, 11, 16, 23, 32, 45, 64, 90, 128, 181, 256, 362, 512, 724, 1024)

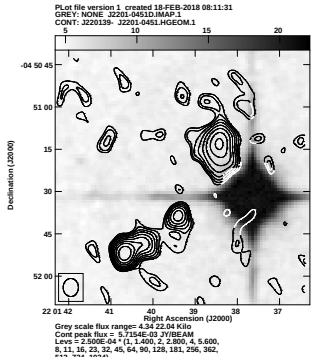
PLot file version 1 created 18-FEB-2018 08:11:31
GREY: NONE J2201-0451D.IMAP.1
CONT: J220139- J2201-0451.HGEOM.1
Declination (J2000)
Right Ascension (J2000)
Grey scale flux range= 4.34 22.04 Kilo
Cont peak flux = 5.7154E-03 JY/BEAM
Levs = 2.500E-04 * (1, 1.400, 2, 2.800, 4, 5.600, 8, 11, 16, 23, 32, 45, 64, 90, 128, 181, 256, 362, 512, 724, 1024)

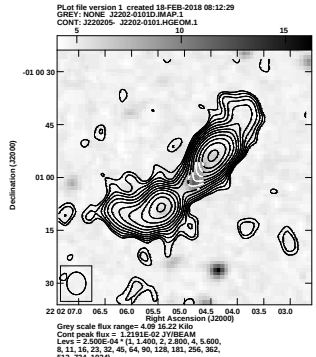
PLot file version 1 created 18-FEB-2018 08:12:29
GREY: NONE J2202-0101D.IMAP.1
CONT: J220205- J2202-0101.HGEOM.1
Declination (J2000)
Right Ascension (J2000)
Grey scale flux range= 4.09 16.22 Kilo
Cont peak flux = 1.2191E-02 JY/BEAM
Levs = 2.500E-04 * (1, 1.400, 2, 2.800, 4, 5.600, 8, 11, 16, 23, 32, 45, 64, 90, 128, 181, 256, 362, 512, 724, 1024)

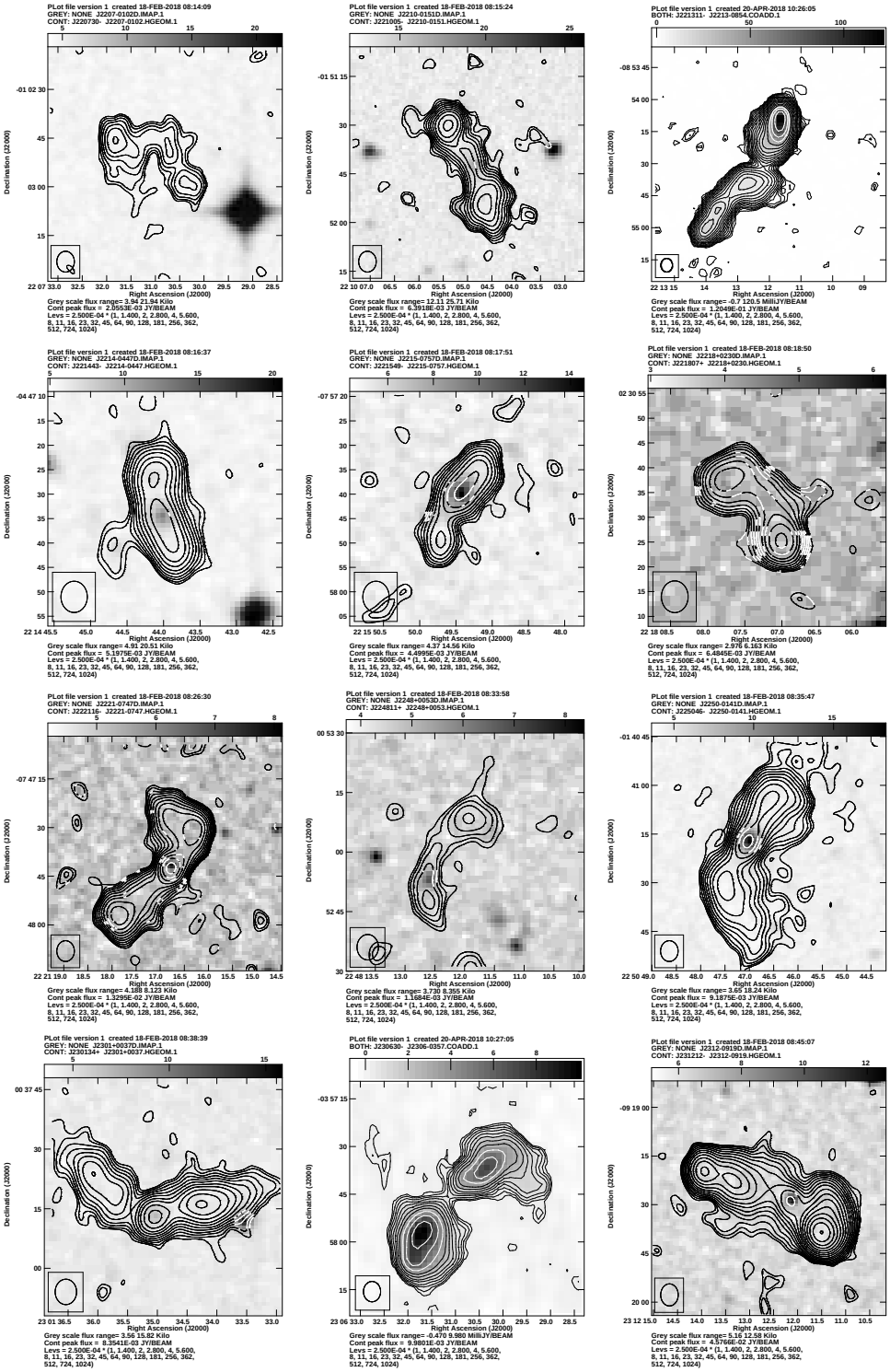
PLot file version 1 created 18-FEB-2018 08:14:09
GREY: NONE J2207-0102D.IMAP.1
CONT: J220730- J2207-0102.HGEOM.1
Declination (J2000)
Right Ascension (J2000)
Grey scale flux range= 3.94 21.94 Kilo
Cont peak flux = 2.0553E-03 JY/BEAM
Levs = 2.500E-04 * (1, 1.400, 2, 2.800, 4, 5.600, 8, 11, 16, 23, 32, 45, 64, 90, 128, 181, 256, 362, 512, 724, 1024)
PLot file version 1 created 18-FEB-2018 08:15:24
GREY: NONE J2210-0151D.IMAP.1
CONT: J221005- J2210-0151.HGEOM.1
Declination (J2000)
Right Ascension (J2000)
Grey scale flux range= 12.11 25.71 Kilo
Cont peak flux = 6.3918E-03 JY/BEAM
Levs = 2.500E-04 * (1, 1.400, 2, 2.800, 4, 5.600, 8, 11, 16, 23, 32, 45, 64, 90, 128, 181, 256, 362, 512, 724, 1024)
PLot file version 1 created 20-APR-2018 10:26:05
BOTH: J221311- J2213-0854.COADD.1
Declination (J2000)
Right Ascension (J2000)
Grey scale flux range= -0.7 120.5 MILLIJY/BEAM
Cont peak flux = 1.2049E-01 JY/BEAM
Levs = 2.500E-04 * (1, 1.400, 2, 2.800, 4, 5.600, 8, 11, 16, 23, 32, 45, 64, 90, 128, 181, 256, 362, 512, 724, 1024)
PLot file version 1 created 18-FEB-2018 08:16:37
GREY: NONE J2214-0447D.IMAP.1
CONT: J221443- J2214-0447.HGEOM.1
Declination (J2000)
Right Ascension (J2000)
Grey scale flux range= -4.91 20.51 Kilo
Cont peak flux = 5.1975E-03 JY/BEAM
Levs = 2.500E-04 * (1, 1.400, 2, 2.800, 4, 5.600, 8, 11, 16, 23, 32, 45, 64, 90, 128, 181, 256, 362, 512, 724, 1024)
PLot file version 1 created 18-FEB-2018 08:17:51
GREY: NONE J2215-0757D.IMAP.1
CONT: J221548- J2215-0757.HGEOM.1
Declination (J2000)
Right Ascension (J2000)
Grey scale flux range= 4.37 14.56 Kilo
Cont peak flux = 4.4989E-03 JY/BEAM
Levs = 2.500E-04 * (1, 1.400, 2, 2.800, 4, 5.600, 8, 11, 16, 23, 32, 45, 64, 90, 128, 181, 256, 362, 512, 724, 1024)
PLot file version 1 created 18-FEB-2018 08:18:50
GREY: NONE J2218+0230D.IMAP.1
CONT: J221807+ J2218+0230.HGEOM.1
Declination (J2000)
Right Ascension (J2000)
Grey scale flux range= 2.976 6.163 Kilo
Cont peak flux = 6.4845E-03 JY/BEAM
Levs = 2.500E-04 * (1, 1.400, 2, 2.800, 4, 5.600, 8, 11, 16, 23, 32, 45, 64, 90, 128, 181, 256, 362, 512, 724, 1024)
PLot file version 1 created 18-FEB-2018 08:26:30
GREY: NONE J2221-0747D.IMAP.1
CONT: J222116- J2221-0747.HGEOM.1
Declination (J2000)
Right Ascension (J2000)
Grey scale flux range= 4.189 8.123 Kilo
Cont peak flux = 1.3295E-02 JY/BEAM
Levs = 2.500E-04 * (1, 1.400, 2, 2.800, 4, 5.600, 8, 11, 16, 23, 32, 45, 64, 90, 128, 181, 256, 362, 512, 724, 1024)
PLot file version 1 created 18-FEB-2018 08:33:58
GREY: NONE J2248+0053D.IMAP.1
CONT: J224811+ J2248+0053.HGEOM.1
Declination (J2000)
Right Ascension (J2000)
Grey scale flux range= 3.730 8.355 Kilo
Cont peak flux = 1.1684E-03 JY/BEAM
Levs = 2.500E-04 * (1, 1.400, 2, 2.800, 4, 5.600, 8, 11, 16, 23, 32, 45, 64, 90, 128, 181, 256, 362, 512, 724, 1024)
PLot file version 1 created 18-FEB-2018 08:35:47
GREY: NONE J2250-0141D.IMAP.1
CONT: J225046- J2250-0141.HGEOM.1
Declination (J2000)
Right Ascension (J2000)
Grey scale flux range= 3.65 18.24 Kilo
Cont peak flux = 8.1879E-03 JY/BEAM
Levs = 2.500E-04 * (1, 1.400, 2, 2.800, 4, 5.600, 8, 11, 16, 23, 32, 45, 64, 90, 128, 181, 256, 362, 512, 724, 1024)
PLot file version 1 created 18-FEB-2018 08:38:39
GREY: NONE J2301+0037D.IMAP.1
CONT: J230134+ J2301+0037.HGEOM.1
Declination (J2000)
Right Ascension (J2000)
Grey scale flux range= 3.56 15.82 Kilo
Cont peak flux = 8.3541E-03 JY/BEAM
Levs = 2.500E-04 * (1, 1.400, 2, 2.800, 4, 5.600, 8, 11, 16, 23, 32, 45, 64, 90, 128, 181, 256, 362, 512, 724, 1024)
PLot file version 1 created 20-APR-2018 10:27:05
BOTH: J230630- J2306-0357.COADD.1
Declination (J2000)
Right Ascension (J2000)
Grey scale flux range= -0.470 9.980 MILLIJY/BEAM
Cont peak flux = 9.9801E-03 JY/BEAM
Levs = 2.500E-04 * (1, 1.400, 2, 2.800, 4, 5.600, 8, 11, 16, 23, 32, 45, 64, 90, 128, 181, 256, 362, 512, 724, 1024)
PLot file version 1 created 18-FEB-2018 08:45:07
GREY: NONE J2312-0919D.IMAP.1
CONT: J231212- J2312-0919.HGEOM.1
Declination (J2000)
Right Ascension (J2000)
Grey scale flux range= 5.16 12.58 Kilo
Cont peak flux = 4.5766E-02 JY/BEAM
Levs = 2.500E-04 * (1, 1.400, 2, 2.800, 4, 5.600, 8, 11, 16, 23, 32, 45, 64, 90, 128, 181, 256, 362, 512, 724, 1024)

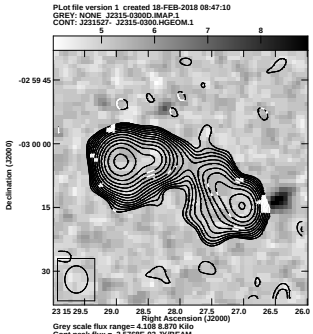
PLot file version 1 created 18-FEB-2018 08:47:10
GREY: NONE J2315-0300D.IMAP.1
CONT: J231527- J2315-0300.HGEOM.1
Declination (J2000)
Right Ascension (J2000)
Grey scale flux range= 4.109 8.870 Kilo
Cont peak flux = 2.5768E-02 JY/BEAM
Levs = 2.500E-04 * (1, 1.400, 2, 2.800, 4, 5.600, 8, 11, 16, 23, 32, 45, 64, 90, 128, 181, 256, 362, 512, 724, 1024)

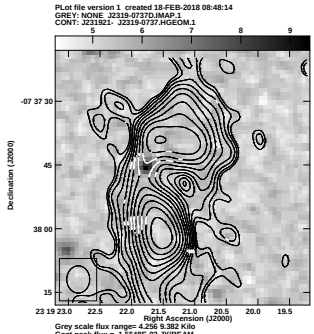
PLot file version 1 created 18-FEB-2018 08:48:14
GREY: NONE J2319-0737D.IMAP.1
CONT: J231921- J2319-0737.HGEOM.1
Declination (J2000)
Right Ascension (J2000)
Grey scale flux range= 4.256 9.382 Kilo
Cont peak flux = 1.5548E-02 JY/BEAM
Levs = 2.500E-04 * (1, 1.400, 2, 2.800, 4, 5.600, 8, 11, 16, 23, 32, 45, 64, 90, 128, 181, 256, 362, 512, 724, 1024)

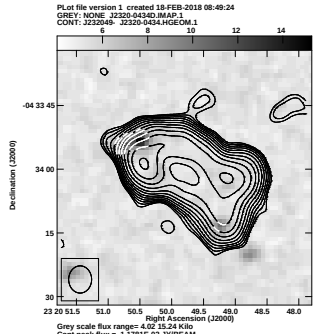
PLot file version 1 created 18-FEB-2018 08:49:24
GREY: NONE J2320-0434D.IMAP.1
CONT: J232049- J2320-0434.HGEOM.1
Declination (J2000)
Right Ascension (J2000)
Grey scale flux range= 4.02 15.24 Kilo
Cont peak flux = 1.1781E-02 JY/BEAM
Levs = 2.500E-04 * (1, 1.400, 2, 2.800, 4, 5.600, 8, 11, 16, 23, 32, 45, 64, 90, 128, 181, 256, 362, 512, 724, 1024)

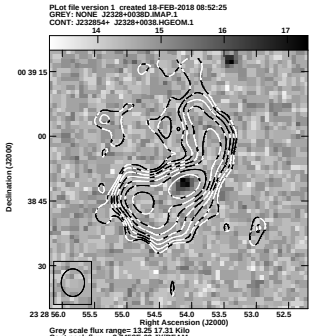
PLot file version 1 created 18-FEB-2018 08:52:25
GREY: NONE J2328+0038D.IMAP.1
CONT: J232854+ J2328+0038.HGEOM.1
Declination (J2000)
Right Ascension (J2000)
Grey scale flux range= 13.25 17.31 Kilo
Cont peak flux = 2.7458E-03 JY/BEAM
Levs = 2.500E-04 * (1, 1.400, 2, 2.800, 4, 5.600, 8, 11, 16, 23, 32, 45, 64, 90, 128, 181, 256, 362, 512, 724, 1024)

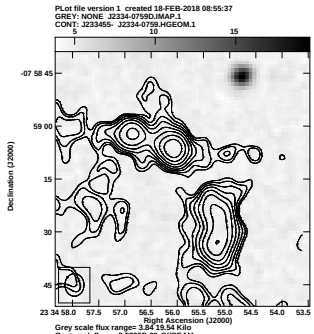
PLot file version 1 created 18-FEB-2018 08:55:37
GREY: NONE J2334-0759D.IMAP.1
CONT: J233455- J2334-0759.HGEOM.1
Declination (J2000)
Right Ascension (J2000)
Grey scale flux range= 3.84 15.54 Kilo
Cont peak flux = 3.7209E-03 JY/BEAM
Levs = 2.500E-04 * (1, 1.400, 2, 2.800, 4, 5.600, 8, 11, 16, 23, 32, 45, 64, 90, 128, 181, 256, 362, 512, 724, 1024)

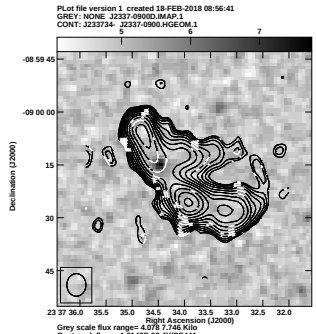
PLot file version 1 created 18-FEB-2018 08:56:41
GREY: NONE J2337-0900D.IMAP.1
CONT: J233734- J2337-0900.HGEOM.1
Declination (J2000)
Right Ascension (J2000)
Grey scale flux range= 4.078 7.746 Kilo
Cont peak flux = 1.2143E-02 JY/BEAM
Levs = 2.500E-04 * (1, 1.400, 2, 2.800, 4, 5.600, 8, 11, 16, 23, 32, 45, 64, 90, 128, 181, 256, 362, 512, 724, 1024)

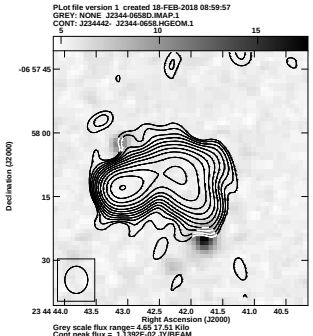
PLot file version 1 created 18-FEB-2018 08:59:57
GREY: NONE J2344-0658D.IMAP.1
CONT: J234442- J2344-0658.HGEOM.1
Declination (J2000)
Right Ascension (J2000)
Grey scale flux range= 4.65 17.51 Kilo
Cont peak flux = 1.1392E-02 JY/BEAM
Levs = 2.500E-04 * (1, 1.400, 2, 2.800, 4, 5.600, 8, 11, 16, 23, 32, 45, 64, 90, 128, 181, 256, 362, 512, 724, 1024)

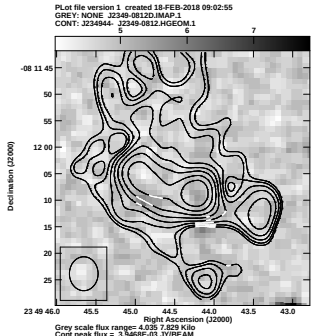
PLot file version 1 created 18-FEB-2018 09:02:55
GREY: NONE J2349-0812D.IMAP.1
CONT: J234944- J2349-0812.HGEOM.1
Declination (J2000)
Right Ascension (J2000)
Grey scale flux range= 4.035 7.829 Kilo
Cont peak flux = 3.9468E-03 JY/BEAM
Levs = 2.500E-04 * (1, 1.400, 2, 2.800, 4, 5.600, 8, 11, 16, 23, 32, 45, 64, 90, 128, 181, 256, 362, 512, 724, 1024)

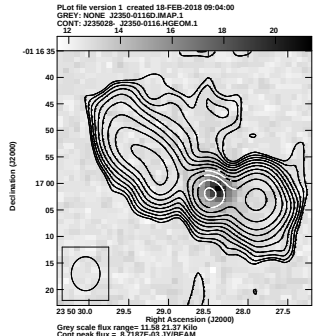
PLot file version 1 created 18-FEB-2018 09:04:00
GREY: NONE J2350-0116D.IMAP.1
CONT: J235028- J2350-0116.HGEOM.1
Declination (J2000)
Right Ascension (J2000)
Grey scale flux range= 11.58 21.37 Kilo
Cont peak flux = 8.7187E-03 JY/BEAM
Levs = 2.500E-04 * (1, 1.400, 2, 2.800, 4, 5.600, 8, 11, 16, 23, 32, 45, 64, 90, 128, 181, 256, 362, 512, 724, 1024)

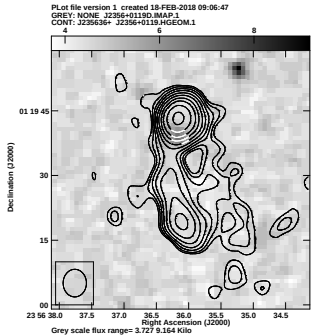
PLot file version 1 created 18-FEB-2018 09:06:47
GREY: NONE J2356+0119D.IMAP.1
CONT: J235636+ J2356+0119.HGEOM.1
Declination (J2000)
Right Ascension (J2000)
Grey scale flux range= 3.727 9.164 Kilo
Cont peak flux = 6.3902E-03 JY/BEAM
Levs = 2.500E-04 * (1, 1.400, 2, 2.800, 4, 5.600, 8, 11, 16, 23, 32, 45, 64, 90, 128, 181, 256, 362, 512, 724, 1024)

Appendix B

All contour images of FIRST NAT sources

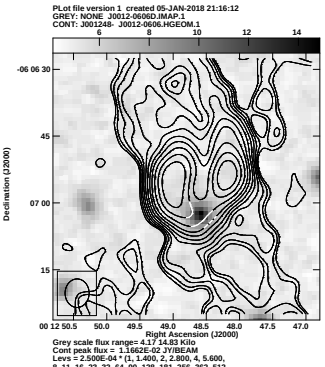
PLot file version 1 created 05-JAN-2018 21:16:12
GREY: NONE J0012-0606D.IMAP.1
CONT: J001248- J0012-0606.HGEOM.1
Declination (J2000)
Right Ascension (J2000)
Grey scale flux range= 4.17 14.83 Kilo
Cont peak flux = 1.1662E-02 JYBEAM
Levs = 2.500E-04 * (1, 1.400, 2, 2.800, 4, 5.600, 8, 11, 16, 23, 32, 64, 90, 128, 181, 256, 362, 512, 724, 1024)

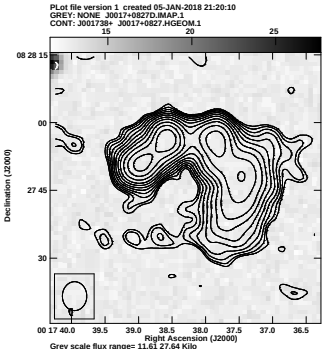
PLot file version 1 created 05-JAN-2018 21:20:10
GREY: NONE J0017+0827D.IMAP.1
CONT: J001738+ J0017+0827.HGEOM.1
Declination (J2000)
Right Ascension (J2000)
Grey scale flux range= 11.61 27.64 Kilo
Cont peak flux = 1.0925E-02 JYBEAM
Levs = 2.500E-04 * (1, 1.400, 2, 2.800, 4, 5.600, 8, 11, 16, 23, 32, 64, 90, 128, 181, 256, 362, 512, 724, 1024)

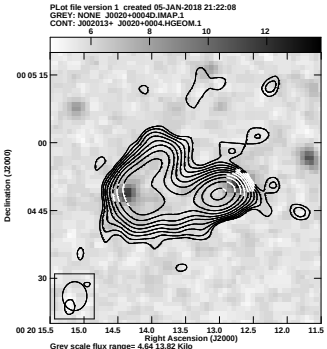
PLot file version 1 created 05-JAN-2018 21:22:08
GREY: NONE J0020+0004D.IMAP.1
CONT: J002013+ J0020+0004.HGEOM.1
Declination (J2000)
Right Ascension (J2000)
Grey scale flux range= 4.64 13.82 Kilo
Cont peak flux = 6.3899E-03 JYBEAM
Levs = 2.500E-04 * (1, 1.400, 2, 2.800, 4, 5.600, 8, 11, 16, 23, 32, 64, 90, 128, 181, 256, 362, 512, 724, 1024)

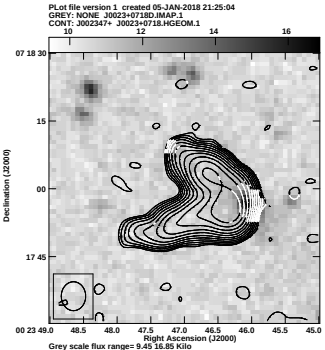
PLot file version 1 created 05-JAN-2018 21:25:04
GREY: NONE J0023+0718D.IMAP.1
CONT: J002347+ J0023+0718.HGEOM.1
Declination (J2000)
Right Ascension (J2000)
Grey scale flux range= 9.45 16.85 Kilo
Cont peak flux = 1.2135E-02 JYBEAM
Levs = 2.500E-04 * (1, 1.400, 2, 2.800, 4, 5.600, 8, 11, 16, 23, 32, 64, 90, 128, 181, 256, 362, 512, 724, 1024)

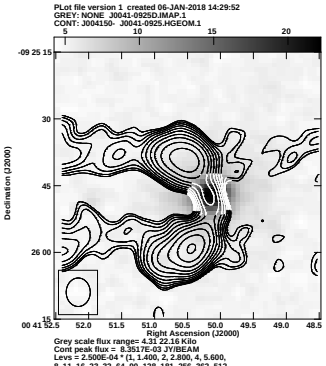
PLot file version 1 created 06-JAN-2018 14:29:52
GREY: NONE J0041-0925D.IMAP.1
CONT: J004150- J0041-0925.HGEOM.1
Declination (J2000)
Right Ascension (J2000)
Grey scale flux range= 4.31 22.16 Kilo
Cont peak flux = 8.3517E-03 JYBEAM
Levs = 2.500E-04 * (1, 1.400, 2, 2.800, 4, 5.600, 8, 11, 16, 23, 32, 64, 90, 128, 181, 256, 362, 512, 724, 1024)

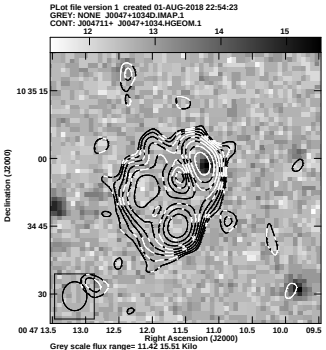
PLot file version 1 created 01-AUG-2018 22:54:23
GREY: NONE J0047+1034D.IMAP.1
CONT: J004711+ J0047+1034.HGEOM.1
Declination (J2000)
Right Ascension (J2000)
Grey scale flux range= 11.42 15.51 Kilo
Cont peak flux = 3.8412E-03 JYBEAM
Levs = 2.500E-04 * (1, 1.400, 2, 2.800, 4, 5.600, 8, 11, 16, 23, 32, 45, 64, 90, 128, 181, 256, 362, 512, 724, 1024)

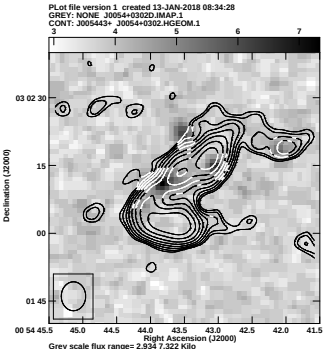
PLot file version 1 created 13-JAN-2018 08:34:28
GREY: NONE J0054+0302D.IMAP.1
CONT: J005443+ J0054+0302.HGEOM.1
Declination (J2000)
Right Ascension (J2000)
Grey scale flux range= 2.934 7.322 Kilo
Cont peak flux = 3.7787E-03 JYBEAM
Levs = 2.500E-04 * (1, 1.400, 2, 2.800, 4, 5.600, 8, 11, 16, 23, 32, 64, 90, 128, 181, 256, 362, 512, 724, 1024)

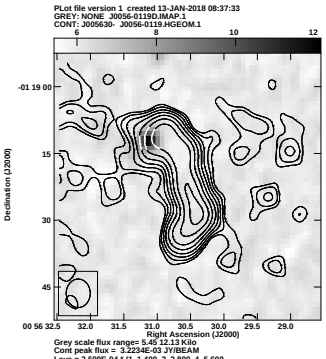
PLot file version 1 created 13-JAN-2018 08:37:33
GREY: NONE J0056-0119D.IMAP.1
CONT: J005630- J0056-0119.HGEOM.1
Declination (J2000)
Right Ascension (J2000)
Grey scale flux range= 5.45 12.13 Kilo
Cont peak flux = 3.2234E-03 JYBEAM
Levs = 2.500E-04 * (1, 1.400, 2, 2.800, 4, 5.600, 8, 11, 16, 23, 32, 64, 90, 128, 181, 256, 362, 512, 724, 1024)

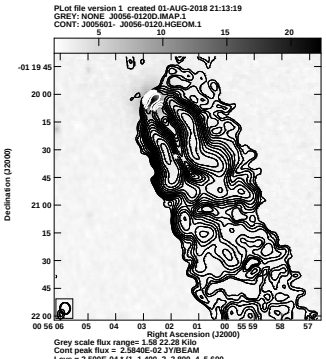
PLot file version 1 created 01-AUG-2018 21:13:19
GREY: NONE J0056-0120D.IMAP.1
CONT: J005601- J0056-0120.HGEOM.1
Declination (J2000)
Right Ascension (J2000)
Grey scale flux range= 1.58 22.28 Kilo
Cont peak flux = 2.5840E-02 JYBEAM
Levs = 2.500E-04 * (1, 1.400, 2, 2.800, 4, 5.600, 8, 11, 16, 23, 32, 45, 64, 90, 128, 181, 256, 362, 512, 724, 1024)

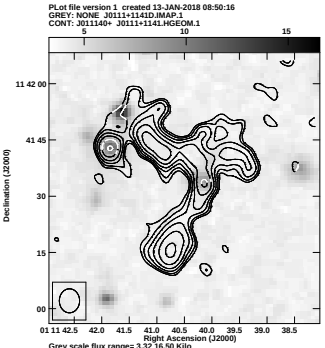
PLot file version 1 created 13-JAN-2018 08:50:16
GREY: NONE J0111+1141D.IMAP.1
CONT: J011140+ J0111+1141.HGEOM.1
Declination (J2000)
Right Ascension (J2000)
Grey scale flux range= 3.32 16.50 Kilo
Cont peak flux = 1.7368E-03 JYBEAM
Levs = 2.500E-04 * (1, 1.400, 2, 2.800, 4, 5.600, 8, 11, 16, 23, 32, 64, 90, 128, 181, 256, 362, 512, 724, 1024)

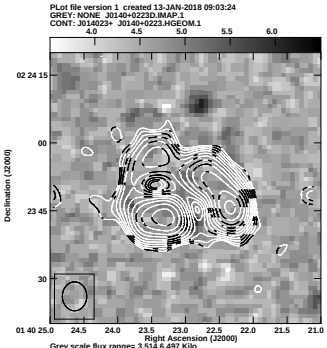
PLot file version 1 created 13-JAN-2018 09:03:24
GREY: NONE J0140+0223D.IMAP.1
CONT: J014023+ J0140+0223.HGEOM.1
Declination (J2000)
Right Ascension (J2000)
Grey scale flux range= 3.514 6.497 Kilo
Cont peak flux = 8.3378E-03 JYBEAM
Levs = 2.500E-04 * (1, 1.400, 2, 2.800, 4, 5.600, 8, 11, 16, 23, 32, 64, 90, 128, 181, 256, 362, 512, 724, 1024)

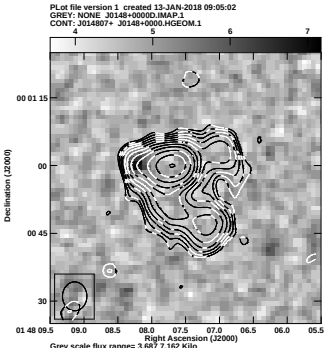
PLot file version 1 created 13-JAN-2018 09:05:02
GREY: NONE J0148+0000D.IMAP.1
CONT: J014807+ J0148+0000.HGEOM.1
Declination (J2000)
Right Ascension (J2000)
Grey scale flux range= 3.687 7.162 Kilo
Cont peak flux = 8.0780E-03 JYBEAM
Levs = 2.500E-04 * (1, 1.400, 2, 2.800, 4, 5.600, 8, 11, 16, 23, 32, 64, 90, 128, 181, 256, 362, 512, 724, 1024)

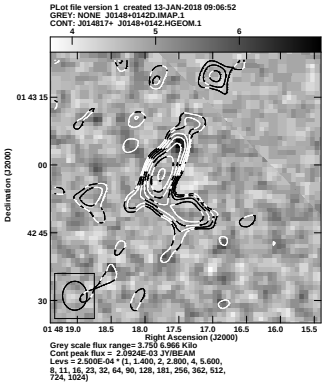
PLot file version 1 created 13-JAN-2018 09:06:52
GREY: NONE J0148+0142D.IMAP.1
CONT: J0148I7+ J0148+0142.HGEOM.1
Declination (J2000)
Right Ascension (J2000)
Grey scale flux range= 3.750 6.966 Kilo
Cont peak flux = 2.0924E-03 JY/BEAM
Levs = 2.500E-04 * (1, 1.400, 2, 2.800, 4, 5.600, 8, 11, 16, 23, 32, 64, 90, 128, 181, 256, 362, 512, 724, 1024)

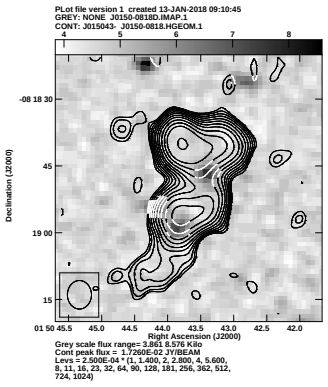
PLot file version 1 created 13-JAN-2018 09:10:45
GREY: NONE J0150-0818D.IMAP.1
CONT: J015043- J0150-0818.HGEOM.1
Declination (J2000)
Right Ascension (J2000)
Grey scale flux range= 3.861 8.576 Kilo
Cont peak flux = 1.7260E-02 JY/BEAM
Levs = 2.500E-04 * (1, 1.400, 2, 2.800, 4, 5.600, 8, 11, 16, 23, 32, 64, 90, 128, 181, 256, 362, 512, 724, 1024)

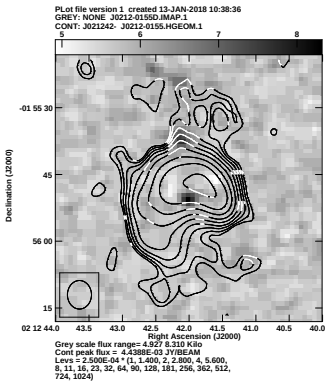
PLot file version 1 created 13-JAN-2018 10:38:36
GREY: NONE J0212-0155D.IMAP.1
CONT: J021242- J0212-0155.HGEOM.1
Declination (J2000)
Right Ascension (J2000)
Grey scale flux range= 4.927 8.310 Kilo
Cont peak flux = 4.4388E-03 JY/BEAM
Levs = 2.500E-04 * (1, 1.400, 2, 2.800, 4, 5.600, 8, 11, 16, 23, 32, 64, 90, 128, 181, 256, 362, 512, 724, 1024)

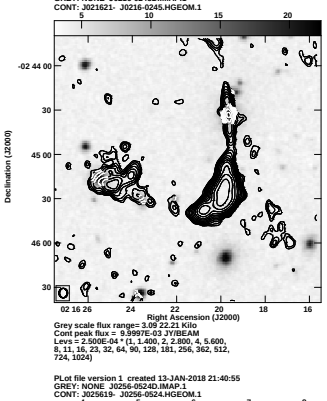
PLot file version 1 created 13-JAN-2018 10:42:10
GREY: NONE J0216-0245D.IMAP.1
CONT: J021621- J0216-0245.HGEOM.1
Declination (J2000)
Right Ascension (J2000)
Grey scale flux range= 3.09 22.21 Kilo
Cont peak flux = 9.9997E-03 JY/BEAM
Levs = 2.500E-04 * (1, 1.400, 2, 2.800, 4, 5.600, 8, 11, 16, 23, 32, 64, 90, 128, 181, 256, 362, 512, 724, 1024)

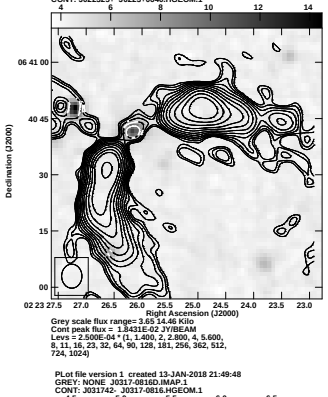
PLot file version 1 created 13-JAN-2018 10:43:35
GREY: NONE J0223+0640D.IMAP.1
CONT: J022325+ J0223+0640.HGEOM.1
Declination (J2000)
Right Ascension (J2000)
Grey scale flux range= 3.65 14.46 Kilo
Cont peak flux = 1.8431E-02 JY/BEAM
Levs = 2.500E-04 * (1, 1.400, 2, 2.800, 4, 5.600, 8, 11, 16, 23, 32, 64, 90, 128, 181, 256, 362, 512, 724, 1024)

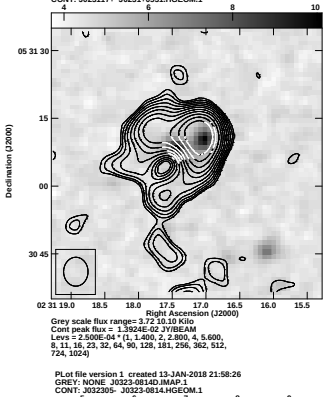
PLot file version 1 created 13-JAN-2018 10:48:23
GREY: NONE J0231+0531D.IMAP.1
CONT: J023117+ J0231+0531.HGEOM.1
Declination (J2000)
Right Ascension (J2000)
Grey scale flux range= 3.72 10.10 Kilo
Cont peak flux = 1.3924E-02 JY/BEAM
Levs = 2.500E-04 * (1, 1.400, 2, 2.800, 4, 5.600, 8, 11, 16, 23, 32, 64, 90, 128, 181, 256, 362, 512, 724, 1024)

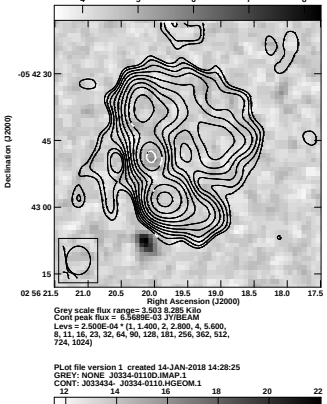
PLot file version 1 created 13-JAN-2018 21:40:55
GREY: NONE J0256-0524D.IMAP.1
CONT: J025619- J0256-0524.HGEOM.1
Declination (J2000)
Right Ascension (J2000)
Grey scale flux range= 3.503 8.285 Kilo
Cont peak flux = 6.5889E-03 JY/BEAM
Levs = 2.500E-04 * (1, 1.400, 2, 2.800, 4, 5.600, 8, 11, 16, 23, 32, 64, 90, 128, 181, 256, 362, 512, 724, 1024)

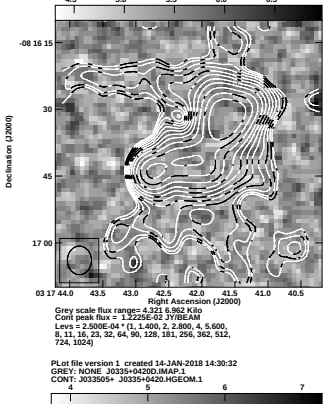
PLot file version 1 created 13-JAN-2018 21:49:48
GREY: NONE J0317-0816D.IMAP.1
CONT: J031742- J0317+0816.HGEOM.1
Declination (J2000)
Right Ascension (J2000)
Grey scale flux range= 4.321 6.962 Kilo
Cont peak flux = 1.3225E-02 JY/BEAM
Levs = 2.500E-04 * (1, 1.400, 2, 2.800, 4, 5.600, 8, 11, 16, 23, 32, 64, 90, 128, 181, 256, 362, 512, 724, 1024)

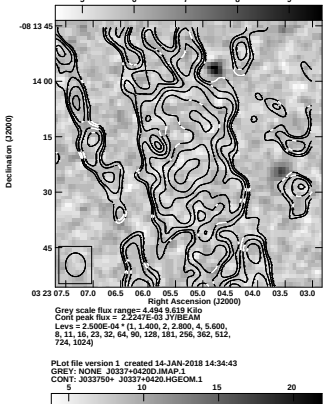
PLot file version 1 created 13-JAN-2018 21:58:26
GREY: NONE J0323-0814D.IMAP.1
CONT: J032305- J0323-0814.HGEOM.1
Declination (J2000)
Right Ascension (J2000)
Grey scale flux range= 4.494 9.619 Kilo
Cont peak flux = 2.2347E-03 JY/BEAM
Levs = 2.500E-04 * (1, 1.400, 2, 2.800, 4, 5.600, 8, 11, 16, 23, 32, 64, 90, 128, 181, 256, 362, 512, 724, 1024)

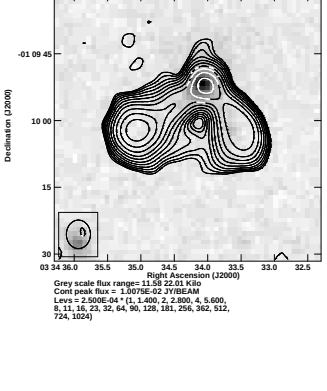
PLot file version 1 created 14-JAN-2018 14:28:25
GREY: NONE J0334-0110D.IMAP.1
CONT: J033434- J0334-0110.HGEOM.1
Declination (J2000)
Right Ascension (J2000)
Grey scale flux range= 11.58 22.01 Kilo
Cont peak flux = 1.0075E-02 JY/BEAM
Levs = 2.500E-04 * (1, 1.400, 2, 2.800, 4, 5.600, 8, 11, 16, 23, 32, 64, 90, 128, 181, 256, 362, 512, 724, 1024)

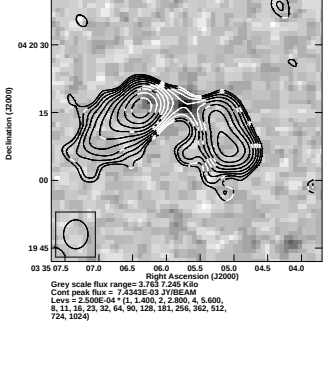
PLot file version 1 created 14-JAN-2018 14:30:32
GREY: NONE J0335+0420D.IMAP.1
CONT: J033505+ J0335+0420.HGEOM.1
Declination (J2000)
Right Ascension (J2000)
Grey scale flux range= 3.763 7.245 Kilo
Cont peak flux = 7.2343E-03 JY/BEAM
Levs = 2.500E-04 * (1, 1.400, 2, 2.800, 4, 5.600, 8, 11, 16, 23, 32, 64, 90, 128, 181, 256, 362, 512, 724, 1024)

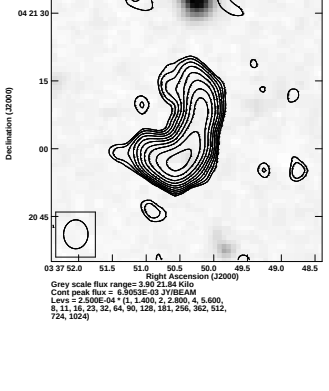
PLot file version 1 created 14-JAN-2018 14:34:43
GREY: NONE J0337+0420D.IMAP.1
CONT: J033750+ J0337+0420.HGEOM.1
Declination (J2000)
Right Ascension (J2000)
Grey scale flux range= 3.90 21.84 Kilo
Cont peak flux = 6.9053E-03 JY/BEAM
Levs = 2.500E-04 * (1, 1.400, 2, 2.800, 4, 5.600, 8, 11, 16, 23, 32, 64, 90, 128, 181, 256, 362, 512, 724, 1024)

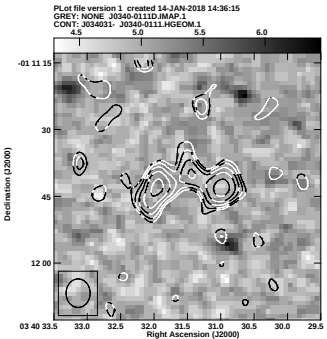

Grey scale flux range= 4.309 6.444 Kilo
Cont peak flux = 1.2082E-03 JY/BEAM
Levs = 2.500E-04 * (1, 1.400, 2, 2.800, 4, 5.600, 8, 11, 16, 23, 32, 64, 90, 128, 181, 256, 362, 512, 724, 1024)

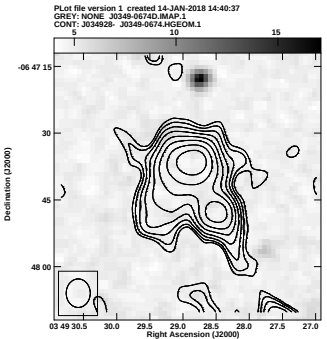

Grey scale flux range= 4.05 17.07 Kilo
Cont peak flux = 3.5671E-03 JY/BEAM
Levs = 2.500E-04 * (1, 1.400, 2, 2.800, 4, 5.600, 8, 11, 16, 23, 32, 64, 90, 128, 181, 256, 362, 512, 724, 1024)

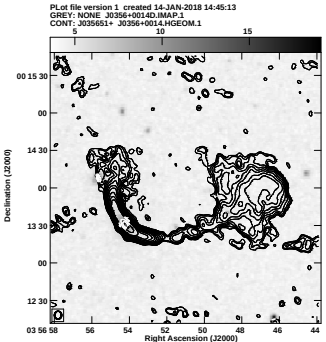

Grey scale flux range= 3.63 19.06 Kilo
Cont peak flux = 2.7392E-02 JY/BEAM
Levs = 2.500E-04 * (1, 1.400, 2, 2.800, 4, 5.600, 8, 11, 16, 23, 32, 64, 90, 128, 181, 256, 362, 512, 724, 1024)

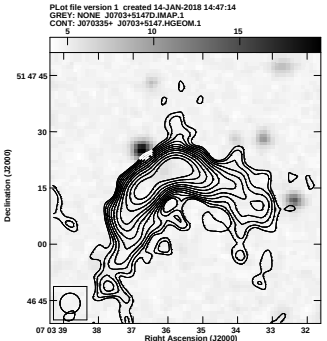

Grey scale flux range= 4.03 19.65 Kilo
Cont peak flux = 1.4489E-02 JY/BEAM
Levs = 2.500E-04 * (1, 1.400, 2, 2.800, 4, 5.600, 8, 11, 16, 23, 32, 64, 90, 128, 181, 256, 362, 512, 724, 1024)

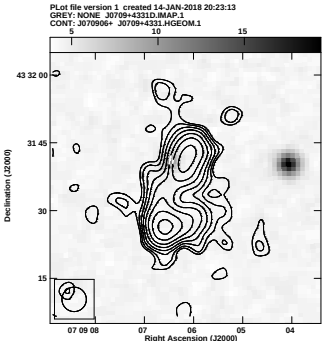

Grey scale flux range= 3.80 19.38 Kilo
Cont peak flux = 3.0967E-03 JY/BEAM
Levs = 2.500E-04 * (1, 1.400, 2, 2.800, 4, 5.600, 8, 11, 16, 23, 32, 64, 90, 128, 181, 256, 362, 512, 724, 1024)

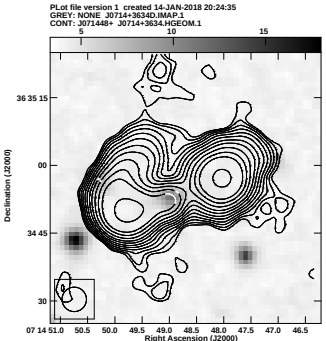

Grey scale flux range= 3.38 17.96 Kilo
Cont peak flux = 2.0534E-02 JY/BEAM
Levs = 2.500E-04 * (1, 1.400, 2, 2.800, 4, 5.600, 8, 11, 16, 23, 32, 64, 90, 128, 181, 256, 362, 512, 724, 1024)

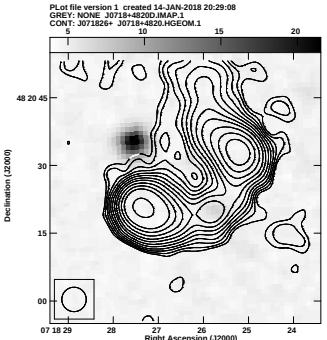

Grey scale flux range= 3.88 21.48 Kilo
Cont peak flux = 2.0120E-02 JY/BEAM
Levs = 2.500E-04 * (1, 1.400, 2, 2.800, 4, 5.600, 8, 11, 16, 23, 32, 64, 90, 128, 181, 256, 362, 512, 724, 1024)

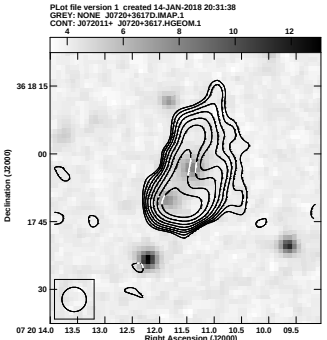

Grey scale flux range= 3.42 13.03 Kilo
Cont peak flux = 3.9398E-03 JY/BEAM
Levs = 2.500E-04 * (1, 1.400, 2, 2.800, 4, 5.600, 8, 11, 16, 23, 32, 64, 90, 128, 181, 256, 362, 512, 724, 1024)

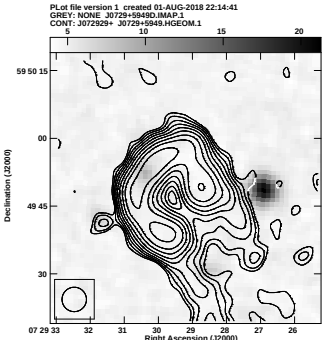

Grey scale flux range= 3.94 21.24 Kilo
Cont peak flux = 5.3914E-03 JY/BEAM
Levs = 2.500E-04 * (1, 1.400, 2, 2.800, 4, 5.600, 8, 11, 16, 23, 32, 45, 64, 90, 128, 181, 256, 362, 512, 724, 1024)

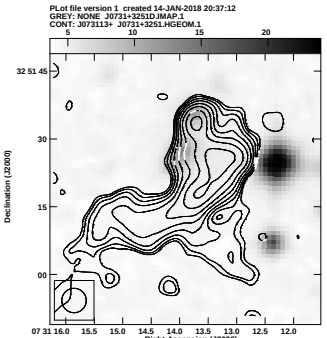

Grey scale flux range= 3.72 23.91 Kilo
Cont peak flux = 3.2577E-03 JY/BEAM
Levs = 2.500E-04 * (1, 1.400, 2, 2.800, 4, 5.600, 8, 11, 16, 23, 32, 64, 90, 128, 181, 256, 362, 512, 724, 1024)

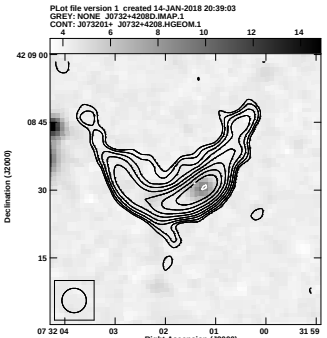

Grey scale flux range= 3.50 14.81 Kilo
Cont peak flux = 4.0288E-03 JY/BEAM
Levs = 2.500E-04 * (1, 1.400, 2, 2.800, 4, 5.600, 8, 11, 16, 23, 32, 64, 90, 128, 181, 256, 362, 512, 724, 1024)

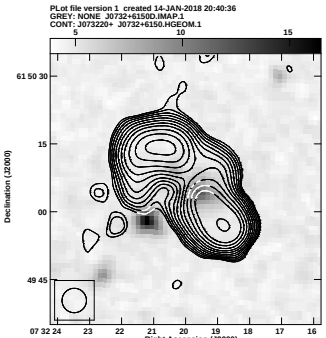

Grey scale flux range= 3.86 16.43 Kilo
Cont peak flux = 1.7267E-02 JY/BEAM
Levs = 2.500E-04 * (1, 1.400, 2, 2.800, 4, 5.600, 8, 11, 16, 23, 32, 64, 90, 128, 181, 256, 362, 512, 724, 1024)

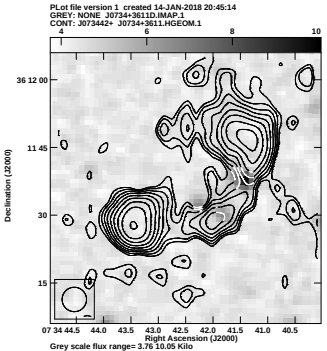
PLot file version 1 created 14-JAN-2018 20:45:14
GREY: NONE J0734+3611D.IMAP.1
CONT: J073442+ J0734+3611.HGEOM.1
Declination (J2000)
Right Ascension (J2000)
Grey scale flux range= 3.76 10.05 Kilo
Cont peak flux = 4.1063E-03 JY/BEAM
Levs = 2.500E-04 * (1, 1.400, 2, 2.800, 4, 5.600, 8, 11, 16, 23, 32, 64, 90, 128, 181, 256, 362, 512, 724, 1024)

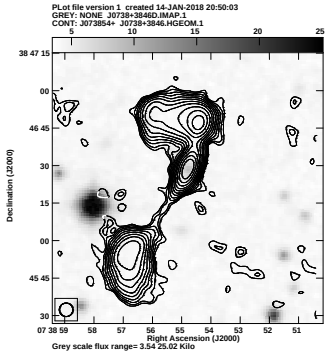
PLot file version 1 created 14-JAN-2018 20:50:03
GREY: NONE J0738+3846D.IMAP.1
CONT: J073854+ J0738+3846.HGEOM.1
Declination (J2000)
Right Ascension (J2000)
Grey scale flux range= 3.54 25.02 Kilo
Cont peak flux = 1.1385E-03 JY/BEAM
Levs = 2.500E-04 * (1, 1.400, 2, 2.800, 4, 5.600, 8, 11, 16, 23, 32, 64, 90, 128, 181, 256, 362, 512, 724, 1024)

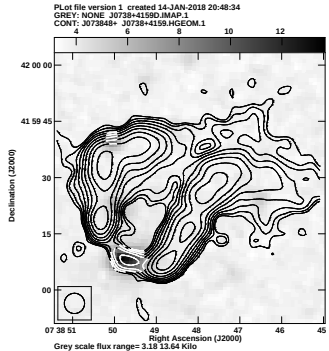
PLot file version 1 created 14-JAN-2018 20:48:34
GREY: NONE J0738+4159D.IMAP.1
CONT: J073848+ J0738+4159.HGEOM.1
Declination (J2000)
Right Ascension (J2000)
Grey scale flux range= 3.18 13.64 Kilo
Cont peak flux = 4.7710E-03 JY/BEAM
Levs = 2.500E-04 * (1, 1.400, 2, 2.800, 4, 5.600, 8, 11, 16, 23, 32, 64, 90, 128, 181, 256, 362, 512, 724, 1024)

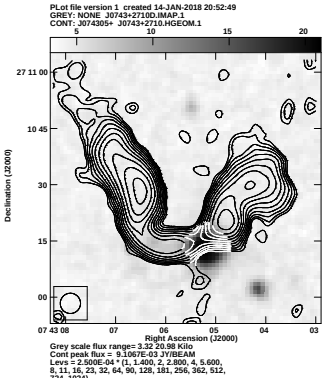
PLot file version 1 created 14-JAN-2018 20:52:49
GREY: NONE J0743+2710D.IMAP.1
CONT: J074305+ J0743+2710.HGEOM.1
Declination (J2000)
Right Ascension (J2000)
Grey scale flux range= 3.32 20.98 Kilo
Cont peak flux = 9.1067E-03 JY/BEAM
Levs = 2.500E-04 * (1, 1.400, 2, 2.800, 4, 5.600, 8, 11, 16, 23, 32, 64, 90, 128, 181, 256, 362, 512, 724, 1024)

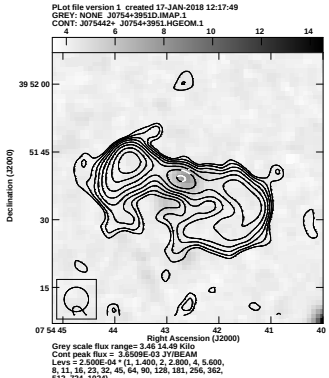
PLot file version 1 created 17-JAN-2018 12:17:49
GREY: NONE J0754+3951D.IMAP.1
CONT: J075442+ J0754+3951.HGEOM.1
Declination (J2000)
Right Ascension (J2000)
Grey scale flux range= 3.46 14.49 Kilo
Cont peak flux = 3.8509E-03 JY/BEAM
Levs = 2.500E-04 * (1, 1.400, 2, 2.800, 4, 5.600, 8, 11, 16, 23, 32, 45, 64, 90, 128, 181, 256, 362, 512, 724, 1024)

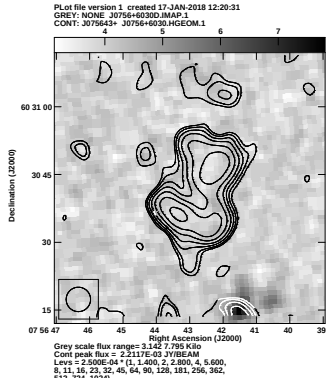
PLot file version 1 created 17-JAN-2018 12:20:31
GREY: NONE J0756+6030D.IMAP.1
CONT: J075643+ J0756+6030.HGEOM.1
Declination (J2000)
Right Ascension (J2000)
Grey scale flux range= 3.142 7.795 Kilo
Cont peak flux = 2.2117E-03 JY/BEAM
Levs = 2.500E-04 * (1, 1.400, 2, 2.800, 4, 5.600, 8, 11, 16, 23, 32, 45, 64, 90, 128, 181, 256, 362, 512, 724, 1024)

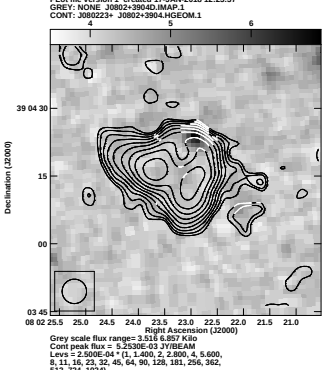
PLot file version 1 created 17-JAN-2018 12:23:37
GREY: NONE J0802+3904D.IMAP.1
CONT: J080223+ J0802+3904.HGEOM.1
Declination (J2000)
Right Ascension (J2000)
Grey scale flux range= 3.516 6.857 Kilo
Cont peak flux = 5.2530E-03 JY/BEAM
Levs = 2.500E-04 * (1, 1.400, 2, 2.800, 4, 5.600, 8, 11, 16, 23, 32, 45, 64, 90, 128, 181, 256, 362, 512, 724, 1024)

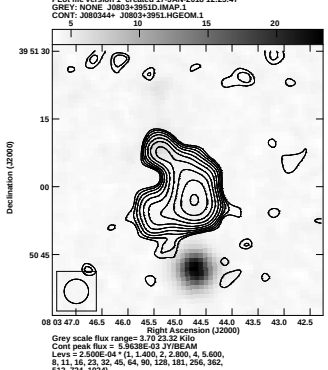
PLot file version 1 created 17-JAN-2018 12:25:47
GREY: NONE J0803+3951D.IMAP.1
CONT: J080344+ J0803+3951.HGEOM.1
Declination (J2000)
Right Ascension (J2000)
Grey scale flux range= 3.70 23.32 Kilo
Cont peak flux = 5.3638E-03 JY/BEAM
Levs = 2.500E-04 * (1, 1.400, 2, 2.800, 4, 5.600, 8, 11, 16, 23, 32, 45, 64, 90, 128, 181, 256, 362, 512, 724, 1024)

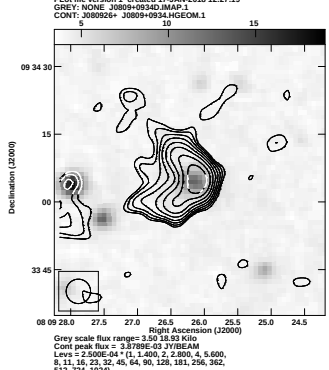
PLot file version 1 created 17-JAN-2018 12:27:19
GREY: NONE J0809+0934D.IMAP.1
CONT: J080926+ J0809+0934.HGEOM.1
Declination (J2000)
Right Ascension (J2000)
Grey scale flux range= 3.50 18.93 Kilo
Cont peak flux = 3.8788E-03 JY/BEAM
Levs = 2.500E-04 * (1, 1.400, 2, 2.800, 4, 5.600, 8, 11, 16, 23, 32, 45, 64, 90, 128, 181, 256, 362, 512, 724, 1024)

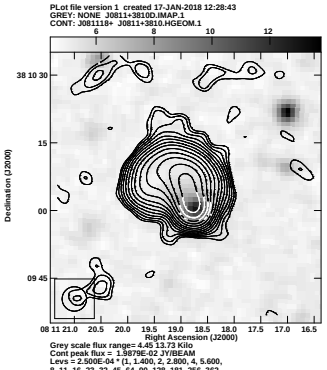
PLot file version 1 created 17-JAN-2018 12:28:43
GREY: NONE J0811+3810D.IMAP.1
CONT: J081118+ J0811+3810.HGEOM.1
Declination (J2000)
Right Ascension (J2000)
Grey scale flux range= 4.45 13.73 Kilo
Cont peak flux = 1.9879E-02 JY/BEAM
Levs = 2.500E-04 * (1, 1.400, 2, 2.800, 4, 5.600, 8, 11, 16, 23, 32, 45, 64, 90, 128, 181, 256, 362, 512, 724, 1024)

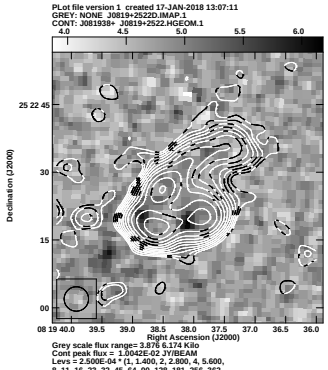
PLot file version 1 created 17-JAN-2018 13:07:11
GREY: NONE J0819+2522D.IMAP.1
CONT: J081938+ J0819+2522.HGEOM.1
Declination (J2000)
Right Ascension (J2000)
Grey scale flux range= 3.876 6.174 Kilo
Cont peak flux = 1.0042E-02 JY/BEAM
Levs = 2.500E-04 * (1, 1.400, 2, 2.800, 4, 5.600, 8, 11, 16, 23, 32, 45, 64, 90, 128, 181, 256, 362, 512, 724, 1024)

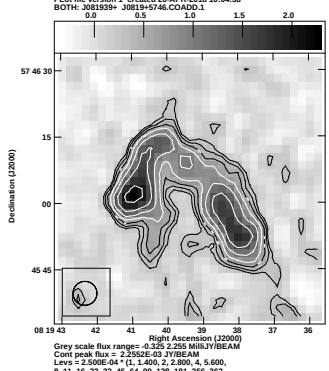
PLot file version 1 created 20-APR-2018 10:04:38
BOTH: J081939+ J0819+5746.COADD.1
Declination (J2000)
Right Ascension (J2000)
Grey scale flux range= -0.325 2.255 MilliJY/BEAM
Cont peak flux = 2.2552E-03 JY/BEAM
Levs = 2.500E-04 * (1, 1.400, 2, 2.800, 4, 5.600, 8, 11, 16, 23, 32, 45, 64, 90, 128, 181, 256, 362, 512, 724, 1024)

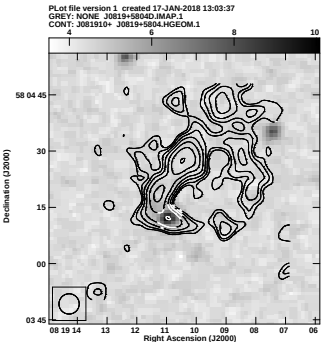
PLot file version 1 created 17-JAN-2018 13:03:37
GREY: NONE J0819+5804D.IMAP.1
CONT: J081910+ J0819+5804.HGEOM.1
Declination (J2000)
Right Ascension (J2000)
Grey scale flux range= 3.53 10.06 Kilo
Cont peak flux = 2.0212E-03 JY/BEAM
Levs = 2.500E-04 * (1, 1.400, 2, 2.800, 4, 5.600, 8, 11, 16, 23, 32, 45, 64, 90, 128, 181, 256, 362, 512, 724, 1024)

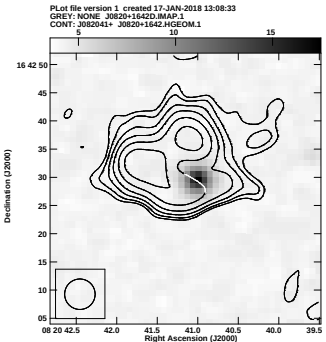
PLot file version 1 created 17-JAN-2018 13:08:33
GREY: NONE J0820+1642D.IMAP.1
CONT: J082041+ J0820+1642.HGEOM.1
Declination (J2000)
Right Ascension (J2000)
Grey scale flux range= 3.58 17.44 Kilo
Cont peak flux = 1.8965E-03 JY/BEAM
Levs = 2.500E-04 * (1, 1.400, 2, 2.800, 4, 5.600, 8, 11, 16, 23, 32, 45, 64, 90, 128, 181, 256, 362, 512, 724, 1024)

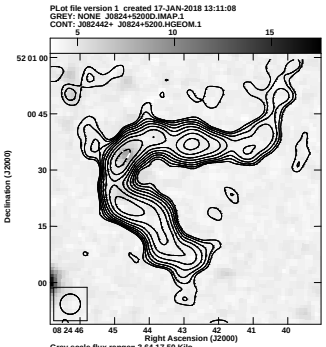
PLot file version 1 created 17-JAN-2018 13:11:08
GREY: NONE J0824+5200D.IMAP.1
CONT: J082442+ J0824+5200.HGEOM.1
Declination (J2000)
Right Ascension (J2000)
Grey scale flux range= 3.64 17.50 Kilo
Cont peak flux = 4.4685E-03 JY/BEAM
Levs = 2.500E-04 * (1, 1.400, 2, 2.800, 4, 5.600, 8, 11, 16, 23, 32, 45, 64, 90, 128, 181, 256, 362, 512, 724, 1024)

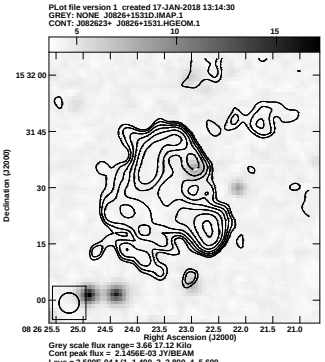
PLot file version 1 created 17-JAN-2018 13:14:30
GREY: NONE J0826+1531D.IMAP.1
CONT: J082623+ J0826+1531.HGEOM.1
Declination (J2000)
Right Ascension (J2000)
Grey scale flux range= 3.66 17.12 Kilo
Cont peak flux = 2.1456E-03 JY/BEAM
Levs = 2.500E-04 * (1, 1.400, 2, 2.800, 4, 5.600, 8, 11, 16, 23, 32, 45, 64, 90, 128, 181, 256, 362, 512, 724, 1024)

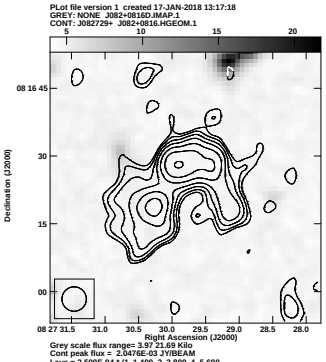
PLot file version 1 created 17-JAN-2018 13:17:18
GREY: NONE J082+0816D.IMAP.1
CONT: J082729+ J082+0816.HGEOM.1
Declination (J2000)
Right Ascension (J2000)
Grey scale flux range= 3.97 21.69 Kilo
Cont peak flux = 2.9476E-03 JY/BEAM
Levs = 2.500E-04 * (1, 1.400, 2, 2.800, 4, 5.600, 8, 11, 16, 23, 32, 45, 64, 90, 128, 181, 256, 362, 512, 724, 1024)

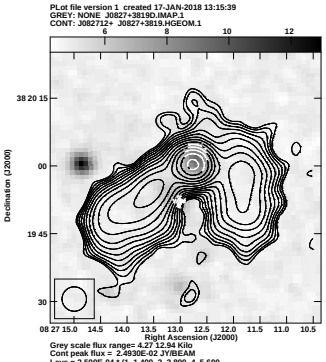
PLot file version 1 created 17-JAN-2018 13:15:39
GREY: NONE J0827+3819D.IMAP.1
CONT: J082712+ J0827+3819.HGEOM.1
Declination (J2000)
Right Ascension (J2000)
Grey scale flux range= 4.27 12.94 Kilo
Cont peak flux = 2.4930E-02 JY/BEAM
Levs = 2.500E-04 * (1, 1.400, 2, 2.800, 4, 5.600, 8, 11, 16, 23, 32, 45, 64, 90, 128, 181, 256, 362, 512, 724, 1024)

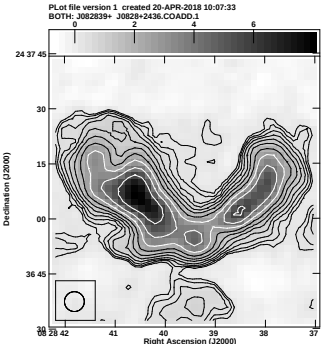
PLot file version 1 created 20-APR-2018 10:07:33
BOTH: J082839+ J0828+2436.COADD.1
Declination (J2000)
Right Ascension (J2000)
Grey scale flux range= -0.645 7.998 MilliJY/BEAM
Cont peak flux = 7.9982E-03 JY/BEAM
Levs = 2.500E-04 * (1, 1.400, 2, 2.800, 4, 5.600, 8, 11, 16, 23, 32, 45, 64, 90, 128, 181, 256, 362, 512, 724, 1024)

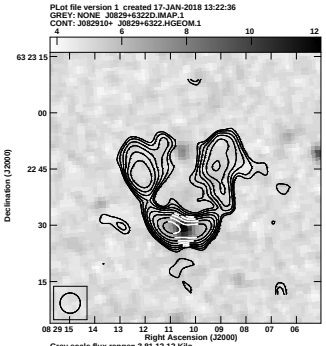
PLot file version 1 created 17-JAN-2018 13:22:36
GREY: NONE J0829+6322D.IMAP.1
CONT: J082910+ J0829+6322.HGEOM.1
Declination (J2000)
Right Ascension (J2000)
Grey scale flux range= 3.81 12.12 Kilo
Cont peak flux = 3.3267E-03 JY/BEAM
Levs = 2.500E-04 * (1, 1.400, 2, 2.800, 4, 5.600, 8, 11, 16, 23, 32, 45, 64, 90, 128, 181, 256, 362, 512, 724, 1024)

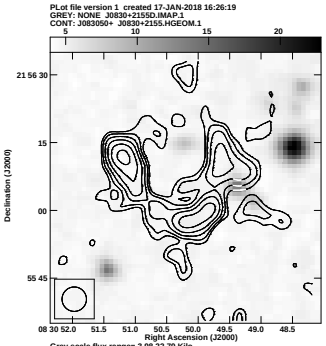
PLot file version 1 created 17-JAN-2018 16:26:19
GREY: NONE J0830+2155D.IMAP.1
CONT: J083050+ J0830+2155.HGEOM.1
Declination (J2000)
Right Ascension (J2000)
Grey scale flux range= 3.88 22.79 Kilo
Cont peak flux = 1.5844E-03 JY/BEAM
Levs = 2.500E-04 * (1, 1.400, 2, 2.800, 4, 5.600, 8, 11, 16, 23, 32, 45, 64, 90, 128, 181, 256, 362, 512, 724, 1024)

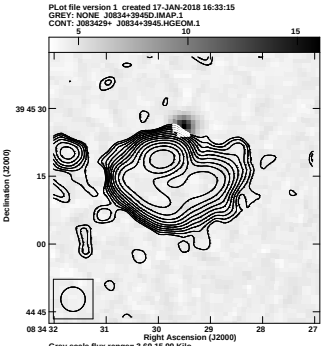
PLot file version 1 created 17-JAN-2018 16:33:15
GREY: NONE J0834+3945D.IMAP.1
CONT: J083429+ J0834+3945.HGEOM.1
Declination (J2000)
Right Ascension (J2000)
Grey scale flux range= 3.69 15.99 Kilo
Cont peak flux = 1.5072E-02 JY/BEAM
Levs = 2.500E-04 * (1, 1.400, 2, 2.800, 4, 5.600, 8, 11, 16, 23, 32, 45, 64, 90, 128, 181, 256, 362, 512, 724, 1024)

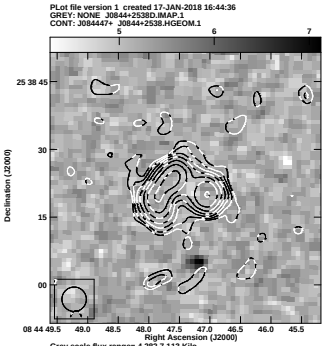
PLot file version 1 created 17-JAN-2018 16:44:36
GREY: NONE J0844+2538D.IMAP.1
CONT: J084447+ J0844+2538.HGEOM.1
Declination (J2000)
Right Ascension (J2000)
Grey scale flux range= 4.282 7.113 Kilo
Cont peak flux = 2.3682E-03 JY/BEAM
Levs = 2.500E-04 * (1, 1.400, 2, 2.800, 4, 5.600, 8, 11, 16, 23, 32, 45, 64, 90, 128, 181, 256, 362, 512, 724, 1024)

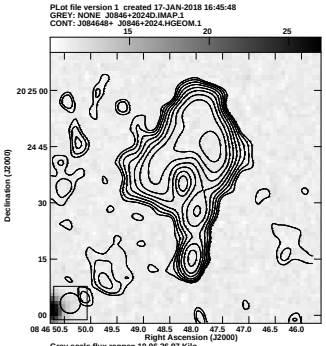
PLot file version 1 created 17-JAN-2018 16:45:48
GREY: NONE J0846+2024D.IMAP.1
CONT: J084648+ J0846+2024.HGEOM.1
Declination (J2000)
Right Ascension (J2000)
Grey scale flux range= 10.06 26.97 Kilo
Cont peak flux = 5.2246E-03 JY/BEAM
Levs = 2.500E-04 * (1, 1.400, 2, 2.800, 4, 5.600, 8, 11, 16, 23, 32, 45, 64, 90, 128, 181, 256, 362, 512, 724, 1024)

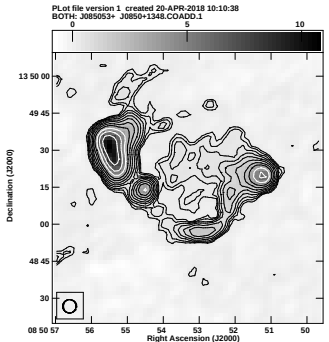
PLot file version 1 created 20-APR-2018 10:10:38
BOTH: J085053+ J0850+1348.COADD.1
Declination (J2000)
Right Ascension (J2000)
Grey scale flux range= -0.69 10.74 MilliJY/BEAM
Cont peak flux = 1.0744E-02 JY/BEAM
Levs = 2.500E-04 * (1, 1.400, 2, 2.800, 4, 5.600, 8, 11, 16, 23, 32, 45, 64, 90, 128, 181, 256, 362, 512, 724, 1024)

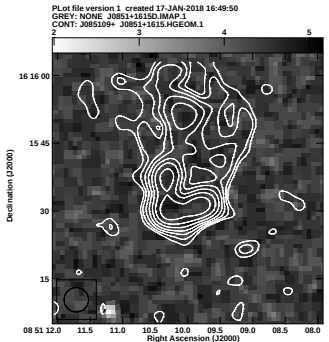
PLot file version 1 created 17-JAN-2018 16:49:50
GREY: NONE J0851+1615D.IMAP.1
CONT: J085109+ J0851+1615.HGEOM.1
Declination (J2000)
Right Ascension (J2000)
Grey scale flux range= 1.989 5.153 Kilo
Cont peak flux = 2.6956E-03 JY/BEAM
Levs = 2.500E-04 * (1, 1.400, 2, 2.800, 4, 5.600, 8, 11, 16, 23, 32, 45, 64, 90, 128, 181, 256, 362, 512, 724, 1024)

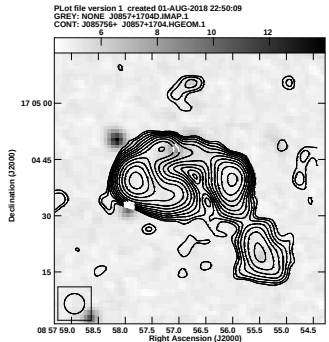
PLot file version 1 created 01-AUG-2018 22:50:09
GREY: NONE J0857+1704D.IMAP.1
CONT: J085756+ J0857+1704.HGEOM.1
Declination (J2000)
Right Ascension (J2000)
Grey scale flux range= 4.36 13.95 Kilo
Cont peak flux = 1.3574E-02 JY/BEAM
Levs = 2.500E-04 * (1, 1.400, 2, 2.800, 4, 5.600, 8, 11, 16, 23, 32, 45, 64, 90, 128, 181, 256, 362, 512, 724, 1024)

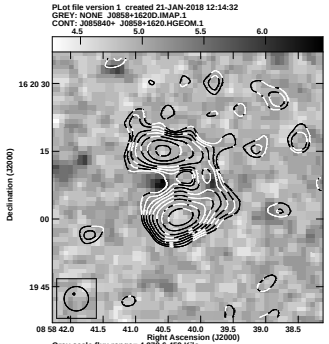
PLot file version 1 created 21-JAN-2018 12:14:32
GREY: NONE J0858+1620D.IMAP.1
CONT: J085840+ J0859+1620.HGEOM.1
Declination (J2000)
Right Ascension (J2000)
Grey scale flux range= 4.278 6.459 Kilo
Cont peak flux = 3.4447E-03 JY/BEAM
Levs = 2.500E-04 * (1, 1.400, 2, 2.800, 4, 5.600, 8, 11, 16, 23, 45, 64, 90, 181, 256, 362, 512, 724, 1024)

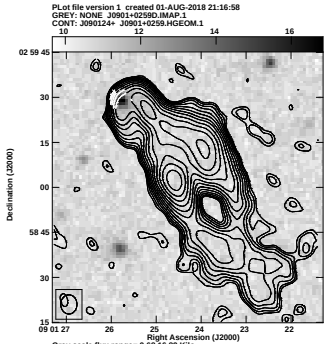
PLot file version 1 created 01-AUG-2018 21:16:58
GREY: NONE J0901+0259D.IMAP.1
CONT: J090124+ J0901+0259.HGEOM.1
Declination (J2000)
Right Ascension (J2000)
Grey scale flux range= 9.68 16.82 Kilo
Cont peak flux = 1.4630E-02 JY/BEAM
Levs = 2.500E-04 * (1, 1.400, 2, 2.800, 4, 5.600, 8, 11, 16, 23, 32, 45, 64, 90, 128, 181, 256, 362, 512, 724, 1024)

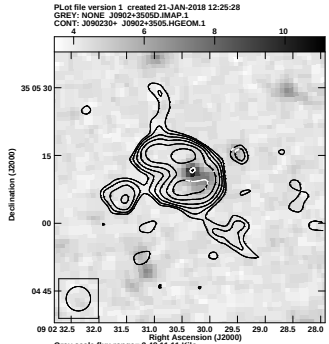
PLot file version 1 created 21-JAN-2018 12:25:28
GREY: NONE J0902+3505D.IMAP.1
CONT: J090230+ J0902+3505.HGEOM.1
Declination (J2000)
Right Ascension (J2000)
Grey scale flux range= 3.48 11.11 Kilo
Cont peak flux = 1.7062E-03 JY/BEAM
Levs = 2.500E-04 * (1, 1.400, 2, 2.800, 4, 5.600, 8, 11, 16, 23, 45, 64, 90, 181, 256, 362, 512, 724, 1024)

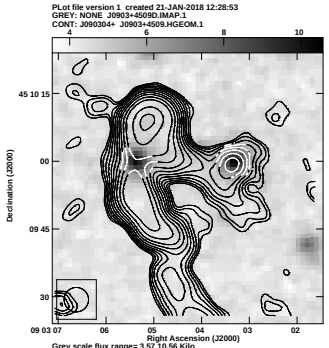
PLot file version 1 created 21-JAN-2018 12:28:53
GREY: NONE J0903+4509D.IMAP.1
CONT: J090304+ J0903+4509.HGEOM.1
Declination (J2000)
Right Ascension (J2000)
Grey scale flux range= 3.57 10.56 Kilo
Cont peak flux = 1.7732E-02 JY/BEAM
Levs = 2.500E-04 * (1, 1.400, 2, 2.800, 4, 5.600, 8, 11, 16, 23, 45, 64, 90, 181, 256, 362, 512, 724, 1024)

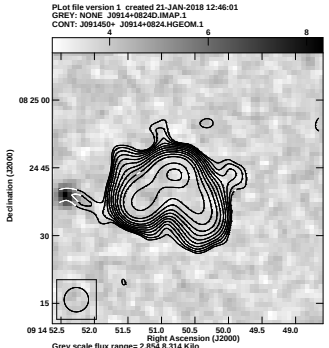
PLot file version 1 created 21-JAN-2018 12:46:01
GREY: NONE J0914+0824D.IMAP.1
CONT: J091450+ J0914+0824.HGEOM.1
Declination (J2000)
Right Ascension (J2000)
Grey scale flux range= 2.854 8.314 Kilo
Cont peak flux = 1.7630E-02 JY/BEAM
Levs = 2.500E-04 * (1, 1.400, 2, 2.800, 4, 5.600, 8, 11, 16, 23, 45, 64, 90, 181, 256, 362, 512, 724, 1024)

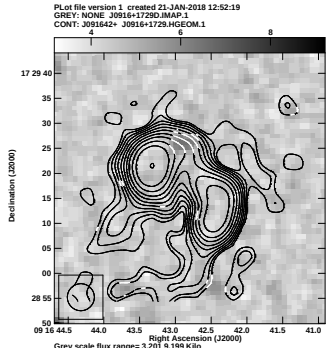
PLot file version 1 created 21-JAN-2018 12:52:19
GREY: NONE J0916+1729D.IMAP.1
CONT: J091642+ J0916+1729.HGEOM.1
Declination (J2000)
Right Ascension (J2000)
Grey scale flux range= 3.201 9.199 Kilo
Cont peak flux = 1.1364E-02 JY/BEAM
Levs = 2.500E-04 * (1, 1.400, 2, 2.800, 4, 5.600, 8, 11, 16, 23, 45, 64, 90, 181, 256, 362, 512, 724, 1024)

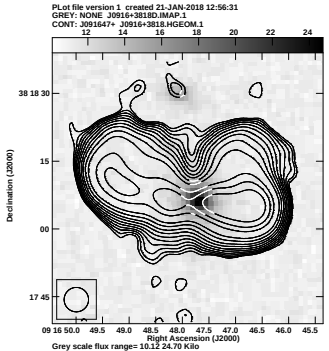
PLot file version 1 created 21-JAN-2018 12:56:31
GREY: NONE J0916+3818D.IMAP.1
CONT: J091647+ J0916+3818.HGEOM.1
Declination (J2000)
Right Ascension (J2000)
Grey scale flux range= 10.12 24.70 Kilo
Cont peak flux = 3.3934E-02 JY/BEAM
Levs = 2.500E-04 * (1, 1.400, 2, 2.800, 4, 5.600, 8, 11, 16, 23, 45, 64, 90, 181, 256, 362, 512, 724, 1024)

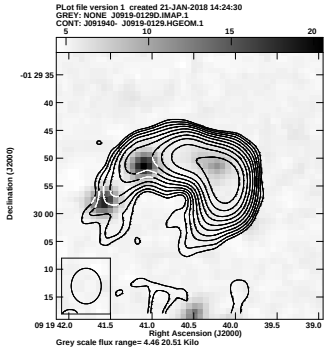
PLot file version 1 created 21-JAN-2018 14:24:30
GREY: NONE J0919-0129D.IMAP.1
CONT: J091940- J0919-0129.HGEOM.1
Declination (J2000)
Right Ascension (J2000)
Grey scale flux range= 4.46 20.51 Kilo
Cont peak flux = 9.0356E-03 JY/BEAM
Levs = 2.500E-04 * (1, 1.400, 2, 2.800, 4, 5.600, 8, 11, 16, 23, 45, 64, 90, 181, 256, 362, 512, 724, 1024)

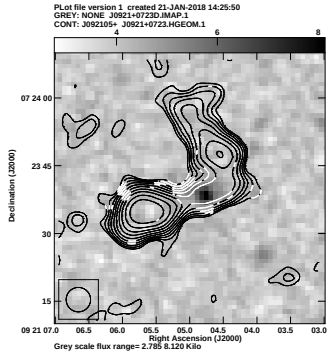
PLot file version 1 created 21-JAN-2018 14:25:50
GREY: NONE J0921+0723D.IMAP.1
CONT: J092105+ J0921+0723.HGEOM.1
Declination (J2000)
Right Ascension (J2000)
Grey scale flux range= 2.785 8.120 Kilo
Cont peak flux = 8.7888E-03 JY/BEAM
Levs = 2.500E-04 * (1, 1.400, 2, 2.800, 4, 5.600, 8, 11, 16, 23, 45, 64, 90, 181, 256, 362, 512, 724, 1024)

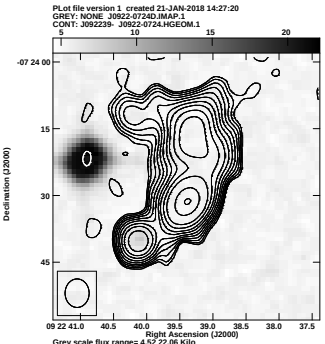
PLot file version 1 created 21-JAN-2018 14:27:20
GREY: NONE J0922-0724D.IMAP.1
CONT: J0922S9- J0922-0724.HGEOM.1
Declination (J2000)
Right Ascension (J2000)
Grey scale flux range= 4.52 22.06 Kilo
Cont peak flux = 1.532E-02 JY/BEAM
Levs = 2.500E-04 * (1, 1.400, 2, 2.800, 4, 5.600, 8, 11, 16, 23, 45, 64, 90, 181, 256, 362, 512, 724, 1024)

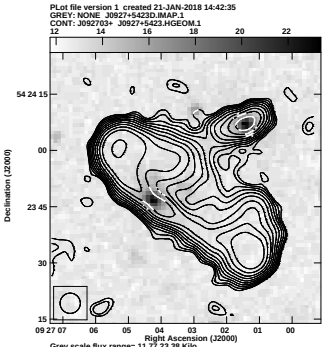
PLot file version 1 created 21-JAN-2018 14:42:35
GREY: NONE J0927+5423D.IMAP.1
CONT: J0927O3+ J0927+5423.HGEOM.1
Declination (J2000)
Right Ascension (J2000)
Grey scale flux range= 11.77 23.38 Kilo
Cont peak flux = 1.262E-02 JY/BEAM
Levs = 2.500E-04 * (1, 1.400, 2, 2.800, 4, 5.600, 8, 11, 16, 23, 45, 64, 90, 181, 256, 362, 512, 724, 1024)

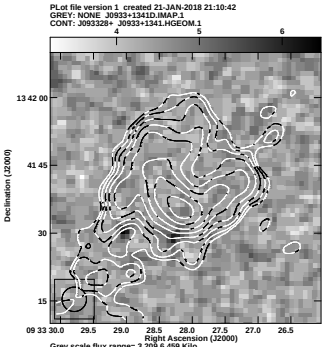
PLot file version 1 created 21-JAN-2018 21:10:42
GREY: NONE J0933+1341D.IMAP.1
CONT: J0933Z8+ J0933+1341.HGEOM.1
Declination (J2000)
Right Ascension (J2000)
Grey scale flux range= 3.209 6.459 Kilo
Cont peak flux = 3.312E-03 JY/BEAM
Levs = 2.500E-04 * (1, 1.400, 2, 2.800, 4, 5.600, 8, 11, 16, 23, 45, 64, 90, 181, 256, 362, 512, 724, 1024)

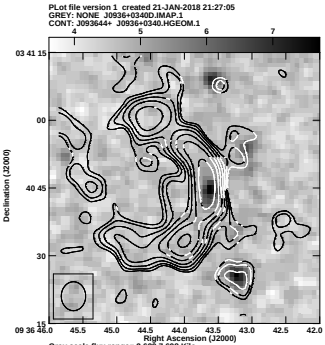
PLot file version 1 created 21-JAN-2018 21:27:05
GREY: NONE J0936+0340D.IMAP.1
CONT: J0936I4+ J0936+0340.HGEOM.1
Declination (J2000)
Right Ascension (J2000)
Grey scale flux range= 3.629 7.698 Kilo
Cont peak flux = 2.881E-03 JY/BEAM
Levs = 2.500E-04 * (1, 1.400, 2, 2.800, 4, 5.600, 8, 11, 16, 23, 45, 64, 90, 181, 256, 362, 512, 724, 1024)

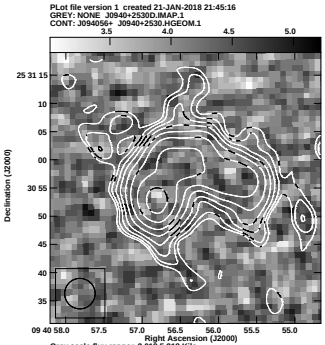
PLot file version 1 created 21-JAN-2018 21:45:16
GREY: NONE J0940+2530D.IMAP.1
CONT: J0940S6+ J0940+2530.HGEOM.1
Declination (J2000)
Right Ascension (J2000)
Grey scale flux range= 3.018 5.218 Kilo
Cont peak flux = 3.180E-03 JY/BEAM
Levs = 2.500E-04 * (1, 1.400, 2, 2.800, 4, 5.600, 8, 11, 16, 23, 45, 64, 90, 181, 256, 362, 512, 724, 1024)

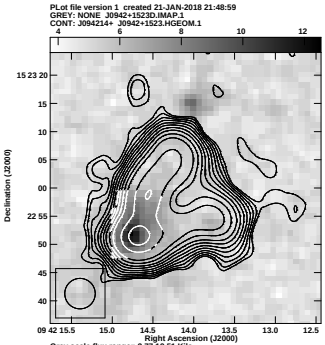
PLot file version 1 created 21-JAN-2018 21:48:59
GREY: NONE J0942+1523D.IMAP.1
CONT: J0942I4+ J0942+1523.HGEOM.1
Declination (J2000)
Right Ascension (J2000)
Grey scale flux range= 3.77 12.51 Kilo
Cont peak flux = 1.852E-02 JY/BEAM
Levs = 2.500E-04 * (1, 1.400, 2, 2.800, 4, 5.600, 8, 11, 16, 23, 45, 64, 90, 181, 256, 362, 512, 724, 1024)

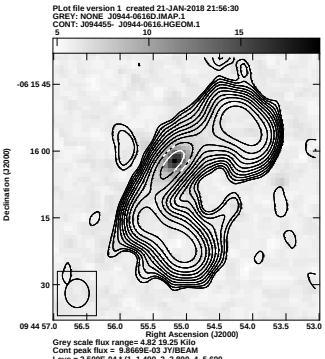
PLot file version 1 created 21-JAN-2018 21:56:30
GREY: NONE J0944-0616D.IMAP.1
CONT: J0944I5- J0944-0616.HGEOM.1
Declination (J2000)
Right Ascension (J2000)
Grey scale flux range= 4.82 19.25 Kilo
Cont peak flux = 9.866E-03 JY/BEAM
Levs = 2.500E-04 * (1, 1.400, 2, 2.800, 4, 5.600, 8, 11, 16, 23, 45, 64, 90, 181, 256, 362, 512, 724, 1024)

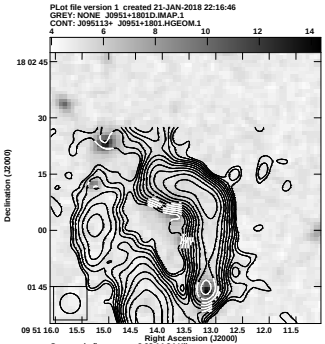
PLot file version 1 created 21-JAN-2018 22:16:46
GREY: NONE J0951+1801D.IMAP.1
CONT: J0951I3+ J0951+1801.HGEOM.1
Declination (J2000)
Right Ascension (J2000)
Grey scale flux range= 3.98 14.34 Kilo
Cont peak flux = 7.720E-03 JY/BEAM
Levs = 2.500E-04 * (1, 1.400, 2, 2.800, 4, 5.600, 8, 11, 16, 23, 45, 64, 90, 181, 256, 362, 512, 724, 1024)

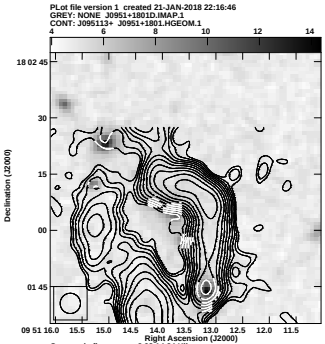
PLot file version 1 created 21-JAN-2018 22:16:46
GREY: NONE J0951+1801D.IMAP.1
CONT: J0951I3+ J0951+1801.HGEOM.1
Declination (J2000)
Right Ascension (J2000)
Grey scale flux range= 3.98 14.34 Kilo
Cont peak flux = 7.720E-03 JY/BEAM
Levs = 2.500E-04 * (1, 1.400, 2, 2.800, 4, 5.600, 8, 11, 16, 23, 45, 64, 90, 181, 256, 362, 512, 724, 1024)

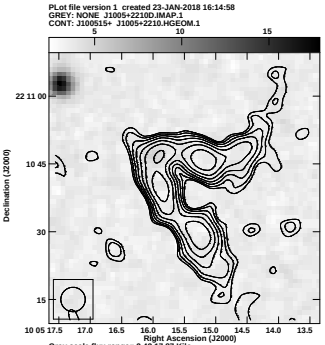
PLot file version 1 created 23-JAN-2018 16:14:58
GREY: NONE J1005+2210D.IMAP.1
CONT: J1005I5+ J1005+2210.HGEOM.1
Declination (J2000)
Right Ascension (J2000)
Grey scale flux range= 2.43 17.87 Kilo
Cont peak flux = 2.870E-03 JY/BEAM
Levs = 2.500E-04 * (1, 1.400, 2, 2.800, 4, 5.600, 8, 11, 16, 23, 32, 45, 64, 90, 128, 181, 256, 362, 512, 724, 1024)

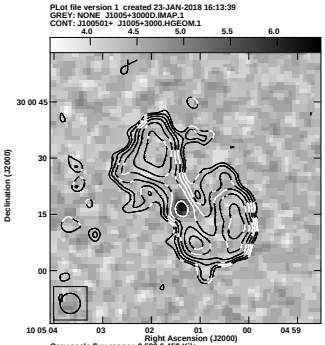
PLot file version 1 created 23-JAN-2018 16:13:39
GREY: NONE J1005+3000D.IMAP.1
CONT: J1005I3+ J1005+3000.HGEOM.1
Declination (J2000)
Right Ascension (J2000)
Grey scale flux range= 3.580 6.459 Kilo
Cont peak flux = 1.734E-03 JY/BEAM
Levs = 2.500E-04 * (1, 1.400, 2, 2.800, 4, 5.600, 8, 11, 16, 23, 32, 45, 64, 90, 128, 181, 256, 362, 512, 724, 1024)

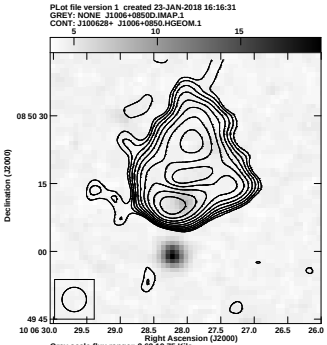
PLot file version 1 created 23-JAN-2018 16:16:31
GREY: NONE J1006+0850D.IMAP.1
CONT: J1006I8+ J1006+0850.HGEOM.1
Declination (J2000)
Right Ascension (J2000)
Grey scale flux range= 3.63 19.75 Kilo
Cont peak flux = 7.640E-03 JY/BEAM
Levs = 2.500E-04 * (1, 1.400, 2, 2.800, 4, 5.600, 8, 11, 16, 23, 32, 45, 64, 90, 128, 181, 256, 362, 512, 724, 1024)

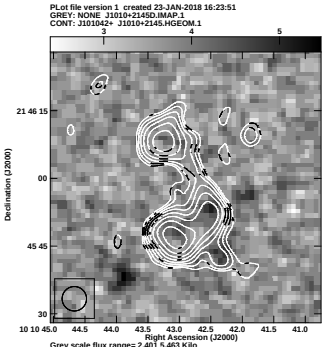
PLot file version 1 created 23-JAN-2018 16:23:51
GREY: NONE J1010+2145D.IMAP.1
CONT: J101042+ J1010+2145.HGEOM.1
Declination (J2000)
Right Ascension (J2000)
Grey scale flux range= 2.401 5.463 Kilo
Cont peak flux = 3.3976E-03 JY/BEAM
Levs = 2.500E-04 * (1, 1.400, 2, 2.800, 4, 5.600,
8, 11, 16, 23, 32, 45, 64, 90, 128, 181, 256, 362,
512, 724, 1024)

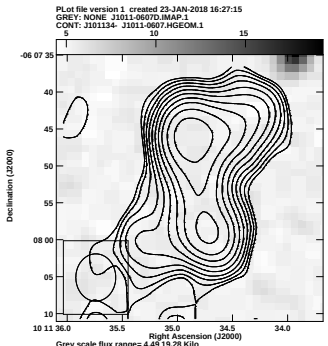
PLot file version 1 created 23-JAN-2018 16:27:15
GREY: NONE J1011-0607D.IMAP.1
CONT: J101134- J1011-0607.HGEOM.1
Declination (J2000)
Right Ascension (J2000)
Grey scale flux range= 4.49 19.28 Kilo
Cont peak flux = 7.8684E-03 JY/BEAM
Levs = 2.500E-04 * (1, 1.400, 2, 2.800, 4, 5.600,
8, 11, 16, 23, 32, 45, 64, 90, 128, 181, 256, 362,
512, 724, 1024)

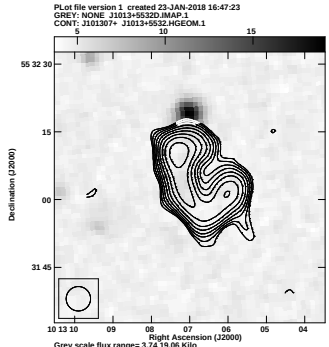
PLot file version 1 created 23-JAN-2018 16:47:23
GREY: NONE J1013+5532D.IMAP.1
CONT: J101307+ J1013+5532.HGEOM.1
Declination (J2000)
Right Ascension (J2000)
Grey scale flux range= 3.74 19.06 Kilo
Cont peak flux = 5.2491E-03 JY/BEAM
Levs = 2.500E-04 * (1, 1.400, 2, 2.800, 4, 5.600,
8, 11, 16, 23, 32, 45, 64, 90, 128, 181, 256, 362,
512, 724, 1024)

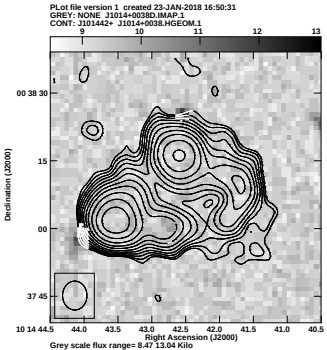
PLot file version 1 created 23-JAN-2018 16:50:31
GREY: NONE J1014+0038D.IMAP.1
CONT: J101442+ J1014+0038.HGEOM.1
Declination (J2000)
Right Ascension (J2000)
Grey scale flux range= 8.47 13.04 Kilo
Cont peak flux = 1.0511E-02 JY/BEAM
Levs = 2.500E-04 * (1, 1.400, 2, 2.800, 4, 5.600,
8, 11, 16, 23, 32, 45, 64, 90, 128, 181, 256, 362,
512, 724, 1024)

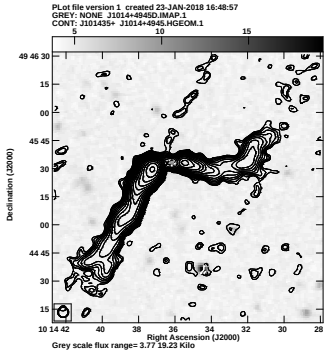
PLot file version 1 created 23-JAN-2018 16:48:57
GREY: NONE J1014+4945D.IMAP.1
CONT: J101435+ J1014+4945.HGEOM.1
Declination (J2000)
Right Ascension (J2000)
Grey scale flux range= 3.77 19.23 Kilo
Cont peak flux = 6.8796E-02 JY/BEAM
Levs = 2.500E-04 * (1, 1.400, 2, 2.800, 4, 5.600,
8, 11, 16, 23, 32, 45, 64, 90, 128, 181, 256, 362,
512, 724, 1024)

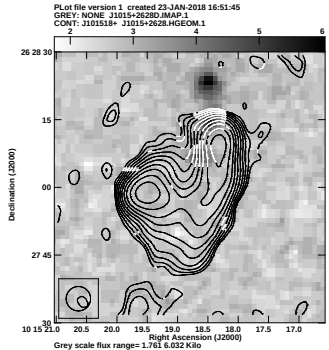
PLot file version 1 created 23-JAN-2018 16:51:45
GREY: NONE J1015+2628D.IMAP.1
CONT: J101518+ J1015+2628.HGEOM.1
Declination (J2000)
Right Ascension (J2000)
Grey scale flux range= 1.761 6.032 Kilo
Cont peak flux = 7.6583E-03 JY/BEAM
Levs = 2.500E-04 * (1, 1.400, 2, 2.800, 4, 5.600,
8, 11, 16, 23, 32, 45, 64, 90, 128, 181, 256, 362,
512, 724, 1024)

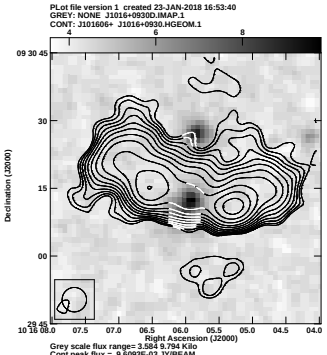
PLot file version 1 created 23-JAN-2018 16:53:40
GREY: NONE J1016+0930D.IMAP.1
CONT: J101606+ J1016+0930.HGEOM.1
Declination (J2000)
Right Ascension (J2000)
Grey scale flux range= 3.584 9.794 Kilo
Cont peak flux = 9.6093E-03 JY/BEAM
Levs = 2.500E-04 * (1, 1.400, 2, 2.800, 4, 5.600,
8, 11, 16, 23, 32, 45, 64, 90, 128, 181, 256, 362,
512, 724, 1024)

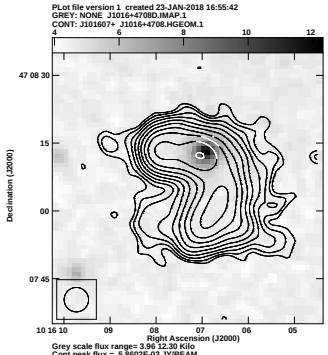
PLot file version 1 created 23-JAN-2018 16:55:42
GREY: NONE J1016+4708D.IMAP.1
CONT: J101607+ J1016+4708.HGEOM.1
Declination (J2000)
Right Ascension (J2000)
Grey scale flux range= 3.96 12.30 Kilo
Cont peak flux = 5.8602E-03 JY/BEAM
Levs = 2.500E-04 * (1, 1.400, 2, 2.800, 4, 5.600,
8, 11, 16, 23, 32, 45, 64, 90, 128, 181, 256, 362,
512, 724, 1024)

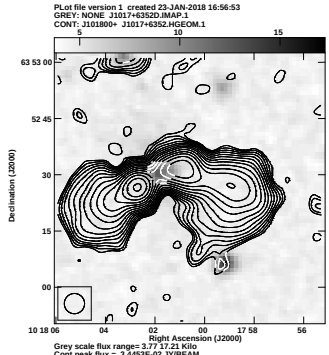
PLot file version 1 created 23-JAN-2018 16:56:53
GREY: NONE J1017+6352D.IMAP.1
CONT: J101800+ J1017+6352.HGEOM.1
Declination (J2000)
Right Ascension (J2000)
Grey scale flux range= 3.77 17.21 Kilo
Cont peak flux = 3.4453E-02 JY/BEAM
Levs = 2.500E-04 * (1, 1.400, 2, 2.800, 4, 5.600,
8, 11, 16, 23, 32, 45, 64, 90, 128, 181, 256, 362,
512, 724, 1024)

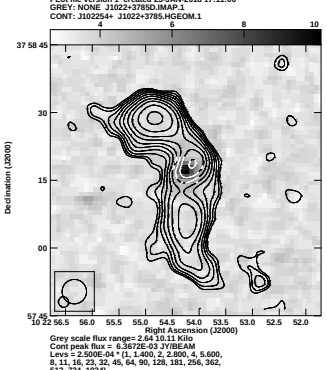
PLot file version 1 created 23-JAN-2018 17:11:00
GREY: NONE J1022+3785D.IMAP.1
CONT: J102254+ J1022+3785.HGEOM.1
Declination (J2000)
Right Ascension (J2000)
Grey scale flux range= 2.64 10.11 Kilo
Cont peak flux = 6.3672E-03 JY/BEAM
Levs = 2.500E-04 * (1, 1.400, 2, 2.800, 4, 5.600,
8, 11, 16, 23, 32, 45, 64, 90, 128, 181, 256, 362,
512, 724, 1024)

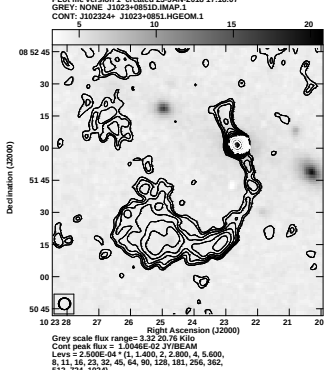
PLot file version 1 created 23-JAN-2018 17:18:07
GREY: NONE J1023+0851D.IMAP.1
CONT: J102324+ J1023+0851.HGEOM.1
Declination (J2000)
Right Ascension (J2000)
Grey scale flux range= 3.32 20.76 Kilo
Cont peak flux = 1.0046E-02 JY/BEAM
Levs = 2.500E-04 * (1, 1.400, 2, 2.800, 4, 5.600,
8, 11, 16, 23, 32, 45, 64, 90, 128, 181, 256, 362,
512, 724, 1024)

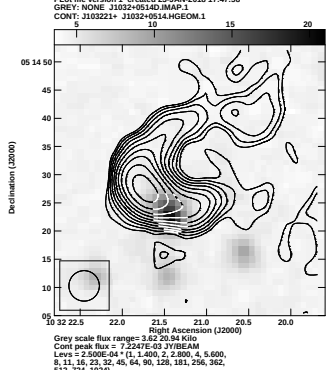
PLot file version 1 created 23-JAN-2018 17:47:58
GREY: NONE J1032+0514D.IMAP.1
CONT: J103221+ J1032+0514.HGEOM.1
Declination (J2000)
Right Ascension (J2000)
Grey scale flux range= 3.62 20.94 Kilo
Cont peak flux = 7.2247E-03 JY/BEAM
Levs = 2.500E-04 * (1, 1.400, 2, 2.800, 4, 5.600,
8, 11, 16, 23, 32, 45, 64, 90, 128, 181, 256, 362,
512, 724, 1024)

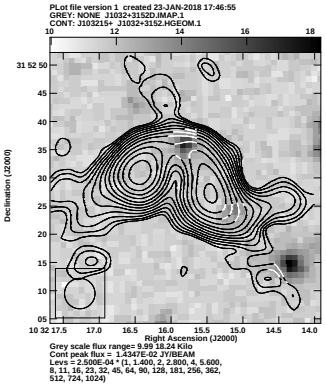
PLot file version 1 created 23-JAN-2018 17:46:55
GREY: NONE J1032+3152D.IMAP.1
CONT: J103215+ J1032+3152.HGEOM.1
Declination (J2000)
Right Ascension (J2000)
Grey scale flux range= 9.99 18.24 Kilo
Cont peak flux = 1.43476-02 JY/BEAM
Levs = 2.500E-04 * (1, 1.400, 2, 2.800, 4, 5.600, 8, 11, 16, 23, 32, 45, 64, 90, 128, 181, 256, 362, 512, 724, 1024)

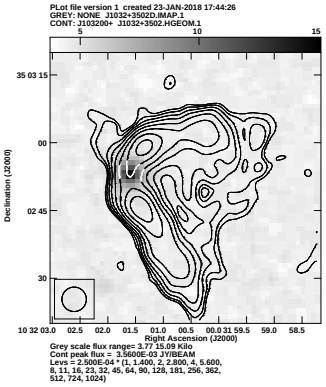
PLot file version 1 created 23-JAN-2018 17:44:26
GREY: NONE J1032+3502D.IMAP.1
CONT: J103200+ J1032+3502.HGEOM.1
Declination (J2000)
Right Ascension (J2000)
Grey scale flux range= 3.77 15.09 Kilo
Cont peak flux = 3.5609E-03 JY/BEAM
Levs = 2.500E-04 * (1, 1.400, 2, 2.800, 4, 5.600, 8, 11, 16, 23, 32, 45, 64, 90, 128, 181, 256, 362, 512, 724, 1024)

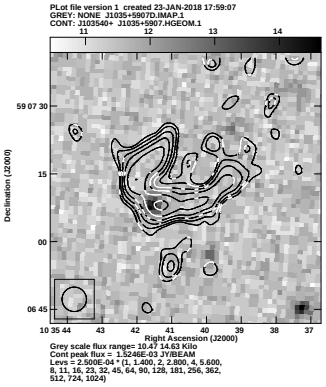
PLot file version 1 created 23-JAN-2018 17:59:07
GREY: NONE J1035+5907D.IMAP.1
CONT: J103540+ J1035+5907.HGEOM.1
Declination (J2000)
Right Ascension (J2000)
Grey scale flux range= 10.47 14.63 Kilo
Cont peak flux = 1.5246E-03 JY/BEAM
Levs = 2.500E-04 * (1, 1.400, 2, 2.800, 4, 5.600, 8, 11, 16, 23, 32, 45, 64, 90, 128, 181, 256, 362, 512, 724, 1024)

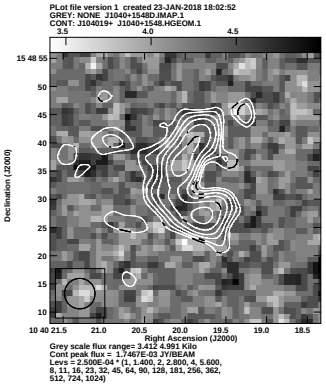
PLot file version 1 created 23-JAN-2018 18:02:52
GREY: NONE J1040+1548D.IMAP.1
CONT: J104019+ J1040+1548.HGEOM.1
Declination (J2000)
Right Ascension (J2000)
Grey scale flux range= 3.412 4.991 Kilo
Cont peak flux = 1.7467E-03 JY/BEAM
Levs = 2.500E-04 * (1, 1.400, 2, 2.800, 4, 5.600, 8, 11, 16, 23, 32, 45, 64, 90, 128, 181, 256, 362, 512, 724, 1024)

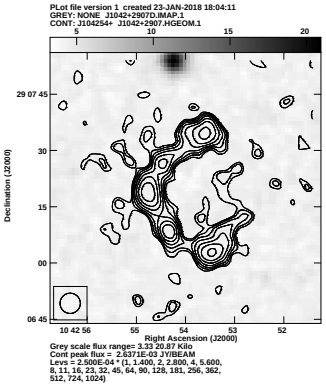
PLot file version 1 created 23-JAN-2018 18:04:11
GREY: NONE J1042+2907D.IMAP.1
CONT: J104254+ J1042+2907.HGEOM.1
Declination (J2000)
Right Ascension (J2000)
Grey scale flux range= 3.33 20.87 Kilo
Cont peak flux = 2.6371E-03 JY/BEAM
Levs = 2.500E-04 * (1, 1.400, 2, 2.800, 4, 5.600, 8, 11, 16, 23, 32, 45, 64, 90, 128, 181, 256, 362, 512, 724, 1024)

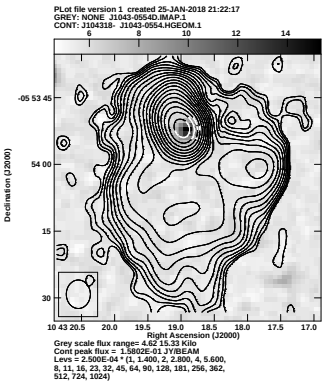
PLot file version 1 created 25-JAN-2018 21:22:17
GREY: NONE J1043-0540.IMAP.1
CONT: J104318- J1043-0554.HGEOM.1
Declination (J2000)
Right Ascension (J2000)
Grey scale flux range= 4.62 15.33 Kilo
Cont peak flux = 1.5802E-03 JY/BEAM
Levs = 2.500E-04 * (1, 1.400, 2, 2.800, 4, 5.600, 8, 11, 16, 23, 32, 45, 64, 90, 128, 181, 256, 362, 512, 724, 1024)

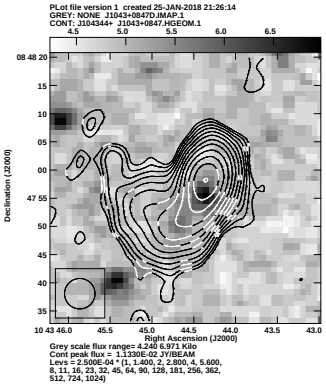
PLot file version 1 created 25-JAN-2018 21:26:14
GREY: NONE J1043+0847D.IMAP.1
CONT: J104344+ J1043+0847.HGEOM.1
Declination (J2000)
Right Ascension (J2000)
Grey scale flux range= 4.240 6.971 Kilo
Cont peak flux = 1.1330E-02 JY/BEAM
Levs = 2.500E-04 * (1, 1.400, 2, 2.800, 4, 5.600, 8, 11, 16, 23, 32, 45, 64, 90, 128, 181, 256, 362, 512, 724, 1024)

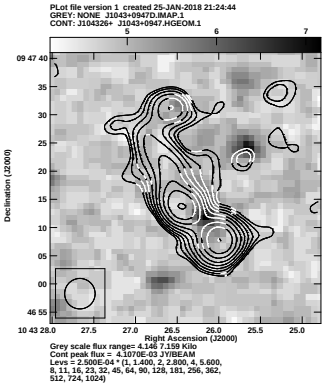
PLot file version 1 created 25-JAN-2018 21:24:44
GREY: NONE J1043+0947D.IMAP.1
CONT: J104326+ J1043+0947.HGEOM.1
Declination (J2000)
Right Ascension (J2000)
Grey scale flux range= 4.146 7.159 Kilo
Cont peak flux = 4.1070E-03 JY/BEAM
Levs = 2.500E-04 * (1, 1.400, 2, 2.800, 4, 5.600, 8, 11, 16, 23, 32, 45, 64, 90, 128, 181, 256, 362, 512, 724, 1024)

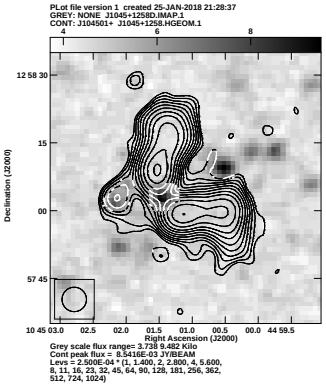
PLot file version 1 created 25-JAN-2018 21:28:37
GREY: NONE J1045+1258D.IMAP.1
CONT: J104501+ J1045+1258.HGEOM.1
Declination (J2000)
Right Ascension (J2000)
Grey scale flux range= 3.738 9.482 Kilo
Cont peak flux = 8.5416E-03 JY/BEAM
Levs = 2.500E-04 * (1, 1.400, 2, 2.800, 4, 5.600, 8, 11, 16, 23, 32, 45, 64, 90, 128, 181, 256, 362, 512, 724, 1024)

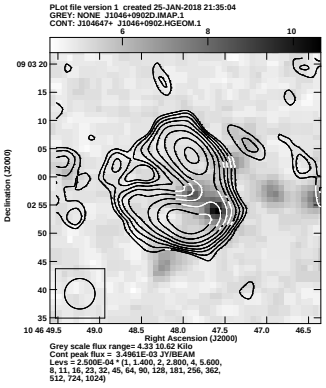
PLot file version 1 created 25-JAN-2018 21:35:04
GREY: NONE J1046+0902D.IMAP.1
CONT: J104647+ J1046+0902.HGEOM.1
Declination (J2000)
Right Ascension (J2000)
Grey scale flux range= 4.33 10.62 Kilo
Cont peak flux = 3.4961E-03 JY/BEAM
Levs = 2.500E-04 * (1, 1.400, 2, 2.800, 4, 5.600, 8, 11, 16, 23, 32, 45, 64, 90, 128, 181, 256, 362, 512, 724, 1024)

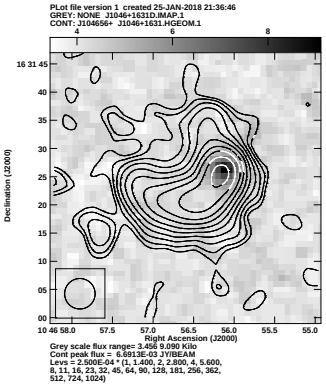
PLot file version 1 created 25-JAN-2018 21:36:46
GREY: NONE J1046+1631D.IMAP.1
CONT: J104656+ J1046+1631.HGEOM.1
Declination (J2000)
Right Ascension (J2000)
Grey scale flux range= 3.456 9.090 Kilo
Cont peak flux = 6.6913E-03 JY/BEAM
Levs = 2.500E-04 * (1, 1.400, 2, 2.800, 4, 5.600, 8, 11, 16, 23, 32, 45, 64, 90, 128, 181, 256, 362, 512, 724, 1024)

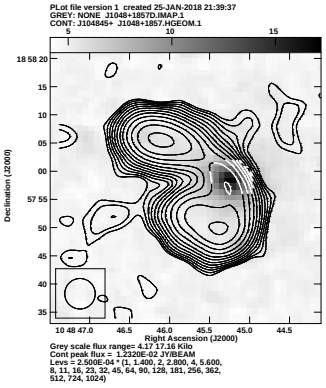
PLot file version 1 created 25-JAN-2018 21:39:37
GREY: NONE J1048+1857D.IMAP.1
CONT: J104845+ J1048+1857.HGEOM.1
Declination (J2000)
Right Ascension (J2000)
Grey scale flux range= 4.17 17.16 Kilo
Cont peak flux = 1.2320E-02 JY/BEAM
Levs = 2.500E-04 * (1, 1.400, 2, 2.800, 4, 5.600, 8, 11, 16, 23, 32, 45, 64, 90, 128, 181, 256, 362, 512, 724, 1024)

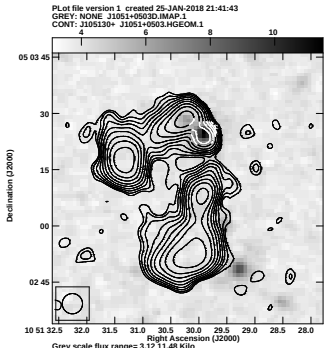
PLot file version 1 created 25-JAN-2018 21:41:43
GREY: NONE J1051+0503D.IMAP.1
CONT: J105130+ J1051+0503.HGEOM.1
Declination (J2000)
Right Ascension (J2000)
Grey scale flux range= 3.12 11.48 Kilo
Cont peak flux = 5.6728E-03 JY/BEAM
Levs = 2.500E-04 * (1, 1.400, 2, 2.800, 4, 5.600, 8, 11, 16, 23, 32, 45, 64, 90, 128, 181, 256, 362, 512, 724, 1024)

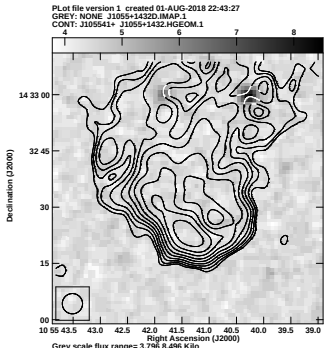
PLot file version 1 created 01-AUG-2018 22:43:27
GREY: NONE J1055+1432D.IMAP.1
CONT: J1055541+ J1055+1432.HGEOM.1
Declination (J2000)
Right Ascension (J2000)
Grey scale flux range= 3.796 8.496 Kilo
Cont peak flux = 5.4166E-03 JY/BEAM
Levs = 2.500E-04 * (1, 1.400, 2, 2.800, 4, 5.600, 8, 11, 16, 23, 32, 45, 64, 90, 128, 181, 256, 362, 512, 724, 1024)

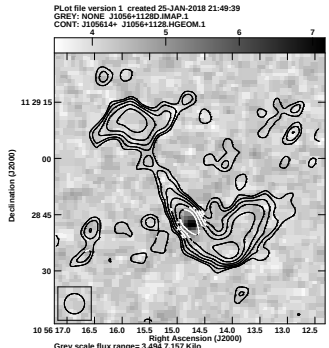
PLot file version 1 created 25-JAN-2018 21:49:39
GREY: NONE J1056+1128D.IMAP.1
CONT: J1056141+ J1056+1128.HGEOM.1
Declination (J2000)
Right Ascension (J2000)
Grey scale flux range= 3.494 7.157 Kilo
Cont peak flux = 1.9953E-03 JY/BEAM
Levs = 2.500E-04 * (1, 1.400, 2, 2.800, 4, 5.600, 8, 11, 16, 23, 32, 45, 64, 90, 128, 181, 256, 362, 512, 724, 1024)

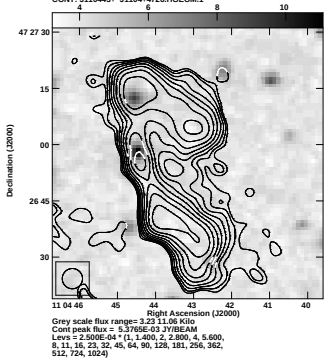
PLot file version 1 created 25-JAN-2018 21:53:10
GREY: NONE J1104+4726D.IMAP.1
CONT: J110443+ J1104+4726.HGEOM.1
Declination (J2000)
Right Ascension (J2000)
Grey scale flux range= 3.23 11.06 Kilo
Cont peak flux = 5.3765E-03 JY/BEAM
Levs = 2.500E-04 * (1, 1.400, 2, 2.800, 4, 5.600, 8, 11, 16, 23, 32, 45, 64, 90, 128, 181, 256, 362, 512, 724, 1024)

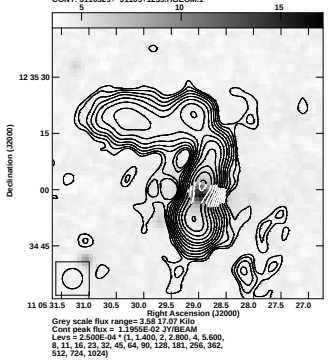
PLot file version 1 created 25-JAN-2018 21:56:16
GREY: NONE J1105+1235D.IMAP.1
CONT: J110529+ J1105+1235.HGEOM.1
Declination (J2000)
Right Ascension (J2000)
Grey scale flux range= 3.58 17.07 Kilo
Cont peak flux = 1.1955E-02 JY/BEAM
Levs = 2.500E-04 * (1, 1.400, 2, 2.800, 4, 5.600, 8, 11, 16, 23, 32, 45, 64, 90, 128, 181, 256, 362, 512, 724, 1024)

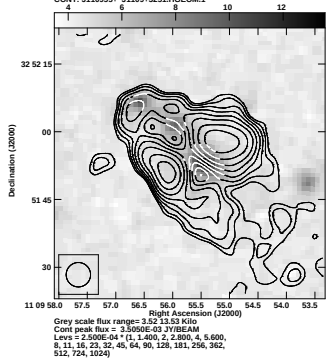
PLot file version 1 created 25-JAN-2018 22:12:51
GREY: NONE J1109+3251D.IMAP.1
CONT: J110955+ J1109+3251.HGEOM.1
Declination (J2000)
Right Ascension (J2000)
Grey scale flux range= 3.52 13.53 Kilo
Cont peak flux = 3.5050E-03 JY/BEAM
Levs = 2.500E-04 * (1, 1.400, 2, 2.800, 4, 5.600, 8, 11, 16, 23, 32, 45, 64, 90, 128, 181, 256, 362, 512, 724, 1024)

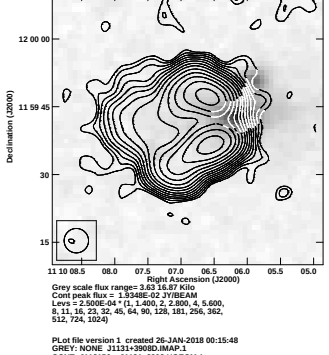
PLot file version 1 created 25-JAN-2018 22:14:09
GREY: NONE J1110+1159D.IMAP.1
CONT: J111006+ J1110+1159.HGEOM.1
Declination (J2000)
Right Ascension (J2000)
Grey scale flux range= 3.63 16.87 Kilo
Cont peak flux = 1.9348E-02 JY/BEAM
Levs = 2.500E-04 * (1, 1.400, 2, 2.800, 4, 5.600, 8, 11, 16, 23, 32, 45, 64, 90, 128, 181, 256, 362, 512, 724, 1024)

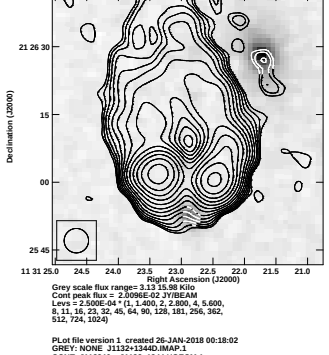
PLot file version 1 created 26-JAN-2018 00:10:57
GREY: NONE J1131+2126D.IMAP.1
CONT: J113122+ J1131+2126.HGEOM.1
Declination (J2000)
Right Ascension (J2000)
Grey scale flux range= 3.13 15.98 Kilo
Cont peak flux = 2.0096E-02 JY/BEAM
Levs = 2.500E-04 * (1, 1.400, 2, 2.800, 4, 5.600, 8, 11, 16, 23, 32, 45, 64, 90, 128, 181, 256, 362, 512, 724, 1024)

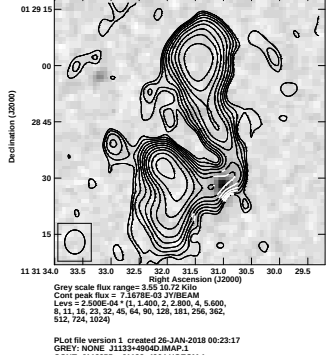
PLot file version 1 created 26-JAN-2018 00:12:29
GREY: NONE J1131+0128D.IMAP.1
CONT: J113131+ J1131+0128.HGEOM.1
Declination (J2000)
Right Ascension (J2000)
Grey scale flux range= 3.55 10.72 Kilo
Cont peak flux = 7.1678E-03 JY/BEAM
Levs = 2.500E-04 * (1, 1.400, 2, 2.800, 4, 5.600, 8, 11, 16, 23, 32, 45, 64, 90, 128, 181, 256, 362, 512, 724, 1024)

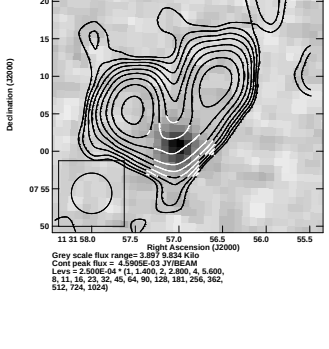
PLot file version 1 created 26-JAN-2018 00:15:48
GREY: NONE J1131+3908D.IMAP.1
CONT: J113156+ J1131+3908.HGEOM.1
Declination (J2000)
Right Ascension (J2000)
Grey scale flux range= 3.897 9.834 Kilo
Cont peak flux = 4.5905E-03 JY/BEAM
Levs = 2.500E-04 * (1, 1.400, 2, 2.800, 4, 5.600, 8, 11, 16, 23, 32, 45, 64, 90, 128, 181, 256, 362, 512, 724, 1024)

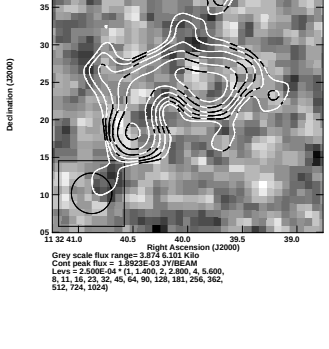
PLot file version 1 created 26-JAN-2018 00:18:02
GREY: NONE J1132+1344D.IMAP.1
CONT: J113240+ J1132+1344.HGEOM.1
Declination (J2000)
Right Ascension (J2000)
Grey scale flux range= 3.874 6.101 Kilo
Cont peak flux = 1.8923E-03 JY/BEAM
Levs = 2.500E-04 * (1, 1.400, 2, 2.800, 4, 5.600, 8, 11, 16, 23, 32, 45, 64, 90, 128, 181, 256, 362, 512, 724, 1024)

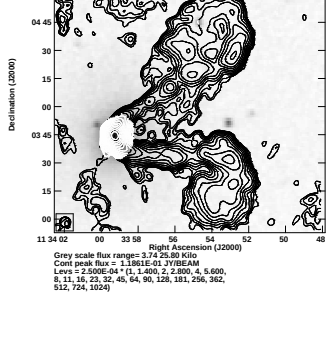
PLot file version 1 created 26-JAN-2018 00:23:17
GREY: NONE J1133+4904D.IMAP.1
CONT: J113355+ J1133+4904.HGEOM.1
Declination (J2000)
Right Ascension (J2000)
Grey scale flux range= 3.74 25.80 Kilo
Cont peak flux = 1.1861E-01 JY/BEAM
Levs = 2.500E-04 * (1, 1.400, 2, 2.800, 4, 5.600, 8, 11, 16, 23, 32, 45, 64, 90, 128, 181, 256, 362, 512, 724, 1024)

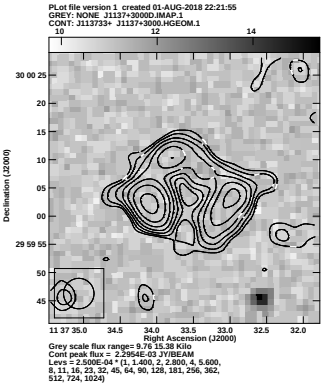
PLot file version 1 created 01-AUG-2018 22:21:55
GREY: NONE J1137+3000D.IMAP.1
CONT: J113733+ J1137+3000.HGEOM.1
Declination (J2000)
Right Ascension (J2000)
Grey scale flux range= 9.76 15.38 Kilo
Cont peak flux = 2.2954E-03 JY/BEAM
Levs = 2.500E-04 * (1, 1.400, 2, 2.800, 4, 5.600, 8, 11, 16, 23, 32, 45, 64, 90, 128, 181, 256, 362, 512, 724, 1024)

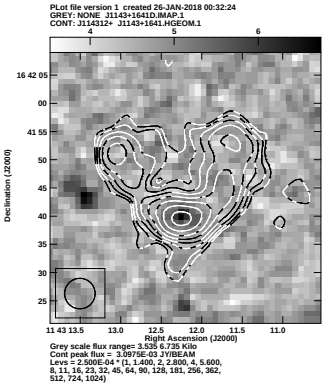
PLot file version 1 created 26-JAN-2018 00:32:24
GREY: NONE J1143+1641D.IMAP.1
CONT: J114312+ J1143+1641.HGEOM.1
Declination (J2000)
Right Ascension (J2000)
Grey scale flux range= 3.535 6.735 Kilo
Cont peak flux = 3.0975E-03 JY/BEAM
Levs = 2.500E-04 * (1, 1.400, 2, 2.800, 4, 5.600, 8, 11, 16, 23, 32, 45, 64, 90, 128, 181, 256, 362, 512, 724, 1024)

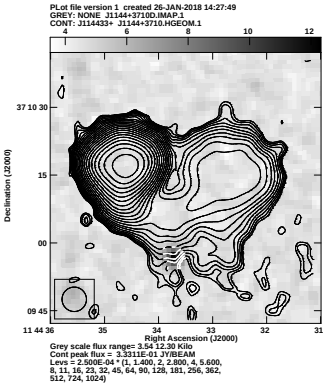
PLot file version 1 created 26-JAN-2018 14:27:49
GREY: NONE J1144+3710D.IMAP.1
CONT: J114433+ J1144+3710.HGEOM.1
Declination (J2000)
Right Ascension (J2000)
Grey scale flux range= 3.54 12.30 Kilo
Cont peak flux = 3.3311E-01 JY/BEAM
Levs = 2.500E-04 * (1, 1.400, 2, 2.800, 4, 5.600, 8, 11, 16, 23, 32, 45, 64, 90, 128, 181, 256, 362, 512, 724, 1024)

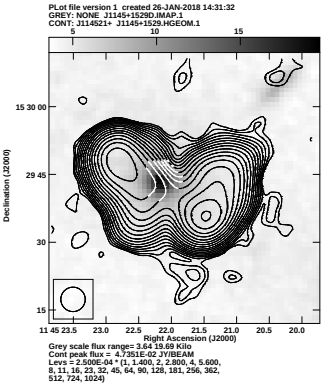
PLot file version 1 created 26-JAN-2018 14:31:32
GREY: NONE J1145+1529D.IMAP.1
CONT: J114521+ J1145+1529.HGEOM.1
Declination (J2000)
Right Ascension (J2000)
Grey scale flux range= 3.64 19.69 Kilo
Cont peak flux = 4.7351E-02 JY/BEAM
Levs = 2.500E-04 * (1, 1.400, 2, 2.800, 4, 5.600, 8, 11, 16, 23, 32, 45, 64, 90, 128, 181, 256, 362, 512, 724, 1024)

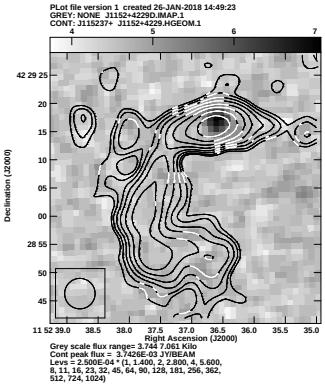
PLot file version 1 created 26-JAN-2018 14:49:23
GREY: NONE J1152+4229D.IMAP.1
CONT: J115237+ J1152+4229.HGEOM.1
Declination (J2000)
Right Ascension (J2000)
Grey scale flux range= 3.744 7.061 Kilo
Cont peak flux = 3.7426E-03 JY/BEAM
Levs = 2.500E-04 * (1, 1.400, 2, 2.800, 4, 5.600, 8, 11, 16, 23, 32, 45, 64, 90, 128, 181, 256, 362, 512, 724, 1024)

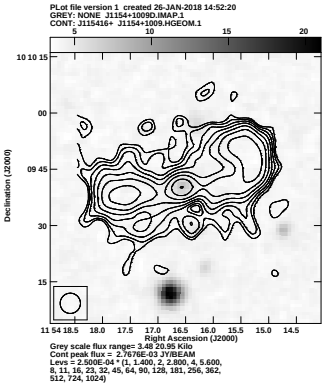
PLot file version 1 created 26-JAN-2018 14:52:20
GREY: NONE J1154+1009D.IMAP.1
CONT: J115416+ J1154+1009.HGEOM.1
Declination (J2000)
Right Ascension (J2000)
Grey scale flux range= 3.48 20.95 Kilo
Cont peak flux = 2.7676E-03 JY/BEAM
Levs = 2.500E-04 * (1, 1.400, 2, 2.800, 4, 5.600, 8, 11, 16, 23, 32, 45, 64, 90, 128, 181, 256, 362, 512, 724, 1024)

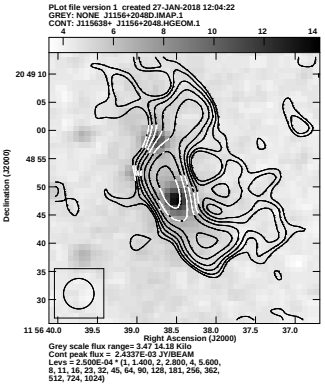
PLot file version 1 created 27-JAN-2018 12:04:22
GREY: NONE J1156+2048D.IMAP.1
CONT: J115638+ J1156+2048.HGEOM.1
Declination (J2000)
Right Ascension (J2000)
Grey scale flux range= 3.47 14.18 Kilo
Cont peak flux = 2.4337E-03 JY/BEAM
Levs = 2.500E-04 * (1, 1.400, 2, 2.800, 4, 5.600, 8, 11, 16, 23, 32, 45, 64, 90, 128, 181, 256, 362, 512, 724, 1024)

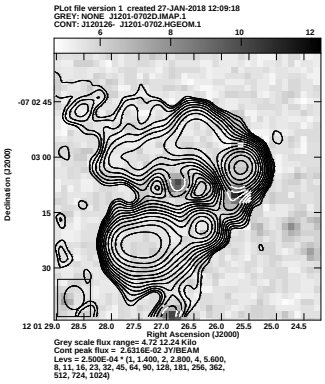
PLot file version 1 created 27-JAN-2018 12:09:18
GREY: NONE J1201-0702D.IMAP.1
CONT: J120126- J1201-0702.HGEOM.1
Declination (J2000)
Right Ascension (J2000)
Grey scale flux range= 4.72 12.24 Kilo
Cont peak flux = 2.6316E-02 JY/BEAM
Levs = 2.500E-04 * (1, 1.400, 2, 2.800, 4, 5.600, 8, 11, 16, 23, 32, 45, 64, 90, 128, 181, 256, 362, 512, 724, 1024)

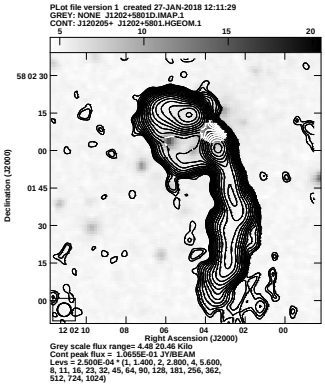
PLot file version 1 created 27-JAN-2018 12:11:29
GREY: NONE J1202+5801D.IMAP.1
CONT: J120205+ J1202+5801.HGEOM.1
Declination (J2000)
Right Ascension (J2000)
Grey scale flux range= 4.48 20.46 Kilo
Cont peak flux = 1.0655E-01 JY/BEAM
Levs = 2.500E-04 * (1, 1.400, 2, 2.800, 4, 5.600, 8, 11, 16, 23, 32, 45, 64, 90, 128, 181, 256, 362, 512, 724, 1024)

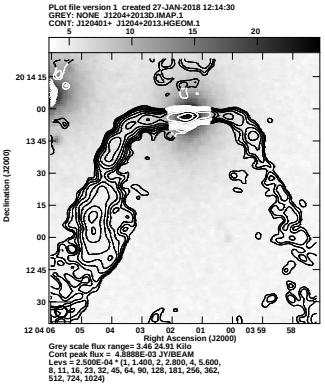
PLot file version 1 created 27-JAN-2018 12:14:30
GREY: NONE J1204+2013D.IMAP.1
CONT: J120401+ J1204+2013.HGEOM.1
Declination (J2000)
Right Ascension (J2000)
Grey scale flux range= 3.46 24.91 Kilo
Cont peak flux = 4.8888E-03 JY/BEAM
Levs = 2.500E-04 * (1, 1.400, 2, 2.800, 4, 5.600, 8, 11, 16, 23, 32, 45, 64, 90, 128, 181, 256, 362, 512, 724, 1024)

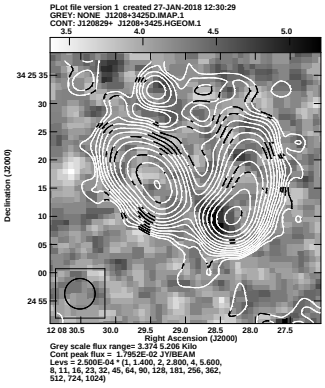
PLot file version 1 created 27-JAN-2018 12:30:29
GREY: NONE J1208+3425D.IMAP.1
CONT: J120829+ J1208+3425.HGEOM.1
Declination (J2000)
Right Ascension (J2000)
Grey scale flux range= 3.374 5.206 Kilo
Cont peak flux = 1.7952E-02 JY/BEAM
Levs = 2.500E-04 * (1, 1.400, 2, 2.800, 4, 5.600, 8, 11, 16, 23, 32, 45, 64, 90, 128, 181, 256, 362, 512, 724, 1024)

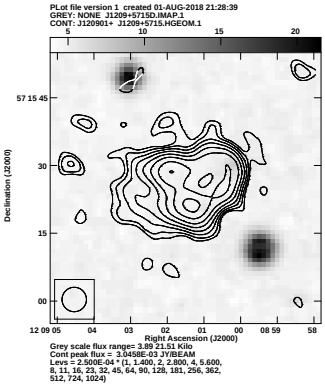
PLot file version 1 created 01-AUG-2018 21:28:39
GREY: NONE J1209+5715D.IMAP.1
CONT: J120901+ J1209+5715.HGEOM.1
Declination (J2000)
Right Ascension (J2000)
Grey scale flux range= 3.89 21.51 Kilo
Cont peak flux = 3.0459E-03 JY/BEAM
Levs = 2.500E-04 * (1, 1.400, 2, 2.800, 4, 5.600, 8, 11, 16, 23, 32, 45, 64, 90, 128, 181, 256, 362, 512, 724, 1024)

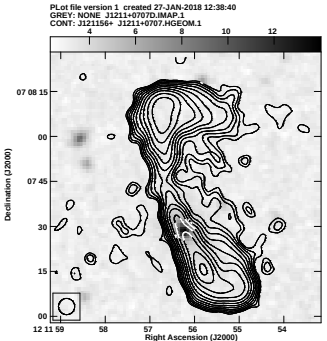
PLot file version 1 created 27-JAN-2018 12:38:40
GREY: NONE J1211+0707D.IMAP.1
CONT: J121156+ J1211+0707.HGEOM.1
Declination (J2000)
Right Ascension (J2000)
Grey scale flux range= 2.34 14.00 Kilo
Cont peak flux = 1.2147E-02 JY/BEAM
Levs = 2.500E-04 * (1, 1.400, 2, 2.800, 4, 5.600, 8, 11, 16, 23, 32, 45, 64, 90, 128, 181, 256, 362, 512, 724, 1024)

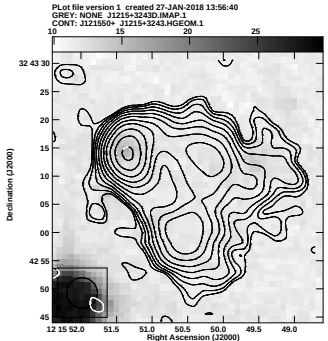
PLot file version 1 created 27-JAN-2018 13:56:40
GREY: NONE J1215+3243D.IMAP.1
CONT: J121550+ J1215+3243.HGEOM.1
Declination (J2000)
Right Ascension (J2000)
Grey scale flux range= 9.93 29.78 Kilo
Cont peak flux = 8.5009E-03 JY/BEAM
Levs = 2.500E-04 * (1, 1.400, 2, 2.800, 4, 5.600, 8, 11, 16, 23, 32, 45, 64, 90, 128, 181, 256, 362, 512, 724, 1024)

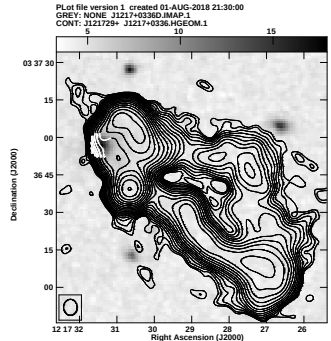
PLot file version 1 created 01-AUG-2018 21:30:00
GREY: NONE J1217+0336D.IMAP.1
CONT: J121729+ J1217+0336.HGEOM.1
Declination (J2000)
Right Ascension (J2000)
Grey scale flux range= 3.36 17.87 Kilo
Cont peak flux = 9.1554E-02 JY/BEAM
Levs = 2.500E-04 * (1, 1.400, 2, 2.800, 4, 5.600, 8, 11, 16, 23, 32, 45, 64, 90, 128, 181, 256, 362, 512, 724, 1024)

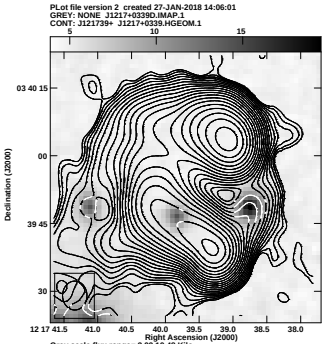
PLot file version 2 created 27-JAN-2018 14:06:01
GREY: NONE J1217+0339D.IMAP.1
CONT: J121739+ J1217+0339.HGEOM.1
Declination (J2000)
Right Ascension (J2000)
Grey scale flux range= 3.92 19.48 Kilo
Cont peak flux = 1.5879E-01 JY/BEAM
Levs = 2.500E-04 * (1, 1.400, 2, 2.800, 4, 5.600, 8, 11, 16, 23, 32, 45, 64, 90, 128, 181, 256, 362, 512, 724, 1024)

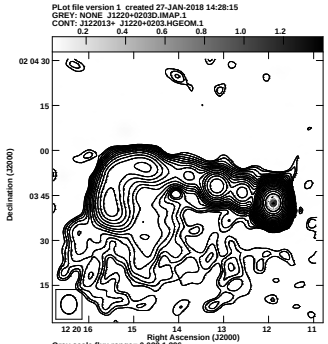
PLot file version 1 created 27-JAN-2018 14:28:15
GREY: NONE J1220+0203D.IMAP.1
CONT: J122013+ J1220+0203.HGEOM.1
Declination (J2000)
Right Ascension (J2000)
Grey scale flux range= 0.033 1.396
Cont peak flux = 3.1787E-01 JY/BEAM
Levs = 2.500E-04 * (1, 1.400, 2, 2.800, 4, 5.600, 8, 11, 16, 23, 32, 45, 64, 90, 128, 181, 256, 362, 512, 724, 1024)

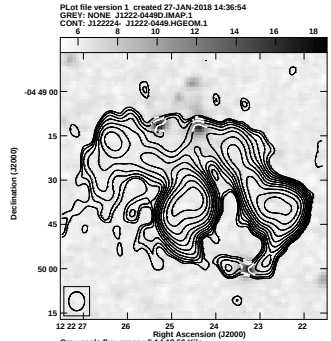
PLot file version 1 created 27-JAN-2018 14:36:54
GREY: NONE J1222-0449D.IMAP.1
CONT: J122224- J1222-0449.HGEOM.1
Declination (J2000)
Right Ascension (J2000)
Grey scale flux range= 5.14 18.56 Kilo
Cont peak flux = 1.0210E-02 JY/BEAM
Levs = 2.500E-04 * (1, 1.400, 2, 2.800, 4, 5.600, 8, 11, 16, 23, 32, 45, 64, 90, 128, 181, 256, 362, 512, 724, 1024)

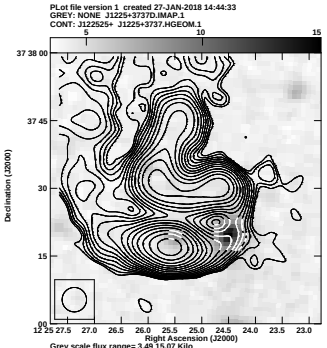
PLot file version 1 created 27-JAN-2018 14:44:33
GREY: NONE J1225+3737D.IMAP.1
CONT: J122525+ J1225+3737.HGEOM.1
Declination (J2000)
Right Ascension (J2000)
Grey scale flux range= 3.49 15.07 Kilo
Cont peak flux = 4.0674E-02 JY/BEAM
Levs = 2.500E-04 * (1, 1.400, 2, 2.800, 4, 5.600, 8, 11, 16, 23, 32, 45, 64, 90, 128, 181, 256, 362, 512, 724, 1024)

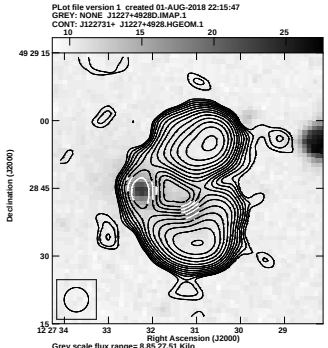
PLot file version 1 created 01-AUG-2018 22:15:47
GREY: NONE J1227+4928D.IMAP.1
CONT: J122731+ J1227+4928.HGEOM.1
Declination (J2000)
Right Ascension (J2000)
Grey scale flux range= 8.85 27.51 Kilo
Cont peak flux = 1.7472E-02 JY/BEAM
Levs = 2.500E-04 * (1, 1.400, 2, 2.800, 4, 5.600, 8, 11, 16, 23, 32, 45, 64, 90, 128, 181, 256, 362, 512, 724, 1024)

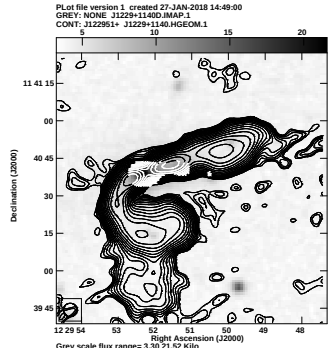
PLot file version 1 created 27-JAN-2018 14:49:00
GREY: NONE J1229+1140D.IMAP.1
CONT: J122951+ J1229+1140.HGEOM.1
Declination (J2000)
Right Ascension (J2000)
Grey scale flux range= 3.30 21.52 Kilo
Cont peak flux = 6.0725E-02 JY/BEAM
Levs = 2.500E-04 * (1, 1.400, 2, 2.800, 4, 5.600, 8, 11, 16, 23, 32, 45, 64, 90, 128, 181, 256, 362, 512, 724, 1024)

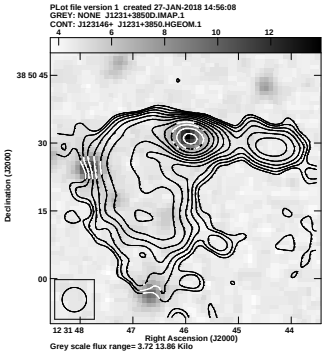
PLot file version 1 created 27-JAN-2018 14:56:08
GREY: NONE J1231+3850D.IMAP.1
CONT: J123146+ J1231+3850.HGEOM.1
Declination (J2000)
Right Ascension (J2000)
Grey scale flux range= 3.72 13.86 Kilo
Cont peak flux = 9.0314E-03 JY/BEAM
Levs = 2.500E-04 * (1, 1.400, 2, 2.800, 4, 5.600, 8, 11, 16, 23, 32, 45, 64, 90, 128, 181, 256, 362, 512, 724, 1024)

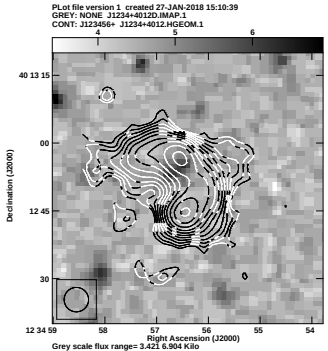
PLot file version 1 created 27-JAN-2018 15:10:39
GREY: NONE J1234+4012D.IMAP.1
CONT: J123456+ J1234+4012.HGEOM.1
Declination (J2000)
Right Ascension (J2000)
Grey scale flux range= 3.421 6.904 Kilo
Cont peak flux = 8.4677E-03 JY/BEAM
Levs = 2.500E-04 * (1, 1.400, 2, 2.800, 4, 5.600, 8, 11, 16, 23, 32, 45, 64, 90, 128, 181, 256, 362, 512, 724, 1024)

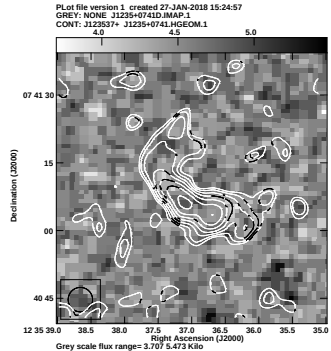
PLot file version 1 created 27-JAN-2018 15:24:57
GREY: NONE J1235+0741D.IMAP.1
CONT: J123537+ J1235+0741.HGEOM.1
Declination (J2000)
Right Ascension (J2000)
Grey scale flux range= 3.707 5.473 Kilo
Cont peak flux = 2.2504E-03 JY/BEAM
Levs = 2.500E-04 * (1, 1.400, 2, 2.800, 4, 5.600, 8, 11, 16, 23, 32, 45, 64, 90, 128, 181, 256, 362, 512, 724, 1024)

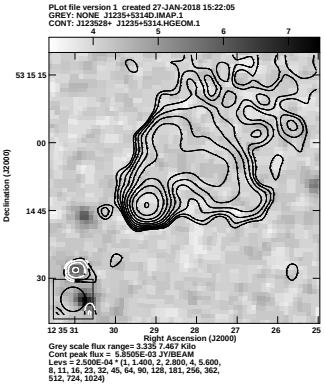
PLot file version 1 created 27-JAN-2018 15:22:05
GREY: NONE J1235+5314D.IMAP.1
CONT: J1235+5314.HGEOM.1
Declination (J2000)
Right Ascension (J2000)
Grey scale flux range= 3.335 7.467 Kilo
Cont peak flux = 5.8505E-03 JY/BEAM
Levs = 2.500E-04 * (1, 1.400, 2, 2.800, 4, 5.600, 8, 11, 16, 23, 32, 45, 64, 90, 128, 181, 256, 362, 512, 724, 1024)

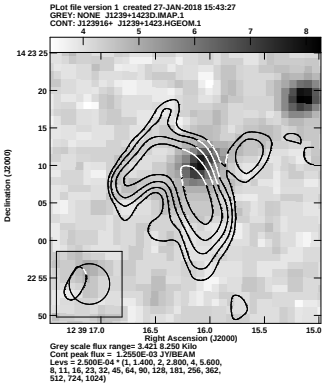
PLot file version 1 created 27-JAN-2018 15:43:27
GREY: NONE J1239+1423D.IMAP.1
CONT: J1239+1+ J1239+1423.HGEOM.1
Declination (J2000)
Right Ascension (J2000)
Grey scale flux range= 3.421 8.250 Kilo
Cont peak flux = 1.2550E-03 JY/BEAM
Levs = 2.500E-04 * (1, 1.400, 2, 2.800, 4, 5.600, 8, 11, 16, 23, 32, 45, 64, 90, 128, 181, 256, 362, 512, 724, 1024)

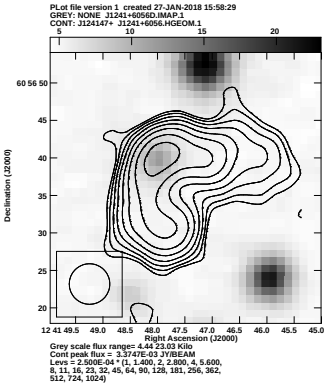
PLot file version 1 created 27-JAN-2018 15:58:29
GREY: NONE J1241+6056D.IMAP.1
CONT: J124147+ J1241+6056.HGEOM.1
Declination (J2000)
Right Ascension (J2000)
Grey scale flux range= 4.44 23.03 Kilo
Cont peak flux = 3.3747E-03 JY/BEAM
Levs = 2.500E-04 * (1, 1.400, 2, 2.800, 4, 5.600, 8, 11, 16, 23, 32, 45, 64, 90, 128, 181, 256, 362, 512, 724, 1024)

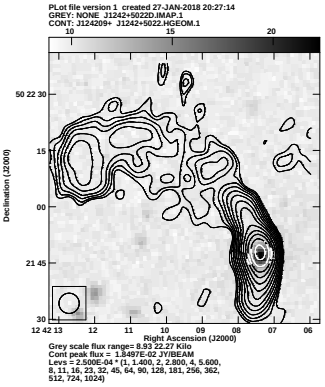
PLot file version 1 created 27-JAN-2018 20:27:14
GREY: NONE J1242+5022D.IMAP.1
CONT: J124209+ J1242+5022.HGEOM.1
Declination (J2000)
Right Ascension (J2000)
Grey scale flux range= 8.93 22.27 Kilo
Cont peak flux = 1.8497E-02 JY/BEAM
Levs = 2.500E-04 * (1, 1.400, 2, 2.800, 4, 5.600, 8, 11, 16, 23, 32, 45, 64, 90, 128, 181, 256, 362, 512, 724, 1024)

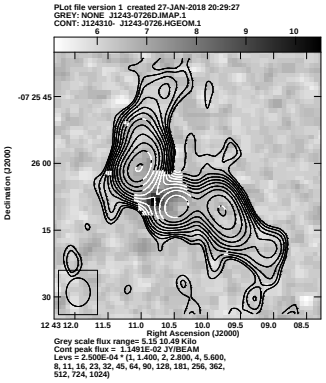
PLot file version 1 created 27-JAN-2018 20:29:27
GREY: NONE J1243-0726D.IMAP.1
CONT: J124310- J1243-0726.HGEOM.1
Declination (J2000)
Right Ascension (J2000)
Grey scale flux range= 5.15 10.49 Kilo
Cont peak flux = 1.1481E-02 JY/BEAM
Levs = 2.500E-04 * (1, 1.400, 2, 2.800, 4, 5.600, 8, 11, 16, 23, 32, 45, 64, 90, 128, 181, 256, 362, 512, 724, 1024)

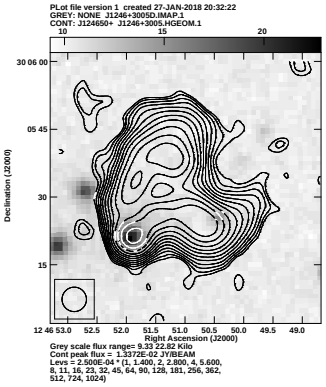
PLot file version 1 created 27-JAN-2018 20:32:22
GREY: NONE J1246+3005D.IMAP.1
CONT: J124650+ J1246+3005.HGEOM.1
Declination (J2000)
Right Ascension (J2000)
Grey scale flux range= 9.33 22.82 Kilo
Cont peak flux = 1.3372E-02 JY/BEAM
Levs = 2.500E-04 * (1, 1.400, 2, 2.800, 4, 5.600, 8, 11, 16, 23, 32, 45, 64, 90, 128, 181, 256, 362, 512, 724, 1024)

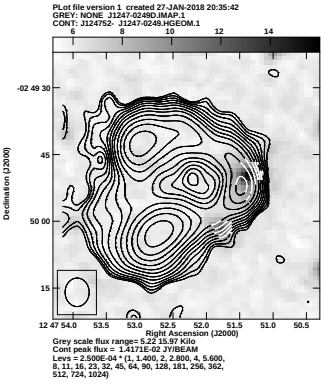
PLot file version 1 created 27-JAN-2018 20:35:42
GREY: NONE J1247-0248D.IMAP.1
CONT: J124752- J1247-0248.HGEOM.1
Declination (J2000)
Right Ascension (J2000)
Grey scale flux range= 5.22 15.97 Kilo
Cont peak flux = 1.4171E-02 JY/BEAM
Levs = 2.500E-04 * (1, 1.400, 2, 2.800, 4, 5.600, 8, 11, 16, 23, 32, 45, 64, 90, 128, 181, 256, 362, 512, 724, 1024)

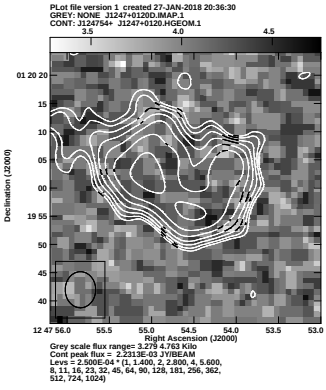
PLot file version 1 created 27-JAN-2018 20:36:30
GREY: NONE J1247+0120D.IMAP.1
CONT: J124754+ J1247+0120.HGEOM.1
Declination (J2000)
Right Ascension (J2000)
Grey scale flux range= 3.279 4.763 Kilo
Cont peak flux = 2.2313E-03 JY/BEAM
Levs = 2.500E-04 * (1, 1.400, 2, 2.800, 4, 5.600, 8, 11, 16, 23, 32, 45, 64, 90, 128, 181, 256, 362, 512, 724, 1024)

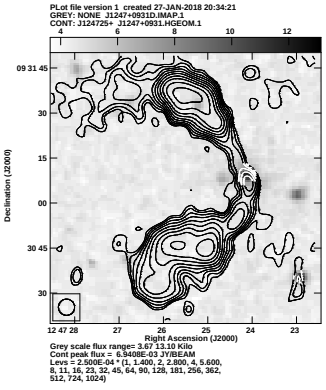
PLot file version 1 created 27-JAN-2018 20:34:21
GREY: NONE J1247+0931D.IMAP.1
CONT: J124725+ J1247+0931.HGEOM.1
Declination (J2000)
Right Ascension (J2000)
Grey scale flux range= 3.67 13.10 Kilo
Cont peak flux = 6.9408E-03 JY/BEAM
Levs = 2.500E-04 * (1, 1.400, 2, 2.800, 4, 5.600, 8, 11, 16, 23, 32, 45, 64, 90, 128, 181, 256, 362, 512, 724, 1024)

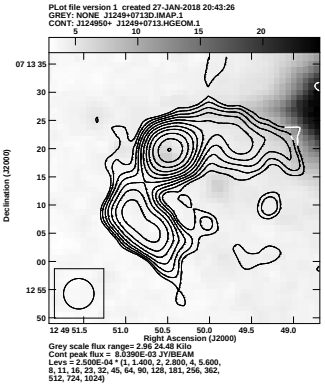
PLot file version 1 created 27-JAN-2018 20:43:26
GREY: NONE J1249+0713D.IMAP.1
CONT: J124950+ J1249+0713.HGEOM.1
Declination (J2000)
Right Ascension (J2000)
Grey scale flux range= 2.96 24.48 Kilo
Cont peak flux = 8.0390E-03 JY/BEAM
Levs = 2.500E-04 * (1, 1.400, 2, 2.800, 4, 5.600, 8, 11, 16, 23, 32, 45, 64, 90, 128, 181, 256, 362, 512, 724, 1024)

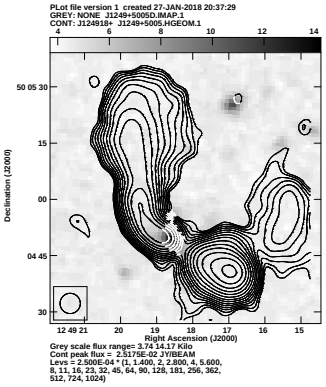
PLot file version 1 created 27-JAN-2018 20:37:29
GREY: NONE J1249+5005D.IMAP.1
CONT: J124918+ J1249+5005.HGEOM.1
Declination (J2000)
Right Ascension (J2000)
Grey scale flux range= 3.74 14.17 Kilo
Cont peak flux = 2.5175E-02 JY/BEAM
Levs = 2.500E-04 * (1, 1.400, 2, 2.800, 4, 5.600, 8, 11, 16, 23, 32, 45, 64, 90, 128, 181, 256, 362, 512, 724, 1024)

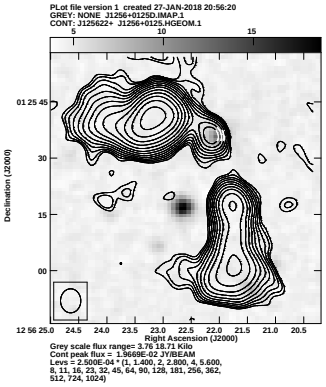
PLot file version 1 created 27-JAN-2018 20:56:20
GREY: NONE J1256+0125D.IMAP.1
CONT: J125622+ J1256+0125.HGEOM.1
Declination (J2000)
Right Ascension (J2000)
Grey scale flux range= 3.76 18.71 Kilo
Cont peak flux = 1.9698E-02 JY/BEAM
Levs = 2.500E-04 * (1, 1.400, 2, 2.800, 4, 5.600, 8, 11, 16, 23, 32, 45, 64, 90, 128, 181, 256, 362, 512, 724, 1024)

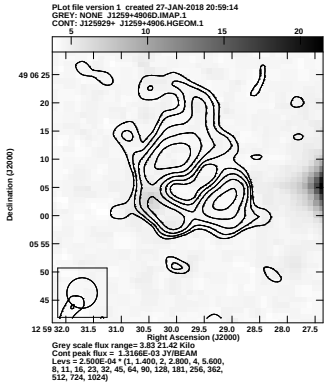
PLot file version 1 created 27-JAN-2018 20:59:14
GREY: NONE J1259+6006D.IMAP.1
CONT: J125929+ J1259+4806.HGEOM.1
Declination (J2000)
Right Ascension (J2000)
Grey scale flux range= 3.83 21.42 Kilo
Cont peak flux = 1.3166E-03 JY/BEAM
Levs = 2.500E-04 * (1, 1.400, 2, 2.800, 4, 5.600, 8, 11, 16, 23, 32, 45, 64, 90, 128, 181, 256, 362, 512, 724, 1024)

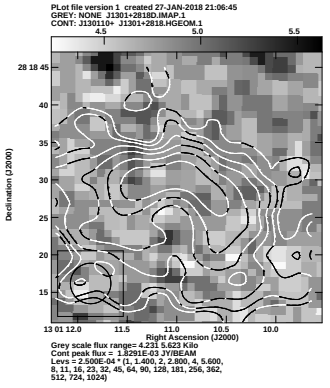
PLot file version 1 created 27-JAN-2018 21:06:45
GREY: NONE J1301+2818D.IMAP.1
CONT: J130110+ J1301+2818.HGEOM.1
Declination (J2000)
Right Ascension (J2000)
Grey scale flux range= 4.231 5.623 Kilo
Cont peak flux = 1.8291E-03 JY/BEAM
Levs = 2.500E-04 * (1, 1.400, 2, 2.800, 4, 5.600, 8, 11, 16, 23, 32, 45, 64, 90, 128, 181, 256, 362, 512, 724, 1024)

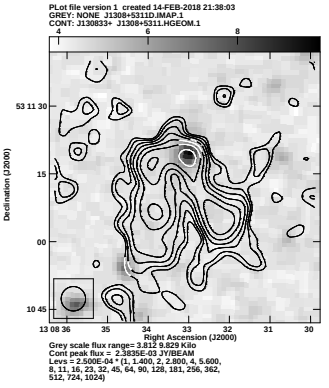
PLot file version 1 created 14-FEB-2018 21:38:03
GREY: NONE J1308+5311D.IMAP.1
CONT: J130833+ J1308+5311.HGEOM.1
Declination (J2000)
Right Ascension (J2000)
Grey scale flux range= 3.812 9.829 Kilo
Cont peak flux = 2.3835E-03 JY/BEAM
Levs = 2.500E-04 * (1, 1.400, 2, 2.800, 4, 5.600, 8, 11, 16, 23, 32, 45, 64, 90, 128, 181, 256, 362, 512, 724, 1024)

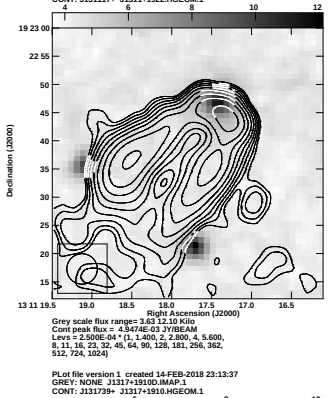
PLot file version 1 created 14-FEB-2018 21:45:16
GREY: NONE J1311+1922D.IMAP.1
CONT: J131117+ J1311+1922.HGEOM.1
Declination (J2000)
Right Ascension (J2000)
Grey scale flux range= 3.63 12.10 Kilo
Cont peak flux = 4.9474E-03 JY/BEAM
Levs = 2.500E-04 * (1, 1.400, 2, 2.800, 4, 5.600, 8, 11, 16, 23, 32, 45, 64, 90, 128, 181, 256, 362, 512, 724, 1024)

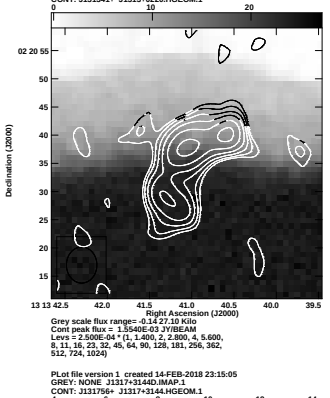
PLot file version 1 created 14-FEB-2018 23:04:16
GREY: NONE J1313+0220D.IMAP.1
CONT: J131341+ J1313+0220.HGEOM.1
Declination (J2000)
Right Ascension (J2000)
Grey scale flux range= -0.14 27.10 Kilo
Cont peak flux = 1.5540E-03 JY/BEAM
Levs = 2.500E-04 * (1, 1.400, 2, 2.800, 4, 5.600, 8, 11, 16, 23, 32, 45, 64, 90, 128, 181, 256, 362, 512, 724, 1024)

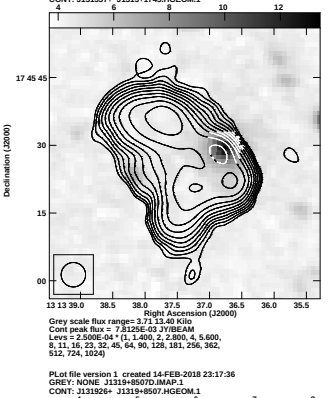
PLot file version 1 created 14-FEB-2018 23:02:33
GREY: NONE J1313+1745D.IMAP.1
CONT: J131337+ J1313+1745.HGEOM.1
Declination (J2000)
Right Ascension (J2000)
Grey scale flux range= 3.71 13.40 Kilo
Cont peak flux = 7.8125E-03 JY/BEAM
Levs = 2.500E-04 * (1, 1.400, 2, 2.800, 4, 5.600, 8, 11, 16, 23, 32, 45, 64, 90, 128, 181, 256, 362, 512, 724, 1024)

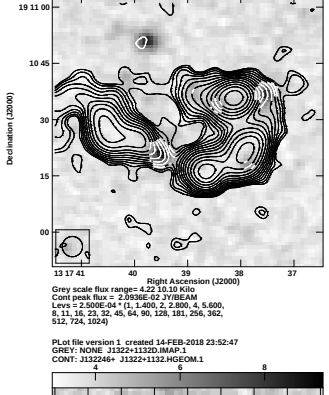
PLot file version 1 created 14-FEB-2018 23:13:37
GREY: NONE J1317+1910D.IMAP.1
CONT: J131739+ J1317+1910.HGEOM.1
Declination (J2000)
Right Ascension (J2000)
Grey scale flux range= 4.22 10.10 Kilo
Cont peak flux = 2.0936E-02 JY/BEAM
Levs = 2.500E-04 * (1, 1.400, 2, 2.800, 4, 5.600, 8, 11, 16, 23, 32, 45, 64, 90, 128, 181, 256, 362, 512, 724, 1024)

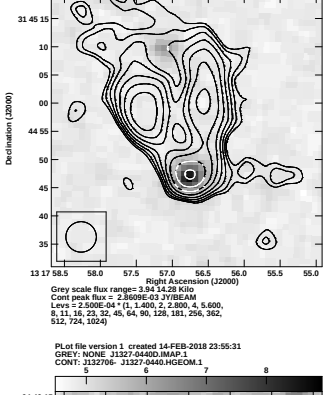
PLot file version 1 created 14-FEB-2018 23:15:05
GREY: NONE J1317+3144D.IMAP.1
CONT: J131756+ J1317+3144.HGEOM.1
Declination (J2000)
Right Ascension (J2000)
Grey scale flux range= 3.94 14.28 Kilo
Cont peak flux = 2.8609E-03 JY/BEAM
Levs = 2.500E-04 * (1, 1.400, 2, 2.800, 4, 5.600, 8, 11, 16, 23, 32, 45, 64, 90, 128, 181, 256, 362, 512, 724, 1024)

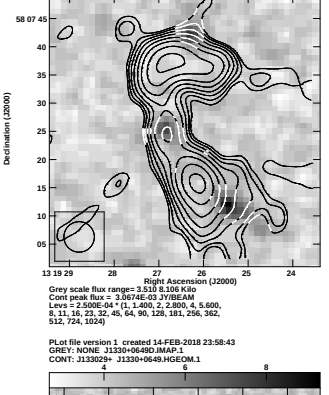
PLot file version 1 created 14-FEB-2018 23:17:36
GREY: NONE J1319+8507D.IMAP.1
CONT: J131926+ J1319+8507.HGEOM.1
Declination (J2000)
Right Ascension (J2000)
Grey scale flux range= 3.510 8.106 Kilo
Cont peak flux = 3.0674E-03 JY/BEAM
Levs = 2.500E-04 * (1, 1.400, 2, 2.800, 4, 5.600, 8, 11, 16, 23, 32, 45, 64, 90, 128, 181, 256, 362, 512, 724, 1024)

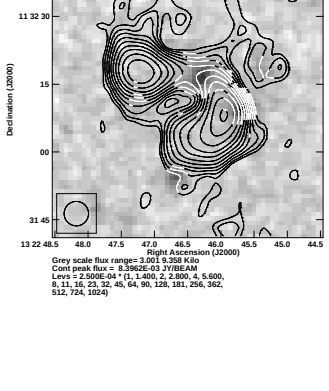
PLot file version 1 created 14-FEB-2018 23:52:47
GREY: NONE J1322+1132D.IMAP.1
CONT: J132246+ J1322+1132.HGEOM.1
Declination (J2000)
Right Ascension (J2000)
Grey scale flux range= 3.001 9.358 Kilo
Cont peak flux = 8.3962E-03 JY/BEAM
Levs = 2.500E-04 * (1, 1.400, 2, 2.800, 4, 5.600, 8, 11, 16, 23, 32, 45, 64, 90, 128, 181, 256, 362, 512, 724, 1024)

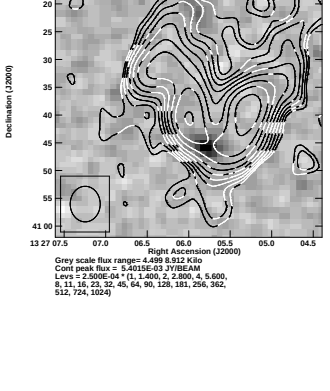
PLot file version 1 created 14-FEB-2018 23:55:31
GREY: NONE J1327-0440D.IMAP.1
CONT: J132706- J1327-0440.HGEOM.1
Declination (J2000)
Right Ascension (J2000)
Grey scale flux range= 4.499 8.912 Kilo
Cont peak flux = 5.4015E-03 JY/BEAM
Levs = 2.500E-04 * (1, 1.400, 2, 2.800, 4, 5.600, 8, 11, 16, 23, 32, 45, 64, 90, 128, 181, 256, 362, 512, 724, 1024)

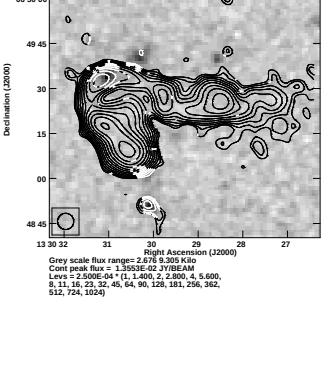
PLot file version 1 created 14-FEB-2018 23:58:43
GREY: NONE J1330+0649D.IMAP.1
CONT: J133029+ J1330+0649.HGEOM.1
Declination (J2000)
Right Ascension (J2000)
Grey scale flux range= 2.676 9.305 Kilo
Cont peak flux = 1.3553E-02 JY/BEAM
Levs = 2.500E-04 * (1, 1.400, 2, 2.800, 4, 5.600, 8, 11, 16, 23, 32, 45, 64, 90, 128, 181, 256, 362, 512, 724, 1024)

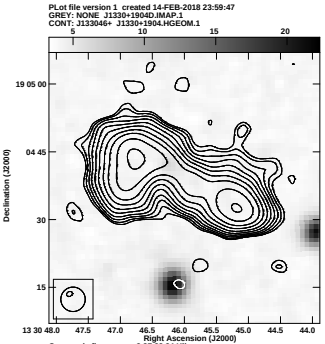
PLot file version 1 created 14-FEB-2018 23:59:47
GREY: NONE J1330+1904D.IMAP.1
CONT: J133046+ J1330+1904.HGEOM.1
Declination (J2000)
Right Ascension (J2000)
Grey scale flux range= 3.37 22.24 Kilo
Cont peak flux = 6.2118E-03 JY/BEAM
Levs = 2.500E-04 * (1, 1.400, 2, 2.800, 4, 5.600, 8, 11, 16, 23, 32, 45, 64, 90, 128, 181, 256, 362, 512, 724, 1024)

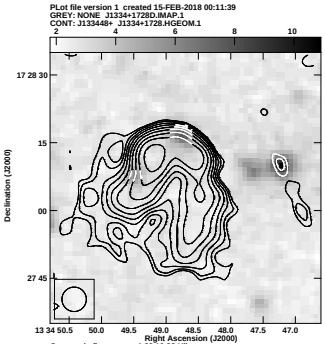
PLot file version 1 created 15-FEB-2018 00:11:39
GREY: NONE J1334+1728D.IMAP.1
CONT: J133448+ J1334+1728.HGEOM.1
Declination (J2000)
Right Ascension (J2000)
Grey scale flux range= 1.82 10.88 Kilo
Cont peak flux = 5.2052E-03 JY/BEAM
Levs = 2.500E-04 * (1, 1.400, 2, 2.800, 4, 5.600, 8, 11, 16, 23, 32, 45, 64, 90, 128, 181, 256, 362, 512, 724, 1024)

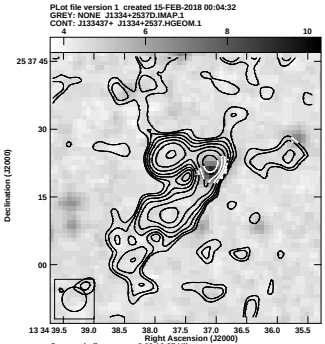
PLot file version 1 created 15-FEB-2018 00:04:32
GREY: NONE J1334+2537D.IMAP.1
CONT: J133437+ J1334+2537.HGEOM.1
Declination (J2000)
Right Ascension (J2000)
Grey scale flux range= 3.69 10.27 Kilo
Cont peak flux = 2.5046E-03 JY/BEAM
Levs = 2.500E-04 * (1, 1.400, 2, 2.800, 4, 5.600, 8, 11, 16, 23, 32, 45, 64, 90, 128, 181, 256, 362, 512, 724, 1024)

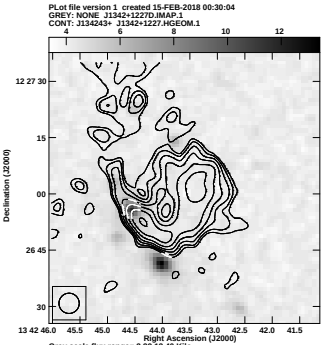
PLot file version 1 created 15-FEB-2018 00:30:04
GREY: NONE J1342+1227D.IMAP.1
CONT: J134243+ J1342+1227.HGEOM.1
Declination (J2000)
Right Ascension (J2000)
Grey scale flux range= 3.39 13.40 Kilo
Cont peak flux = 2.0689E-03 JY/BEAM
Levs = 2.500E-04 * (1, 1.400, 2, 2.800, 4, 5.600, 8, 11, 16, 23, 32, 45, 64, 90, 128, 181, 256, 362, 512, 724, 1024)

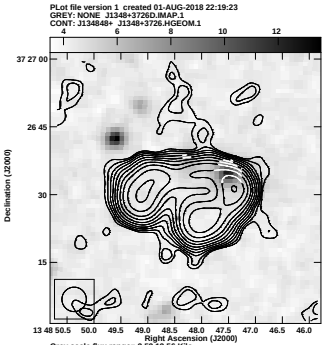
PLot file version 1 created 01-AUG-2018 22:19:23
GREY: NONE J1348+3726D.IMAP.1
CONT: J134848+ J1348+3726.HGEOM.1
Declination (J2000)
Right Ascension (J2000)
Grey scale flux range= 3.53 13.56 Kilo
Cont peak flux = 8.1467E-03 JY/BEAM
Levs = 2.500E-04 * (1, 1.400, 2, 2.800, 4, 5.600, 8, 11, 16, 23, 32, 45, 64, 90, 128, 181, 256, 362, 512, 724, 1024)

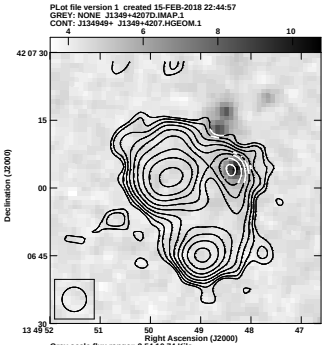
PLot file version 1 created 15-FEB-2018 22:44:57
GREY: NONE J1349+4207D.IMAP.1
CONT: J134949+ J1349+4207.HGEOM.1
Declination (J2000)
Right Ascension (J2000)
Grey scale flux range= 3.54 10.74 Kilo
Cont peak flux = 4.6062E-03 JY/BEAM
Levs = 2.500E-04 * (1, 1.400, 2, 2.800, 4, 5.600, 8, 11, 16, 23, 32, 45, 65, 90, 128, 181, 256, 362, 512, 724, 1024)

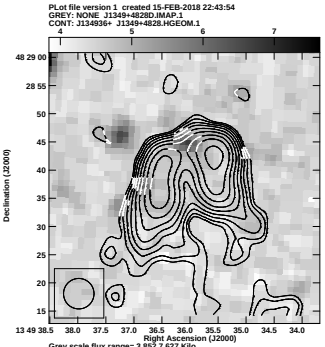
PLot file version 1 created 15-FEB-2018 22:43:54
GREY: NONE J1349+4828D.IMAP.1
CONT: J134936+ J1349+4828.HGEOM.1
Declination (J2000)
Right Ascension (J2000)
Grey scale flux range= 3.852 7.627 Kilo
Cont peak flux = 4.7889E-03 JY/BEAM
Levs = 2.500E-04 * (1, 1.400, 2, 2.800, 4, 5.600, 8, 11, 16, 23, 32, 45, 65, 90, 128, 181, 256, 362, 512, 724, 1024)

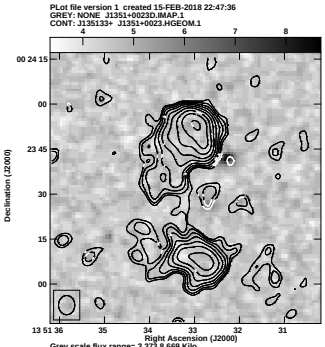
PLot file version 1 created 15-FEB-2018 22:47:36
GREY: NONE J1351+0023D.IMAP.1
CONT: J135133+ J1351+0023.HGEOM.1
Declination (J2000)
Right Ascension (J2000)
Grey scale flux range= 3.373 8.669 Kilo
Cont peak flux = 2.2006E-03 JY/BEAM
Levs = 2.500E-04 * (1, 1.400, 2, 2.800, 4, 5.600, 8, 11, 16, 23, 32, 45, 65, 90, 128, 181, 256, 362, 512, 724, 1024)

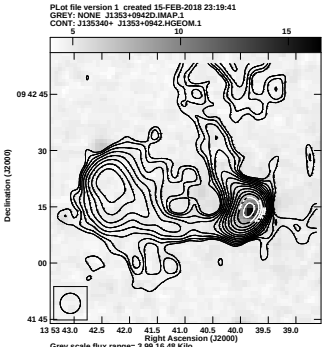
PLot file version 1 created 15-FEB-2018 23:19:41
GREY: NONE J1353+0942D.IMAP.1
CONT: J135340+ J1353+0942.HGEOM.1
Declination (J2000)
Right Ascension (J2000)
Grey scale flux range= 3.99 16.48 Kilo
Cont peak flux = 1.8951E-02 JY/BEAM
Levs = 2.500E-04 * (1, 1.400, 2, 2.800, 4, 5.600, 8, 11, 16, 23, 32, 45, 65, 90, 128, 181, 256, 362, 512, 724, 1024)

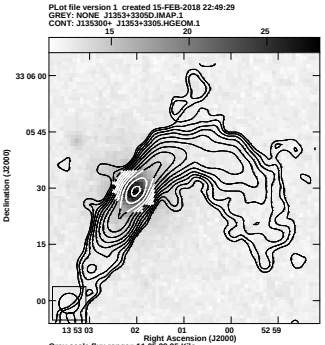
PLot file version 1 created 15-FEB-2018 22:49:29
GREY: NONE J1353+3305D.IMAP.1
CONT: J135300+ J1353+3305.HGEOM.1
Declination (J2000)
Right Ascension (J2000)
Grey scale flux range= 11.05 28.35 Kilo
Cont peak flux = 8.8894E-03 JY/BEAM
Levs = 2.500E-04 * (1, 1.400, 2, 2.800, 4, 5.600, 8, 11, 16, 23, 32, 45, 65, 90, 128, 181, 256, 362, 512, 724, 1024)

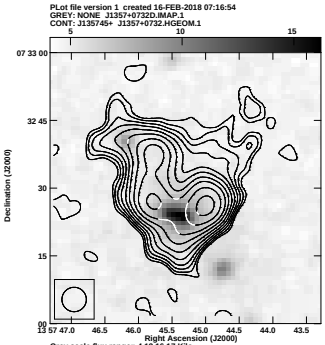
PLot file version 1 created 16-FEB-2018 07:16:54
GREY: NONE J1357+0732D.IMAP.1
CONT: J135745+ J1357+0732.HGEOM.1
Declination (J2000)
Right Ascension (J2000)
Grey scale flux range= 4.13 16.17 Kilo
Cont peak flux = 6.7480E-03 JY/BEAM
Levs = 2.500E-04 * (1, 1.400, 2, 2.800, 4, 5.600, 8, 11, 16, 23, 32, 45, 65, 90, 128, 181, 256, 362, 512, 724, 1024)

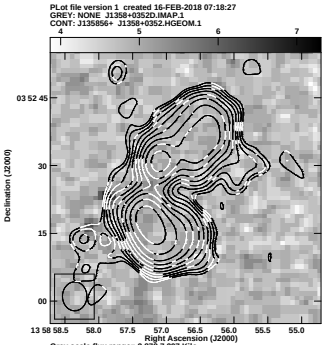
PLot file version 1 created 16-FEB-2018 07:18:27
GREY: NONE J1358+0352D.IMAP.1
CONT: J135856+ J1358+0352.HGEOM.1
Declination (J2000)
Right Ascension (J2000)
Grey scale flux range= 3.878 7.297 Kilo
Cont peak flux = 7.9148E-03 JY/BEAM
Levs = 2.500E-04 * (1, 1.400, 2, 2.800, 4, 5.600, 8, 11, 16, 23, 32, 45, 65, 90, 128, 181, 256, 362, 512, 724, 1024)

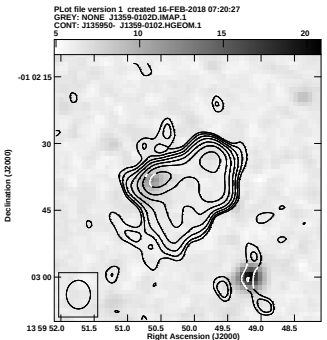
PLot file version 1 created 16-FEB-2018 07:20:27
GREY: NONE J1359-0102D.IMAP.1
CONT: J1359S0- J1359-0102.HGEOM.1
Declination (J2000)
Right Ascension (J2000)
Grey scale flux range= 4.95 20.79 Kilo
Cont peak flux = 2.3927E-03 JY/BEAM
Levs = 2.500E-04 * (1, 1.400, 2, 2.800, 4, 5.600, 8, 11, 16, 23, 32, 45, 65, 90, 128, 181, 256, 362, 512, 724, 1024)

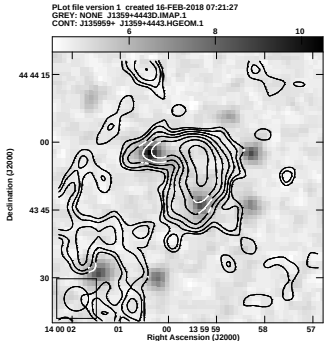
PLot file version 1 created 16-FEB-2018 07:21:27
GREY: NONE J1359+4443D.IMAP.1
CONT: J1359S9+ J1359+4443.HGEOM.1
Declination (J2000)
Right Ascension (J2000)
Grey scale flux range= 4.24 10.48 Kilo
Cont peak flux = 2.4520E-03 JY/BEAM
Levs = 2.500E-04 * (1, 1.400, 2, 2.800, 4, 5.600, 8, 11, 16, 23, 32, 45, 65, 90, 128, 181, 256, 362, 512, 724, 1024)

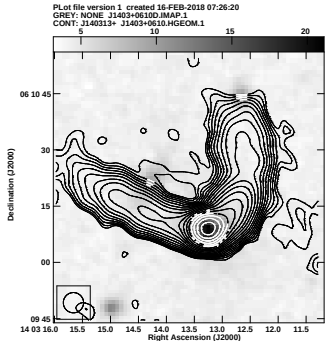
PLot file version 1 created 16-FEB-2018 07:26:20
GREY: NONE J1403+0610D.IMAP.1
CONT: J140313+ J1403+0610.HGEOM.1
Declination (J2000)
Right Ascension (J2000)
Grey scale flux range= 3.23 21.06 Kilo
Cont peak flux = 1.1300E-01 JY/BEAM
Levs = 2.500E-04 * (1, 1.400, 2, 2.800, 4, 5.600, 8, 11, 16, 23, 32, 45, 65, 90, 128, 181, 256, 362, 512, 724, 1024)

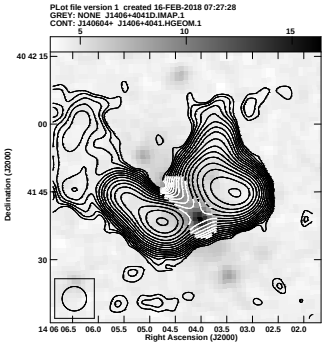
PLot file version 1 created 16-FEB-2018 07:27:28
GREY: NONE J1406+4041D.IMAP.1
CONT: J140604+ J1406+4041.HGEOM.1
Declination (J2000)
Right Ascension (J2000)
Grey scale flux range= 3.62 16.33 Kilo
Cont peak flux = 4.7021E-02 JY/BEAM
Levs = 2.500E-04 * (1, 1.400, 2, 2.800, 4, 5.600, 8, 11, 16, 23, 32, 45, 65, 90, 128, 181, 256, 362, 512, 724, 1024)

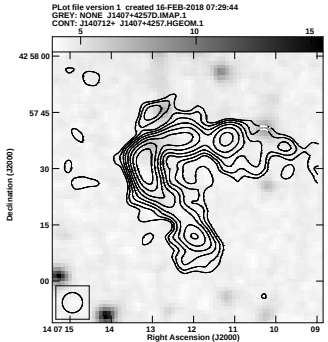
PLot file version 1 created 16-FEB-2018 07:29:44
GREY: NONE J1407+4257D.IMAP.1
CONT: J140712+ J1407+4257.HGEOM.1
Declination (J2000)
Right Ascension (J2000)
Grey scale flux range= 3.81 15.46 Kilo
Cont peak flux = 3.6742E-03 JY/BEAM
Levs = 2.500E-04 * (1, 1.400, 2, 2.800, 4, 5.600, 8, 11, 16, 23, 32, 45, 65, 90, 128, 181, 256, 362, 512, 724, 1024)

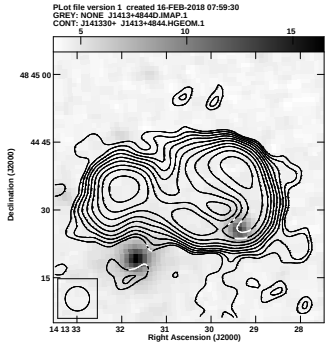
PLot file version 1 created 16-FEB-2018 07:59:30
GREY: NONE J1413+4844D.IMAP.1
CONT: J141330+ J1413+4844.HGEOM.1
Declination (J2000)
Right Ascension (J2000)
Grey scale flux range= 3.75 16.43 Kilo
Cont peak flux = 7.5510E-03 JY/BEAM
Levs = 2.500E-04 * (1, 1.400, 2, 2.800, 4, 5.600, 8, 11, 16, 23, 32, 45, 65, 90, 128, 181, 256, 362, 512, 724, 1024)

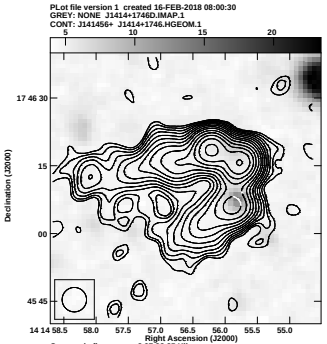
PLot file version 1 created 16-FEB-2018 08:00:30
GREY: NONE J1414+1746D.IMAP.1
CONT: J141456+ J1414+1746.HGEOM.1
Declination (J2000)
Right Ascension (J2000)
Grey scale flux range= 3.97 23.35 Kilo
Cont peak flux = 1.8129E-02 JY/BEAM
Levs = 2.500E-04 * (1, 1.400, 2, 2.800, 4, 5.600, 8, 11, 16, 23, 32, 45, 65, 90, 128, 181, 256, 362, 512, 724, 1024)

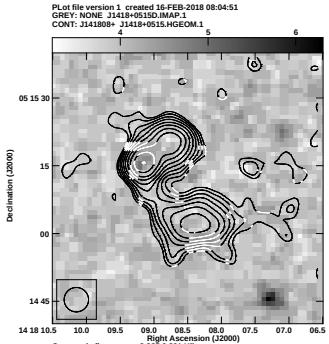
PLot file version 1 created 16-FEB-2018 08:04:51
GREY: NONE J1418+0515D.IMAP.1
CONT: J141808+ J1418+0515.HGEOM.1
Declination (J2000)
Right Ascension (J2000)
Grey scale flux range= 3.23 6.301 Kilo
Cont peak flux = 5.7879E-03 JY/BEAM
Levs = 2.500E-04 * (1, 1.400, 2, 2.800, 4, 5.600, 8, 11, 16, 23, 32, 45, 65, 90, 128, 181, 256, 362, 512, 724, 1024)

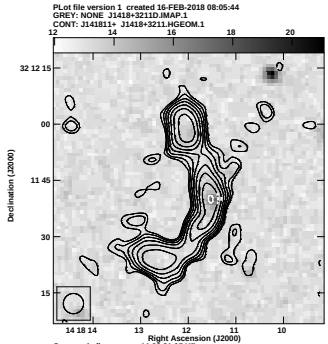
PLot file version 1 created 16-FEB-2018 08:05:44
GREY: NONE J1418+3211D.IMAP.1
CONT: J141811+ J1418+3211.HGEOM.1
Declination (J2000)
Right Ascension (J2000)
Grey scale flux range= 11.98 21.05 Kilo
Cont peak flux = 2.8377E-03 JY/BEAM
Levs = 2.500E-04 * (1, 1.400, 2, 2.800, 4, 5.600, 8, 11, 16, 23, 32, 45, 65, 90, 128, 181, 256, 362, 512, 724, 1024)

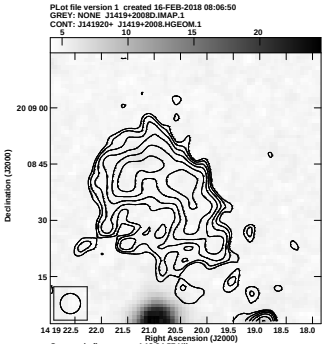
PLot file version 1 created 16-FEB-2018 08:06:50
GREY: NONE J1419+2008D.IMAP.1
CONT: J141920+ J1419+2008.HGEOM.1
Declination (J2000)
Right Ascension (J2000)
Grey scale flux range= 4.18 24.57 Kilo
Cont peak flux = 1.7665E-03 JY/BEAM
Levs = 2.500E-04 * (1, 1.400, 2, 2.800, 4, 5.600, 8, 11, 16, 23, 32, 45, 65, 90, 128, 181, 256, 362, 512, 724, 1024)

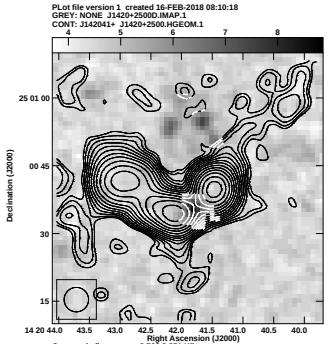
PLot file version 1 created 16-FEB-2018 08:10:18
GREY: NONE J1420+2500D.IMAP.1
CONT: J142041+ J1420+2500.HGEOM.1
Declination (J2000)
Right Ascension (J2000)
Grey scale flux range= 3.708 8.851 Kilo
Cont peak flux = 2.7609E-02 JY/BEAM
Levs = 2.500E-04 * (1, 1.400, 2, 2.800, 4, 5.600, 8, 11, 16, 23, 32, 45, 65, 90, 128, 181, 256, 362, 512, 724, 1024)

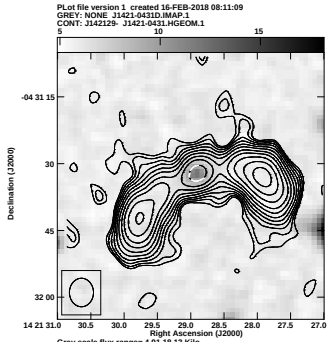
PLot file version 1 created 16-FEB-2018 08:11:09
GREY: NONE J1421-0431D.IMAP.1
CONT: J142129- J1421-0431.HGEOM.1
Declination (J2000)
Right Ascension (J2000)
Grey scale flux range= 4.91 18.13 Kilo
Cont peak flux = 9.5473E-03 JY/BEAM
Levs = 2.500E-04 * (1, 1.400, 2, 2.800, 4, 5.600, 8, 11, 16, 23, 32, 45, 65, 90, 128, 181, 256, 362, 512, 724, 1024)

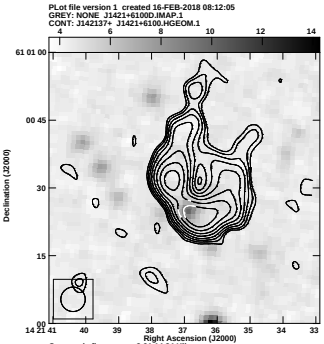
PLot file version 1 created 16-FEB-2018 08:12:05
GREY: NONE J1421+6100D.IMAP.1
CONT: J142137+ J1421+6100.HGEOM.1
Declination (J2000)
Right Ascension (J2000)
Grey scale flux range= 3.61 14.24 Kilo
Cont peak flux = 3.8303E-03 JY/BEAM
Levs = 2.500E-04 * (1, 1.400, 2, 2.800, 4, 5.600, 8, 11, 16, 23, 32, 45, 65, 90, 128, 181, 256, 362, 512, 724, 1024)

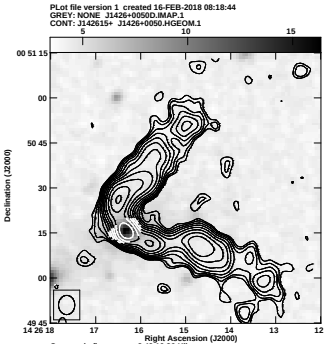
PLot file version 1 created 16-FEB-2018 08:18:44
GREY: NONE J1426+0050D.IMAP.1
CONT: J142615+ J1426+0050.HGEOM.1
Declination (J2000)
Right Ascension (J2000)
Grey scale flux range= 3.49 16.30 Kilo
Cont peak flux = 8.3665E-03 JY/BEAM
Levs = 2.500E-04 * (1, 1.400, 2, 2.800, 4, 5.600, 8, 11, 16, 23, 32, 45, 65, 90, 128, 181, 256, 362, 512, 724, 1024)

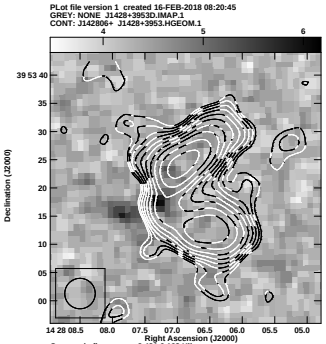
PLot file version 1 created 16-FEB-2018 08:20:45
GREY: NONE J1428+3953D.IMAP.1
CONT: J142806+ J1428+3953.HGEOM.1
Declination (J2000)
Right Ascension (J2000)
Grey scale flux range= 3.481 6.168 Kilo
Cont peak flux = 7.0665E-03 JY/BEAM
Levs = 2.500E-04 * (1, 1.400, 2, 2.800, 4, 5.600, 8, 11, 16, 23, 32, 45, 65, 90, 128, 181, 256, 362, 512, 724, 1024)

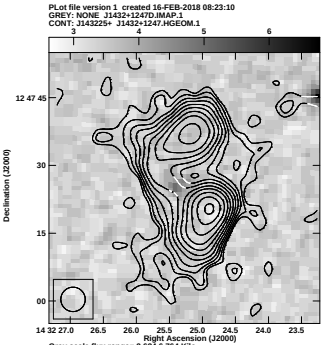
PLot file version 1 created 16-FEB-2018 08:23:10
GREY: NONE J1432+1247D.IMAP.1
CONT: J143225+ J1432+1247.HGEOM.1
Declination (J2000)
Right Ascension (J2000)
Grey scale flux range= 2.634 6.764 Kilo
Cont peak flux = 8.4749E-03 JY/BEAM
Levs = 2.500E-04 * (1, 1.400, 2, 2.800, 4, 5.600, 8, 11, 16, 23, 32, 45, 65, 90, 128, 181, 256, 362, 512, 724, 1024)

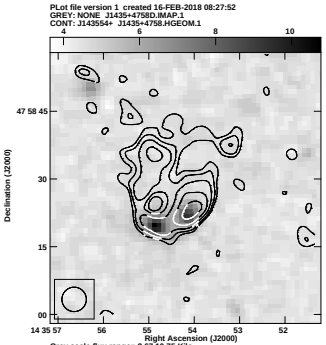
PLot file version 1 created 16-FEB-2018 08:27:52
GREY: NONE J1435+4758D.IMAP.1
CONT: J143554+ J1435+4758.HGEOM.1
Declination (J2000)
Right Ascension (J2000)
Grey scale flux range= 3.67 10.75 Kilo
Cont peak flux = 1.1977E-03 JY/BEAM
Levs = 2.500E-04 * (1, 1.400, 2, 2.800, 4, 5.600, 8, 11, 16, 23, 32, 45, 65, 90, 128, 181, 256, 362, 512, 724, 1024)

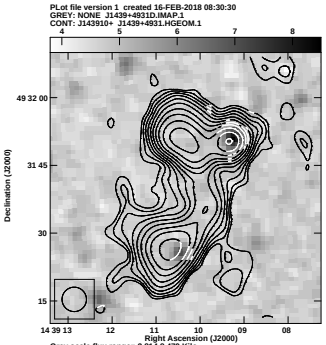
PLot file version 1 created 16-FEB-2018 08:30:30
GREY: NONE J1439+4931D.IMAP.1
CONT: J143910+ J1439+4931.HGEOM.1
Declination (J2000)
Right Ascension (J2000)
Grey scale flux range= 3.814 8.479 Kilo
Cont peak flux = 8.1898E-03 JY/BEAM
Levs = 2.500E-04 * (1, 1.400, 2, 2.800, 4, 5.600, 8, 11, 16, 23, 32, 45, 65, 90, 128, 181, 256, 362, 512, 724, 1024)

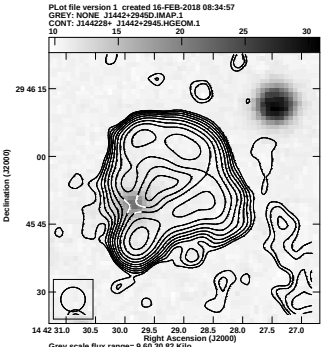
PLot file version 1 created 16-FEB-2018 08:34:57
GREY: NONE J1442+2945D.IMAP.1
CONT: J144228+ J1442+2945.HGEOM.1
Declination (J2000)
Right Ascension (J2000)
Grey scale flux range= 9.60 30.82 Kilo
Cont peak flux = 7.0787E-03 JY/BEAM
Levs = 2.500E-04 * (1, 1.400, 2, 2.800, 4, 5.600, 8, 11, 16, 23, 32, 45, 65, 90, 128, 181, 256, 362, 512, 724, 1024)

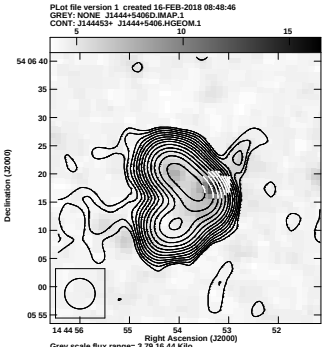
PLot file version 1 created 16-FEB-2018 08:48:46
GREY: NONE J1444+5406D.IMAP.1
CONT: J144453+ J1444+5406.HGEOM.1
Declination (J2000)
Right Ascension (J2000)
Grey scale flux range= 3.79 16.44 Kilo
Cont peak flux = 2.0022E-02 JY/BEAM
Levs = 2.500E-04 * (1, 1.400, 2, 2.800, 4, 5.600, 8, 11, 16, 23, 32, 45, 65, 90, 128, 181, 256, 362, 512, 724, 1024)

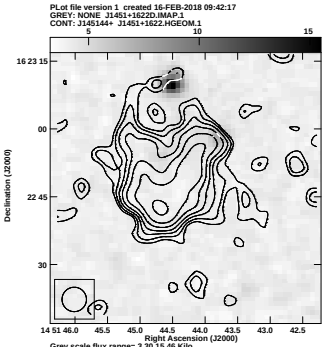
PLot file version 1 created 16-FEB-2018 09:42:17
GREY: NONE J1451+1622D.IMAP.1
CONT: J145144+ J1451+1622.HGEOM.1
Declination (J2000)
Right Ascension (J2000)
Grey scale flux range= 3.30 15.46 Kilo
Cont peak flux = 2.1331E-03 JY/BEAM
Levs = 2.500E-04 * (1, 1.400, 2, 2.800, 4, 5.600, 8, 11, 16, 23, 32, 45, 64, 90, 128, 181, 256, 362, 512, 724, 1024)

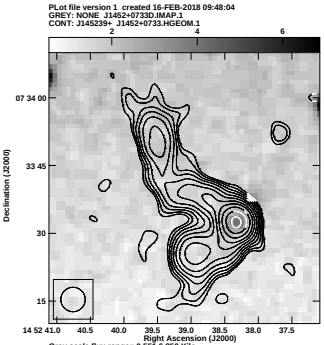
PLot file version 1 created 16-FEB-2018 09:48:04
GREY: NONE J1452+0733D.IMAP.1
CONT: J145239+ J1452+0733.HGEOM.1
Declination (J2000)
Right Ascension (J2000)
Grey scale flux range= 0.551 6.850 Kilo
Cont peak flux = 8.8451E-03 JY/BEAM
Levs = 2.500E-04 * (1, 1.400, 2, 2.800, 4, 5.600, 8, 11, 16, 23, 32, 45, 64, 90, 128, 181, 256, 362, 512, 724, 1024)

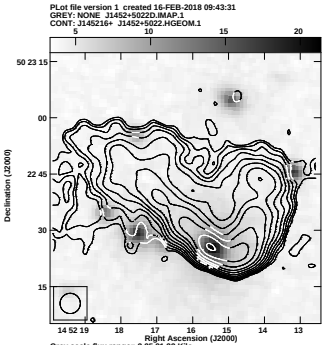
PLot file version 1 created 16-FEB-2018 09:43:31
GREY: NONE J1452+5022D.IMAP.1
CONT: J145216+ J1452+5022.HGEOM.1
Declination (J2000)
Right Ascension (J2000)
Grey scale flux range= 3.35 21.33 Kilo
Cont peak flux = 8.2998E-03 JY/BEAM
Levs = 2.500E-04 * (1, 1.400, 2, 2.800, 4, 5.600, 8, 11, 16, 23, 32, 45, 64, 90, 128, 181, 256, 362, 512, 724, 1024)

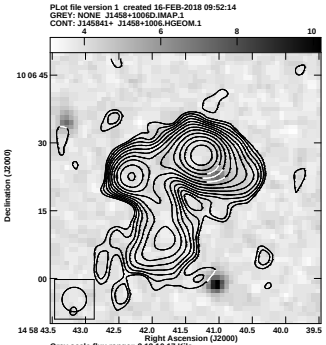
PLot file version 1 created 16-FEB-2018 09:52:14
GREY: NONE J1458+1006D.IMAP.1
CONT: J145841+ J1458+1006.HGEOM.1
Declination (J2000)
Right Ascension (J2000)
Grey scale flux range= 3.13 10.17 Kilo
Cont peak flux = 1.5019E-02 JY/BEAM
Levs = 2.500E-04 * (1, 1.400, 2, 2.800, 4, 5.600, 8, 11, 16, 23, 32, 45, 64, 90, 128, 181, 256, 362, 512, 724, 1024)

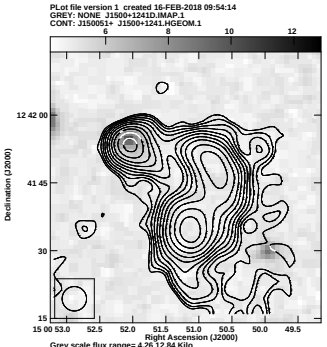
PLot file version 1 created 16-FEB-2018 09:54:14
GREY: NONE J1509+1241D.IMAP.1
CONT: J150051+ J1509+1241.HGEOM.1
Declination (J2000)
Right Ascension (J2000)
Grey scale flux range= 4.26 12.84 Kilo
Cont peak flux = 1.0207E-02 JY/BEAM
Levs = 2.500E-04 * (1, 1.400, 2, 2.800, 4, 5.600, 8, 11, 16, 23, 32, 45, 64, 90, 128, 181, 256, 362, 512, 724, 1024)

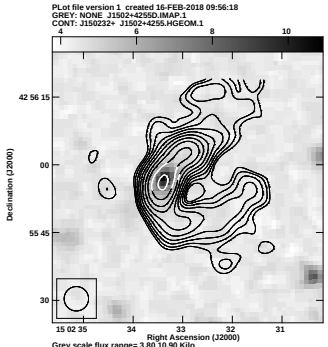
PLot file version 1 created 16-FEB-2018 09:56:18
GREY: NONE J1502+4255D.IMAP.1
CONT: J150232+ J1502+4255.HGEOM.1
Declination (J2000)
Right Ascension (J2000)
Grey scale flux range= 3.80 10.90 Kilo
Cont peak flux = 6.2989E-03 JY/BEAM
Levs = 2.500E-04 * (1, 1.400, 2, 2.800, 4, 5.600, 8, 11, 16, 23, 32, 45, 64, 90, 128, 181, 256, 362, 512, 724, 1024)

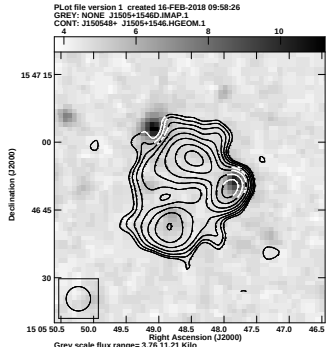
PLot file version 1 created 16-FEB-2018 09:58:26
GREY: NONE J1505+1546D.IMAP.1
CONT: J150548+ J1505+1546.HGEOM.1
Declination (J2000)
Right Ascension (J2000)
Grey scale flux range= 3.76 11.21 Kilo
Cont peak flux = 3.3055E-03 JY/BEAM
Levs = 2.500E-04 * (1, 1.400, 2, 2.800, 4, 5.600, 8, 11, 16, 23, 32, 45, 64, 90, 128, 181, 256, 362, 512, 724, 1024)

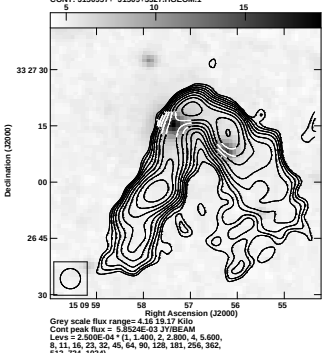
PLot file version 1 created 16-FEB-2018 10:00:53
GREY: NONE J1509+3227D.IMAP.1
CONT: J150957+ J1509+3227.HGEOM.1
Declination (J2000)
Right Ascension (J2000)
Grey scale flux range= 4.16 19.17 Kilo
Cont peak flux = 5.8524E-03 JY/BEAM
Levs = 2.500E-04 * (1, 1.400, 2, 2.800, 4, 5.600, 8, 11, 16, 23, 32, 45, 64, 90, 128, 181, 256, 362, 512, 724, 1024)

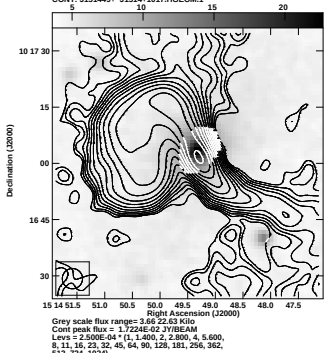
PLot file version 1 created 16-FEB-2018 10:10:00
GREY: NONE J1514+1017D.IMAP.1
CONT: J151449+ J1514+1017.HGEOM.1
Declination (J2000)
Right Ascension (J2000)
Grey scale flux range= 3.66 22.53 Kilo
Cont peak flux = 1.7224E-02 JY/BEAM
Levs = 2.500E-04 * (1, 1.400, 2, 2.800, 4, 5.600, 8, 11, 16, 23, 32, 45, 64, 90, 128, 181, 256, 362, 512, 724, 1024)

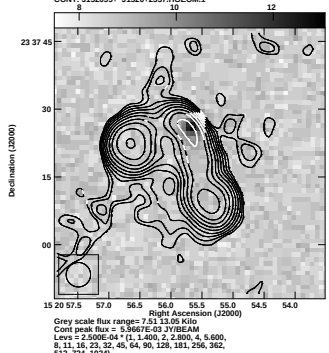
PLot file version 1 created 16-FEB-2018 10:11:56
GREY: NONE J1520+2337D.IMAP.1
CONT: J152059+ J1520+2337.HGEOM.1
Declination (J2000)
Right Ascension (J2000)
Grey scale flux range= 7.51 13.05 Kilo
Cont peak flux = 5.9667E-03 JY/BEAM
Levs = 2.500E-04 * (1, 1.400, 2, 2.800, 4, 5.600, 8, 11, 16, 23, 32, 45, 64, 90, 128, 181, 256, 362, 512, 724, 1024)

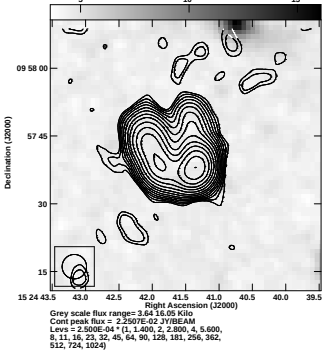
PLot file version 1 created 16-FEB-2018 10:18:54
GREY: NONE J1524+0957D.IMAP.1
CONT: J152441+ J1524+0957.HGEOM.1
Declination (J2000)
Right Ascension (J2000)
Grey scale flux range= 3.64 16.05 Kilo
Cont peak flux = 2.2507E-02 JY/BEAM
Levs = 2.500E-04 * (1, 1.400, 2, 2.800, 4, 5.600, 8, 11, 16, 23, 32, 45, 64, 90, 128, 181, 256, 362, 512, 724, 1024)

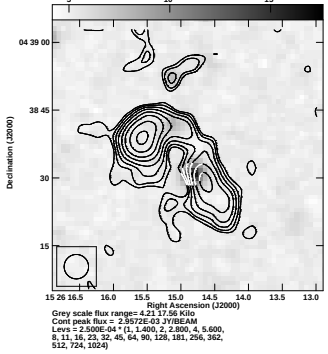
PLot file version 1 created 16-FEB-2018 10:21:13
GREY: NONE J1526+0438D.IMAP.1
CONT: J152614+ J1526+0438.HGEOM.1
Declination (J2000)
Right Ascension (J2000)
Grey scale flux range= 4.21 17.56 Kilo
Cont peak flux = 2.9572E-03 JY/BEAM
Levs = 2.500E-04 * (1, 1.400, 2, 2.800, 4, 5.600, 8, 11, 16, 23, 32, 45, 64, 90, 128, 181, 256, 362, 512, 724, 1024)

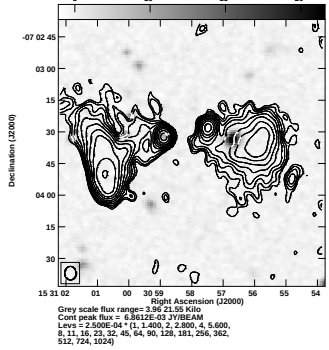
PLot file version 1 created 16-FEB-2018 10:33:03
GREY: NONE J1530-0703D.IMAP.1
CONT: J153058- J1530-0703.HGEOM.1
Declination (J2000)
Right Ascension (J2000)
Grey scale flux range= 3.96 21.55 Kilo
Cont peak flux = 6.8612E-03 JY/BEAM
Levs = 2.500E-04 * (1, 1.400, 2, 2.800, 4, 5.600, 8, 11, 16, 23, 32, 45, 64, 90, 128, 181, 256, 362, 512, 724, 1024)

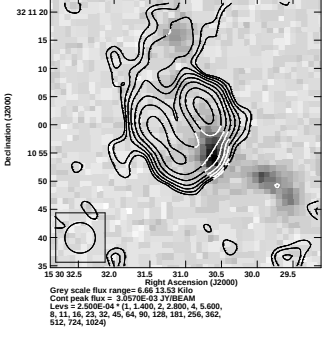
PLot file version 1 created 16-FEB-2018 10:31:55
GREY: NONE J1530+3210D.IMAP.1
CONT: J153031+ J1530+3210.HGEOM.1
Declination (J2000)
Right Ascension (J2000)
Grey scale flux range= 6.66 13.53 Kilo
Cont peak flux = 3.0570E-03 JY/BEAM
Levs = 2.500E-04 * (1, 1.400, 2, 2.800, 4, 5.600, 8, 11, 16, 23, 32, 45, 64, 90, 128, 181, 256, 362, 512, 724, 1024)

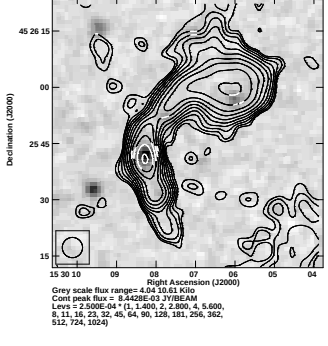
PLot file version 1 created 16-FEB-2018 10:30:50
GREY: NONE J1530+4525D.IMAP.1
CONT: J153007+ J1530+4525.HGEOM.1
Declination (J2000)
Right Ascension (J2000)
Grey scale flux range= 4.04 10.61 Kilo
Cont peak flux = 8.4428E-03 JY/BEAM
Levs = 2.500E-04 * (1, 1.400, 2, 2.800, 4, 5.600, 8, 11, 16, 23, 32, 45, 64, 90, 128, 181, 256, 362, 512, 724, 1024)

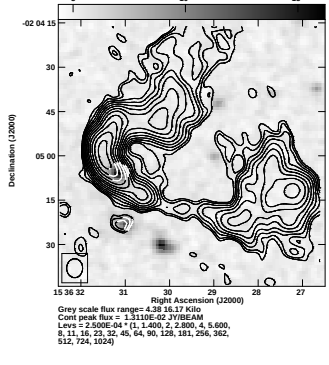
PLot file version 1 created 16-FEB-2018 10:44:53
GREY: NONE J1536-0204D.IMAP.1
CONT: J153629- J1536-0204.HGEOM.1
Declination (J2000)
Right Ascension (J2000)
Grey scale flux range= 4.38 16.17 Kilo
Cont peak flux = 1.3110E-02 JY/BEAM
Levs = 2.500E-04 * (1, 1.400, 2, 2.800, 4, 5.600, 8, 11, 16, 23, 32, 45, 64, 90, 128, 181, 256, 362, 512, 724, 1024)

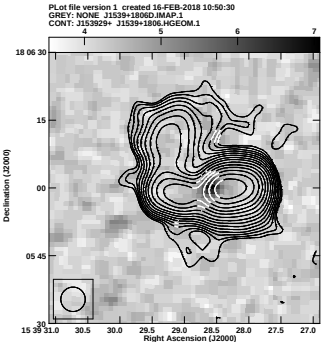
PLot file version 1 created 16-FEB-2018 10:50:30
GREY: NONE J1539+1806D.IMAP.1
CONT: J153929+ J1539+1806.HGEOM.1
Declination (J2000)
Right Ascension (J2000)
Grey scale flux range= 3.548 7.061 Kilo
Cont peak flux = 2.9896E-02 JY/BEAM
Levs = 2.500E-04 * (1, 1.400, 2, 2.800, 4, 5.600, 8, 11, 16, 23, 32, 45, 64, 90, 128, 181, 256, 362, 512, 724, 1024)

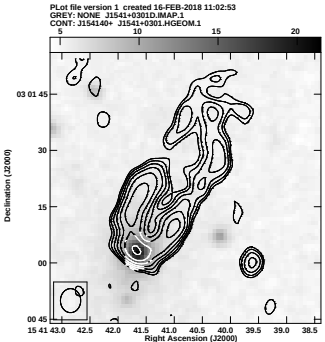
PLot file version 1 created 16-FEB-2018 11:02:53
GREY: NONE J1541+0301D.IMAP.1
CONT: J154140+ J1541+0301.HGEOM.1
Declination (J2000)
Right Ascension (J2000)
Grey scale flux range= 4.42 21.45 Kilo
Cont peak flux = 2.1180E-03 JY/BEAM
Levs = 2.500E-04 * (1, 1.400, 2, 2.800, 4, 5.600, 8, 11, 16, 23, 32, 45, 64, 90, 128, 181, 256, 362, 512, 724, 1024)

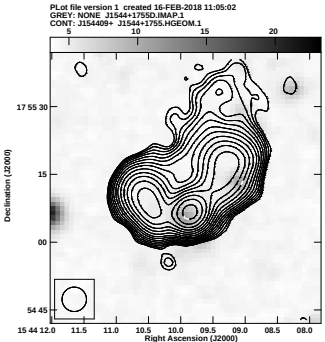
PLot file version 1 created 16-FEB-2018 11:05:02
GREY: NONE J1544+1755D.IMAP.1
CONT: J154409+ J1544+1755.HGEOM.1
Declination (J2000)
Right Ascension (J2000)
Grey scale flux range= 3.70 23.27 Kilo
Cont peak flux = 3.3271E-02 JY/BEAM
Levs = 2.500E-04 * (1, 1.400, 2, 2.800, 4, 5.600, 8, 11, 16, 23, 32, 45, 64, 90, 128, 181, 256, 362, 512, 724, 1024)

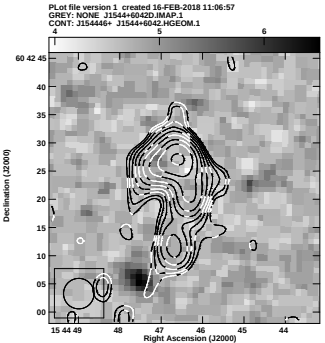
PLot file version 1 created 16-FEB-2018 11:06:57
GREY: NONE J1544+6042D.IMAP.1
CONT: J154446+ J1544+6042.HGEOM.1
Declination (J2000)
Right Ascension (J2000)
Grey scale flux range= 3.952 6.525 Kilo
Cont peak flux = 4.2780E-03 JY/BEAM
Levs = 2.500E-04 * (1, 1.400, 2, 2.800, 4, 5.600, 8, 11, 16, 23, 32, 45, 64, 90, 128, 181, 256, 362, 512, 724, 1024)

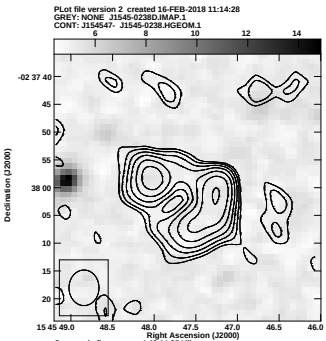
PLot file version 2 created 16-FEB-2018 11:14:28
GREY: NONE J1545-0238D.IMAP.1
CONT: J154547- J1545-0238.HGEOM.1
Declination (J2000)
Right Ascension (J2000)
Grey scale flux range= 4.42 14.85 Kilo
Cont peak flux = 2.0777E-03 JY/BEAM
Levs = 2.500E-04 * (1, 1.400, 2, 2.800, 4, 5.600, 8, 11, 16, 23, 32, 45, 64, 90, 128, 181, 256, 362, 512, 724, 1024)

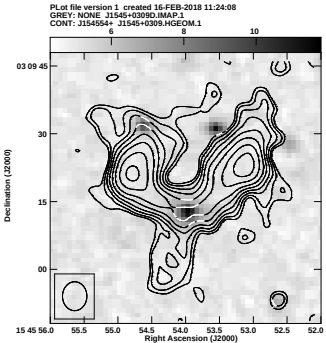
PLot file version 1 created 16-FEB-2018 11:24:08
GREY: NONE J1545+0309D.IMAP.1
CONT: J154554+ J1545+0309.HGEOM.1
Declination (J2000)
Right Ascension (J2000)
Grey scale flux range= 4.33 11.77 Kilo
Cont peak flux = 3.3146E-03 JY/BEAM
Levs = 2.500E-04 * (1, 1.400, 2, 2.800, 4, 5.600, 8, 11, 16, 23, 32, 45, 64, 90, 128, 181, 256, 362, 512, 724, 1024)

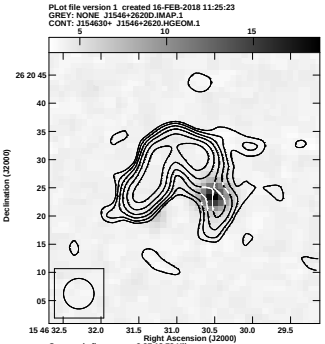
PLot file version 1 created 16-FEB-2018 11:25:23
GREY: NONE J1546+2620D.IMAP.1
CONT: J154630+ J1546+2620.HGEOM.1
Declination (J2000)
Right Ascension (J2000)
Grey scale flux range= 3.27 18.78 Kilo
Cont peak flux = 1.9220E-03 JY/BEAM
Levs = 2.500E-04 * (1, 1.400, 2, 2.800, 4, 5.600, 8, 11, 16, 23, 32, 45, 64, 90, 128, 181, 256, 362, 512, 724, 1024)

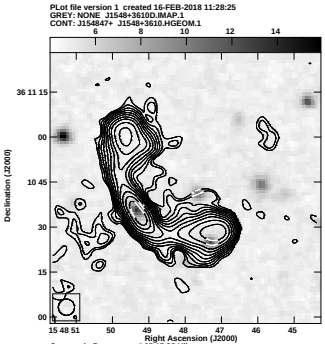
PLot file version 1 created 16-FEB-2018 11:28:25
GREY: NONE J1548+3610D.IMAP.1
CONT: J154847+ J1548+3610.HGEOM.1
Declination (J2000)
Right Ascension (J2000)
Grey scale flux range= 4.05 15.88 Kilo
Cont peak flux = 1.0436E-02 JY/BEAM
Levs = 2.500E-04 * (1, 1.400, 2, 2.800, 4, 5.600, 8, 11, 16, 23, 32, 45, 64, 90, 128, 181, 256, 362, 512, 724, 1024)

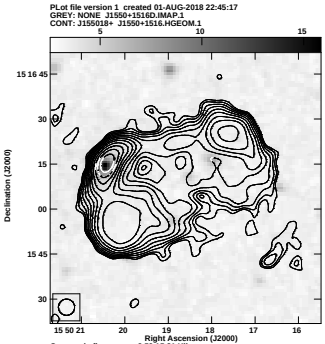
PLot file version 1 created 01-AUG-2018 22:45:17
GREY: NONE J1550+1516D.IMAP.1
CONT: J155018+ J1550+1516.HGEOM.1
Declination (J2000)
Right Ascension (J2000)
Grey scale flux range= 2.59 15.81 Kilo
Cont peak flux = 1.5572E-02 JY/BEAM
Levs = 2.500E-04 * (1, 1.400, 2, 2.800, 4, 5.600, 8, 11, 16, 23, 32, 45, 64, 90, 128, 181, 256, 362, 512, 724, 1024)

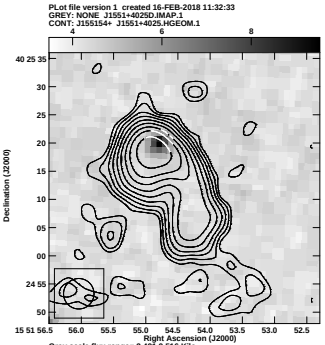
PLot file version 1 created 16-FEB-2018 11:32:33
GREY: NONE J1551+4025D.IMAP.1
CONT: J155154+ J1551+4025.HGEOM.1
Declination (J2000)
Right Ascension (J2000)
Grey scale flux range= 3.491 9.516 Kilo
Cont peak flux = 5.6045E-03 JY/BEAM
Levs = 2.500E-04 * (1, 1.400, 2, 2.800, 4, 5.600, 8, 11, 16, 23, 32, 45, 64, 90, 128, 181, 256, 362, 512, 724, 1024)

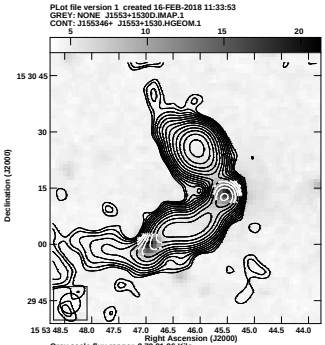
PLot file version 1 created 16-FEB-2018 11:33:53
GREY: NONE J1553+1530D.IMAP.1
CONT: J155346+ J1553+1530.HGEOM.1
Declination (J2000)
Right Ascension (J2000)
Grey scale flux range= 3.72 21.26 Kilo
Cont peak flux = 1.8954E-02 JY/BEAM
Levs = 2.500E-04 * (1, 1.400, 2, 2.800, 4, 5.600, 8, 11, 16, 23, 32, 45, 64, 90, 128, 181, 256, 362, 512, 724, 1024)

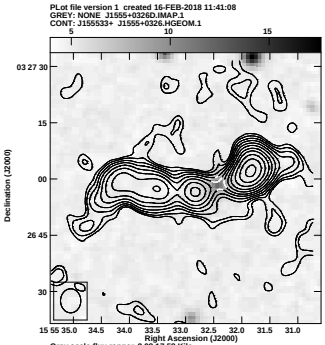
PLot file version 1 created 16-FEB-2018 11:41:08
GREY: NONE J1555+0326D.IMAP.1
CONT: J155533+ J1555+0326.HGEOM.1
Declination (J2000)
Right Ascension (J2000)
Grey scale flux range= 3.98 17.58 Kilo
Cont peak flux = 8.8783E-03 JY/BEAM
Levs = 2.500E-04 * (1, 1.400, 2, 2.800, 4, 5.600, 8, 11, 16, 23, 32, 45, 64, 90, 128, 181, 256, 362, 512, 724, 1024)

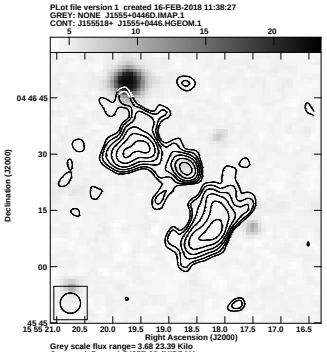
PLot file version 1 created 16-FEB-2018 11:38:27
GREY: NONE J1555+0446D.IMAP.1
CONT: J155518+ J1555+0446.HGEOM.1
Declination (J2000)
Right Ascension (J2000)
Grey scale flux range= 3.68 23.39 Kilo
Cont peak flux = 1.7485E-03 JY/BEAM
Levs = 2.500E-04 * (1, 1.400, 2, 2.800, 4, 5.600, 8, 11, 16, 23, 32, 45, 64, 90, 128, 181, 256, 362, 512, 724, 1024)

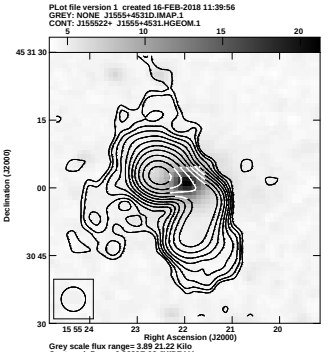
PLot file version 1 created 16-FEB-2018 11:39:56
GREY: NONE J1555+4531D.IMAP.1
CONT: J155522+ J1555+4531.HGEOM.1
Declination (J2000)
Right Ascension (J2000)
Grey scale flux range= 3.89 21.22 Kilo
Cont peak flux = 9.9239E-03 JY/BEAM
Levs = 2.500E-04 * (1, 1.400, 2, 2.800, 4, 5.600, 8, 11, 16, 23, 32, 45, 64, 90, 128, 181, 256, 362, 512, 724, 1024)

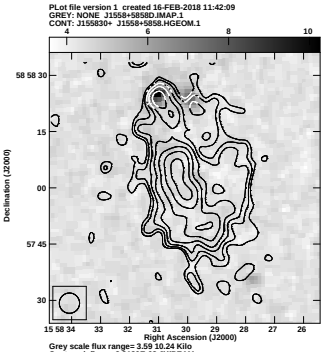
PLot file version 1 created 16-FEB-2018 11:42:09
GREY: NONE J1558+5858D.IMAP.1
CONT: J155830+ J1558+5858.HGEOM.1
Declination (J2000)
Right Ascension (J2000)
Grey scale flux range= 3.59 10.24 Kilo
Cont peak flux = 2.3130E-03 JY/BEAM
Levs = 2.500E-04 * (1, 1.400, 2, 2.800, 4, 5.600, 8, 11, 16, 23, 32, 45, 64, 90, 128, 181, 256, 362, 512, 724, 1024)

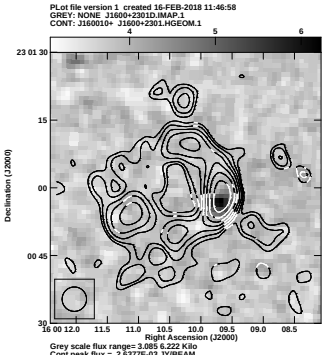
PLot file version 1 created 16-FEB-2018 11:46:58
GREY: NONE J1600+2301D.IMAP.1
CONT: J160010+ J1600+2301.HGEOM.1
Declination (J2000)
Right Ascension (J2000)
Grey scale flux range= 3.085 6.222 Kilo
Cont peak flux = 2.6377E-03 JY/BEAM
Levs = 2.500E-04 * (1, 1.400, 2, 2.800, 4, 5.600, 8, 11, 16, 23, 32, 45, 64, 90, 128, 181, 256, 362, 512, 724, 1024)

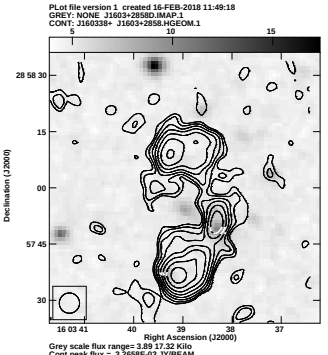
PLot file version 1 created 16-FEB-2018 11:49:18
GREY: NONE J1603+2858D.IMAP.1
CONT: J160338+ J1603+2858.HGEOM.1
Declination (J2000)
Right Ascension (J2000)
Grey scale flux range= 3.89 17.32 Kilo
Cont peak flux = 3.2658E-03 JY/BEAM
Levs = 2.500E-04 * (1, 1.400, 2, 2.800, 4, 5.600, 8, 11, 16, 23, 32, 45, 64, 90, 128, 181, 256, 362, 512, 724, 1024)

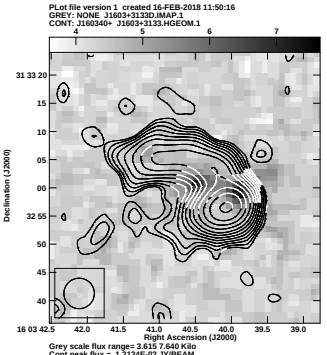
PLot file version 1 created 16-FEB-2018 11:50:16
GREY: NONE J1603+3133D.IMAP.1
CONT: J160340+ J1603+3133.HGEOM.1
Declination (J2000)
Right Ascension (J2000)
Grey scale flux range= 3.615 7.640 Kilo
Cont peak flux = 1.2124E-02 JY/BEAM
Levs = 2.500E-04 * (1, 1.400, 2, 2.800, 4, 5.600, 8, 11, 16, 23, 32, 45, 64, 90, 128, 181, 256, 362, 512, 724, 1024)

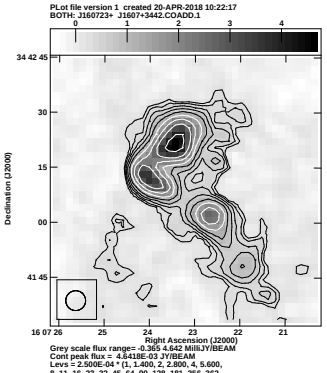
PLot file version 1 created 20-APR-2018 10:22:17
BOTH: J160723+ J1607+3442.COADD.1
Declination (J2000)
Right Ascension (J2000)
Grey scale flux range= -0.365 4.642 MilliJY/BEAM
Cont peak flux = 4.6418E-03 JY/BEAM
Levs = 2.500E-04 * (1, 1.400, 2, 2.800, 4, 5.600, 8, 11, 16, 23, 32, 45, 64, 90, 128, 181, 256, 362, 512, 724, 1024)

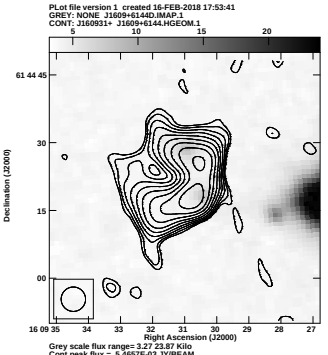
PLot file version 1 created 16-FEB-2018 17:53:41
GREY: NONE J1609+6144D.IMAP.1
CONT: J160931+ J1609+6144.HGEOM.1
Declination (J2000)
Right Ascension (J2000)
Grey scale flux range= 3.27 23.87 Kilo
Cont peak flux = 5.4657E-03 JY/BEAM
Levs = 2.500E-04 * (1, 1.400, 2, 2.800, 4, 5.600, 8, 11, 16, 23, 32, 45, 64, 90, 128, 181, 256, 362, 512, 724, 1024)

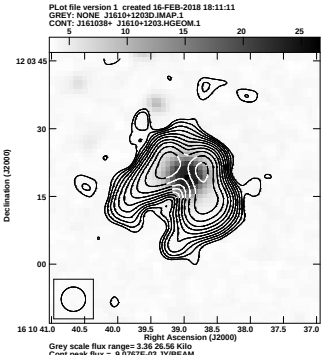
PLot file version 1 created 16-FEB-2018 18:11:11
GREY: NONE J1610+1203D.IMAP.1
CONT: J161038+ J1610+1203.HGEOM.1
Declination (J2000)
Right Ascension (J2000)
Grey scale flux range= 3.36 26.56 Kilo
Cont peak flux = 9.0767E-03 JY/BEAM
Levs = 2.500E-04 * (1, 1.400, 2, 2.800, 4, 5.600, 8, 11, 16, 23, 32, 45, 64, 90, 128, 181, 256, 362, 512, 724, 1024)

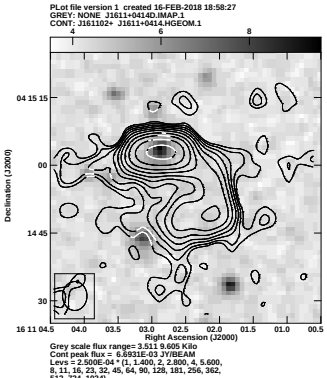
PLot file version 1 created 16-FEB-2018 18:58:27
GREY: NONE J1611+0414D.IMAP.1
CONT: J161102+ J1611+0414.HGEOM.1
Declination (J2000)
Right Ascension (J2000)
Grey scale flux range= 3.511 9.605 Kilo
Cont peak flux = 6.6931E-03 JY/BEAM
Levs = 2.500E-04 * (1, 1.400, 2, 2.800, 4, 5.600, 8, 11, 16, 23, 32, 45, 64, 90, 128, 181, 256, 362, 512, 724, 1024)

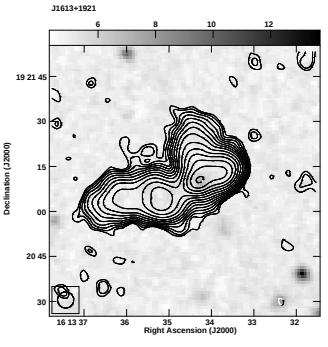
J1613+1921
Declination (J2000)
Right Ascension (J2000)
Levs = 2.500E-04 * (1, 1.4, 2, 2.8, 4, 5.7, 8, 11, 16, 23, 32, 45, 64, 90, 128, 181, 256, 362, 512, 724, 1024)

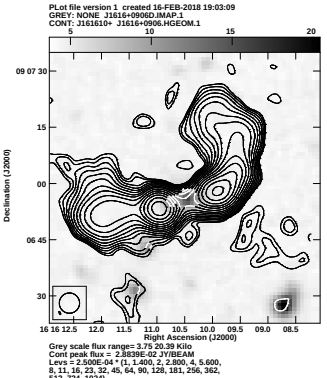
PLot file version 1 created 16-FEB-2018 19:03:09
GREY: NONE J1616+0906D.IMAP.1
CONT: J161610+ J1616+0906.HGEOM.1
Declination (J2000)
Right Ascension (J2000)
Grey scale flux range= 3.75 20.39 Kilo
Cont peak flux = 2.8839E-02 JY/BEAM
Levs = 2.500E-04 * (1, 1.400, 2, 2.800, 4, 5.600, 8, 11, 16, 23, 32, 45, 64, 90, 128, 181, 256, 362, 512, 724, 1024)

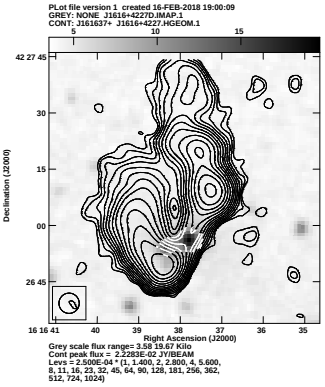
PLot file version 1 created 16-FEB-2018 19:00:09
GREY: NONE J1616+4227D.IMAP.1
CONT: J161637+ J1616+4227.HGEOM.1
Declination (J2000)
Right Ascension (J2000)
Grey scale flux range= 3.58 19.67 Kilo
Cont peak flux = 2.2283E-02 JY/BEAM
Levs = 2.500E-04 * (1, 1.400, 2, 2.800, 4, 5.600, 8, 11, 16, 23, 32, 45, 64, 90, 128, 181, 256, 362, 512, 724, 1024)

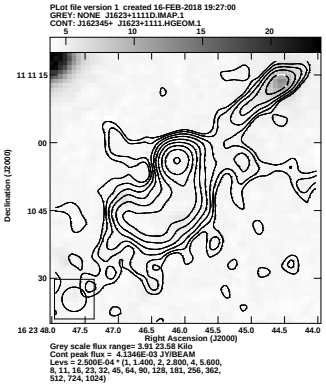
PLot file version 1 created 16-FEB-2018 19:27:00
GREY: NONE J1623+1111D.IMAP.1
CONT: J162345+ J1623+1111.HGEOM.1
Declination (J2000)
Right Ascension (J2000)
Grey scale flux range= 3.91 23.58 Kilo
Cont peak flux = 4.1346E-03 JY/BEAM
Levs = 2.500E-04 * (1, 1.400, 2, 2.800, 4, 5.600, 8, 11, 16, 23, 32, 45, 64, 90, 128, 181, 256, 362, 512, 724, 1024)

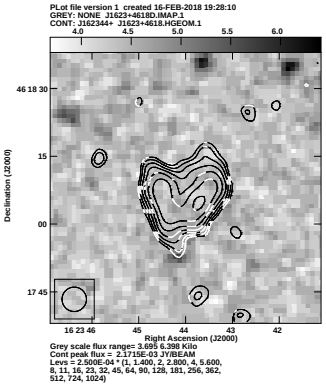
PLot file version 1 created 16-FEB-2018 19:28:10
GREY: NONE J1623+4618D.IMAP.1
CONT: J162344+ J1623+4618.HGEOM.1
Declination (J2000)
Right Ascension (J2000)
Grey scale flux range= 3.695 6.398 Kilo
Cont peak flux = 2.1715E-03 JY/BEAM
Levs = 2.500E-04 * (1, 1.400, 2, 2.800, 4, 5.600, 8, 11, 16, 23, 32, 45, 64, 90, 128, 181, 256, 362, 512, 724, 1024)

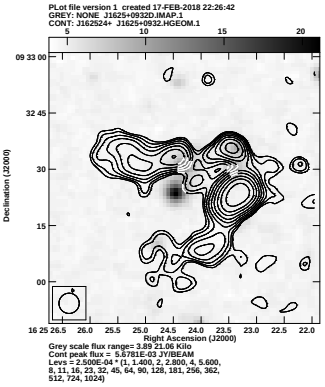
PLot file version 1 created 17-FEB-2018 22:26:42
GREY: NONE J1625+0932D.IMAP.1
CONT: J162524+ J1625+0932.HGEOM.1
Declination (J2000)
Right Ascension (J2000)
Grey scale flux range= 3.89 21.06 Kilo
Cont peak flux = 5.8781E-03 JY/BEAM
Levs = 2.500E-04 * (1, 1.400, 2, 2.800, 4, 5.600, 8, 11, 16, 23, 32, 45, 64, 90, 128, 181, 256, 362, 512, 724, 1024)

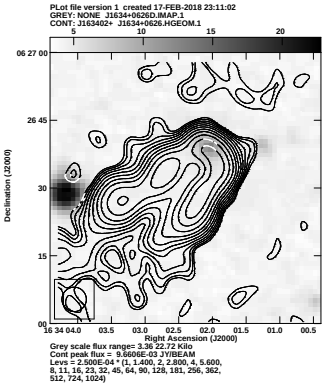
PLot file version 1 created 17-FEB-2018 23:11:02
GREY: NONE J1634+0626D.IMAP.1
CONT: J163402+ J1634+0626.HGEOM.1
Declination (J2000)
Right Ascension (J2000)
Grey scale flux range= 3.36 22.72 Kilo
Cont peak flux = 9.6606E-03 JY/BEAM
Levs = 2.500E-04 * (1, 1.400, 2, 2.800, 4, 5.600, 8, 11, 16, 23, 32, 45, 64, 90, 128, 181, 256, 362, 512, 724, 1024)

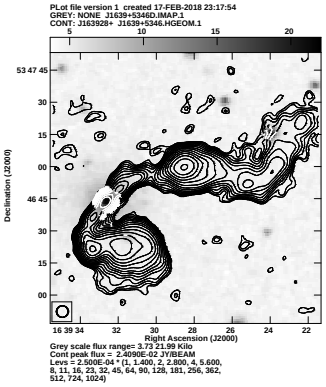
PLot file version 1 created 17-FEB-2018 23:17:54
GREY: NONE J1639+5346D.IMAP.1
CONT: J163928+ J1639+5346.HGEOM.1
Declination (J2000)
Right Ascension (J2000)
Grey scale flux range= 3.73 21.99 Kilo
Cont peak flux = 2.4090E-02 JY/BEAM
Levs = 2.500E-04 * (1, 1.400, 2, 2.800, 4, 5.600, 8, 11, 16, 23, 32, 45, 64, 90, 128, 181, 256, 362, 512, 724, 1024)

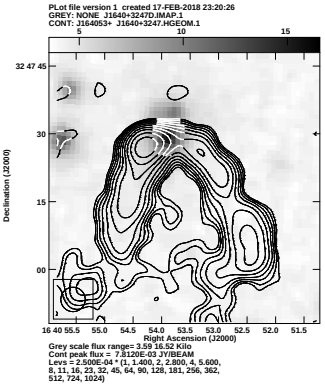
PLot file version 1 created 17-FEB-2018 23:20:26
GREY: NONE J1640+3247D.IMAP.1
CONT: J164053+ J1640+3247.HGEOM.1
Declination (J2000)
Right Ascension (J2000)
Grey scale flux range= 3.59 16.52 Kilo
Cont peak flux = 7.8120E-03 JY/BEAM
Levs = 2.500E-04 * (1, 1.400, 2, 2.800, 4, 5.600, 8, 11, 16, 23, 32, 45, 64, 90, 128, 181, 256, 362, 512, 724, 1024)

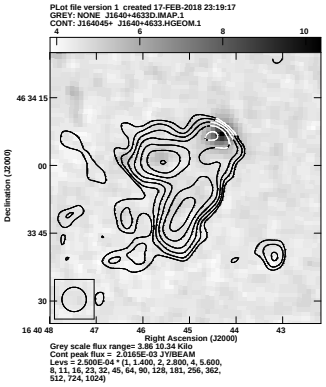
PLot file version 1 created 17-FEB-2018 23:19:17
GREY: NONE J1640+4633D.IMAP.1
CONT: J164045+ J1640+4633.HGEOM.1
Declination (J2000)
Right Ascension (J2000)
Grey scale flux range= 3.86 10.34 Kilo
Cont peak flux = 2.0165E-03 JY/BEAM
Levs = 2.500E-04 * (1, 1.400, 2, 2.800, 4, 5.600, 8, 11, 16, 23, 32, 45, 64, 90, 128, 181, 256, 362, 512, 724, 1024)

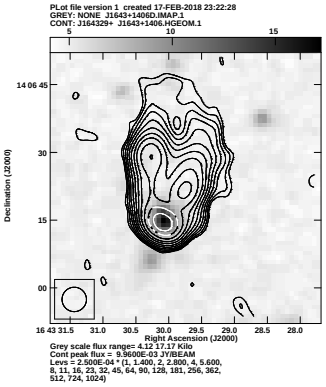
PLot file version 1 created 17-FEB-2018 23:22:28
GREY: NONE J1643+1406D.IMAP.1
CONT: J164329+ J1643+1406.HGEOM.1
Declination (J2000)
Right Ascension (J2000)
Grey scale flux range= 4.12 17.17 Kilo
Cont peak flux = 9.9600E-03 JY/BEAM
Levs = 2.500E-04 * (1, 1.400, 2, 2.800, 4, 5.600, 8, 11, 16, 23, 32, 45, 64, 90, 128, 181, 256, 362, 512, 724, 1024)

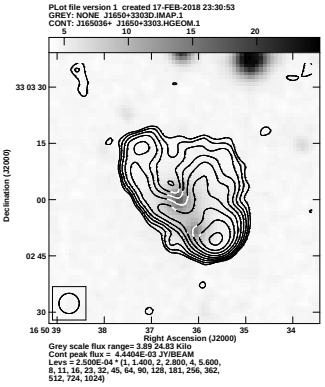
PLot file version 1 created 17-FEB-2018 23:30:53
GREY: NONE J1650+3303D.IMAP.1
CONT: J165036+ J1650+3303.HGEOM.1
Declination (J2000)
Right Ascension (J2000)
Grey scale flux range= 3.89 24.83 Kilo
Cont peak flux = 4.4804E-03 JY/BEAM
Levs = 2.500E-04 * (1, 1.400, 2, 2.800, 4, 5.600, 8, 11, 16, 23, 32, 45, 64, 90, 128, 181, 256, 362, 512, 724, 1024)

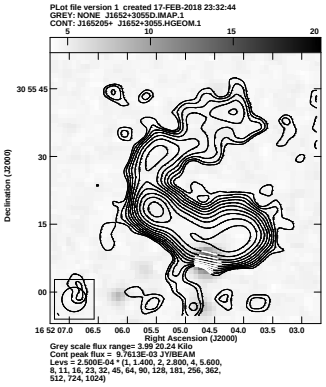
PLot file version 1 created 17-FEB-2018 23:32:44
GREY: NONE J1652+3055D.IMAP.1
CONT: J165205+ J1652+3055.HGEOM.1
Declination (J2000)
Right Ascension (J2000)
Grey scale flux range= 3.99 20.24 Kilo
Cont peak flux = 9.7613E-03 JY/BEAM
Levs = 2.500E-04 * (1, 1.400, 2, 2.800, 4, 5.600, 8, 11, 16, 23, 32, 45, 64, 90, 128, 181, 256, 362, 512, 724, 1024)

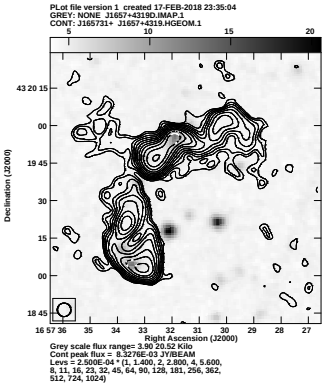
PLot file version 1 created 17-FEB-2018 23:35:04
GREY: NONE J1657+4319D.IMAP.1
CONT: J165731+ J1657+4319.HGEOM.1
Declination (J2000)
Right Ascension (J2000)
Grey scale flux range= 3.90 20.52 Kilo
Cont peak flux = 8.3276E-03 JY/BEAM
Levs = 2.500E-04 * (1, 1.400, 2, 2.800, 4, 5.600, 8, 11, 16, 23, 32, 45, 64, 90, 128, 181, 256, 362, 512, 724, 1024)

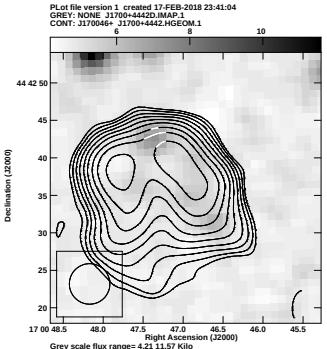
PLot file version 1 created 17-FEB-2018 23:41:04
GREY: NONE J1700+4442D.IMAP.1
CONT: J170046+ J1700+4442.HGEOM.1
Declination (J2000)
Right Ascension (J2000)
Grey scale flux range= 4.21 11.57 Kilo
Cont peak flux = 5.2122E-03 JY/BEAM
Levs = 2.500E-04 * (1, 1.400, 2, 2.800, 4, 5.600, 8, 11, 16, 23, 32, 45, 64, 90, 128, 181, 256, 362, 512, 724, 1024)

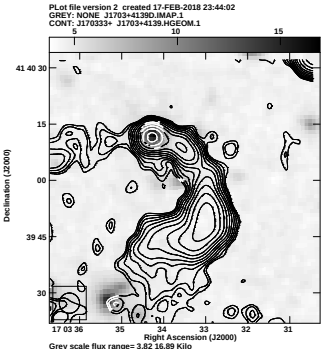
PLot file version 2 created 17-FEB-2018 23:44:02
GREY: NONE J1703+4139D.IMAP.1
CONT: J170333+ J1703+4139.HGEOM.1
Declination (J2000)
Right Ascension (J2000)
Grey scale flux range= 3.82 16.89 Kilo
Cont peak flux = 1.0398E-02 JY/BEAM
Levs = 2.500E-04 * (1, 1.400, 2, 2.800, 4, 5.600, 8, 11, 16, 23, 32, 45, 64, 90, 128, 181, 256, 362, 512, 724, 1024)

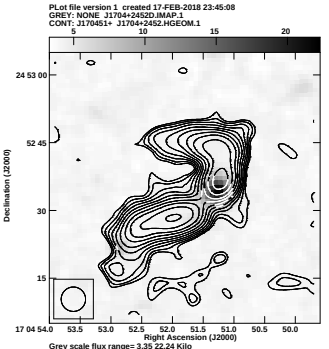
PLot file version 1 created 17-FEB-2018 23:45:08
GREY: NONE J1704+2452D.IMAP.1
CONT: J170451+ J1704+2452.HGEOM.1
Declination (J2000)
Right Ascension (J2000)
Grey scale flux range= 3.35 22.24 Kilo
Cont peak flux = 7.0899E-03 JY/BEAM
Levs = 2.500E-04 * (1, 1.400, 2, 2.800, 4, 5.600, 8, 11, 16, 23, 32, 45, 64, 90, 128, 181, 256, 362, 512, 724, 1024)

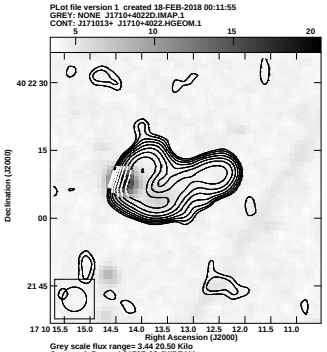
PLot file version 1 created 18-FEB-2018 00:11:55
GREY: NONE J1710+4022D.IMAP.1
CONT: J171013+ J1710+4022.HGEOM.1
Declination (J2000)
Right Ascension (J2000)
Grey scale flux range= 3.44 20.50 Kilo
Cont peak flux = 4.0173E-03 JY/BEAM
Levs = 2.500E-04 * (1, 1.400, 2, 2.800, 4, 5.600, 8, 11, 16, 23, 32, 45, 64, 90, 128, 181, 256, 362, 512, 724, 1024)

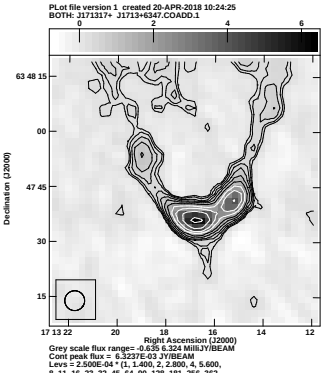
PLot file version 1 created 20-APR-2018 10:24:25
BOTH: J171317+ J1713+6347.COADD.1
Declination (J2000)
Right Ascension (J2000)
Grey scale flux range= -0.635 6.324 MilliJY/BEAM
Cont peak flux = 6.3237E-03 JY/BEAM
Levs = 2.500E-04 * (1, 1.400, 2, 2.800, 4, 5.600, 8, 11, 16, 23, 32, 45, 64, 90, 128, 181, 256, 362, 512, 724, 1024)

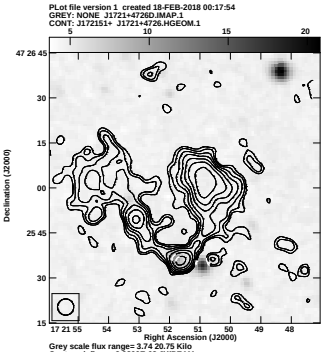
PLot file version 1 created 18-FEB-2018 00:17:54
GREY: NONE J1721+4726D.IMAP.1
CONT: J172151+ J1721+4726.HGEOM.1
Declination (J2000)
Right Ascension (J2000)
Grey scale flux range= 3.74 20.75 Kilo
Cont peak flux = 2.6806E-03 JY/BEAM
Levs = 2.500E-04 * (1, 1.400, 2, 2.800, 4, 5.600, 8, 11, 16, 23, 32, 45, 64, 90, 128, 181, 256, 362, 512, 724, 1024)

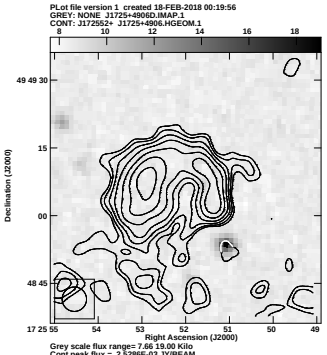
PLot file version 1 created 18-FEB-2018 00:19:56
GREY: NONE J1725+4906D.IMAP.1
CONT: J172552+ J1725+4906.HGEOM.1
Declination (J2000)
Right Ascension (J2000)
Grey scale flux range= 7.66 19.00 Kilo
Cont peak flux = 2.5286E-03 JY/BEAM
Levs = 2.500E-04 * (1, 1.400, 2, 2.800, 4, 5.600, 8, 11, 16, 23, 32, 45, 64, 90, 128, 181, 256, 362, 512, 724, 1024)

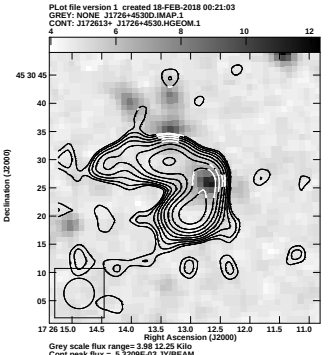
PLot file version 1 created 18-FEB-2018 00:21:03
GREY: NONE J1726+4530D.IMAP.1
CONT: J172613+ J1726+4530.HGEOM.1
Declination (J2000)
Right Ascension (J2000)
Grey scale flux range= 3.98 12.25 Kilo
Cont peak flux = 5.3209E-03 JY/BEAM
Levs = 2.500E-04 * (1, 1.400, 2, 2.800, 4, 5.600, 8, 11, 16, 23, 32, 45, 64, 90, 128, 181, 256, 362, 512, 724, 1024)

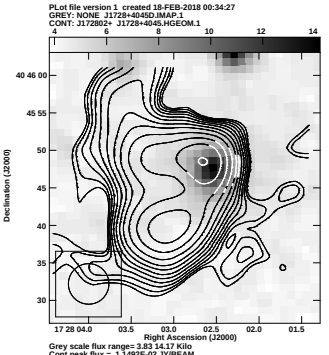
PLot file version 1 created 18-FEB-2018 00:34:27
GREY: NONE J1728+4045D.IMAP.1
CONT: J172802+ J1728+4045.HGEOM.1
Declination (J2000)
Right Ascension (J2000)
Grey scale flux range= 3.83 14.17 Kilo
Cont peak flux = 1.1492E-02 JY/BEAM
Levs = 2.500E-04 * (1, 1.400, 2, 2.800, 4, 5.600, 8, 11, 16, 23, 32, 45, 64, 90, 128, 181, 256, 362, 512, 724, 1024)

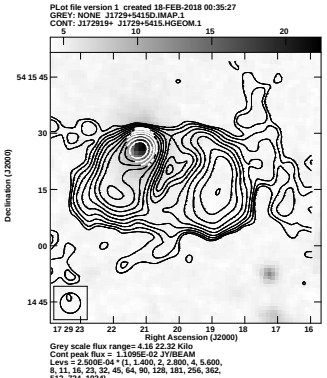
PLot file version 1 created 18-FEB-2018 00:35:27
GREY: NONE J1729+5415D.IMAP.1
CONT: J172919+ J1729+5415.HGEOM.1
Declination (J2000)
Right Ascension (J2000)
Grey scale flux range= 4.16 22.32 Kilo
Cont peak flux = 1.1095E-02 JY/BEAM
Levs = 2.500E-04 * (1, 1.400, 2, 2.800, 4, 5.600, 8, 11, 16, 23, 32, 45, 64, 90, 128, 181, 256, 362, 512, 724, 1024)

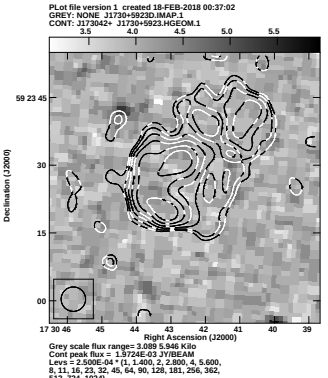
PLot file version 1 created 18-FEB-2018 00:37:02
GREY: NONE J1730+5823D.IMAP.1
CONT: J173042+ J1730+5923.HGEOM.1
Declination (J2000)
Right Ascension (J2000)
Grey scale flux range= 3.089 5.946 Kilo
Cont peak flux = 1.9724E-03 JY/BEAM
Levs = 2.500E-04 * (1, 1.400, 2, 2.800, 4, 5.600, 8, 11, 16, 23, 32, 45, 64, 90, 128, 181, 256, 362, 512, 724, 1024)

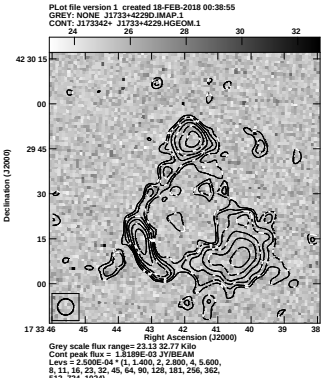
PLot file version 1 created 18-FEB-2018 00:38:55
GREY: NONE J1733+4229D.IMAP.1
CONT: J173342+ J1733+4229.HGEOM.1
Declination (J2000)
Right Ascension (J2000)
Grey scale flux range= 23.13 32.77 Kilo
Cont peak flux = 1.8189E-03 JY/BEAM
Levs = 2.500E-04 * (1, 1.400, 2, 2.800, 4, 5.600, 8, 11, 16, 23, 32, 45, 64, 90, 128, 181, 256, 362, 512, 724, 1024)

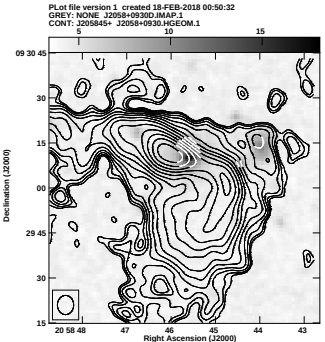
PLot file version 1 created 18-FEB-2018 00:50:32
GREY: NONE J2058+0930D.IMAP.1
CONT: J205845+ J2058+0930.HGEOM.1
Declination (J2000)
Right Ascension (J2000)
Grey scale flux range= 3.42 18.10 Kilo
Cont peak flux = 2.1142E-02 JY/BEAM
Levs = 2.500E-04 * (1, 1.400, 2, 2.800, 4, 5.600, 8, 11, 16, 23, 32, 45, 64, 90, 128, 181, 256, 362, 512, 724, 1024)

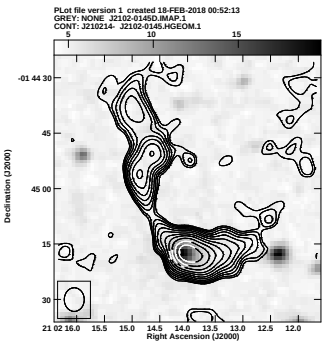
PLot file version 1 created 18-FEB-2018 00:52:13
GREY: NONE J2102-0145D.IMAP.1
CONT: J210214- J2102-0145.HGEOM.1
Declination (J2000)
Right Ascension (J2000)
Grey scale flux range= 4.21 19.82 Kilo
Cont peak flux = 1.0704E-02 JY/BEAM
Levs = 2.500E-04 * (1, 1.400, 2, 2.800, 4, 5.600, 8, 11, 16, 23, 32, 45, 64, 90, 128, 181, 256, 362, 512, 724, 1024)

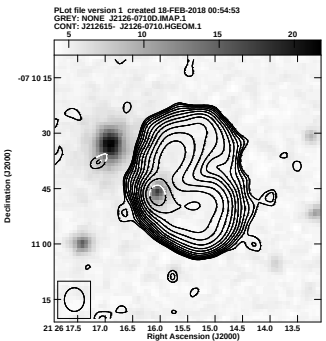
PLot file version 1 created 18-FEB-2018 00:54:53
GREY: NONE J2126-0710D.IMAP.1
CONT: J212615- J2126-0710.HGEOM.1
Declination (J2000)
Right Ascension (J2000)
Grey scale flux range= 4.08 21.72 Kilo
Cont peak flux = 2.0810E-02 JY/BEAM
Levs = 2.500E-04 * (1, 1.400, 2, 2.800, 4, 5.600, 8, 11, 16, 23, 32, 45, 64, 90, 128, 181, 256, 362, 512, 724, 1024)

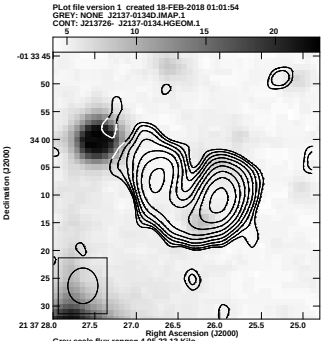
PLot file version 1 created 18-FEB-2018 01:01:54
GREY: NONE J2137-0134D.IMAP.1
CONT: J213726- J2137-0134.HGEOM.1
Declination (J2000)
Right Ascension (J2000)
Grey scale flux range= 4.05 23.13 Kilo
Cont peak flux = 4.5553E-03 JY/BEAM
Levs = 2.500E-04 * (1, 1.400, 2, 2.800, 4, 5.600, 8, 11, 16, 23, 32, 45, 64, 90, 128, 181, 256, 362, 512, 724, 1024)

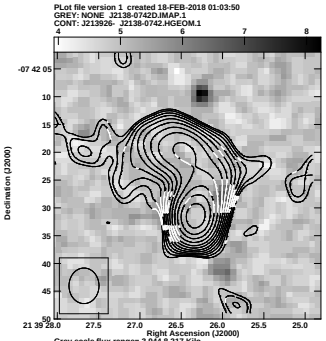
PLot file version 1 created 18-FEB-2018 01:03:50
GREY: NONE J2138-0742D.IMAP.1
CONT: J213926- J2138-0742.HGEOM.1
Declination (J2000)
Right Ascension (J2000)
Grey scale flux range= 3.944 8.217 Kilo
Cont peak flux = 1.4227E-02 JY/BEAM
Levs = 2.500E-04 * (1, 1.400, 2, 2.800, 4, 5.600, 8, 11, 16, 23, 32, 45, 64, 90, 128, 181, 256, 362, 512, 724, 1024)

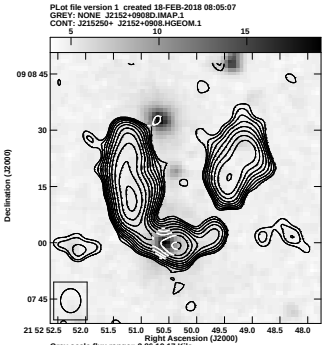
PLot file version 1 created 18-FEB-2018 08:05:07
GREY: NONE J2152+0908D.IMAP.1
CONT: J215250+ J2152+0908.HGEOM.1
Declination (J2000)
Right Ascension (J2000)
Grey scale flux range= 3.86 19.17 Kilo
Cont peak flux = 8.8854E-03 JY/BEAM
Levs = 2.500E-04 * (1, 1.400, 2, 2.800, 4, 5.600, 8, 11, 16, 23, 32, 45, 64, 90, 128, 181, 256, 362, 512, 724, 1024)

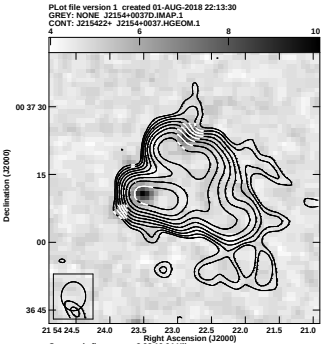
PLot file version 1 created 01-AUG-2018 22:13:30
GREY: NONE J2154+0037D.IMAP.1
CONT: J215422+ J2154+0037.HGEOM.1
Declination (J2000)
Right Ascension (J2000)
Grey scale flux range= 3.98 10.04 Kilo
Cont peak flux = 5.2565E-03 JY/BEAM
Levs = 2.500E-04 * (1, 1.400, 2, 2.800, 4, 5.600, 8, 11, 16, 23, 32, 45, 64, 90, 128, 181, 256, 362, 512, 724, 1024)

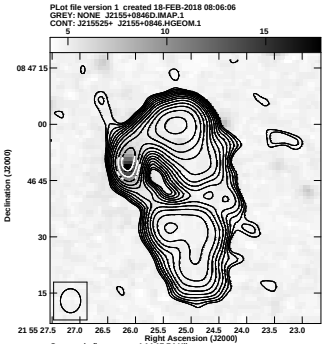
PLot file version 1 created 18-FEB-2018 08:06:06
GREY: NONE J2155+0846D.IMAP.1
CONT: J215525+ J2155+0846.HGEOM.1
Declination (J2000)
Right Ascension (J2000)
Grey scale flux range= 4.14 17.74 Kilo
Cont peak flux = 1.8196E-02 JY/BEAM
Levs = 2.500E-04 * (1, 1.400, 2, 2.800, 4, 5.600, 8, 11, 16, 23, 32, 45, 64, 90, 128, 181, 256, 362, 512, 724, 1024)

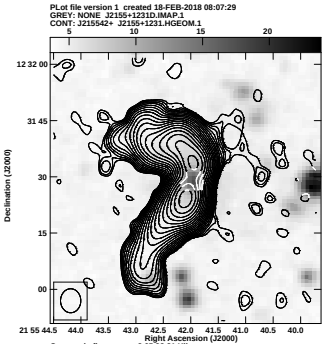
PLot file version 1 created 18-FEB-2018 08:07:29
GREY: NONE J2155+1231D.IMAP.1
CONT: J215542+ J2155+1231.HGEOM.1
Declination (J2000)
Right Ascension (J2000)
Grey scale flux range= 3.65 23.81 Kilo
Cont peak flux = 1.5798E-01 JY/BEAM
Levs = 2.500E-04 * (1, 1.400, 2, 2.800, 4, 5.600, 8, 11, 16, 23, 32, 45, 64, 90, 128, 181, 256, 362, 512, 724, 1024)

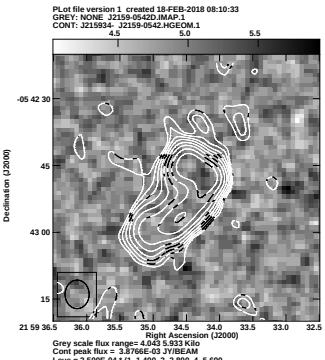
PLot file version 1 created 18-FEB-2018 08:10:33
GREY: NONE J2159-0542D.IMAP.1
CONT: J215934- J2159-0542.HGEOM.1
Declination (J2000)
Right Ascension (J2000)
Grey scale flux range= 4.043 5.933 Kilo
Cont peak flux = 3.8766E-03 JY/BEAM
Levs = 2.500E-04 * (1, 1.400, 2, 2.800, 4, 5.600, 8, 11, 16, 23, 32, 45, 64, 90, 128, 181, 256, 362, 512, 724, 1024)

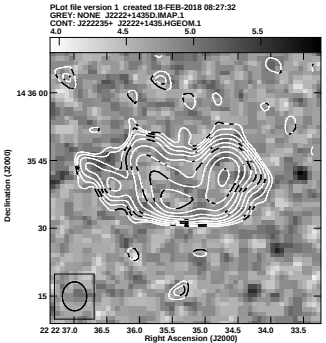
PLot file version 1 created 18-FEB-2018 08:27:32
GREY: NONE J2222+1435D.IMAP.1
CONT: J222235+ J2222+1435.HGEOM.1
Declination (J2000)
Right Ascension (J2000)
Grey scale flux range= 3.939 5.940 Kilo
Cont peak flux = 4.2738E-03 JY/BEAM
Levs = 2.500E-04 * (1, 1.400, 2, 2.800, 4, 5.600, 8, 11, 16, 23, 32, 45, 64, 90, 128, 181, 256, 362, 512, 724, 1024)

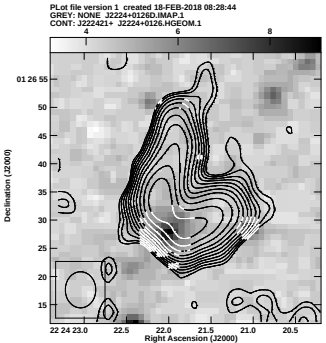
PLot file version 1 created 18-FEB-2018 08:28:44
GREY: NONE J2224+0126D.IMAP.1
CONT: J222421+ J2224+0126.HGEOM.1
Declination (J2000)
Right Ascension (J2000)
Grey scale flux range= 3.238 9.088 Kilo
Cont peak flux = 1.1106E-02 JY/BEAM
Levs = 2.500E-04 * (1, 1.400, 2, 2.800, 4, 5.600, 8, 11, 16, 23, 32, 45, 64, 90, 128, 181, 256, 362, 512, 724, 1024)

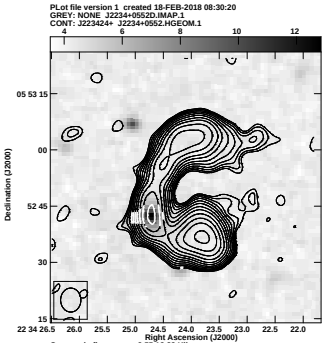
PLot file version 1 created 18-FEB-2018 08:30:20
GREY: NONE J2234+0552D.IMAP.1
CONT: J223424+ J2234+0552.HGEOM.1
Declination (J2000)
Right Ascension (J2000)
Grey scale flux range= 3.55 12.82 Kilo
Cont peak flux = 1.2283E-02 JY/BEAM
Levs = 2.500E-04 * (1, 1.400, 2, 2.800, 4, 5.600, 8, 11, 16, 23, 32, 45, 64, 90, 128, 181, 256, 362, 512, 724, 1024)

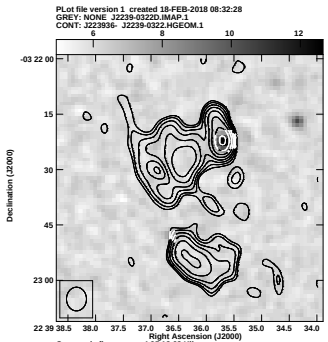
PLot file version 1 created 18-FEB-2018 08:32:28
GREY: NONE J2239-0322D.IMAP.1
CONT: J223936- J2239-0322.HGEOM.1
Declination (J2000)
Right Ascension (J2000)
Grey scale flux range= 4.95 12.63 Kilo
Cont peak flux = 2.9218E-03 JY/BEAM
Levs = 2.500E-04 * (1, 1.400, 2, 2.800, 4, 5.600, 8, 11, 16, 23, 32, 45, 64, 90, 128, 181, 256, 362, 512, 724, 1024)

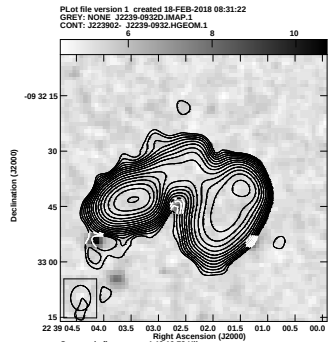
PLot file version 1 created 18-FEB-2018 08:31:22
GREY: NONE J2239-0932D.IMAP.1
CONT: J223902- J2239-0932.HGEOM.1
Declination (J2000)
Right Ascension (J2000)
Grey scale flux range= 4.40 10.72 Kilo
Cont peak flux = 3.2663E-02 JY/BEAM
Levs = 2.500E-04 * (1, 1.400, 2, 2.800, 4, 5.600, 8, 11, 16, 23, 32, 45, 64, 90, 128, 181, 256, 362, 512, 724, 1024)

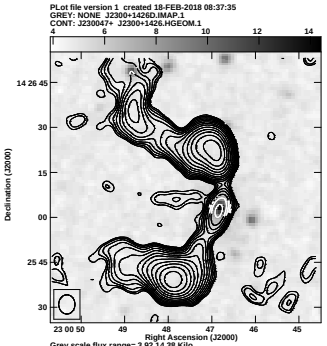
PLot file version 1 created 18-FEB-2018 08:37:35
GREY: NONE J2300+1426D.IMAP.1
CONT: J230047+ J2300+1426.HGEOM.1
Declination (J2000)
Right Ascension (J2000)
Grey scale flux range= 3.92 14.38 Kilo
Cont peak flux = 2.1015E-02 JY/BEAM
Levs = 2.500E-04 * (1, 1.400, 2, 2.800, 4, 5.600, 8, 11, 16, 23, 32, 45, 64, 90, 128, 181, 256, 362, 512, 724, 1024)

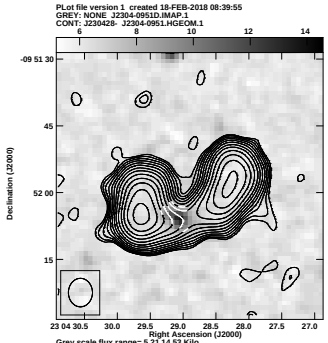
PLot file version 1 created 18-FEB-2018 08:39:55
GREY: NONE J2304-0951D.IMAP.1
CONT: J230428- J2304-0951.HGEOM.1
Declination (J2000)
Right Ascension (J2000)
Grey scale flux range= 5.21 14.53 Kilo
Cont peak flux = 1.8816E-02 JY/BEAM
Levs = 2.500E-04 * (1, 1.400, 2, 2.800, 4, 5.600, 8, 11, 16, 23, 32, 45, 64, 90, 128, 181, 256, 362, 512, 724, 1024)

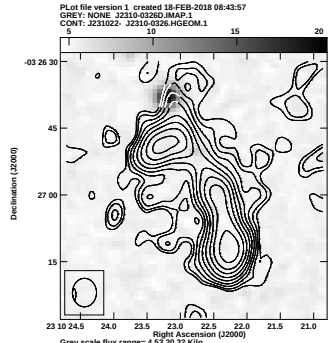
PLot file version 1 created 18-FEB-2018 08:43:57
GREY: NONE J2310-0326D.IMAP.1
CONT: J231022- J2310-0326.HGEOM.1
Declination (J2000)
Right Ascension (J2000)
Grey scale flux range= 4.53 20.32 Kilo
Cont peak flux = 5.3114E-03 JY/BEAM
Levs = 2.500E-04 * (1, 1.400, 2, 2.800, 4, 5.600, 8, 11, 16, 23, 32, 45, 64, 90, 128, 181, 256, 362, 512, 724, 1024)

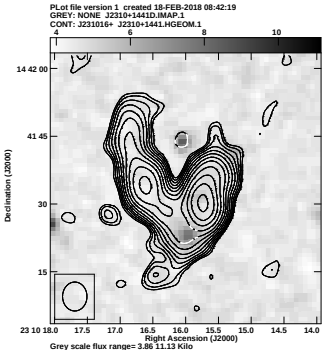
PLot file version 1 created 18-FEB-2018 08:42:19
GREY: NONE J2310+1441D.IMAP.1
CONT: J231016+ J2310+1441.HGEOM.1
Declination (J2000)
Right Ascension (J2000)
Grey scale flux range= 3.86 11.13 Kilo
Cont peak flux = 1.2458E-02 JY/BEAM
Levs = 2.500E-04 * (1, 1.400, 2, 2.800, 4, 5.600, 8, 11, 16, 23, 32, 45, 64, 90, 128, 181, 256, 362, 512, 724, 1024)

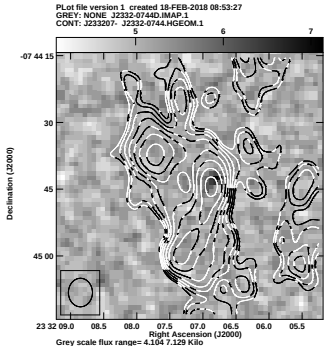
PLot file version 1 created 18-FEB-2018 08:53:27
GREY: NONE J2332-0744D.IMAP.1
CONT: J233207- J2332-0744.HGEOM.1
Declination (J2000)
Right Ascension (J2000)
Grey scale flux range= 4.104 7.129 Kilo
Cont peak flux = 3.1478E-03 JY/BEAM
Levs = 2.500E-04 * (1, 1.400, 2, 2.800, 4, 5.600, 8, 11, 16, 23, 32, 45, 64, 90, 128, 181, 256, 362, 512, 724, 1024)

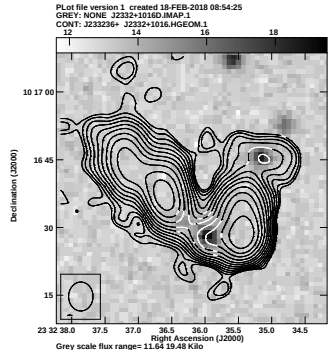
PLot file version 1 created 18-FEB-2018 08:54:25
GREY: NONE J2332+1016D.IMAP.1
CONT: J233236+ J2332+1016.HGEOM.1
Declination (J2000)
Right Ascension (J2000)
Grey scale flux range= 11.64 19.48 Kilo
Cont peak flux = 1.5931E-02 JY/BEAM
Levs = 2.500E-04 * (1, 1.400, 2, 2.800, 4, 5.600, 8, 11, 16, 23, 32, 45, 64, 90, 128, 181, 256, 362, 512, 724, 1024)

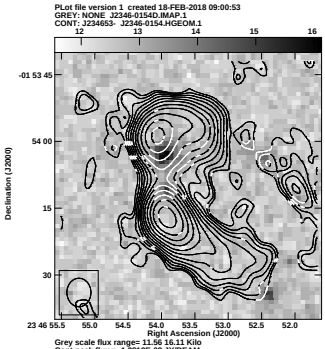
PLot file version 1 created 18-FEB-2018 09:00:53
GREY: NONE J2346-0154D.IMAP.1
CONT: J234653- J2346-0154.HGEOM.1
Declination (J2000)
Right Ascension (J2000)
Grey scale flux range= 11.56 16.11 Kilo
Cont peak flux = 1.3813E-02 JY/BEAM
Levs = 2.500E-04 * (1, 1.400, 2, 2.800, 4, 5.600, 8, 11, 16, 23, 32, 45, 64, 90, 128, 181, 256, 362, 512, 724, 1024)

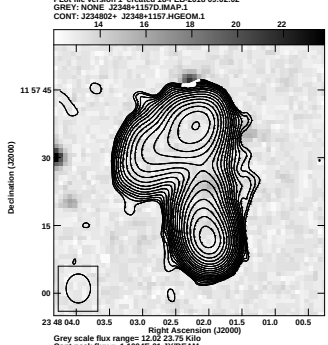
PLot file version 1 created 18-FEB-2018 09:02:02
GREY: NONE J2348+1157D.IMAP.1
CONT: J234802+ J2348+1157.HGEOM.1
Declination (J2000)
Right Ascension (J2000)
Grey scale flux range= 12.02 23.75 Kilo
Cont peak flux = 1.1004E-01 JY/BEAM
Levs = 2.500E-04 * (1, 1.400, 2, 2.800, 4, 5.600, 8, 11, 16, 23, 32, 45, 64, 90, 128, 181, 256, 362, 512, 724, 1024)

Appendix C

All contour images of LoTSS BT sources

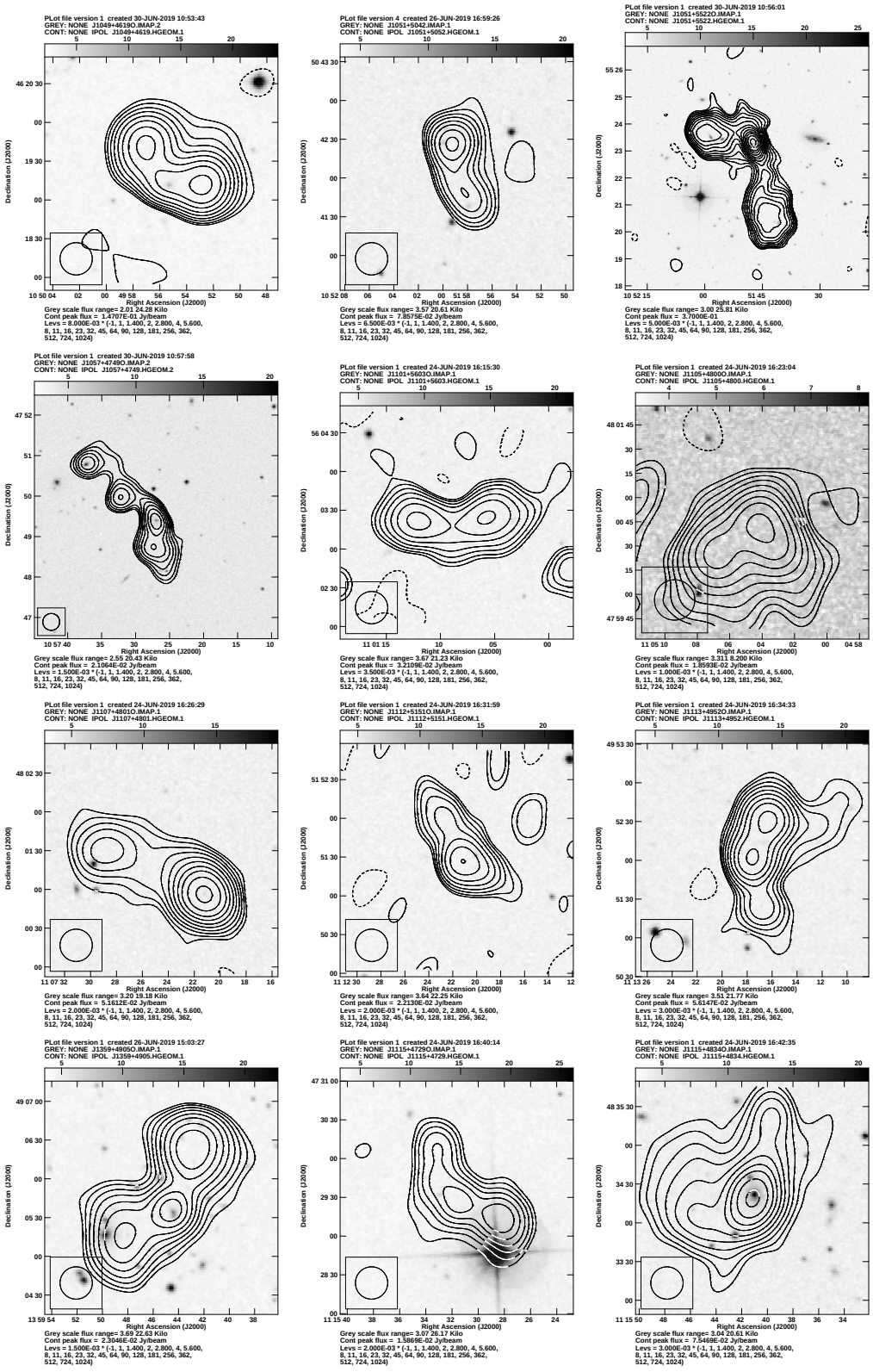

Figure 8: LoTSS image of Wide Angle Tail (NAT) radio sources (contours) overlaid on the DSS2 red image (gray scale).

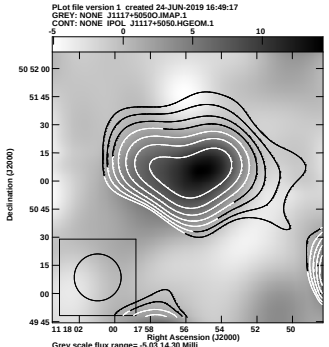
PLot file version 1 created 24-JUN-2019 16:49:17
GREY: NONE J1117+5050O.IMAP-1
CONT: NONE IPOL J1117+5050.HGEOM.1
Declination (J2000)
Right Ascension (J2000)
Grey scale flux range= -5.03 14.30 Milli
Cont peak flux = 2.1667E-02 Jy/beam
Levs = 2.000E-03 * (-1, 1, 1.400, 2, 2.800, 4, 5.600, 8, 11, 16, 23, 32, 45, 64, 90, 128, 181, 256, 362, 512, 724, 1024)

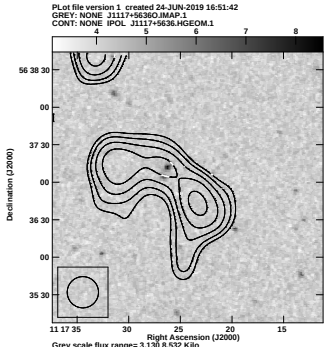
PLot file version 1 created 24-JUN-2019 16:51:42
GREY: NONE J1117+5636O.IMAP-1
CONT: NONE IPOL J1117+5636.HGEOM.1
Declination (J2000)
Right Ascension (J2000)
Grey scale flux range= 3.130 8.532 Kilo
Cont peak flux = 9.1226E-03 Jy/beam
Levs = 2.000E-03 * (-1, 1, 1.400, 2, 2.800, 4, 5.600, 8, 11, 16, 23, 32, 45, 64, 90, 128, 181, 256, 362, 512, 724, 1024)

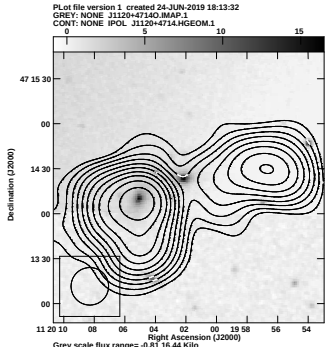
PLot file version 1 created 24-JUN-2019 18:13:32
GREY: NONE J1120+4714O.IMAP-1
CONT: NONE IPOL J1120+4714.HGEOM.1
Declination (J2000)
Right Ascension (J2000)
Grey scale flux range= -0.81 16.44 Kilo
Cont peak flux = 9.5549E-02 Jy/beam
Levs = 3.000E-03 * (-1, 1, 1.400, 2, 2.800, 4, 5.600, 8, 11, 16, 23, 32, 45, 64, 90, 128, 181, 256, 362, 512, 724, 1024)

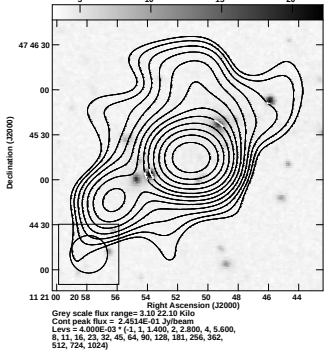
PLot file version 1 created 24-JUN-2019 18:16:28
GREY: NONE J1120+4746O.IMAP-1
CONT: NONE IPOL J1120+4746.HGEOM.1
Declination (J2000)
Right Ascension (J2000)
Grey scale flux range= 3.10 22.10 Kilo
Cont peak flux = 2.4514E-01 Jy/beam
Levs = 4.000E-03 * (-1, 1, 1.400, 2, 2.800, 4, 5.600, 8, 11, 16, 23, 32, 45, 64, 90, 128, 181, 256, 362, 512, 724, 1024)

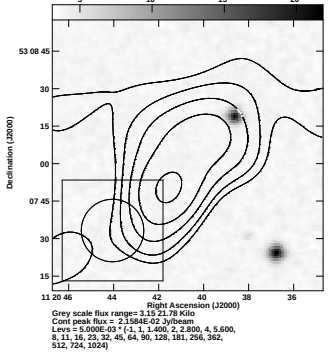
PLot file version 1 created 24-JUN-2019 18:20:35
GREY: NONE J1120+5308.IMAP-1
CONT: NONE IPOL J1120+5308.HGEOM.1
Declination (J2000)
Right Ascension (J2000)
Grey scale flux range= 3.15 21.78 Kilo
Cont peak flux = 2.1584E-02 Jy/beam
Levs = 5.000E-03 * (-1, 1, 1.400, 2, 2.800, 4, 5.600, 8, 11, 16, 23, 32, 45, 64, 90, 128, 181, 256, 362, 512, 724, 1024)

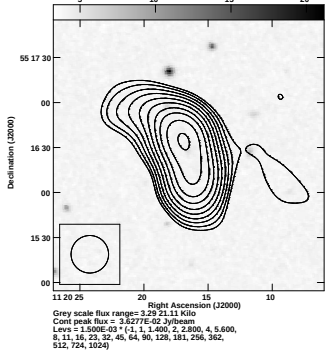
PLot file version 1 created 24-JUN-2019 18:22:51
GREY: NONE J1120+5516O.IMAP-1
CONT: NONE IPOL J1120+5516.HGEOM.1
Declination (J2000)
Right Ascension (J2000)
Grey scale flux range= 3.29 21.11 Kilo
Cont peak flux = 3.6277E-02 Jy/beam
Levs = 1.500E-03 * (-1, 1, 1.400, 2, 2.800, 4, 5.600, 8, 11, 16, 23, 32, 45, 64, 90, 128, 181, 256, 362, 512, 724, 1024)

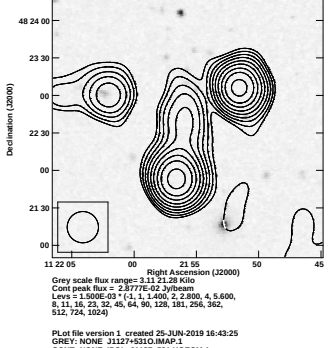
PLot file version 1 created 24-JUN-2019 18:25:23
GREY: NONE J1121+4822O.IMAP-1
CONT: NONE IPOL J1121+4822.HGEOM.1
Declination (J2000)
Right Ascension (J2000)
Grey scale flux range= 3.11 21.28 Kilo
Cont peak flux = 2.8777E-02 Jy/beam
Levs = 1.500E-03 * (-1, 1, 1.400, 2, 2.800, 4, 5.600, 8, 11, 16, 23, 32, 45, 64, 90, 128, 181, 256, 362, 512, 724, 1024)

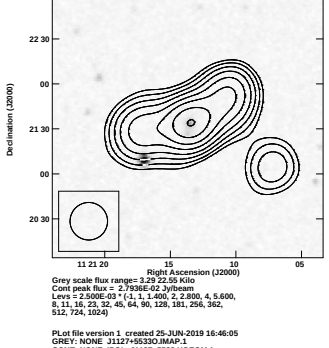
PLot file version 1 created 30-JUN-2019 11:00:51
GREY: NONE J1121+5421O.IMAP-3
CONT: NONE IPOL J1121+5421.HGEOM.2
Declination (J2000)
Right Ascension (J2000)
Grey scale flux range= 3.29 22.95 Kilo
Cont peak flux = 2.7936E-02 Jy/beam
Levs = 2.500E-03 * (-1, 1, 1.400, 2, 2.800, 4, 5.600, 8, 11, 16, 23, 32, 45, 64, 90, 128, 181, 256, 362, 512, 724, 1024)

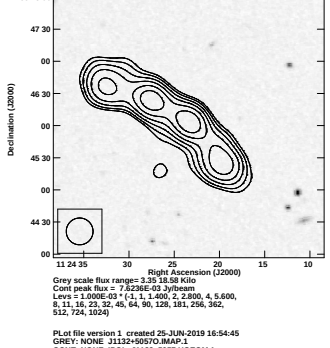
PLot file version 1 created 25-JUN-2019 16:39:17
GREY: NONE J1124+5546O.IMAP-1
CONT: NONE IPOL J1124+5546.HGEOM.1
Declination (J2000)
Right Ascension (J2000)
Grey scale flux range= 3.35 18.58 Kilo
Cont peak flux = 7.6236E-03 Jy/beam
Levs = 1.000E-03 * (-1, 1, 1.400, 2, 2.800, 4, 5.600, 8, 11, 16, 23, 32, 45, 64, 90, 128, 181, 256, 362, 512, 724, 1024)

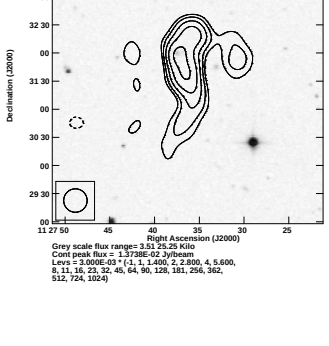
PLot file version 1 created 25-JUN-2019 16:43:25
GREY: NONE J1127+5310.IMAP-1
CONT: NONE IPOL J1127+531.HGEOM.1
Declination (J2000)
Right Ascension (J2000)
Grey scale flux range= 3.51 25.25 Kilo
Cont peak flux = 1.3738E-02 Jy/beam
Levs = 3.000E-03 * (-1, 1, 1.400, 2, 2.800, 4, 5.600, 8, 11, 16, 23, 32, 45, 64, 90, 128, 181, 256, 362, 512, 724, 1024)

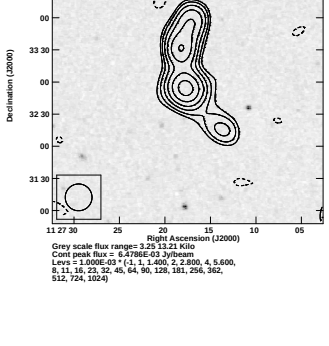
PLot file version 1 created 25-JUN-2019 16:46:05
GREY: NONE J1127+5533O.IMAP-1
CONT: NONE IPOL J1127+5533.HGEOM.1
Declination (J2000)
Right Ascension (J2000)
Grey scale flux range= 3.25 13.21 Kilo
Cont peak flux = 6.4786E-03 Jy/beam
Levs = 1.000E-03 * (-1, 1, 1.400, 2, 2.800, 4, 5.600, 8, 11, 16, 23, 32, 45, 64, 90, 128, 181, 256, 362, 512, 724, 1024)

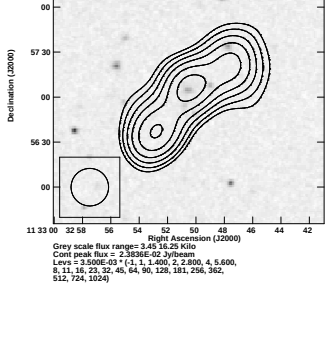
PLot file version 1 created 25-JUN-2019 16:54:45
GREY: NONE J1132+5057O.IMAP-1
CONT: NONE IPOL J1132+5057.HGEOM.1
Declination (J2000)
Right Ascension (J2000)
Grey scale flux range= 3.45 16.25 Kilo
Cont peak flux = 2.3836E-02 Jy/beam
Levs = 3.500E-03 * (-1, 1, 1.400, 2, 2.800, 4, 5.600, 8, 11, 16, 23, 32, 45, 64, 90, 128, 181, 256, 362, 512, 724, 1024)

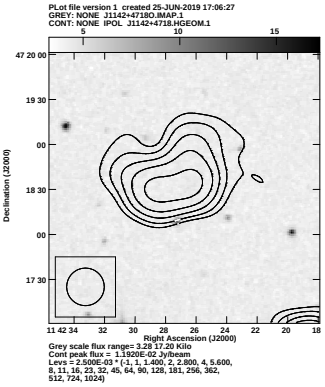
PLot file version 1 created 25-JUN-2019 17:06:27
GREY: NONE J1142+4718O.IMAP.1
CONT: NONE IPOL J1142+4718.HGEOM.1
Declination (J2000)
Right Ascension (J2000)
Grey scale flux range= 3.28 17.20 Kilo
Cont peak flux = 1.1920E-02 Jy/beam
Levs = 2.500E-03 * (-1, 1, 1.400, 2, 2.800, 4, 5.600, 8, 11, 16, 23, 32, 45, 64, 90, 128, 181, 256, 362, 512, 724, 1024)

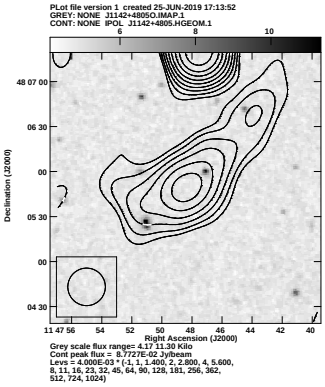
PLot file version 1 created 25-JUN-2019 17:13:52
GREY: NONE J1142+4805O.IMAP.1
CONT: NONE IPOL J1142+4805.HGEOM.1
Declination (J2000)
Right Ascension (J2000)
Grey scale flux range= 4.17 11.30 Kilo
Cont peak flux = 8.7727E-02 Jy/beam
Levs = 4.000E-03 * (-1, 1, 1.400, 2, 2.800, 4, 5.600, 8, 11, 16, 23, 32, 45, 64, 90, 128, 181, 256, 362, 512, 724, 1024)

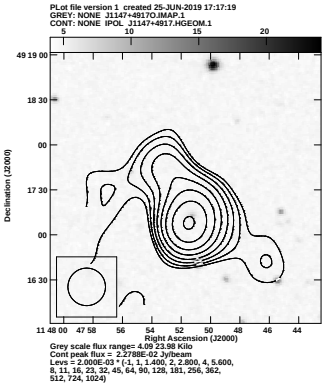
PLot file version 1 created 25-JUN-2019 17:17:19
GREY: NONE J1147+4917O.IMAP.1
CONT: NONE IPOL J1147+4917.HGEOM.1
Declination (J2000)
Right Ascension (J2000)
Grey scale flux range= 4.09 23.98 Kilo
Cont peak flux = 2.2788E-02 Jy/beam
Levs = 2.000E-03 * (-1, 1, 1.400, 2, 2.800, 4, 5.600, 8, 11, 16, 23, 32, 45, 64, 90, 128, 181, 256, 362, 512, 724, 1024)

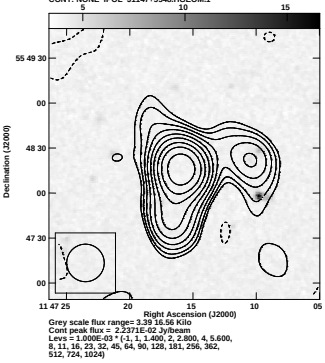
PLot file version 1 created 25-JUN-2019 17:20:20
GREY: NONE J1147+5548O.IMAP.1
CONT: NONE IPOL J1147+5548.HGEOM.1
Declination (J2000)
Right Ascension (J2000)
Grey scale flux range= 3.39 16.56 Kilo
Cont peak flux = 2.2371E-02 Jy/beam
Levs = 1.000E-03 * (-1, 1, 1.400, 2, 2.800, 4, 5.600, 8, 11, 16, 23, 32, 45, 64, 90, 128, 181, 256, 362, 512, 724, 1024)

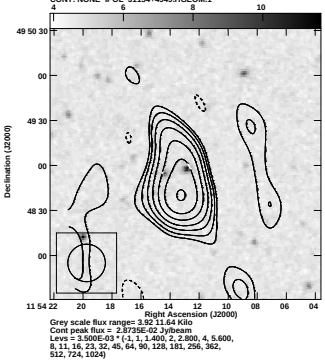
PLot file version 1 created 25-JUN-2019 18:17:53
GREY: NONE J1154+4949O.IMAP.1
CONT: NONE IPOL J1154+4949.HGEOM.1
Declination (J2000)
Right Ascension (J2000)
Grey scale flux range= 3.92 11.64 Kilo
Cont peak flux = 2.8735E-02 Jy/beam
Levs = 3.500E-03 * (-1, 1, 1.400, 2, 2.800, 4, 5.600, 8, 11, 16, 23, 32, 45, 64, 90, 128, 181, 256, 362, 512, 724, 1024)

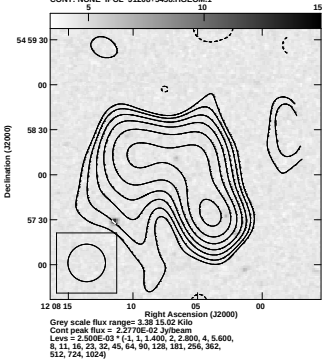
PLot file version 1 created 25-JUN-2019 18:26:45
GREY: NONE J1208+5458O.IMAP.1
CONT: NONE IPOL J1208+5458.HGEOM.1
Declination (J2000)
Right Ascension (J2000)
Grey scale flux range= 3.38 15.02 Kilo
Cont peak flux = 2.2770E-02 Jy/beam
Levs = 2.500E-03 * (-1, 1, 1.400, 2, 2.800, 4, 5.600, 8, 11, 16, 23, 32, 45, 64, 90, 128, 181, 256, 362, 512, 724, 1024)

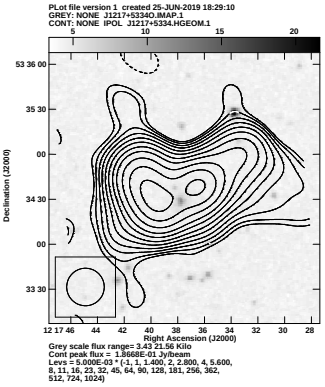
PLot file version 1 created 25-JUN-2019 18:29:10
GREY: NONE J1217+5334O.IMAP.1
CONT: NONE IPOL J1217+5334.HGEOM.1
Declination (J2000)
Right Ascension (J2000)
Grey scale flux range= 3.43 21.56 Kilo
Cont peak flux = 1.8668E-01 Jy/beam
Levs = 5.000E-03 * (-1, 1, 1.400, 2, 2.800, 4, 5.600, 8, 11, 16, 23, 32, 45, 64, 90, 128, 181, 256, 362, 512, 724, 1024)

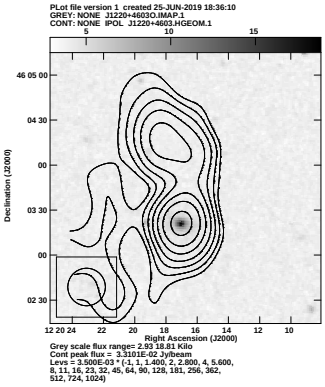
PLot file version 1 created 25-JUN-2019 18:36:10
GREY: NONE J1220+4603O.IMAP.1
CONT: NONE IPOL J1220+4603.HGEOM.1
Declination (J2000)
Right Ascension (J2000)
Grey scale flux range= 2.93 18.81 Kilo
Cont peak flux = 3.3101E-02 Jy/beam
Levs = 3.500E-03 * (-1, 1, 1.400, 2, 2.800, 4, 5.600, 8, 11, 16, 23, 32, 45, 64, 90, 128, 181, 256, 362, 512, 724, 1024)

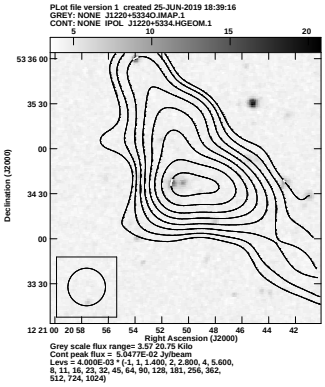
PLot file version 1 created 25-JUN-2019 18:39:16
GREY: NONE J1220+5334O.IMAP.1
CONT: NONE IPOL J1220+5334.HGEOM.1
Declination (J2000)
Right Ascension (J2000)
Grey scale flux range= 3.57 20.75 Kilo
Cont peak flux = 5.0477E-02 Jy/beam
Levs = 4.000E-03 * (-1, 1, 1.400, 2, 2.800, 4, 5.600, 8, 11, 16, 23, 32, 45, 64, 90, 128, 181, 256, 362, 512, 724, 1024)

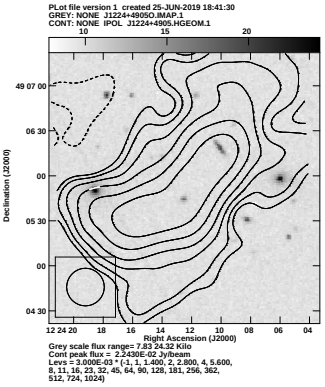
PLot file version 1 created 25-JUN-2019 18:41:30
GREY: NONE J1224+4905O.IMAP.1
CONT: NONE IPOL J1224+4905.HGEOM.1
Declination (J2000)
Right Ascension (J2000)
Grey scale flux range= 7.83 24.32 Kilo
Cont peak flux = 2.2430E-02 Jy/beam
Levs = 3.000E-03 * (-1, 1, 1.400, 2, 2.800, 4, 5.600, 8, 11, 16, 23, 32, 45, 64, 90, 128, 181, 256, 362, 512, 724, 1024)

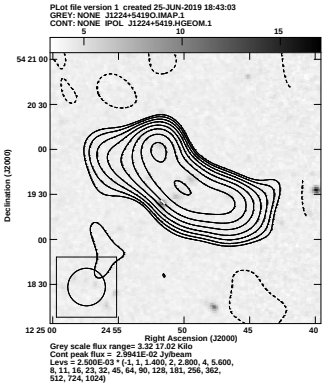
PLot file version 1 created 25-JUN-2019 18:43:03
GREY: NONE J1224+5419O.IMAP.1
CONT: NONE IPOL J1224+5419.HGEOM.1
Declination (J2000)
Right Ascension (J2000)
Grey scale flux range= 3.32 17.02 Kilo
Cont peak flux = 2.9941E-02 Jy/beam
Levs = 2.500E-03 * (-1, 1, 1.400, 2, 2.800, 4, 5.600, 8, 11, 16, 23, 32, 45, 64, 90, 128, 181, 256, 362, 512, 724, 1024)

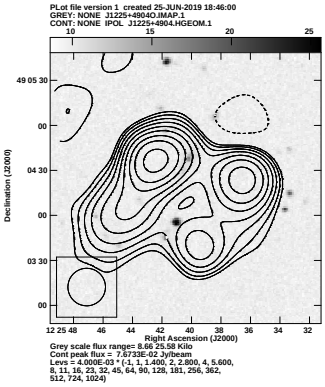
PLot file version 1 created 25-JUN-2019 18:46:00
GREY: NONE J1225+4904O.IMAP.1
CONT: NONE IPOL J1225+4904.HGEOM.1
Declination (J2000)
Right Ascension (J2000)
Grey scale flux range= 8.66 25.58 Kilo
Cont peak flux = 7.6733E-02 Jy/beam
Levs = 4.000E-03 * (-1, 1, 1.400, 2, 2.800, 4, 5.600, 8, 11, 16, 23, 32, 45, 64, 90, 128, 181, 256, 362, 512, 724, 1024)

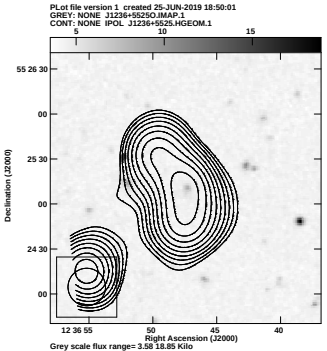
PLot file version 1 created 25-JUN-2019 18:50:01
GREY: NONE J1236+5525O.IMAP.1
CONT: NONE IPOL J1236+5525.HGEOM.1
Declination (J2000)
Right Ascension (J2000)
Grey scale flux range= 3.58 18.85 Kilo
Cont peak flux = 8.3667E-02 Jy/beam
Levs = 4.000E-03 * (-1, 1, 1.400, 2, 2.800, 4, 5.600, 8, 11, 16, 23, 32, 45, 64, 90, 128, 181, 256, 362, 512, 724, 1024)

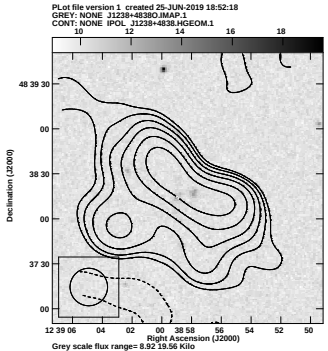
PLot file version 1 created 25-JUN-2019 18:52:18
GREY: NONE J1238+4838O.IMAP.1
CONT: NONE IPOL J1238+4838.HGEOM.1
Declination (J2000)
Right Ascension (J2000)
Grey scale flux range= 8.92 19.56 Kilo
Cont peak flux = 3.7213E-02 Jy/beam
Levs = 5.000E-03 * (-1, 1, 1.400, 2, 2.800, 4, 5.600, 8, 11, 16, 23, 32, 45, 64, 90, 128, 181, 256, 362, 512, 724, 1024)

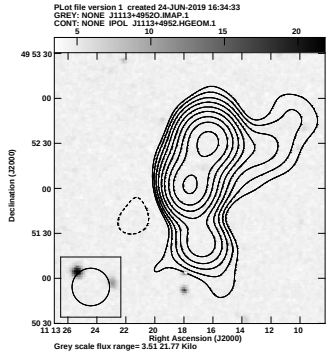
PLot file version 1 created 28-JUN-2019 16:34:33
GREY: NONE J1113+4952O.IMAP.1
CONT: NONE IPOL J1113+4952.HGEOM.1
Declination (J2000)
Right Ascension (J2000)
Grey scale flux range= 3.51 21.77 Kilo
Cont peak flux = 5.8147E-02 Jy/beam
Levs = 3.000E-03 * (-1, 1, 1.400, 2, 2.800, 4, 5.600, 8, 11, 16, 23, 32, 45, 64, 90, 128, 181, 256, 362, 512, 724, 1024)

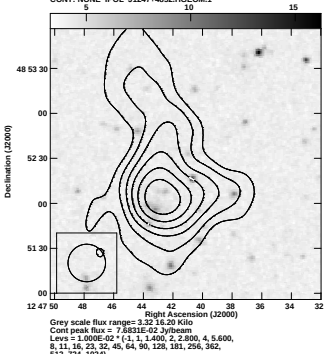
PLot file version 1 created 26-JUN-2019 13:12:38
GREY: NONE J1247+4852O.IMAP.1
CONT: NONE IPOL J1247+4852.HGEOM.1
Declination (J2000)
Right Ascension (J2000)
Grey scale flux range= 3.32 16.20 Kilo
Cont peak flux = 7.8831E-02 Jy/beam
Levs = 1.000E-02 * (-1, 1, 1.400, 2, 2.800, 4, 5.600, 8, 11, 16, 23, 32, 45, 64, 90, 128, 181, 256, 362, 512, 724, 1024)

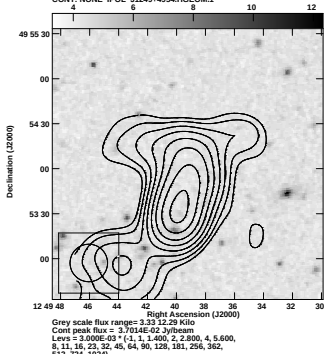
PLot file version 1 created 26-JUN-2019 13:19:02
GREY: NONE J1249+4954O.IMAP.1
CONT: NONE IPOL J1249+4954.HGEOM.1
Declination (J2000)
Right Ascension (J2000)
Grey scale flux range= 3.33 12.29 Kilo
Cont peak flux = 3.7014E-02 Jy/beam
Levs = 3.000E-03 * (-1, 1, 1.400, 2, 2.800, 4, 5.600, 8, 11, 16, 23, 32, 45, 64, 90, 128, 181, 256, 362, 512, 724, 1024)

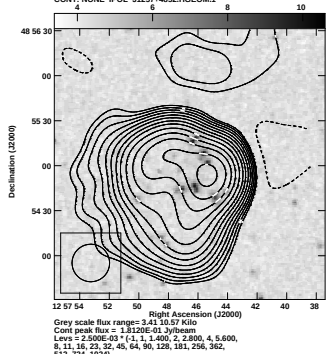
PLot file version 1 created 26-JUN-2019 13:21:56
GREY: NONE J1257+4852O.IMAP.1
CONT: NONE IPOL J1257+4852.HGEOM.1
Declination (J2000)
Right Ascension (J2000)
Grey scale flux range= 3.41 10.57 Kilo
Cont peak flux = 1.8120E-01 Jy/beam
Levs = 2.500E-03 * (-1, 1, 1.400, 2, 2.800, 4, 5.600, 8, 11, 16, 23, 32, 45, 64, 90, 128, 181, 256, 362, 512, 724, 1024)

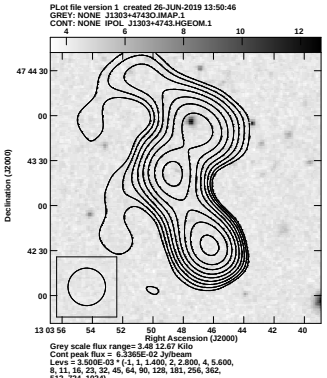
PLot file version 1 created 26-JUN-2019 13:50:46
GREY: NONE J1303+4743O.IMAP.1
CONT: NONE IPOL J1303+4743.HGEOM.1
Declination (J2000)
Right Ascension (J2000)
Grey scale flux range= 3.48 12.67 Kilo
Cont peak flux = 6.3360E-02 Jy/beam
Levs = 3.500E-03 * (-1, 1, 1.400, 2, 2.800, 4, 5.600, 8, 11, 16, 23, 32, 45, 64, 90, 128, 181, 256, 362, 512, 724, 1024)

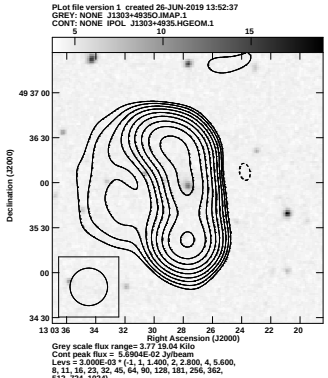
PLot file version 1 created 26-JUN-2019 13:52:37
GREY: NONE J1303+4935O.IMAP.1
CONT: NONE IPOL J1303+4935.HGEOM.1
Declination (J2000)
Right Ascension (J2000)
Grey scale flux range= 3.77 19.04 Kilo
Cont peak flux = 5.6904E-02 Jy/beam
Levs = 3.000E-03 * (-1, 1, 1.400, 2, 2.800, 4, 5.600, 8, 11, 16, 23, 32, 45, 64, 90, 128, 181, 256, 362, 512, 724, 1024)

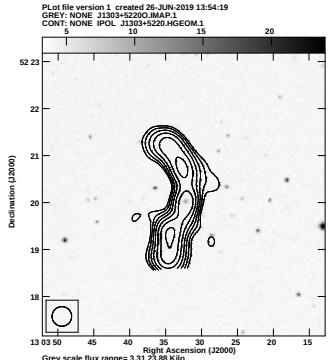
PLot file version 1 created 26-JUN-2019 13:54:19
GREY: NONE J1303+5220O.IMAP.1
CONT: NONE IPOL J1303+5220.HGEOM.1
Declination (J2000)
Right Ascension (J2000)
Grey scale flux range= 3.31 23.88 Kilo
Cont peak flux = 1.7633E-02 Jy/beam
Levs = 2.000E-03 * (-1, 1, 1.400, 2, 2.800, 4, 5.600, 8, 11, 16, 23, 32, 45, 64, 90, 128, 181, 256, 362, 512, 724, 1024)

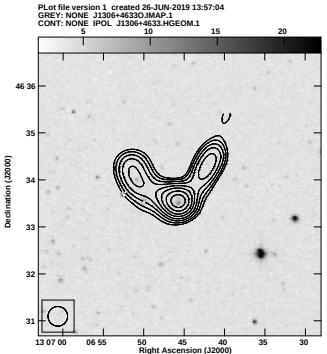
PLot file version 1 created 26-JUN-2019 13:57:04
GREY: NONE J1306+4633O.IMAP.1
CONT: NONE IPOL J1306+4633.HGEOM.1
Declination (J2000)
Right Ascension (J2000)
Grey scale flux range= 1.72 22.68 Kilo
Cont peak flux = 8.2796E-01 Jy/beam
Levs = 6.000E-02 * (-1, 1, 1.400, 2, 2.800, 4, 5.600, 8, 11, 16, 23, 32, 45, 64, 90, 128, 181, 256, 362, 512, 724, 1024)

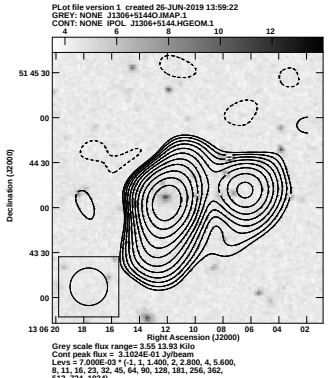
PLot file version 1 created 26-JUN-2019 13:59:22
GREY: NONE J1306+5144O.IMAP.1
CONT: NONE IPOL J1306+5144.HGEOM.1
Declination (J2000)
Right Ascension (J2000)
Grey scale flux range= 3.55 13.93 Kilo
Cont peak flux = 3.1024E-01 Jy/beam
Levs = 7.000E-03 * (-1, 1, 1.400, 2, 2.800, 4, 5.600, 8, 11, 16, 23, 32, 45, 64, 90, 128, 181, 256, 362, 512, 724, 1024)

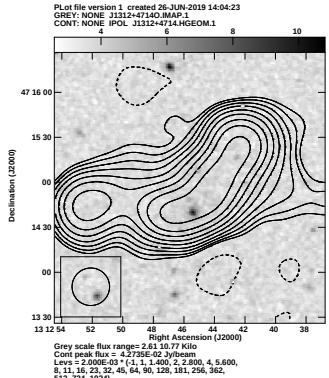
PLot file version 1 created 26-JUN-2019 14:04:23
GREY: NONE J1312+4714O.IMAP.1
CONT: NONE IPOL J1312+4714.HGEOM.1
Declination (J2000)
Right Ascension (J2000)
Grey scale flux range= 2.61 10.77 Kilo
Cont peak flux = 4.2735E-02 Jy/beam
Levs = 2.000E-03 * (-1, 1, 1.400, 2, 2.800, 4, 5.600, 8, 11, 16, 23, 32, 45, 64, 90, 128, 181, 256, 362, 512, 724, 1024)

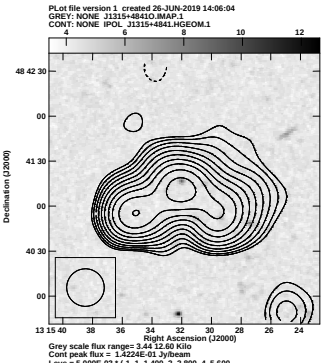
PLot file version 1 created 26-JUN-2019 14:06:04
GREY: NONE J1315+4841O.IMAP.1
CONT: NONE IPOL J1315+4841.HGEOM.1
Declination (J2000)
Right Ascension (J2000)
Grey scale flux range= 3.44 12.60 Kilo
Cont peak flux = 1.4224E-01 Jy/beam
Levs = 5.000E-03 * (-1, 1, 1.400, 2, 2.800, 4, 5.600, 8, 11, 16, 23, 32, 45, 64, 90, 128, 181, 256, 362, 512, 724, 1024)

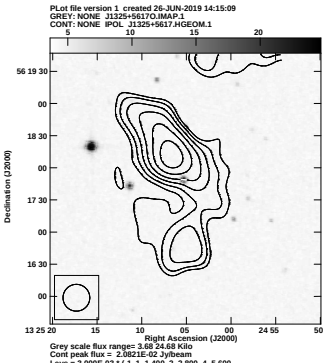
PLot file version 1 created 26-JUN-2019 14:15:09
GREY: NONE J1325+5617O.IMAP.1
CONT: NONE IPOL J1325+5617.HGEOM.1
Declination (J2000)
Right Ascension (J2000)
Grey scale flux range= 3.68 24.68 Kilo
Cont peak flux = 2.0821E-02 Jy/beam
Levs = 3.000E-03 * (-1, 1, 1.400, 2, 2.800, 4, 5.600, 8, 11, 16, 23, 32, 45, 64, 90, 128, 181, 256, 362, 512, 724, 1024)

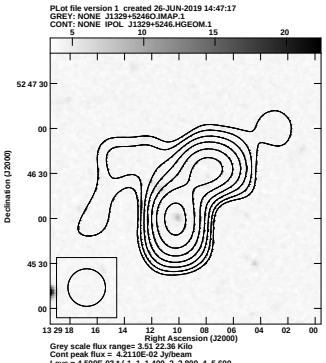
PLot file version 1 created 26-JUN-2019 14:47:17
GREY: NONE J1329+5246O.IMAP.1
CONT: NONE IPOL J1329+5246.HGEOM.1
Declination (J2000)
Right Ascension (J2000)
Grey scale flux range= 3.51 22.36 Kilo
Cont peak flux = 4.2110E-02 Jy/beam
Levs = 4.500E-03 * (-1, 1, 1.400, 2, 2.800, 4, 5.600, 8, 11, 16, 23, 32, 45, 64, 90, 128, 181, 256, 362, 512, 724, 1024)

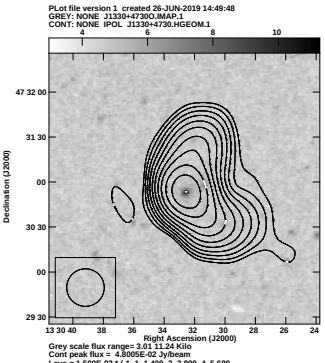
PLot file version 1 created 26-JUN-2019 14:49:48
GREY: NONE J1330+4730O.IMAP.1
CONT: NONE IPOL J1330+4730.HGEOM.1
Declination (J2000)
Right Ascension (J2000)
Grey scale flux range= 3.01 11.24 Kilo
Cont peak flux = 4.8005E-02 Jy/beam
Levs = 1.500E-03 * (-1, 1, 1.400, 2, 2.800, 4, 5.600, 8, 11, 16, 23, 32, 45, 64, 90, 128, 181, 256, 362, 512, 724, 1024)

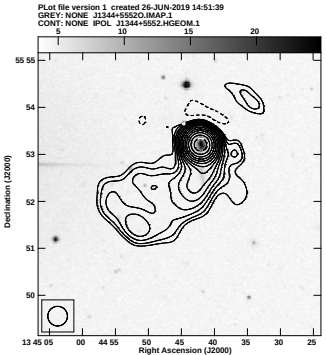
PLot file version 1 created 26-JUN-2019 14:51:39
GREY: NONE J1344+5552O.IMAP.1
CONT: NONE IPOL J1344+5552.HGEOM.1
Declination (J2000)
Right Ascension (J2000)
Grey scale flux range= 3.59 24.81 Kilo
Cont peak flux = 3.5148E-01 Jy/beam
Levs = 3.000E-03 * (-1, 1, 1.400, 2, 2.800, 4, 5.600, 8, 11, 16, 23, 32, 45, 64, 90, 128, 181, 256, 362, 512, 724, 1024)

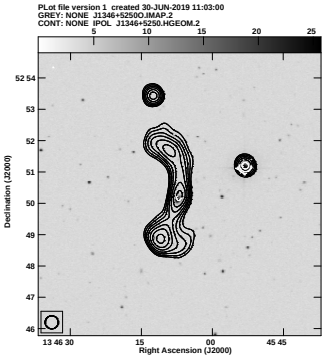
PLot file version 1 created 30-JUN-2019 11:03:00
GREY: NONE J1346+5250O.IMAP.2
CONT: NONE IPOL J1346+5250.HGEOM.2
Declination (J2000)
Right Ascension (J2000)
Grey scale flux range= 0.01 25.63 Kilo
Cont peak flux = 2.7076E-02 Jy/beam
Levs = 3.000E-03 * (-1, 1, 1.400, 2, 2.800, 4, 5.600, 8, 11, 16, 23, 32, 45, 64, 90, 128, 181, 256, 362, 512, 724, 1024)

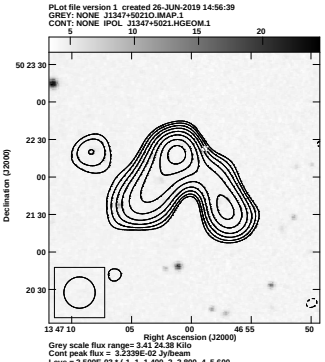
PLot file version 1 created 26-JUN-2019 14:56:39
GREY: NONE J1347+5021O.IMAP.1
CONT: NONE IPOL J1347+5021.HGEOM.1
Declination (J2000)
Right Ascension (J2000)
Grey scale flux range= 3.41 24.38 Kilo
Cont peak flux = 3.2339E-02 Jy/beam
Levs = 2.500E-03 * (-1, 1, 1.400, 2, 2.800, 4, 5.600, 8, 11, 16, 23, 32, 45, 64, 90, 128, 181, 256, 362, 512, 724, 1024)

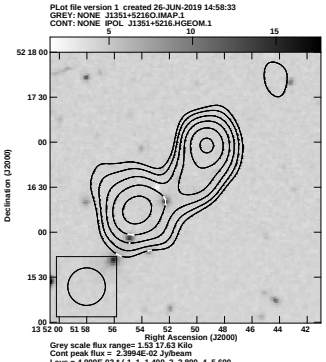
PLot file version 1 created 26-JUN-2019 14:58:33
GREY: NONE J1351+5216O.IMAP.1
CONT: NONE IPOL J1351+5216.HGEOM.1
Declination (J2000)
Right Ascension (J2000)
Grey scale flux range= 1.53 17.63 Kilo
Cont peak flux = 2.3994E-02 Jy/beam
Levs = 4.000E-03 * (-1, 1, 1.400, 2, 2.800, 4, 5.600, 8, 11, 16, 23, 32, 45, 64, 90, 128, 181, 256, 362, 512, 724, 1024)

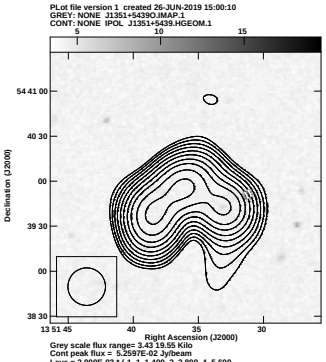
PLot file version 1 created 26-JUN-2019 15:00:10
GREY: NONE J1351+5439O.IMAP.1
CONT: NONE IPOL J1351+5439.HGEOM.1
Declination (J2000)
Right Ascension (J2000)
Grey scale flux range= 3.43 19.55 Kilo
Cont peak flux = 5.2597E-02 Jy/beam
Levs = 2.000E-03 * (-1, 1, 1.400, 2, 2.800, 4, 5.600, 8, 11, 16, 23, 32, 45, 64, 90, 128, 181, 256, 362, 512, 724, 1024)

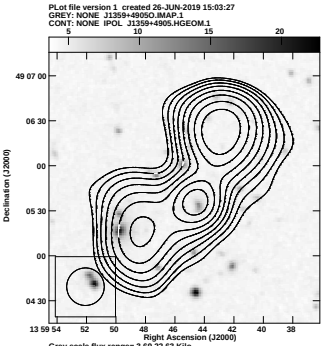
PLot file version 1 created 26-JUN-2019 15:03:27
GREY: NONE J1359+4905O.IMAP.1
CONT: NONE IPOL J1359+4905.HGEOM.1
Declination (J2000)
Right Ascension (J2000)
Grey scale flux range= 3.69 22.63 Kilo
Cont peak flux = 2.3046E-02 Jy/beam
Levs = 1.500E-03 * (-1, 1, 1.400, 2, 2.800, 4, 5.600, 8, 11, 16, 23, 32, 45, 64, 90, 128, 181, 256, 362, 512, 724, 1024)

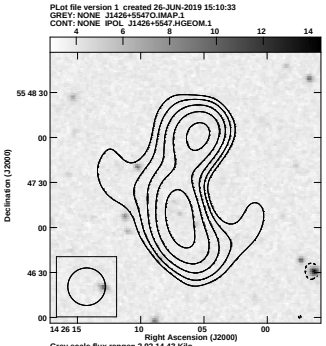
PLot file version 1 created 26-JUN-2019 15:10:33
GREY: NONE J1426+5547O.IMAP.1
CONT: NONE IPOL J1426+5547.HGEOM.1
Declination (J2000)
Right Ascension (J2000)
Grey scale flux range= 2.92 14.43 Kilo
Cont peak flux = 1.7501E-02 Jy/beam
Levs = 3.500E-03 * (-1, 1, 1.400, 2, 2.800, 4, 5.600, 8, 11, 16, 23, 32, 45, 64, 90, 128, 181, 256, 362, 512, 724, 1024)

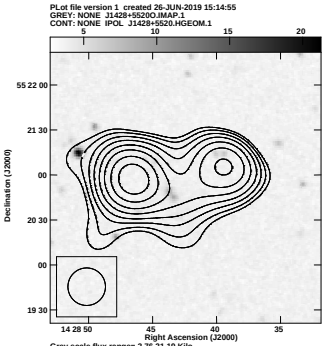
PLot file version 1 created 26-JUN-2019 15:14:55
GREY: NONE J1428+5520O.IMAP.1
CONT: NONE IPOL J1428+5520.HGEOM.1
Declination (J2000)
Right Ascension (J2000)
Grey scale flux range= 2.76 21.19 Kilo
Cont peak flux = 6.3204E-02 Jy/beam
Levs = 4.500E-03 * (-1, 1, 1.400, 2, 2.800, 4, 5.600, 8, 11, 16, 23, 32, 45, 64, 90, 128, 181, 256, 362, 512, 724, 1024)

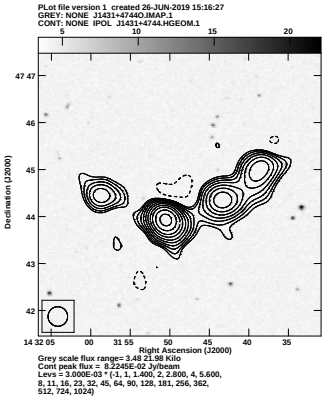
PLot file version 1 created 26-JUN-2019 15:16:27
GREY: NONE J1431+4744O.IMAP.1
CONT: NONE IPOL J1431+4744.HGEOM.1
Declination (J2000)
Right Ascension (J2000)
Grey scale flux range= 3.48 21.98 Kilo
Cont peak flux = 8.2245E-02 Jy/beam
Levs = 3.000E-03 * (-1, 1, 1.400, 2, 2.800, 4, 5.600, 8, 11, 16, 23, 32, 45, 64, 90, 128, 181, 256, 362, 512, 724, 1024)

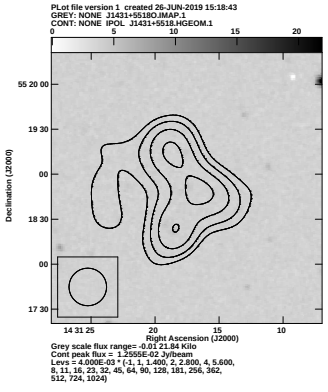
PLot file version 1 created 26-JUN-2019 15:18:43
GREY: NONE J1431+5518O.IMAP.1
CONT: NONE IPOL J1431+5518.HGEOM.1
Declination (J2000)
Right Ascension (J2000)
Grey scale flux range= -0.01 21.84 Kilo
Cont peak flux = 1.2555E-02 Jy/beam
Levs = 4.000E-03 * (-1, 1, 1.400, 2, 2.800, 4, 5.600, 8, 11, 16, 23, 32, 45, 64, 90, 128, 181, 256, 362, 512, 724, 1024)

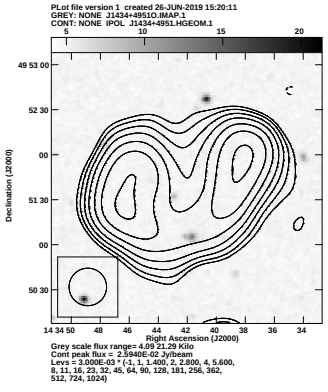
PLot file version 1 created 26-JUN-2019 15:20:11
GREY: NONE J1434+4951O.IMAP.1
CONT: NONE IPOL J1434+4951.HGEOM.1
Declination (J2000)
Right Ascension (J2000)
Grey scale flux range= 4.09 21.29 Kilo
Cont peak flux = 2.5940E-02 Jy/beam
Levs = 3.000E-03 * (-1, 1, 1.400, 2, 2.800, 4, 5.600, 8, 11, 16, 23, 32, 45, 64, 90, 128, 181, 256, 362, 512, 724, 1024)

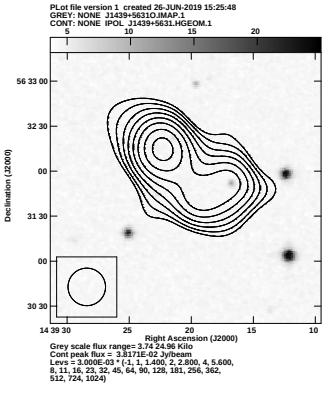
PLot file version 1 created 26-JUN-2019 15:25:48
GREY: NONE J1439+5631O.IMAP.1
CONT: NONE IPOL J1439+5631.HGEOM.1
Declination (J2000)
Right Ascension (J2000)
Grey scale flux range= 3.74 24.96 Kilo
Cont peak flux = 3.8171E-02 Jy/beam
Levs = 3.000E-03 * (-1, 1, 1.400, 2, 2.800, 4, 5.600, 8, 11, 16, 23, 32, 45, 64, 90, 128, 181, 256, 362, 512, 724, 1024)

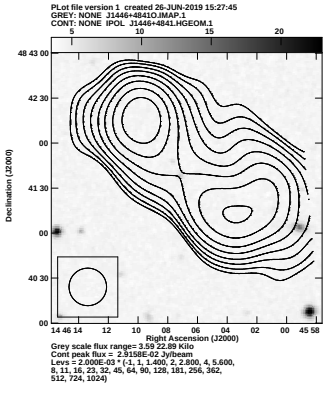
PLot file version 1 created 26-JUN-2019 15:27:45
GREY: NONE J1446+4841O.IMAP.1
CONT: NONE IPOL J1446+4841.HGEOM.1
Declination (J2000)
Right Ascension (J2000)
Grey scale flux range= 3.59 22.89 Kilo
Cont peak flux = 2.5158E-02 Jy/beam
Levs = 2.000E-03 * (-1, 1, 1.400, 2, 2.800, 4, 5.600, 8, 11, 16, 23, 32, 45, 64, 90, 128, 181, 256, 362, 512, 724, 1024)

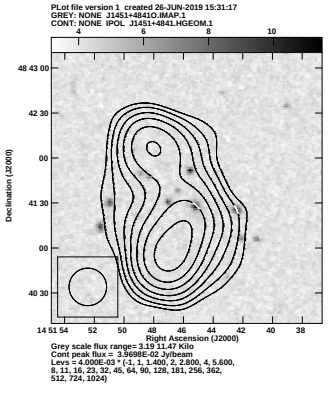
PLot file version 1 created 26-JUN-2019 15:31:17
GREY: NONE J1451+4841O.IMAP.1
CONT: NONE IPOL J1451+4841.HGEOM.1
Declination (J2000)
Right Ascension (J2000)
Grey scale flux range= 3.19 11.47 Kilo
Cont peak flux = 3.9698E-02 Jy/beam
Levs = 4.000E-03 * (-1, 1, 1.400, 2, 2.800, 4, 5.600, 8, 11, 16, 23, 32, 45, 64, 90, 128, 181, 256, 362, 512, 724, 1024)

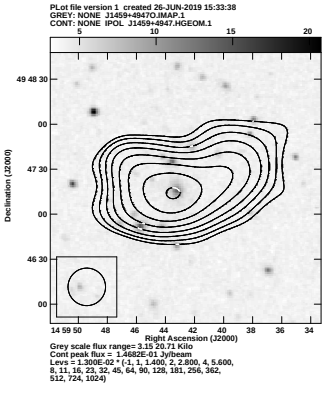
PLot file version 1 created 26-JUN-2019 15:33:38
GREY: NONE J1459+4947O.IMAP.1
CONT: NONE IPOL J1459+4947.HGEOM.1
Declination (J2000)
Right Ascension (J2000)
Grey scale flux range= 3.15 20.71 Kilo
Cont peak flux = 1.4682E-01 Jy/beam
Levs = 1.300E-02 * (-1, 1, 1.400, 2, 2.800, 4, 5.600, 8, 11, 16, 23, 32, 45, 64, 90, 128, 181, 256, 362, 512, 724, 1024)

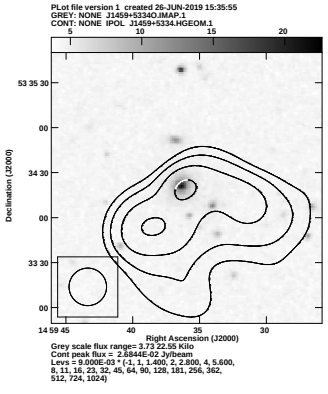
PLot file version 1 created 26-JUN-2019 15:35:55
GREY: NONE J1459+5334O.IMAP.1
CONT: NONE IPOL J1459+5334.HGEOM.1
Declination (J2000)
Right Ascension (J2000)
Grey scale flux range= 3.73 22.55 Kilo
Cont peak flux = 2.5844E-02 Jy/beam
Levs = 9.000E-03 * (-1, 1, 1.400, 2, 2.800, 4, 5.600, 8, 11, 16, 23, 32, 45, 64, 90, 128, 181, 256, 362, 512, 724, 1024)

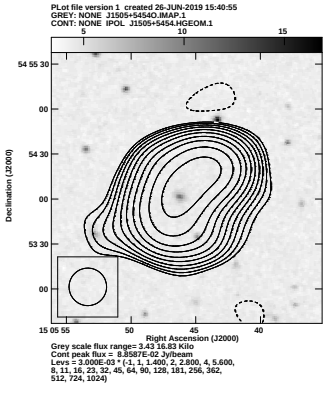
PLot file version 1 created 26-JUN-2019 15:40:55
GREY: NONE J1505+5454O.IMAP.1
CONT: NONE IPOL J1505+5454.HGEOM.1
Declination (J2000)
Right Ascension (J2000)
Grey scale flux range= 3.43 16.83 Kilo
Cont peak flux = 8.8587E-02 Jy/beam
Levs = 3.000E-03 * (-1, 1, 1.400, 2, 2.800, 4, 5.600, 8, 11, 16, 23, 32, 45, 64, 90, 128, 181, 256, 362, 512, 724, 1024)

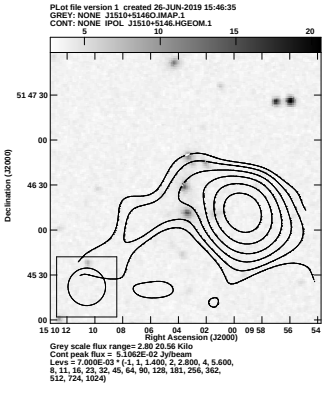
PLot file version 1 created 26-JUN-2019 15:46:35
GREY: NONE J1510+5146O.IMAP.1
CONT: NONE IPOL J1510+5146.HGEOM.1
Declination (J2000)
Right Ascension (J2000)
Grey scale flux range= 2.80 20.56 Kilo
Cont peak flux = 5.1062E-02 Jy/beam
Levs = 7.000E-03 * (-1, 1, 1.400, 2, 2.800, 4, 5.600, 8, 11, 16, 23, 32, 45, 64, 90, 128, 181, 256, 362, 512, 724, 1024)

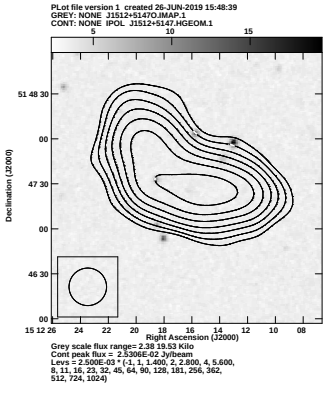
PLot file version 1 created 26-JUN-2019 15:48:39
GREY: NONE J1512+5147O.IMAP.1
CONT: NONE IPOL J1512+5147.HGEOM.1
Declination (J2000)
Right Ascension (J2000)
Grey scale flux range= 2.38 19.53 Kilo
Cont peak flux = 2.5306E-02 Jy/beam
Levs = 2.500E-03 * (-1, 1, 1.400, 2, 2.800, 4, 5.600, 8, 11, 16, 23, 32, 45, 64, 90, 128, 181, 256, 362, 512, 724, 1024)

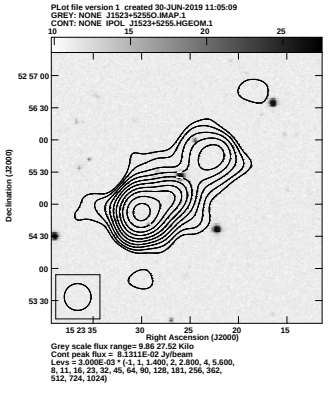
PLot file version 1 created 30-JUN-2019 11:05:09
GREY: NONE J1523+5255O.IMAP.1
CONT: NONE IPOL J1523+5255.HGEOM.1
Declination (J2000)
Right Ascension (J2000)
Grey scale flux range= 9.86 27.52 Kilo
Cont peak flux = 8.1311E-02 Jy/beam
Levs = 3.000E-03 * (-1, 1, 1.400, 2, 2.800, 4, 5.600, 8, 11, 16, 23, 32, 45, 64, 90, 128, 181, 256, 362, 512, 724, 1024)

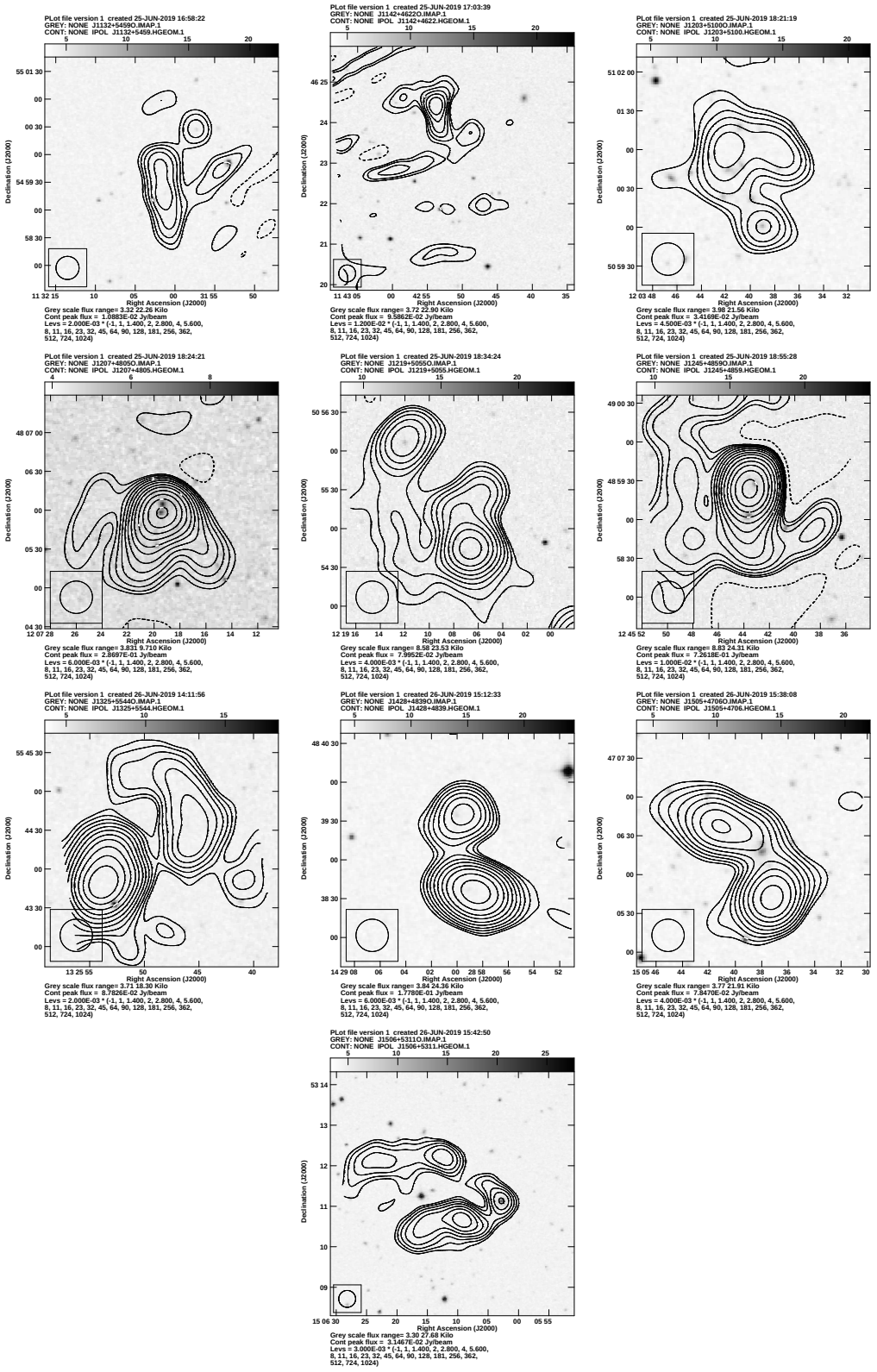

Figure 8: LoTSS image of Narrow Angle Tail (NAT) radio sources (contours) overlaid on the DSS2 red image (gray scale).